THE ROLE OF CALMODULIN IN THE REGULATION OF CALCIUM SIGNALLING PROTEINS IN HEALTH AND DISEASE

A thesis submitted in accordance with the conditions governing candidates for the degree of

Philosophiæ Doctor in Cardiff University

BRIAN LEWIS CALVER

IONIC CELL SIGNALLING
SIR GERAINT EVANS WALES HEART RESEARCH INSTITUTE
INSTITUTE OF MOLECULAR & EXPERIMENTAL MEDICINE
SCHOOL OF MEDICINE

2018

TABLE OF CONTENTS

DECLARATION

This work has not previously been accepted in substance for any degree and is not concurrently submitted in candidature for any degree.

Signed……(Candidate) Date …….

Statement 1

This thesis is being submitted in partial fulfilment of the requirements for the degree of PhD.

Signed…….(Candidate) Date …….

Statement 2

This thesis is the result of my own independent work, except where otherwise stated. Explicit references acknowledge other sources. The thesis has not been edited by a third party beyond what is permitted by Cardiff University's Policy on the Use of Third Party Editors by Research Degree Students. The views expressed are my own.

Signed…….(Candidate) Date …….

Statement 3

I hereby give consent for my thesis, if accepted, to be available for photocopying and inter-library loan, and for the title and summary to be made available to outside organisations.

Signed…….(Candidate) Date …….

Statement 4

I hereby give consent for my thesis, if accepted, to be available for photocopying and inter-library loans after the expiry of a bar on access previously approved by the Graduate Development Committee.

Signed…….(Candidate) Date …….

ACKNOWLEDGEMENTS

As a part-time, mature student, I could never have completed this PhD without the help and support of many people over the years. Firstly, I wish to thank my supervisors Prof. Anthony Lai, Prof. Karl Swann and Dr Pierre Rizkallah for allowing me the opportunity to work within their areas of research in pursuit of my studies. I am very grateful to Prof. Lai for supporting both me and the work in my thesis, sage guidance and advice, and giving me the time and freedom to work on it.

I will be forever grateful to Dr Michail Nomikos for his encouragement, confidence in me, and persuading me to embrace calcium signalling and PLCζ in the first place, and that you never work alone! I would like to thank Dr Maria Theodoridou for her help and advice with techniques, patience and good humour throughout. I thank our previous PTY students Helen Hu, Emily Matthews, Adrian Smith, Morgan Lofty and last but not least PTY/honours student/research assistant extraordinaire Luke Buntwal for their help in expressing and purifying the proteins, without their efforts and enthusiasm this thesis would be far poorer and have been less enjoyable. A big thank you to Dr Andy Tee for providing a safe harbour after the storm and for the many helpful discussions during the preparation of my thesis.

In particular, I would like to thank the following people. Dr Angelos Thanassoulas for help and advice in designing, performing and analysing the ITC and Ca^{2+} affinity experiments. Dr Konrad Beck for performing CD experiments, preparing the figures, patient explanations and interesting discussions. Dr David Cole for permitting me to work in his lab and use of the ITC microcalorimeter. Dr Pierre Rizkallah for his help and advice with setting up crystallisation experiments, harvesting

and shooting crystals, and subsequent analysis. Dr Lynda Blayney for help and advice with ryanodine binding assays. Dr Vyronia Vasilakopoulou for design and synthesis of RyR2 peptides. Dr David Edwards for advice and support when things got tricky. Also the comradeship of all past fellow students and staff of the gone but not forgotten WHRI, especially Junaid Kashir, Monika Seidel, Bevan Cumbes, Rienk Doetjes (RIP), Peter Wilson, Ajay Sharma, Peter Gapper and Wendy Scaccia.

My love and gratitude to my family. My mother, father and sister, Monica, Malcolm and Michelle for their love, support and patience during the seemingly neverending years of study despite not being entirely sure what exactly it was that I was doing with all that time. I will be eternally grateful to my wife Christine for her love, support and faith in me throughout the years regardless of my doubts, and patience during the not infrequent absences both in mind and body. Not to mention all the advice and help she has given me during the preparation of this thesis whilst also caring for our three young children. Finally, my sons Elliot, Rhys and Osian, a constant and very welcome reminder of life outside the lab. Born during my studies, it must seem that I am always working on my thesis but they have never begrudged it and their unconditional love and affection never cease to amaze me. I know they will just be delighted that I can go to the park with them more now.

DEDICATION

TO

MY WIFE AND SONS

CHRISTINE, ELLIOT, RHYS & OSIAN

SUMMARY

Calcium ions (Ca^{2+}) are major secondary signalling messengers, controlling many biological processes. Signalling relies on the activity of multiple proteins to bind, sequester, transport, release and respond to Ca^{2+}. Phospholipase C (PLC) catalyses the production of inositol 1,4,5-trisphosphate (IP_3) which stimulates the intracellular release of Ca^{2+} via IP_3 receptor (IP_3R). Another primary Ca^{2+} release channel is the ryanodine receptor (RyR). In response to changes in Ca^{2+} concentration the Ca^{2+} sensitive protein calmodulin (CaM) binds to and releases multiple proteins, including PLC and RyR ,altering function and regulating activity.

The sperm-specific PLCζ isoform stimulates oocyte activation upon fertilisation by triggering, via IP_3, subsequent Ca^{2+} release events to produce the oscillations in the Ca^{2+} concentration required for embryogenesis. Dysfunctional PLCζ causes male infertility and subfertility. The structure of PLCζ and the full mechanism of action are unknown. Recently, a novel inhibitory interaction between PLCζ and CaM was observed.

The cardiac-specific RyR2 isoform releases Ca^{2+} in cardiac myocytes during the heartbeat. Dysfunctional RyR2 activity causes life-threatening arrhythmias. CaM binding to RyR2 inhibits Ca^{2+} release, and dysfunctional CaM binding is arrhythmogenic. Mutations in CaM and the CaM-binding sites of RyR2 cosegregate with arrhythmias.

This thesis develops the tools for subsequent investigation of the structure of PLCζ, interaction between PLCζ and CaM, altered characteristics of interaction with

RyR2 by arrhythmogenic CaM mutations. Varying fusion partners and expressed amino acid coordinates improved the yield and solubility of recombinant PLCζ. Recombinant CaM protein recapitulated established parameters of CaM and Ca^{2+} dependent interactions between RyR2 and CaM. Arrhythmia patient mutations of CaM perturbed these divergently without altering protein secondary structure. However, the mutations altered the Ca^{2+} binding affinity and thermal stability of CaM. Ca^{2+} dependent binding between CaM and PLCζ occurred between the C-lobe of CaM with contribution from the N-lobe and no Ca^{2+}-free binding was observed.

PUBLICATIONS AND ABSTRACTS ARISING FROM THIS THESIS

Work included in this thesis has been presented in the following:

Publications

"Distinctive malfunctions of calmodulin mutations associated with heart RyR2-mediated arrhythmic disease." *BBA*, (2015) 1850(11), 2168–2176. (Joint first author).

"Altered RyR2 regulation by the calmodulin F90L mutation associated with idiopathic ventricular fibrillation and early sudden cardiac death." *FEBS Lett*. (2014) 588(17), 2898-902. (Co-author)

Abstracts to meetings and learned societies

Biophysical Society Meeting 2018, San Francisco: "Calmodulin Mutations Associated with Congenital Cardiac Disease Display Novel Biophysical and Biochemical Characteristics" (Poster presentation co-author)

Qatar University Research Forum & Exhibition 2018, Doha: "Calmodulin interacts and regulates enzyme activity of sperm PLC-zeta: a potentially vital role in human fertilization" (Poster presentation co-author)

Biophysical Society Meeting 2017, New Orleans: "Calmodulin Interacts and Regulates Enzyme Activity of the Mammalian Sperm Phospholipase C." (Poster presentation co-author)

Biochemical Society Focused Meeting 2014, "Calcium Signalling: The Next Generation", London: "Molecular characterization of CaM mutations associated with severe ventricular arrhythmia and sudden cardiac death." (Poster presentation author)

ABBREVIATIONS, ACRONYMS AND TERMINOLOGY

% (v/v)	Percentage concentration of a solution by volume of solute
% (w/v)	Percentage concentration of a solution by mass of solute
$(CH_3)_2AsO_2H$	Cacodylic acid
$(CH_3)_2AsO_2Na$	Sodium cacodylate
[^{3}H]ryanodine	Tritiated ryanodine
[Ca^{2+}]	Calcium ion concentration
[-T·ΔSb]	Entropic term
[ΔGb]	Gibbs free energy change
[ΔHb]	Binding enthalpy
[θ]	Molar ellipticity
°C	Degree Celsius
3′-end	Three prime end, nucleotide strand terminus with a hydroxyl group bound to the third carbon in the sugar-ring,
3D	Three-dimensional
^{3}H	Tritium
5′-end	Five prime end, nucleotide strand terminus with a phosphate group bound to the fifth carbon in the sugar ring.
6xHis	Hexahistidine
Å	Angstrom
AEBSF	4-Benzenesulfonyl fluoride hydrochloride
AP	Action potential
apoCaM	Calcium free calmodulin

APS	Ammonium persulfate
Arg	Arginine
ARM1	Armadillo repeat domain
ARVD/C	Arrhythmogenic right ventricular dysplasia/cardiomyopathy
Asn	Asparagine
Asp	Aspartic acid
ATP	Adenosine-5'-triphosphate
bar(g)	Gauge pressure in bar
Bis-Tris	1,3-Bis(tris (hydroxymethyl)methylamino)propane
bp	Base pairs
Br-Sol	Bridging solenoid
BSA	Bovine serum albumin
C2 domain	Conserved protein domain which targets cell membranes
Ca^{2+}	Calcium Ion
CaBP	Calcium binding protein
$CaCl_2$	Calcium chloride
cADPr	Cyclic adenosine diphosphate ADP-ribose
Calmodulin	Calcium-modulated protein
CaM	Calmodulin
CaMBD1	Calmodulin binding domain 1
CaMBD2	Calmodulin binding domain 2
CaMBD3	Calmodulin binding domain 3
CaMKII	Calmodulin-dependent kinase II

CaMLD	Calmodulin-like domain
CaM^{MUT}	Recombinant mutant CaM, mutation expressed in superscript
CaM^{WT}	Recombinant wild-type CaM
$Ca_V1.1$	An L-type VGCC or dihydropyridine receptor in skeletal muscle
$Ca_V1.2$	An L-type VGCC in cardiac muscle
CAX	Calcium hydrogen exchanger
CBP	Calmodulin binding protein/peptide
CCD	Central core disease
CCP4	Collaborative Computational Project number 4
CD	Circular dichroism
C-domain	The domain of protein closest to the C-terminus
CICR	Calcium-induced calcium release
CIP	Calf intestinal phosphate
C-lobe	Protein lobe on the C-terminus side of the flexible linker
cm	Centimetre (10^{-3} x m)
CNG	Cyclic nucleotide-gated ion channels
cpm	Counts per minute
CPVT	Catecholaminergic polymorphic ventricular tachycardia
CRAC	Calcium release-activated calcium channels
Cryo-EM	Cryogenic electron microscopy
C-Sol	Core solenoid
CTD	The α-helical C-terminal domain of IP_3R
C-terminus	Carboxyl-terminal, polypeptide terminal with a free carboxyl group

D	Denatured conformation
Da	Dalton
DAD	Delayed afterdepolarisation
DAG	sn-1,2 Diacylglycerol
DI H_2O	Deionised water
DLS	Dynamic light scattering
DNA	Deoxyribonucleic acid
dNTPs	Nucleoside triphosphates
DsbA	Disulfide bond formation protein A
DsbC	Disulfide bond formation protein C
dsDNA	Double-stranded DNA
DTT	Dithiothreitol
EAD	Early afterdepolarisation
EC_{50}	Half maximal effective concentration
E-CC	Excitation-contraction coupling
ECF	Extracellular fluid
ECG	Electrocardiogram
ECL	Enhanced Chemiluminescent
EDTA	Ethylenediamine tetraacetic acid
EF-Hand	Conserved protein domain which binds calcium ions
EGTA	Ethylene glycol tetraacetic acid
ER	Endoplasmic reticulum
FKBP	FK506-binding protein

FKBP12	FK506-binding protein – 12.0 kDa
FKBP12.6	FK506-binding protein–12.6 kDa cardiac isoform
FRET	Fluorescence resonance energy transfer
FS1	Fine screen 1
FS2	Fine screen 2
FS3	Fine screen 3
g	Gram
GA	Golgi apparatus
GC content	Guanine-cytosine content
Gln	Glutamine
Glu	Glutamic acid
Gly	Glycine
GOF	Gain of function
GST	Glutathione S-transferase
h	Hour
HCl	Hydrochloric acid
HD	The α-helical domain of IP_3R
HEPES	4-(2-hydroxyethyl)-1-piperazineethanesulfonic acid
HF	Heart failure
His	Histidine
holoCaM	calcium saturated calmodulin
hPLCζ	Human PLCζ
HRP	Horseradish peroxidase

hRyR2	Human ryanodine receptor 2
HS	Mutation hot spot
HS-loop	Mutation hot spot loop
I	Intermediate conformation
IBC	The IP_3 binding core of IP_3R
IgG	Immunoglobulin G
Ile	Isoleucine
IMS	Industrial methylated spirits
Intein	Intervening protein sequence
IP_3	Inositol triphosphate
IP_3R	Inositol trisphosphate receptor
IP_3R1, IP_3R2 & IP_3R3	Isoforms 1,2 & 3 of IP_3R
IPTG	Iso-Propyl β-D-1-thio-galactopyranoside
ITC	Isothermal titration calorimetry
I_{to1}	Voltage-gated K^+ channel
IVT	Idiopathic ventricular tachycardia/fibrillation
J	Joule
JCSG	Joint Centre for Structural Genomics
K	Kelvin
K^+	Potassium Ion
kb	Kilobase pairs (10^3 x bp)
KCl	Potassium chloride

K_d	Dissociation constant
kDa	Kilo Dalton (10^3 x Da)
KH_2PO_4	Potassium dihydrogen phosphate
K_{ir} & IRK	Inwardly rectifying potassium channels
kJ	Kilojoule (10^3 x J)
KOH	Potassium hydroxide
kPa	Kilopascal (10^3 x Pa)
K_V7.1 & K_V11.1	Voltage gated potassium channels
L	Litre
LB	Lysogeny broth
LCP	Left-circularly polarized light
Leu	Leucine
LNK	Helical linker domain of IP_3R
Lobes	Protein regions joined by flexible linker enabling movement
LOF	Loss of function
LQTS	Long QT syndrome
Lys	Lysine
M	Molar concentration (mol/L)
mAKAP	Muscle A-kinase anchoring protein
MBP	Maltose binding protein
MCS	Multiple cloning site
MCU	Mitochondrial calcium uniporter
MDa	Mega Daltons (10^6 x Da)

MES	2-(N-morpholino)ethanesulfonic acid
Met	Methionine
mg	Milligram (10^{-3} x g)
Mg^{2+}	Magnesium Ion
$MgCl_2$	Magnesium chloride
MH	Malignant hyperthermia
MI	Myocardial infarction
min	Minute
ml	Millilitre (10^{-3} x L)
mM	Milimolar (10^{-3} x mol/L)
MOPS	2-(N-morpholino)ethanesulfonic acid
MPD	2-Methyl-2,4-pentanediol
mPLCζ	Mouse PLCζ
mV	Millivolts (10^{3} x V)
M_W	Molecular weight
M_WCO	Molecular weight cut off
n	Number of experiments
N	Native conformation
N	Stoichiometry
Na^{+}	Sodium ion
Na_2HPO_4	Sodium phosphate dibasic
NAADP	Nicotinic acid dinucleotide phosphate
NaCl	Sodium chloride

Na^+/K^+-ATPase	ATP dependent Na^+-K^+ ion pump
NaOAc	Sodium acetate
NaOH	Sodium hydroxide
$Na_V1.5$	Voltage-gated sodium channel
NCX	Sodium/calcium exchanger
NCX	Sodium ion calcium exchanger
N-domain	The domain of protein closest to the N-terminus
ng	Nanogram (10^{-9} x g)
Ni-NTA	Ni-NTA agarose NTA with co-ordinated nickel ion coupled to agarose resin
nl	Nanolitre (10^{-9} x L)
N-lobe	Protein lobe on the N-terminus side of the flexible linker
nM	Nanomolar (10^{-9} x mol/L)
nm	Nanometre (10^{-9} x m)
NMR	Nuclear magnetic resonance
NTA	Nitrilotriacetic acid
NTD	N-terminal domain
N-terminus	Amino-terminal, the end of a polypeptide bearing a free amine group
NusA	N-utilization substance protein A
OD	Optical density
OD_{260}	Optical density at 260 nm
OD_{280}	Optical density at 280 nm
OD_{600}	Optical density at 600 nm

Orai1	Plasma membrane protein component of CRAC
P4D3	Phosphodiesterase 4D3
PACT	pH, anion and cation testing
PBS	Phosphate buffered saline
PCR	Polymerase chain reaction
PDB	Protein data bank
PEG	Polyethylene glycol
PEG-6000	Polyethylene glycol average M_W 6000
PFR	Pore-forming region
PH domain	Pleckstrin homology domain, a conserved domain that binds phospholipids
Phe	Phenylalanine
PIP_2	Phosphatidylinositol 4,5-bisphosphate
PIPES	Piperazine-N,N′-bis(2-ethanesulfonic acid)
PI-PLC	Phosphoinositide phospholipase C
PKA	Protein kinase A
PKA	Protein kinase A
PLB	Phospholamban
PLCζ	Sperm-specific PI-PLC isoform ζ
PLCδ1	Ubiquitous PI-PLC isoform δ1
PMCA	Plasma membrane calcium ATPase
P_O	Open probability
POI	Protein of interest
PP1	Type 1 phosphatase

PP2A	Type 2A phosphatase
PP2B	Type 2B phosphatase
Pro	Proline
PVDF	Polyvinylidene fluoride
pVSD	Pseudo-voltage sensor domain
RCF	Relative centrifugal force
RCP	Right Circularly Polarized light
R_H	Hydrodynamic radius
RNA	Ribonucleic acid
rpm	Revolutions per minute
Ruthenium red	Ammoniated ruthenium oxychloride
Ry	Ryanodine
RY	RyR repeat domain
RyR	Ryanodine receptor
RyR1	Ryanodine receptor 1, skeletal muscle isoform
RyR2	Ryanodine receptor 2, cardiac muscle isoform
s	Second
S1, S2, S3, S4, S5 & S6	Six membrane-spanning TM helices of RyR
SCD	Sudden cardiac death
sd	Standard deviation
SD	Suppressor domain of IP_3R
SDM	Site-directed mutagenesis
SDS	Sodium dodecyl sulfate

SDS-PAGE	Sodium dodecyl sulfate-polyacrylamide gel electrophoresis or denaturing polyacrylamide gel electrophoresis
SEC	Size exclusion chromatography
SEM	The standard error of the mean
Ser	Serine
SER	Smooth endoplasmic reticulum
SERCA	Sarco/endoplasmic reticulum calcium ATPases
SK	Small conductance calcium-activated potassium channels
SOCC	Store-operated calcium channel
SOCE	Store-operated calcium entry
SOICR	Store overload-induced calcium release
SPCA	Secretory-pathway calcium-transport ATPases
SPRY domain	Conserved protein domain thought to act as a protein interaction module
SR	Sarcoplasmic reticulum
STIM1	An SER/SR protein component of CRAC
SUMO	Small ubiquitin-like modifier
T-tubules	Transverse Tubules
TAE	Tris buffered, acetate and EDTA solution
TBS	Tris-buffered saline solution
TdP	Torsades de pointes
TEMED	Tetramethylethylenediamine
TEV	Tobacco etch virus
Thr	Threonine

TIM barrel	A conserved protein fold first identified in triose-phosphate isomerase
TM	Transmembrane
T_M	Melting temperature
TM and CTD	Trans-membrane and C-terminal domain of RyR
TM1, TM2, TM3, TM4, TM5 & TM6	Six TM α-helices of IP_3R
TMD	The transmembrane domain of IP_3R
TmX	The transmembrane helix of RyR
TPC2	Two-pore channel 2
Tris	Tris hydroxymethylaminomethane
TRP	Transient receptor potential channels
Trx	Thioredoxin
Tyr	Tyrosine
UV	Ultraviolet
Val	Valine
VGCC	Voltage-gated calcium channel
VT	Ventricular tachycardia
W	Watt
WHRI	Wales Heart Research Institute
x *g*	Multiple of the acceleration of gravity
XY domain	Catalytic TIM barrel domain with two halves, X and Y, separated by a linker sequence.
XY linker	Polypeptide joining X and Y halves of TIM barrel domain

β-AR	β-Adrenergic receptor
βME	β-Mercaptoethanol
β-TF	β-Trefoil fold domain
Δελ	Molar circular dichroism at a specified wavelength
ΔG	Gibbs free energy
ΔHvH	van't Hoff transition enthalpy
λEM	Emission wavelength
λEX	Excitation wavelength
µg	Microgram (10^{-6} x g)
µJ	Microjoule (10^{-6}xJ)
µl	Microlitre (10^{-6} x L)
µM	Micromolar (10^{-6} x mol/L)
µm	Micrometre (10^{-6} x m)

LIST OF FIGURES

LIST OF TABLES

LIST OF EQUATIONS

LIST OF CONTENTS

Chapter 1 - INTRODUCTION

1.1 General Introduction

Calcium is the fifth most common element and most abundant metal in organisms serving an electrolytic and structural role. The Calcium ion (Ca^{2+}) is a critical component of cellular biochemistry and physiology, regulating multiple aspects of cell function, proliferation, differentiation and apoptosis (Bootman *et al.*, 2012). In all cell types, Ca^{2+} is an essential secondary messenger in signal transduction pathways and a required co-factor for many enzymatic reactions (Berridge, Lipp and Bootman, 2000). However, Ca^{2+} is an ambivalent signalling molecule; un-controlled Ca^{2+} levels can lead to cell dysfunction and uncontrolled cell death (Campbell, 1987).

Ca^{2+} is highly reactive and ubiquitous in the environment. Sustained high cytosolic concentrations of free Ca^{2+} results in the precipitation of phosphates causing aggregation of proteins and nucleic acids, and organelle damage as phospholipid membranes are damaged (Jaiswal, 2001). Early single cell organisms probably first developed control of intracellular Ca^{2+} concentrations to enable survival in the Ca^{2+} rich environments in which they evolved. (Case *et al.*, 2007). Due to environmental ubiquity, low cytosolic concentrations and unique physiochemical properties, single-cell organisms evolved and adapted to use Ca^{2+} as a versatile signalling molecule (Verkhratsky and Parpura, 2014; Plattner and Verkhratsky, 2015).

Due to the deleterious effects of elevated Ca^{2+} on the cell and the sensitivity of many cellular proteins to Ca^{2+}, the concentration of Ca^{2+} ($[Ca^{2+}]$) in the cytosol is controlled rigorously to be four orders of magnitude lower than the extracellular

environment (Clapham, 2007). The low basal [Ca^{2+}] also means that small, energetically favourable amounts of Ca^{2+} will trigger a response. Multiple proteins maintain the concentration gradient by buffering free Ca^{2+}, and translocating Ca^{2+} both out of the cytosol and into intracellular Ca^{2+} stores, e.g. the Endoplasmic Reticulum (ER) as can be seen in Figure 1-1, (Berridge, Bootman and Roderick, 2003).

Any given cell type expresses a unique profile of proteins with a range of binding affinities for Ca^{2+} (Bootman, Lipp and Berridge, 2001). Inter and intracellular calcium-binding proteins (CaBP) that bind Ca^{2+} reversibly fall into two broad groups, Ca^{2+} buffers and Ca^{2+} sensors. Ca^{2+} buffers bind Ca^{2+} regulating Ca^{2+} concentrations in the cell. The Ca^{2+} sensors bind Ca^{2+} with optimal efficiency at ambient (≤ μM) concentrations (Carafoli *et al.*, 2001). Upon Ca^{2+} binding to a Ca^{2+} sensor, protein function alters due to changes in protein conformation and charge, “activating” the protein. The regulation of the enzymatic activity of proteins by Ca^{2+} is allosteric, Ca^{2+} does not contribute to the catalysis of reactions at active sites. The binding of Ca^{2+} to Ca^{2+} sensors does not contribute to control of Ca^{2+} concentration (Carafoli *et al.*, 2001). Rather, Ca^{2+} sensors trigger downstream signalling pathways or induce other proteins to do so, and process and transmit Ca^{2+} signals to targets. Therefore, the expression profile enables the cell to detect, translate and respond appropriately to Ca^{2+} signals (Bootman, Lipp and Berridge, 2001).

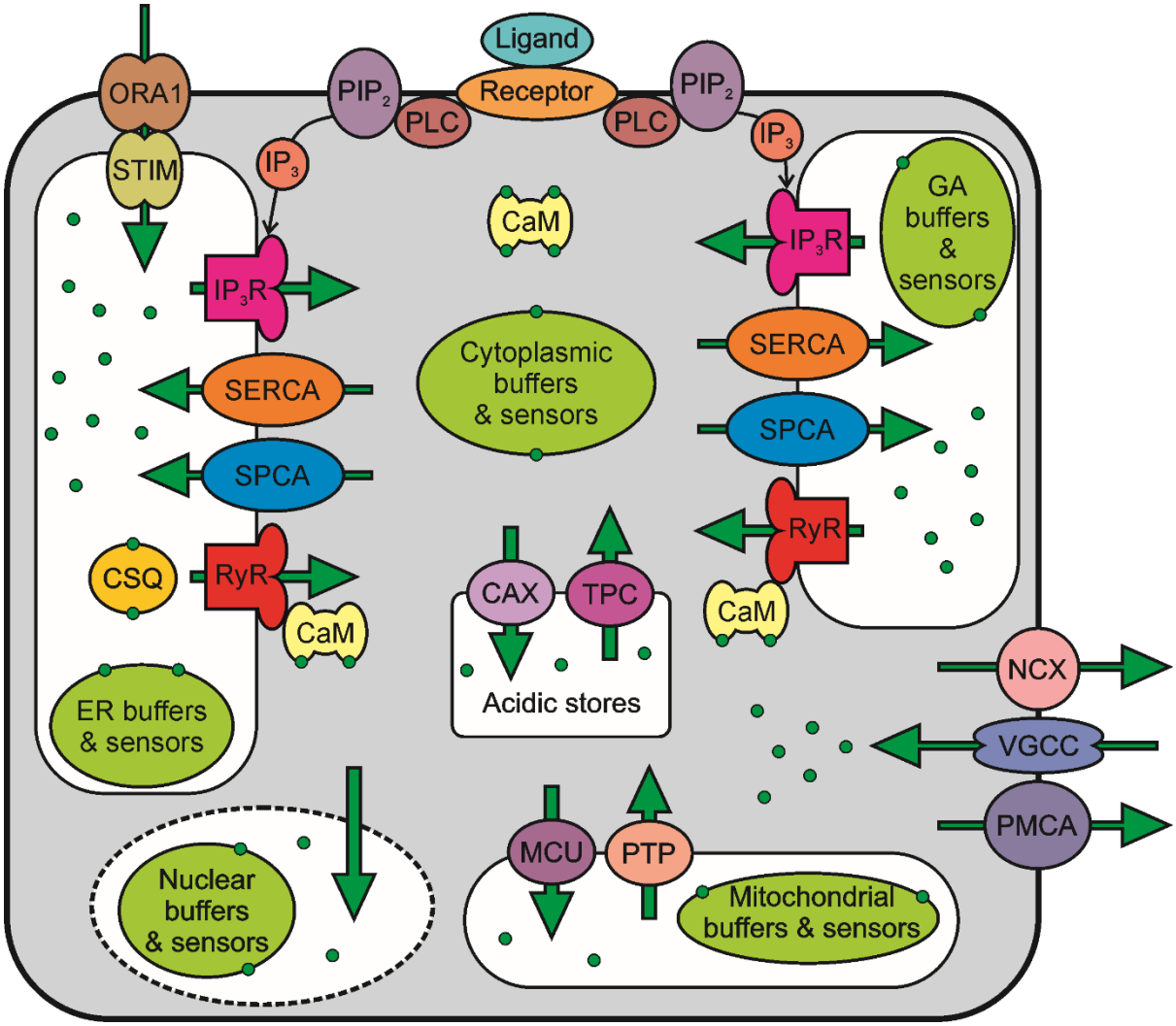

Figure 1-1 The Cell Maintains Resting [Ca^{2+}] by Transporting Ca^{2+} out of the Cytoplasm and Sequestering Ca^{2+} in Discrete Pools in the Cytoplasm and Organelles

Diagram showing the Ca^{2+} transportation and storage proteins of a typical eukaryotic cell which together contribute to Ca^{2+} homeostasis. The activity of these proteins enables Ca^{2+} signalling by rapidly altering cytoplasmic [Ca^{2+}] via the interplay between Ca^{2+} release and uptake mechanisms. Green circles and arrows depict Ca^{2+} and the flow of Ca^{2+} respectively.

During Ca^{2+} signalling, there is an influx of Ca^{2+} into the cytosol in response to stimuli. Ca^{2+} enters from the extracellular medium and intracellular stores through specific ion channels embedded in the cytoplasmic and endo- membranes shown in Figure 1-1. The Ca^{2+} influx results in a transient increase in cytosolic [Ca^{2+}] as Ca^{2+} reuptake mechanisms rapidly restore the resting [Ca^{2+}]. The triggering of downstream signalling cascades is dependent on the specific binding of Ca^{2+} and proteins. Both the unique expression profile of Ca^{2+} responsive proteins and, the scale, duration and location of the transients dictate the response of any given cell to the stimuli. Therefore, the regulation of ion channel activity by chemical agents, proteins, lipids and Ca^{2+} itself is a critical aspect of Ca^{2+} signalling (Berridge, Lipp and Bootman, 2000).

1.2 Calcium Signalling

The biochemical roles of Ca^{2+} regulating enzymatic activity, ion channel permeability, ion pump action and characteristics of cytoskeletal components enables Ca^{2+} to act as a versatile secondary messenger. Ca^{2+} is ubiquitous, acting as a secondary messenger in many varied cell types and organs. Therefore Ca^{2+} plays a key role physiological processes including motility, initiation of gene expression, cell growth, differentiation and proliferation, apoptosis, immune response, neurogenesis, muscle contraction, neuronal transmission, exocrine and endocrine gland secretion, fertilisation and the cardiac cycle (Berridge, Lipp and Bootman, 2000; Berridge, Bootman and Roderick, 2003).

The nuclear envelope separates the nucleoplasm from the cytoplasm and is poorly permeable to ions and molecules (Schermelleh et al., 2008; Ljubojevic et al.,

2014). Nucleoplasmic [Ca2+] increases and decreases with cytoplasmic [Ca2+] primarily due to passive diffusion through Nuclear pore complexes (NPCs) (Bootman et al., 2009). NPCs occur throughout the nuclear membrane and are porous to ions and small molecules while associated transport systems facilitate the movement of larger molecules e.g. proteins. (Görlich and Kutay, 1999; Ljubojevic et al., 2014). Nuclear Ca2+ transients are varied spatially and temporally. diffusion being augmented by differences in distribution and location of NPCs in relation to Ca2+ channels, NPC regulation by Ca2+ and ATP, nuclear, perinuclear, and cytosolic structures e.g. nuclear invaginations and nuclear membrane ion receptors, channels and pumps (Greer and Greenberg, 2008; Barbado et al., 2009; Dewenter et al., 2017).

Ca2+ dependent gene expression enables long-term effects from the transient Ca2+ signal in many cell types including cardiomyocytes, neurons and lymphocytes (Greer and Greenberg, 2008; Bengtson and Bading, 2012; Naranjo and Mellström, 2012; Monaco et al., 2016; Dewenter et al., 2017). Gene expression can be regulated by Ca2+ indirectly through proteins that activate and regulate transcription factors which bind Ca2+ or are associated with Ca2+ signalling complexes, directly through Ca2+ binding transcription factors, or via subunits and fragments of Ca2+ channels which act as transcription factors (Barbado et al., 2009). Ca2+ dependent alterations to gene expression are involved in physiological and pathological processes including ventricular remodelling, neuroadaptation, immune activation and adaption of the Ca2+ Homeostatome itself (Greer and Greenberg, 2008; Naranjo and Mellström, 2012; Monaco et al., 2016; Dewenter et al., 2017). The ability of Ca2+ to control gene transcription enables influence of synaptic transmission and membrane de-

polarisation to protein expression in excitable cells (Greer and Greenberg, 2008; Barbado et al., 2009).

During Ca^{2+} signalling, cells are stimulated by a variety of factors to release Ca^{2+} ions from intracellular stores and permit entry of extracellular Ca^{2+} via plasma membrane ion channels (Bootman, Berridge and Roderick, 2002; Roderick, Berridge and Bootman, 2003). Ca^{2+} can act directly on cellular components or induce the further localised release of Ca^{2+} from Ca^{2+} sensitive Ca^{2+} channels in a process known as Ca^{2+} induced Ca^{2+} release (CICR) (Fabiato and Fabiato, 1975, 1978). Many proteins bear specific high-affinity binding sites for Ca^{2+} and will readily bind Ca^{2+} inducing changes in protein shape and charge which dictate protein function. The ability of Ca^{2+} to alter local electrostatic fields and protein conformations confer the versatility as a universal signal molecule (Carafoli *et al.*, 2001). The quintessential Ca^{2+} sensor is the ubiquitous Ca^{2+} binding protein Calmodulin (CaM) that transduces Ca^{2+} signals in a wide variety of signalling pathways (Chin and Means, 2000).

Unsurprisingly given the ubiquity and versatility of Ca^{2+} as a messenger and a signal transducer, aberrant Ca^{2+} signals and concentrations are a critical contributory factor in disease and clinical disorders (Berridge, 2012). Dysfunctional Ca^{2+} handling results in a variety of cellular defects that can lead to a broad spectrum of disease and disorders, including Alzheimer`s, cardiovascular and psychiatric diseases, infertility, and cancer (Bojarski, Herms and Kuznicki, 2008; Roderick and Cook, 2008; Borges *et al.*, 2009; Bejarano *et al.*, 2012; Berridge, 2012; Goonasekera and Molkentin, 2012).

Ca^{2+} acts as a vital second messenger during two significant processes of life, the heartbeat and fertilisation (Miao and Williams, 2012; Capel and Terrar, 2015; Huang *et al.*, 2016). In both processes, CaM has been shown to be a vital element of the Ca^{2+} signalling pathways (Courtot, Pesty and Lefèvre, 1999; Sorensen, Søndergaard and Overgaard, 2013).

1.2.1 Regulation of Cytosolic Calcium

1.2.1.1 Resting Calcium Equilibrium

At rest, the concentration of free Ca^{2+} in mammalian cells equilibrates at 10 nM to 100 nM compared to 1 to 2 mM typically found in the surrounding extracellular fluid (ECF) (Boal, 2012). The equilibrium in Ca^{2+} concentration is the result of the combined action of the Ca^{2+} Homeostasome, a set of proteins which function as buffers, pumps and ion channels for Ca^{2+} as shown in Figure 1-1 (Schwaller, 2012). Ca^{2+} buffers are intracellular proteins capable of binding Ca^{2+} (Schwaller, 2010). While Ca^{2+} channels are passive conduits which permit the flow of Ca^{2+} along the concentration gradient. (Gadsby, 2009) Ca^{2+} pumps actively transport Ca^{2+} against the concentration gradient driven by either ATP hydrolysis or coupled to the thermodynamically movement of another ion e.g. Sodium (Gadsby, 2009). These proteins sequester Ca^{2+}, transfer it to intracellular stores and export it to the ECF (Berridge, Lipp and Bootman, 2000). In addition to maintaining the resting equilibrium of Ca^{2+} these proteins shape the temporal and spatial characteristics of Ca^{2+} transients (Berridge, Bootman and Roderick, 2003).

1.2.1.2 Intracellular Calcium Stores

Ca^{2+} stores are membrane-bound organelles which sequester Ca^{2+} into intracellular membrane compartments. Free Ca^{2+}in the cytosol is transported into the lumen of the organelles via specific ion pumps. The sarcoplasmic reticulum (SR) and smooth endoplasmic reticulum (SER) are the primary Ca^{2+} stores in myocytes and all other cell types respectively (Berridge, 2002). The acidic organelles, lysosomes, lysosome-related organelles, secretory vesicles, vacuoles and acidocalcisomes are other essential Ca^{2+} stores (Patel and Docampo, 2010). Mitochondria and the Golgi Apparatus (GA) also take up and store free Ca^{2+} from the cytosol (Contreras *et al.*, 2010; Yang *et al.*, 2015)

1.2.1.3 Calcium Buffers

Ca^{2+} buffers are mobile cytosolic proteins that modulate cytosolic Ca^{2+} transients by binding Ca^{2+} with affinities ranging from 200 nM–1.5 µM without triggering downstream signalling; examples include parvalbumins α and β, calbindin-D9k, calbindin-D28k and calretinin (Schwaller, 2010). Unique protein expression profiles of Ca^{2+} buffers confer the specific buffering capacities of different excitatory cell types and enables cell function (Fierro and Llano, 1996; Lips and Keller, 1998; Lee *et al.*, 2000; Delvendahl *et al.*, 2015).

At basal [Ca^{2+}], Ca^{2+} buffers will be Ca^{2+} free. With increasing [Ca^{2+}], the buffers co-operatively bind Ca^{2+} with rising affinity at an increasing rate. While no conformational change that triggers a signalling pathway occurs, some authors report conformational changes and Ca^{2+} sensing activities (Schwaller, 2009). As [Ca^{2+}] re-

equilibrates, Ca^{2+} dissociates from the buffer modulating the temporal-spatial dynamics of the Ca^{2+} transient. (Faas *et al.*, 2007; Schwaller, 2009). The uptake and release of Ca^{2+} by a specific buffer will depend on the binding affinity with metal ions, the kinetics of binding and dissociation with Ca^{2+} and intracellular protein concentration and mobility.

1.2.1.4 Calcium Transporters

The efflux of Ca^{2+} across the plasma membrane from the cytosol to the ECF is against the concentration gradient. Translocation of Ca^{2+} is by two ion-specific membrane transporters, Plasma Membrane Ca^{2+} ATPase (PMCA), and the Sodium ion (Na^{+}) Ca^{2+} exchanger (NCX) (Blaustein and Lederer, 1999; Brini *et al.*, 2013).

PCMA is a member of the type-II phosphorylation ATPase (P-type) superfamily and uses the energy liberated from adenosine-5'-triphosphate (ATP) hydrolysis to translocate Ca^{2+} across the plasma membrane with high affinity at a low rate of transfer (Pedersen and Carafoli, 1987; Axelsen and Palmgren, 1998). NCX is a Ca^{2+} specific uniporter and cation exchanger superfamily member that uses the electrochemical gradient of Na^{+} to export Ca^{2+} at low-affinity and a high rate of transfer while importing three Na^{+} (Cai and Lytton, 2004; Liao *et al.*, 2012). NCX also imports Ca^{2+} at elevated Na^{+} and during excitation-contraction coupling (E-CC) in response to membrane depolarisation (Philipson and Nicoll, 2000). The two transporters play different roles in cellular Ca^{2+} signalling, PMCA exports Ca^{2+} at basal [Ca^{2+}] maintaining resting [Ca^{2+}], and NCX exports Ca^{2+} at a high rate when [Ca^{2+}] is elevated allowing rapid clearance. Also, NCX can prolong Ca^{2+} transients by importing Ca^{2+} co-operatively and locally in

response to ion gradients and the activity of co-localised ion transporters to which it is coupled (Khananshvili, 2014).

Cytosolic Ca^{2+} is imported into intracellular stores by specific ion pumps embedded in the plasma membrane of organelles. The membranes of SR/SER and GA contain P-type ATPase superfamily members, Sarco/endoplasmic reticulum Ca^{2+} ATPases (SERCA) and Secretory-pathway Ca^{2+}-transport ATPases Ca^{2+} ATPases (SPCA). Cell and tissue-specific isoforms of SERCA, splice variants of three homologous genes, are present in ER membranes and translocate Ca^{2+} from the cytosol into the lumens of the SR and SER (Periasamy and Kalyanasundaram, 2007). SERCA and SPCA are present in membranes of the GA, and both import Ca^{2+} into trans-Golgi bodies but only SPCA imports into cis-Golgi (Van Baelen *et al.*, 2004; Lissandron *et al.*, 2010).

Compared to the cytosol, there is a high concentration of protons (H^+) in the lumen of acidic stores. Ca^{2+} translocates into the acidic stores' lumen at a high rate with low affinity via Ca^{2+}/ H^+ exchanger (CAX), a Ca^{2+}/cation antiporter superfamily member. CAX uses the concentration gradient to drive transfer of H^+ out of, and Ca^{2+} into the lumen (Patel and Docampo, 2010; Melchionda *et al.*, 2016). The mitochondrial Ca^{2+} uniporter (MCU) complex imports cytosolic Ca^{2+} into the mitochondrial matrix (Baughman *et al.*, 2011; De Stefani *et al.*, 2011).

1.2.2 The Influx of Extracellular Calcium

A key event in the initiation of biochemical and physiological processes controlled by Ca^{2+} is the influx Ca^{2+} from either or both the extracellular space and intracellular

stores. Ca^{2+} crosses membranes via transmembrane protein complexes that form ion channels in response to ligands, ions or changes in transmembrane potential. Voltage-gated calcium channels (VGCC) and calcium release-activated Ca^{2+} channels (CRAC) mediate the entry of extracellular Ca^{2+} into many cell types.

1.2.2.1 Voltage-Gated Calcium Channels

The primary entry point for extracellular Ca^{2+} into the cytosol of electrically excitable cells e.g. muscle, nerve, glial and pancreatic β cells are VGCCs (Catterall, 2011). VGCCs are members of the voltage-gated ion channel superfamily and conduct Ca^{2+} through the plasma membrane in response to an action potential (AP) and membrane depolarisation. An activated VGCC conducts approximately $1x10^6$ Ca^{2+} per second, enabling rapid changes in cytosolic [Ca^{2+}] (Clapham, 2007). Alterations in the transmembrane potential of surrounding plasma membrane trigger VGCCs to undergo a conformational change forming an ion channel (Catterall, Wisedchaisri and Zheng, 2017). The ion channel selectively allows Ca^{2+} but not Sodium ions (Na^+), to follow the concentration gradient into the cytosol (Tang *et al.*, 2014). There are five main types of VGCC; L, P/Q, R, N and T classified according to the threshold of activation, electrophysiology, pharmacology and cellular distribution (Snutch *et al.*, 1990). While L and T type VGCCs are expressed in many cell types both excitatory and non-excitatory, P/Q, R, and N are found mainly in neuronal cells (Catterall, 2000).

1.2.2.2 Calcium Release-Activated Channels

During Store-Operated Ca^{2+} Entry (SOCE), depleted intracellular Ca^{2+} stores refill from the ECF via protein complexes, calcium release-activated Ca^{2+} (CRAC) channels

(Stathopulos and Ikura, 2017). The most significant components of CRAC channels are two transmembrane proteins, STIM1 an SER/SR protein and Orai1 a plasma membrane protein (Prakriya, 2009). In response to low luminal [Ca^{2+}], STIM1 translocates to ER/plasma membrane junctions and recruits Orai1 to form a Ca^{2+} selective ion channel (Hogan and Rao, 2015).

1.2.2.3 Transient Receptor Potential Channel

Members of the Transient receptor potential (TRP) channel superfamily are cation channels permeable to Ca2+ found across the animal kingdom (Smani *et al.*, 2015) (Montell, 2001)(Moiseenkova-Bell and Wensel, 2011). Distantly related to voltage-gated ion channels, including VGCCs, TPR channels are contentiously involved in SOCE and interact with IP3R and L-type VGCCs (Harteneck, Klose and Krautwurst, 2011)(Harteneck, Klose and Krautwurst, 2011)(Sabourin, Robin and Raddatz, 2011).; Based on structural characteristics TRP channels are divided into seven groups not all of which are represented in every class of animal (Smani *et al.*, 2015)(Fliniaux *et al.*, 2018).

Functioning as either receptor-, second messenger- or store-operated channels in a variety of systems and organs, TRP channels permit entry of Ca2+ and other ions resulting in membrane depolarisation and the activation of Ca2+-dependent mechanisms.(Clapham, 2003). In addition to the plasma membrane, TRP channels are located on the membranes of the intracellular stores and are involved in localised Ca2+ release events required for cell survival and proliferation, autophagy and apoptosis. (Fliniaux *et al.*, 2018)(La Rovere *et al.*, 2016). The gating of TRP channels

can be regulated by a range of stimuli including physical e.g. osmotic pressure, temperature change, mechanical stress and vibration, chemical i.e. a variety of endogenous or exogenous ligands, and the depletion of intracellular Ca2+-stores (Harteneck, Klose and Krautwurst, 2011)(Harteneck, Klose and Krautwurst, 2011). The majority of TRP channel superfamily members are permeable to monovalent and divalent cations, but some are selective for monovalent cations e.g. TRPM4 and TRPM5 and others are Ca2+ selective e.g. TRPV5 and TRPV6 (Smani *et al.*, 2015).

Ca2+ specific TRP channels are expressed in many cells types and involved in diverse physiological functions including; cardiomyocytes controlling aspects of cardiac function e.g contractility, conduction and pacemaking, in vascular smooth muscle involved in vascular tone, remodelling and angiogenesis, and pancreatic β cells promoting insulin secretion (Jacobson and Philipson, 2007; Inoue, Jian and Kawarabayashi, 2009; Islam, 2010; Sabourin, Robin and Raddatz, 2011; La Rovere *et al.*, 2016). Dysfunctional activity TRP channels permeable to Ca2+ is a physiopathological mechanism in clinical conditions including cardiovascular disease, cancer and type-2 diabetes mellitus (Smani *et al.*, 2015)

1.2.2.4 Sperm-Specific Cation Channels

Increased cytosolic Ca2+ is required for spermatazoan (sperm) motility and function prior to fertilisation e.g activation, capacitation, chemotaxis and flagellum hyperactivity (Marquez, Ignotz and Suarez, 2007; Chung *et al.*, 2014). Cation channels of sperm (CatSper channels) are sperm-specific, ion channels required for male fertility which permit entry of the extracellular Ca^{2+} required for sperm activity (Ren *et al.*, 2001;

Kirichok, Navarro and Clapham, 2006; Navarro *et al.*, 2008; Singh and Rajender, 2015). The activity of CatSper channels is pH and low voltage dependent and active channels are permeable to both Ca^{2+} and other monovalent and divalent ions (Sun *et al.*, 2017). CatSper channels are activated by multiple mechanisms notably PKA-dependent phosphorylation controlled by cAMP following G-protein receptor ligand binding, and direct stimulation by progesterone and prostaglandin in the oviduct (Brenker *et al.*, 2012; Orta *et al.*, 2018).

1.2.2.5 Purinergic Ion Channels

Ca2+ signalling can also be the result of stimulation by extracellular purines and pyrimidines of members of the purinergic receptor superfamily expressed on the plasma membranes of a variety cell types (Burnstock and Ralevic, 2013; Glaser, Resende and Ulrich, 2013; Burnstock, 2017). Purinergic receptors are divided into two main families further divided into subtypes based on ligand specificity, biochemical and pharmacological characteristics, molecular structure and mechanisms of signal transduction mechanisms (Ralevic and Burnstock, 1998). The P1 family and P2Y subtypes are G-protein coupled receptors (Ralevic and Burnstock, 1998).

However, the P2X subfamily contains plasma membrane ion channels which become permeable to Ca2+ upon the binding of extracellular ATP (North, 2002). Binding of ATP to the extracellular surface of the P2X receptor results in a conformational change in the ion channel and the opening of the ion-permeable pore, permitting cations, including Ca2+, entry (Kawate *et al.*, 2011). Cation entry results in cell membrane depolarisation and activation of Ca2+-sensitive intracellular

processes(Koshimizu *et al.*, 2000; Shigetomi and Kato, 2004). Dependent on the subtype ATP stimulation of the P2X receptor can result in a rapidly dissipating or prolonged influx of extracellular Ca2+ (North, 2016)

P2X receptors are found throughout the animal kingdom, expressed by many cell types in a wide range of tissues (North, 2002). Entry of extracellular Ca2+ via P2X receptors in repsonse to ATP binding is involved in multiple physiological processes including; vascular tone modulation, neuronal-glial and synaptic transmission, pain perception, cardiac rhythm and contractility, aggregation of platelets, contraction of vas deferens during ejaculation and bladder during urination, activation of macrophages and apoptosis, (Burnstock, 2000, 2013; Chizh and Illes, 2001; Vassort, 2001; Gachet, 2006; Fowler, Griffiths and de Groat, 2008; Wewers and Sarkar, 2009; Kawano *et al.*, 2012).

1.2.3 The Release of Calcium from Intracellular Stores

The ER is the primary intracellular store of Ca^{2+} (Verkhratsky, 2005). The release of Ca^{2+} from the ER is via two Ca^{2+} sensitive Ca^{2+}channels, inositol 1,4,5-trisphosphate receptor (IP_3R) and ryanodine receptor (RyR) (Cancela *et al.*, 2000). IP_3R and RyR are not closely related sharing only approximately 30% sequence identity but are homologous structurally with a high degree of similarity between structures and biological function (Seo *et al.*, 2012). The release of Ca^{2+} from stores in the Golgi and Nuclear envelope are biologically distinct to release from the ER (Pinton, Pozzan and Rizzuto, 1998; Gerasimenko *et al.*, 2003). However, recent data indicate that Nicotinic Acid Dinucleotide Phosphate (NAADP) stimulated Ca^{2+} release from acidic stores and the release of Ca^{2+} from the ER are linked (Cancela, 2001; Patel and Brailoiu, 2012).

The endo-lysosomal transmembrane protein Two-Pore Channel 2 (TPC2), releases Ca^{2+} from acidic stores in response to NAADP stimulation (Brailoiu *et al.*, 2009; Calcraft *et al.*, 2009). TPC2 is a member of the voltage-gated ion channel superfamily, permeable to Ca^{2+}, sensitive to NAADP and localised to the membranes of acidic organelles (Patel, 2015). Other Ca^{2+} permeable channels present on acidic organelles include members of the TPR and P2X famil**ie**s, RyR and IP_3R channels, and potentially VGCCs (Yoo *et al.*, 2001; Kiselyov *et al.*, 2005; Karacsonyi, Miguel and Puertollano, 2007; Qureshi *et al.*, 2007; Miklavc *et al.*, 2010; Huang *et al.*, 2014; Tian *et al.*, 2015).

The release of Ca^{2+} from acidic stores and the ER sensitises IP_3R and RyR, to stimulation by signalling molecules (Kilpatrick *et al.*, 2013; Morgan *et al.*, 2013). TPC mediated Ca2+ release could potentially be stimulated by a positive feedback mechanism involving a novel Ca2+ sensitive NAADP synthase similar to one already identified in sperm (Vasudevan, Galione and Churchill, 2008). Communication between the ER and endo-lysosomal system results in augmented Ca^{2+} release amplifying the Ca^{2+} signal and modifying the characteristics of Ca^{2+} transients (Morgan, 2016).

1.2.4 Sensing Calcium

1.2.4.1 Intracellular Calcium-Binding Proteins

Within eukaryotic cells, hundreds of CaBP bind Ca^{2+} with a million-fold range of binding affinities from resting cytosolic [Ca^{2+}] upwards classified as either Ca^{2+} sensors or Ca^{2+} buffers (Berridge, Lipp and Bootman, 2000; Zhou, Xue and Yang, 2013). Ca^{2+} sensors

are intracellular CaBP that modulate cellular processes in response to changes in cytosolic [Ca^{2+}] stimulated by alterations in the binding of Ca^{2+}(Hiraoki and Vogel, 1987). Ca^{2+} buffers are CaBP that modulate changes in cytosolic [Ca^{2+}] as described in 1.2.1.3 but are increasingly shown to have functions that correspond to an additional Ca^{2+}sensing role (Schwaller, 2009). In the post-proteomic era, calciomics, a combination of predictive and mass throughput experimental techniques to identify CaBPs and map the downstream interactions, elucidates the roles of Ca^{2+} sensors further (Zhou, Xue and Yang, 2013).

The Ca^{2+} binding EF-Hand domains confer the ability of most CaBPs to bind Ca^{2+}; other CaBPs include annexins and C2-region containing proteins that both bind phospholipids in a Ca^{2+} dependent manner (Niki *et al.*, 1996). Annexins contain multiple conserved copies of 17 residue consensus sequence, the "endonexin fold" which binds Ca^{2+} (Geisow *et al.*, 1986; Thiel, Weber and Gerke, 1991). The 130 residue C2 domain motif was identified first in Ca^{2+} sensitive PKC isoforms then subsequently in other structurally distinct Ca^{2+} sensitive proteins which share biological properties, e.g. Ca^{2+} dependent membrane translocation and common intracellular receptors (Nishizuka, 1992; Nalefski and Falke, 1996).

1.2.4.2 EF-Hand Domains

First identified as a Ca^{2+} binding region in parvalbumin between the “E” and “F” helices; an EF-hand is a ~30 residue helix-loop-helix structural motif resembling the spread thumb and forefinger of a human hand with the remaining fingers folded as shown in Figure 1-2 (Kretsinger and Nockolds, 1973). The loop that joins the two α-helices is a conserved consensus sequence of ~12 residues with side chains that co-ordinate and bind one Ca^{2+}, also shown in Figure 1-2 (Hiraoki and Vogel, 1987). Upon Ca^{2+} binding EF-hands, domains undergo conformational changes to adopt an open confirmation compared to the closed conformation in a Ca^{2+} free state (Yap *et al.*, 1999). Predicted to occur in other CaBP, various putative EF-hand sequences containing the consensus sequence were subsequently identified in multiple Ca^{2+} binding and sensitive proteins (Hiraoki and Vogel, 1987; Lewit-Bentley and Réty, 2000). Recently, proteomic analysis has identified 865 protein sequences containing EF-hands divided into 156 subfamilies that belong to one of six different groups (Kawasaki and Kretsinger, 2017).

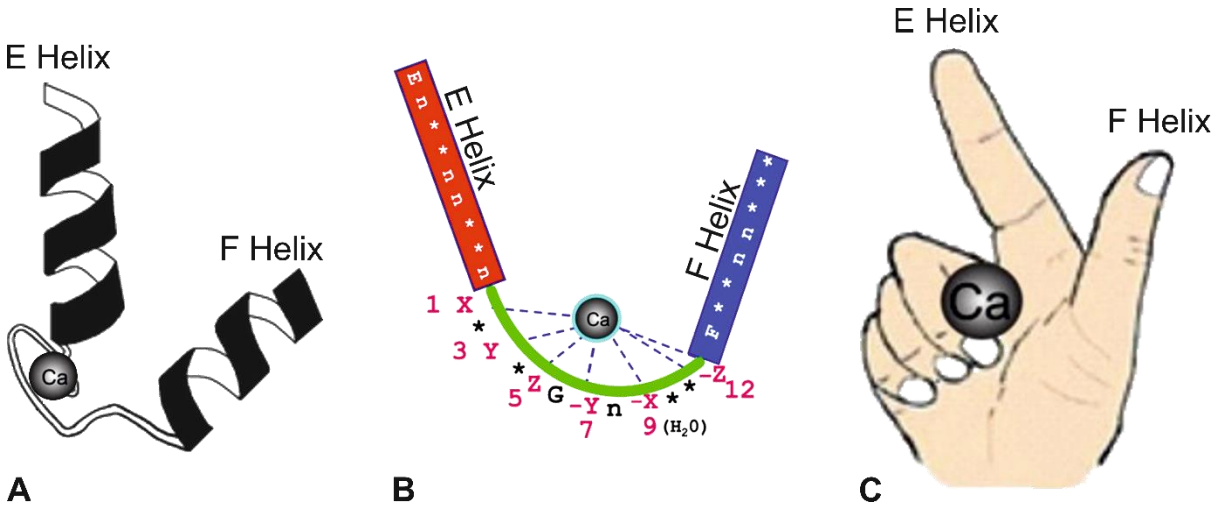

Figure 1-2 The Helix Loop Helix of the Ca^{2+} Binding EF-Hand Motif Resembles a Human Hand

(A) 3D structure of a typical canonical EF-hand motif, the Ca^{2+} binding pocket is in the 12-residue loop separating the E and F helix. **(B)** Cartoon of the canonical EF-hand Ca^{2+}-binding motif, Ca^{2+} is chelated by ligands from the residues in the loop. **(C)** Illustration showing the comparison of the helix loop helix motif to a partially folded human hand. Adaption of image republished with permission (Zhou, Xue and Yang, 2013).

1.2.4.3 Propagation of Intracellular Calcium Signals

Multicellular responses to Ca^{2+} signalling mechanisms are coordinated resulting in propagating rises in intracellular [Ca^{2+}] known as intercellular Ca^{2+} waves (ICWs) emanating from a trigger cell that initiates the ICW. ICWs are the result of the release of Ca^{2+} from internal stores triggered by a variety of stimuli and occur in a wide diversity of cell types, ICWs are propagated by inter-cell communication by intra-cellular and extra-cellular messengers via gap junctions or paracrine signalling respectively. (Leybaert and Sanderson, 2012)

ICWs can following a radial or spiral path across hundreds of cells at a frequency of ~10–20 μm/s lasting for up to 1 min. The characteristics of ICWs are dependent on multiple factors including the cell types involved, how the signal is propagated both within and between cells and the type and strength of the initial stimulus, and regeneration of the messenger. Both IP_3R and RyR release Ca^{2+} during ICW propagation. However, due to Ca^{2+} homeostatic mechanisms, IP_3 appears to have a far more significant role in the propagation of ICWs between cells via gap junctions (Leybaert and Sanderson, 2012).

1.2.5 The Role of Calcium Signalling in Cardiac Muscle Contraction

1.2.5.1 Striated Muscle

Cardiac and skeletal muscle are both forms of striated muscle tissue. Both consist of the tube-shaped myocytes containing a cytoplasm packed with myofibrils, rod-like structures composed of repeating units, sarcomeres. Sarcomeres are the basic units of striated muscle tissue and bordered at either end by structures known as Z-lines.

Each sarcomere is composed of parallel alternating filaments of two long fibrous proteins, actin and myosin with the actin filaments anchored to one of the Z-lines. During the contraction and relaxation of striated muscle tissue, the filaments slide past each other shortening or lengthening the sarcomere.

Myosin has a globular head that binds to actin forming a cross-bridge between two filaments. Powered by ATP hydrolysis the myosin head moves, pulling the actin along so that the actin slides across the myosin filament. The distance between the Z-lines shortens and the muscle tissue contracts. The myosin head detaches, returns to its original position and forms a new cross-bridge on another part of the actin filament. The cycle repeats itself shortening the sarcomere and the muscle tissue contracts further. If new bridges do not form, the actin filament slides back along the myosin filament the sarcomere lengthens, and the muscle tissue relaxes.

1.2.5.2 Excitation-Contraction Coupling

E-CC is the electrophysical process by which an electrical signal, the action potential (AP), is converted into a physical response, the shortening of the sarcomeres (Sandow, 1952). An AP propagates along the myocyte membrane into the transverse-tubules (T-tubules), invaginations that penetrate the interior of the myocyte and are surrounded by the terminal cisternae of the SR.. The sarcolemma of the T-tubules is enriched with VGCC which are in close apposition to RyRs in the terminal cisternae.

In response to membrane depolarisation, VGCC undergo conformational change resulting in the the entry of extracellular Ca2+ into the cell and release of Ca2+ from the SR via the RyR channels. In skeletal muscle the VGCC are directly coupled

to RyR1 and VGCC opening activates the RyR1 channel allosterically. In cardiac muscle VGCC and RyR2 are in close proximity and the extracellular Ca^{2+} strimulates RyR channel opening. The Ca^{2+} release from the SR indirectly activates the shortening of the sarcomeres resulting in muscle contraction.

The myosin filaments associate with another protein troponin C (TnC) which blocks the formation of the cross-bridges. Therefore, actin does not slide over myosin, and the muscle tissue remains relaxed. TnC contains four EF-hand motifs so is capable of binding Ca^{2+} (Kretsinger and Barry, 1975). Upon Ca^{2+} binding, TnC changes conformation exposing the actin-myosin binding sites. The cycle of cross-bridge formation, movement, detachment and formation can commence. actin slides across myosin shortening the sarcomere and the muscles tissue contracts.

The influx of extracellular Ca^{2+} ceases in response to cessation of the AP. Also, the release of intracellular Ca^{2+} will fall due to store depletion and channel closure. The cytosolic [Ca^{2+}] will then fall as Ca^{2+} homeostatic mechanisms, e.g. SERCA pumps, restore resting cytoplasmic [Ca^{2+}]. At low [Ca^{2+}] Ca^{2+} bound to TnC is released, and TnC returns to a Ca^{2+} free conformation blocking cross-bridge formation. Without cross-bridges forming actin slides back, the sarcomere lengthens, and the muscle tissue relaxes.

1.2.5.3 Role of Calcium in the Cardiac Cycle

During the cardiac cycle E–CC links AP to myocardial contraction via changes of cytoplasmic [Ca^{2+}]. The contractile force is mainly dependent on the quantity of Ca^{2+} bound to TnC, which is in turn dependent on the size and length of the Ca^{2+} transient.

However, the proper cardiac function also requires cardiac relaxation so that the atria can refill before the next contraction. Contraction and relaxation are the product of increased and decreased [Ca^{2+}] respectively. Therefore, both the initiation and termination of the release of Ca^{2+} are tightly regulated (Eisner *et al.*, 2017).

During heart failure (HF) the contractile force of the heart is reduced. Despite HF being aetiologically complex the inappropriate release of Ca^{2+} from the SR via misfunctioning RyR channels is frequently observed. Dysfunctional Ca^{2+} handling due to reduced RyR2 activity, failure to terminate CICR and the leak of SR Ca^{2+} appear to be important causative factors of reduced contractile force during HF. Dysfunctional activity in RyR2 channel is believed to be acquired due to changes within RyR2 and the macromolecular signalling complex during HF. The molecular alterations are the result of oxidation and phosphorylation of RyR2 and modulating proteins and could be both causative of and the result of HF pathology (Zima *et al.*, 2014).

A significant cause of sudden cardiac death (SCD) during non-ischaemic HF is cardiac arrhythmias, with SR Ca^{2+} leak causing delayed afterdepolarisations (DADs) believed to play a prominent role (Schlotthauer and Bers, 2000; Pogwizd, 2004). In otherwise normal hearts inherited defects in the proteins responsible for Ca^{2+} handling during the cardiac cycle can also cause inappropriate Ca^{2+} release. The dysfunctional Ca^{2+} release causes DADs leading to ventricular polymorphism and tachycardia which can result in myocardial infarction (MI) and SCD (Schlotthauer and Bers, 2000; Ter Keurs and Boyden, 2007).

Since 1995 it has become apparent that mutations in the genes that encode cardiac ion channels cause inherited arrhythmic cardiac syndromes by disturbing the flow of ions during the cardiac cycle (Curran *et al.*, 1995; Wang *et al.*, 1995).

1.2.6 The Role of Calcium at Fertilisation

1.2.6.1 Gametes Before Fertilisation

In sexually reproducing organisms at fertilisation two haploid gametes from two organisms of the same species fuse to produce a diploid single cell zygote. The zygote, which contains genetic information from both parent organisms undergoes successive rounds of mitotic cell division and differentiation to produce a new, offspring organism.

In animals, morphologically different gametes are produced by the male and female organisms in testes and ovaries respectively. The male gametocytes are the small motile spermatozoan (sperm), and the female gametocytes are the large, non-motile oocytes. The gametocytes are the result of male and female germ cells undergoing meiotic division, differentiation, morphological development and maturation (Kupker, Diedrich and Edwards, 1998). The cell cycle of a mature oocyte is arrested during meiosis to prevent sperm-free embryonic cell cycles from occurring; in mammalian oocytes, the cell cycle is arrested during metaphase II of meiosis (Dupré, Haccard and Jessus, 2011).

1.2.6.2 Fertilisation

Mammalian fertilisation occurs in the oviduct where chemotaxis enables mature, hyperactive capacitive sperm to locate and surround the oocyte (Suarez and Pacey, 2006). The sperm interacts with the zona pellucida (ZP), the extracellular matrix of glycoproteins surrounding the plasma membrane of the mature oocyte (Bianchi and Wright, 2016). The ZP contains proteins suggested to endow a lock-and-key type mechanism that excludes sperm from a species different to the oocyte conferring species selectivity (Conner and Hughes, 2003; Conner *et al.*, 2005). Upon reaching the oocyte, triggered by an unknown mechanism the sperm acrosome releases enzymes that catalyse the acrosomal reaction which is required for the sperm to penetrate the ZP and fertilise the oocyte (Bedford, 2011). Once beyond the ZP, the fertilising sperm traverses the perivitelline space between the ZP and oocyte plasma membrane and the plasma membranes of the sperm and oocyte fuse (Bianchi and Wright, 2016).

1.2.6.3 Polyspermy Block

However, if more than one sperm penetrates the ZP and fuses with the oocyte, fertilisation is polyspermic resulting in a potentially non-viable polyploidal embryo (Jacobs *et al.*, 1978; Michelmann, Bonhoff and Mettler, 1986; Zaragoza *et al.*, 2000; Liu, 2011) To avoid polyspermy upon fertilisation the penetration of the oocyte by additional sperm is blocked (Austin and Braden, 1956). The exocytosis of cortical granules (CGs), secretory vesicles in the cortex of the unfertilised oocyte, “hardens” the ZP so to be impenetrable to sperm (Gardner and Evans, 2006). The exact

composition of the CG is unknown but includes proteases, peroxidases and glycosaminoglycans the nett result of the actions of which is to biochemically alter the ZP and perivitelline space to no longer support the binding and passage of sperm (Liu, 2011).

In all animals, a substantial transient increase in cytosolic [Ca^{2+}] concentration is the first signalling event in the activation of an oocyte at fertilisation (Stricker, 1999; Runft, Jaffe and Mehlmann, 2002). The temporal pattern of the [Ca^{2+}] transients varies across the animal kingdom from a single increase in jellyfish and frogs to a series of prolonged repetitive Ca^{2+} transients, or Ca^{2+} oscillations in mammals and ascidians (Stricker, 1999). A series of Ca^{2+} oscillations typical in mammalian oocytes are shown in Figure 1-3.

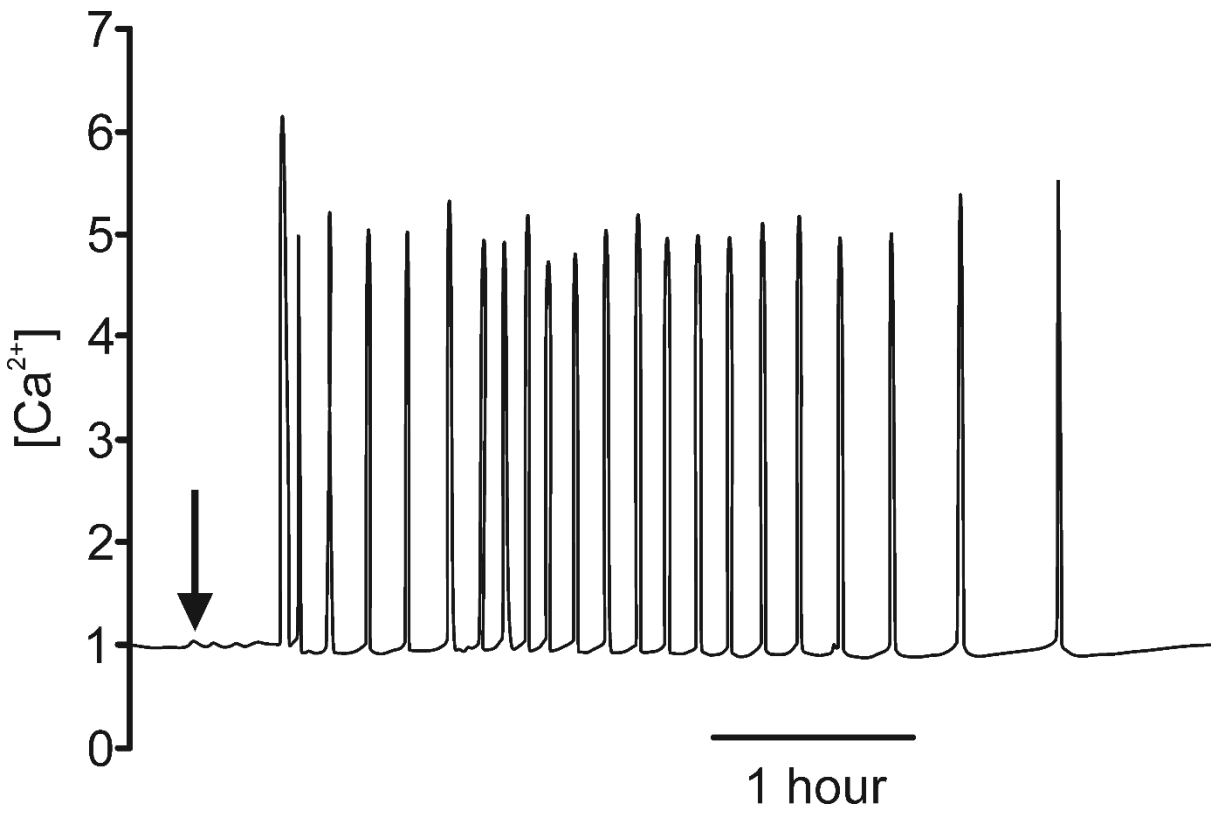

Figure 1-3 Following Fertilisation Cytoplasmic [Ca^{2+}] of Oocytes Fluctuates in a Repetitive, Regular Pattern

The typical pattern of Ca^{2+} oscillation in mature MII mouse oocytes following *in vitro* fertilisation. The arrow indicates the time of insemination, and [Ca^{2+}] is monitored with a fluorescent Ca^{2+} probe. Reprinted with permission (Deng and Sun, 1996)

1.3 Calmodulin

1.3.1 Background

Expressed in all eukaryotic cells, CaM is a primary transducer of Ca^{2+} signals regulating a broad spectrum of physiological processes (Chin and Means, 2000; Clapham, 2007). Processes in which CaM plays a regulatory role include cellular growth, proliferation, signalling, metabolism, motility, ion transport, cytoskeletal architecture and function, apoptosis, autophagy, phospholipid turnover, gene expression, protein folding and phosphorylation/dephosphorylation, osmosis, reproduction, muscle contraction, memory and inflammation (Berchtold and Villalobo, 2014). More than 300 distinct proteins are known to bind to CaM including enzymes, myosins, receptors and ion channels [http://calcium.uhnres.utoronto.ca/ctdb] (Yap *et al.*, 2000). The interaction of CaM with a protein either directly induces a physiological response or provokes a subsequent signalling pathway (Yamniuk and Vogel, 2004).

1.3.1.1 Discovery

During the 1970s several groups independently identified Ca modulating protein or calmodulin (CaM), a protein capable of binding Ca^{2+} that also individually activated different enzymes (Marx, 1980). CaM has been identified in many eukaryotic species and widely distributed in vertebrate and invertebrate animal tissues (Brostrom and Wolff, 1981). CaM is also present in plant, fungi and protist species (Kuźnicki, Kuźnicki and Drabikowski, 1979; Muthukumar, Nickerson and Nickerson, 1987; Zhu *et al.*, 2015). Ca^{2+} binding EF-hand proteins homologous to CaM that mediate Ca^{2+} signalling also occur in bacteria (Domínguez, Guragain and Patrauchan, 2015). Postulated to have been present in the last common ancestor of plants, fungi and

animals, CaM is conserved in all eukaryotic lineages playing a pivotal role in Ca^{2+} signalling (Friedberg and Rhoads, 2001; Plattner and Verkhratsky, 2015).

1.3.1.2 Genetics of Calmodulin

Amongst vertebrates, CaM is highly conserved with 100% sequence identity (Friedberg and Rhoads, 2001). In mammals, three paralogous non-identical genes with variable flanking sequences, *CALM1*, *CALM2* and *CALM3* express identical CaM protein in response to different stimuli (Sengupta, Friedberg and Detera-Wadleigh, 1987; Fischer *et al.*, 1988; Pegues and Friedberg, 1990; Toutenhoofd *et al.*, 1998). Expression of the paralogous genes as multiple mRNA species with differing untranslated sequences that enable localisation is proposed to result in dedicated pools of CaM at specific cellular locations (Toutenhoofd *et al.*, 1998)

1.3.1.3 The Relationship Between Structure and Function of Calmodulin

CaMs all belong to the CaM subfamily of the EF-hand protein family (Kawasaki and Kretsinger, 2017). Mammalian CaM consists of 148 amino acids with a molecular mass of 17 kDa and contains four “helix-loop-helix” EF-hand Ca^{2+} binding domains (Watterson, Sharief and Vanaman, 1980). Therefore, CaM contains four Ca^{2+} binding sites comprised of eight α-helices. The 3D structure of CaM resembles a “dumbbell” shape of an N-terminal lobe (N-lobe) containing the first pair of EF-hands (EFI and EFII) separated by a short flexible linker from the C-terminal lobe (C-lobe) containing the second pair of EF-hands (EFIII and EF IV)

The flexible linker of CaM permits the N- and C-lobes a high degree of independent movement and function (Chou *et al.*, 2001). However, the binding

properties of each lobe is a product of interaction with the other (Sorensen and Shea, 1998). The flexibility of CaM and autonomy of the lobes permits CaM to adopt the range of conformational states required to interact with a variety of target proteins (Yamniuk and Vogel, 2004; Ikura and Ames, 2006). Dependent on the target protein the lobes of CaM may have different and specific roles (Kung *et al.*, 1992; Ohya and Botstein, 1994; Persechini, Stemmer and Ohashi, 1996).

1.3.2 Activity of Cam

1.3.2.1 Calcium Binding Affinity of Calmodulin

Dependent on experimental conditions, the binding affinity between CaM and Ca^{2+} varies as the dissociation constant (K_d) can range between 300 to 5000 nM; while at an approximation of physiological ionic conditions K_d is ~1 μM, within the range of intracellular Ca^{2+} oscillations (Linse, Helmersson and Forsen, 1991; Alaimo *et al.*, 2014; Hoffman *et al.*, 2014). The binding affinity between CaM and Ca^{2+} can be increased or reduced by the binding of a target protein (Villarroel *et al.*, 2014).

The Ca^{2+} binding affinity of the C-lobe is an order of magnitude greater than that of N-lobe, the degree of magnitude varies with the ionic strength of the surroundings (Potter *et al.*, 1983; Linse, Helmersson and Forsen, 1991). The binding of Ca^{2+} to CaM is cooperative and sequential, the first Ca^{2+} binds to the two sites in the C-lobe and then to the two sites in the N-lobe (Crouchl and Klee, 1980). In the presence of CaM binding partners the Ca^{2+} affinity of the lobes increases and Ca^{2+} binding is positively co-operative (Olwin and Storm, 1985; Yazawa *et al.*, 1987). The interaction with and regulation of protein binding targets by CaM may be dependent

on the level of saturation dictating the occupation of Ca^{2+} binding sites, i.e. which and how many Ca^{2+} binding sites are occupied (Wang *et al.*, 1980; Haiech, Klee and Demaille, 1981). However, common Ca^{2+} dependent CaM interactions with enzymes require 3-4 Ca^{2+} binding sites to be occupied (Carafoli and Klee, 1992).

1.3.2.2 Calmodulin Conformational Change Mediated by Calcium-Binding

At basal [Ca^{2+}], CaM exists in a Ca^{2+} free state (apoCaM) with the Ca^{2+} binding sites unoccupied and adopts a “closed” conformation as shown in Figure 1-4 (Finn and Forsén, 1995; Zhang, Tanaka and Ikura, 1995). At increasing [Ca^{2+}], the Ca^{2+} sites of CaM are rapidly occupied resulting in Ca^{2+} saturated state (holoCaM) accompanied by conformational change as shown in Figure 1-4 (Babu, Bugg and Cook, 1988). HoloCaM and apoCaM bind different overlapping sets of proteins transducing changes in [Ca^{2+}] to control of cellular function (Jurado, Chockalingam and Jarrett, 1999).

The open conformation adopted by holoCaM exposes hydrophobic patches on the two lobes of CaM forming a methionine (Met) rich binding pocket which enables CaM to engulf target sequences as shown in Figure 1-4 (Zhang, Tanaka and Ikura, 1995). The Met residues in the binding pocket enable CaM to target the side chains of aromatic hydrophobic residues separated by aliphatic residues that occur in Ca^{2+} dependent-binding motifs; consensus amino acid sequences that bind CaM and classified according to the relative position of conserved hydrophobic residues (Rhoads and Friedberg, 1997; Kursula, 2014b). The binding of holoCaM to a major binding partner, Ca^{2+}/CaM dependent kinase II (CaMKII) is shown in Figure 1-4.

The conformational states of the N- and C-lobes of CaM alter reversibly and autonomously (Martin and Bayley, 1986). Dependent on surrounding conditions; apoCaM can contain a C-lobe in a different conformational state, stabilised by subsequent Ca^{2+} binding, than the N-lobe, (Masino, Martin and Bayley, 2000). In the absence of Ca^{2+}, the apoCaM N-lobe adopts a closed conformation while the C-lobe is in a partially open conformation; providing limited access to the hydrophobic patches which may enable Ca^{2+} free binding of CaM to target sequences (Swindells and Ikura, 1996).

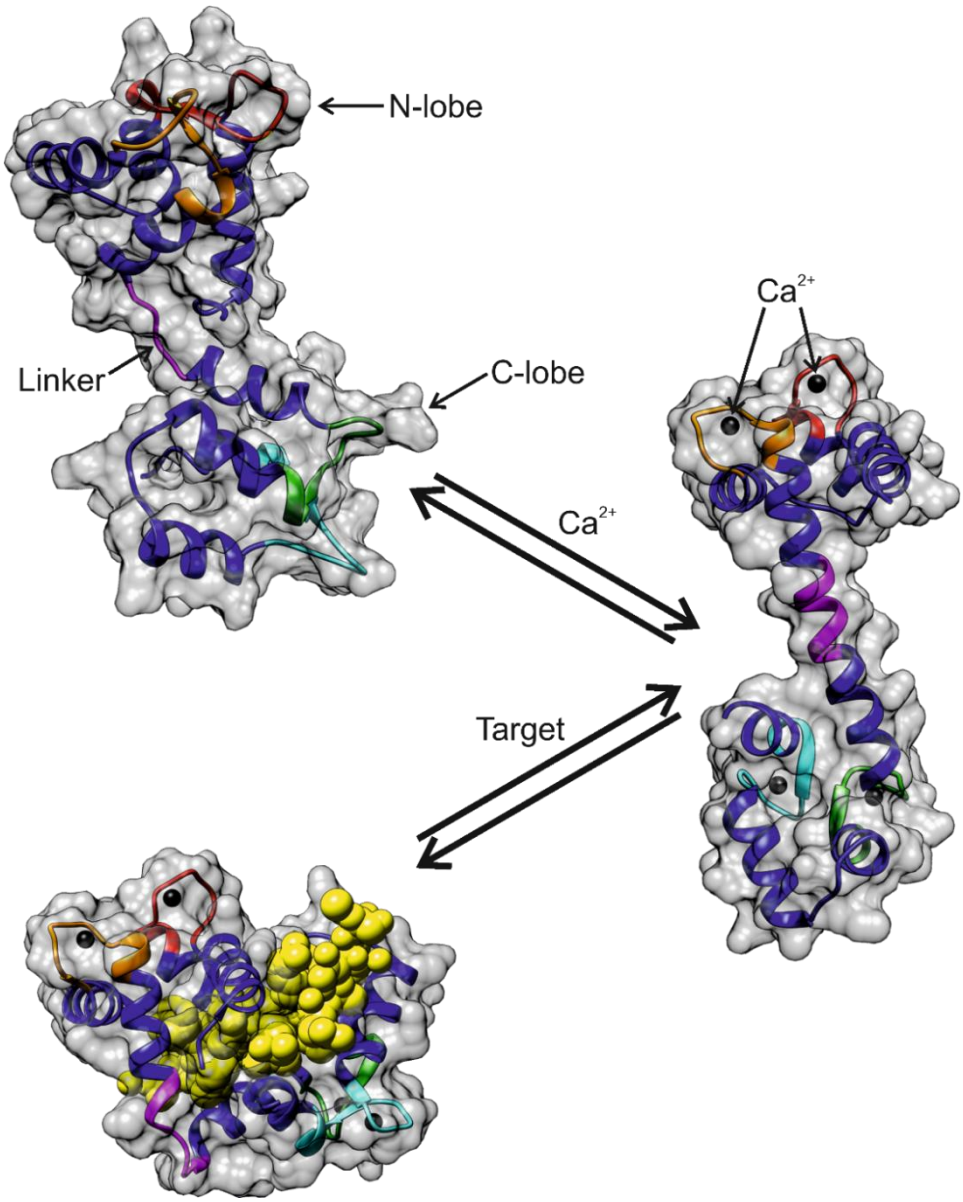

Figure 1-4 The Ca^{2+} Induced Conformational Change Enables Calmodulin to Bind Target Proteins

Molecular models of apoCaM, holoCaM and holoCaM bound to a peptide corresponding to CaM-binding domain of CaMKII. Ca^{2+} ions bind to the four binding sites (red, orange, green and cyan) of apoCaM inducing a conformational change in CaM with the alpha-helical content increasing (magenta). HoloCaM can bind and engulf target sequences, e.g. CaMKII peptide (yellow). Structures derived from RCSB PDB (rcsb.org) entries 1QX5, 1CLL and 3GP2 (Berman, 2000). Molecular graphics and analyses performed with UCSF Chimera (Pettersen *et al.*, 2004)

1.3.2.3 Complex and Dynamic Binding of Calmodulin to Target Proteins

Binding between CaM and target proteins is complex and dynamic varying with the target and Ca^{2+} binding. Salt bridges and hydrogen bonds formed between CaM and the target binding sequences assist target orientation and induce structural changes within the α-heliices of the flexible linker of CaM (Kurokawa *et al.*, 2001; Kursula, 2014a). The relative contribution of each CaM lobe and EF-hand α-helices to overall target binding can vary resulting in a range of different binding complex conformations (Villarroel *et al.*, 2014).

CaM can bind to a target in a parallel orientation with both lobes in the same orientation (Juranic *et al.*, 2010; Rodríguez-Castañeda *et al.*, 2010). Alternatively, the individual lobes of CaM can be bound to the target in an antiparallel orientation to each other (Houdusse *et al.*, 2006; Mori *et al.*, 2008; de Diego *et al.*, 2010; Lau, Procko and Gaudet, 2012). The lobes can be bound in close enough proximity to be on adjacent sequences, to overlap or be displaced by each other (Mori *et al.*, 2008; de Diego *et al.*, 2010; Lau, Procko and Gaudet, 2012). The lobes can also bind to non-adjacent locations to bridge distant residues within the same sequence or span distant residues in spatially adjacent domains (Fallon *et al.*, 2005; de Diego *et al.*, 2010; Juranic *et al.*, 2010; Rodríguez-Castañeda *et al.*, 2010). Multiple binding complexes between CaM and the same target protein indicate the lobes of CaM can slide and rotatate forwards and backwards along the target between different binding sites (de Diego *et al.*, 2010).

1.3.2.4 Calmodulin as Ca^{2+}-Sensing Subunits or Localised Binding Domains

In many cases, apoCaM is “pre-bound” to the target protein or forms part of a protein complex, typically via the C-lobe (Jurado, Chockalingam and Jarrett, 1999; Alaimo *et al.*, 2014). The high-affinity binding between apoCaM and targets creates localised Ca^{2+} signalling that enables CaM to be effective despite finite cytosolic levels and provide specific localised responses to global and local Ca^{2+} signals (Saucerman and Bers, 2012). ApoCaM binds to target proteins in a Ca^{2+} independent manner via the IQ CaM-binding motif (IQ motif), a consensus amino acid sequence, (Rhoads and Friedberg, 1997). The binding of apoCaM can be via both lobes or by the C-lobe alone (Houdusse *et al.*, 2006; C. Wang *et al.*, 2012). Multiple examples of both holo and apoCaM binding to target proteins via only the C-lobe, but not the N-lobe alone, have been observed. Also, few examples of contact between the target protein and the N-lobe of bound apoCaM are known (Villarroel *et al.*, 2014).

1.3.2.5 Binding Targets of Calmodulin

A primary binding target of CaM is Ca^{2+}/CaM dependent kinase (CaMK) family members and isoforms. CaMKs are serine (Ser)/threonine (Thr)-specific protein kinases that phosphorylate proteins; notable examples include the multifunctional CaMKI, II & IV, and the specific myosin light chain kinase and CaMKIII (Wayman *et al.*, 2011). Substrates of CaMK isoforms participate in diverse cellular functions, processes, and signalling cascades including gene transcription, biosynthesis, ion transport, cardiomyocyte Ca^{2+} homeostasis, oocyte meiotic arrest, T-cell activation, memory and muscle contraction (Braun and Schulman, 1995). Dysfunctional

regulation of CaMKII is associated with Alzheimer's disease, Angelman syndrome, and heart arrhythmia (Yamauchi, 2005; Couchonnal and Anderson, 2008).

Other enzymes targeted by CaM include Ca^{2+} transport ATPase, cyclic nucleotide phosphodiesterase, the phosphatase calcineurin, phosphorylase kinase and nitric oxide synthase (Means *et al.*, 1991; Vogel, 1994; James, Vorherr and Carafoli, 1995). CaM also modulates cell growth and movement by interacting with cytoskeletal proteins such as caldesmon, brush border myosin, and myristoylated alanine-rich C kinase substrate (Means *et al.*, 1991; Vogel, 1994; James, Vorherr and Carafoli, 1995).

CaM modulates the ion flow into, out of, and within cells by modulating ion channels, often acting as a constitutive or dissociable Ca^{2+} sensing subunit. Ion channels to which CaM binds and regulates include RyR, IP_3R, TRP, and voltage-gated ion channels, small conductance Ca^{2+}-activated potassium ion (K^+) channels (SK), inwardly rectifying potassium channels (K_{ir}, IRK), cyclic nucleotide-gated ion channels (CNG), and PMCA (Saimi and Kung, 2002; Brini *et al.*, 2013).

1.3.2.6 Calmodulin: A Multifunctional Calcium Signal Transducer

The differing Ca^{2+} binding affinities of the N- and C-lobes modulate regulation of target proteins by CaM in response to Ca^{2+}, enabling a specific response by CaM according to the spatiotemporal characteristics of $[Ca^{2+}]$ changes (Tadross, Dick and Yue, 2008). Meanwhile, structural flexibility and conformational plasticity enable CaM to adapt in order to recognise, bind and regulate a plethora of target proteins allowing CaM to

regulate a diverse variety of cellular processes in response to [Ca^{2+}] changes (Yamniuk and Vogel, 2004; Kursula, 2014b; Villarroel *et al.*, 2014).

1.3.2.7 Calmodulin and Human Disease

Due to the wide-ranging direct and indirect roles of CaM, CaM is required for cell cycle progression in all eukaryotic organisms tested to date and deletion of CALM is fatal (Davis *et al.*, 1986; Kahl and Means, 2003). Potentially any mutations in CaM could be deleterious if not lethal. However, there is a high degree of redundancy as three identical CaM encoding genes, i.e. six alleles could be expressed in any given cell. Nevertheless, CaM participates in many of the processes the derangement of which is aetiological in human disease, e.g. Alzheimer's disease (Clapham, 2007).

In cardiomyocytes, CaM regulates many of the ion channels and cytoplasmic regulators in the cardiac AP and so controls the excitability threshold, E-CC and refractory period (Tang, 2002). Dysfunctional binding of CaM to targets and mutations in CaM binding sites of cardiac ion channels RyR2 and voltage-gated ion channels have been associated with inherited cardiac arrhythmias (Tan *et al.*, 2002; Ghosh, Nunziato and Pitt, 2006; Shamgar *et al.*, 2006; Uchinoumi *et al.*, 2010; Xu *et al.*, 2010; Blaich *et al.*, 2012; Limpitikul *et al.*, 2014). Recently dominant mutations in CaM encoding genes predicted to cause single amino acid substitutions have been identified in clinical cases of cardiac arrhythmia (Sorensen, Søndergaard and Overgaard, 2013; George, 2015).

1.4 Phospholipase Cζ

1.4.1 Inositol 1,4,5-Trisphosphate Receptor

1.4.1.1 The Release of Calcium from IP_3 Sensitive Intracellular Stores

In direct response to stimulation by the secondary messenger IP_3, Ca^{2+} is released from intracellular Ca^{2+} stores, particularly those in the ER, (Burgess *et al.*, 1984; Prentki, Wollheim and Lew, 1984; Meyer, Holowka and Stryer, 1988). Extracellular agonists stimulate the production of IP_3, so IP_3 enables the mobilisation of Ca^{2+} in response to receptor activation in many cell types (Berridge, 1984, 1993; Berridge and Irvine, 1984). The IP_3R channel, the target of IP_3 is a 1.2 MDa tetrameric protein complex integral to ER membranes which becomes Ca^{2+} permeable in response to IP_3 binding (Supattapone *et al.*, 1988; Ferris *et al.*, 1989). Studies of native and recombinant protein have revealed the functional and structural characteristics of IP_3R channels and subunits; the best-characterised subunit is IP_3R1 (Fedorenko *et al.*, 2014). The exact molecular mechanism by which IP_3 binding at extreme N-terminus of the IP_3R causes pore opening at the opposite end is unknown. A substantial conformational change in the receptor accompanies IP_3 binding (Mignery and Südhof, 1990). However, the linkage between IP_3 binding and channel opening is complex. It is likely that several of the receptor subunits first bind IP_3 and then Ca^{2+} before the pore opens (Marchant and Taylor, 1997).

1.4.1.2 Isoforms of IP_3 Receptor

In mammals, there are three isoforms of IP_3R subunit, IP_3R1, IP_3R2 and IP_3R3, which have differing affinities for IP_3; (Blondel *et al.*, 1994; Newton, Mignery and Südhof,

1994; Yamada *et al.*, 1994; Yamamoto-Hino *et al.*, 1994; Joseph, 1996). IP_3R1 is the most commonly expressed isoform, but many cell types express two or three isoforms in different combinations and proportions (Taylor, Genazzani and Morris, 1999). There are four alternative splicing sites in IP_3R1 and two in IP_3R2. The full physiological significance and functional impact of splice variants are unclear (Nakade, Maeda and Mikoshiba, 1991; Yoshikawa *et al.*, 1996; Futatsugi, Kuwajima and Mikoshiba, 1998; Boehning *et al.*, 2001; Peinelt *et al.*, 2009). The specific spatiotemporal expression pattern of IP_3R isoforms and splice variants could enable tissue and development specific expression of functionally diverse IP_3R channels (Nakagawa, Okano, *et al.*, 1991; Nakagawa, Shiota, *et al.*, 1991). Potentially there is a multitude of different IP_3R channels with a diversity of function as channels can be hetero-tetrameric combinations of any of the isoforms and splice variants (Foskett *et al.*, 2007). However, recent data indicate the function of heterotetrameric channels resembles that of a homotetrameric channel of one of the constituent subunits rather than a blend of all the subunits present (Chandrasekhar, Alzayady and Yule, 2015).

IP_3R isoforms share 60-80% sequence identity, and a highly conserved domain structure consisting of a cytosolic IP_3 binding region near the N-terminal, a central region containing phosphorylation and regulatory protein binding sites, and Ca^{2+} channel domain close to the C terminal (Michikawa *et al.*, 1994). IP_3 binds to the N-terminal region independently of the C-terminal, but tetramer formation and Ca^{2+} release require the C-terminal (Mignery *et al.*, 1990; Miyawaki *et al.*, 1991; Nakade, Maeda and Mikoshiba, 1991; Michikawa *et al.*, 1994). Channel gating requires interaction between the N-terminus and the C-terminus of adjacent subunits

(Boehning, 2000). Also, the interaction between CaM, ATP and Ca^{2+} binding sites and residues within the C-terminal and central regions modulate channel response to IP_3 (Maeda *et al.*, 1991; Sienaert *et al.*, 2002).

1.4.1.3 Structure of IP_3 Receptor Ion Channel

EM images of IP_3R have been published at increasing resolution in the presence and absence of ligands (Q. Jiang *et al.*, 2002; da Fonseca *et al.*, 2003; Hamada, Terauchi and Mikoshiba, 2003; Serysheva *et al.*, 2003; Ludtke *et al.*, 2011). The resolution and contrast of EM images were hampered by various factors which were gradually overcome (Baker, Fan and Serysheva, 2017). The highest contrast single-particle structure published to date is a 4.7 Å resolution cryogenic electron microscopy (Cryo-EM) image of rat IP_3R1 in a closed conformation, shown in Figure 1-5 (Fan *et al.*, 2015; Baker, Fan and Serysheva, 2017). This model redefined the existing domain architecture and elucidated several areas of ambiguity from previous models to one of IP_3R1 containing ten domains seen in Figure 1-5 (Fan *et al.*, 2015; Baker, Fan and Serysheva, 2017). Crucial interactions link ligand binding to channel gating and opening (Chan *et al.*, 2010; Yamazaki *et al.*, 2010). Movement and changes in the intradomain interactions are critical for channel permeability (Li *et al.*, 2013).

Viewed from the membrane plane, IP_3R resembles a mushroom, with a “cap like” cytoplasmic region on top of a smaller transmembrane region as shown in Figure 1-5. When viewed from cytoplasm and lumen, the cytoplasmic and transmembrane region are square-shaped structures with four-fold rotational symmetry around a central “plug”. The cytoplasmic structure is 220 Å wide, and the transmembrane

structure is 120 Å wide, the combined height is 190 Å (Ludtke *et al.*, 2011). The cytoplasmic region accounts for 89 % of the total protein mass and contains both N- and C- termini (Fan *et al.*, 2015; Baker, Fan and Serysheva, 2017).

The tetrameric architecture of IP_3R1 channel is constructed around a central core which runs along the axis of four-fold symmetry. The structural and functional integrity of the IP_3R channel may be the result of the combined interactions throughout the entire central core stabilising subunit interfaces. The central core consists of two coiled α-helical bundles, a right-handed coil spanning the transmembrane region and a left-handed coil spanning most of the cytoplasmic region, connected by helical linker domains (LNK) (Fan *et al.*, 2015; Baker, Fan and Serysheva, 2017). To the central core, each subunit contributes an α-helix (TM6) from the transmembrane domain (TMD) to the transmembrane bundle, an α-helical C-terminal domain (CTD) to the cytoplasmic bundle and an LNK to join them (Fan *et al.*, 2015; Baker, Fan and Serysheva, 2017).

In the presence of Ca^{2+}, the IP_3R channel adopts a wider, windmill shaped configuration with each sail of the windmill anchored at the central plug (Q. Jiang *et al.*, 2002; da Fonseca *et al.*, 2003; Hamada, Terauchi and Mikoshiba, 2003; Serysheva *et al.*, 2003). However, while the windmill configuration is indicative of channel opening no change in channel conformation in the presence of IP_3 has been observed (Taylor, da Fonseca and Morris, 2004).

1.4.1.4 Activation of the IP_3 Receptor

The exact mechanism of IP_3R1 activation, how IP_3-induced changes in conformation lead to channel gating, remains unrevealed. The IP_3 binding site and ion channel are separated, so there must be a coupling mechanism to transmit ligand binding to the pore to produce a specific gating event. Pore gating could be the result of interaction between the cytosolic helix connecting the fourth and fifth transmembrane helices and the N-terminal of adjacent IP_3R subunits (Taylor and Tovey, 2010). Direct coupling between the ligand binding and TMD was proposed as the mechanism (Ludtke *et al.*, 2011). Recently, the identification of discrete intra-subunit and inter-subunit interfaces suggests a new route via which ligand binding signals propagate to the TMD.

Channel activation appears to be the result of complex interplay between the binding of primary ligands and modulating intracellular signals. Activation of the tetrameric IP_3R1 channel relies on interactions between domains both within the same and neighbouring subunits that occur near potential regulatory sites. Binding of a single IP_3 molecule to one subunit elicits conformational changes in domains of two neighbouring subunits, cascading activation to the channel pore. Several intracellular regulatory molecules modulate channel gating resulting in a functional response in the channel. Modulation could be the result of allosteric interaction at locations mechanically coupled to the IP_3 binding sites to propagate the signal.

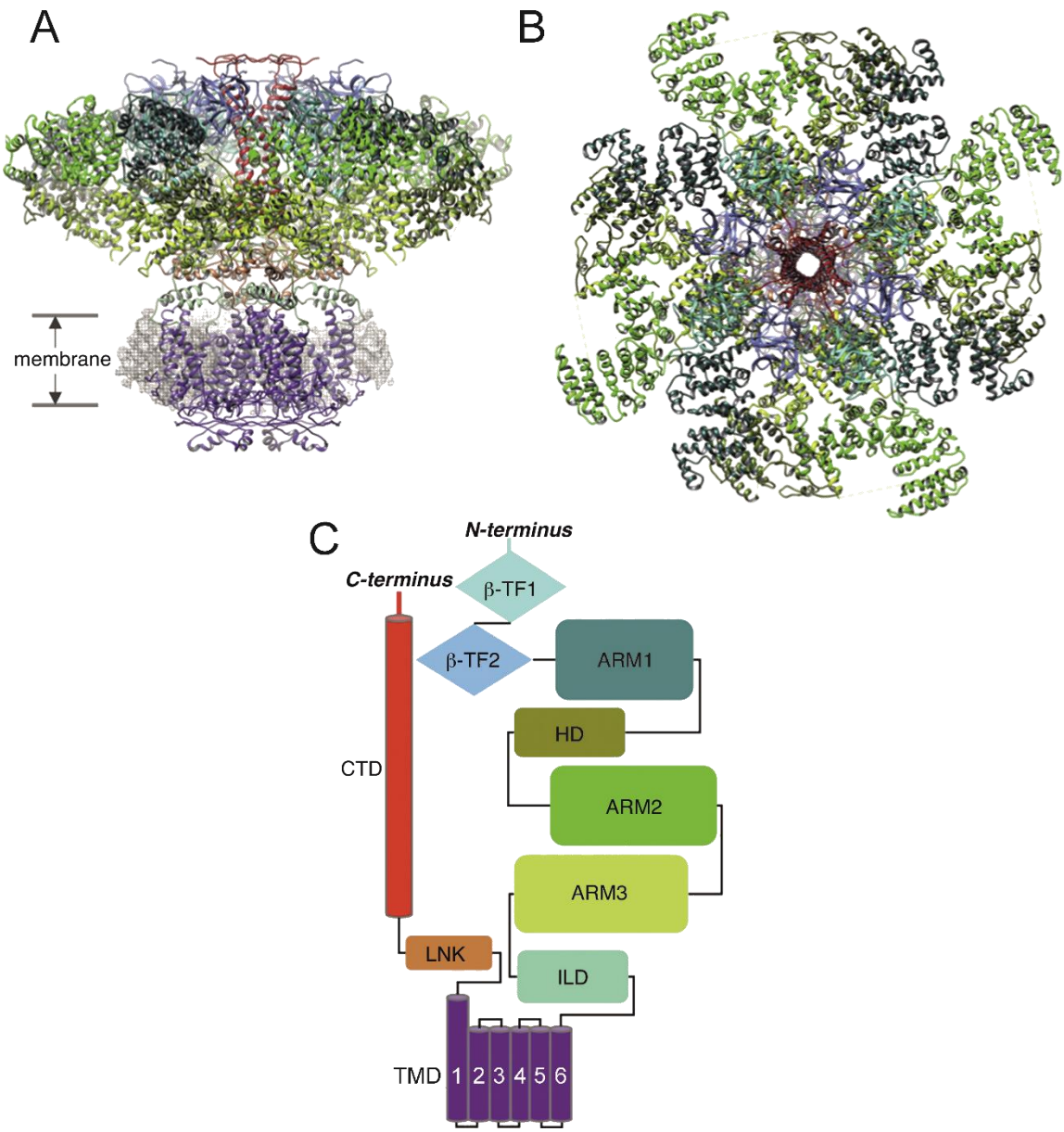

Figure 1-5 The Tetrameric IP_3R1 Channel Consists of Subunits Each Containing Ten Domains That Contribute to the Function and Formation of the Ca^{2+} Channel

The proposed structure of rat cerebellar IP_3R1 based on single-particle Cryo-EM republished with permission (Baker, Fan and Serysheva, 2017). (A&B) The overall structure of the closed rat IP_3R at a resolution varying from 3.6 Å to 6.5 Å. The tetrameric structure of IP_3R1 is domain-coloured with the same scheme as in **(C)**. **(A)** View along the membrane plane, the channel is orientated so that the cytosolic domain is above the semi-transparent grey mesh which indicates the observed detergent–phospholipid belt. **(B)** cytosolic view of the channel. **(C)** Domain organisation of a rat IP_3R1 protomer.

1.4.1.5 Domain Architecture of IP_3 Receptor

The N-terminal region of IP_3R1 contains two β-Trefoil fold domains (β-TF1&2), an Armadillo repeat domain (ARM1), an α-helical domain (HD) followed by two more ARM domains (ARM2&3) (Baker, Fan and Serysheva, 2017) The β-TF domains and a portion of ARM1 contribute to the "Suppressor domain" (SD) and "IP_3 binding core" (IBC) (Baker, Fan and Serysheva, 2017). The IBC binds IP_3 with high binding affinity and contains basic residues conserved amongst IP_3R isoforms that are essential for specific binding of inositol phosphates (Yoshikawa *et al.*, 1996, 1999; Uchiyama *et al.*, 2002; Bultynck *et al.*, 2004). The SD and the IBC interact directly, and removal of the SD results in enhanced binding of IP_3 by IBC (Yoshikawa *et al.*, 1996, 1999; Bultynck *et al.*, 2004).

Removing the SD increases IP_3 binding affinity by one order of magnitude in all IP_3R isoforms (Uchiyama *et al.*, 2002; Iwai *et al.*, 2007). Differences in the SD mediated suppression of IP_3 binding is responsible for IP_3R isoform-specific ligand binding affinities (Iwai *et al.*, 2007). In addition to suppressing ligand binding, Ca^{2+} release requires the SD to be present (Uchida *et al.*, 2003; Szlufcik *et al.*, 2006). Movement and changes in the interaction of SD and other IP_3R domains are critical for channel permeability (Li *et al.*, 2013). Interaction of crucial residues in the N-terminal and CTD link ligand binding to channel gating and opening (Chan *et al.*, 2010; Yamazaki *et al.*, 2010). Upon IP_3 binding the induced conformational changes are transmitted and propagated via flexible linking sequences resulting in pore opening (Chan *et al.*, 2007; Rossi *et al.*, 2009).

Within the SD is a loop of exposed amino acids known as a Hot Spot loop (HS-loop) (Chan *et al.*, 2010). The HS-loop contains residues essential for channel activation and becomes accessible in the presence of Ca^{2+} (Anyatonwu and Joseph, 2009; Yamazaki *et al.*, 2010). The N terminal regions of the four subunits form a ring around the plug, with the HS-loop of each participating in extensive intersubunit interactions with the N terminals of the adjacent subunits, which hold the tetramer together (Seo *et al.*, 2012). There are electrostatic interactions at two points between the SD and the IBC, (Seo *et al.*, 2012; Fan *et al.*, 2015). The SD and IP_3-binding site face each other indicating that the SD suppresses ligand binding through allosteric interference (Lin, Baek and Lu, 2011; Seo *et al.*, 2012). Domain movement induced by IP_3 binding disrupts some of the allosteric interactions causing the SD to move and rotate. Movement and rotation of the SD shift the position of the HS-loop resulting in altered interactions with other parts of the channel (Stathopulos *et al.*, 2012; Li *et al.*, 2013).

ARM1-3 dominate the cytoplasmic region, the external surfaces of which slope inward towards the central plug and contain multiple putative binding sites for modulatory proteins (Baker, Fan and Serysheva, 2017). Due to the modular domain architecture, IP_3R can bind many modulators, and alternative splicing can produce a variety of recognition interfaces (Mikoshiba, 2007, 2015). Binding sites include those for Ca^{2+} and CaBPs including holoCaM, apoCaM (Sienaert *et al.*, 2002; Taylor and Tovey, 2010). A flexible domain architecture probably facilitates propagation of ligand-evoked signals towards the ion-conduction pathway (Baker, Fan and Serysheva, 2017).

Inter- and intra-subunit interactions couple IP_3 binding to activation of the channel gate. The intrasubunit interface between β-TF domains is dynamic and permits β-TF1 to twist in response to IP_3 binding (Lin, Baek and Lu, 2011; Seo *et al.*, 2012). The SD interacts with β-TF, ARM2 and ARM3 domains in adjacent subunits. These interactions include multiple non-contiguous residues, specific helices, and regions linked to modulation of channel activation containing phosphorylation and Ca^{2+} binding sites (Miyakawa *et al.*, 2001; Tu *et al.*, 2003; Soulsby *et al.*, 2004).

The cytoplasmic region domains are connected to the channel-forming transmembrane region by the “intervening lateral” domain (ILD) and LNK. The TMD contains six α-helices (TM1 to TM6) within which is the α-helical pore-forming region (PFR) and three luminal loops. Following TM6, LNK connects the TMD to the CTD. Thus the entire cytoplasmic region can communicate with the transmembrane region, CTDs and ILDs (Baker, Fan and Serysheva, 2017).

The TMD helices mediate oligomerisation of the subunits to form the IP_3R channel and membrane integration (Michikawa *et al.*, 1994; Joseph *et al.*, 1997; Galvan *et al.*, 1999). An intraluminal loop connects the fifth and sixth helices and contains a PFR. Residues in the PFRs of the four subunits contribute to the central pore of the channel which conducts Ca^{2+} across the membrane. Similar to other tetrameric channels, the influence between the N and C termini of adjacent IP_3R subunits is a vital part of channel function (Boehning, 2000).

Salt bridges between adjacent subunits stabilise the cytoplasmic bundle which is lined with negatively charged residues potentially assisting the translocation of Ca^{2+}

into the cytosol (Baker, Fan and Serysheva, 2017). The ring of four IBC containing HS-loops is arranged around the cytoplasmic bundle. Electrostatic interactions between the adjacent subunits confirm previous biochemical studies of native channels showing the close association of N-and C-terminals (Boehning, 2000). Feasibly, the proximity of the cytoplasmic bundle and the IBC enables the bundle to sense IP_3 binding and undergo a conformational change in response transmitting the IP_3 signal to the TMD (Baker, Fan and Serysheva, 2017). The transmission of ligand binding via the CTD is consistent with previous deletion studies demonstrating that the absence of CTD residues disrupts channel gating (Schug and Joseph, 2006).

Channel gating appears to be the result of physical and electrochemical properties of residues lining the channel (Baker, Fan and Serysheva, 2017). The selectivity filter could be a ring of positively charged Histidine (His) residues from the four PFRs in the lumenal opening, residues that repel Ca^{2+} and prevent it from entering the vestibule. As the channel passes through the membrane, it is lined by Glycine (Gly) residues in the TM6 helices which might permit the channel to flex. The physical gate for ion-permeation may be a point of constriction closer to the cytosolic end of the channel formed by a series of hydrophobic residues, in TM6. The hydrophobic residues form a 5 Å pore through which hydrated Ca^{2+} (8-10 Å) cannot pass. Potentially, structural changes at activation widen the channel permitting Ca^{2+} to pass (Baker, Fan and Serysheva, 2017). Higher resolution images are required to predict the positions of TM1-5 which adopt an increasingly parallel position to the to the plasma membrane (Ludtke *et al.*, 2011; Murray *et al.*, 2013).

1.4.2 Generation of The Inositol 1,4,5-Trisphosphate Signal

Extracellular agonist stimulation results in phosphoinositide hydrolysis leading to an increase in cytosolic IP_3 concentration which induces an increase in [Ca^{2+}] (Hokin, R.; Hokin, 1953; Berridge and Lipke, 1979; Berridge *et al.*, 1983; Streb *et al.*, 1983). The lipid IP_3 is an organic molecule that acts as a secondary messenger for intracellular signal transduction provoking the release of Ca^{2+} from intracellular stores (Berridge, 2009). The IP_3 stimulated Ca^{2+} signalling pathway regulates a large number of cellular processes both directly by generating Ca^{2+} signals and indirectly by modulating Ca^{2+} signals produced by other signalling pathways (Berridge, 2009).

The structure of IP_3 is an inositol ring with three phosphate groups at carbons 1, 4, and 5 and three hydroxyl groups at carbons 2, 3, and 6. IP_3 is produced by the specific hydrolysis of the phospholipid phosphatidylinositol 4,5-bisphosphate (PIP_2), a minor cell membrane component as shown in Figure 1-6 (Czech, 2000). The hydrolysis of PIP_2 is catalysed by isoforms of phosphoinositide-specific phospholipase C (PI-PLC) (EC 3.1.4.11) (Essen *et al.*, 1997; Ellis *et al.*, 1998). The soluble IP_3 diffuses across the cytoplasm and binds to IP_3R on the SER membranes. The binding of IP_3 to IP_3R results in a conformational change leading to the consequential opening of the IP_3R channel and release of Ca^{2+} from the SER as shown in Figure 1-6 (Berridge, 2009).

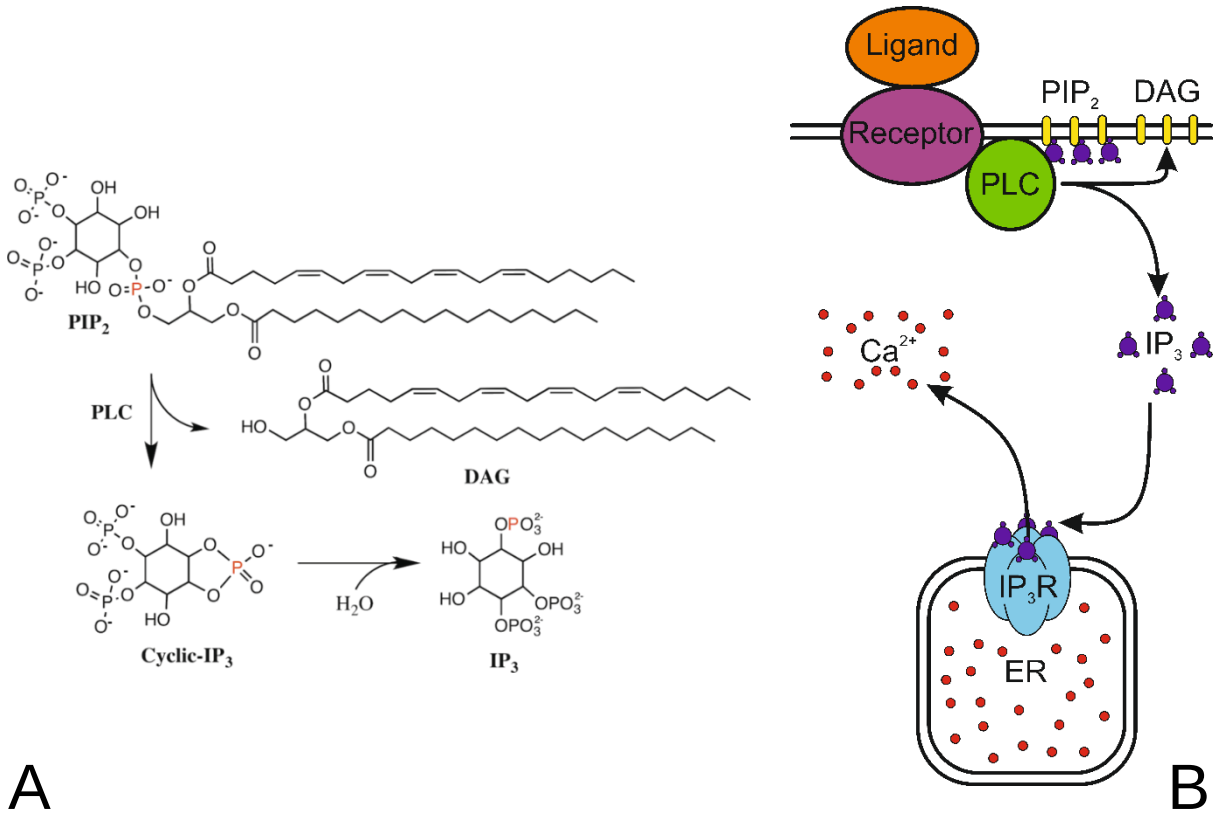

Figure 1-6 PI-PLC Cleaves the Membrane-Bound PIP_2 Yielding Ca^{2+} Release Inducing IP_3

(A) PI-PLC selectively catalyses the hydrolysis of PIP_2 on the glycerol side of the phosphodiester bond to form DAG and an enzyme-bound intermediate, cyclic IP_3, which hydrolyses to IP_3. **(B)** Schematic diagram showing a typical IP_3 signalling cascade. Stimulation of a receptor (R) at the cell surface leads to the activation of PI-PLC, which catalyses the hydrolysis of PIP_2 to yield IP_3 and DAG. IP_3 diffuses to the (ER), and binds to the IP_3R channel, resulting in the release of Ca^{2+} into the cytoplasm. Adapted and republished according to Creative Commons Attribution 4.0 International Public License from images by credited authors. **(A)** (Walker *et al.*, 2009) **(B)** (Lmyates16).

The ubiquitous mammalian PI-PLC family play an essential role in activating the phosphoinositide intracellular signal transduction pathway that regulates various cellular functions (Suh *et al.*, 2008). Consisting of fourteen distinct identified isoforms the PI-PLC family is divided into six sub-families, termed β, γ, δ, ε, ζ and η dependent on domain organisation and mode of activation, shown in Figure 1-7 (Kadamur and Ross, 2013). All PI-PLC isoforms share the same basic core domain structure; a tandem pair of EF-hands, an extended TIM barrel XY catalytic domain and a C2 domain, all isoforms bar PLCζ also possess an N-terminal pleckstrin homology domain (PH domain) (Kadamur and Ross, 2013). PI-PLC isoforms directly participate in the phosphoinositide signalling pathway, catalysing the hydrolysis of PIP_2 and giving rise to two crucial second messenger molecules: IP_3 and sn-1,2 diacylglycerol (DAG) (Suh *et al.*, 2008). While expression of PI-PLC isoforms is widespread the levels and patterns of expression vary between isoforms as does, sensitivity to Ca^{2+}, regulation of activity and cellular localisation (Suh *et al.*, 2008; Kadamur and Ross, 2013).

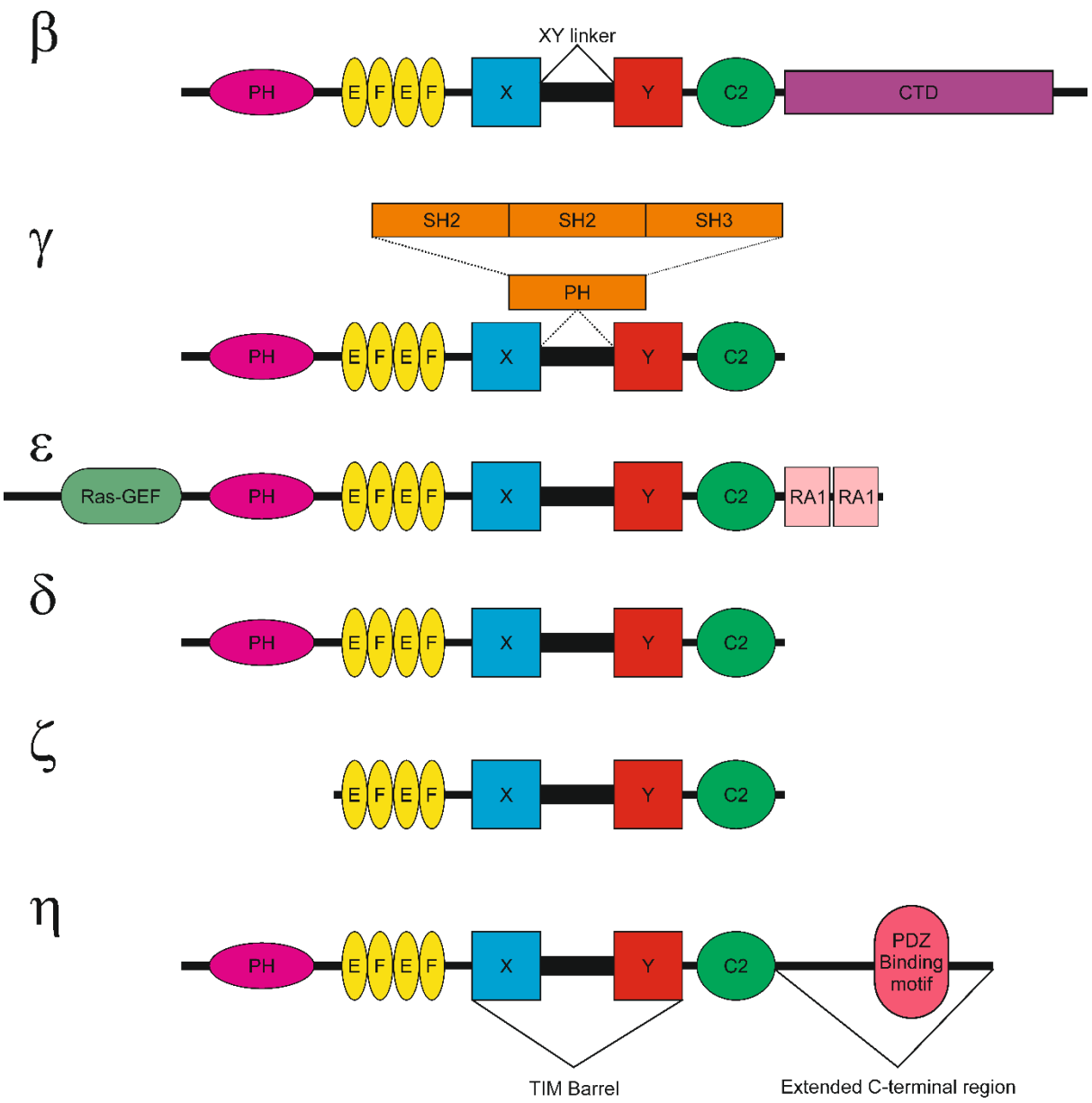

Figure 1-7 All Isoforms of PI-PLC Share a Conserved Core Structure

The domain organisation of mammalian PI-PLC isoforms. The domains not already mentioned in the main text are, a C-terminal domain (CTD), Src homology 2/3 (SH2/SH3), Ras association (RA), Ras GDP/GTP exchange factor (Ras GEF), N- and C-terminal portions of the TIM barrel (X and Y).

Cellular membranes are enriched with PIP_2 where PIP_2 is a substrate for PI-PLC isoforms in response to extracellular signals (Czech, 2000). Both PIP_2 and derived molecules act as signalling molecules as shown in Figure 1-8. The hydrolysis of PIP_2 also yields DAG which remains membrane-bound (Eichmann *et al.*, 2012). IP_3 and DAG both act as secondary messengers activating different signal transduction pathways (Berridge, 1984). DAG activates and localises protein kinase C (PKC) family members at cell membranes (Antal and Newton, 2014). The signal transduction pathways of PKC isozymes regulate a myriad of diverse cellular processes and responses including permeability, contraction, migration, hypertrophy, proliferation, apoptosis, and secretion, and play a vital role in the aetiology of many diseases (Dempsey *et al.*, 2000). Also, phosphorylation of PIP_2, IP_3 and DAG yields the signalling molecules phosphatidylinositol 3,4,5-trisphosphate (PIP_3), the poly-phosphorylated inositols (IP_n) and phosphatidic acid (PA) respectively.

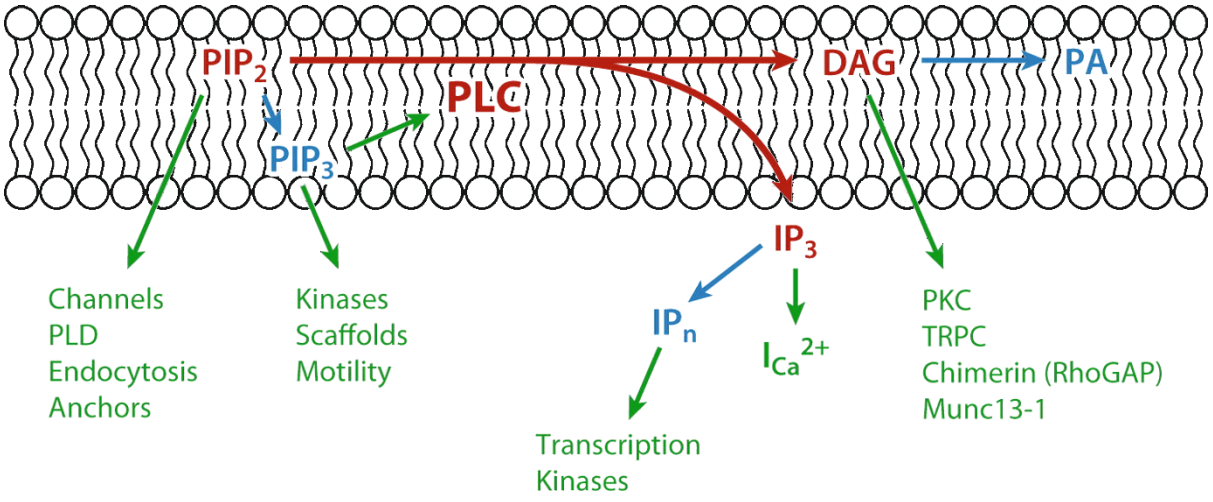

Figure 1-8 The Membrane Phospholipid PIP_2 and Derivatives Are Signalling Molecules for Diverse Cell Signalling Pathways

Schematic illustration of the signalling roles played by PIP_2 and the derived phospholipid phosphatidylinositol 3,4,5-trisphosphate (PIP_3), and the cleavage products of PIP_2 and PIP_3. Isoforms of PI-PLC catalyse PIP_2 hydrolysis to yield DAG and IP_3 which are both signalling molecules and precursors of the signalling molecules, phosphatidic acid (PA) and inositol polyphosphates (IP_n) respectively. The major PI-PLC catalysed reaction is red and other signalling metabolites are blue. The regulatory targets are green and include phospholipase D (PLD), and protein kinase C. (PKC). The principal target of IP_3 is the IP_3R channels increasing intracellular [Ca^{2+}] ($I_{Ca^{2+}}$). Republished with permission (Kadamur and Ross, 2013)

The versatile IP_3 signalling system regulates a myriad of cellular processes in a multitude of cell types because the system is capable of inducing complex Ca^{2+} signals (Berridge, 2009). The complexity of Ca^{2+} signals is the result of Ca^{2+} release events elicited by IP_3 varying both spatially and temporally (Thomas *et al.*, 1996; Clapham, 2007).

IP_3 stimulation induces Ca^{2+} oscillations, rapid rises and falls of [Ca^{2+}] separated by regular intervals of basal [Ca^{2+}] (Berridge and Dupont, 1994; Thomas *et al.*, 1996; Clapham, 2007). The duration of the intervals, i.e. the frequency of the oscillations, can vary, e.g. between 60 s to 3-4 min for hepatocytes and fertilised oocytes respectively (Cuthbertson and Cobbold, 1985; Miyazaki *et al.*, 1986; Woods, Cuthbertson and Cobbold, 1986; Cheek *et al.*, 1993). The sensitivity of IP_3R to internal Ca^{2+} store load could mean that the rate of store loading is determining the Ca^{2+} oscillation frequency (Berridge, 2009). The frequency of the Ca^{2+} oscillations has been proposed to encode the transduced signal (Smedler and Uhlén, 2014). The mechanisms by which IP_3 induces a repetitive transient response are under investigation.

IP_3 is capable of stimulating Ca^{2+} signals at specific sites that can remain localised or can propagate into intracellular Ca^{2+} waves. (Berridge and Dupont, 1994; Thomas *et al.*, 1996; Clapham, 2007). IP_3 initiated Ca^{2+} signals occur in three categories of increasing scale, “blips”, “puffs” and “waves” that perform different functions and combine to produce a more significant signal overall (Parker, Choi and Yao, 1996; Bootman, Lipp and Berridge, 2001).

Ca^{2+} “blips” are small localised increases in [Ca^{2+}] due to the release of Ca^{2+} by a limited number of individual channels through stimulation by IP_3 (Parker, Choi and Yao, 1996). Blips may play a role in the initiation of global Ca^{2+} transients in cells with smaller IP_3R clusters (Qi *et al.*, 2014). Ca^{2+} “puffs” are larger localised increases in [Ca^{2+}] due to the coordinated release of Ca^{2+} by multiple clustered IP_3R channels. A Ca^{2+} “blip” initiates the coordinated release of Ca^{2+}, the Ca^{2+} from the blip synergises with IP_3 to induce simultaneous CICR within the IP_3R cluster (Swillens *et al.*, 1999). Ca^{2+} puffs regulate specific physiological cell functions in a spatially restricted manner due to co-localisation of IP_3R cluster with Ca^{2+} responsive effector proteins (Marchant and Parker, 2000; Bootman, Lipp and Berridge, 2001; Bootman *et al.*, 2012). CICR by the Ca^{2+} sensitive IP_3R could provide a positive feedback mechanism to allow Ca^{2+} transients to regenerate as Ca^{2+} released by IP_3 stimulation provokes further Ca^{2+} release via IP_3R, but high Ca^{2+} inhibits IP_3R activity (Bezprozvanny, Watras and Ehrlich, 1991; Finch, Turner and Goldin, 1991).

1.4.3 Role Of PLCζ In Fertilisation

1.4.3.1 Oocyte Activation

As previously stated before fertilisation mammalian oocyte cell cycle is paused at metaphase II. At fertilisation, the oocyte “activates” upon sperm fusion, and the cell cycle resumes. The cortical reaction and so CG exocytosis and the ZP hardening is triggered by and requires the transient increase in [Ca^{2+}] that occurs upon fertilisation (Ducibella, 1996; Abbott, Allison, 2001). Similarly, resumption and completion of meiosis and commencement of mitosis requires the increase in [Ca^{2+}] (Kline and Kline,

1992; Swann and Ozil, 1994; Schultz and Kopf, 1995; Runft, Jaffe and Mehlmann, 2002)

During mammalian fertilisation, the increase in cytosolic Ca^{2+} in the egg occurs as a series of long-lasting, repetitive Ca^{2+} oscillations of constant amplitude. The oscillations are both necessary and sufficient for all the events of egg activation (Stricker, 1999; Runft, Jaffe and Mehlmann, 2002). The Ca^{2+} oscillations vary in frequency and duration between species from 2min to 1h intervals between calcium spikes (Fissore *et al.*, 1992; Kline and Kline, 1992).

The temporal pattern of Ca^{2+} oscillations is species specific, commencing shortly after gamete fusion, and lasts for a few hours until after meiosis finishes (Fissore *et al.*, 1992; Kline and Kline, 1992; Stricker, 1999). Ca^{2+} oscillations also occur during the first of rounds of cell division cycles in embryos controlling nuclear envelope breakdown and the beginning of anaphase (Steinhardt, 1990; Ciapa *et al.*, 1994; Kono *et al.*, 1996; Groigno and Whitaker, 1998). Oocytes are sensitive to the precise temporal pattern of Ca^{2+} oscillations which are necessary, sufficient and required for all the events of oocyte activation and subsequent events in embryo development (Ducibella *et al.*, 2002; Ducibella, Schultz and Ozil, 2006; Malcuit, Kurokawa and Fissore, 2006; Stitzel and Seydoux, 2007; Yu *et al.*, 2007; Wong *et al.*, 2010).

1.4.3.2 Initiation of Calcium Oscillations

Four different mechanisms for initiation of Ca^{2+} at fertilisation in mammals were proposed; “Ca^{2+} bomb”, “Ca^{2+} conduit” “Contact” and “Sperm Factor”, Figure 1-9 (Nomikos, Swann and Lai, 2012).

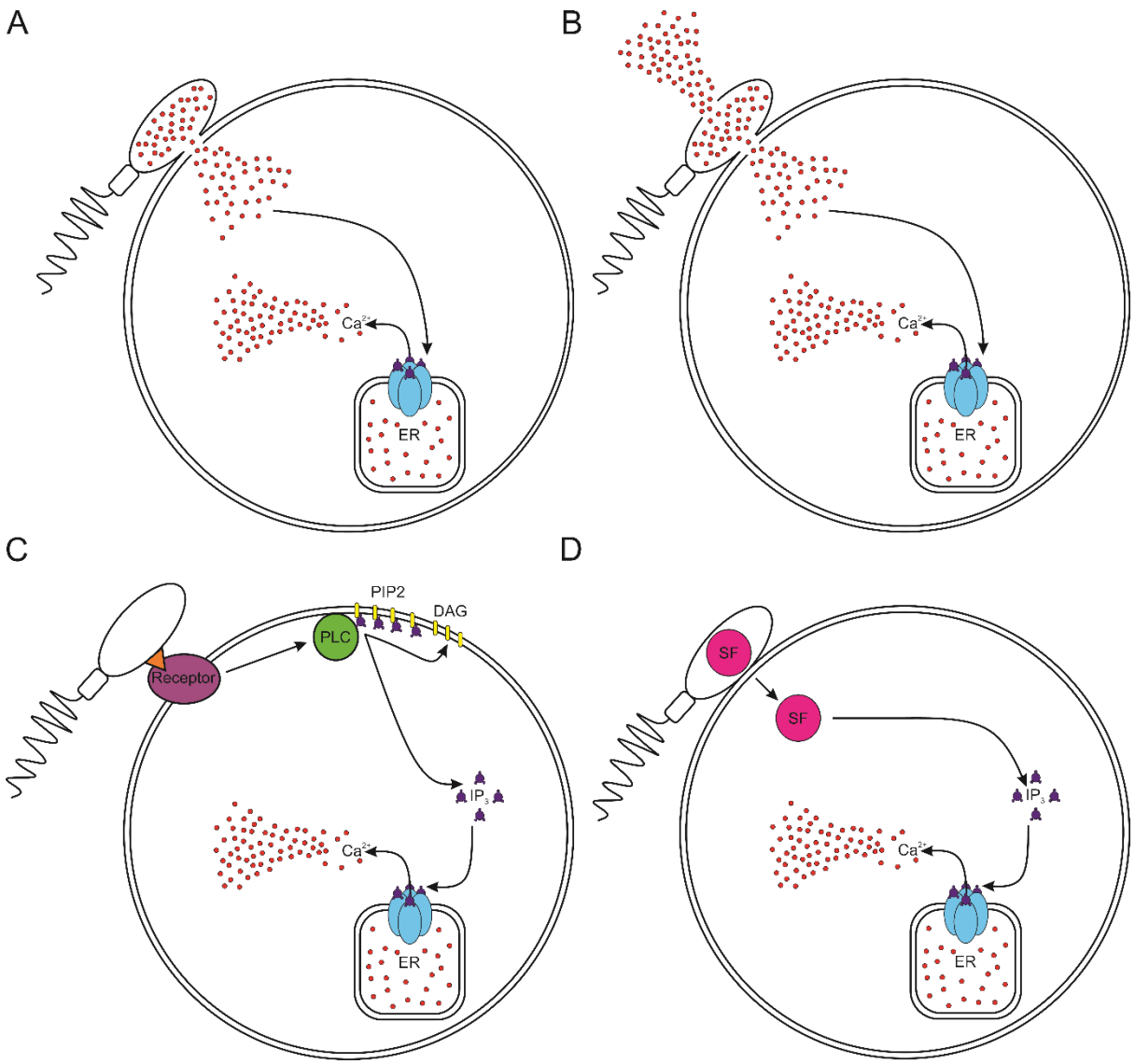

Figure 1-9 The Proposed Mechanisms for Sperm Initiated Ca^{2+} Release at Fertilisation

Illustration depicting the four models proposed for oocyte activation by fertilising sperm. **(A)** Ca^{2+} bomb. **(B)** Conduit. **(C)** Contact **(D)** Sperm factor

The “Ca^{2+} bomb” proposed that upon fertilisation a bolus of Ca^{2+} enters the oocyte cytosol from the sperm triggering CICR (Jaffe, 1983). ‘Ca^{2+} conduit’ hypothesised that the fusion of the sperm head and oolemma created a conduit permitting extracellular Ca^{2+} to flow into the ooplasm leading to store overload-induced calcium release (SOICR) (Jaffe, 1991). The ‘contact’ hypothesis suggested that a receptor-ligand interaction on the surface of the gametes upon fertilisation initiated an intracellular signalling cascade that stimulated SER Ca^{2+} release (Jaffe, 1991). In the “Sperm Factor” hypothesis, sperm was proposed to contain a soluble proteinaceous factor that upon entering the oocyte cytoplasm stimulated SER Ca^{2+} release (Stricker, 1997). The initial evidence was the observation that injection of cytosolic sperm extracts directly into the egg triggered Ca^{2+} oscillations and the pattern was identical to that seen during *In vitro* Fertilisation (IVF) (Swann, 1990). Eventually, the weight of experimental evidence discounted the first three hypotheses and indicated that the “Sperm Factor” hypothesis was the most likely explanation (Nomikos, Swann and Lai, 2012). A yet to be identified isoform of PI-PLC was proposed as the sperm factor based on experimental evidence that the increase in [Ca^{2+}] was the result of Ca^{2+} release from SER via IP_3R stimulated by the secondary messenger IP_3 (Rice *et al.*, 2000).

Both oocyte activation and Ca^{2+} oscillations were inhibited by blocking IP_3R and stimulated by IP_3 oscillations (Miyazaki *et al.*, 1992; Brind, Swann and Carroll, 2000; Jellerette *et al.*, 2000; Jones and Nixon, 2000; Wu *et al.*, 2001). IP_3 triggered, mediated and was required for the signal transduction cascade upon fertilisation that induced Ca^{2+} release from the SER via IP_3R to ultimately induce the cortical reaction, CG

exocytosis and the block on polyspermy (Cran, Moor and Irvine, 1988; Miyazaki, 1988; Kurasawa, Schultz and Kopf, 1989; Ducibella *et al.*, 1993; Xu, Kopf and Schultz, 1994). Knockdown, down-regulation and up-regulation experiments indicating the involvement of the IP_3 and the IP_3R in fertilisation suggested a potential Sperm Factor could be a PI-PLC isoform enzyme (Miyazaki *et al.*, 1992, 1993). Sperm cytosolic extracts displayed a high level of PI-PLC enzymatic activity *in vitro* (Rice *et al.*, 2000). However, recombinant proteins corresponding to the then known PI-PLC isoforms expressed in sperm failed to initiate the anticipated Ca^{2+} oscillations (Jones *et al.*, 2000; Parrington *et al.*, 2002).

1.4.3.3 Discovery of PLCζ

A database search identified a novel isoform of PI-PLC expressed only in sperm, termed PLCζ (Saunders *et al.*, 2002). Fertilising sperm were proposed to introduce PLCζ into the cytoplasm of the oocyte in addition to genetic information as shown in Figure 1-10. The soluble PLCζ catalyses the lysis of PIP_2 in the membrane of intracellular vesicles dispersed throughout the cytoplasm to produce IP_3 which stimulates IP_3R to release Ca^{2+}, and DAG (Swann and Yu, 2008; Nomikos, Swann and Lai, 2012). The Ca^{2+} oscillations stimulate a cascade of downstream events involving multiple oocyte proteins including protein kinase C (PKC) and CaMKII and DAG levels enabling the arrest on cell cycle at MII to be released and the completion of meiosis (Yeste *et al.*, 2017).

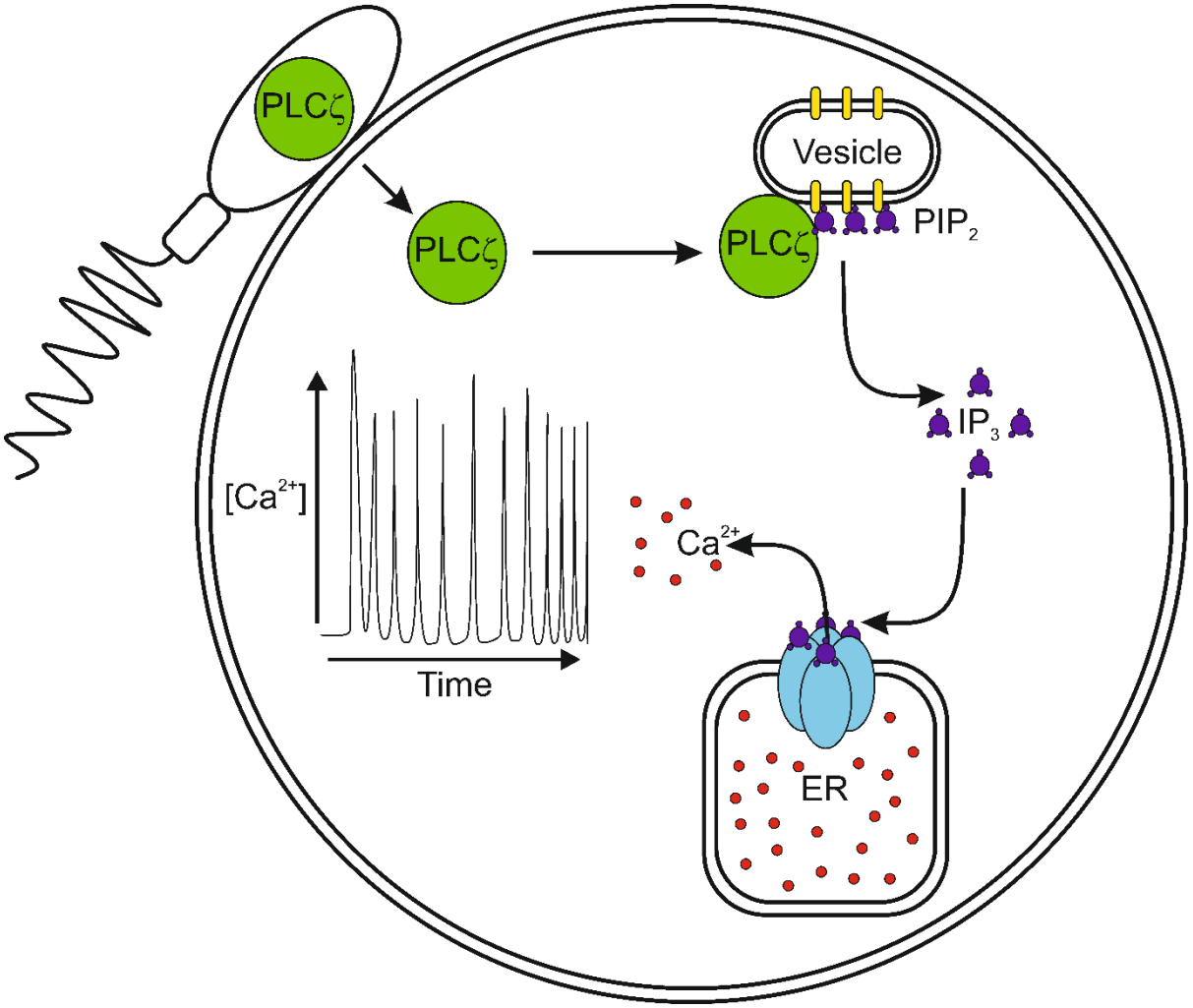

Figure 1-10 The Sperm Protein PLCζ Triggers Activation of the Oocyte at Fertilisation

Illustration showing oocyte activation at fertilisation stimulated by the products of the hydrolytic reaction catalysed by the sperm protein PLCζ. Following the fusion of sperm and oocyte membranes PLCζ is released from the sperm into the oocyte. PLCζ diffuses across the ooplasm and targets a distinct intracellular vesicular membrane containing the membrane-bound substrate, PIP_2. PLCζ catalysed PIP_2 hydrolysis produces two secondary messengers, IP_3 and DAG. IP_3 stimulates the IP_3R channels on the SER membrane to release Ca^{2+} from intracellular stores to produce the oscillations in $[Ca^{2+}]$ required for oocyte activation. Adapted from (Nomikos, Kashir and Lai, 2017) with the publisher's standard permission for non-commercial reuse.

1.4.3.4 Experimental Evidence for PLCζ as the Sperm Factor

Microinjection of complementary RNA (cRNA) and recombinant protein corresponding to PLCζ from various species into mouse oocytes triggered Ca^{2+} oscillations similar to those observed at fertilisation (Cox *et al.*, 2002; Saunders *et al.*, 2002; Kouchi *et al.*, 2004). Native sperm extracts lost the ability to trigger Ca^{2+} oscillations in mouse oocytes when PLCζ was removed by immunodepletion with an anti-PLCζ antibody (Saunders *et al.*, 2002). Additionally, the sperm of transgenic mice expressing short hairpin RNAs had reduced amounts of PLCζ and initiated prematurely terminating Ca^{2+} oscillations when used for IVF (Knott *et al.*, 2005). To date, the accumulated evidence has confirmed PLCζ to be the most widely accepted and only plausible candidate for the sperm factor (Nomikos, Kashir and Lai, 2017).

The importance of PLCζ in mammalian fertilisation has been highlighted by some clinical reports that directly linked the absence of or abnormal forms of PLCζ with documented cases of male infertility and failure of intracytoplasmic sperm injection (ICSI) during IVF treatment. (Yoon *et al.*, 2008; Heytens *et al.*, 2009; Kashir *et al.*, 2012). In two unrelated male infertility cases different mutations in the gene encoding PLCζ were demonstrated to both impair Ca^{2+} oscillations *in vivo* while *in vitro* one mutation abolished PIP_2 binding while the other abolished PI-PLC enzymatic activity (Nomikos, Elgmati, Theodoridou, Brian L. Calver, *et al.*, 2011; Nomikos, Stamatiadis, *et al.*, 2017). Additionally, recombinant human PLCζ (hPLCζ) can phenotypically rescue the failed activation of mouse oocytes expressing dysfunctional

PLCζ, leading to efficient blastocyst formation; a prototype of male factor infertility reinforcing the potential of PLCζ as a therapeutic agent (Nomikos *et al.*, 2013).

1.4.4 Structure and Domain Organisation of PLCζ

PLCζ is the smallest known isoform of mammalian PI-PLC with the most straightforward domain structure containing domains common to all PI-PLC isoforms, (Kadamur and Ross, 2013). PLCζ shares greatest sequence homology with PLCδ1. However, PLCζ has a Ca^{2+} sensitivity 100-fold greater than PLCδ1 for optimal PIP_2 hydrolysis (Kouchi *et al.*, 2005; Nomikos *et al.*, 2005). Meanwhile, the *in vitro* enzymatic activity of PLCδ1 is ~ 5 fold greater than PLCζ, but PLCζ is more potent in eliciting Ca^{2+} oscillations in oocytes (Nomikos, Elgmati, Theodoridou, Georgilis, *et al.*, 2011; Theodoridou *et al.*, 2013).

Currently, there is no published tertiary structure for PLCζ. The 3D crystal structure of the closely related PLCδ1 has been published (Ferguson *et al.*, 1995; Essen *et al.*, 1996). Based on the 3D structure of PLCδ1, the predicted domain organisation of PLCζ is a tandem pair of EF-hands at the N-terminus, followed by an XY catalytic domain and a C2 domain at the C-terminus, Figure 1-11 (Saunders *et al.*, 2002). In contrast to PLCδ1 and unique amongst all the other isoforms, PLCζ lacks a Pleckstrin Homology (PH) domain which is required for the interaction of PLCδ1 with its substrate (Kadamur and Ross, 2013).

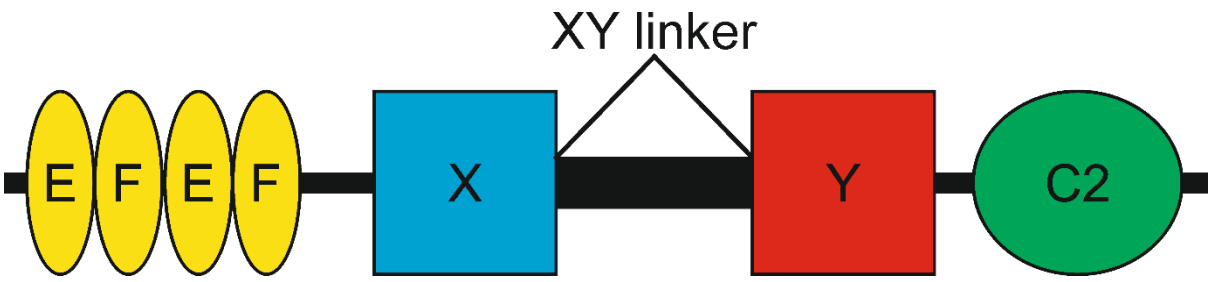

Figure 1-11 PLCζ Contains Core Structure Conserved in PI-PLC Isozymes but Lacks a PH Domain

Schematic diagram of the predicted domain organisation of the sperm-specific PI-PLC isoform PLCζ. The mouse isoform is also predicted to contain a nuclear localisation signal in the XY linker.

1.4.4.1 EF-Hands

The N-terminal of PLCζ contains two pairs of EF-hand domains that are similar to those found in PLCδ1 (Saunders *et al.*, 2002). In PLCδ1 the EF-hands form a flexible link between the XY catalytic domain and the PH domain and contain Ca^{2+} binding sites comparable to those found in other Ca^{2+} binding proteins (Essen *et al.*, 1996; Kouchi *et al.*, 2005). However, PLCζ is 100-fold more sensitive to [Ca^{2+}] than PLCδ1 with an EC_{50} of 80 nM, which is within the range of reported basal [Ca^{2+}] in oocytes. The EF-hands of PLCζ appears to confer the high Ca^{2+} sensitivity. Deletion of either or both PLCζ EF-hands abolishes the ability of PLCζ to induce Ca^{2+} oscillations *in vivo* mouse oocytes while the ability to lyse PIP_2 *in vitro* remained intact albeit with reduced Ca^{2+} sensitivity (Kouchi *et al.*, 2005; Nomikos *et al.*, 2005). Notably, the reduction in sensitivity increases the EC_{50} to a level beyond oocyte basal [Ca^{2+}] indicating why an EF-hand deletion mutant would be inactive *in vivo* and so unable to initiate Ca^{2+} oscillations. (Nomikos *et al.*, 2005). However, it appears that the high Ca^{2+} sensitivity of PLCζ compared to PLCδ1 is not solely endowed by the EF-hands, but the overall tertiary structure of PLCζ plays a role. Compared to wildtype, the Ca^{2+} sensitivity of PLCδ1 chimaera was increased when containing PLCζ EF-hands and lacking a PH domain but not to the same level as PLCζ (Theodoridou *et al.*, 2013).

Additionally, the first half of the first pair of the EF-hands of PLCζ contains a cluster of basic amino acid residues. Sequentially neutralising the electropositive residues with mutagenesis reduced the ability of PLCζ to bind PIP_2 (Nomikos *et al.*, 2015). Potentially, the positively charged residues in the EF-hands and the XY linker

could facilitate the association of PLCζ with the negatively charged PIP_2 through electrostatic interactions. The electrostatic interactions allow PIP_2 to access and bind to the catalytic domain of PLCζ. Also, similar to the XY linker, the EF-hands are believed to contain an NLS as mutagenesis of critical residues disrupts translocation of PLCζ to the nucleus (Kuroda *et al.*, 2006).

The precise mechanisms by which PLCζ targets subcellular locations are yet to be confirmed (Nomikos, Kashir and Lai, 2017). All other PI-PLC isoforms possess a PH domain which enables association with membranes that are essential for function, e.g. the PH domain of PLCδ1 enables the enzyme to target the main pool of the substrate, PIP_2, in the plasma membrane (Lemmon *et al.*, 1995; Várnai and Balla, 1998; Dowler *et al.*, 2000). However, recombinant PLCζ expressed in oocytes does not localise at the oolemma but disperses throughout the ooplasm indicating that PLCζ does not have a mechanism to target PIP_2 in the oolemma or the main substrate pool is located in another membrane (Yoda *et al.*, 2004).

1.4.4.2 XY Catalytic Domain

The highly conserved catalytic domain of PLCζ displays 64% similarity with that of PLCδ1 and retains the five essential active site residues found within the catalytic domain of PLCδ1 (H311, Q341, D343, H356 and Q390) (Saunders *et al.*, 2002). Mutagenesis in mouse PLCζ (mPLCζ) of the residue corresponding to H^{343} of PLCδ1 resulted in the abolition of *in vitro* PIP_2 hydrolytic enzyme activity and the ability of PLCζ to induce Ca^{2+} oscillations in mouse oocytes. Similarly so did the mutation of the corresponding residue in mPLCζ to an hPLCζ mutation linked to a clinical case of male

infertility (Saunders *et al.*, 2002; Nomikos, Elgmati, Theodoridou, Brian L. Calver, *et al.*, 2011).

Like all other PI-PLC isoforms, the XY catalytic domain of PLCζ consists of two halves of an extended TIM barrel catalytic domain joined together by a discrete region, the XY linker (Bunney and Katan, 2011). The XY linker of PLCζ is longer than that of PLCδ1, is predominately basic and is potentially involved in substrate targeting (Nomikos, Elgmati, Theodoridou, Brian L Calver, *et al.*, 2011; Nomikos, Elgmati, Theodoridou, Georgilis, *et al.*, 2011). Between PI-PLC isoforms XY linkers vary from unstructured polypeptide sequences to multiple domains. In all isoforms except PLCζ disruption or removal of the XY linker induces activity (Kadamur and Ross, 2013). Unique amongst PI-PLC isoforms the PLCζ XY linker contains a distinctive cluster of positively charged amino acid residues which enables and is required for the enzyme to target PIP_2 containing membranes and bind to PIP_2 (Nomikos *et al.*, 2007; Nomikos, Elgmati, Theodoridou, Brian L Calver, *et al.*, 2011). Also, in contrast to other isoforms, the disruption and removal of the PLCζ XY linker inhibits enzymatic activity and does not induce enzyme activation (Kurokawa *et al.*, 2007; Nomikos, Elgmati, Theodoridou, Georgilis, *et al.*, 2011).

The PLCζ XY linker contains a nuclear localisation signal (NLS) which potentially mediates the translocation and sequestration of PLCζ to the nucleus for degradation (Larman *et al.*, 2004). In mice, the nuclear localisation of PLCζ correlates with the cessation of Ca^{2+} oscillations and pronucleus formation (Larman *et al.*, 2004). Mutation of the NLS results in PLCζ remaining in the cytoplasm of mouse oocytes and

Ca^{2+} oscillations to continue past the formation of the pronucleus. (Kuroda *et al.*, 2006; Ito, Shikano, Kuroda, *et al.*, 2008; Ito, Shikano, Oda, *et al.*, 2008). However, while putative NLS is present in PLCζ from other species, PLCζ translocation to the nucleus is only observed in mice (Ito, Shikano, Oda, *et al.*, 2008). The precise mechanism by which Ca^{2+} oscillations terminate in other species is currently unknown.

1.4.4.3 C2 Domain

C2 domains are ~120 amino acid structural motifs found in numerous proteins capable of binding phospholipids in either a Ca^{2+}-dependent or -independent manner (Nalefski and Falke, 1996). The majority of C2 domains bind Ca^{2+}, which is required for the activity of the protein (Zheng *et al.*, 2000). The C2 domain of PLCδ1 binds three perhaps four Ca^{2+} ions and then recruits PLCδ1 to the plasma membrane where the C2 domain forms a complex with phosphatidylserine (PS) (Rizo and Südhof, 1998; Hurley and Misra, 2000). The formation of the complex is believed to enhance enzymatic activity by bringing the catalytic site into contact with the substrate in the plasma membrane and displacing the auto-inhibitory XY linker (Williams, 1999; Kadamur and Ross, 2013).

While the C2 domain of PLCζ shares homology with the PLCδ1 C2 domain, the predicted C2 domain of PLCζ lacks the Ca^{2+} binding sites identified in PLCδ1 (Swann *et al.*, 2006; Swann and Lai, 2013). There are C2 domains that do not bind or require Ca^{2+} to bind phospholipids with relatively low affinity and specificity, e.g. C2 domains of *Aplysia* PKC isoform II and human Class II phosphoinositide 3-kinase (Arcaro *et al.*, 1998; Pepio, Fan and Sossin, 1998; Hurley and Misra, 2000).

The specific role played by the C2 domain of PLCζ is currently unclear. The C2 domain is required for PLCζ function and is essential for oocyte activation. Deletion of the C2 domain abolished the ability of PLCζ to elicit Ca^{2+} oscillations in oocytes. Recombinant PLCζ lacking the C2 domain retained *in vitro* enzymatic activity albeit at a reduced rate, although Ca^{2+} sensitivity was unaffected (Nomikos *et al.*, 2005). The PLCζ C2 domain has been demonstrated to bind the membrane phospholipids including phosphatidylinositol 3-phosphate (PI3P) and phosphatidylinositol 5-phosphate (PI5P) at low affinity, but not PIP_2 (Kouchi *et al.*, 2005; Nomikos, Elgmati, Theodoridou, Brian L Calver, *et al.*, 2011). The C2 domain associating with PI3P may localise PLCζ at the target membrane in the ooplasm bearing the substrate PIP_2. Alternatively, the PLCζ C2 domain binding PI3P maybe a regulatory mechanism as the presence of PI3P reduces PLCζ *in vitro* PIP_2 hydrolytic activity (Kouchi *et al.*, 2005).

Phosphoinositides are important signalling molecules mediating critical sub-cellular processes such as ion channel gating, cytoskeleton organisation, intracellular membrane trafficking and targeting of proteins to specific subcellular compartments (Di Paolo and De Camilli, 2006; Balla, 2013). PI 3-phosphate species include PI3P, phosphatidylinositol 3,4-bisphosphate (PI(3,4)P2), phosphatidylinositol 3,5-bisphosphate (PI(3,5)P2), and phosphatidylinositol 3,4,5-trisphosphate (PI(3,4,5)P3). (Marat and Haucke, 2016) Different PI 3-phosphates are distributed as components of the plasma membrane and distinct endosomal vesicle membranes (Cantley, 2002; Vicinanza et al., 2008).

All PI 3-phosphate species are products of phosphorylation at the 3-position of the inositol ring of phosphatidylinositol and its derivatives (Marat and Haucke, 2016).The distinct pools of PI 3-phosphates are the products of different PI kinases with differing substrate specificities and sub-cellular locations (Balla, 2013; Raiborg, Schink and Stenmark, 2013). Meanwhile, specific PI phosphatases enable a rapid turnover of PI 3-phosphates (Hsu and Mao, 2015).

The distinct sub-cellular locations and rapid turnover of PI 3-phosphate species enables function as regulators of biological processes at intracellular membranes, (Balla, 2013; Raiborg, Schink and Stenmark, 2013). PI3P is the predominant species found on early endosomes and plays an important role in autophagy (Vicinanza et al., 2008; Mayinger, 2012).

1.4.5 Regulation of PLCζ

The regulation of mammalian PI-PLC isoforms is diverse, but all are regulated by Ca^{2+} (Kadamur and Ross, 2013). Unlike other PI-PLC isoforms the only known regulatory ligand of PLCζ is Ca^{2+}, to which PLCζ is extremely sensitive (Nomikos *et al.*, 2005). Upon injection PLCζ is active in the low [Ca^{2+}] environment of the ooplasm but remains inactive at far higher [Ca^{2+}] in the sperm (Nomikos, Kashir and Lai, 2017). Immunological studies have revealed that within the sperm, PLCζ is compartmentalised into populations which could be functionally and physiologically distinct (Kashir, Nomikos and Lai, 2018). The observed compartmentalisation or enzymatic inactivation have both been proposed as mechanisms for the inactivity of PLCζ in sperm (Nomikos, Kashir and Lai, 2017).

The localisation of PLCζ within the cytoplasm is also unique amongst PI-PLC isoforms. In somatic cells, PI-PLC is localised and restricted to the nuclear and plasma membranes, the main pools of PIP_2 (Kadamur and Ross, 2013). However, PLCζ does not localise to the oolemma but at small vesicles throughout the ooplasm which also contain PIP_2 (Yu *et al.*, 2012). The targeted depletion of PIP_2 from the oolemma does not affect PLCζ, or sperm-induced Ca^{2+} oscillations but does abolish PLCδ1-induced Ca^{2+} oscillations (Yu *et al.*, 2012). Conversely, targetted depletion of PIP_2 from the small vesicles inhibits both PLCζ and sperm-induced Ca^{2+} oscillations (Yu *et al.*, 2012). Ca^{2+} oscillations in oocytes upon fertilisation appear to the result of IP_3 liberated by PLCζ specifically targetting and hydrolysing membrane-bound PIP_2 in intracellular vesicles. An unknown mechanism achieves this novel form of PI-mediated Ca^{2+} signalling.

While cytosolic sperm extracts induce Ca^{2+} oscillations in nerve and liver cells, expression of transfected PLCζ in Chinese Hamster Ovarian (CHO) cells does not result in changes in Ca^{2+} homeostasis, despite the relatively higher [Ca^{2+}] compared to oocytes (Currie *et al.*, 1992; Berrie *et al.*, 1996; Phillips *et al.*, 2011). Notably, CHO cells lack intracellular organelles bearing PIP_2. However, microinjection into mouse oocytes of PLCζ-expressing CHO cells or the cytosolic extract does trigger Ca^{2+} oscillations, indicating that PLCζ may only be active in oocytes (Phillips *et al.*, 2011).

The specific targetted activity of PLCζ solely in oocytes indicates that oocytes contain an “egg factor”, essential for PIP_2 hydrolysis catalysed by PLCζ. The egg factor could be a binding target or receptor located on the PIP_2 bearing intracellular vesicles

which enables PLCζ to localise to the specific substrate pool in the ooplasm. Once localised to PIP_2, electrostatic interactions between electropositive residues in EF-hand and XY linker, and electronegative PIP_2 enable the active site of PLCζ to orientate to and come in contact with PIP_2 as shown in Figure 1-12. The highly specific interaction between the egg factor and PLCζ would explain the lower potency of other mammalian PI-PLC isoforms in triggering Ca^{2+}oscillations in mouse oocytes. The identification of an oocyte receptor for PLCζ will have significant implications for understanding a broader range of infertility cases, reproductive medicine and for animal reproductive technologies.

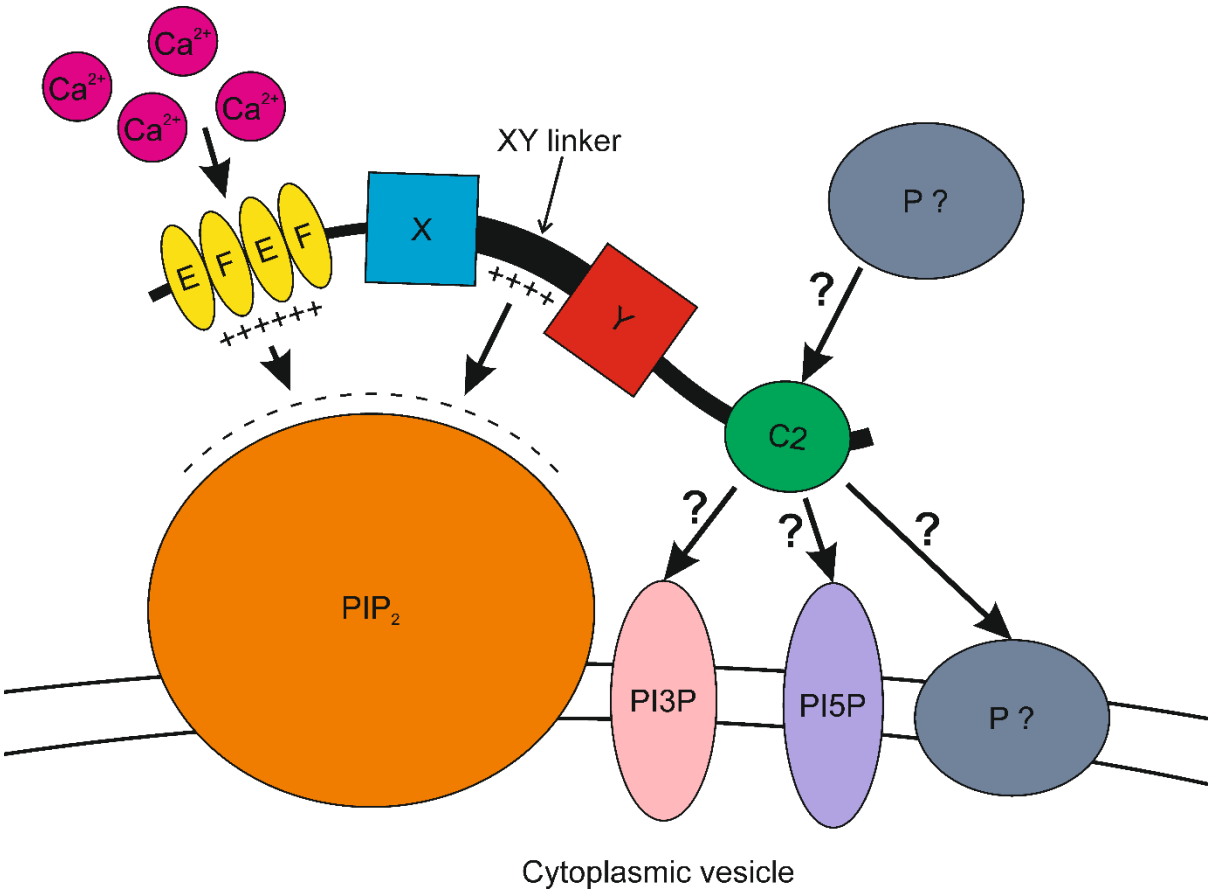

Figure 1-12 PLCζ Targets PIP2 Stores in the Ooplasm via an Unresolved Mechanism Where Electrostatic Interactions Bring the Substrate and Enzyme Catalytic Site in Close Proximity.

Schematic diagram of the proposed mechanism for PLCζ enzymatic activity in mammalian oocytes. Upon entry to the ooplasm from the fertilising sperm, PLCζ associates specifically with the membrane of an unknown vesicle. Potentially, the interaction between the C2 domain and either PI_3P, PI_5P or an unidentified cytosolic or membrane protein (P ?) mediates the association. At the target membrane PLCζ associates with PIP_2 via electrostatic interactions between positively charged residues in the first EF-hand domain and the C-terminal of the XY-linker with the negatively charged PIP2. Subsequently, the XY domain catalyses the enzymatic cleavage of PIP_2. The EF-hand domains confer the high sensitivity of PLCζ to Ca^{2+} which enables enzymatic activity at the nanomolar resting [Ca^{2+}] in the oocyte. Reproduced with permission (Nomikos, Kashir and Lai, 2017).

1.5 Ryanodine Receptor

1.5.1 Ryanodine Receptor Channel

The release of Ca^{2+} from intracellular stores in the SER and SR in myocytes is mediated by RyRs, large-conductance Ca^{2+} specific channels (Meissner, 2017). There are three mammalian RyR isoforms, RyR1, RyR2 and RyR3 first identified in skeletal, cardiac and epithelial tissue respectively (Takeshima *et al.*, 1989; Otsus *et al.*, 1990; Giannini *et al.*, 1992). Ca^{2+} stimulates but excess Ca^{2+} inhibits the release of Ca^{2+} by RyR (Bezprozvanny, Watras and Ehrlich, 1991).

RyR activity is also regulated and modulated by endogenous and exogenous ligands (Zalk, Lehnart and Marks, 2007). Magnesium ions (Mg^{2+}) inhibit RyR channel activity while adenine nucleotides, ATP and cyclic Adenosine Diphosphate (ADP)-ribose (cADPr) stimulate channel activity (Fill and Copello, 2002; Meissner, 2004; Zalk, Lehnart and Marks, 2007).

Exogenous ligands of RyR have been widely utilised to probe channel characteristics and function. The plant alkaloid ryanodine binds to open RyR channels with high affinity and “locks” the channel in an open conformation in a dose-dependent manner, see 1.5.1.2 for more details. (Fleischer *et al.*, 1985; Pessah *et al.*, 1986; Hymel *et al.*, 1988; Lai *et al.*, 1988). Caffeine and 4-chloroform-cresol (CmC) stimulate channel activity by increasing the sensitivity of RyR to Ca^{2+} (Rousseau *et al.*, 1988). The inorganic dye ammoniated ruthenium oxychloride (Ruthenium red) is a potent inhibitor of RyR mediated SR Ca^{2+} release (Ma, 1993).

Pharmacologically active molecules, i.e. drugs, that modify RyR channel function e.g. local anaesthetics procaine and tetracaine, and postsynaptic muscle relaxant dantrolene, inhibit channel activity and block SR Ca^{2+} release (Xu, Jones and Meissner, 1993; Koulen and Thrower, 2001; Zhao *et al.*, 2001; Shannon, Ginsburg and Bers, 2002). In susceptible patients, volatile anaesthetics trigger malignant hyperthermia (MH) which was treated historically with procaine but now with dantrolene which blocks the pathological SR Ca^{2+} release (MacLennan and Phillips, 1992; Harrison, 1998; Koulen and Thrower, 2001; Zhao *et al.*, 2001)

RyR channels are ~2 MDa homotetramers containing four ~550 kDa identical subunits of the same isoform (Imagawa *et al.*, 1987; Lai *et al.*, 1988). In myocytes the RyR channel is part of and forms the scaffold for a large macromolecular signalling complex, the best characterised in normal and pathological states is RyR2 (Landstrom, Dobrev and Wehrens, 2017).

The complex consists of four ~12 kDa FK506-binding proteins (FKBP) and a variety of accessory proteins including CaM, CaMKII, cyclic AMP-dependent protein kinase A (PKA), Types 1, 2A and 2B phosphatase (PP1, PP2A and PP2B), c-AMP specific phosphodiesterase 4D3 (P4D3) and muscle A-kinase anchoring protein (mAKAP) and spinophilin (Fill and Copello, 2002; Zalk, Lehnart and Marks, 2007; Meissner, 2017). RyR also interacts with transmembrane and luminal proteins including calsequestrin via triadin and Junctin. RyR2 is regulated by luminal [Ca^{2+}]; either directly by luminal Ca^{2+} binding to RyR2 or indirectly by calsequestrin-2, triadin and junctin activity stimulated by luminal Ca^{2+} binding (Chen *et al.*, 2013).

Two forms of FKBP, the 12 kDa FKBP12 and 12.6 kDa FKBP 12.6 interact with and maintain the stability of RyR1 and RyR2 channels respectively (Brillantes *et al.*, 1994; Marx *et al.*, 2000). The interaction of FKBPs with the RyR channels promotes coupled gating of RyR (Marx, Ondrias and Marks, 1998; Marx *et al.*, 2001). DuringHF, hyperphosphorylation of RyR2 has been linked to dissociation of FKBP12.6 from RyR2; leading to altered channel function and changed stoichiometry in the macromolecular signalling complex (Marx *et al.*, 2000).

Changes in the redox state of the channel can either stimulate or inhibit channel activity (Lanner *et al.*, 2010). RyR contains multiple amino acid residues vulnerable to attack by reactive oxygen and nitrogen species. Proteins associated with RyR also contain sensitive residues (Meissner, 2017). Oxidation and nitrosylation modulates RyR channel activity, so Ca^{2+} release appears to be regulated by changes to the oxidative state of the cell that occurs during both healthy and pathological muscle function (Sutko and Airey, 1996; Zucchi and Ronca-Testoni, 1997; Fill and Copello, 2002; Meissner, 2004, 2017; Zalk, Lehnart and Marks, 2007; Betzenhauser and Marks, 2010; Lanner *et al.*, 2010).

RyR phosphorylation is an important regulatory mechanism of RyR channel function (Shan *et al.*, 2010). RyR1 and RyR2 both contain multiple potential phosphorylation sites, and PKA and CaMKII phosphorylate several of the Ser residues (Suko *et al.*, 1993; Huke and Bers, 2008; Meissner, 2017). PKA anchors to the RyR complexes via mAKAP, and in response to β-Adrenergic Receptor (β-AR) stimulation phosphorylates specific residues which reduce FKBP binding and increases channel activity (Kapiloff, Jackson and Airhart, 2001; Zalk, Lehnart and Marks, 2007). P4D3

also anchors via mAKAP and is believed to inhibit β-AR stimulated PKA phosphorylation which is cAMP-dependent (Lehnart *et al.*, 2005). Physiological β-AR-mediated stimulation of PKA is part of the “flight or fight” response (Shan *et al.*, 2010). However, dysfunctional PKA phosphorylation of RyR2 and P4D3 deficiency have been associated with dissociation of FKBP12.6, the leak of Ca^{2+} from the SR via RyR2 and linked with HF and stress-induced arrhythmias (Marx *et al.*, 2000; Lehnart *et al.*, 2005). Treatment with β-AR agonists reduces RyR2 phosphorylation and restores RyR2 channel function and signalling complex stoichiometry. Recently, both increased and abolished PKA mediated phosphorylation of RyR2 were shown to increase the leak of SR Ca^{2+} (Bovo *et al.*, 2017).PP1, PP2A and PP2B are present in RyR macromolecular complexes via anchoring proteins and could also dephosphorylate potential phosphorylated residues in RyR (Meissner, 2017).

In response to CaM transduced Ca^{2+} signals, CaMKII phosphorylates distinct RyR residues (Maier and Bers, 2002; Wehrens *et al.*, 2004). In the heart, CaMKII activation results in increased release of SR Ca^{2+} and elevated heart rates with greater contractile force during (Maier and Bers, 2002). Increased CaMKII activity associated with aberrant Ca^{2+} release via RyR2 is also observed during HF and cardiac arrhythmia in both patients and animal models (Hoch *et al.*, 1999; Kirchhefer *et al.*, 1999; van Oort *et al.*, 2010; Respress *et al.*, 2012; Li *et al.*, 2014). The roles and purpose of phosphorylation of specific RyR residues by particular kinases are under active investigation (Meissner, 2017).

The multifunctional Ca^{2+} binding protein CaM binds to both RyR1 and RyR2 and regulates channel activity in a Ca^{2+}-dependent manner (Fruen *et al.*, 2003). The

binding of CaM to both RyR1 and RyR2 is at a ratio of 4:1 with a CaM molecule binding to each tetramer sub-unit (Moore *et al.*, 1999; Balshaw *et al.*, 2001). CaM regulates RyR channel activity differently depending on RyR isoform. At low [Ca^{2+}] CaM activates RyR1 channels but inhibits channel activity at high [Ca^{2+}] (Tripathy *et al.*, 1995). However, CaM does not activate RyR2 channels at low [Ca^{2+}] but does inhibit channel opening at high [Ca^{2+}] (Meissner and Henderson, 1987; Fruen *et al.*, 2000)

The multiple modifications of RyR that modulate channel function show that RyR channels are a focal point for multiple separate and interacting pathways that regulate Ca^{2+} release from the SR.

1.5.1.1 Background

Ca^{2+} release from the SR, initiated by and coupled to changes in the potential difference across the T-Tubule membrane was long known, but not the channel responsible (Schneider, 1981; Martonosi, 1984). At Triad junctions a regular array of structures, “feet”, spanning the membranes were observed and isolated in vesicles of junctional SR from striated muscle (Franzini-Armstrong, 1970; Campbell, Franzini-Armstrong and Shamoo, 1980). SR vesicles of junctional membrane released Ca^{2+} in response to Ca^{2+}, consistent with whole muscle and skinned SR fibres. A single channel type was responsible for the Ca^{2+} release, which was enhanced by ATP and caffeine, and inhibited by Mg^{2+}, CaM, procaine and Ruthenium Red (Nagasaki and Kasai, 1983; Ikemoto, Antoniu and Mészáros, 1985; Meissner, 1986a; Meissner, Darling and Eveleth, 1986). Junctional SR membrane incorporated into bilayers

became ion permeable in response to Ca^{2+} and ATP (Smith, Coronado and Meissner, 1985; Smith, Coronado and Meissner, 1986).

1.5.1.2 Discovery of Ryanodine Receptor

Previously, the botanical alkaloid toxin ryanodine had been shown to interfere with muscle contraction and relaxation. First used as an arrow-head poison and then a commercial insecticide, ryanodine is extracted from the stem and roots of the tropical Central and South American plant *Ryania speciosa* (Rogers *et al.*, 1948). In mammals, ryanodine causes muscular spasms, paralysis and rigidity, leading to hypotension, circulatory and respiratory failure, and death (Procita, 1958). Treatment of mammalian striated and cardiac muscle with ryanodine results in prolonged contracture and reduced contractile force respectively (Jenden and Fairhurst, 1969). However, a complex picture emerged of ryanodine stimulating and inhibiting both the release and uptake of Ca^{2+} by the SR fraction of skeletal muscle (Fairhurst and Jenden, 1966; Fairhurst and Hasselbach, 1970; Fairhurst, 1974; Jones *et al.*, 1979). The high-affinity binding of ryanodine to SR Ca^{2+} channel competitively inhibits the ability of Ruthenium Red to block Ca^{2+} release (Fleischer *et al.*, 1985).

Changes in extracellular Ca^{2+} accompany ryanodine induced contractile failure of cardiac muscle (Hilgemann, Delay and Langer, 1983; Hunter, Haworth and Berkoff, 1983; Sutko and Kenyon, 1983; Hilgemann, 1986). The Ca^{2+} permeability of ER membranes derived from skeletal and cardiac muscle is increased or decreased by ryanodine in a dose-dependent manner (Meissner, 1986b; Lattanzio *et al.*, 1987). Vesicles of junctional SR membrane contain a Ca^{2+} channel which releases Ca^{2+} in

specific gating events stimulated by Ca^{2+} and ATP (Smith, Coronado and Meissner, 1985; Smith, Coronado and Meissner, 1986; Smith, Coronado and Meissner, 1986; Rousseau *et al.*, 1986). After ryanodine treatment cardiac and skeletal ER Ca^{2+} channels had increased open probability (P_O), lower conductance and reduced sensitivity to inhibitors and activators (Rousseau, Smith and Meissner, 1987).

The SR "feet" are large, multimeric protein assemblies which conduct Ca^{2+} through the SR and bind ryanodine (Campbell *et al.*, 1987; Imagawa *et al.*, 1987; Inui, Saito and Fleischer, 1987b, 1987a; Wang *et al.*, 1987). The purified "feet" contained a large ryanodine binding protein termed the RyR (Inui, Saito and Fleischer, 1987b). RyR purified to homogeneity from both skeletal and cardiac muscle could conduct Ca^{2+} similar to native channels (Lai *et al.*, 1988; Anderson *et al.*, 1989)

RyR is a ~2 MDa homotetrameric Ca^{2+} channel consisting of four 550 kDa subunits (Imagawa *et al.*, 1987; Lai *et al.*, 1988). At basal Ca^{2+} RyR is closed, P_O increases with rising Ca^{2+} until reaching maximal P_O at 10 µM Ca^{2+}, but at higher Ca^{2+} levels the P_O is reduced (Meissner, Darling and Eveleth, 1986; Bezprozvanny, Watras and Ehrlich, 1991). RyR is locked in an open conformation with reduced conductance when ryanodine concentrations are below 10 mM. However, at higher concentrations of ryanodine, the channel becomes locked into a non-conducting state (Nagasaki and Fleischer, 1988).

1.5.1.3 Isoforms of Ryanodine Receptor

The three isoforms of RyR are well conserved containing 70% sequence similarity (Rossi and Sorrentino, 2002). The pre-dominate isoforms in skeletal and cardiac

muscle are RyR1 and RyR2 respectively, both express at low levels in other cell types, and all three isoforms express to varying levels in a wide range of tissues. However, the most widely distributed isoform is RyR3. RyR3 is expressed in nerve, and both smooth and slow-twitch skeletal muscle cells in diverse organs: bladder, brain, kidneys, lungs, spleen and uterus; and tissues: oesophageal, gastrointestinal, neuronal and vascular (Ledbetter *et al.*, 1994; Giannini *et al.*, 1995; Lanner *et al.*, 2010).The opening of all three isoforms can be induced by Ca^{2+} (Meissner, Darling and Eveleth, 1986). RyR1 activation occurs upon a small [Ca^{2+}] increase as Ca^{2+} binds to stimulatory ion binding sites with specific high affinity for Ca^{2+}. At high [Ca^{2+}], Ca^{2+} binds to inhibitory ion binding sites that are less selective and have low-affinity for Ca^{2+} (Meissner, Darling and Eveleth, 1986; Meissner, 1994; Meissner *et al.*, 1997).

Striated muscle contraction, i.e. skeletal and cardiac muscle, requires RyR1 and RyR2 respectively for E-CC to convert an electrical signal to a mechanical contraction in myocytes. During E-CC, an AP induces Ca^{2+} to be released from the SR via RyR. At the maximal opening, high [Ca^{2+}] induces RyR channel closing, and Ca^{2+} uptake mechanisms reduce [Ca^{2+}]. The high cytoplasmic [Ca^{2+}] activates actin-myosin cross-bridging, and the myofilaments slide over each shortening the sarcomere. When [Ca^{2+}] falls the actin-myosin bridges release, the myofibrils retract, and the sarcomere lengthens. The shortening and lengthening of the sarcomere results in the contraction and relaxation of the muscle fibre.

1.5.1.4 Structure of Ryanodine Receptor

There is currently no 3D structure of full-length RyR derived from X-ray crystallography. The structure of RyR1 is the best characterised of the RyR isoforms as its size, and relative stability rendered it more amenable to single particle negative stain and Cryo-EM studies (Saito *et al.*, 1988; Radermacher *et al.*, 1994). Low-resolution Cryo-EM studies revealed RyR2 architecture, structural homology with IP_3R, the secondary structure of the channel sub-unit and pore, and gating and opening related structural movement (Serysheva *et al.*, 2005, 2008; Samsó *et al.*, 2009). Improvements in Cryo-EM technology and methodology have been used to resolve the structure of RyR1 in closed conformation to near-atomic resolution (Bai, McMullan and Scheres, 2015; Efremov *et al.*, 2015; Yan *et al.*, 2015; Zalk *et al.*, 2015).

When viewed from the membrane plane, RyR has a mushroom-like appearance similar to IP_3R, most of the protein is in the cytoplasm and forms a cap-like structure connected to the stalk like transmembrane structure, Figure 1-13 (Hamilton and Serysheva, 2009). The dimensions of the cap are 280 x 280 x 120 Å, and the cytosolic view of RyR resembles a square with clamp-shaped regions located at the corners of the assembly connected to the central rim and the stalk. Meanwhile, the luminal view is of a smaller square shaped structure, and the dimensions of the TM domain are 120 x 120 x 60 Å. The entire structure has four-fold rotational symmetry around a central “pore” (Saito *et al.*, 1988; Radermacher *et al.*, 1994).

Recent Cryo-EM studies of both RyR1 and RyR2 in open conformation have elucidated the structural basis of channel gating and opening (Bai *et al.*, 2016; des

Georges *et al.*, 2016; Peng *et al.*, 2016; Wei *et al.*, 2016). The highest resolution structures published to date comprise approximately 85 % of the structure of RyR1 at 3.8 Å (Zalk and Marks, 2017). X-ray crystallography of RyR fragments revealing the structure of crucial domains have been published (Tung *et al.*, 2010; Sharma *et al.*, 2012; Yuchi, Lau and Van Petegem, 2012; Lau and Van Petegem, 2014; Yuchi *et al.*, 2015). The highest resolution Cryo-EM image of RyR2 in open and closed conformation at 4.4- and 4.2-Å respectively revealed a structure with similar overall architecture and domain organisation to RyR1 (Peng *et al.*, 2016).

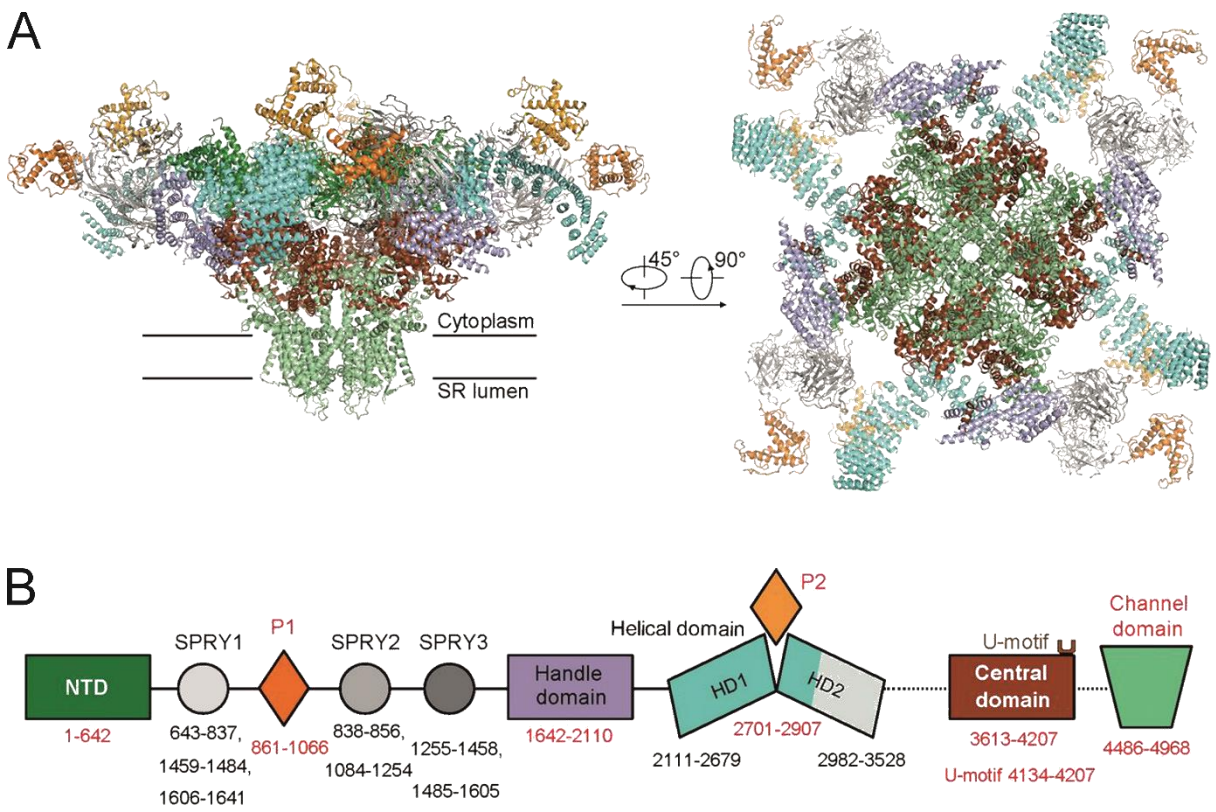

Figure 1-13 The Tetrameric RyR2 Channel Consists of Identical Subunits Containing Multiple Domains That Contribute to the Function and Formation of the Ion Channel

Current proposed structure of RyR2 based on Cyro EM republished with permission (Peng *et al.*, 2016). **(A)** The overall structure of the closed porcine RyR2 at a nominal resolution of 4.2 Å. The tetrameric structure of pRyR2 is domain-coloured with the same scheme as in **(B)**. The left-hand image shows the transmembrane view while the right-hand shows the cytoplasmic view. **(B)** Domain organisation of a pRyR2 protomer. The domain boundaries are indicated, with the reliably assigned boundaries labelled red.

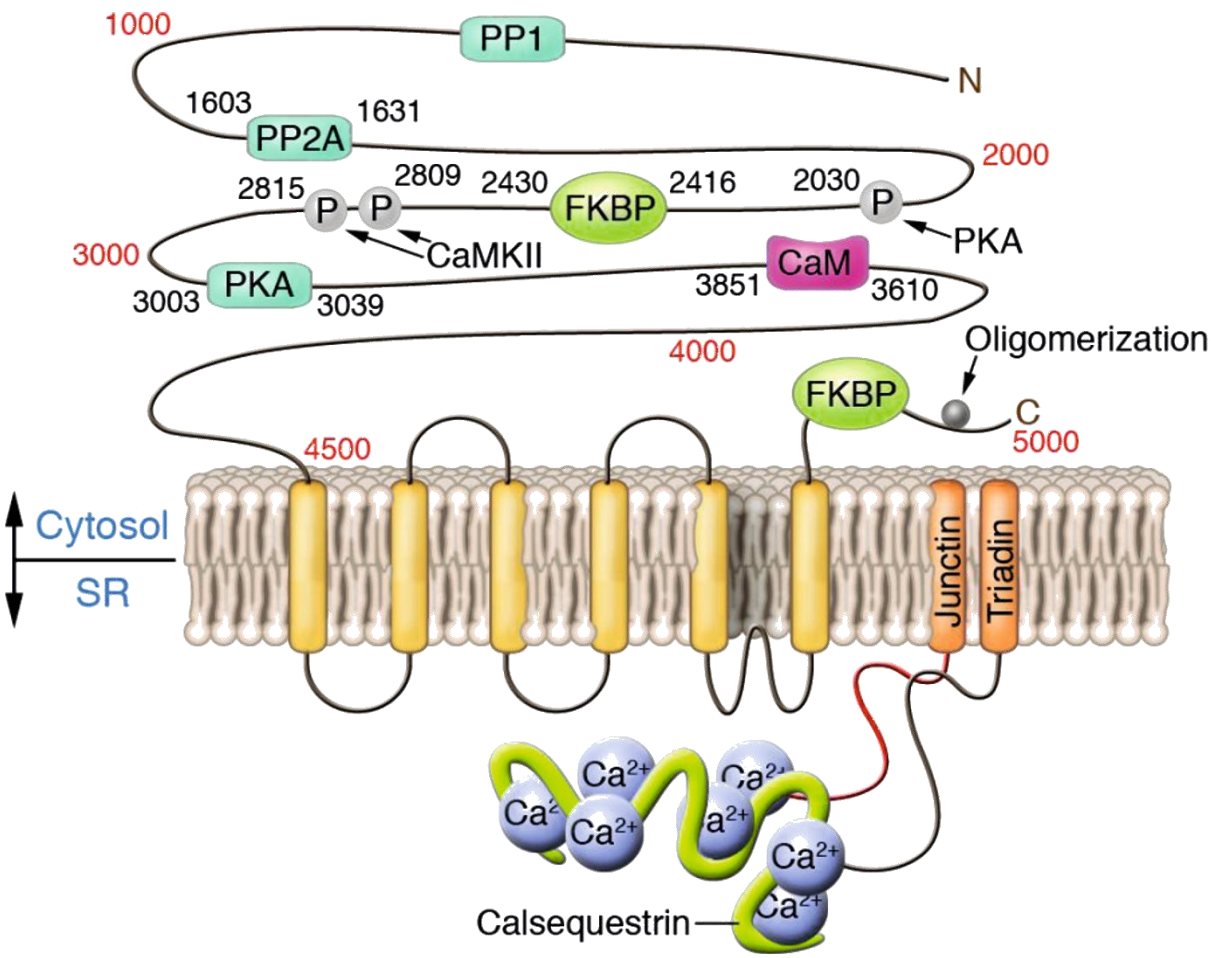

Figure 1-14 The Cytosolic Portion of RyR2 Subunits Contains Regulatory Binding Sites

Schematic illustration of the predicted structure of RyR2 and interacting SR luminal proteins calsequestrin, junctin, and triadin. The cytoplasmic region of RyR2 shows the location of interaction sites for ancillary proteins, phosphorylation (P) and phosphatase (PP). Reprinted with permission (Priori and Napolitano, 2005)

1.5.1.5 Proposed Ryanodine Receptor Domain Organisation

RyR consists of multiple motifs and domains summarised as five main domains, N-terminal domain (NTD), bridging solenoid (Br-Sol), the core solenoid (C-Sol), trans-membrane and C-terminal Domain (TM and CTD) as can be seen in Figure 1-15 (Zalk and Marks, 2017). The cap is the largest assembly in RyR and contains the NTD, three SPRY domains, two RyR repeat (RY) domains (RYR1&2 and RYR3&4) and BrB (Zalk and Marks, 2017). The scaffold for the regulatory proteins and related anchoring proteins comprising the cytoplasmic portion of the macromolecular signalling complex, e.g. FKBP12.6, CaM, PKA, CaMKII and their anchoring proteins, PP1 and PP2A, PDE4D3 as shown in Figure 1-14. The cytoplasmic complex controls channel pore opening and closing allosterically. The channel activation is modulated by the accessory proteins which regulate conformational changes in the pore and the TM segments altering the P_O of the channel (des Georges *et al.*, 2016; Peng *et al.*, 2016).

The crystal structure of the first 559 amino acids of RyR1 contains two β-trefoil domains and a domain containing a bundle of five α-helices (Tung *et al.*, 2010). Docking the RyR N-terminal crystal structure onto the Cryo-EM map reveals the β-trefoil domains from each subunit forming a vestibule around the four-fold axis at the centre of the cap. There are disease-associated mutation hotspots (HS) where the β-trefoil domains of different sub-units interact (Tung *et al.*, 2010). Comparably, the N-terminal region of IP_3R1 also folds into domains in the full-length receptor which are similarly arranged and superimposable on the corresponding domains of RyR1 (Seo *et al.*, 2012). Interactions between two NTDs of neighbouring subunits modulate channel gating allosterically by stabilising the closed conformation of the channel, one

of these domains contains a disease associated mutation hot spot (HS) (Kimlicka *et al.*, 2013; des Georges *et al.*, 2016; Peng *et al.*, 2016). The channelopathy associated mutations in the HS disrupt interdomain interactions destabilising channel closed conformation increasing RyR1 P_O and mean channel open time, and increasing pro-arrhythmic SR Ca^{2+} leak in RyR2 (Yamamoto, El-Hayek and Ikemoto, 2000; Shtifman *et al.*, 2002; Yang *et al.*, 2006). Docking crystal structures of the N-terminal region reveals that specific SPRY domains are exposed to binding with FKBP and BrB domains of adjacent subunits (Lau and Van Petegem, 2014; Yuchi *et al.*, 2015; Zalk and Marks, 2017). Disease mutation clusters occur at points of interdomain interaction between BrB and other domains (Zalk and Marks, 2017). Docking crystal structures of RyR domains also revealed the location of residues phosphorylated by PKA, at the top of the cytoplasmic cap (Zalk and Marks, 2017). RyR channel P_O increases upon PKA phosphorylation, and such modification at the position could modify the interaction between domains and accessory proteins promoting channel open conformation (Zalk and Marks, 2017).

The cap is connected to the channel pore by the C-Sol, a rigid structure with inter and intrasubunit domain interactions that transmit ligand binding signals from the cap to the channel pore. The C-Sol also contains putative binding sites for Ca^{2+}, caffeine and ATP (des Georges *et al.*, 2016). The central core of each subunit interacts with specific NTDs in the same and adjacent subunits. A pair of high affinity Ca^{2+} binding EF-hand motifs interacts with TMR of the neighbouring subunit (Xiong *et al.*, 1998; Zalk and Marks, 2017). The EF-hands are proposed to play a role in cytosolic Ca^{2+} activation of RyR acting as a Ca^{2+} sensor or conformational switch (Efremov *et*

al., 2015; Zalk *et al.*, 2015). In RyR1 the EF-hands are required for channel activation and regulation (Fessenden *et al.*, 2004; Xiong *et al.*, 2006; Gomez and Yamaguchi, 2014). However, the EF-hands are not required for the activation of RyR2 by cytosolic Ca^{2+} but are essential for correct regulation of luminal [Ca^{2+}] by SOCIR (Guo *et al.*, 2016). In both RyR2 and RyR3, there appears to be an alternative Ca^{2+} sensing site; a conserved glutamic acid (Glu) residue endows cytosolic Ca^{2+} sensitivity on both isoforms (Zhao *et al.*, 1999; Li and Chen, 2001). The C-Sol also contains a U motif which envelopes the CTD enabling conformational changes induced by ligand binding to the cap to be transmitted to the pore aperture via the CTD if activators are bound (Zalk *et al.*, 2015; Zalk and Marks, 2017).

The pore of the RyR channel is formed by the TMD which contains six membrane-spanning transmembrane (TM) helices (S1-S6) similar to 6TM cation channel superfamily members (Zalk and Marks, 2017). The organisation of S1–S4 resembles voltage sensors in other 6TM channels but lacks most of the positive residues so is termed a pseudo-voltage sensor domain (pVSD). The first two helices S1 and S2 are joined by a long, disordered, negatively charged luminal loop. The S2 and S3 helices are bundled together to form a unique motif conserved within RyRs termed VSC, which is near the cytosolic EF-hands so may contribute to modulating channel gating in response to conformational changes. The channel is formed by S5 and S6 which are connected to the pVSD via a juxtamembrane S4–S5 cytosolic linker.

Each subunit contributes to the ion pore an S6 consisting of a short pore helix and an extended segment which narrows and terminates beyond the cytosolic side of the membrane. The luminal entrance is lined with eight negatively charged residues

from each sub-unit forming the selectivity filter. The luminal loops joining the TM helices form a negatively charged vestibule which carries on a third of the way through the membrane and appears to concentrate Ca^{2+} in the luminal opening of the pore (Zalk *et al.*, 2015). The narrowest part of the ion pore is where S6 is enclosed by the amphipathic S4–S5 linker forming the pore aperture with a single gate containing an Isoleucine (Ile) residue.

Additionally, seven acidic residues at the carboxyl end of S6 form negatively charged 'rings' on the cytosolic side of the aperture resemble those in IP_3R1 and presumably play a similar role (Xu *et al.*, 2006; Fan *et al.*, 2015). The cytosolic extension of S6 terminates at the CTD connecting the CTD with the pore aperture. Zinc fingers in the CTD stiffen the hinge connecting S6 and CTD (Yan *et al.*, 2015). The CTD contains binding sites for the RyR activators Ca^{2+}, ATP, and caffeine (des Georges *et al.*, 2016). The extension of S6 resembles that found in IP_3R1 where the H6 of the TMD directly connects the pore and IBC (Fan *et al.*, 2015).

In some Cryo-EM structures of RyR1, an additional helix has also been observed near pVSD and S5 of neighbouring subunits as can be seen in Figure 1-15 (Zalk *et al.*, 2015; des Georges *et al.*, 2016). The transmembrane (TM) helix, TmX is believed to form a TM hairpin occurring upstream of S1 and could play a modulatory role but requires further investigation (Zalk and Marks, 2017).

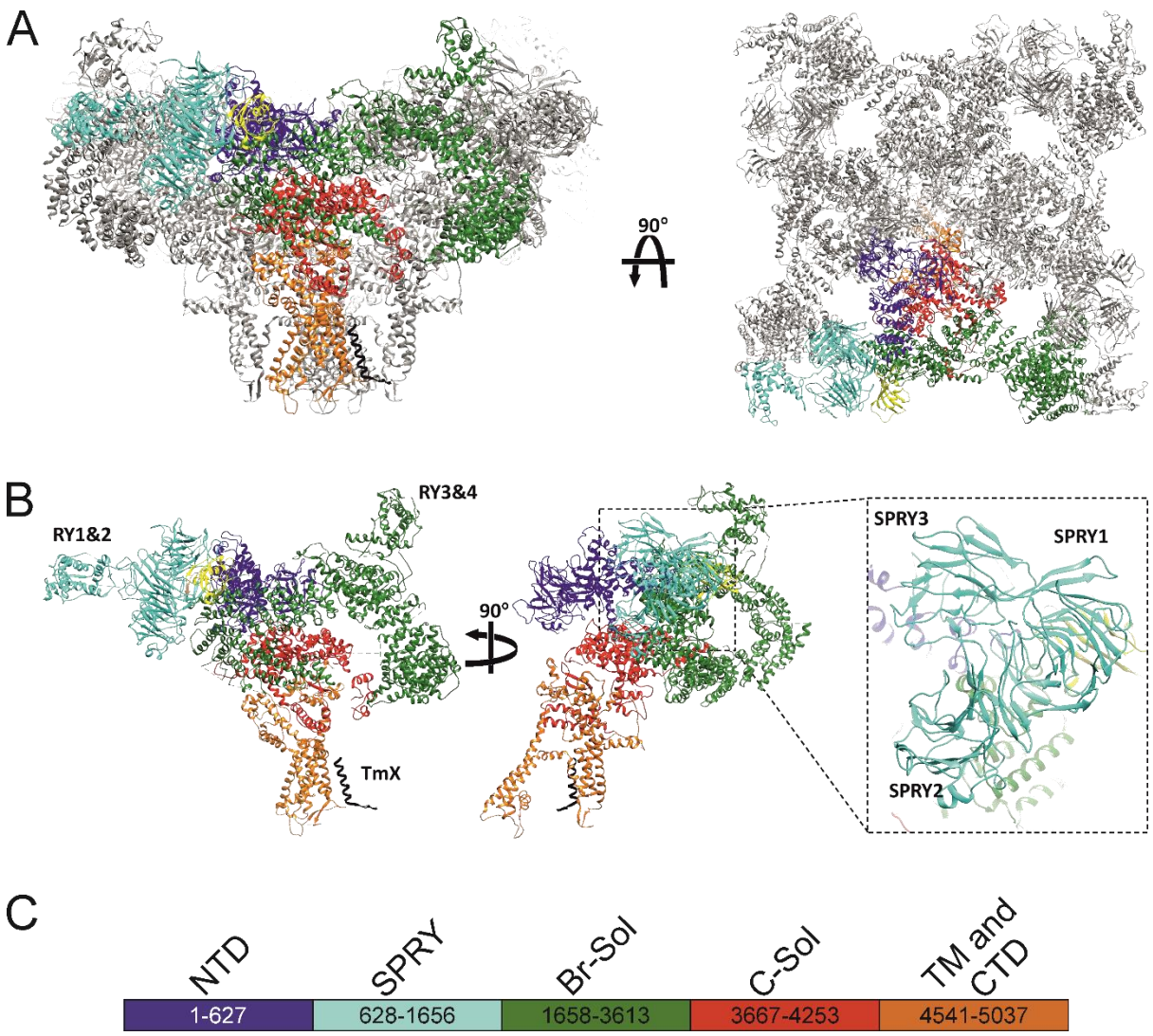

Figure 1-15 RyR Can Be Divided into Five Main Domains

Model of the 3D structure of RyR1 based on Cryo-EM images and assigned domains republished with permission (Zalk and Marks, 2017). **(A)** The overall structure of the closed RyR1 with a single subunit highlighted with the location of assigned domains. The left-hand image shows the transmembrane view while the right-hand shows the cytoplasmic view. **(B)** An individual RyR1 subunit annotated with the locations of RY1&2 and RY3&4 and inset with the orientation of the three SPRY domains. Each subunit of RyR1 can be divided into five main domains which are coloured in both **(A)** and **(B)** with the same scheme as in **(C)**. The modulatory subunit calstabin and the recently identified TmX, are shown yellow and black respectively. **(C)** The colour code and boundaries of the five main domains.

1.5.2 Regulation of Ryanodine Receptor 2 by Calmodulin

Potentially, Ca^{2+} regulates CICR directly by binding to RyR and indirectly by binding to CaM which regulates both L-type VGCCs and RyR2. ApoCaM acts as a partial agonist of channel activity, while partial Ca^{2+} saturation of CaM results in inhibition of channel activity (Tripathy *et al.*, 1995; Rodney *et al.*, 2000; Tang, 2002). All RyR isoforms bind both apo- and holoCaM (Tripathy *et al.*, 1995; Yamaguchi *et al.*, 2005). CaM binds to RyR1 at a ratio of four to one, i.e. one CaM per subunit regardless of Ca^{2+} saturation, but the location of binding depends on Ca^{2+} saturation (Moore *et al.*, 1999). ApoCaM prebound to RyR1 retains the ability to bind Ca^{2+} sequentially (Newman *et al.*, 2014). The relative position of CaM on the surface of RyR2 changes upon Ca^{2+} binding (Wagenknecht *et al.*, 1994, 1997; Samsó and Wagenknecht, 2002).

The binding of holoCaM to RyR1 and RyR2 occurs within a highly conserved region (CaMBD2) predicted to be adjacent to the binding site of FKBP (Takeshima *et al.*, 1989; Moore *et al.*, 1999; J. Zhang *et al.*, 2003; Yamaguchi *et al.*, 2003). All isoforms contain three CaM binding domains (CaMBD), accessible regions predicted to bind CaM containing strictly conserved residues (Huang *et al.*, 2013). In the presence of Ca^{2+}, CaM binds to the highly conserved CaMBD2 of RyR1 (Maximciuc *et al.*, 2006). HoloCaM binds to all three domains in both RyR1 and RyR2, while apoCaM binds to CaMBD2 weakly and CaMBD3 with higher affinity. There are RyR isoform-specific differences between the binding of CaM to the CaMBD1&3. HoloCaM has a fourfold lower binding affinity for the CaMBD2 of RyR1 compared to RyR2. In the presence of Ca^{2+}, binding of CaM and CaMBD3 is of high affinity in RyR1, while it is strong and complex in RyR2 (Lau, Chan and Van Petegem, 2014). The CaM-like

domain (CaMLD) (RyR2$^{4064–4210}$), a Ca^{2+} binding region containing EF-hand motifs that resemble CaM, is also predicted to interact CaMBD2(Xiong *et al.*, 2006).

Binding between CaM and CaMBD1 is calcium-dependent, both CaM lobes contribute to binding to RyR1 but the N-lobe drives binding in RyR2 as the C-lobe only interacts weakly. The affinity of the N-lobe for CaMBD1 is greater than the reduced affinity that occurs when the C-lobe is bound to CaMBD2 (Lau, Chan and Van Petegem, 2014).

The lobes of CaM bind independently to different but contiguous sections of CaMBD2 (Maximciuc *et al.*, 2006; Lau, Chan and Van Petegem, 2014). Binding to RyR1 CaMBD2 is preferable over binding to CaMBD1 for both lobes (Newman *et al.*, 2014). While both lobes contribute, binding is driven by the C-lobe upon C-lobe binding the N-lobe affinity is reduced (Lau, Chan and Van Petegem, 2014). The affinity between CaMBD2 of RyR1 and lobes of apoCaM is lower than the holoCaM lobes, in the absence of Ca^{2+} the apoCaM C-lobe affinity is reduced, and N-lobe cannot bind (Newman *et al.*, 2014). In a Ca^{2+} free state, CaM is bound to RyR1 CaMBD2 mainly via the C-lobe, with N-lobe available to interact elsewhere. The binding of Ca^{2+} to prebound CaM increases the likelihood of CaM being predominately bound to CaMBD2 via both lobes changing the interaction of CaM with the RyR channel (Her *et al.*, 2016).

Binding of CaM to CaMBD3 is Ca^{2+} independent in both RyR isoforms. The high-affinity binding of RyR1 CaMBD3 and holoCaM is contributed to by both lobes which have lower specific binding affinities. In the presence of Ca^{2+}, the CaM N-lobe

binds to one site in CaMBD3 of RyR2 and competes with the C-lobe for its binding site. Both lobes of apoCaM bind CaMBD3 of RyR2 and only the N-lobe of apoCaM binds CaMBD3 of RyR1 (Lau, Chan and Van Petegem, 2014).

RyR isoform-specific differences in CaMBD2 sequence between RyR2 and RyR1 do not impart differences in regulation by CaM (Yamaguchi *et al.*, 2003). The CaMLD and N terminal sequences, both outside of CaMBD2 appear to confer differential regulation of RyR1 and RyR2 in response to Ca^{2+} (Xu *et al.*, 2017).

Independent binding of the lobes of CaM could enable Ca^{2+} dependent interaction with different regions of RyR, even neighbouring subunits, allowing CaM to fine-tune the response of RyR to Ca^{2+}. Additionally, the presence or absence of CaM bound to specific locations could interrupt or permit intra-subunit interactions within RyR. Variations in the regulatory sequences between RyR isoforms would explain the ability of CaM to induce an isoform-specific response when binding to a conserved site.

1.5.3 The Function of the Ryanodine Receptor

1.5.3.1 Skeletal Muscle

During E-CC in skeletal muscle, the signal transmits across the junction of two terminal cisternae of the SR and a T-tubule known as the Triad. In the Triad, RyR1 in the SR and the $Ca_V1.1$, an L-type VGCC in the T-Tubule occur in tetrads of four $Ca_V1.1$ to one RyR1. The $Ca_V1.1$ and RyR1 are in close enough proximity to be conformationally coupled. Upon the depolarisation of the sarcolemma, $Ca_V1.1$ undergoes a

conformational change which induces the same in RyR1 causing the channel pore to open and Ca^{2+} to be released (Bannister and Beam, 2013).

1.5.3.2 Cardiac Muscle

Signal transmission in cardiac myocytes occurs across Diads, the juxtaposition of one terminal cisterna and a T-tubule on the sarcomere Z-line. The $Ca_V1.2$ an L-type VGCC and RyR2 occur nearby on the T-Tubule and SR respectively. In contrast to RyR1, RyR2 and the VGCC are not conformationally coupled. As can be seen in Figure 1-16 $Ca_V1.2$ opening releases Ca^{2+} into the cleft between the sarcolemma and the SR membrane inducing CICR by RyR2 (Donald M Bers, 2002; Eisner *et al.*, 2017).

Dysfunctional Ca^{2+} release and failure of Ca^{2+} handling from the SR is a significant cause of cardiac arrhythmias in congenital cardiac rhythm disorders and HF (Ter Keurs and Boyden, 2007; Zima *et al.*, 2014). Knowledge of the mechanisms will provide insight into the pathophysiology of disease and potential targets for therapeutic intervention.

The need to keep Ca^{2+} release under tight regulatory control means it is unsurprising that RyR is modulated by multiple effector molecules which bind to the sizeable cytoplasmic structure as shown in Figure 1-14. Additionally, regulation of the channel by molecules in the SR/ER lumen, have been reported. In particular, raised luminal [Ca^{2+}] increases P_O during SOICR (Entman *et al.*, 1979; Jiang *et al.*, 2004; Jones, Guo and Chen, 2017).

To date all binding sites for regulatory ions in RyR2 have not been confirmed (Peng *et al.*, 2016). Several reports propose that RyR2 contains EF-hand motifs with

high Ca^{2+} binding affinity and conserved residues near the C-terminal, that act as Ca^{2+} sensors. Improvements to the known structure of RyR2 and further investigation of how RyR2 and modulators interact will elucidate how channel regulation ensures the timely and correct release of Ca^{2+} in response to Ca^{2+} during the cardiac cycle.

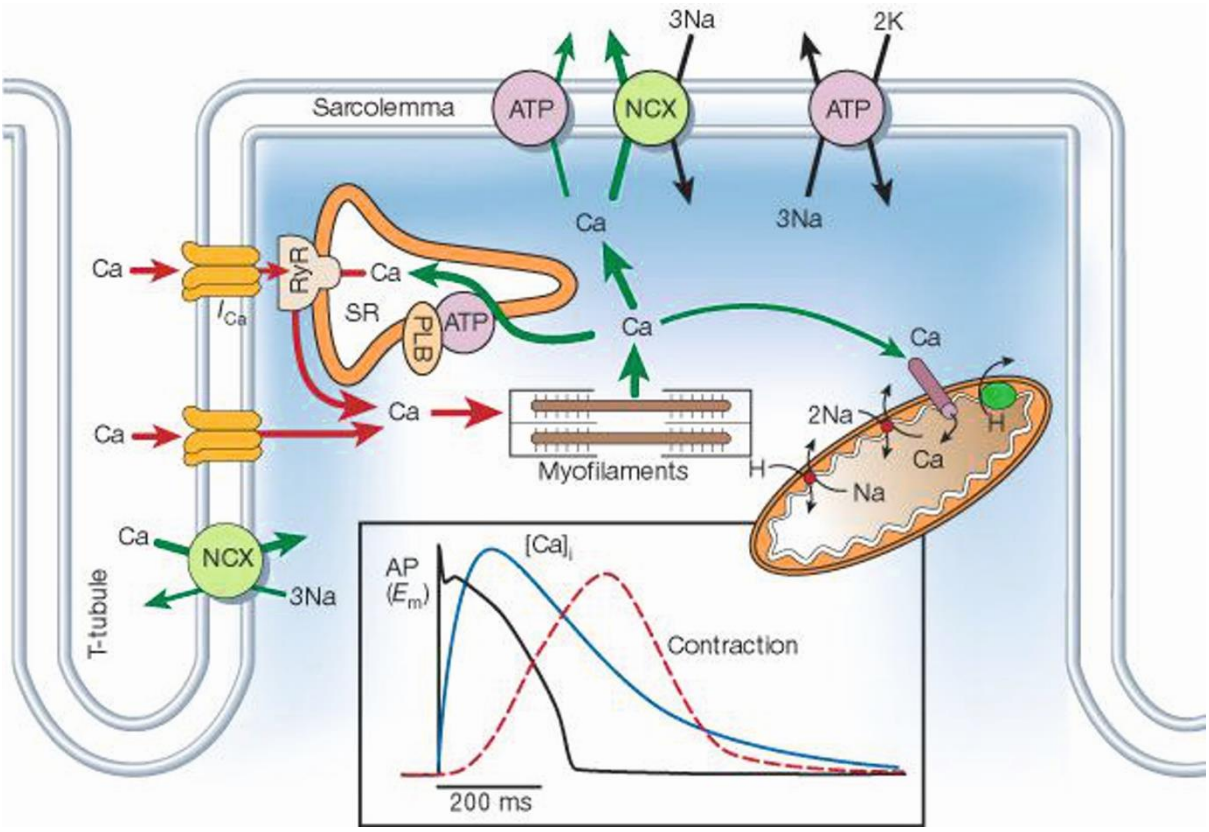

Figure 1-16 Action Potentials Are Converted to Mechanical Contractions in Ventricular Myocytes by the Flow of Ions

Schematic diagram showing ion flow, particularly Ca^{2+} transport, in a ventricular myocyte during E-CC. Upon AP reaching the T-tubule, VGCCs (orange) permit Ca^{2+} to enter the sarcomere and stimulate RyR to release Ca^{2+} from the SR stimulating myofilament contraction The inset shows the time course of an AP, Ca^{2+} transient and contraction measured in a rabbit ventricular myocyte at 37 °C. In this diagram, the transport of Ca^{2+} into the SR is represented by phospholamban (PLB) and ATPase (ATP). Reprinted with permission (Donald M. Bers, 2002)

1.6 Channelopathies and Primary Cardiac Electrical Disease

The electrophysiology of cardiomyocytes is defined by the activity of cardiac ion channels which shape the characteristics of the AP. Membrane depolarisation is the result of an influx of cations, i.e. Ca^{2+} and Na^{+} via ion channels, while the efflux of cations, i.e. K^{+} results in the subsequent repolarisation. Alterations to either cation influx or efflux due to genetic changes in ion channel can profoundly change AP duration (Kass, 1997). Inherited or acquired disturbances to ion channel function are termed channelopathies and are linked to many human diseases including cardiac arrhythmias (Ashcroft, 2006). Inherited cardiac channelopathies are clinically and genetically heterogeneous congenital cardiac disorders associated with sudden death, ventricular tachycardia (VT) and cardiac arrhythmia due to aberrant ion channel function (Ackerman *et al.*, 2011; Bastiaenen and Behr, 2011).

The most common forms of cardiac channelopathy are believed to occur in the general population at a rate of 1 in 2000-3000 and be responsible for ~50 % of SCD due arrhythmia (Behr *et al.*, 2008; Schwartz *et al.*, 2009). Amongst genetic arrhythmia patients mutations have been identified in nearly all the genes encoding cardiac ion channel subunits and associated proteins (Abriel and Zaklyazminskaya, 2013). The mutations result in altered ion channel characteristics leading to changes in either membrane depolarisation or repolarisation during cardiac AP.

Potential difference on the surface of the body that corresponds to the membrane potential of cardiomyocytes during the cardiac cycle can be recorded by an electrocardiogram (ECG). The characteristic ECG trace during a heartbeat with sinus rhythm is the result of a wave of depolarisations initiated at sinoatrial node,

spreading through the atrium to the atrioventricular node, on to the bundle of His and then the Purkinje fibres and spreading out throughout the ventricles as can be seen in Figure 1-17. An ECG can be used to diagnose, categorise and in the treatment of heart disease by ascertaining heartbeat rate and rhythm, structure and electrical function of the heart, the size and position of the heart chambers, and damage to the heart muscle or electrical system. During an arrhythmia, additional polarisations initiated spontaneously in other parts of the heart disrupt the wave of depolarisations resulting in an abnormal ECG Figure 1-17.

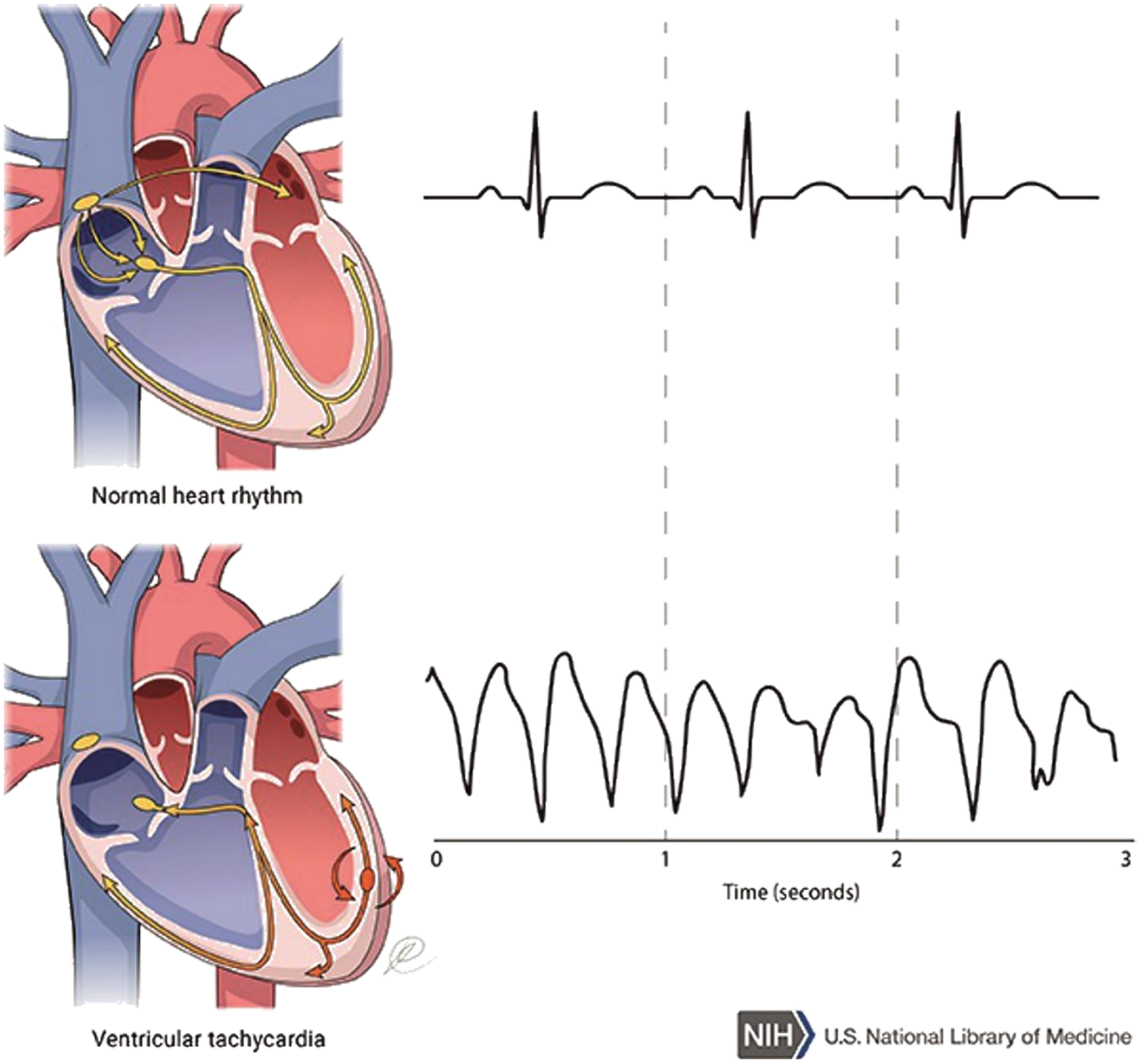

Figure 1-17 Cardiac Arrhythmia Results from Additional Depolarisation Events Disrupting Regular Depolarisation Originating in the Sinoatrial Node

Illustration of the wave of depolarisations and corresponding ECG in normal and during an episode of VT. Top, a normal sinus rhythm initiated in the sinoatrial node and typical ECG. Bottom shows an arrhythmic heartbeat caused by additional waves of depolarisation initiated in ventricles during an episode of VT. Illustration: Pubic Domain obtained from Genetics Home Reference (National Library of Medicine, 2018)

An illustration of a generic surface ECG and ventricular cardiac AP are shown in Figure 1-18. As can be seen in Figure 1-18, the ventricular cardiac AP can be divided into five phases. Before and after a cardiac AP is Phase 4, the resting membrane potential which is the result of a balance in the flow of ions into and out of the cell. The balanced ion flux is maintained by the action of the ATP dependent Na^+-K^+ ion pump (Na^+/K^+-ATPase) exporting three Na^+ in exchange for two K^+ and the NCX which imports three Na^+ in exchange for exporting one Ca^{2+} from the cell (Morad and Tung, 1982).

Phase 0, the start of the cardiac AP corresponds to the rapid influx of Na^+ through the voltage-gated Na^+ channel $Na_V1.5$, followed by Ca^{2+} through $Ca_V1.2$ in response to membrane depolarisation. The cardiac AP peaks at the start of Phase 1, the $Na_V1.5$ channels inactivate and I_{to1}, a voltage-gated K^+ channel, flicker open causing a transient efflux of K^+ and a dip in the membrane potential (Niwa and Nerbonne, 2010). The increase in $[Ca^{2+}]$ continues into Phase 2 which corresponds to systole.

During Phase 2 the Ca^{2+} influx is offset by the efflux of K^+ through SK channels (Gu *et al.*, 2018). Additionally, the raised $[Ca^{2+}]$ increases NCX activity which in turn increases the activity of Na^+/K^+-ATPase. The net result of the ion fluxes is that the membrane potential remains constant during Phase 2 and the cardiac AP plateaus (Santana, Cheng and Lederer, 2010). In Phase 2 myocyte contraction in response to an AP during E-CC is dependent on CICR occurring. The increased $[Ca^{2+}]$ induces RyR2 activation and the influx of Ca^{2+} from the SR. SR Ca^{2+} binds to TnC resulting in myocardial contraction.

Following contraction, the cardiomyocytes relax as diastole begins corresponding to Phase 3 of the cardiac AP. The increased [Ca^{2+}] induces increased activation of SK channels, the plateau of Phase 2 ends and Phase 3 begins (Gu *et al.*, 2018). During Phase 3, SK channels, Na^+/K^+-ATPase and NCX begin to restore resting ion concentrations. The membrane repolarises, with decreasing membrane potential the VGCCs close and the K_{ir} and IRK channels open, further reducing membrane potential (Lopatin and Nichols, 2001). The [Ca^{2+}] returns to resting levels due to inactivations of VGCCs and then RyR2 as Ca^{2+} homeostatic mechanisms take up Ca^{2+} (van der Werf and Wilde, 2013). With reduced [Ca^{2+}], myocardial contraction halts and the heart muscle relaxes. Membrane potential decreases until resting potential is achieved as diastole continues into phase 4 to await the initiation of the next cardiac AP (Santana, Cheng and Lederer, 2010).

The inward and outward fluxes of Na^+ Ca^{2+} and K^+ through the interlinked activities of ion channels in response to ion concentrations and membrane potential shape the cardiac AP. The cardiac AP and ion concentrations also dictate the influx of Ca^{2+} which in turn regulates cardiomyocyte contractility (Bartos, Grandi and Ripplinger, 2015). Acquired and congenital dysfunctions of the cardiac ion channels can alter both the cardiac AP and cardiac function (Nerbonne and Kass, 2005). Consequently, arrhythmia patients with cardiac channelopathies of the various ion channels display altered and characteristic ECGs which can share basic features depending on the type of channelopathy (Abriel and Zaklyazminskaya, 2013).

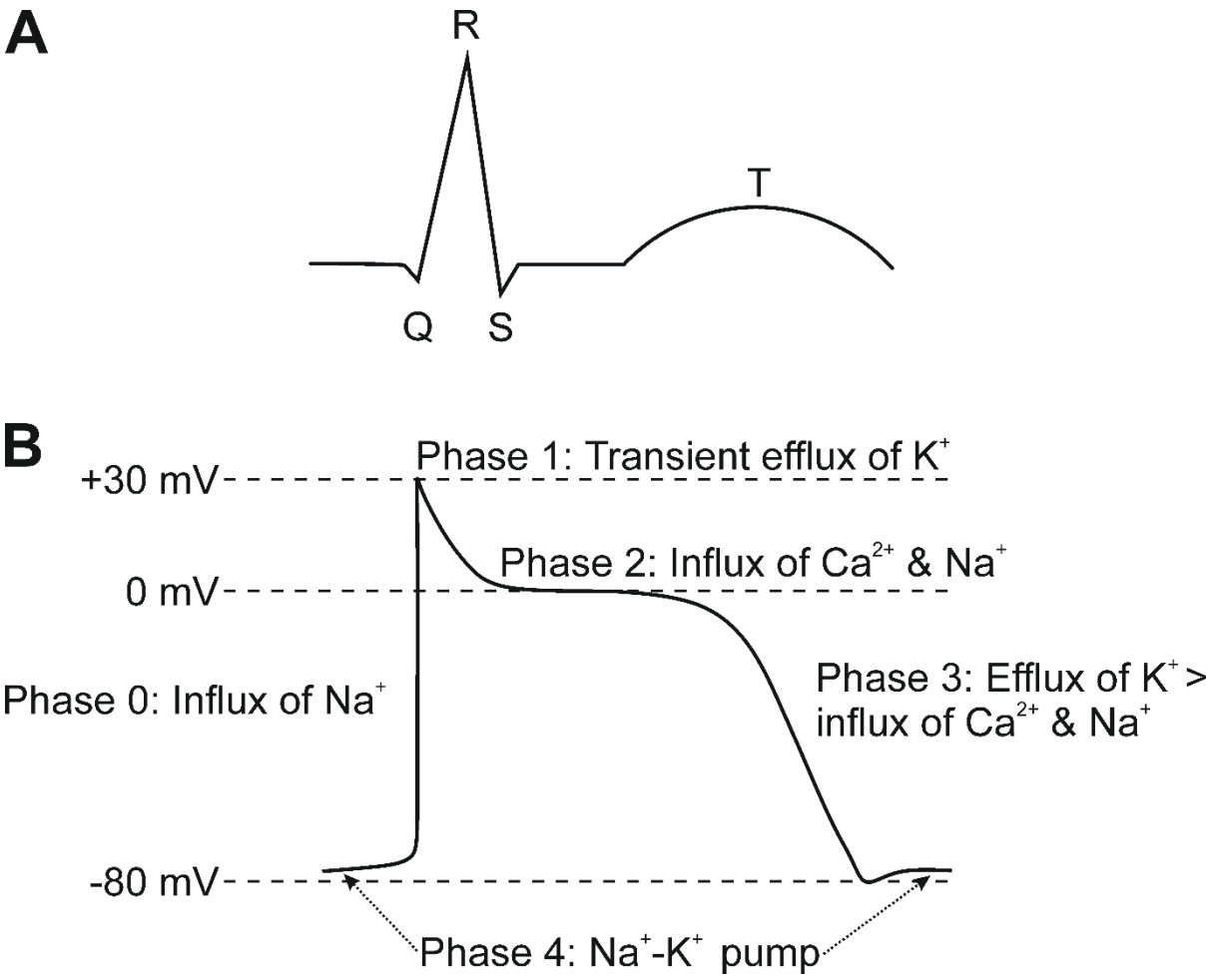

Figure 1-18 ECG Measure Cardiac Rhythm and Ventricular Cardiac Action Potential

Illustration showing a surface ECG trace and the ventricular cardiac AP for normal sinus rhythm. **(A)** An ECG trace showing the QRS complex and the T wave associated with ventricle depolarisation and repolarisation respectively. Q is a negative deflection on the isoelectric line that precedes ventricular contraction, R is the positive deflection which corresponds to the peak of the ventricular contraction, S is the downward deflection immediately after the ventricular contraction and T is the recovery of the ventricles. **(B)** The five phases of ventricular cardiac AP are annotated with changes in ion flow that occur at each phase. Republished in accordance with Creative Commons Attribution 4.0 International Public License from (Kwon and Kim, 2017) ©creative commons.

Channelopathies that alter the flow of ions can result in “afterdepolarisations”, abnormal cardiomyocyte depolarisation events that interrupt phases 2, 3, or 4. The membrane depolarisation results in tachycardia, arrhythmia and fibrillation (Clusin, 2003). Afterdepolarizations during Phases 2 or 3 are known as early afterdepolarisations (EADs). EADs are the result of the aberrant initiation of failed APs during repolarisation. The aberrant AP is caused by enhanced Ca^{2+} channel activation and dysfunctional Na^{2+} channel opening during Phase 2 and Phase 3 respectively. Delayed afterdepolarizations (DADs) occur during phase 4 and are not the result of an AP but are the result of raised [Ca^{2+}] due to the spontaneous release of Ca^{2+} from the SR. Ca^{2+} homeostatic mechanisms reduce [Ca^{2+}] particularly the NCX. NCX activity causes an increase in AP and membrane depolarisation due to the import of three Na^{+} for every one Ca^{2+} (Clusin, 2003).

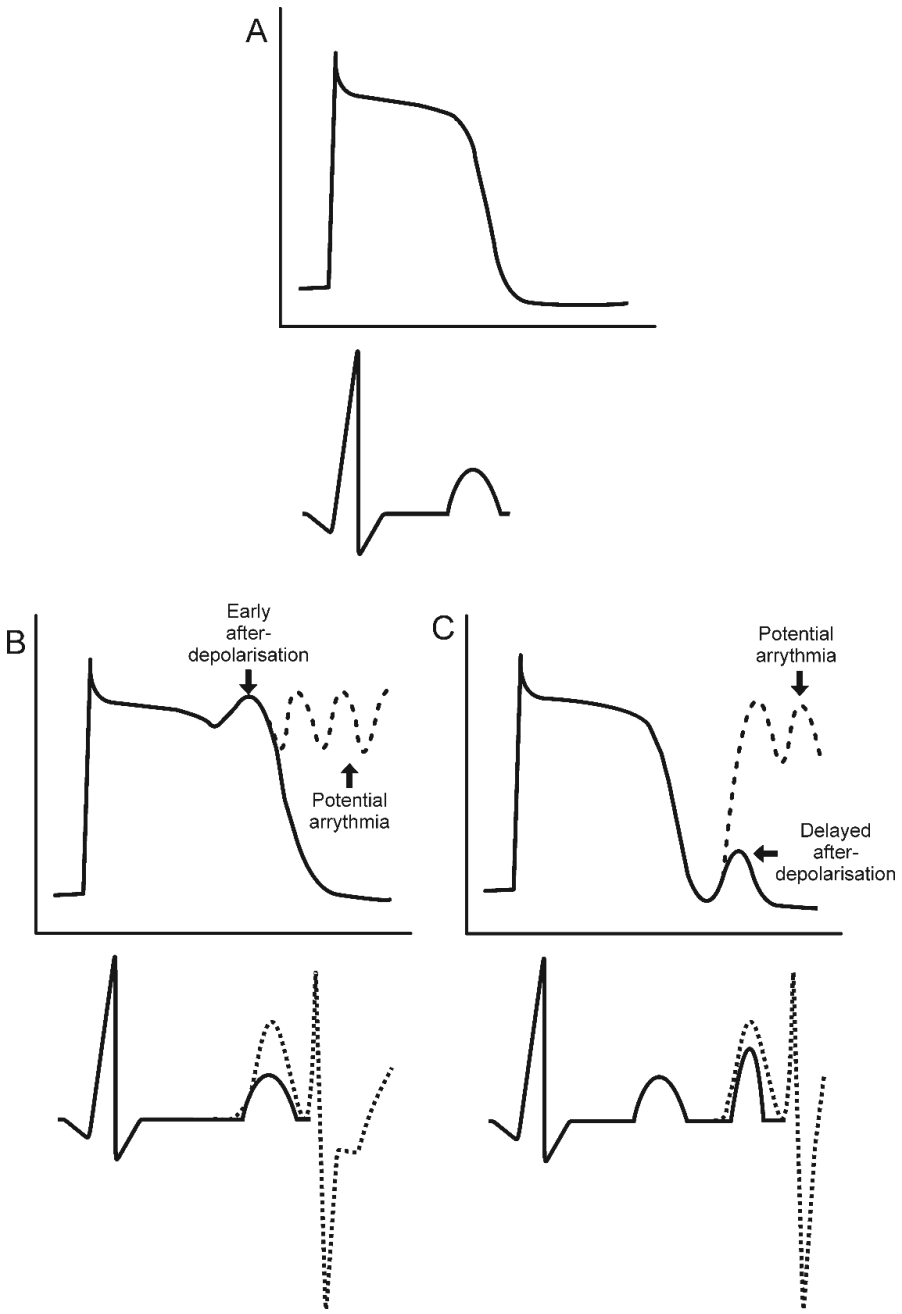

Figure 1-19 Early And Delayed Afterdepolarisations in Cardiac AP are Potentially Arrhythmogenic

Illustration of ventricular cardiac AP and corresponding ECG during normal sinus rhythm **(A)** and arrhythmias (B and C). Both Early afterdepolarisation **(B)** and Delayed afterdepolarisation **(C)** alter cardiac rhythm to have a prolonged QT interval or an additional depolarisation event respectively, both of which are potentially arrhythmogenic.

1.6.1 Cardiac Arrhythmias

1.6.1.1 Congenital Channelopathies

MI and SCD are both outcomes of heart disease, the leading cause of which is coronary artery disease (Thomas *et al.*, 2018). However, in a small percentage of SCD cases, there is no existing cardiac disease nor any structural defects in the heart. Channelopathies, inherited abnormalities in ion channel function in morphically normal hearts can result in altered electrical behaviour which leads to cardiac arrhythmias and SCD. Amongst survivors of MI with unknown origin, 54% were diagnosed with an arrhythmogenic channelopathy. (Maury *et al.*, 2010). While CPVT and LQTS were each diagnosed in 13% of cases, the 44% of cases that were undiagnosed were classed as IVT (Krahn *et al.*, 2009).

1.6.1.2 Catecholaminergic Polymorphic Ventricular Tachycardia

First described over 40 years ago, catecholaminergic polymorphic ventricular tachycardia (CPVT) is a highly malignant, inheritable, cardiac ion channelopathy associated with MI and SCD particularly in young people with morphologically normal hearts (Reid *et al.*, 1975; Leenhardt *et al.*, 1995). CPVT is rare with an estimated prevalence of 1:10,000 (van der Werf and Wilde, 2013). RyR2 mutations with CPVT characteristics occur 1.5 % of Sudden Infant Deaths Syndrome cases (Tester *et al.*, 2007) and 12 % of deaths unexplained by autopsy (Tester *et al.*, 2012). CPVT is characterised by potentially life-threatening ventricular arrhythmias triggered by catecholamine stimulation during psychological and emotional stress or physical exertion (Behere and Weindling, 2016). Individuals with CPVT have normal resting

heart rhythm and no detectable abnormalities nor structural heart defects. Once provoked the polymorphic or bidirectional ventricular arrhythmias can become progressively rapid and degenerate into ventricular tachycardia (VT) and ventricular fibrillation (VF), Figure 1-20, resulting in syncope and SCD (Reid *et al.*, 1975; Leenhardt *et al.*, 1995; Loar *et al.*, 2015).

Typically, diagnosis of CPVT follows the patient presenting with stress-induced syncope, or cardiac arrest successfully treated with defibrillation or CPR. Screening of families with a history of stress or exercise-induced arrhythmias and SCD or trios of cases with asymptomatic parents reveal a genetic cause, typically a mutation in RyR2. Generally diagnosed in the first two decades of life at the median age of 15 ± 10 years (Hayashi *et al.*, 2009). Prognosis is poor with 50% mortality in undiagnosed cases falling to 13% in treated cases; post diagnosis cerebral damage is not uncommon especially if the first instance was severe and the survival rate at 10 years post-diagnosis is 40% (Leenhardt *et al.*, 1995; Sumitomo, 2003; Hayashi *et al.*, 2009).

The diagnosis of CPVT is problematic as resting ECG is normal and exercise ECG can be complicated, Figure 1-20 (van der Werf and Wilde, 2013; Sumitomo, 2016). The initial cardiac events of CPVT can be dizzy spells or syncope but the severe first manifestation of the disease can be fatal, or subsequent fatal events can occur before diagnosis.

The pathogenic mechanism of CPVT is the aberrant release of Ca^{2+} during diastole from the SR via RyR2 channels. The increase in $[Ca^{2+}]$ during phase 4 of the cardiac AP results in DADs which make the sufferer prone to arrhythmia and especially

vulnerable to VT induced by β-adrenergic stimulation during emotional stress or physical exercise (Sumitomo, 2003; van der Werf and Wilde, 2013). Mutations in *RYR2* the gene encoding RyR2, are the leading cause of CPVT (Laitinen *et al.*, 2001; Priori *et al.*, 2001). Mutations in the genes encoding RyR2 associated proteins, e.g. *CASQ2* encoding calsequestrin-2, which are components of the macromolecular signalling complex are also associated with CPVT (Lahat, Pras, *et al.*, 2001). Multiple hypotheses have been proposed to explain how different mutations alter the activity of the RyR2 channel (Sumitomo, 2016). However, the net results of the mutations is a gain-of-function (GOF) in RyR2 causing increased P_O resulting in the diastolic leak of Ca^{2+} (Sumitomo, 2003).

Pathogenic mutations in the gene encoding RyR2 are the primary cause of CPVT accounting for between 50-79 % of cases depending on population (Laitinen *et al.*, 2001; Priori *et al.*, 2001; Sumitomo, 2016). The sequence encoding the CaM-binding region of RyR2 is one of the critical regions in which mutations have been observed to cluster (Xu *et al.*, 2010). The second major cause of CPVT accounting for 3-5 % of cases was found to be via *CASQ2* mutations, the gene encoding calsequestrin (Ackerman *et al.*, 2011; Faggioni, Kryshtal and Knollmann, 2012). CPVT of differing levels of severity have been associated with both autosomal dominant and recessive mutations in *CASQ2* with varying characteristics and penetrance (Lahat, Eldar, *et al.*, 2001; Lahat, Pras, *et al.*, 2001; Postma *et al.*, 2002; de la Fuente *et al.*, 2008; Roux-Buisson *et al.*, 2011; Josephs *et al.*, 2017). Calsequestrin-2 regulates RyR2 alongside another SR luminal protein, triadin. Mutation of *TRD*, the gene encoding triadin, has also been associated with CPVT (Roux-Buisson *et al.*, 2012). An

early onset, fully penetrant, highly malignant recessive form of CPVT in a single family mapped to a novel locus on chromosome 7p14-p22, but no causative mutation in candidate genes was identified (Bhuiyan *et al.*, 2007). Mutations in two other genes, *KCNJ2* and *ANK2*, have also been proposed to result in a CPVT phenotype, but previously other mutations in these genes were associated with forms of LQTS (Mohler *et al.*, 2004; Vega *et al.*, 2009).

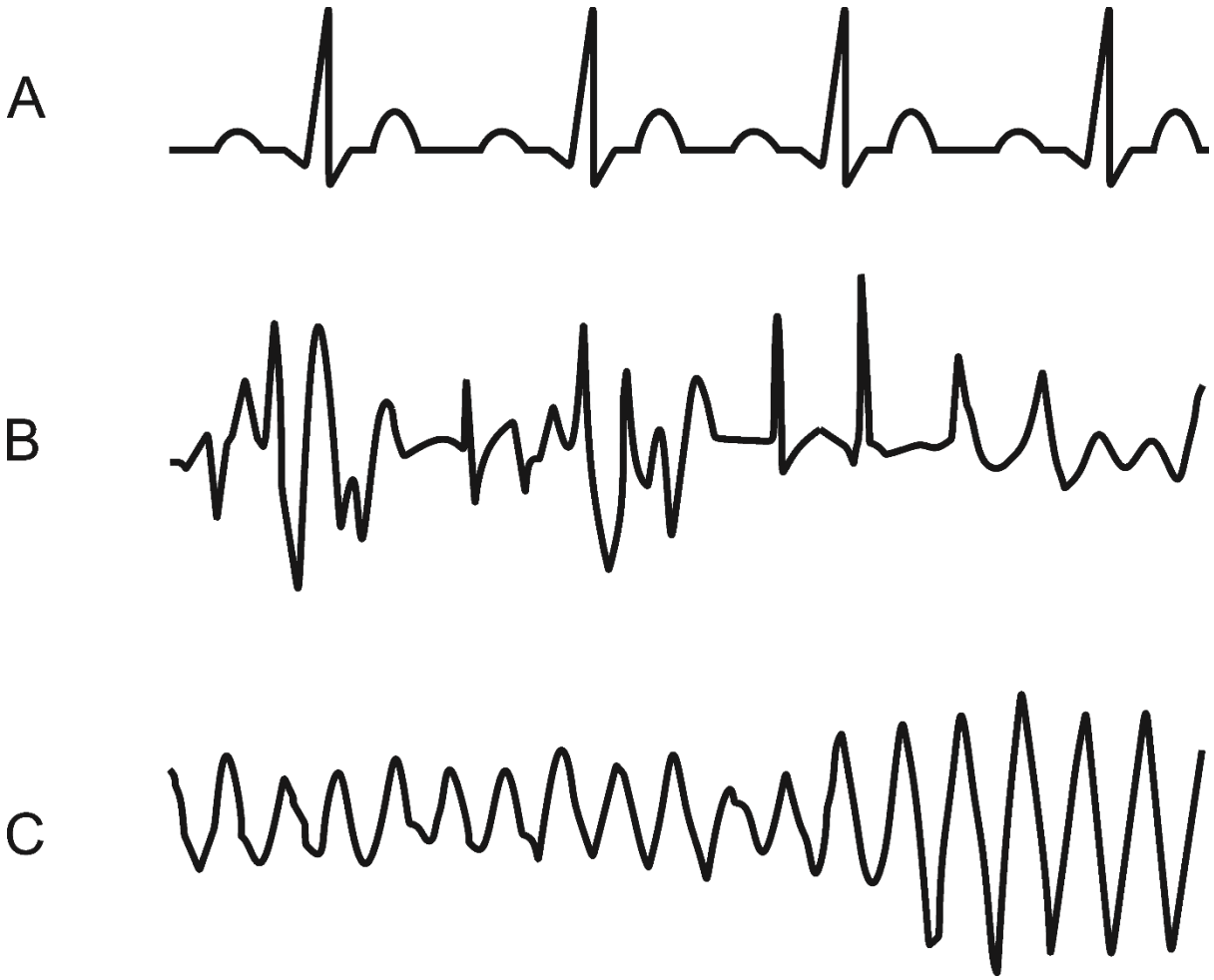

Figure 1-20 The ECG of CPVT Patients Changes from Rhythmic to Arrhythmic During Exercise

Illustration of the ECG of a CPVT sufferer showing the initial normal sinus rhythm at rest **(A)** which during exercise becomes arrhythmic (B and C). The cardiac rhythm becomes tachycardic **(B)** and has the potential to degenerate into fibrillation **(C)**.

1.6.1.3 Long QT Syndrome

Long QT arrhythmias are a heterogeneous group of acquired and congenital cardiac electrical diseases which share characteristic ECG abnormalities including prolongation of the QT interval and disturbed T waves (Shah, Park and Alweis, 2019). While in the majority of clinical cases long QT is acquired, the prevalence of the congenital long QT syndrome (LQTS) is estimated to be 1 in 2000 (Schwartz *et al.*, 2009; Shah, Park and Alweis, 2019). LQTS is an inherited cardiac channelopathy which results in abnormal ventricular repolarisation events that appear on an ECG as prolonged QT intervals and can cause lethal ventricular arrhythmias (Priori *et al.*, 2003; Goldenberg, Zareba and Moss, 2008; Roden, 2008).

The prolonged QT interval has the potential to progress to the characteristic abnormal heart rhythm torsades de pointes (TdP) which can degenerate into VT and lead to SCD (Schwartz, Periti and Malliani, 1975). LQTS can be accompanied by deafness from birth, is associated with syncope, ventricular arrhythmia and SCD, and is a significant cause of sudden death in young people (Schwartz, Periti and Malliani, 1975). The initial presentation is dizzy spells and syncope which can be associated with exercise or stress (Diercks *et al.*, 2004). In arrhythmia patients with an ECG displaying a prolonged QT interval and no secondary causes, congenital LQTS is confirmed by scoring from set diagnostic criteria and genotyping in 15 susceptibility genes (Priori *et al.*, 2013).

Currently, 15 types of “classical” LQTS and an additional two types which also result in congenital deafness are recognised (Priori *et al.*, 2013; Nakano and Shimizu,

2016). Genetic studies have linked 235 different mutations spread across 15 genes with LQTS, with 80% of cases genotype positive in one of the three major susceptibility genes commonly associated with the three main types of LQTS (Napolitano *et al.*, 2005; Shimizu *et al.*, 2009; Nakano and Shimizu, 2016).

The prolonged QT interval appears to be the result of EAD during phase 3 of the cardiac AP (Goldenberg, Zareba and Moss, 2008). Mutations in the K^+ channels are characterised as causing a loss of function (LOF) which results in a reduced efflux of K^+. Meanwhile, the Na^+ channel mutations result in a GOF with increased Na^+ influx which in turn causes increased in Ca^{2+} influx (Moss, 2005). All the changes in ion channel activity result in a rise in TMP and an arrhythmogenic prolongation in cardiac AP (Nakano and Shimizu, 2016).

Mutations in additional genes *KCNJ2*, *CACNA1C* and *SCN4B* that encode K^+, Ca^{2+} and Na^+ selective channels respectively, have been linked with rarer, familial forms of LQTS and prolonged QT interval (Goldenberg, Zareba and Moss, 2008). The mutations result in reduced K^+ efflux and increased influx of Ca^{2+} and Na^+ leading to an increased cardiac AP and proarrhythmic EADs during phase 3 of the cardiac AP (Plaster *et al.*, 2001; Splawski *et al.*, 2004; Medeiros-Domingo *et al.*, 2007). AEDs which extend membrane repolarisation and prolong QT intervals can also be caused by dysfunctional activity in ion channel associated proteins (Goldenberg, Zareba and Moss, 2008). Mutations in genes for ankyrin B a cytoskeletal protein that interacts with NCX and IP_3R, and caveolin-3 which interacts with a voltage-gated Na^+ channel have been linked with types of LQTS (Mohler *et al.*, 2003; Vatta *et al.*, 2006).

In arrhythmia patients, a diagnosis of congenital LQTS follows an ECG meeting set criteria including a prolonged QT interval and positive genotype for a pathogenic mutation in an LQTS associated gene (Priori *et al.*, 2013). LQTS is associated with mutations in 15 susceptibility genes. Like CPVT there is an increasing number of loci. However, 72-80 % of LQTS cases harbour mutations in one of three genes encoding ion channels of electrophysiological importance (Napolitano *et al.*, 2005; Shimizu, 2008; Kapplinger *et al.*, 2009). The three major LQTS susceptibility genes are *KCNQ1* and *KCNH2* which encode the voltage-gated K^+ channels $K_V7.1$ and $K_V11.1$, and *SCN5A* encoding the voltage-gated Na^+ channel $Na_V1.5$. (Wang *et al.*, 1995; Ghosh, Nunziato and Pitt, 2006; Cordeiro *et al.*, 2010). Mutations in *KCNQ1*, *KCNH2*, and *SCN5A* are associated with 30%–35%, 25%–40%,5%–10% of LQTS cases, respectively (Ackerman *et al.*, 2011).

Notable amongst the remaining susceptibility genes is *CACNA1C* the gene encoding the α-1 $Ca_V1.2$ subunit of the L-type VGCC. Mutations in *CACNA1C* are associated with Timothy syndrome (TS), a rare multisystem disorder with a range of severe symptoms throughout the body including a malignant form of LQTS (Splawski *et al.*, 2004, 2005). A milder form of LQTS lacking the typical TS characteristics is also associated with *CACNA1C* mutations (Boczek *et al.*, 2013; Fukuyama *et al.*, 2014; Wemhöner *et al.*, 2015). Some of the LQTS only *CACNA1C* mutations occur in the C-terminus cytoplasmic domain (Fukuyama *et al.*, 2014; Wemhöner *et al.*, 2015). $Ca_V1.2$ contains multiple CaM-binding sites including a CaM-binding region with an IQ motif in the C-terminus cytoplasmic domain (Asmara *et al.*, 2010).

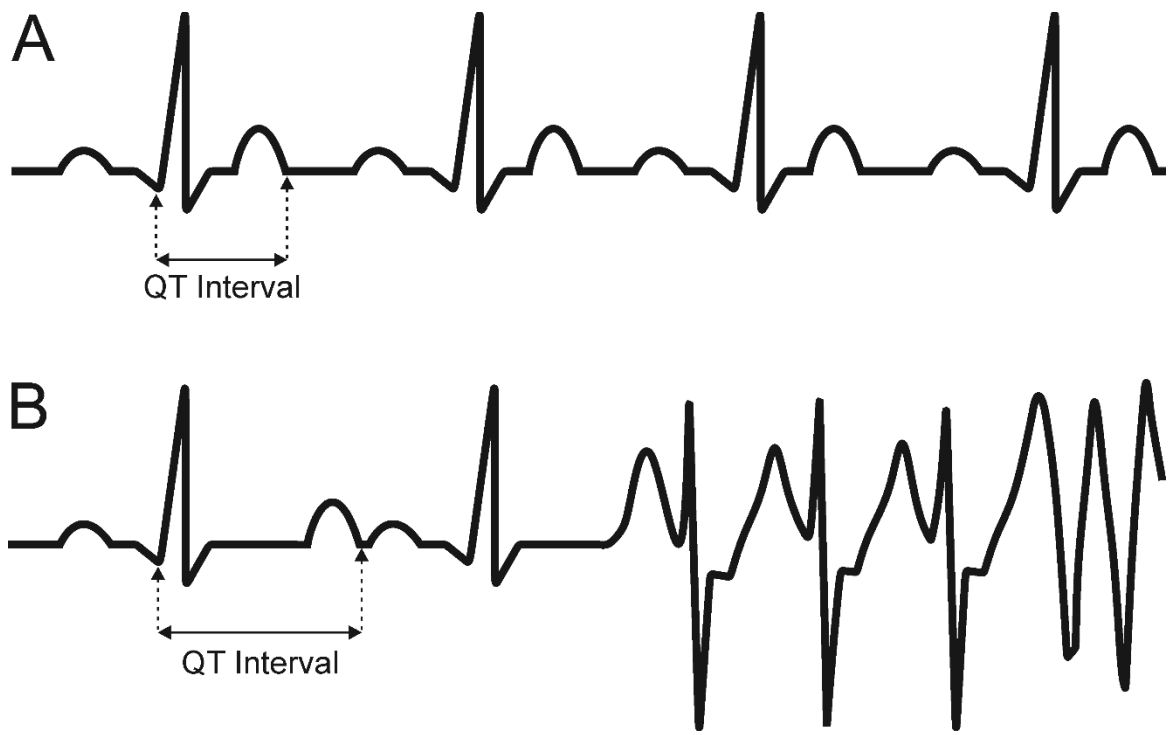

Figure 1-21 A Prolonged QT Interval is Potentially Arrhythmogenic

Illustration of the ECG of normal sinus rhythm **(A)** compared to that of an LQTS sufferer **(B)**. The prolonged QT interval at rest can degenerate into tachycardia and fibrillation during exercise.

1.6.1.4 Idiopathic Ventricular Tachycardia

The classification Idiopathic Ventricular Tachycardia/Fibrillation (IVT) applies to cardiac arrhythmias of unknown origin in morphologically normal hearts characterised by rapid onset VF leading to syncope, MI and SCD. The aetiology may remain unknown despite extensive clinical investigation and could be a novel genotype, genetic loci or phenotype, e.g. ECG not fitting established criteria (Maury *et al.*, 2010). The established channelopathies, i.e. CPVT, LQTS, were described initially as IVT until characteristics and aetiologies were defined (Visser *et al.*, 2016). Despite advances in genetic screening enabling increased diagnosis of channelopathies, arrhythmias with novel characteristics, genetic background or both are still described as IVT (Wijeyeratne and Behr, 2017). Potentially, any change to the flow of ions in cardiac myocytes will disrupt physiological cardiac AP leading to arrhythmia (Ackerman *et al.*, 2011). Therefore, the cause of IVT could be monogenic, polygenic or multifactorial including inherited characteristics. Interestingly, IVT cases with novel arrhythmia phenotypes also carry putative CPVT mutations in *RYR2* (Kron, Ellenbogen and Abbate, 2015; Fujii *et al.*, 2017).

1.6.2 Ryanodine Receptor Channelopathies

1.6.2.1 Disease-Causing Mutations of the Ryanodine Receptor

RyR1 and RyR2 are encoded by *RYR1* and *RYR2* respectively. Mutations in RYR1 & *RYR2* show strong linkage to diseases of skeletal and cardiac muscle (Manning *et al.*, 1998; Laitinen *et al.*, 2001). The shared characteristic of the pathogenic mutations is an inappropriate release of Ca^{2+}. The aberrant Ca^{2+} release can manifest as large

spontaneous Ca^{2+} release resulting in delayed de-polarisation or a stream of Ca^{2+} through a “leaky” channel leading to reduced [Ca^{2+}] in the SR and muscle weakness (Betzenhauser and Marks, 2010; Priori and Chen, 2011; Reddish *et al.*, 2017; Jungbluth *et al.*, 2018). Additionally, the inability of RyR2 to maintain a stable closed conformation due to acquired defects is instrumental in the clinical hallmarks observed during HF (Fischer, Maier and Sossalla, 2013).

RyR1 channelopathies constitute a significant cause of congenital myopathies, in particular, Central Core Disease (CCD) and the associated condition MH (Jungbluth *et al.*, 2018). To date, ~300 mutations linked to CCD, MH and other congenital myopathies have been identified throughout RyR1 (MacLennan and Zvaritch, 2011). The majority cluster in three hot spots (HS) corresponding to the amino-terminal $RyR1^{1-614}$ (HS1), a central region $RyR^{2101-2458}$ (HS2) and the pore-forming C-terminal of $RyR1^{3916-4990}$ (HS3) (MacLennan and Zvaritch, 2011; Reddish *et al.*, 2017).

Channelopathies of RyR2 commonly result in the arrhythmogenic disorder CPVT (Betzenhauser and Marks, 2010). Mutations in *RYR2* and *CASQ2* the genes encoding the components of the SR Ca^{2+} channel complex in cardiomyocytes are linked to CPVT1 and CPVT2 respectively (Liu and Priori, 2008). Mutations in *RYR2* were found to cosegregate in families with a history of CPVT and SCD (Laitinen *et al.*, 2001). Approximately 70 *RYR2* mutations associated with CPVT1 occur in three HS, $RyR^{277-466}$ (HS1), $RyR^{22246-2534}$ (HS2), and $RyR^{23778-4967}$ (HS3), (Priori and Chen, 2011; Priori and Napolitano, 2014). The HS correspond to those for CCD/MH in RyR1 and occur in regions highly conserved in RyR across species and between isoforms (MacLennan and Zvaritch, 2011; Priori and Chen, 2011).

The shared locations and effects of the RyR mutations suggest shared mechanisms for induction of dysfunctional Ca^{2+} release by the SR channels. Proposed disease mechanisms include a lowered threshold for SOICR, the reduced binding affinity of FKBP12.6, and “domain unzipping” the disruption of inter-domain interactions (Liu and Priori, 2008).

1.6.2.2 Pathological Store Overload-Induced Calcium Release

Mutations in *RYR1* can result in CCD, MH or a mixed phenotype (CCD/MH) of RYR1 depending on the mutation carried in the protein. The mutations characterised show dysfunctional RyR1 activity; varying levels of Ca^{2+} leakage and spontaneous release of Ca^{2+} (Tilgen *et al.*, 2001; Dirksen and Avila, 2004; Brini *et al.*, 2005; Sato, Pollock and Stowell, 2010). A reduction in SR [Ca^{2+}] and increase in cytosolic [Ca^{2+}] is observed in CCD and CCD/MH mutants but not in MH mutants (Tilgen *et al.*, 2001; Dirksen and Avila, 2004; Brini *et al.*, 2005). The leak of Ca^{2+} is pronounced in CCD, yet small enough in mutations linked to MH to be compensated for by the Ca^{2+} uptake mechanism of the cell (Dirksen and Avila, 2004; Brini *et al.*, 2005). Compared to wildtype, the channels of both MH/CCD and MH mutants are hypersensitive to agonists while CCD mutants show reduced sensitivity or are hypersensitive (Brini *et al.*, 2005; Sato, Pollock and Stowell, 2010).

The effect of the mutations on channel opening is inconsistent with a higher P_O, potentially due to coincidental alterations in the ryanodine binding site (Sato, Pollock and Stowell, 2010). Reduced sensitivity to cytosolic Ca^{2+} and Excitation-Contraction

Uncoupling have been proposed as the pathophysiological mechanism of the mutations linked to CCD alone (Avila, O'Brien and Dirksen, 2001; Du *et al.*, 2004).

Dysfunctional SOICR due to a reduction in the threshold of luminal [Ca^{2+}] required for channel activation has also been proposed as the disease mechanism for both MH/CCD and CPVT linked mutations. In MH/CCD sufferers the activation threshold is further reduced by volatile anaesthetics, increasing the sensitivity of RyR1 to changes in luminal [Ca^{2+}] and increasing the likelihood of spontaneous channel opening (Priori and Chen, 2011). The resulting raised cytosolic [Ca^{2+}] leads to hypermetabolism. In CPVT patients during exercise, β-adrenergic stimulation induces enhanced Ca^{2+} uptake by the SR raising the luminal [Ca^{2+}] beyond the abnormally lowered threshold for Ca2+ release increasing the likelihood of spontaneous Ca^{2+} release (MacLennan and Chen, 2009).

RYR2 mutations were identified in families and cases with a history of ventricular arrhythmias and SCD, and characterised in cell models. A gain-of-function (GOF), manifested as increased SOICR activity was identified. Generally, all showed a higher propensity and frequency of spontaneous Ca^{2+} oscillations, reduced store content and higher sensitivity to agonists, especially under conditions mimicking catecholaminergic stress. While increased channel opening due to SOICR was observed at lower luminal [Ca^{2+}] levels sensitivity to cytosolic Ca^{2+} was inconsistent. (D. Jiang *et al.*, 2002; Jiang *et al.*, 2004, 2005; Jones *et al.*, 2008; Liu *et al.*, 2013; Wangüemert *et al.*, 2015). No change in binding or interaction between FKBP12.6 and RyR2 was observed (Jiang *et al.*, 2005; Jones *et al.*, 2008).

Previously, enhanced agonist-induced Ca^{2+} release in cardiomyocytes bearing CPVT associated mutations was observed despite no change in RyR2–FKBP12.6 binding (George, Higgs and Lai, 2003). Accordingly, it was proposed that CPVT1 is the results of a reduction in the luminal [Ca^{2+}] threshold required for activation causing pathological SOICR (MacLennan and Chen, 2009). A notion that has been encouraged by the identification of mutations of cardiac-specific calsequestrin-2 linked to CPVT2 (Faggioni, Kryshtal and Knollmann, 2012).

Mutagenesis of a critical highly conserved residue in RyR2 abolishes SOICR but not CICR and protects against VT induced by excess Ca^{2+} (Chen *et al.*, 2014). An *RYR2* mutation linked to CPVT, characterised with dysfunctional SOICR and intact binding with FKBP12 and 12.6 binding, but the termination threshold of SOICR regulated by FKBP is elevated (Zhang *et al.*, 2016). Conversely, a novel RyR2 mutation was identified in an arrhythmia patient displaying normal RyR2 channel CICR activity with altered gating. The mutation was characterised as loss of function (LOF) because levels of spontaneous channel openings and SOICR were reduced due to loss of sensitivity to luminal Ca^{2+} (Jiang *et al.*, 2007).

1.6.2.3 Dysfunctional FKBP Binding

In HF animal models, partial disassociation of FKBP12.6 from RyR results in conformational change, dysfunctional regulation and defective Ca^{2+} release from the SR (Yamamoto, 1999; Ono *et al.*, 2000; Yano *et al.*, 2000). RyR channels unable to bind FKBP12.6 are more sensitive to cytosolic Ca^{2+} lowering the activation threshold of the channel (Marx *et al.*, 2000). Treatment with β-blockers restores FKBP12.6

binding resulting in corrected RyR2 structure and function, and improved cardiac performance (Reiken *et al.*, 2001, 2003; Doi *et al.*, 2002). In HF models, the cardioprotective Ca^{2+} channel antagonist JTV519 enhances binding between and prevents disassociation of RyR2 and FKBP12.6, stabilising the closed channel conformation (Kohno *et al.*, 2003; Wehrens, 2004). Treatment with JTV519 ameliorates the severity of HF by restoring the correct conformation of RyR2 preventing the leak of Ca^{2+}, LV remodelling, ventricular arrhythmias which can cause SCD, and improving cardiac and skeletal function (Yano *et al.*, 2003; Wehrens, 2004; Wehrens *et al.*, 2005). FKBP12.6 improves heart function in failing hearts in mice following MI (Huang *et al.*, 2006).

However, some studies have identified mutations associated with CPVT which show spontaneous Ca^{2+} release but no alteration to RyR2/FKBP binding (George, Higgs and Lai, 2003; Jiang *et al.*, 2005; Jones *et al.*, 2008).

1.6.2.4 Domain Unzipping

The interaction between the N-terminal and central domains of RyR1 regulates channel function through the formation of a “domain switch”, conformational constraints that stabilise and maintain the closed state of the SR Ca^{2+} channel. The release of the interdomain contacts, in response to E-CC or pharmacological antagonists, lowers the threshold for channel opening, increasing P_O. Mutations in HS1 and HS2 of RYR1 change the residues of the N-terminal and central region causing “domain unzipping” due to poor, weakened or absent interactions. The loss of interactions results in a hypersensitive SR Ca^{2+} channel with increased P_O and the

likelihood of inappropriate opening (Yamamoto, El-Hayek and Ikemoto, 2000; Yamamoto and Ikemoto, 2002). The muscle relaxant dantrolene used to treat MH inhibits aberrant Ca^{2+} release by blocking domain unzipping of RyR1 (Kobayashi *et al.*, 2005).

In failing hearts, Ca^{2+} leaks from the SR via RyR2 channels which no longer bind FKBP12.6 and are destabilised by domain unzipping (Oda *et al.*, 2005). Therapeutic restoration of the interdomain interactions with dantrolene stops the Ca^{2+} leakage and improves contractile function (Yamamoto *et al.*, 2008; Kobayashi *et al.*, 2009). Mutagenesis of critical residues in CaMBD2 disrupting CaM binding result in a cardiomyopathic phenotype (Yamaguchi *et al.*, 2007). Recapitulation of an arrhythmogenic mutation in an animal model, a single base substitution in RyR2, disrupted CaM binding and intra-subunit interactions. Alterations in channel function resulted in spontaneous Ca^{2+} release in response to low levels of Ca^{2+} leading to a CPVT phenotype. Treatment with excess CaM and therapeutic agents (dantrolene) restored interactions, resolved the aberrant Ca^{2+} release and cardiac arrhythmias (Uchinoumi *et al.*, 2010; Xu *et al.*, 2010). Recently, an induced HF animal model which included disrupted CaM binding and arrhythmias was corrected by a modified CaM with a higher affinity for RyR2, corrected and restored CaM binding (Kato *et al.*, 2017).

1.6.2.5 CPVT: The Result of Diverse Pathological Mechanisms

The aetiology of congenital arrhythmogenic disorders is the dysfunctional release of Ca^{2+} from the SR (Priori and Chen, 2011). The conformational changes required for RyR2 channel function likely involve multiple functional domains which have mapped

to the location of many CPVT associated mutants (George *et al.*, 2007). Potentially, a mutation in any of these domains could disrupt the interactions resulting in similar phenotypes. Additionally, mutations in critical residues also adversely affect channel function directly. Any mutation mediated mechanism disrupting channel function has the potential to lead to a ventricular arrhythmia which could be classified as CPVT (Ackerman *et al.*, 2011).

Mutations associated with CPVT with no alteration in SOICR that cause LOF by increasing cytosolic Ca^{2+} sensitivity and GOF by reducing Ca^{2+} permeation have been reported (Marjamaa *et al.*, 2011; Roston *et al.*, 2017). Also, an *RYR2* mutant identified in a high penetrance severe form of CPVT was shown to have increased sensitivity to both luminal and cytosolic Ca^{2+} and abnormal PKA phosphorylation potentially altering FKBP binding (Loaiza *et al.*, 2013). By altering conformational stability, an *RYR2* mutant can both induce aberrant Ca^{2+} release and alter the penetrance of CPVT by affecting the expression of the mutated protein (Liu *et al.*, 2017). Recently, a novel RyR2 mutation caused CPVT characterised with an abnormal Ca^{2+} release due to an over tight CaMLD and CaMBD interaction preventing CaM binding and stabilising the closed conformation (Nishimura *et al.*, 2018)

Other arrhythmogenic conditions associated with *RYR2* mutations display a diversity of phenotypes and altered RyR2 channel characteristics. Two *RYR2* mutations cosegregated in families with histories of VF and SCD which were not linked to exercise or physiological stress classified as a form of IVT (Paech *et al.*, 2014). Also, of four *RYR2* mutations associated with a short-coupled variant of TdP (scTdP), a form of IVT, three displayed spontaneous Ca^{2+} oscillations and alterations to the

luminal [Ca^{2+}] indicating abnormal SOICR events. The fourth showed few sporadic Ca^{2+} transients, no change in luminal [Ca^{2+}], and significant release of Ca^{2+} in response to agonist stimulation but low channel activity (Fujii *et al.*, 2017). A RyR2 mutation was linked to a phenotype of arrhythmogenic right ventricular cardiomyopathy/dysplasia (ARVC/D) spectrum including aspects of CPVT (Stattin *et al.*, 2012). However, an *RYR2* mutation mediated CPVT phenotype can be modified by other congenital abnormalities to induce CPVT treatment responsive IVT (Kron, Ellenbogen and Abbate, 2015). Mutations of RyR2 can result in phenotypes that result in a diagnosis of LQTS, IVT, bradycardia or ARVC/D (Stattin *et al.*, 2012; Roux-Buisson *et al.*, 2014; Leinonen *et al.*, 2018; Miyata *et al.*, 2018)

Historically, there was a variety of clinical impediments which prevented the correct, timely, (mostly 2-3 years but as much as nine years) diagnosis of CPVT and distinguish it from LQTS (Siegers *et al.*, 2014; Behere and Weindling, 2016). There are an estimated 30% of CPVT cases misdiagnosed as “LQTS with normal QT intervals” or “concealed LQTS” (Priori, Napolitano and Schwartz, 1999; Medeiros-Domingo *et al.*, 2009). The sheer size of *RYR2* hampered thorough analysis with molecular diagnosis by screening for mutations limited to regions known to contain disease-associated mutations.

Increasingly, large cohort studies are analysing greater portions of the entire *RYR2* coding sequence of SCD, and unclassified, CPTV, LQTS and IVT arrhythmia cases. These studies have challenged the previously held views that RyR2 mutations are rare, that deleterious and disease-causing mutations only occur in HS1-3, and produced only a CPVT1 phenotype with the first cardiac event related to physical or

emotional stress (Tester *et al.*, 2005, 2007; van der Werf and Wilde, 2013; Tanaka *et al.*, 2015; Roston *et al.*, 2018). Of cases lacking LQTS causing mutations but diagnosed as LQTS, 6% were found to contain potential CPVT *RYR2* mutations; this rose to 31% of cases classified as “atypical/possible LQTS” (Tester *et al.*, 2005; Medeiros-Domingo *et al.*, 2009). A case of arrhythmia was recently reported with a prolonged QT interval later diagnosed as CPVT that harboured an arrhythmogenic *RYR2* mutation (Tanaka *et al.*, 2015). Also, molecular autopsies in cohorts of sudden unexplained fatalities with no structural heart defects have revealed a high prevalence of CPVT associated *RYR2* mutations with the first instance of the disease being SCD (Tester *et al.*, 2004, 2012; Tester and Ackerman, 2006; Larsen *et al.*, 2013; Roston *et al.*, 2018).

The corollary of improved screening in arrhythmia cases is that mutations in novel loci that confer susceptibility to CPVT and other cardiac arrhythmias are being identified. As can be seen in Figure 1-22 mutations in multiple overlapping genes that encode ion channels and associated proteins have been linked to forms of CPVT, LQTS or both.

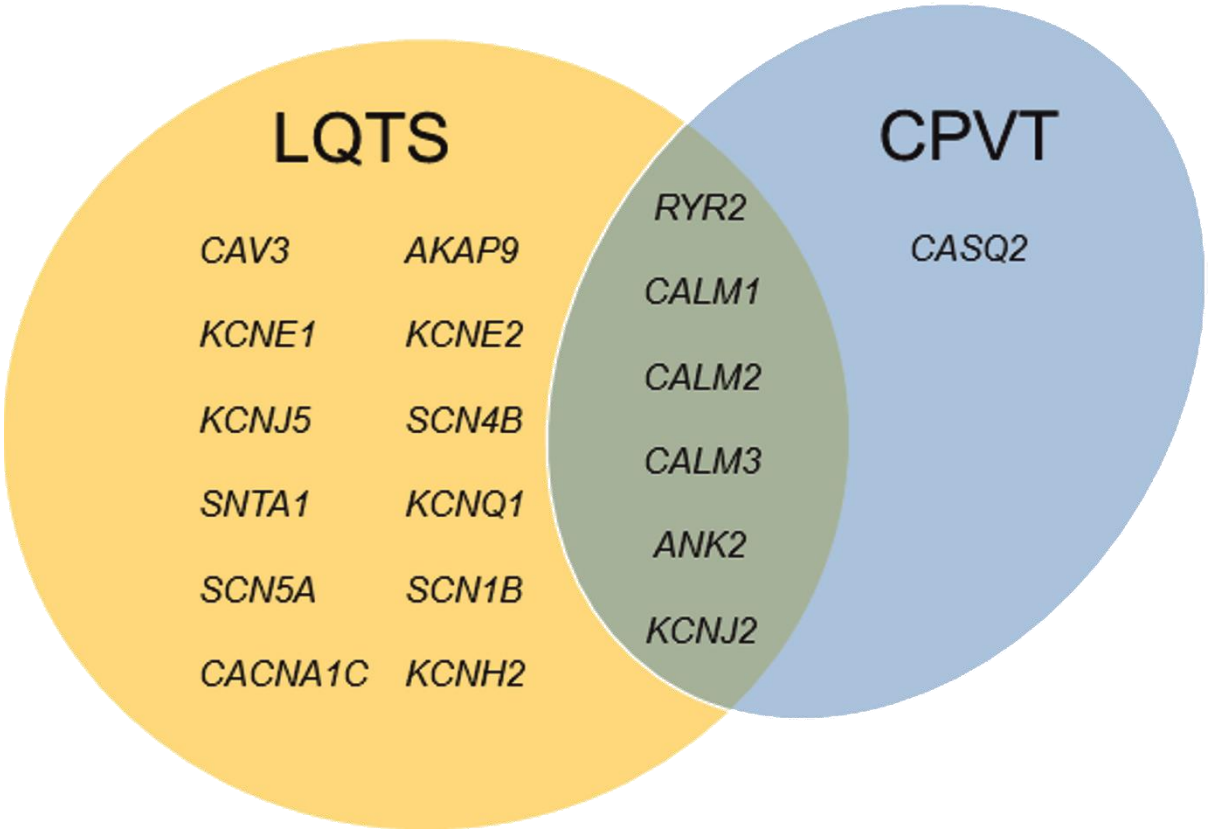

Figure 1-22 Mutations in Multiple Overlapping Genes Associate with LQTS and CPVT

Venn diagram showing the genes, the pathological variations of which are associated with LQTS, CPVT or both. The genes encode cardiac ion channels or associated proteins. Other channelopathies, e.g. Brugada syndrome or Short QT syndrome are associated with some of the genes listed in addition to being associated with other genes. Image after figure first published (Fernández-Falgueras et al., 2017)

1.7 Aims and Objectives

1.7.1 Hypothesis

PLCζ is a sperm-specific PI-PLC isozyme with unique biochemical characteristics. Structural and biophysical analysis of bacterially expressed, recombinant PLCζ will help to unravel the complicated regulatory mechanism of this enzyme, which is required for life to begin. X-ray diffraction data to determine the high-resolution 3D structure of PLCζ would reveal potential lipid, protein and ion binding sites necessary for function and regulation. Due to the sperm-specific expression of PLCζ it is unfeasible to extract enough native protein for crystallisation. Therefore, recombinant protein will be required, the functionality of which can be confirmed with an existing activity assay.

A key question is the existence and identity of a binding partner for PLCζ which may regulate activity. Recently, a novel interaction and regulation of PLCζ by the ubiquitous Ca^{2+} sensing regulatory protein CaM was demonstrated (Nomikos, Thanassoulas, *et al.*, 2017). CaM regulates a wide variety of cellular processes by interacting with and modulating the activity of many diverse proteins in response to changes in Ca^{2+}. Recombinant CaM could be used to investigate the structure of PLCζ by acting as a binding partner to facilitate crystallisation while also investigating the nature of a binding complex between the two. However, fidelity and functionality of the recombinant CaM produced will require confirmation by biophysical analysis. Also, existing assays will be used to measure and confirm the regulation of RyR2 by recombinant CaM.

RyR2 is the cardiac-specific Ca^{2+} channel which regulates intracellular Ca^{2+} release during the heartbeat and is a major binding partner of CaM. Recently, mutations in the genes encoding CaM have been associated with clinical cases of cardiac arrhythmia including CPVT. CPVT is commonly associated with mutations in the gene encoding RyR2. Given the role of CaM in regulating so many proteins including ion channels involved in cardiac function, the exact pathophysiological mechanisms of the CaM mutants are currently an area of intense study. Biophysical and functional analysis using existing assays can be used to characterise the mutations and assess any alterations in the ability of CaM to interact with and regulate RyR2.

This thesis will investigate strategies to elucidate the 3D structure of PLCζ, whether CaM interacts specifically with PLCζ and whether derangement of the regulation of RyR2 by CaM is an aetiological factor in new inherited cardiac arrhythmias.

1.7.2 Project Aims

Investigate interaction of PLCζ with ions and other proteins, i.e. Ca^{2+} and CaM.

Characterise mutations of CaM linked with arrhythmogenic channelopathies particularly Ca^{2+} binding properties, and interaction with and regulation of RyR2. Altered interaction between mutant CaM and RyR2 maybe pathogenic and could provide insight into the regulation of RyR2 activity by CaM.

Produce protein crystals to elucidate the tertiary structures of PLCζ or individual domains, CaM mutants, and binding complex of wild-type CaM and PLCζ. The CaM

tertiary structures could reveal pathogenic mutation mediated alterations to the structure of CaM. Meanwhile, the tertiary structure of full length, domains and binding complexes of PLCζ may inform the mechanism and regulation of PLCζ activity with particular reference to the role of CaM binding.

1.7.3 Project Objectives

The following work will be carried out to address the above aims.

- Molecular cloning of DNA sequences corresponding to PLCζ and CaM into plasmids for bacterial expression.
- Optimisation of bacterial expression of recombinant protein suitable for purification to yield soluble protein, preferably untagged corresponding to full-length and truncated PLCζ and wild-type CaM, and full-length mutant CaM
- Establish and demonstrate fidelity and functionality of recombinant protein using established activity and functional assays.

Chapter 2 - MATERIALS AND METHODS

2.1 Materials

Unless stated otherwise, chemicals and reagents used in this study were of analytical grade and obtained from either Fisher Scientific or Sigma-Aldrich. Unless there is a stated supplier, all solutions were laboratory prepared. All deionised water (DI H_2O) used in this study was Ultrapure Type I produced using a PURELAB® Option-Q Water purification system (ELGA LabWater). All solutions were stored at room temperature unless otherwise stated. The pH of buffers containing sodium chloride (NaCl) was adjusted with either hydrochloric acid (HCl) or sodium Hydroxide (NaOH), while either potassium hydroxide (KOH) or HCl was used to adjust the pH of buffers containing potassium chloride (KCl).

2.1.1 Microbiology

Glassware, plasticware, growth media, antibiotics and reagents used were all pre-sterilised. Solutions sterilised by filtration were passed through 0.22 µm Millex-GP Syringe Filters (Merck). Autoclave sterilisation conditions were 121 °C for 22 min. The absorbance of cultures was measured using disposable 1.5 ml semi-micro cuvettes (Fisher). Pipette tips (VWR) were racked, sealed and sterilised by autoclave before use. Pre-sterilised spreaders were from Microspec. All other plasticware was obtained pre-sterilised from Fisher Scientific and Greiner Bio-One.

2.1.1.1 General Microbiology Reagents

- Calcium chloride ($CaCl_2$), 1 M stock prepared using $CaCl_2 \cdot 2H_2O$, filter sterilised and stored at 4°C.

- IPTG (Formedium), 1 M stock prepared as required, filter sterilised and kept on ice.
- Glycerol, 50 % (w/v) stock, sterilised by autoclave
- 70 % Industrial Methylated Spirits (IMS), 70 % (v/v) Pure Methylated Spirit (94% (v/v)).
- Ethanol, Molecular Biology Grade Absolute Ethanol (200 Proof).

2.1.1.2 Preparation of Liquid Bacterial Media

Lennox formulation of Lysogeny Broth (LB) was used throughout and was prepared by dissolving LB Medium Lennox (Formedium) in DI H_2O (20 g/L). The suspension was sterilised immediately by autoclave. Sterilised LB was kept sealed and stored at room temperature until use. Before the addition of antibiotics, LB was cooled until <50°C and then stored at 4 °C until use.

2.1.1.3 Preparation of Solid Bacterial Media

LB-agar was prepared by preparing LB as described in 2.1.1.2 but with the addition of Agar (Sigma) (15 g/L) before sterilisation. The molten LB-agar was cooled until <50 °C before the addition of antibiotics if required. The molten LB-agar was then poured into a Petri dish and allowed to set (LB-agar plate). LB-agar plates were sealed with parafilm and stored inverted at 4 °C until required, for no longer than one month.

2.1.1.4 Antibiotics

The stock solutions and working dilutions of the antibiotics used in this study are in Table 2-1. Ethanol was used to prepare stock solutions of chloramphenicol. DI H_2O was used to prepare stock solutions of all other antibiotics which were also filter sterilised and aliquoted into single-use aliquots. All stock antibiotic solutions were stored at -20 °C. The stock antibiotics were added directly to bacterial media to achieve the working dilution outlined in Table 2-1. Unless stated otherwise, all media contained antibiotics appropriate for the bacterial strain and plasmid being cultured.

Table 2-1 Selective antibiotics used in this study

Antibiotic	Supplier	Stock solution	Working solution
Kanamycin	Formedium	10 mg/ml	100 µg/ml
Ampicillin	Formedium	100 mg/ml	100 µg/ml
Chloramphenicol	Merck	34 mg/ml	68 µg/ml
Streptomycin	Fisher Scientific	50 mg/ml	50 µg/ml

2.1.1.5 Bacterial Strains

The strains of *E.coli* used in this study, source, purpose and antibiotic resistance are summarised in Table 2-2. Unless stated otherwise, all bacteria strains were cultured in the presence of the selective antibiotics.

Table 2-2 Bacterial strains used in this study

Strain	Use	Source	Selection
BL21(DE3)	Protein expression	Invitrogen	None
BL21(DE3)pLysS	Protein expression	Invitrogen	Chloramphenicol
Rosetta™ (DE3)	Protein expression	Invitrogen	Chloramphenicol
Rosetta™(DE3)pLysS	Protein expression	Invitrogen	Chloramphenicol
Rosetta-gami™ 2(DE3)	Protein expression	Invitrogen	Chloramphenicol
TOP10	Cloning and plasmid propagation	Invitrogen	None
BL21-CodonPlus(DE3)-RILP	Protein expression	Stratagene	Ampicillin
XL10 Gold Ultracompetent	Site-directed mutageneisis	Stratagene	Chloramphenicol
CH184	Protein expression		Streptomycin

2.1.2 Protein Biochemistry

2.1.2.1 General Lab Reagents

- Sodium dodecyl sulfate (SDS), 10 % (w/v) stored for six months at room temperature.
- Phosphate-buffered saline (PBS), prepared as required by dissolving PBS tablets (Sigma) in DI H2O per product instructions to yield 10 mM Sodium phosphate dibasic (Na2HPO4), 1.8 mM Potassium dihydrogen phosphate (KH2PO4) buffer, pH 7.4, 37 mM NaCl, 2.7 mM KCl.
- Lysozyme, lyophilised powder from chicken egg white 50000 units/mg, (Merck).
- Bovine serum albumin (BSA), 2 mg/ml BSA standard (BioRad).
- Protease inhibitors, cOmplete™, ethylenedinitrilo-tetraacetic acid (EDTA)-free Protease Inhibitor Cocktail tablets (Roche) either added directly to the solution at a ratio of 1 tablet per 50 ml or used to prepare a 10X stock stored at -20 °C until use.
- Tris Buffered Saline (TBS), 10X Stock 200 mM Tris, pH 7.4, 1.37 M NaCl.

2.1.2.2 SDS-PAGE

- Stacking gel buffer, 0.5 M Tris, pH 6.8.
- Separating gel buffer, 1.5 M Tris, pH 8.8.

- 10 % Ammonium persulfate (APS) 10 % (w/v) prepared as required and stored at 4 °C.
- Tetramethylethylenediamine (TEMED).
- Acrylamide, National Diagnostics ProtoGel™, 40 % (w/v) solution acrylamide/methylene bisacrylamide at ratio of 37.5:1 (Geneflow).
- Protein loading buffer, 5X Stock pH 6.8, 0.225 M Tris, 50 % (w/v) glycerol, 5 % (w/v) SDS, 10 % (v/v) β-Mercaptoethanol (β-ME), 0.05 % (w/v) bromophenol blue. Added directly to sample and final sample volume adjusted to 1X.
- SDS-PAGE Running buffer, 10X stock 250 mM Tris, 1.92 M Gly, 1 % (w/v) SDS. Diluted to 1X before use.
- Coomassie stain, 48 % (v/v) Methanol, 42 % (v/v) DI H_2O, 10 % (v/v) glacial acetic acid, 0.2% (w/v) Coomassie brilliant blue R-250.
- Coomassie de-stain, 45 % (v/v) Methanol, 45 % (v/v) DI H_2O, 10 % (v/v) glacial acetic acid.
- Protein molecular weight markers, ColorPlus™ Prestained Protein Ladder, Broad Range (10-230 kDa) and Color Prestained Protein Standard, Broad Range (11–245 kDa) both obtained from NEB. Precision Plus Protein™ All Blue Prestained Protein Standards obtained from BioRad. Dispensed upon on receipt into single-use aliquots and stored at -20 °C until use.

2.1.2.3 Immunoblotting

- Semi-dry transfer buffer, 48 mM Tris, 39 mM Gly, 0.0375 % (w/v) SDS, 20 % (v/v) methanol. Prepared as required.
- Blotting buffer, 1X TBS, 0.1 % (v/v) Tween-20. Prepared when required.
- Blocking buffer, 1X TBS, 0.1 % (v/v) Tween-20, 5%, (w/v) non-fat milk powder. Prepared when required.
- Bradford Reagent, 10 % (v/v) dilution of Bio-Rad Protein Assay Dye Reagent Concentrate (Bio-Rad) prepared as required and kept on ice. Addition of protein to the reagent causes a change in colour from brown to blue.
- Transfer membrane, Immobilon-P PVDF 0.45 µm pore size membrane (Merck). Pre-soaked in methanol for 1 min before use.
- Enhanced Chemiluminescent (ECL) reagents, Amersham ECL Prime Western Blotting Detection Reagent (GE Healthcare) A and B reagents mixed to 1:1 ratio just before use.
- X-ray Film, Amersham Hyperfilm ECL (GE Healthcare).

2.1.2.4 Protein Purification

- Ni-NTA Agarose (Ni-NTA) (Qiagen)
- Amylose resin (NEB)
- Columns, Thompson SINGLE StEP® Empty Columns (Generon)

- Purification buffer compositions varied depending on purification. Made as required and kept on ice.

- Lysis buffer, purification buffer supplemented with lysozyme and protease inhibitors. Made as required and kept on ice

- Cleaving buffer, PBS supplemented with 40 mM 1,3-bis(tris (hydroxymethyl)methylamino)propane (Bis-Tris) and 25 mM imidazole and adjusted to pH 6.

- Elution buffer, compositions varied depending on purification. Made as required and kept on ice.

2.1.2.5 Native Protein Purification

- Pig hearts obtained directly from the abattoir, kept chilled and processed immediately, see page 171.

- Homogenisation buffer, 10 mM PIPES·Na_2, pH 7.4, 0.3 M sucrose, 0.5 mM EDTA, 0.2 mM 4-benzenesulfonyl fluoride hydrochloride (AEBSF), 2 mM Dithiothreitol (DTT) (Formedium), protease inhibitors. Made as required and kept on ice.

- Resuspension buffer, 10 mM PIPES·Na_2, pH 7.4, 0.6 M KCl, 2 mM DTT, 0.2 mM AEBSF, protease inhibitors. Made as required and kept on ice.

2.1.2.6 Circular Dichronism

- 10 mM 2-(N-morpholino)ethanesulfonic acid (MOPS), pH 6.5, 50 mM KCl, including either 1 mM $CaCl_2$ or 1 mM EDTA.

2.1.2.7 Co-Immunoprecipitation

- Stock Buffer, 20 mM Tris-HCl, pH 7.4, 150 mM NaCl.
- Stock Ethylene Glycol Tetraacetic Acid (EGTA), 20 mM Tris-HCl, 1 mM EGTA, pH 7.4, 150 mM NaCl.
- Stock Ca^{2+}, 20 mM Tris-HCl, pH 7.4, 1 mM $CaCl_2 \cdot 2H_2O$, 150 mM NaCl.
- Protein-A beads, Protein A Sepharose® 4 Fast Flow (GE Healthcare).

2.1.2.8 Ryanodine Binding Assay

- General buffer, 20 mM PIPES·Na_2, pH 7.1.
- Stock buffer, 20 mM PIPES·Na_2, 300 mM KCl.
- Stock EGTA, 100 mM EGTA, 20 mM PIPES·Na_2, pH 7.1, 300 mM KCl.
- Stock Ca^{2+}, 100 mM $CaCl_2.2H_2O$, 20 mM PIPES·Na_2, pH 7.1, 300 mM KCl.
- [^{3}H]ryanodine, [9,21-^{3}H(N)]ryanodine, 100 Ci/mmol (Perkin Elmer).
- Unlabelled Stock, 1.5 mM ryanodine (Polvsciences Inc) in General buffer. Dispensed into 50 µL aliquots and stored at -20 °C until use.

- Cold ryanodine, 45 µM Unlabelled Stock in General buffer. Dispensed into 100 µL aliquots and stored at -20 °C until use.
- Hot ryanodine mix, 10 µL [^{3}H]ryanodine, 10 µL Cold Ryanodine, 380 µL General buffer.
- Wash buffer, 20mM Tris, pH 7.4, 200 mM KCl. Stored at 4 °C until use and during use kept on ice.
- Filters, Whatman™ Binder-Free Glass Microfiber Filters GF/F Circles (Fisher Scientific).
- Scintillant, Ultima Gold scintillation cocktail (Perkin Elmer).

2.1.2.9 Isothermal Titration Calorimetry

- ITC buffer, 10 mM 2-(N-morpholino)ethanesulfonic acid (MES), pH 6.5, 150 mM KCl.
- Stock EDTA, 100 mM EDTA in ITC buffer.
- Stock Ca^{2+}, 100 mM $CaCl_2.2H_2O$ in ITC buffer.

2.1.2.10 Crystallisation Experiments

- Stock Ca^{2+}, 100 mM $CaCl_2.2H_2O$ in ITC buffer.
- Cacodylic acid ($(CH_3)_2AsO_2H$) buffer pH 4.4, 50 mM Sodium Cacodylate ($(CH_3)_2AsO_2Na$), 5 mM $CaCl_2$, pH 4.4

- $(CH_3)_2AsO_2H$ pH 5.4 buffer, 50 mM (CH3)2AsO2Na, 5 mM $CaCl_2$, pH 5.4
- 55 % (v/v) 2-Methyl-2,4-pentanediol (MPD), pH 4.4, 50 mM $(CH_3)_2AsO_2Na$), 5 mM $CaCl_2$.
- 55 % (v/v) MPD, pH 5.4, 50 mM $(CH_3)_2AsO_2Na$), 5 mM $CaCl_2$.
- pH 4.2, 50 mM Sodium Acetate (NaOAc), 5 mM $CaCl_2$.
- pH 5.2, 50 mM NaOAc, 5 mM $CaCl_2$.
- 30 % (w/v) Polyethylene glycol 6000 (PEG-6000), pH 4.2, 50 mM NaOAc, 5 mM $CaCl_2$.
- 30 % (w/v) PEG-6000, pH 5.2, 50 mM NaOAc, 5 mM $CaCl_2$.
- JCSG screen, JCSG-plus™ HT-96 (Molecular Dimensions).
- PACT screen, PACT premier™ HT-96 (Molecular Dimensions).
- Fine Screen 3 (FS3), Custom Screen HT-96 as shown in Figure 2-1 (96 x 1 ml).
- Crystallography plate, INTELLI-PLATE 96, 96 well, sitting-drop, vapour diffusion crystallography plate (Art Robbins Instruments).
- Plate seal, SureSeal DWB sealing sheet (Molecular Dimensions).

2.1.3 Antibodies

- anti-CaM: CaM specific mouse monoclonal antibody (Source Bioscience).

- anti-RyR2: human RyR2-specific Ab^{1093}, “in-house” rabbit polyclonal antiserum raised against a peptide of human $RyR2^{4459-4478}$ (Xiao *et al.*, 2002).
- anti-PLCζ: human PLCζ-specific Immunoglobulin G (IgG), “in-house” rabbit polyclonal raised against EF-hand domain $PLC\zeta^{16–31}$ peptide (National Centre for Scientific Research “Demokritos”).
- anti-rabbit-HRP: goat anti-rabbit IgG (whole molecule) conjugated to horse radish peroxidase (HRP) (Sigma Aldrich)
- anti-mouse-HRP: goat anti-mouse IgG (whole molecule) conjugated to HRP (Sigma Aldrich)

2.1.4 Peptides

The RyR2 peptides and $PLC\zeta^{16–31}$ peptides were synthesised by Dr Zilli Sideratou of National Centre for Scientific Research “Demokritos”, Athens, Greece.

PLCζ peptides used in ITC experiments were purchased from LifeTein.

Weighed lyophilised peptides reconstituted with buffer at 10X final concentration, stored at -20 °C and kept on ice during use.

2.1.5 Molecular biology

Sterile or molecular biology grade glassware plastics, growth media, antibiotics and reagents were used as appropriate unless otherwise stated. Autoclave sterilisation conditions were 121 °C for 22 min. Pipette tips (VWR) were racked, sealed and

sterilised by autoclave before use. All other molecular biology grade plastics purchased from Fisher Scientific, Greiner Bio-One and Elkay.

- TAE, 50X Stock 2 M Tris, 2 M glacial acetic acid, 50 mM EDTA. Diluted to 1X with DI H_2O before use.
- Sterile H_2O, DI H_2O sterilised by autoclave.
- DNA loading buffer, 0.25 % (w/v) Orange G, 15 % (w/v) Ficoll Type 4000 (GE Healthcare) in DI H_2O. Added directly to sample and final sample volume adjusted to 1X.
- DNA molecular weight marker, 2-Log DNA Ladder (New England Biolabs (NEB)).
- Agarose, PeqGold Universal-Agarose (Peqlab).
- Ethidium bromide, Ethidium Bromide Solution (10 mg/ml).
- Plasmid miniprep kits, Wizard® Plus SV Minipreps DNA Purification System (Promega).
- Plasmid maxiprep kits, Qiagen Plasmid Maxi Kit (Qiagen).
- Ethanol, Molecular Biology Grade Absolute Ethanol (200 Proof). Also used to prepare 70 % and 95 % (v/v) solutions with DI H_2O for use in maxi and mini preps.
- Isopropanol, 99.9% (HPLC Grade).

- Restriction endonucleases (NEB).
- Calf Intestinal Alkaline Phosphatase (CIP) (NEB).
- Ligase, T4 DNA ligase (NEB).
- Polymerase Chain Reaction (PCR) master mix, Phusion High-Fidelity PCR Master Mix contains Phusion DNA Polymerase, 400 µM of each dNTP and 2X Phusion HF Buffer (Thermo Fisher Scientific). Dispensed into aliquots on the first thaw to prevent repeated freeze-thaw and stored at -20 °C before use.
- Mutagenesis kit, QuikChange II XL Site-Directed Mutagenesis Kit (Stratagene).
- PCR Clean-up kit, QIAquick PCR Purification Kit (Qiagen).
- Gel extraction kit, QIAquick Gel Extraction Kit (Qiagen).

2.1.6 Oligonucleotides

Custom oligonucleotides (primers) were synthesised, purified by desalting and lyophilised by Sigma-Genosys. The primers were reconstituted with sterile DI H_2O to yield a 100 µM stock solution. Working dilutions of primers were prepared from stock and sterile H_2O as required. All primers solutions stored at -20 °C. The primers used in this study are described in Appendix Table I.

Each primer used for cloning was typically 30 base pairs (bp) long and contained specific sequences for the forward and reverse sequences of the required gene. The 5’-end of the primers included a nucleotide clamp of random bases which could be varied to keep the GC content at 50-60 %. Each primer pair was designed to

produce a PCR product containing the nucleotide sequence corresponding to the primary structure of the protein of interest (POI) with a 3'-stop codon. The product could correspond to the sequence encoding the full-length protein or to between specific amino acid coordinates of the protein. The product also included a stop codon flanked by restriction sites compatible with the Multiple cloning sites (MCS). Restriction endonucleases which left overhanging sequences were chosen to ensure ligation in the correct orientation.

The sequences of primers for mutagenesis corresponded to guidelines issued by the manufacturer of the kit. Primers were a minimum of 32 bp and had a high melting temperature. The forward and reverse primers both contained the desired mutation and were complementary for the same sequence surrounding the location of the mutation which was always a single base substitution.

2.1.7 Vectors

2.1.7.1 Summary of Vectors

Table 2-3 is a summary of the protein expression plasmids used in this study, the maps of each plasmid are shown in Appendix Figure I to Appendix Figure IX. Matthias Bochtler (International Institute of Molecular and Cell Biology, Warsaw, Poland) provided the pETMM series of vectors. Xuexun Fang (Jilin University, China) provided the pHSIE vector (Wang *et al.*, 2010; Z. Wang *et al.*, 2012). All contain the *lac* operon, enabling IPTG induced protein expression.

The pAED4-hCaM plasmid (Tan, Mabuchi and Grabarek, 1996) was a kind gift from Zenon Grabarek (Boston Biomedical Research Institute, USA). The pCR3.1-hPLCζ-luciferase (Yu *et al.*, 2007) and the pCR3.1D^{210}R-luciferase (Nomikos *et al.*, 2005) plasmids were a kind gift from Michail Nomikos (Cardiff University).

Table 2-3 Summary of protein expression vectors used in this study

Plasmid	Amino-terminal fusion partners.	**Size (kDa)**
pETMM11	N-Hexa Histidine (6xHis)	**1 kDa**
pETMM20	N-Thioredoxin A (TrxA) 6xHis	**12 kDa**
pETMM30	N-6xHis-Glutathione S-transferase (GST)	**26 kDa**
pETMM41	N- 6xHis-Maltose Binding Protein (MBP)-	**42 kDa**
pETMM50	N-Disulfide oxidoreductase A (DsbA) 6xHis	**21 kDa**
pETMM60	N-N utilization substance A (NusA) 6xHis	**55 kDa**
pETMM70	N-Calmodulin Binding Peptide (CBP)	**4 kDa**
pETMM80	N- Disulfide oxidoreductase C (DsbC)	**24 kDa**
pHSIE	N-6xHis-SUMO2-Intein	**30 kDa**

2.2 Methods

Generic microbiology, biochemistry and molecular biology techniques originate from published protocols (Green and Sambrook, 2012) and methods previously developed and optimised by fellow members of laboratory staff. When applicable, techniques using kits followed manufacturer's recommendations. All procedures were carried out in agreement with local guidelines covered in the WHRI Health and Safety handbooks.

2.2.1 Health and Safety

All experiments and related techniques and procedures described in this study adhered to the relevant COSHH regulations and local rules, i.e., those contained in Wales Heart Research Institute (WHRI) Health and Safety policies and training manuals. The storage conditions, handling and disposal of reagents used in this study were as per the manufacturer's safety data sheets. The generation and handling of genetically modified organisms followed guidelines issued by the Advisory Committee on Genetic Modification.

Before disposal contaminated bacterial liquid media and serological pipettes were disinfected using HAZ-TAB™ Chlorine release tablets (Guest Medical) as per manufacturer's instructions (4 tablets per L of solution to be disinfected). The same disinfectant was used to decontaminate microbiological glassware which was then washed thoroughly with laboratory detergent and rinsed well with DI H_2O. All other contaminated plastics and lab consumables were disinfected by autoclave, 20 min at 136 °C, before disposal. Disposal of all materials contaminated with radioactivity was in line with local rules. All other biohazardous and general laboratory waste treated as clinical waste and disposed of accordingly.

2.2.2 Microbiology Techniques

All microbiological was under aseptic conditions. Once sterilised all procedures were carried out in Class II safety cabinets on surfaces cleaned with 70 % IMS before and after use. Colonies grown on LB-agar plates were picked using sterile pipette tips or loops.

2.2.2.1 Preparation of Chemically Competent E.coli

Chemically competent *E.coli* were prepared in-house by $CaCl_2$ treatment. *E.coli* were streaked onto an LB-agar plate and incubated inverted overnight at 37 °C. A single colony was picked and used to inoculate 10 ml of LB-media which was incubated overnight at 37 °C with shaking at 200 rpm. A 3 ml aliquot of the overnight culture was added to 300 ml selective LB and incubated at 37 °C with shaking at 225 rpm. Bacterial growth was monitored periodically by measuring optical density at 600 nm (OD_{600}). At OD_{600}=0.5 growth was halted by transferring the culture to a pre-chilled 500 ml centrifuge tube and incubated on ice for 1 h. The cells were then centrifuged at 3,000x *g* for 10 min at 4 °C. The supernatant was discarded, and the pellet was re-suspended gently in 150 ml of chilled sterile 50 mM $CaCl_2$ and incubated on ice for 30 min. The cells were centrifuged under the same conditions and the pellet gently re-suspended in 30 ml of sterile 50 mM $CaCl_2$, 20 % (w/v) glycerol. The re-suspended cells were dispensed into aliquots of 100 µL in 1.5 ml microcentrifuge tubes and immediately snap frozen on dry ice for 30 min. The frozen aliquots were stored at -80 °C until use. The cells were found to be capable of efficient transformation for up to 6 months.

2.2.2.2 Transformation of Chemically E.coli

Chemically competent *E.coli* were transformed with plasmid DNA using heat shock. Aliquots of chemically competent *E.coli* were removed from -80 °C and kept on ice. The bacteria were inoculated with 10-100 ng plasmid DNA and mixed gently with the pipette tip. The bacteria were incubated on ice for 30 min, heat shocked at 42 °C in a water bath for 45 s and immediately incubated on ice for further 5 min. A 900 µL aliquot of antibiotic-free LB was added to the cell suspension and incubated at 37 °C for 1 h with shaking at 225 rpm. Following incubation 100 µl cell culture was spread onto an LB-agar plate. Then the remaining culture was centrifuged at top speed in a benchtop micro-centrifuge for 1 min. All bar 100 µL of the supernatant was discarded. The pelleted bacteria were re-suspended in the remaining supernatant and spread onto an LB-agar plate. The spread plates were incubated inverted at 37 °C overnight. Following overnight incubation, the plates were sealed with parafilm and stored inverted for up to 21 days at 4 °C.

2.2.2.3 Expression and Purification of Recombinant Protein

Unless stated otherwise throughout the protein purification process all steps were carried out using chilled buffers either on ice or in a temperature controlled room set to 4 °C.

2.2.2.4 Preparation of Transformed Bacteria

Protein expression strains of *E.coli* were transformed with protein expression plasmids as described. Plates containing the resulting colonies were incubated overnight at 37 °C overnight, sealed and stored at 4 °C until use for no longer than 21 days.

2.2.2.5 The Culture of Transformed E.coli

Colonies of recently transformed *E.coli* were picked and used to inoculate LB, one colony per 10 ml of LB. The inoculated medium was incubated overnight at 37 °C with shaking at 225 rpm. The overnight culture was used to inoculate LB (1 in 100) in vessels, typically Erlenmeyer flasks, of a volume that the volume of LB was 25 % vessel volume. Large culture volumes of a specific transformed *E.coli* were grown in multiple flasks inoculated with a pool of overnight cultures.

2.2.2.6 Induction of Protein Expression

Inoculated flasks were incubated at 37 °C with shaking at 200 rpm, and OD_{600} monitored periodically using a LAMBDA BIO+ spectrophotometer (Perkin-Elmer). When OD_{600}=0.6, the flasks were transferred to 4 °C for a minimum of 30 min. A 1 ml sample of un-induced culture was pelleted and stored at -20 °C for future analysis. Isopropyl β-D-thiogalactopyranoside (IPTG) (Formedium) was added to the flasks to induce protein expression and cultures incubated overnight at 16 °C with shaking at 225 rpm. The following morning a 0.5 ml sample of induced culture was pelleted and stored at -20 °C for future analysis. Identical cultures were pooled, and *E.coli* harvested by centrifugation at 3,000x *g* for 30 min. The resulting pellets were stored immediately at -80 °C until use.

2.2.2.7 Screening of Protein Expression

Pelleted un-induced and induced samples were re-suspended with 5x SDS loading buffer, boiled for 2 min and briefly centrifuged. The resulting crude lysate was separated by denaturing Poly-acrylamide gel electrophoresis (SDS-PAGE).

2.2.2.8 Solubility Assessment

Bacterial pellets from 12 ml induced culture were re-suspended in 20 mM Tris, 1 mM EDTA, 125 mM NaCl. The resuspended *E.coli* were transferred to a 1.5 ml microcentrifuge tube, sonicated briefly (3x10 s pulses on lowest setting) and centrifuged. The supernatant (soluble fraction) was decanted, and the pellet was re-suspended in 8 M urea (insoluble fraction). The fractions were separated by SDS-PAGE.

2.3 Nucleic Acid Methods

2.3.1 Plasmid Propagation

Chemically competent TOP10 *E.coli* were transformed with plasmid DNA as described to produce bacterial colonies bearing the desired plasmid on LB-Agar plates.

2.3.2 Plasmid Purification

2.3.2.1 Small-Scale Plasmid Purification

Plasmids were purified on a small scale by miniprep using Miniprep Kits following the manufacturer's protocol based on the principal of alkaline lysis followed by binding to, purification on and elution from a silica membrane. A single colony of transformed *E.coli* was picked and used to inoculate 10 ml of LB and incubated overnight at 37 °C with shaking at 225 rpm. The incubated culture was centrifuged at 3000x *g* for 10 min, and the supernatant discarded. Using the buffers and purification columns supplied the pelleted cells were resuspended and lysed. The plasmid DNA was immobilised on provided columns and washed. The immobilised plasmid DNA was eluted with sterile H_2O into clean 1.5 ml microcentrifuge tubes.

2.3.2.2 Large-Scale Plasmid Purification

Plasmids were purified at a large scale, plasmid “maxiprep” using QIAGEN Plasmid Maxi Kit (Qiagen) as per the manufacturer’s protocol, based on the principal of alkaline lysis followed by binding to, purification on and elution from an anion exchange resin. A single colony of transformed *E.coli* was picked and used to inoculate 10 ml of selective (if appropriate) LB medium. The inoculated LB was incubated for 8 h at 37 °C with shaking at 225 rpm. LB medium (100-500 ml, 25% culture vessel volume). Following incubation, the cultures were used to inoculate LB at a ratio of 1:500. The inoculated LB was then incubated overnight at 37 °C with shaking at 225 rpm. The culture was centrifuged at 3000x *g* for 10 min, and the supernatant discarded. The pelleted cells were re-suspended, lysed then the plasmid DNA was purified and eluted using the buffers and column supplied according to the manufacturer's protocol. Eluted plasmid DNA was precipitated with Isopropanol then with 70 % (v/v) ethanol as instructed. The pellet was air-dried and reconstituted with 500 µL of sterile H_2O.

2.3.3 Polymerase Chain Reaction

Polymerase chain reactions (PCRs) were carried out using a Veriti® Thermal Cycler (Applied Biosystems) according to PCR reagent manufacturer’s instructions. PCR Master Mix containing optimal Taq DNA polymerase, nucleoside triphosphates (dNTPs), buffer and $MgCl_2$ was used throughout. Typical PCR components and cycling conditions are shown in Table 2-4 and Table 2-5. Analysis of the PCR products was by agarose gel electrophoresis.

Table 2-4 PCR components

Component	Amount
2X PCR Master Mix	25 µL
DNA template	10 ng
Forward Primer	0.5 µM
Reverse Primer	0.5 µM
Sterile H_2O	to a final volume of 50 µL

Table 2-5 Thermocycler parameters for PCR

Cycles	Step	Temperature	Time
1	Initial Denaturation	98 °C	1 min
35	Denaturation	98 °C	10 s
	Elongation	72 °C	30 s/ kilobase (kb)
1	Final elongation	72 °C	10 min
1	Hold	4 °C	∞

2.3.4 Purification of PCR Products

If required for downstream applications, PCR products were purified. For sequencing PCR reactions were purified using PCR purification kit. For molecular sub-cloning PCR products were separated by agarose gel electrophoresis and the desired fragment excised from the gel and DNA extracted using the Gel Purification Kit. Both kits were used according to the manufacturer's instructions. Purified PCR products were eluted in sterile H_2O.

2.3.5 Agarose Gel Electrophoresis

Agarose gels for electrophoresis were prepared at appropriate concentrations (0.6 %-1 % depending on the size of the fragment) by dissolving agarose in TAE with gentle heating. After cooling (~50 °C), ethidium bromide was added to a final concentration of 0.2 µg/ml. Gels were cast and run using Horizontal Electrophoresis System (BioRad) according to manufacturer's instructions. DNA samples were mixed with DNA loading buffer and loaded into the gel wells. A standard DNA molecular weight marker (NEB) was also loaded to check for the correct size DNA fragments. Submarine electrophoresis was performed in a gel tank containing TAE with a constant voltage (80-120 V). The gel was visualised using a ultraviolet (UV) trans-illuminator and image acquired using Gel Doc Gel Documentation system (BioRad) and Quantity One software (BioRad).

2.3.6 Molecular Subcloning

For each construct, three identical 50 µl PCR reactions were pooled and separated using Agarose Gel Electrophoresis. Under UV trans-illumination the correct size band

was excised and DNA extracted from the gel slices as previously described. The purified DNA was incubated with the appropriate restriction endonucleases and the corresponding buffer (NEB) overnight at 37 °C before being heated at 80 °C for 30 min for restriction endonuclease inactivation. The target vector (~1 µg) linearised by digestion under the same conditions was dephosphorylated using CIP (NEB) according to manufacturer's instructions to prevent re-ligation. The insert and linearised vector were purified using QIAquick PCR purification kit (Qiagen) and analysed by agarose gel electrophoresis before ligation.

Ligation reactions were set up according to the manufacturer's instructions. A typical 20 µL ligation reaction contained insert and vector at 10:1 Molar ratio with 4 U of T4 ligase (NEB), 1x T4 Ligation Buffer (NEB) and sterile H_2O to volume. The ligation reaction was incubated overnight at 16 °C. Competent TOP10 *E.coli* transformed with 20 µl (5-100 ng DNA) of the ligation reaction, were spread onto LB-agar plates and resulting colonies screened for the presence of the recombinant plasmid.

2.3.7 Screening of Positive Clones

Colonies were selected and screened for the presence of the recombinant plasmid. Plasmid DNA purified by miniprep from picked colonies was separated alongside empty vector by agarose gel electrophoresis. Plasmids of greater size than the empty vector were selected for further analysis to confirm the presence of an insert.

Presence of the insert in larger plasmids was detected by PCR containing primers specific to the sub-cloned insert and restriction digest with the specific

endonucleases used for sub-cloning. The presence of the insert was then further confirmed by sequencing.

Plasmids were stored in sterile H_2O at -20 °C until use. Stocks of plasmid were replenished by transforming competent TOP10 *E.coli* with a plasmid. The resulting colonies were used to prepare mini-preps and maxi-preps also as described.

2.3.8 DNA Quantification.

The quantity and quality of DNA were estimated by measuring the optical density at 260 nm (OD_{260}) and 280 nm (OD_{280}). The absorbance of a 1:100 dilution sample was measured in quartz cuvettes (Perkin Elmer) using a LAMBDA BIO+ spectrophotometer (Perkin-Elmer) in Chapter 3. While in remaining chapters the absorbance of an undiluted sample was measured using a DS-11 Microvolume Spectrophotometer (DeNovix).

The concentration of double-stranded DNA (dsDNA) was estimated from OD_{260} assuming an extinction coefficient of 0.020 $(\mu g/ml)^{-1}cm^{-1}$, so an OD_{260} of 1 corresponds to 50 µg/ml dsDNA. The purity of the DNA was estimated from the ratio OD_{260}/OD_{280}, a ratio of 1.8-2.0 was deemed to be 90 % pure and free of significant contamination.

2.3.9 Site-Directed Mutagenesis

Site-directed mutagenesis (SDM) was carried out with QuikChange II XL Site-Directed Mutagenesis Kit (Agilent). Each mutagenesis reaction was the substitution of a single base pair. Therefore, if a codon change required the substitution of more than one base, the mutated plasmid was used as template in the reaction to effect subsequent

base changes. Each SDM-PCR was prepared as shown in Table 2-6. The reaction was carried out using a Veriti® Thermal Cycler (Applied Biosystems) using the cycling conditions are shown in Table 2-7. Once the PCR cycle was complete the parental plasmid in the reaction was digested by adding 1.1 µL of supplied *DpnI* and incubating at 37 °C for 1.5 h.

A pre-chilled sterile 14 ml tube was prepared, containing 60 µL of XL10 Gold Ultracompetent cells (Agilent) and 1 µL of the provided β-ME. The treated cells were gently mixed and incubated on ice for 10 min with additional gentle mixing every 2 min. A 4.5 µL aliquot of the digestion reaction was added to the cells and incubated on ice for 30 min. The cells were heat-shocked at 42 °C for 30 s and then incubated on ice for a further 5 min. A 450 µL aliquot of antibiotic-free LB was added, and cells were incubated at 37 °C for 1.5 h with shaking at 200 rpm. The reaction was split into two ~250 µL aliquots which were spread onto two separate LB-agar plates. The plates were incubated for 20 h at 37 °C. Colonies were picked and used to prepare mini-preps as described. The eluted plasmid DNA was separated using agarose gel electrophoresis alongside the parental plasmid. Clones which were of equal size to the parental plasmid were selected for confirmation of identity and presence of the mutation by sequencing.

Table 2-6 Site-directed mutagenesis PCR components

Component	Amount
10x Reaction buffer	5 µL
DNA template	5-50 ng
Forward Primer	125 ng
Reverse Primer	125 ng
dNTP	1.1 µl
Quik solution	3 µl
Nuclease-free water	to a final volume of 50µl

Table 2-7 Thermocycler parameters for site-directed mutagenesis PCR

Cycles	Step	Temperature	Time
1	Denature	95 °C	1 min
18	Denature	95 °C	50 s
	Annealing	60 °C	50 s
	Elongation	68 °C	1 min/kb
1	Final elongation	68 °C	7 min
1	Hold	4 °C	∞

2.3.10 Sequencing

Quality and quantity of DNA for sequencing was estimated as described and confirmed by separating 150 ng of DNA by agarose gel electrophoresis. Samples (30 µl) of plasmids (20 ng/µl) or PCR products (concentration dependent of product size) were submitted to DNA Sequencing & Services (www.dnaseq.co.uk) and sequenced using Applied Biosystems Big-Dye Ver. 3.1 chemistry on an Applied Biosystems model 3730 automated capillary DNA sequencer.

2.4 Recombinant Protein Purification.

2.4.1 General Techniques

2.4.1.1 Re-Suspension of Pelleted Bacteria

Frozen pellets were defrosted on ice and re-suspended in Lysis buffer (10 ml Lysis buffer per L of culture) supplemented with Protease inhibitors and lysozyme (2 mg per ml Lysis buffer). The re-suspended cells were left rolling at 4 °C for 30 min before being lysed by either of the two methods outlined.

2.4.1.2 Lysis of Bacteria by Sonication

Re-suspended cells were transferred to a plastic vessel, typically 50 ml centrifuge tubes for large volumes and 1.5 ml microcentrifuge tubes for small volumes. A VibraCell Ultrasonic Processor (Sonics), fitted with probe appropriate to the volume of re-suspended cells, was used. Amplitude was adjusted so output did not exceed 40 W. Sonication was performed on ice in three 10 s pulses with 1 min intervals in between.

2.4.1.3 High-Pressure Cell Lysis of Bacteria Using a French Pressure Cell Press

Re-suspended cells were passed through a Sansted Pressure Cell homogeniser (Sansted Fluid Power) under pressure. The 10 ml pressure cell and post-lysis heat exchanger were fitted with cooling jackets connected to a circulating ice bath pre-chilled to 4 °C. Both were pre-chilled and kept cold throughout. The homogenising control valve gauge pressure was 1.2 – 1.4 bar(g) which typically resulted in an output of ~150 kPa. The resulting lysate was collected on ice.

2.4.1.4 Clarification of Lysate

Lysates were clarified by centrifugation to remove cell debris, genomic DNA and insoluble material. Large volumes of lysate were centrifuged at 25,000x *g* for 20 min while small volumes at 14,000x *g* for 30 min, both at 4 °C. Following centrifugation, the supernatant was carefully removed ensuring the pellet was not disturbed. The pellet was discarded, and recombinant protein in the supernatant was purified by affinity chromatography as described in the specific methods.

2.4.2 Affinity Chromatography

2.4.2.1 The Principal of Protein Purification by Affinity Chromatography

Affinity chromatography utilises specific interaction between binding partners to separate a biomolecule. The stationary phase is an immobilised binding partner selectively binds a molecule in the mobile phase, a biochemical mixture. In the case of recombinant proteins, a fusion protein is expressed consisting of the POI fused to a protein or peptide sequence with a specific affinity for another molecule. Under stringent conditions, few of the proteins expressed by the host will co-purify with the fusion recombinant protein due to the specificity of the binding. The fusion protein can be recovered by making binding less favourable. The conditions can be altered or a competitor, e.g., a soluble binding partner or a low molecular weight ligand added. Alternatively, the POI alone can be recovered by cleaving within the sequence linking the affinity tag and, POI. A site-specific protease can be added to the mobile phase or conditions altered to induce auto-cleavage.

2.4.2.2 Batch Purification of PLCζ^{D210R} Fusion Proteins

Recombinant PLCζ^{D210R} fusion proteins were purified on a small scale by batch affinity chromatography in 1.5 ml microcentrifuge tubes. The buffer was pH7.4, 20 mM Tris, 200 mM NaCl. Samples were centrifuged for 1 min at 500x *g* and 4 °C at each step to separate mobile and stationary phases.

Bacterial pellets representing 100 ml of culture were re-suspended in lysis buffer. The re-suspended cells were lysed using a French press and resulting lysate clarified.

Clarified lysate was incubated with 100 µL of the appropriate affinity resin at 4 °C for 1 h with rotation. The mixtures of lysate and resin were centrifuged. The supernatant was decanted. The pelleted resin was re-suspended with 5x bed volumes of buffer, centrifuged and the supernatant discarded. The pellet was re-suspended then recovered repeatedly until no protein was detectable in the supernatant with Bradford reagent. The resin was re-suspended in 2x bed volume of elution buffer and centrifuged. The decanted supernatant and the pellet were retained. At each stage, the total protein content of the fractions was monitored using Bradford reagent. All fractions were retained for subsequent analysis by SDS-PAGE.

2.4.2.3 Column Purification of PLCζ^{D210R} Fusion Proteins

The recombinant MBP-6xHis-PLCζ^{D210R} fusion protein was purified on a large scale using column affinity chromatography. The buffer for this purification was pH 8, 50 mM NaH_2PO_4, 500 mM NaCl.

Pelleted bacteria representing 24 L of culture was re-suspended in lysis buffer and lysed by French pressure cell press. The clarified lysate was centrifuged for 20 mins at 20,000x *g* and 4 °C. The clarified lysate was applied to a column packed with either NiNTA or Amylose resin column. Each column was packed with 1 ml resin and pre-equilibrated with column buffer. The lysates were allowed to flow through under gravity and retained. The columns were washed extensively with buffer.

Ni-NTA columns were then washed sequentially with buffer supplemented with increasing concentrations of imidazole at 20, 40 and 60 mM. The bound protein was eluted from the column in 0.5 ml volumes of buffer supplemented with 250 mM imidazole.

Amylose resin columns were washed with buffer supplemented with 1 mM maltose. The bound protein was eluted from the column in 0.5 ml volumes of column buffer supplemented with 10 mM maltose.

At each stage, the total protein content of the fractions was monitored using Bradford reagent. All fractions were retained for subsequent analysis by SDS-PAGE. The total protein content of fractions was monitored by eye using Bradford reagent, washing and elution were halted when protein was observed to decline. Samples of flow-through, all washes and fractions positive for protein were retained for analysis by SDS-PAGE.

2.4.2.4 Intein One-Step Purification

Fusion proteins containing 6xHis-SUMO2-intein were purified on a Ni-NTA column using a modified purification protocol. Unless otherwise stated all the following steps

were carried out at 4 °C with ice-cold buffers to avoid unwanted intein self-cleavage. The buffer was pH 8.5, 50 mM Tris, 300 mM NaCl, 25 mM imidazole. Clarified lysate, washes and elutions were passed through the column under gravity.

Pellets were re-suspended in lysis buffer, and the resuspended cells were lysed with sonication. The lysate was clarified by centrifugation, and the clarified lysate was applied to a Ni–NTA column, packed with 1 ml resin and pre-equilibrated in column buffer. The column was washed with 10 ml of buffer.

Buffer conditions on the column were altered with a 10 ml wash of Cleaving buffer. The column was sealed, 5 ml of Cleaving buffer was applied, and the column incubated at room temperature for 3 h. Following incubation, the column was unsealed, and cleavage fractions collected. Any remaining protein was eluted from the column with 1 ml Elution buffer, Cleaving buffer supplemented with 500 mM imidazole, and elution fraction collected.

At each stage, the total protein content of the fractions was monitored using Bradford reagent. All fractions were retained for subsequent analysis by SDS-PAGE.

2.4.3 Size Exclusion Chromatography

2.4.3.1 The Principal of Size Exclusion Chromatography

Size exclusion chromatography (SEC) separates molecules according to differences in partition coefficient which result from differences in molecular weight (MW) and hydrodynamic radius (R_H) of the molecules. The stationary phase is a matrix of porous resin beads with small regular pores. The M_W and R_H of a molecule dictate how much

the beads absorb it via the pores and so the rate it will migrate through the column. Smaller molecules can enter and migrate through the beads via the pores; larger molecules are less likely to enter the pores and bypass the beads.

Consequently, the larger molecules will elute first and smaller molecules last. The elution profile of the protein can be compared to that of a mixture of proteins of known M_W and R_H separated on the same SEC column, revealing biophysical information on the protein being separated. Due to the scale of dilution, SEC can also be used to change the buffer in which proteins are dissolved.

2.4.3.2 Further Purification of Recombinant Proteins by Size.

Protein samples to be purified by SEC were concentrated, see 2.5.1, to a final volume of 0.5 ml and filter sterilised. Buffers used in gel filtration were vacuum filtered through Whatman® 0.2 µm membrane filter (GE Healthcare). The protein was then injected into ÄKTA FPLC system via 1 ml Superloop™ and applied to a pre-equilibrated Sephadex® GS-100 gel filtration column (all GE Healthcare). A constant flow rate was maintained. Runoff from the column was monitored by UV absorbance and elution fractions collected by the automatic collector. Based on the elution profile, fractions of interest were analysed by SDS-PAGE. The SEC column was calibrated using a Gel Filtration Calibration Kit (GE Healthcare).

2.5 General Protein Methods

2.5.1 Protein Concentration

Proteins were concentrated by ultrafiltration using centrifugal columns containing a membrane with a molecular weight cut off (M_WCO) at least 2 times smaller than the

size of the protein to be retained. Protein solutions of less than 1.5 ml were concentrated with Amicon Ultra 0.5 ml Centrifugal Filters (Merck-Millipore). To concentrate volumes higher than 1.5 ml Vivaspin® Centrifugal Concentrators (Sartorius) were used. Centrifugal columns were handled throughout as per manufacturer's instructions.

2.5.2 Buffer Exchange

If not exchanged by SEC the buffers dissolving proteins were exchanged either by dialysis or ultrafiltration.

2.5.2.1 Dialysis

Protein solution to be dialysed was loaded into SnakeSkin™ Dialysis Tubing (Pierce) with a molecular weight cut off (M_WCO) at least 2 times smaller than the size of the protein to be retained. The dialysis tubing was placed in a container of excess buffer (typically 4 L) and incubated with gentle stirring at 4 °C. The buffer was changed after a minimum of 2 h at least once and dialysis allowed to run overnight.

2.5.2.2 Ultrafiltration

The protein solution was loaded into centrifugal columns of M_WCO and volume appropriate for the size of the protein and starting volume as described in 2.5.1. As per the manufacturer's instructions, the volume of the protein was reduced until the dead volume of the column was reached. The concentrated protein solution was re-suspended in the replacement buffer and the process repeated three times. The

protein solution was then resuspended to a volume suitable for the next steps and recovered from the column.

2.5.3 Quantification of Proteins

Protein concentration was estimated spectrophotometrically by measuring OD at 280 nm (OD_{280}) of the protein solution (diluted into range as required). Initially, a quartz cuvette (Perkin Elmer) and LAMBDA BIO+ spectrophotometer (Perkin-Elmer) was used in Chapter 3. In the remaining chapters, a DS-11 Microvolume Spectrophotometer (DeNovix) was used. Concentration was estimated using the formula. The concentration was confirmed by loading an SDS-PAGE gel with specific amounts of protein alongside known amounts of a standard protein either BSA or lysozyme.

$$[\text{protein}]\ (\text{mg/ml}) = \frac{\text{OD}_{280}}{(\varepsilon \times l) \times \text{M}_W}$$

Equation 2-1 Calculation of protein concentration from UV absorbance

Where ε is the specific molar extinction coefficient of the protein, l is the path length and MW is the molecular weight of the protein.

2.5.4 Denaturing Protein Electrophoresis Electrophoresis

Reducing SDS-polyacrylamide gel electrophoresis (SDS-PAGE) was used to analyse proteins. SDS-PAGE gels were prepared, cast and run using Vertical Electrophoresis System (BioRad) as described below.

2.5.4.1 Preparation of SDS-PAGE Gels

The SDS-PAGE gels prepared comprised of two layers a stacking gel with wells which was always 4 % and a separating gel the concentration of which was dependent on the size of the proteins to be separated. Briefly, a separating gel was prepared according to Table 2-8 using Separating Gel Buffer and poured between two glass plates arranged on a gel casting frame according to the manufacturer's instructions. The polymerisation mixture was overlaid with a layer of isopropanol, and the gel was allowed to polymerise, typically for 1 h. Once gel polymerisation was complete, the isopropanol was decanted and rinsed away with DI H_2O. A 4 % stacking gel mixture was then similarly prepared according to Table 2-8 using Stacking Gel Buffer and poured onto the separating gel. A comb was inserted to form the wells, and the gel allowed to polymerise, typically for 1 h.

Table 2-8 Polyacrylamide gel composition

	Volume of reagent required for specified gel percentage (µl)				
Reagent	4%	8%	10%	12%	15%
40% Acrylamide	1000	2000	2500	3000	3750
DI H_2O	6345	5345	4845	4345	3595
Gel Buffer	2500	2500	2500	2500	2500
10% SDS	100	100	100	100	100
10% APS	50	50	50	50	50
TEMED	5	5	5	5	5

2.5.4.2 Preparation of Samples for SDS-PAGE

Protein samples were mixed with protein loading buffer, incubated at 95 °C for 5 min and spun briefly.

2.5.4.3 Loading and Running SDS-PAGE Gels

The SDS-PAGE gel was clamped into an electrode assembly. The assembly was transferred to a Protean II tank (BioRaD), submerged in running buffer and the comb was removed. The wells were loaded with prepared samples were loaded, typically 20 µl, and M_W markers. Electrophoresis was carried out at constant voltage (typically 140 V) until the dye front reached the bottom of the separating gel. The plates were then removed from the electrode assembly and gel released by separating the plates. The proteins were then either visualised by staining with Coomassie Brilliant Blue R-250 or transferred to PVDF for immunoblotting

2.5.4.4 Staining and De-Staining Of SDS-PAGE Gels

Following transfer to a plastic container the gel was rinsed briefly with DI H_2O and submerged in Coomassie Brilliant Blue R-250 staining solution (Coomassie stain) for 30 min with rocking. The Coomassie stain was decanted. The stained gel was rinsed briefly with destain buffer to remove excess stain and submerged in fresh destain buffer with rocking. The destain buffer was replaced as required until all background staining was removed. An image of the gel was then captured using a flatbed scanner.

2.5.5 Western Blotting

2.5.5.1 Transfer of Proteins to Membranes.

The proteins from the SDS-PAGE gel were transferred to PVDF membrane by Semi-Dry transfer using a Transblot® SD Semi-Dry Transfer Cell (Biorad). Immobilon-P polyvinylidene difluoride (PVDF) (Millipore) was soaked in methanol for 1 min. Both

the SDS-PAGE gel and membrane were submerged in semi-dry transfer buffer with rocking for 30 min at room temperature. Eight pieces of blotting paper were similarly soaked in Transfer buffer. Four pieces of blotting paper were stacked on the cathode followed by the membrane, the SDS-PAGE gel and finally the four remaining pieces of blotting paper. The transfer cell was assembled according to the manufacturer's instructions. The proteins were transferred by electrophoresis at a constant voltage (20 V) for 1 h at room temperature.

2.5.5.2 Western Blot Analysis.

Following protein transfer, the membrane was blocked by incubating it in Tris-buffered saline, 0.1 % Tween 20 (TBS-T) containing 5 % (w/v) non-fat milk protein (Marvel) (TBS-T/Marvel) for 4 h at room temperature or overnight at 4 °C. The membrane was incubated with TBS-T/Marvel containing a primary antibody at room temperature for 2 h with rocking. The membrane was washed for 30 min with TBS-T/Marvel which was replaced with fresh TBS-T/Marvel every 10 min. The membrane was incubated at room temperature for 2 h with rocking in TBS-T/Marvel containing a secondary antibody conjugated to horseradiash peroxidase. The membrane was washed for 30 min with TBS-T which was replaced with fresh TBS-T every 10 min. Immunoreactive bands were detected using West-One (Pierce) and the image captured with Hyperfilm (GE Healthcare life sciences).

2.5.6 Preparation of Cardiac Heavy Sarcoplasmic Reticulum Vesicles

2.5.6.1 Processing of Native Tissue

Approximately 200 g of ventricular muscle was separated from each pig heart and roughly chopped. The chopped material was flash frozen in liquid nitrogen (BOC) and stored at -80 °C until use.

2.5.6.2 Purification of Microsomes

Material from one pig heart was defrosted at room temperature. The defrosted heart muscle was mixed with four volumes of homogenization buffer and homogenised in a blender. The homogenate was centrifuged at 10,500x *g* at 4 °C for 20 min. The supernatant was decanted and retained. The pellet was re-suspended in two volumes of homogenization buffer and homogenised again. The homogenate was centrifuged as before, the supernatant decanted and the pellet discarded. Both supernatants were filtered through cheesecloth and pooled. The pooled supernatant was centrifuged at 100,000x *g* for 45 min at 4 °C. The supernatant was discarded and the pellet re-suspended in 20 ml of resuspension buffer. The suspension was incubated with mild stirring for 1 h in the cold room. The suspension was centrifuged at 100,000x *g* for 45 min at 4 °C, and the supernatant was discarded. The pellet was re-suspended in 3 ml homogenisation buffer and stored at -80°C in small aliquots, typically 800 µL.

2.5.6.3 Quantification of RyR2 Proteins

A sample of the SR vesicles was run on an SDS–PAGE (5.5 %) with a standard curve of BSA 10 to 200 µg/ml (20 µl per lane). The gel was stained, de-stained and scanned

using a GS-800™ Calibrated Imaging Densitometer (BioRad). The protein content of the RyR2 band was determined from the BSA standard curve by densitometry, using Quantity One 1-D Analysis Software (BioRad).

2.6 Biophysical Characterisation of Recombinant Protein

2.6.1 Circular Dichroism

2.6.1.1 The Principal of Circular Dichroism

Circular polar light is produced by superimposing two perpendicular beams of polarised light of equal magnitude that are out of phase. The combined beam will propagate as a helix and can rotate either clockwise or anticlockwise around the direction of propagation. Clockwise rotation is Right Circularly Polarized light (RCP), and anticlockwise rotation is Left Circularly Polarized light (LCP).

Circular Dichroism (CD) is the wavelength dependent difference in absorption of RCP and LCP by optically active chiral molecules, e.g., proteins. The characteristic CD of a specific protein is a product of the secondary structure, particularly the alpha helices present. The absorbance of alternating RCP and LCP at different wavelengths can be measured. The resulting differences in absorbance can be expressed as molar circular dichroism ($\Delta\varepsilon$) and plotted against wavelength. The spectra produced will be characteristic of the secondary structure of the protein. Changes in the CD of a protein accompany alterations in the secondary structure. Therefore, CD can be used to assess the secondary structure of proteins. If the CD spectrum of a protein is already known this will indicate whether the protein is correctly folded and show if the secondary structure is perturbed. Differences in CD between wildtype and mutant

proteins show that the mutation changes the secondary structure. Also, by measuring CD under different conditions, the relative stabilities of proteins can be assessed.

2.6.1.2 Secondary Structure and Thermal Stability of Recombinant Calmodulin Proteins

Recombinant protein was dialysed at 4 °C against excess (≥500 fold) CD buffer with two changes of buffer. To prevent buffer mismatches, at the end of dialysis a portion of the dialysis buffer was sterile filtered and retained to use as a solvent and diluent for all experimental components. Concentrated (10X) stock solutions of EDTA and $CaCl_2$ were prepared in final dialysis buffer and sterile filtered.

Following dialysis, protein samples were centrifuged at 10,000x *g* for 5 min and the supernatant transferred to a fresh tube. The concentration of the protein was estimated and confirmed as previously described. If necessary, the protein was concentrated to a concentration higher than required.

Working solutions of protein in either 1 mM Ca^{2+} or EDTA were prepared by combining concentrated protein with Ca^{2+} or EDTA stock solutions and diluting to volume with CD buffer. Stock solutions of Ca^{2+} and EDTA were diluted with CD buffer to produce 1 mM solutions of each to adjust protein concentrations as required. Before use, protein samples were centrifuged at 10,000x *g* for 5 min and the supernatant transferred to a fresh tube.

CD spectroscopy was measured using an Aviv model 215 CD spectropolarimeter (Aviv Biomedical) equipped with a Peltier thermostatic cell holder according to manufacturer's instructions. The CD across Far-UV spectra of 50 μM

protein was measured in a quartz cuvette with a path length of 0.02 cm at 4 °C in the presence of either 1 mM Ca^{2+} or 1 mM EDTA.

The thermal stability of the recombinant proteins was assessed by measuring the CD at 221 nm in a quartz cuvette with a path length of 0.1 cm with increasing temperature. The protein concentration was 12 µM protein. The temperature range was from 4 °C to 100 °C at 0.5 °C intervals with an average heating rate of *ca*. 30 °C/h. CD was plotted against temperature calibrated to the temperature measured inside the cell. Melting curves of CaM recombinant proteins were fitted using Origin software (OriginLab) assuming either of two transition models. Depending on the collected data either a two-state transition from native conformation (*N*) to the denatured conformation (*D*) or a three-state transition from the *N* to *D* via an intermediate conformation (*I*) was assumed. The coefficients of determination for fitted curves vs measurements were $r^2 > 0.99$.

All CD measurement, data collection and processing were performed by Dr Konrad Beck (School of Dentistry, Cardiff University).

2.6.2 Dynamic Light Scattering

2.6.2.1 The Principal of Dynamic Light Scattering

The size distribution of particles in solutions of recombinant proteins was characterised using dynamic light scattering (DLS). DLS is the measurement over time of the intensity of scattered light from a sample cell containing sub-micron particles and macromolecules, i.e., the protein, in solution. Due to the Brownian motion of the particles in solution, the intensity of scattered light will oscillate around an average

value. Based on the diffusion coefficient which is indicative of the size of the particles present is inferred from the oscillation. Therefore, DLS can be used to assess the average size of the particles present and the frequency of different size particles. DLS data can be used to assess the size of a recombinant protein if it present in oligomers and the extent of any protein aggregation.

2.6.2.2 Dynamic Light Scattering Measurement

All DLS measurements were made using a Zetasizer µV (Malvern Instruments) according to the manufacturer's instructions. Protein samples at working concentration and buffer were centrifuged at 10,000x *g* for 5 min at 4 °C and the supernatant transferred to a fresh tube. A 50 µl aliquot was dispensed into a Microvolume cuvette (Malvern Instruments). The cuvette was placed in the sample holder, and a run of three measurements using the default setting at 20 °C was started. After an initial 2 min equilibration, the system automatically optimised duration and laser settings (intensity and angle) for the measurements. The first measurement then commenced followed by two subsequent measurements using the same settings. Following completion of the run, the sample could be recovered.

Data were collected and pooled, and the DLS controlled using the provided Zetasizer software (Malvern Instruments). For each run, an average profile was generated, and the parameters used to assess the quality of the protein sample. The particle size frequencies were exported and used to generate a histogram in Excel.

2.6.3 Steady State Fluorescence Spectroscopy

2.6.3.1 The Principal of Equilibrium Ca^{2+} Titrations

Fluorescence spectroscopy is used to measure the intrinsic fluorescence of optically active amino acid residues, e.g., tyrosine (Tyr) and phenylalanine (Phe), in proteins. Changes in fluorescence intensity accompanying the conformational changes that occur upon ligand binding can reveal biophysical information.

CaM N-domain contains five Phe residues near Ca^{2+}-binding sites I & II. Similarly, the C-domain contains two Tyr residues close to Sites III & IV. The fluorescence of these residues can be selectively monitored due to discrete excitation and emission wavelengths. Ca^{2+}-dependent changes in the intensities of Tyr and Phe fluorescence have been observed. Therefore, Ca^{2+}-binding at sites I & II and sites III & IV can be monitored simultaneously during titration. So, differences in the kinetics of Ca^{2+}-binding at both the N- and C-domain in CaM recombinant proteins can be measured.

2.6.3.2 Ca^{2+}-Binding Affinity of the N- and C-Terminal Regions of Calmodulin.

The Ca^{2+}-binding affinities of wild-type and mutant recombinant CaM were compared by measuring the intensity of fluorescence emissions.

Purified recombinant proteins were concentrated and dialysed overnight with one change of buffer against pH 7.4, 50 mM HEPES, 100 mM KCl. Following dialysis, a portion of the final dialysis buffer was filtered with a 0.22 µm syringe filter and retained to be used as a solvent and diluent for all stock solutions of experimental

components. Protein samples were centrifuged at 10,000x *g* for 5 min and the supernatant transferred to a fresh tube. The concentration of the protein was estimated as previously described.

Working solutions of 6 μM protein and 10-100 mM $CaCl_2$ in pH7.4, 50 mM HEPES, 100 mM KCl, 0.05 mM EGTA, 5 mM NTA, 1 mM $MgCl_2$ and 4 nM fluo-5N (Invitrogen) were prepared by diluting concentrated stocks with final dialysis buffer. The protein solution was titrated with the Ca^{2+}-rich solution. At each titration, the intrinsic fluorescence emissions were measured at λ_{EX}=250 nm & λ_{EM}=280nm and λ_{EX}=277 nm & λ_{EM}=300 nm. The free Ca^{2+} concentration of each sample was determined following the fluorescence intensity of the Ca^{2+}, indicating dye excitation at $\lambda_{EX}^{467\ nm}$ with a λ_{EM} maximum at 510 nm. The macroscopic K_d for the fluo-5N-Ca^{2+} binding was determined to be 85.3 ± 1.4 μM in the buffer used for this study.

All fluorescence measurements were made using a Quantamaster-4 fluorescence spectrometer (Photon Technology International) with a xenon short arc lamp (Ushio), in a 4 ml quartz cuvette with a 1 cm path-length (Roth). All experiments were carried out using a 0.5 nm excitation slit width and a 3.5 nm emission slit width with a scan rate of 0.5 nm/s and 8 nm bandpasses. An appropriate buffer scan was subtracted from each spectrum. All measurements were repeated at least three times. Origin® 7.0 (OriginLab) software was used for the analysis and plotting of the collected data. Normalised fluorescence intensity signal was plotted against the free Ca^{2+} concentration of the sample, and a nonlinear least-squares curve was fitted using Equation 2-2

$$\bar{Y} = \frac{K_1 \times \left[Ca^{2+}_{free}\right] + 2K_2 \times \left[Ca^{2+}_{free}\right]^2}{2\left(1 + K_1 \times \left[Ca^{2+}_{free}\right] + 2K_2 \times \left[Ca^{2+}_{free}\right]^2\right)}$$

Equation 2-2 Two-site model-independent Adair function

$\bar{Y}$ is the fractional occupancy of the binding sites, $\left[Ca^{2+}_{free}\right]$ is the concentration of free Ca^{2+} in the solution, K_1 is the sum of the microscopic equilibrium constants (k1 + k2) of the two Ca^{2+}-binding sites in question (sites I and II or III and IV depending on the excitation wavelength), and K_2 is the product of the microscopic equilibrium constants and a binding cooperativity constant (k1·k2·kc). The apparent macroscopic K_d are reported as the average value for each pair of Ca^{2+}-binding sites, derived from the square root of K_2.

All Ca^{2+}-affinity fluorescence spectroscopy titrations, data collection and processing were performed by Dr Angelos Thanassoulas (Institute of Nuclear and Radiological Sciences, Energy, Technology and Safety, National Center for Scientific Research “Demokritos”)

2.7 Functional Characterisation of Recombinant Protein

2.7.1 [^{3}H]Ryanodine Binding Assays

2.7.1.1 The Principal of [^{3}H]Ryanodine Binding Assay

The mode of action of the plant alkaloid ryanodine is to target and bind to the RyR Ca^{2+} channel. Ryanodine can bind with the highest affinity when RyR is in an open conformation, more likely at higher concentrations of Ca^{2+}. The binding of ryanodine to RyR can, therefore, be altered by the presence of modulators of P_O, e.g. CaM.

The basis of this assay is to incubate radiolabelled ryanodine ([^{3}H]ryanodine) with RyR rich microsomes, in the presence and absence of modulators of RyR P_O. Unbound ryanodine is removed and the amount of [^{3}H]ryanodine measured.

Differences in radioactivity indicate a difference in the amount of [^{3}H]ryanodine binding and so a difference in the conformational state of RyR. Therefore, this assay allows the measurement of the ability of CaM to alter the conformation of native RyR.

2.7.1.2 Measuring Ryanodine Binding to RyR2

Each [^{3}H]ryanodine binding assay contained 200 µg SR prep with 10 nM ryanodine containing [^{3}H]ryanodine to a final assay volume of 300 µl as shown in Table 2-9. Ryanodine binding buffers at specific free Ca^{2+} concentrations were prepared by combining different proportions of stock EGTA and Ca^{2+}, as calculated by Max Chelator (http://maxchelator.stanford.edu/). CaM^{WT} or CaM^{MUT} were added at a final concentration of 1 µM. Control assays contained an equal volume of the buffer in the which the protein was dissolved.Non-specific binding of ryanodine to proteins in the microsomal fraction was assessed by preparing control reactions containing 10 µM unlabelled ryanodine. The reaction was incubated at 37 °C for 90 min before being halted by the addition of 5 ml of ice-cold Wash buffer. The contents of the test tube were filtered under vacuum through a filter pre-soaked with Wash buffer. The test tube was rinsed with another 5 ml of ice-cold Wash buffer which was passed through the same filter. The filter and 5 ml of scintillant were combined in a scintillation vial with and left overnight at room temperature. The [^{3}H]ryanodine present on the filter was measured using a Tri-carb 2100 TR (Packard Bioscience) in counts per min (cpm) for 1 min.

Table 2-9 The components of [^{3}H]ryanodine binding assay reaction.

Component	Volume
Ryanodine binding buffer at specific free Ca^{2+}	150 µl
Ryanodine hot mix	10 µl
SR Prep (200 µg)	100 µl
Recombinant protein (7.5 µM) or Protein buffer (control) or 10 µL 1.5 mM cold Ry and 30 µL Protein buffer (non-specific binding control)	40 µl

2.7.2 Co-Immunoprecipitation Assay

2.7.2.1 The Principal of Co-Immunoprecipitation Assay

Coimmunoprecipitation (CoIP) is the specific precipitation of a protein out of solution using an antibody bound to a solid substrate. The immobilised protein can be isolated and concentrated for downstream analysis. In this instance, solubilised RyR2 is incubated with anti-RyR2 pre-bound to Sepharose beads. The Sepharose beads with immobilised RyR2 were recovered by centrifugation. The immobilised RyR2 was then incubated with CaM. Following incubation, any unbound CaM was removed by centrifugation and wash steps. The Sepharose beads are recovered and separated by SDS-PAGE Immunoblotting with anti-CaM antibody and densitometry measures the

presence of CaM with anti-CaM antibody and densitometry. Therefore, this assay allows the measurement of the ability of CaM recombinant proteins to bind to native RyR2.

2.7.2.2 Measuring Ability of Recombinant CaM to Bind RyR2

The ability of CaM recombinant proteins to bind RyR2 was assayed at three specific free Ca^{2+} concentrations on different three occasions. For each occasion, cardiac SR microsomes prepared from a different heart were used. ImmunoPrecipitation (IP) buffer at specific free Ca^{2+} concentrations was prepared by combining different proportions of stock Ca^{2+} and stock EGTA. For each assay 300 µg of cardiac microsomes were incubated overnight at 4 °C with rolling in 200 µl of IP buffer at specific free Ca^{2+} concentration. The mixture was centrifuged at 20,000x *g* for 10 min at 4 °C, the supernatant was retained, and the pellet was discarded. At the same time for each assay 4 µl of anti-RyR2 (RyR2-specific Ab^{1093} was incubated overnight at 4°C with 20 µl Protein A Sepharose beads (GE Healthcare) in 200 µl of PBS overnight at 4 °C. The mixture was centrifuged at 1,500x *g* for 2 min at 4 °C and the supernatant discarded. The pellet containing beads with immobilised antibody was re-suspended in IP buffer at a specific free Ca^{2+} concentration and centrifuged under the same conditions twice, on each occasion the supernatant was discarded.

Washed beads and solubilised SR proteins were incubated together with 1 µM of recombinant CaM protein for 6 hours at 4 °C with rolling. The mixture was centrifuged at 1,500x *g* for 2 min at 4 °C and washed twice with the appropriate IP buffer as previously. The washed pellet was re-suspended in 20 µl of loading buffer

and incubated at 80 °C for 5 min. Immunoblotting with the anti-CaM antibody visualised the samples separated by SDS-PAGE.

The relative intensity of the CaM specific bands of the CaM proteins compared to that for CaM^{WT} by densitometry. The films were scanned using a GS-800™ Calibrated Imaging Densitometer (BioRad) and images analysed using Quantity One Software (BioRad). Differences in band intensity between the proteins indicates altered RyR/CaM binding.

2.7.3 Isothermal Titration Calorimetry

2.7.3.1 The Principal of Isothermal Titration Calorimetry

Isothermal Titration Calorimetry (ITC) measures heat produced or absorbed on the interaction of two reactants in solution in this case target proteins and ligands. An ITC system contains two cells constantly kept at the same temperature, a reference cell containing a buffer and a reaction cell containing one excess of one reactant. A syringe is used to titrate the other reactant into the reaction cell, and the power required to keep the cells at the same temperature monitored. Power changes reflect any heat changes that are the direct result of binding. Typically, the syringe dispenses the ligand, and the reaction cell contains the target although reverse titrations of the target into excess ligand are also possible. The concentrations of the reactants are known and so the thermodynamic parameters of the binding reaction calculated. Therefore, this assay allows the direct kinetic measurement of the binding of CaM recombinant proteins and binding partners.

2.7.3.2 General ITC Microcalorimeter Set Up

All Isothermal Titration Calorimetry (ITC) experiments were performed using a MicroCal™ VP-ITC microcalorimeter (GE Healthcare) according to manufacturer's instructions. The concentration of the target protein in the ITC reaction cell was optimised from initial experimental results using the concentration calculated using Equation 2-3. The ligand concentration used in the syringe was calculated from Equation 2-4.

$$m[Cell] = \frac{K_d \times c}{n}$$

Equation 2-3 Calculation of the concentration of ITC analyte

$m[Cell]$ is the concentration of the binding partner in the reaction cell, K_d is the dissociation constant of the binding reaction, c is the Wiseman parameter and n is the stoichiometry of the binding reaction. The Wiseman parameter was assumed to be 100 and K_d was based on previous experimental results and published data.

$$m[Syringe] = m[Cell] \times n \times 10$$

Equation 2-4 Calculation of the concentration of ITC titrant

$m[Syringe]$ is the concentration of the binding partner in the syringe, $m[Cell]$ is the concentration of the binding partner in the reaction cell and n is is the stoichiometry of the binding reaction.

2.7.3.3 Measurement of Calmodulin and Ligand Binding Energetics by ITC

Recombinant protein was dialysed at 4 °C against excess (≥500 fold) ITC buffer with two changes of buffer. Differences in buffer composition cause anomalous heat due to dilution effects so, the same batch of buffer was used throughout a set of

experiments. Therefore, a portion of the final dialysis buffer was sterile filtered and retained to be used as a solvent and diluent for all experimental components.

Following dialysis, protein samples were centrifuged at 10,000x *g* for 5 min and the supernatant transferred to a fresh tube. The concentration of the protein was estimated and confirmed as previously described. If necessary, the protein was concentrated as previously described. Concentrated (10X) stock solutions of the peptides, EDTA and $CaCl_2$ were prepared in ITC buffer and sterile filtered.

Working solutions of protein and peptides were prepared by combining concentrated protein or peptide with either stock Ca^{2+} or EDTA and diluting to volume with ITC buffer. The syringe solution was 0.72 mM peptide, and the cell solution was 72 µM protein both contained either 10 mM EDTA or 10 mM Ca^{2+}. Before use, protein and peptide samples were centrifuged at 10,000x *g* for 5 min and the supernatant transferred to a fresh tube.

The calorimeter was set to allow an initial delay of 300 s followed by 16 injections with a delay of 300 s between each one. The initial injection was of 0.4 µL for 5.1 s followed by 15 injections of 2.55 µL for 5.1 s. The reaction temperature was 25 °C, the stirring speed was 1000 rpm, and the Reference Power was 6 µCal/s. A control reaction of titration of the ligand into buffer was performed and subtracted from the integrated binding data.

The data were fitted assuming a one site binding model using MicroCal™ ORIGIN software (OriginLab) in the expectation that CaM binds to the peptides in a 1:1 ratio. ITC data was processed by Dr Angelos Thanassoulas (Institute of Nuclear

and Radiological Sciences, Energy, Technology and Safety, National Center for Scientific Research “Demokritos”).

2.7.4 Crystallisation Experiments

2.7.4.1 The Principal of Protein Crystallography

Protein crystallisation is the formation of a tightly packed repeating array of individual protein molecules, a protein crystal. A well-ordered uncontaminated crystal will yield a diffraction pattern when exposed to X-rays which can be analysed to reveal the tertiary structure of the protein. If the conditions in a protein solution gradually change to those in which the protein becomes insoluble the protein will precipitate in a controlled manner to form crystals.

Vapour diffusion, either by hanging-drop or sitting-drop format, is commonly used in protein crystallisation. A small drop of concentrated protein combined with a buffered precipitant solution is formed on a surface near a reservoir containing a larger volume of the precipitant solution. In hanging-drop, the drop is suspended above the reservoir on an inverted coverslip, and in sitting-drop crystallisation, the drop is on a ledge next to the reservoir. Both reservoir and drop in a sealed environment so that the conditions between the two slowly equilibrate. If the new conditions are conducive to crystal growth, the protein gradually becomes insoluble and precipitates as well ordered crystals.

The conditions in which a specific protein will crystallise are dependent on the characteristics of the protein. Conditions required will vary widely between proteins, so prediction of conditions is difficult. Many other factors influence protein crystal

formation, and different conditions can result in different packing arrangements. For a specific protein, multiple conditions must be trialled to identify those in which crystals will grow that yield an X-ray diffraction pattern.

2.7.4.2 Screening Conditions for Crystals of Recombinant Calmodulin Proteins.

A 96- deep well plate (master plate) containing buffer solutions $(CH_3)_2AsO_2H$, and NaOAc with precipitants MPD and PEG-6000 respectively were prepared, Figure 2-1. The master plate was orientated so acidity increased across columns 1-6 and 7-12 and precipitant concentration increased from row A-H. The master plate was used to produce two screens of crystallisation conditions, Fine screen 1 (FS1) rows A-H and columns 1-6, Fine screen 2 (FS2) rows A-H and columns 7-12. Fine screen 3 (FS3), a custom screen with the same buffer conditions and orientation as Figure 2-1 was also obtained from a commercial supplier (Molecular Dimensions).

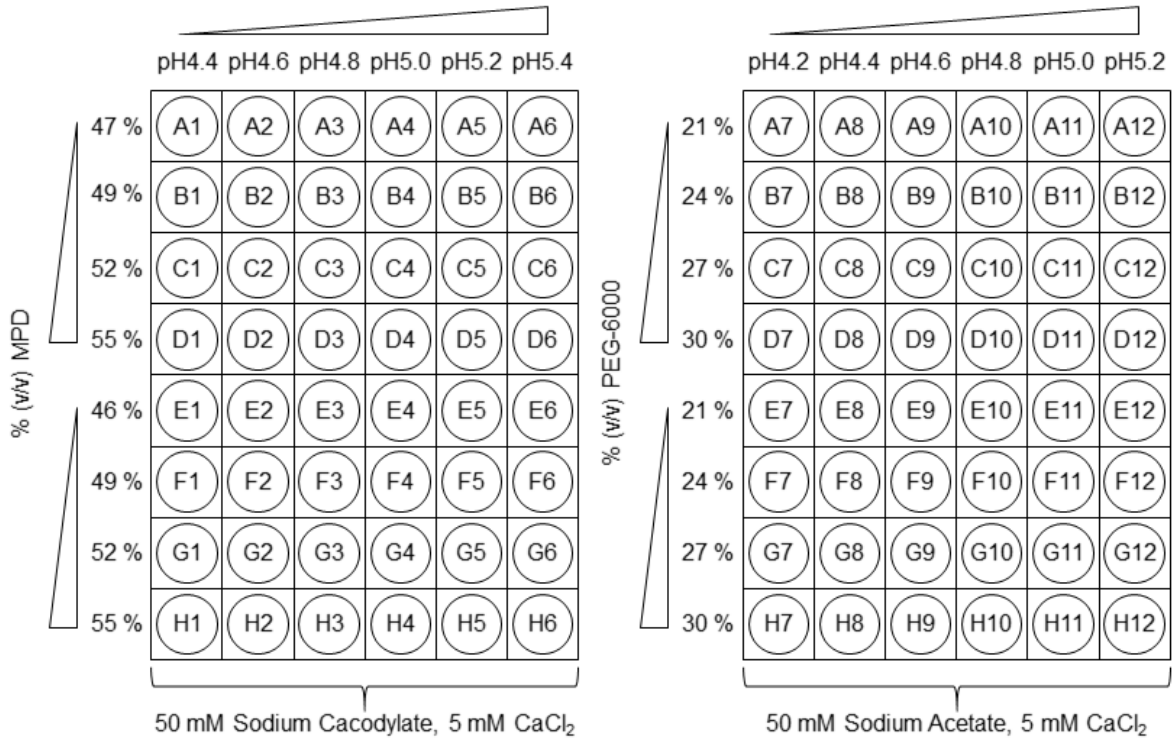

Figure 2-1 Fine Screen Master plate Layout.

A master plate was prepared as above in a deep well 96 well plate comprising two buffers (sodium cacodylate and sodium acetate) of increasing pH, along with titrations of two cryopreservation and precipitants (MPD and PEG-6000).

Two sets of reagents also in deep well plates were obtained, JCSG and PACT (Molecular Dimensions). These reagents form two complimentary screens a systematic grid screen and a sparse matrix screen. Similarly, an additional set of NaOAc buffers supplemented with 0.1 M lithium sulfate and PEG 400 were prepared. The pH ranged from pH4.6 to pH5.6 in increments of pH 0.2 and precipitant from 46 % (w/v) to 52 % (w/v) of PEG 400 in 2 % increments.

Experiments to screen for conditions suitable for the growth of protein crystals were set up on INTELLI-PLATE® 96 Well “sitting drop” vapour diffusion crystallography plates (Art Robbins Instruments) using a Crystal Phoenix Liquid Handling System (Art Robbins Instruments). The conditions used are summarised in Table 2-10 and Table 2-11... The well reservoirs of the crystallisation plate was filled from the corresponding well of the reagent plate. A sitting drop was prepared in the small well by combining, depending on ratio used, 1-2 nl of purified protein and 1-2 nl of reservoir solution. Completed plates were sealed and incubated at either 4 °C or 16 °C. Plates were monitored and observed crystals harvested for further analysis as described in Appendix IV.

Table 2-10 Summary of Crystallisation Experiments with CaM^{WT}

Protein Concentration	Screen	Ratio (Protein:Reservoir solution)	Temperature
9 mg/ml	PACT JCSG FS3	1:1	4°C
		2:1	
		1:1	16°C
		2:1	
20 mg/ml	PACT JCSG FS3	1:1	4°C
		2:1	
		1:1	16°C
		2:1	
		2:1	
20 mg/ml pre-bound to PLCζ peptide	PACT JCSG FS3	1:1	16°C

Protein Concentration	Screen	Ratio (Protein:Reservoir solution)	Temperature
40 mg/ml/ with Lysozyme 20 mg/ml	PACT FS3	1:1	16°C
40 mg/ml with Lysozyme 20 mg/ml	FS3	2:1	16°C

Table 2-11 Summary of Crystallisation Experiments with CaM^{MUT}

Protein (Concentration)	Screen	Ratio (Protein:Reservoir solution)	Temperature
CaM^{F142L} (20 mg/ml)	FS1	1:1	4 °C
		2:1	
		1:2	
		1:1	16 °C
		2:1	
		1:2	
CaM^{D96V} (10 mg/ml)	FS1	1:1	4 °C
		2:1	
		3:1	
		1:1	16 °C
		2:1	
		3:1	

Protein (Concentration)	Screen	Ratio (Protein:Reservoir solution)	Temperature
CaM^{N54I} (11 mg/ml)	FS2	1:1	4 °C
		2:1	
		1:1	16°C
		2:1	
CaM^{N98S} (6 mg/ml)	FS2	1:1	4°C
		2:1	
		1:1	16°C
		2:1	
CaM^{F142L} (20 mg/ml)	FS2	1:1	4°C
		2:1	
		1:1	16°C
		2:1	
CaM^{F90L} (20 mg/ml)	PACT JCSG FS3	1:1	16°C

Chapter 3 - EXPRESSION AND PURIFICATION OF PLCζ

3.1 Chapter Summary

The 3D structure of PLCζ is still to be characterised while the structure of the closest related isoform, PLCδ1, is long established. The major obstacle is the lack of sufficient quantities of soluble pure PLCζ for crystallisation. There are a wide variety of approaches that can be applied to achieve the yields required (Makino, Skretas and Georgiou, 2011; Young, Britton and Robinson, 2012; Rosano and Ceccarelli, 2014). This chapter describes experiments intended to develop tools to increase expression and yield of recombinant PLCζ to a quantity and quality sufficient to set up crystal trays. Two sets of plasmids referred to as the pETMM-D^{210}R and hPLCζ deletion series were set up. The pETMM-D^{210}R series express an inactive mutant of mouse PLCζ (PLCζ^{D210R}) with a variety of affinity tags and solubility partners. The hPLCζ deletion series expresses forty-eight different N- and C-terminal deletion mutants of human PLCζ (hPLCζ) with a Maltose Binding Protein fusion partner. The expression, solubility and large-scale purification yield of the pETMM-D^{210}R series were examined. One construct, MBP-PLCζ^{D210R} was soluble when expressed and could be purified for crystallisation. However, the protein was not stable and did not elute as an intact protein from SEC. Due to the success of expressing soluble recombinant protein with an MBP tag, MBP was chosen as the fusion partner for deletion mutants of human PLCζ. While deletion mutants were expressed, initial studies indicated that the quantity of soluble expressed protein was insufficient for crystallographic studies.

3.2 Introduction

3.2.1 Background

For unknown reasons when using the same prokaryotic expression system the yields of PLCζ proteins are lower than those of PLCδ1. Also, the expression levels and yield of mouse PLCζ (mPLCζ) is higher than human PLCζ (hPLCζ). However, the yield of recombinant protein PLCζ^{D210R} corresponding to the inactive mutant of mPLCζ p(Arg210Asp), was observed to be greater than wild-type mPLCζ when both were expressed as recombinant proteins fused with GST (personal communication, Dr Michail Nomikos, Cardiff University). PLCζ p(Asp210Arg) is a missense mutation in which a conserved aspartic acid (Asp) at position 210 in the X half of the TIM catalytic domain has been substituted for arginine (Arg) abolishing enzymatic activity (Saunders *et al.*, 2002). The equivalent mutation in PLC isoforms also abolishes enzymatic activity but is not predicted to alter the protein structure (Ellis *et al.*, 1998; Katan, 1998; Williams, 1999; Rebecchi and Pentyala, 2000) . Therefore, PLCζ^{D210R} was considered as a candidate for producing enough recombinant protein to produce a 3D crystal structure of mPLCζ. However, the structure of PLCζ^{D210R} would be of a protein that is enzymatically inactive, so correct folding could not be confirmed by activity assay.

Recently, expression of both mouse and human PLCζ was enhanced by the presence of a different solubility partner (Nomikos *et al.*, 2013). Fusion partners can be affinity tags, solubility enhancers or both. The comparative merits of the variety of fusion partners available have been widely reviewed in the literature (Davis *et al.*,

1999; Terpe, 2003; Waugh, 2005; Esposito and Chatterjee, 2006; Young, Britton and Robinson, 2012; Zhao, Li and Liang, 2013; Costa *et al.*, 2014). It is difficult to predict which fusion partner would be optimal for any given target protein. Parallel assessment of different fusion partners has been shown to be a useful tool in optimising production of recombinant proteins (Dummler, Lawrence and de Marco, 2005; Cabrita, Dai and Bottomley, 2006; Hammarström *et al.*, 2009; Bird, 2011; Pacheco *et al.*, 2012; Correa *et al.*, 2014).

The pETMM series of vectors can express a recombinant protein fused to the partners outlined in Table 3-1. Also, the pETMM vectors have similar multiple cloning sites allowing the ligation of a common insert and have the same antibiotic resistance which is convenient for parallel induction of expression. Therefore, the pETMM vectors can be used to screen fusion partners for improvements in the expression of soluble protein.

3.2.2 Rationale and Experimental Plan

To investigate the structure of PLCζ it is desirable to produce recombinant human PLCζ in the quantities required for biophysical and structural studies. In this chapter, a series of plasmids will be designed to express PLCζ^{D210R} with a variety of N-terminal fusion partners to investigate if the yields of PLCζ^{D210R} can be sufficiently improved to generate enough protein for crystallographic studies.

Further optimisation may reveal one or more fusion partner which can increase expression and yield. Use of these fusion partners could be then further optimised by changing the coordinates of the protein expressed. The tertiary structure of other PI-

PLC isoforms has been elucidated by crystallising portions of the full length protein separately.

Table 3-1 Summary of pETMM Expression Vectors

Expression Vector	Size of vector	N-terminal Fusion partner	Size of the fusion partner
pETMM11	5.4 kb	Hexahistidine	**1 kDa**
pETMM20	5.7 kb	Thioredoxin A-Hexahistidine	**13 kDa**
pETMM30	6.0 kb	Hexahistidine- Glutathione S-transferase	**26 kDa**
pETMM41	6.4 kb	Hexahistidine-Maltose binding protein	**43 kDa**
pETMM50	6.0 kb	Disulfide bond formation protein A-Hexahistidine	**22 kDa**
pETMM60	6.8 kb	N-utilisation substance protein A-Hexahistidine	**56 kDa**
pETMM70	5.4 kb	Calmodulin Binding Peptide	**4 kDa**
pETMM80	6.1 kb	Disulfide bond formation protein C	**24 kDa**

3.2.2.1 Fusion Partners

Hexahistidine (6xHis) is an amino acid motif consisting of six His residues with a high affinity for divalent metal ions enabling purification using affinity resin with immobilised nickel ions (Hochuli, Döbeli and Schacher, 1987; Hochuli *et al.*, 1988).

Thioredoxin A (TrxA) reduces disulphide bonds of cytoplasmic proteins in *E.coli* and has been shown to improve expression and solubility (LaVallie *et al.*, 1993, 2000). The crystal structure of recombinant proteins have been resolved with TrxA still attached and the presence of TrxA aided crystal growth (Corsini *et al.*, 2008).

Glutathione S-Transferase (GST) is an *Schistosoma japonicum.* protein that binds to reduced glutathione (GSH) with high affinity so can be purified by affinity chromatography using GSH immobilised on agarose (Smith and Johnson, 1988). Multiple studies have shown while GST has the potential to protect and stabilise recombinant proteins improving solubility, it is a poor solubility enhancer (Costa *et al.*, 2014).

Disulfide bond formation protein A (DsbA) and C (DsbC) are periplasmic *E.coli* proteins which catalyse disulphide bond formation in the periplasmic space ensuring correct protein folding; both increase the solubility of recombinant proteins when expressed in *E.coli* (Collins-Racie *et al.*, 1995; Zhang *et al.*, 2002).

Maltose binding protein (MBP) binds maltose with a high degree of affinity and improves the solubility of recombinant proteins (Pryor and Leiting, 1997; Kapust and Waugh, 1999).

N-utilisation substance protein A (NusA) is an *E.coli* protein with a high predicted solubility which can enhance solubility and prevents aggregation (Davis *et al.*, 1999).

Calmodulin-Binding Peptide (CBP) is a 26 residue peptide with a high affinity for CaM. Fusion proteins containing recombinant CBP can be expressed at high levels and purified to a high degree of purity using CaM affinity chromatography (Stofko-Hahn, Carr and Scott, 1992; Zheng *et al.*, 1997).

3.2.2.2 Deletion Mutations

Another strategy to improve expression in order to have sufficient yield is to express deletion mutations of the target protein with flexible regions omitted to both improve expression and solubility, and aid crystallisation (Derewenda, 2004). This approach has been successful in resolving the 3D structure of PLCδ1 which is derived from crystals produced from two different recombinant proteins representing residues 11-140 and 133-756 (Ellis, Carne and Katan, 1993; Ferguson *et al.*, 1995; Lemmon *et al.*, 1995; Essen *et al.*, 1996). Aggregation or possibly dimerisation of mPLCζ has been observed and appears to be associated with specific domains (unpublished data, laboratory communication).

Therefore, systematic N- and C-terminal deletion mutations of hPLCζ. were designed. Eight N-terminal amino and six C-terminal amino acid coordinates of hPLCζ were selected. Forward primers were designed to yield PCR products corresponding to the amino acid sequence of hPLCζ commencing with Met^{1}, Glu^{29}, Glutamine $(Gln)^{42}$, Tyr^{64}, Thr^{68}, Gln^{100}, Gln^{128}, or Arg^{151}. Reverse primers that would yield PCR products

corresponding to the amino acid sequence of hPLCζ terminating at Arg^{608}, Val^{602}, Arg^{583}, Thr^{572}, Thr^{572}, Glu^{557}or Thr^{524} were designed. Forty-eight recombinant proteins were expressed corresponding to all combinations of the coordinates fused to MBP.

3.3 Results

3.3.1 Construction of PLCζD210R Protein Expression Plasmids

3.3.1.1 Cloning of PLCζD210R into pETMM Vectors

The sequence encoding PLCζ^{D210R} was amplified by PCR from pCR3.1-mPLCζ^{D210R} (Yu *et al.*, 2007) using the primers MzSalIF and MzNotIR, see Figure 3-1, to incorporate a 5'-*SalI* site and a 3'-*NotI* site to facilitate cloning into each of the pETMM expression vectors outlined in Table 3-1. The cloning strategy is outlined in Figure 3-1. The resulting plasmids were termed pETMM11-D^{210}R, pETMM20-D^{210}R, pETMM30-D^{210}R, pETMM41-D^{210}R, pETMM50-D^{210}R, pETMM60-D^{210}R, pETMM70-D^{210}R and pETMM80-D^{210}R. Confirmation of correct clones was carried out by PCR and restriction endonuclease digestion, Figure 3-2.

PCRs containing the cloning primers, and candidate clones were observed to yield a product matching the size of the sequence encoding mPLCζ^{D210R}, Figure 3-2, panel A. The restriction digest liberated two fragments, Figure 3-2, panel B. The smaller fragment is the same for all plasmids and matches the sequence encoding mPLCζ^{D210R}. The larger fragment, different for each plasmid, corresponds to the appropriate vector and indicates that the cloning was successful.

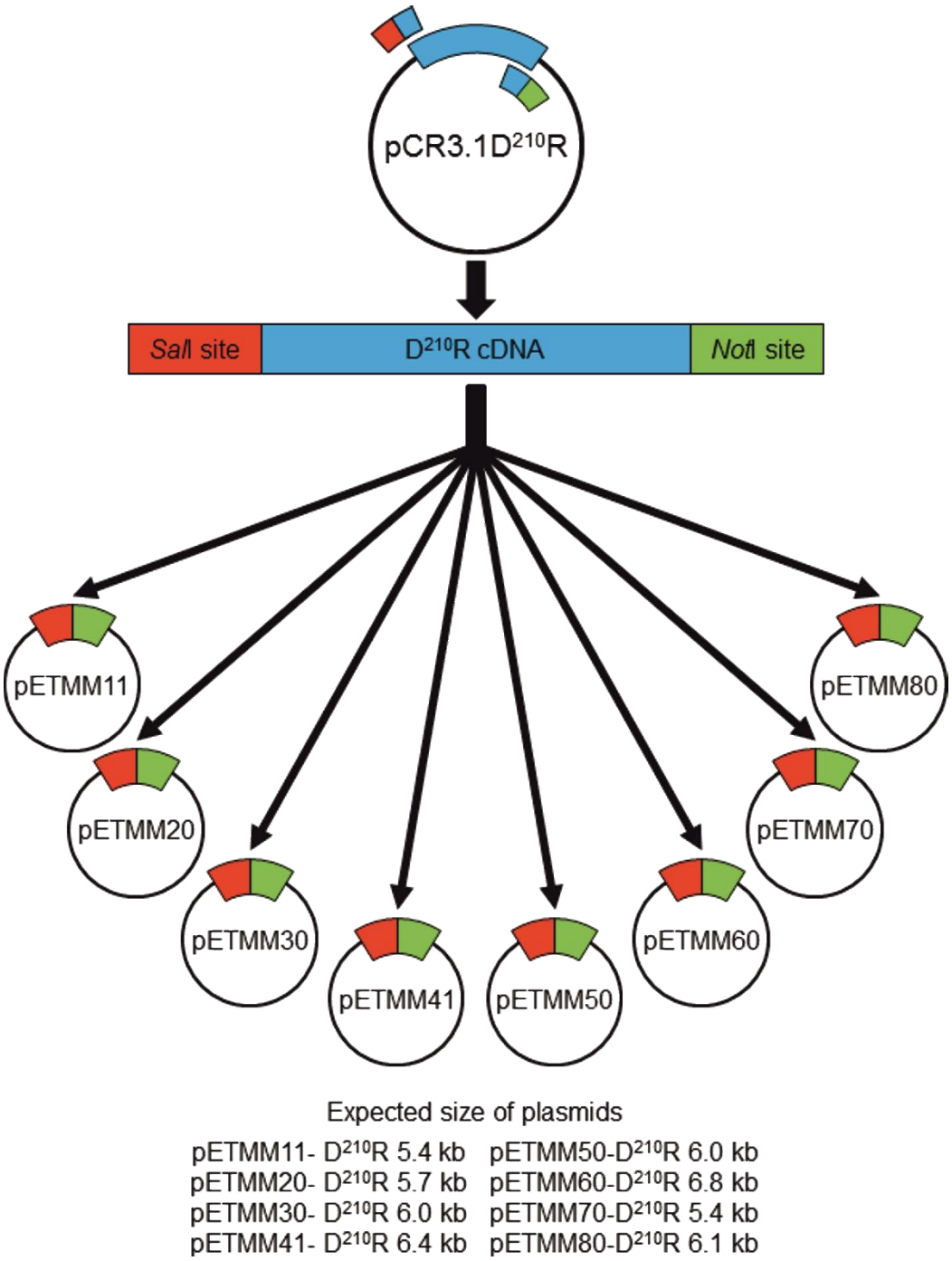

Figure 3-1 Cloning Strategy for Construction of pETMM-D^{210}R Protein Expression Plasmids

A common insert was produced and ligated into eight different vectors using the same enzymes.

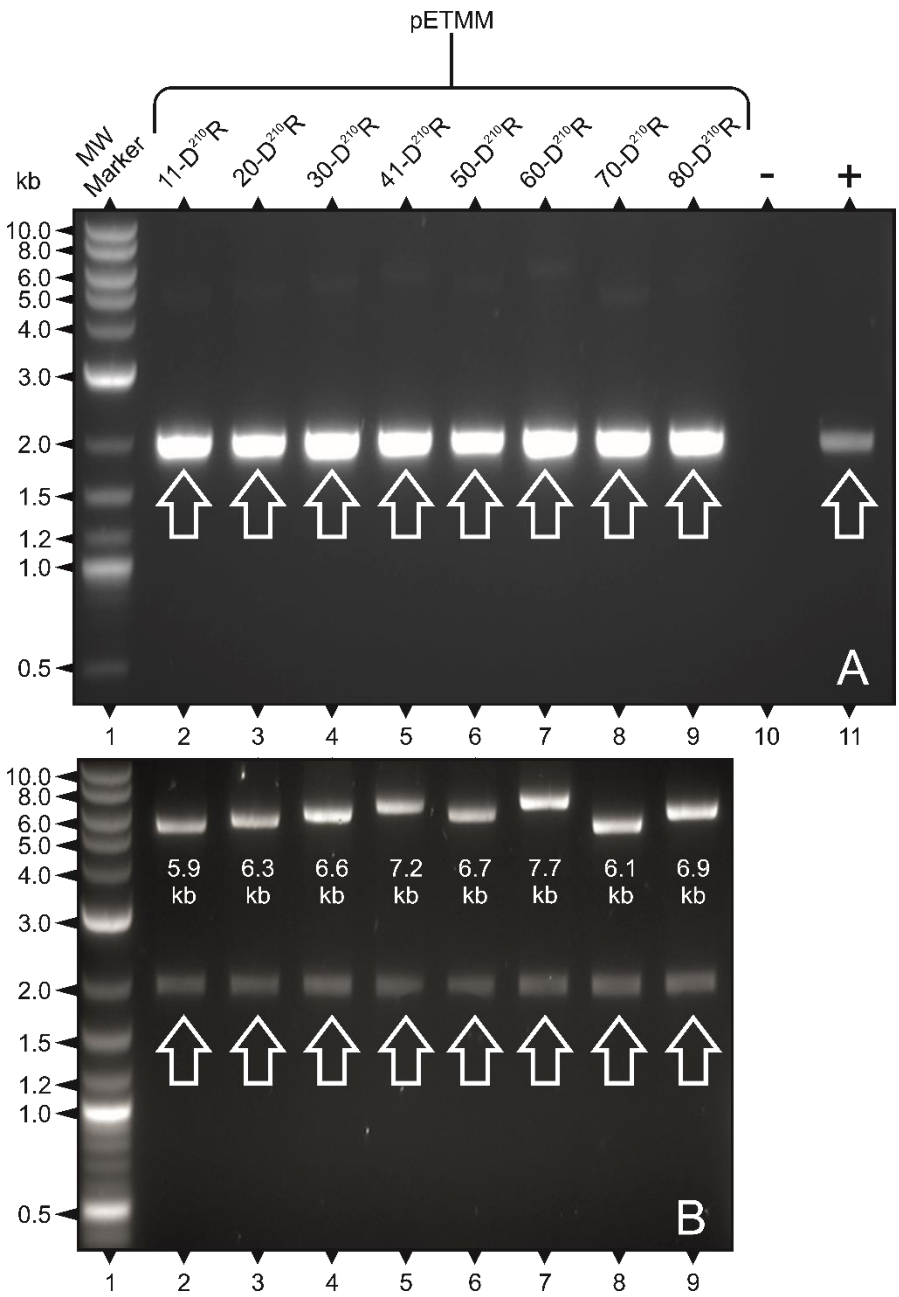

Figure 3-2 Confirmation of pETMM D^{210}R Plasmids.

Agarose gel 1 % (w/v) electrophoresis of PCR and restriction digest products confirmed the identity of candidate clones. **(A)** PCRs except negative control contained a 2.0kb (highlighted) and **(B)** all digests released a 2.0kb fragment and another corresponding to the vector. **(A)** and **(B)**; Lane 1: 2-Log DNA marker (NEB), Lane 2: pETMM11-D^{210}R, Lane 3: pETMM20-D^{210}R, Lane 4: pETMM30-D^{210}R, Lane 5: pETMM41-D^{210}R, Lane 6: pETMM50-D^{210}R, Lane 7: pETMM60-D^{210}R, Lane 8: pETMM70-D^{210}R, Lane 9: pETMM80-D^{210}R. **(A)**; only Lane 10: water, Lane 11: pCR3.1-D^{210}R

3.3.2 Screening Expression and Solubility of PLCζD210R with a Variety of Fusion Partners

3.3.2.1 Screening Expression of PLCζD210R Fusion Proteins

Protein expression *E.coli* strains Rosetta™ (DE3) (R(DE3)) and BL21(DE3) were transformed with the pETMM-D^{210}R plasmids. Both expression strains are BL21 *E.coli* bearing the λDE3 lysogen and both are suitable for recombinant protein expression, The only difference between the strains is the presence of the pRARE plasmid in R(DE3). The pRARE plasmid codes for codon tRNAs found in eukaryotes but rare in prokaryotes. Therefore, protein expression of eukaryotic DNA sequences containing rare codons maybe enhanced in R(DE3) compared to BL21(DE3). Protein expression was induced using conditions previously established as optimal for PLC. Expression could not be induced in BL21(DE3)/pETMM11-D^{210}R as the bacterial culture failed to reach OD_{600}=0.6 on two occasions. The predicted recombinant proteins are shown in Figure 3-3.

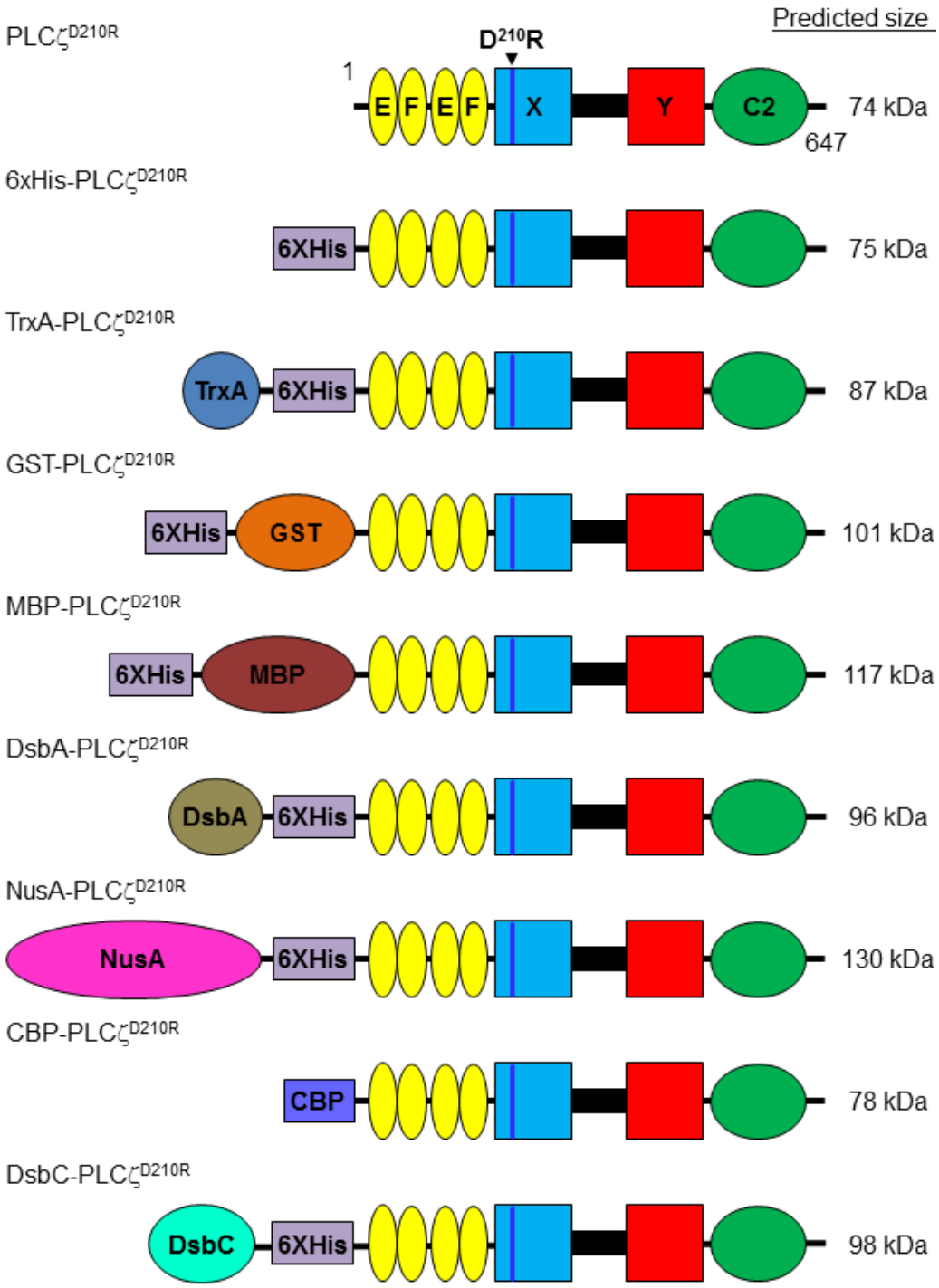

Figure 3-3 PLCζ^{D210R} Expressed with N-Terminal Fusion Partners

Successful induction of expression of E.coli transformed with pETMMD210R plasmids should yield the proteins above.

Expression was initially screened by separating crude lysates using SDS-PAGE, Figure 3-4. Expression levels varied widely with different fusion partners. Between bacterial expression strains, the pattern of expression, excluding 6xHis-$D^{210}R$, was generally similar. However, the expression for individual fusion proteins was higher in R(DE3). When fused with DsbA, DsbC and CBP, $PLC\zeta^{D210R}$ expression was undetectable by Coomassie staining. Protein expression for $PLC\zeta^{D210R}$ fused with either 6xHis or GST was lower than $PLC\zeta^{D210R}$ fused with either TrxA, MBP or NusA.

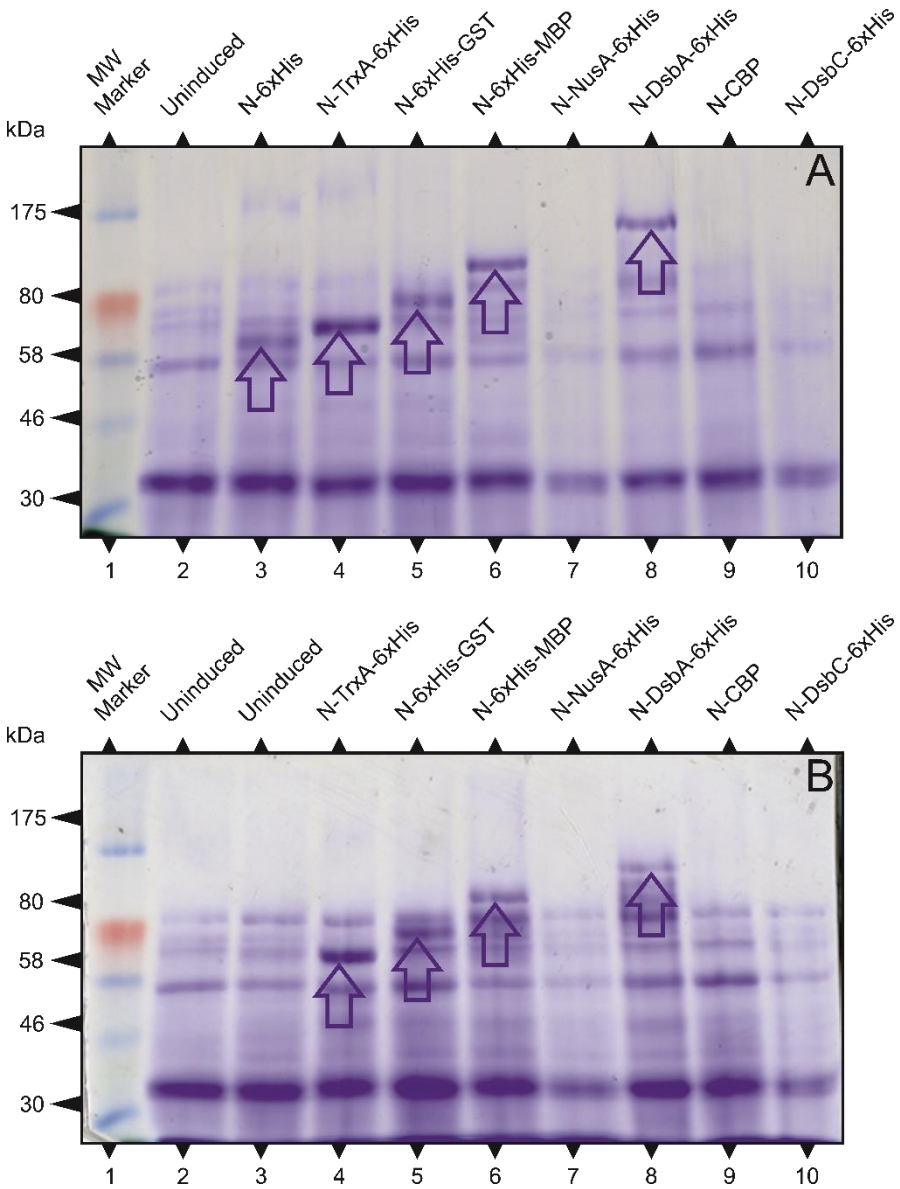

Figure 3-4 PLCζ^{D210R} Expression Varied with Fusion Partner and *E.coli* Strain.

Protein expression was induced in R(DE3) **(A)** and BL21 **(B)** with 0.1 mM IPTG. Crude lysates were separated 7 % (w/v) SDS-PAGE which was stained with Coomasie **(A)** Lane 1: ColorPlus Protein Marker (NEB), Lane 2: Uninduced control Lanes 3-10: crude lysates from induced cultures Lane 3: pETMM11-D^{210}R, Lane 4: pETMM20-D^{210}R, Lane 5: pETMM30-D^{210}R, Lane 6: pETMM41-D^{210}R, Lane 7: pETMM50-D^{210}R, Lane 8: pETMM60-D^{210}R, Lane 9: pETMM70-D^{210}R, Lane 10: pETMM80-D^{210}R **(B)** Lane 1: ColorPlus Protein Marker (NEB), Lanes 2 & 3: Uninduced controls Lanes 4-10: crude lysate from induced cultures Lane 2: R(DE3)/pETMM11-D^{210}R, Lane 4: pETMM20-D^{210}R, Lane 5: pETMM30-D^{210}R, Lane 6: pETMM41-D^{210}R, Lane 7: pETMM50-D^{210}R, Lane 8: pETMM60-D^{210}R, Lane 9: pETMM70-D^{210}R, Lane 10: pETMM80-D^{210}R.

3.3.2.2 Screening Solubility of PLCζD210R Fusion Proteins

The solubility of PLCζ^{D210R} fusion proteins expressed in R(DE3) were assessed by separating soluble and insoluble fractions using SDS-PAGE, Figure 3-5 and Figure 3-6. Only MBP and NusA fusion proteins were detected in the soluble fraction. When PLCζ^{D210R} was fused with 6xHis, GST and TrxA, the fusion proteins were restricted to the insoluble fractions.

Immunoblotting of the soluble and insoluble fractions with anti-PLCζ (Nomikos *et al.*, 2013) confirmed the presence of PLCζ^{D210R} in expressed fusion proteins, Figure 3-5 and Figure 3-6. No PLCζ^{D210} fused to DsbA, DsbC or CBP could be detected confirming lack of expression. Recombinant protein was restricted to the insoluble fractions when fused with 6xHis, TrxA and GST confirming the insolubility of these fusion proteins. The only soluble fractions containing PLCζ^{D210R} were those for R(DE3)/pETMM41-D^{210}R and R(DE3)/pETMM60-D^{210}R. However, the NusA-PLCζ^{D210R} detected was around 60 kDa suggesting that NusA-PLCζ^{D210R} had undergone proteolysis, potentially as a result of sonication.

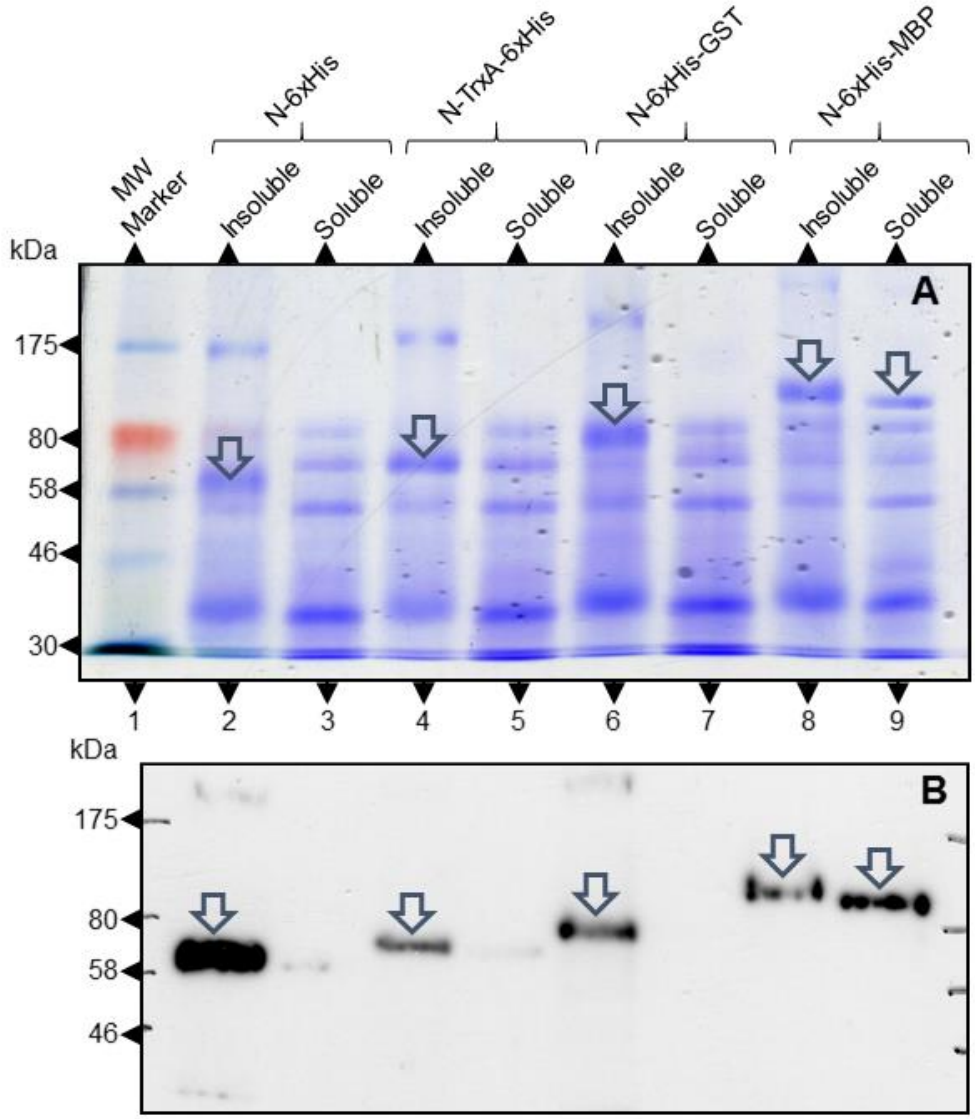

Figure 3-5 MBP-PLCζ^{D210R} Is Expressed and Is Present in the Soluble Fraction

Expression of PLCζ^{D210R} with fusion partners was induced in R(DE3) with 0.1 mM IPTG. The insoluble and soluble fractions were separated by SDS-PAGE **(A)** Coomassie stained 7 % (w/v) gel Lane 1: ColorPlus Prestained Protein Marker (NEB), Lanes 2–9: re-suspended pellet (even lanes) and clarified lysate (odd lanes) of R(DE3) induced with 0.1MM IPTG. Lanes 2&3: pETMM11-D^{210}R, Lanes 4&5: pETMM20-D^{210}R, Lanes 6&7: pETMM30-D^{210}R, Lanes 8&9: pETMM41-D^{210}R **(B)** Corresponding immunoblot to (A). Primary antibody: anti-PLCζ (1:10,000), secondary antibody: anti-rabbit HRP (1: 10,000). Exposure: 30 s.

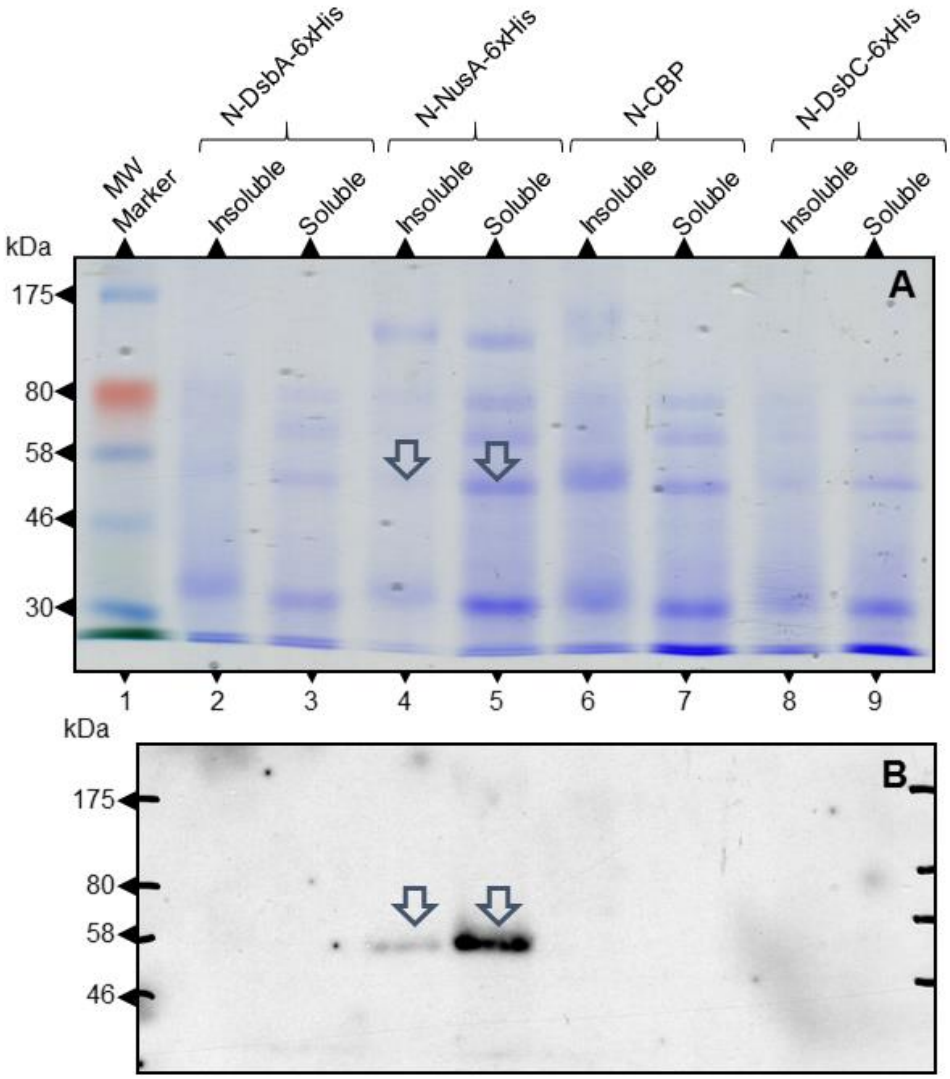

Figure 3-6 Expressed NusA-PLCζ^{D210R} Yielded a Breakdown Product That Was Present in the Soluble Fraction and Was Recognised by IgG Specific for PLCζ EF Hands

Expression of PLCζ^{D210R} with fusion partners was induced in R(DE3) with 0.1mM IPTG. The insoluble and soluble fractions were separated by SDS-PAGE **(A)** Coomassie stained 7 % (w/v) gel Lane 1: ColorPlus Prestained Protein Marker (NEB), Lanes 2–9: Clarified lysate (even numbered lanes) and re-suspended pellet (odd numbered lanes) Lanes 2&3: pETMM50-D^{210}R, Lanes 4&5: pETMM60-D^{210}R, Lanes 6&7: pETMM70-D^{210}R, Lanes 8&9: pETMM80-D^{210}R (**B**) Corresponding immunoblot to **(A)**. Primary antibody: anti-PLCζ (1:10,000), secondary antibody: anti-rabbit HRP (1: 10,000). Exposure: 30 s.

3.3.3 Purification of PLCζD210R Fusion Proteins

3.3.3.1 Small-Scale Purification of PLCζD210R

Based on expression levels and solubility of MBP-PLCζ^{D210R} and NusA-PLCζ^{D210R} in R(DE3), these constructs were chosen for further screening by small-scale purification. MBP-PLCζ^{D210R} and NusA-PLCζ^{D210R} were purified by batch affinity chromatography. SDS-PAGE of the purification fractions, Figure 3-7, revealed the yield of eluted MBP-PLCζ^{D210R} that was greater from the same volume of bacterial culture than NusA-PLCζ^{D210R}. Amylose affinity purification shown in Figure 3-7, panel A appeared to be more effective, as the elution fraction contained a protein band of the expected size while the elution fraction for the nickel resin purification contained no visible bands. NusA-PLCζ^{D210R} was present in most fractions apart from the elution and re-suspended pellet fractions indicating that all bound protein was eluted during washes. Accordingly, MBP-PLCζ^{D210R} was chosen for large-scale expression and purification.

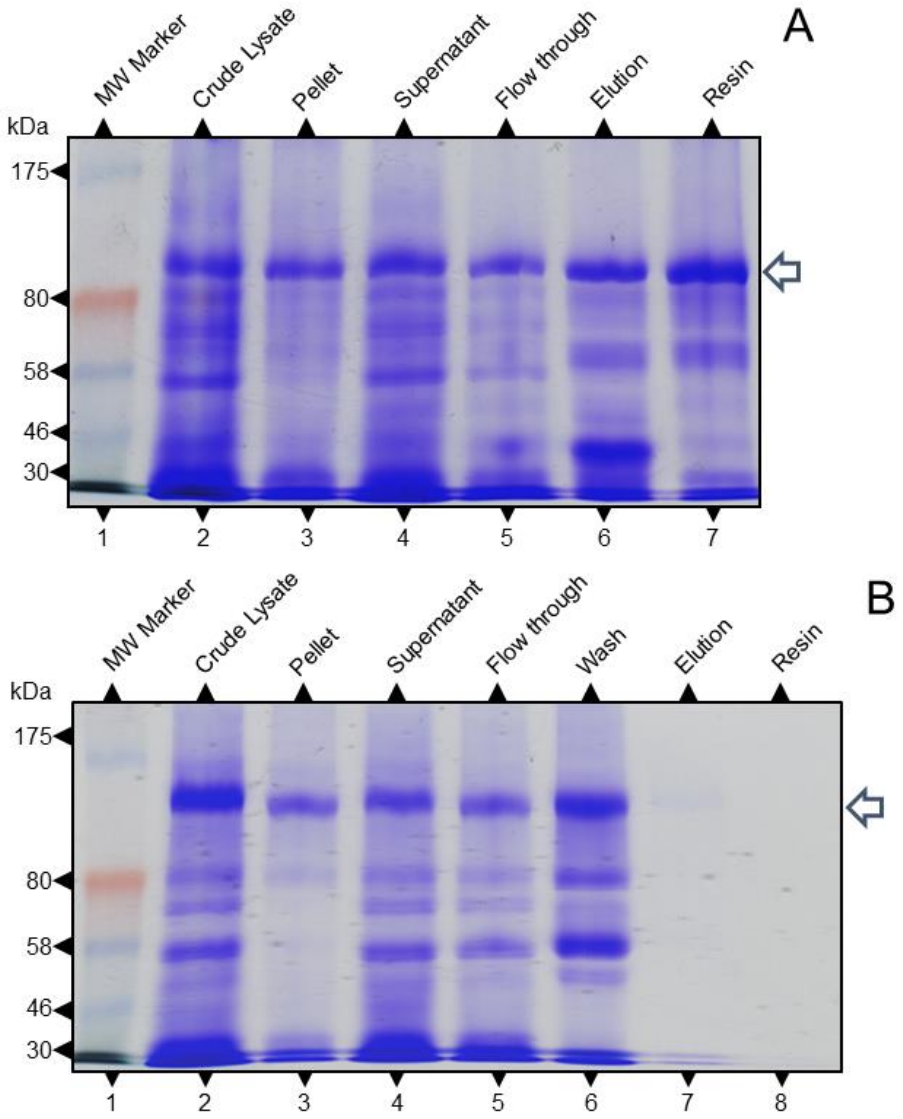

Figure 3-7 MBP-PLCζ^{D210R} Purified by Batch Affinity Purification

Fractions from batch affinity purification of pellets derived from 200 ml culture induced with 0.1 mM IPTG. Fractions of R(DE3)/pETMM41-D^{210}R purified with amylose resin **(A)** and R(DE3)/pETMM60 D^{210}R purified with NiNTA resin **(B)** were separated by 7 % (w/v) SDS-PAGE and stained with Coomassie. **(A)** Lane 1: Color Plus Prestained Protein Marker (NEB), Lane 2: crude lysate, Lane 3: supernatant, Lane 4: resuspended pellet, Lane 5: Flow-through, Lane 6: 10 mM Maltose Elution Lane 7: Resuspended resin. **(B)** Lane 1: Color Plus Prestained Protein Marker (NEB), Lane 2: crude lysate, Lane 3: supernatant, Lane 4: resuspended pellet, Lane 5: Flow-through, Lane 6: 60 mM Imidazole Wash, Lane 7: 250 mM Imidazole Elution, Lane 8: resuspended resin.

3.3.3.2 Large-Scale Expression and Purification of MBP- PLCζD210R

Re-suspended pellets representing 12 l of expression culture were pooled, lysed and clarified. The clarified lysate was split into two equal aliquots. As MBP-PLCζ^{D210R} has two affinity tags, 6xHis and MBP, large-scale purification using Ni-NTA and Amylose resin was performed in parallel to assess relative effectiveness. The aliquots were purified separately by gravity column affinity chromatography using Ni-NTA and amylose resin. Purification fractions were separated by SDS-PAGE, Figure 3-8. The MBP purification elution fractions, Figure 3-8, panel A, showed higher amounts of protein than the 6xHis tag purification, Figure 3-8, panel B. However, a protein band higher than 175 kDa, indicating protein aggregation, was also observed in the elution fractions from the amylose purification, in Figure 3-8, panel A.

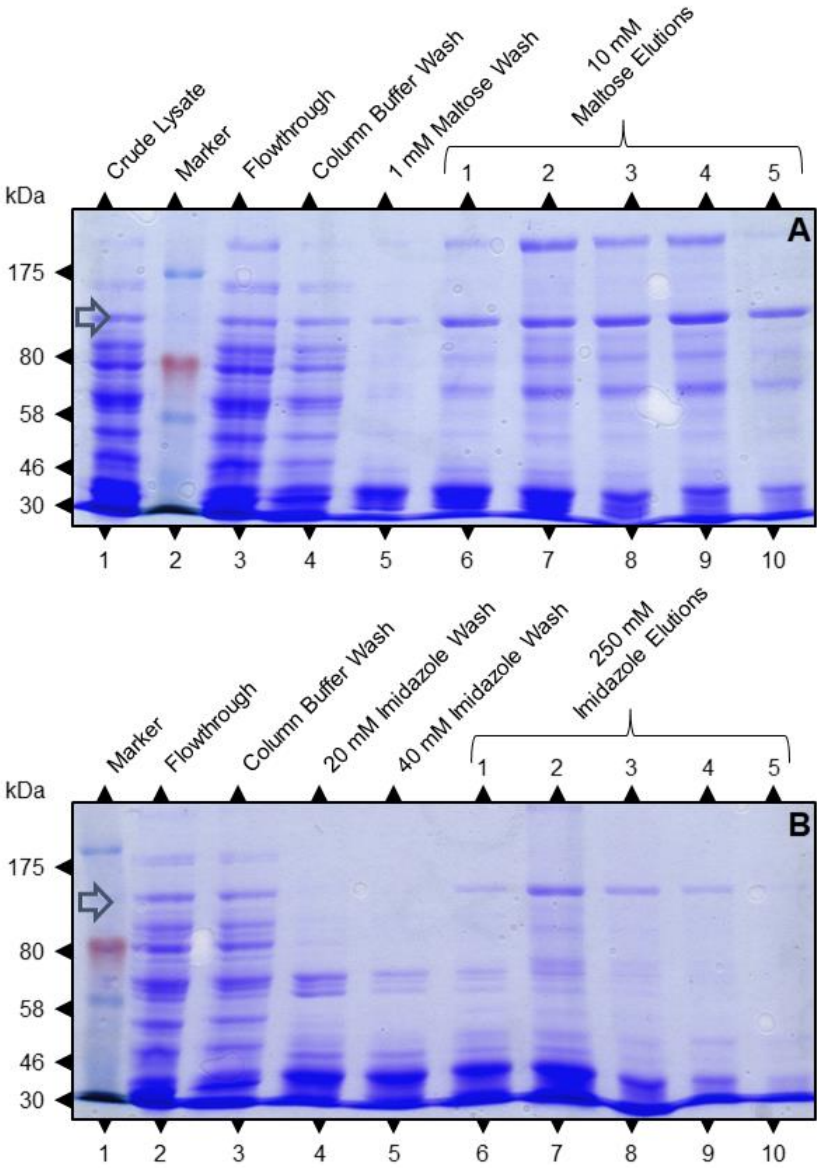

Figure 3-8 Amylose Resin Purification of MBP-PLCζ^{D210R} Contain Greater Recombinant Protein Than Those from Ni-NTA resin purification

Fractions from amylose resin **(A)** and Ni-NTA resin **(B)** column affinity purifications of pellets each derived from 6 L of R(DE3)/pETMM41-D^{210}R culture induced with 0.1 mM IPTG; were separated by 7 % (w/v) SDS-PAGE and stained with Coomasie . **(A)** Lane 1: crude lysate, Lane 2: ColorPlus Prestained Protein Marker (NEB), Lane 3: flowthrough, Lane 4: column wash, Lane 5: 1 mM maltose wash, Lanes 6-10: 10 mM maltose elutions.**(B)** Lane 1: Color Plus Prestained Protein Marker (NEB), Lane 2: crude lysate, Lane 3: flowthrough, Lane 4: column wash, Lane 5: 20 mM imidazole wash, Lane 6: 40 mM imidazole wash Lanes 7-10: 250 mM imidazole elutions**.**

All elution fractions were pooled and purified further using SEC. The UV Trace, Figure 3-9, indicates the protein eluted from the column in two peaks. The first peak corresponds with the void volume, while the second peak corresponds to a protein that is approximately 40 kDa in size. The fractions within both peaks were separated using SDS-PAGE, Figure 3-9 Panels A and B. As can be seen in Panel A, Figure 3-9, elution volume of 45 ml to 47 ml contains a protein of 100 kDa matching the predicted size of MBP-PLCζ^{D210R}. Meanwhile, as can be seen in Panel B, Figure 3-9, elution volume 80 ml to 85 ml contains a protein of 40 kDa matching MBP. These results indicate that MBP-PLCζ^{D210R} is not remaining soluble and intact in the gel filtration buffer. Possibly, MBP-PLCζ^{D210R} is undergoing partial proteolysis releasing MBP, which remains soluble and passes through the column. Meanwhile, intact MBP-PLCζ^{D210R} appears to forms aggregates and is washed out of the column. Another possibility is that PLCζ^{D210R} undergoes dimerisation when in solution, which has been observed but not investigated in other recombinant PLCζ proteins (unpublished data, laboratory communication).

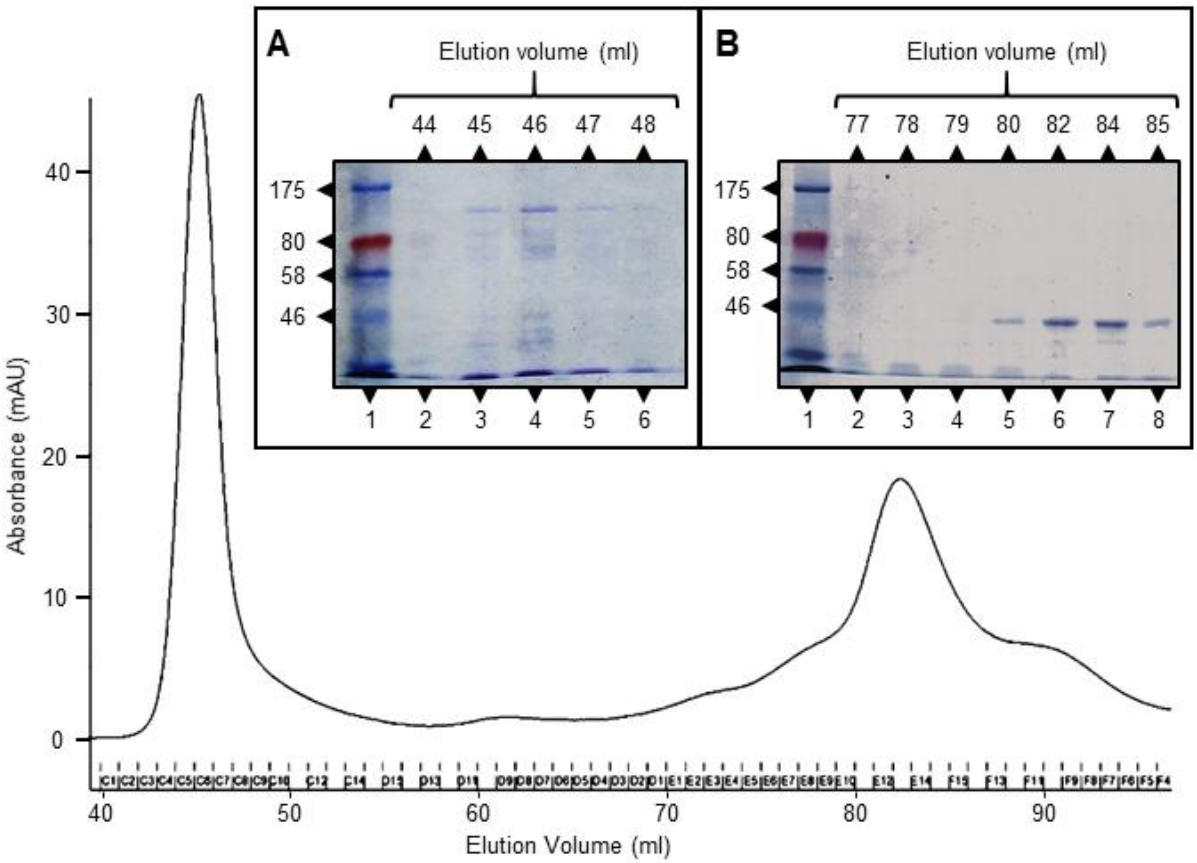

Figure 3-9 MBP-PLCζ^{D210R} Elutes from SEC Column in Two Peaks

Pooled and concentrated purification elution fractions were loaded onto a Superdex 200 SEC Column (GE Healthcare) with a 2 ml Superloop and eluted with pH 7.4 50 mM Tris 100 mM NaCl in two peaks at 46 ml and 84 ml. SEC fractions from within the main peaks were collected and separated by SDS-PAGE. Main figure, UV trace of preparative SEC. Insets, Coomassie stained 7 % (w/v) SDS-PAGE gel elution fractions (volumes as shown) occurring around the volume of 46 ml Panel A and 80 ml Panel B, first lane of panel A & B ColorPlus Prestained Protein Marker (NEB).

3.3.4 Construction of hPLCζ Deletion Mutants

3.3.4.1 Cloning hPLCζ Deletion Mutants into pETMM41

A series of forty-eight N- and C- terminal deletion mutants of hPLCζ proteins were designed. The series comprised all combinations of eight N-terminal and six C-terminal amino acid coordinates of hPLCζ as shown in Figure 3-10. DNA sequences corresponding to these coordinates were amplified by PCR from pCR3.1-hPLCζ (Yu *et al.*, 2007) using primers shown in Table 3-2, which also shows the amino co-ordinates encoded. All forward primers contained a 5'-*Sal*I site followed by the gene-specific region and reverse primers incorporated a 3'-*Not*I site in addition to the gene-specific region to facilitate cloning into pETMM41.

For each plasmid, confirmation of successful cloning was assessed by two PCR reactions. The first PCR reaction contained the insert specific forward cloning primer and the vector specific reverse primer, mmUR(2). The second PCR reaction contained the insert specific reverse cloning primer and a vector specific forward primer, mm41F. The primer sequences are shown in the Appendix Table I. The PCR products were resolved by gel electrophoresis as shown in Figure 3-12 and Figure 3-13. All PCR reactions yielded a DNA product of approximately the correct size. Sequence identity and exact coordinates were confirmed by sequencing with primers specific for sequences flanking the MCS in both the forward and reverse directions.

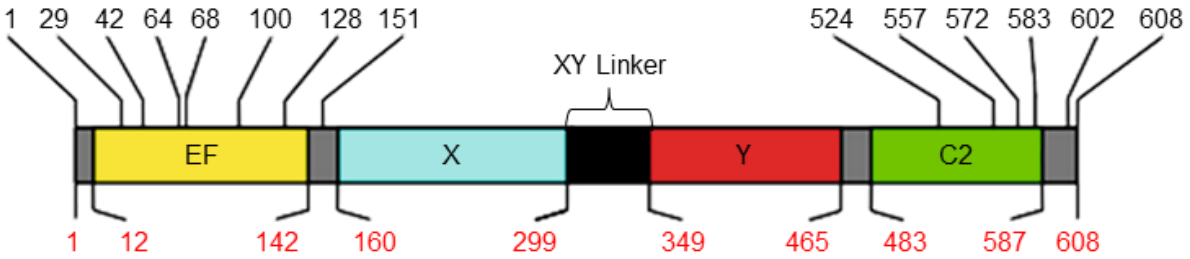

Figure 3-10 Eight N-Terminal and Six C-Terminal Amino Acid Coordinates Selected for hPLCζ Deletion Mutants

The co-ordinates chosen are shown in black and domain boundaries are shown in red.

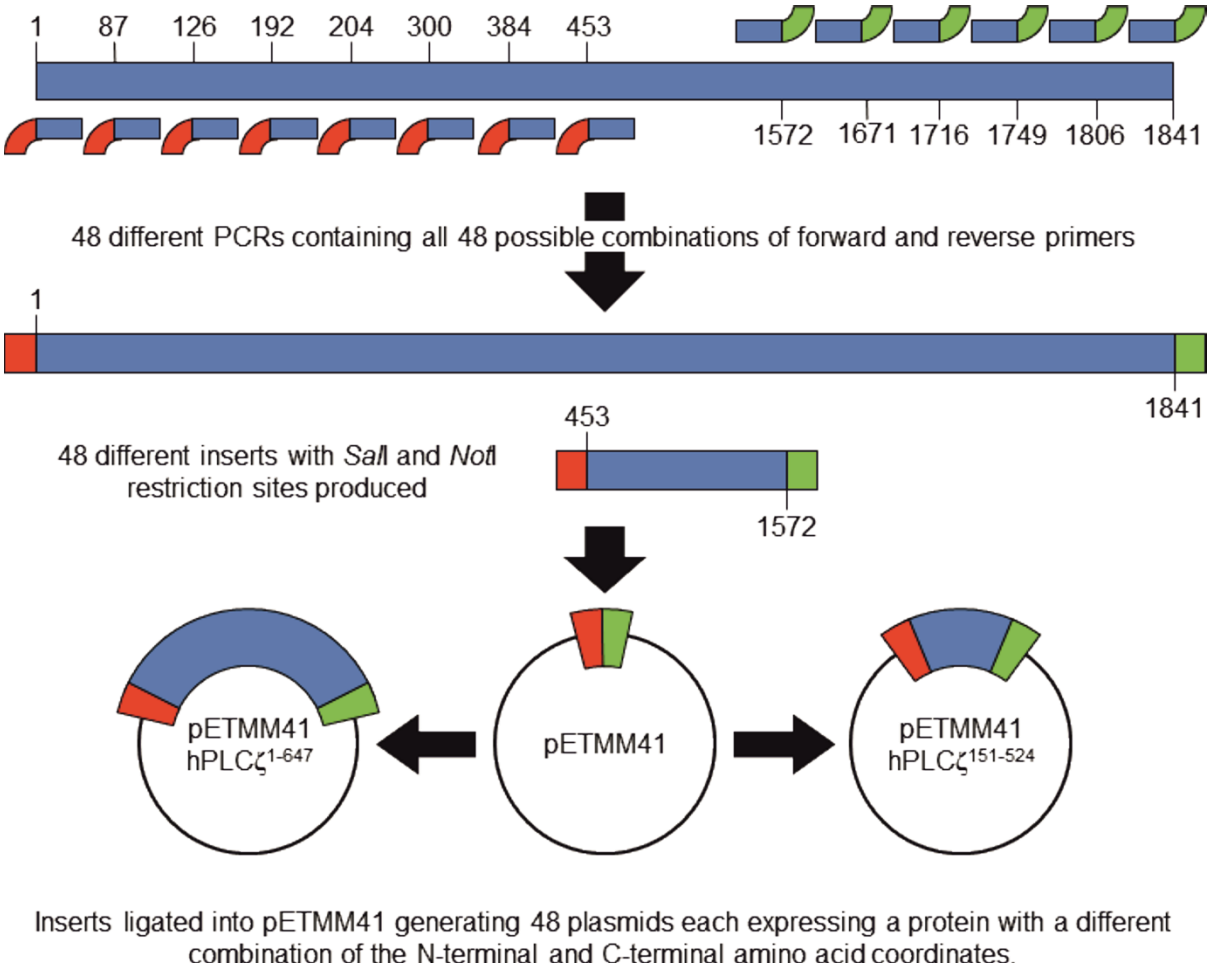

Figure 3-11 Deletion Mutant Cloning Strategy

Eight forward primers with a SalI restriction site overhang (red) and six reverse primers with a NotI restriction site overhang (green) restriction corresponding to the N-terminus and C terminus co-ordinates respectively. The primers were used to generate 48 different inserts corresponding to all the possible combinations. All the inserts were ligated into the pETMM41 vector.

Table 3-2 Primer Pairs for Truncation Series PCR.

Primer	Hz608R	Hz602R	Hz583R	Hz572R	Hz557R	Hz524R
Hz1F	1849bp (Met^{1}-Arg^{608})	1831bp (Met^{1}-Val^{602})	1774bp (Met^{1}-Arg^{583})	1741bp (Met^{1}-Thr^{572})	1696bp (Met^{1}-Glu^{557})	1597bp (Met^{1}-Thr^{524})
Hz29F	1765bp (Glu^{29}-Arg^{608})	1747bp (Glu^{29}-Val^{602})	1690bp (Glu^{29}-Arg^{583}	1657bp (Glu^{29}-Thr^{572})	1612bp (Glu^{29}-Glu^{557})	1513bp (Glu^{29}-Thr^{524})
Hz42F	1726bp (Gln^{42}-Arg^{608})	1708bp (Gln^{42}-Val^{602})	1651bp (Gln^{42}-Arg^{583})	1618bp (Gln^{42}-Thr^{572})	1573bp (Gln^{42}-Glu^{557})	1474bp (Gln^{42}-Thr^{524})
Hz64F	1660bp (Tyr^{64}-Arg^{608})	1642bp (Tyr^{64}-Val^{602})	1585bp (Tyr^{64}-Arg^{583})	1552bp (Tyr^{64}-Thr^{572})	1507bp (Tyr^{64}-Glu^{557})	1408bp (Tyr^{64}-Thr^{524})
Hz68F	1648bp (Thr^{68}-Arg^{608})	1630bp (Thr^{68}-Val^{602})	1573bp (Thr^{68}-Arg^{583})	1540bp (Thr^{68}-Thr^{572})	1495bp (Thr^{68}-Glu^{557})	1396bp (Thr^{68}-Thr^{524})
Hz100F	1552bp (Gln^{100}-Arg^{608})	1534bp (Gln^{100}-Val^{602})	1477bp (Gln^{100}-Arg^{583})	1444bp (Gln^{100}-Thr^{572})	1399bp (Gln^{100}-Glu^{557})	1300bp (Gln^{100}-Thr^{524})
Hz128F	1468bp (Gln^{128}-Arg^{608})	1450bp (Gln^{128}-Val^{602})	1393bp (Gln^{128}-Arg^{583})	1360bp (Gln^{128}-Thr^{572})	1315bp (Gln^{128}-Glu^{557})	1216bp (Gln^{128}-Thr^{524})
Hz151F	1399bp (Arg^{151}-Arg^{608})	1381bp (Arg^{151}-Val^{602})	1324bp (Arg^{151}-Arg^{583})	1291bp (Arg^{151}-Thr^{572})	1246bp (Arg^{151}-Glu^{557})	1147bp (Arg^{151}-Thr^{524})

The size of the resulting PCR product and the amino co-ordinates of hPLCζ encoded are shown

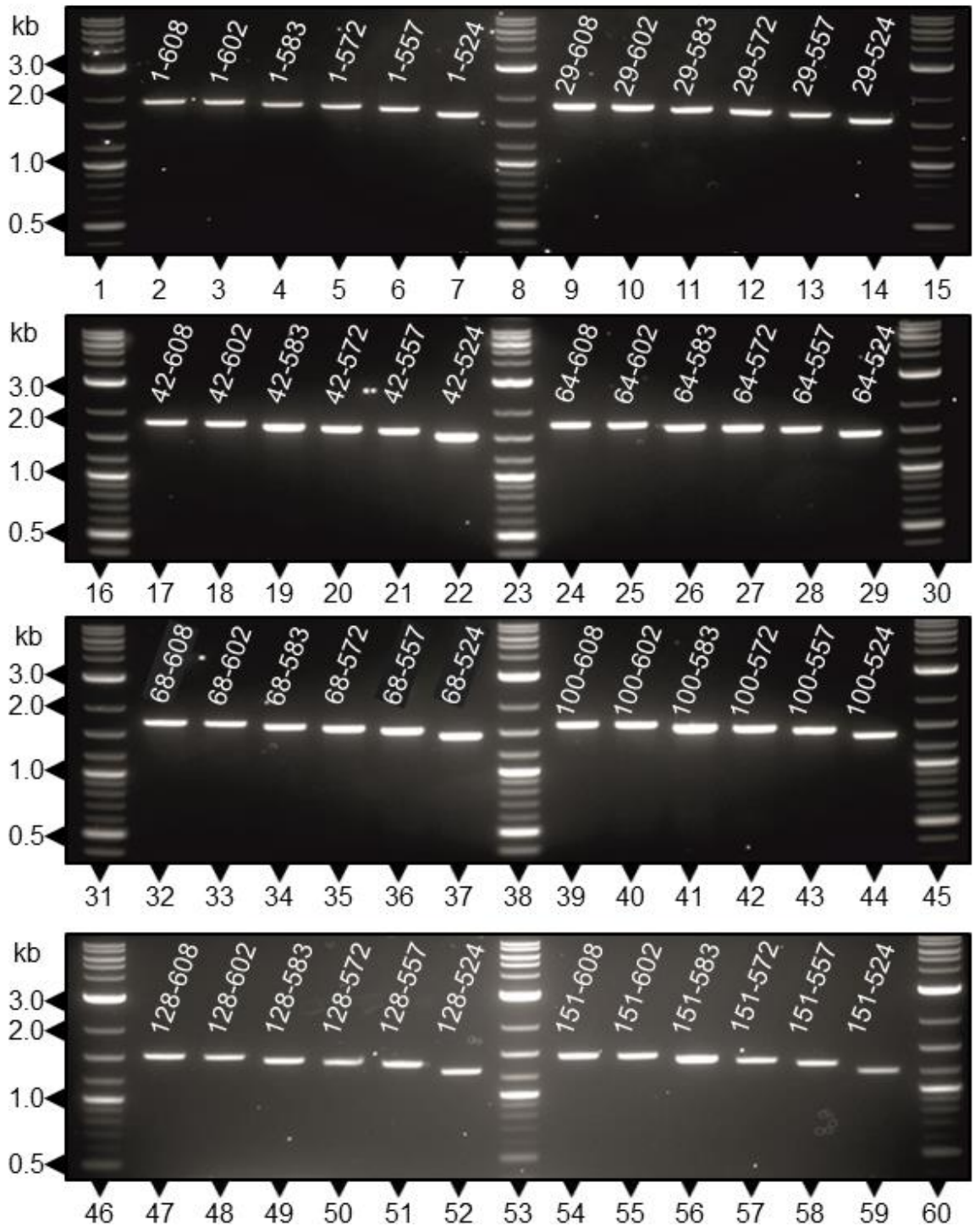

Figure 3-12 Forward Specific PCR Confirmation of hPLCζ Deletion Mutants

Lanes 1, 8, 15, 16, 23, 30, 31, 38 45, 46, 60: 2-Log DNA marker (NEB). Remaining lanes: the products of PCRs containing truncation series plasmids encoding the amino acid coordinates shown as templates, mmUR(2) and forward cloning primer specific for those coordinates.

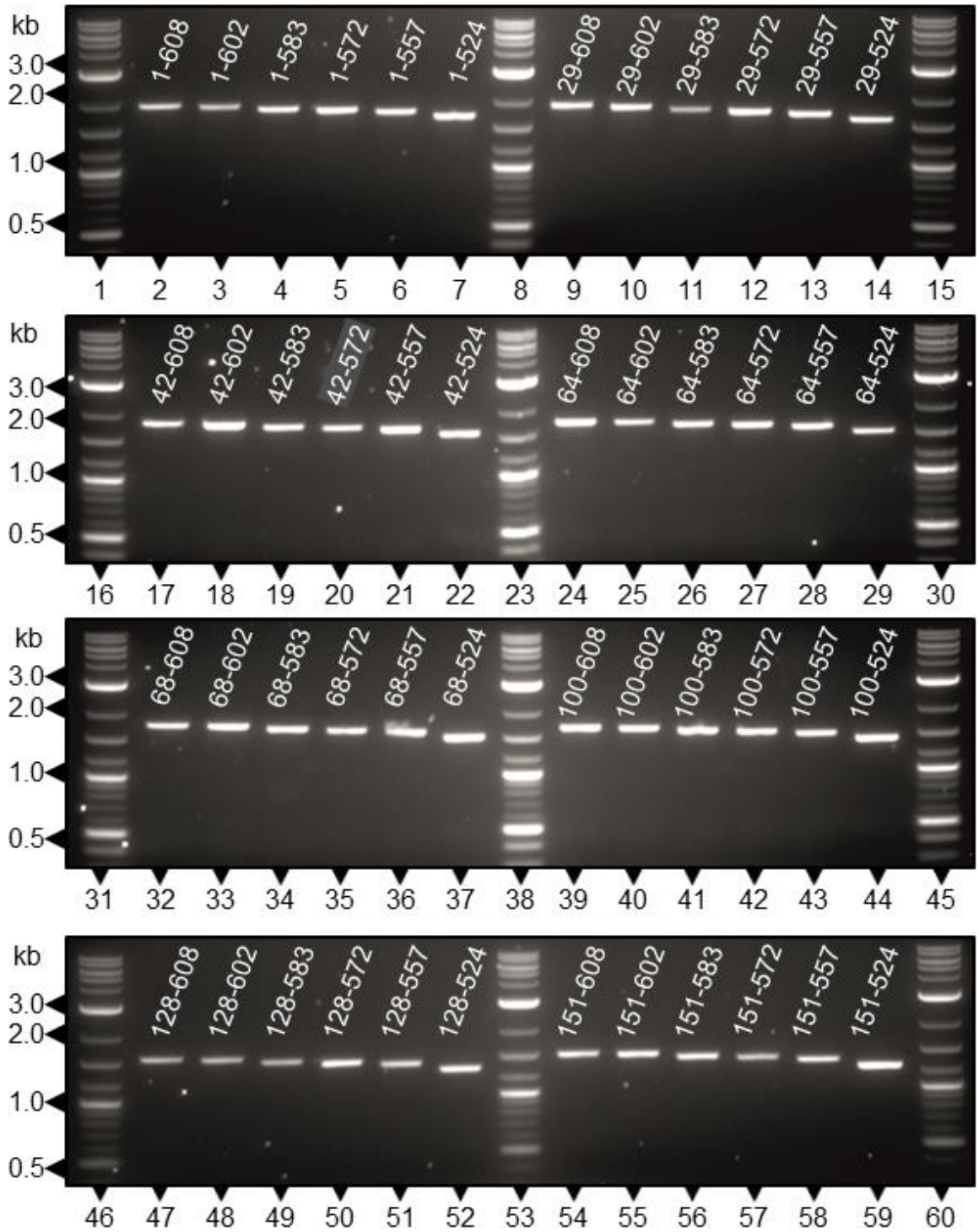

Figure 3-13 Reverse Specific PCR Confirmation of hPLCζ Deletion Mutants

Lanes: 1, 8, 15, 16, 23, 30, 31, 38 45, 46, 60: 2-Log DNA marker (NEB). Remaining lanes: the products of PCRs containing truncation series plasmids encoding the amino acid coordinates shown as templates, mm41F and reverse the cloning primer specific for those coordinates.

3.3.5 Screening Expression and Solubility of hPLCζ Deletion Mutants.

3.3.5.1 Optimising Expression Strain

Additional *E.coli* strains with differing features to enhance recombinant protein expression were available. The Gami(DE3) strain permits enhanced disulfide bond formation and expression of eukaryotic proteins that contain codons rarely used in E. coli. Meanwhile, pLysS indicates the presence of pLysS plasmid expressing T7 lysozyme which reduces basal expression of recombinant proteins enhancing the induced expression of genes toxic to bacteria. The CH184 strain bears mutations resulting in a reduced rate of polypeptide synthesis enabling soluble expression of correctly folded multidomain eukaryotic protein prone to aggregation when expressed in prokaryotes (Siller *et al.*, 2010; Zhu, Dai and Wang, 2016). All could enhance expression of PLCζ so six protein expression *E.coli* strains were screened, BL21(DE3), BL21(DE3)pLysS, CH184, R(DE3), Rosetta™ (DE3)pLysS (R(DE3)pLyS), Rosetta-gami™ 2(DE3) (Gami(DE3)), were transformed with pETMM41-PLCζ$^{1-647}$ and pETMM41-PLCζ$^{151-524}$.

Due to transformation failure on two occasions BL21(DE3)pLysS and Gami(DE3) were not pursued further. Protein expression was induced in the four remaining bacterial strains, and the prepared crude lysates were separated by SDS-PAGE, Figure 3-15. As can be seen in Figure 3-15, the expression for both hPLCζ mutants were only successful in BL21(DE3) with the best overall expression being observed with hPLCζ$^{151-524}$ in BL21(DE3). Expression failed in CH184. In R(DE3), only hPLCζ$^{1-647}$ was expressed and in R(DE3)pLysS, only hPLCζ$^{151-524}$ was expressed.

Therefore, BL21(DE3) was chosen to screen expression of all the deletions hPLCζ mutants.

Aliquots of BL21(DE3) were transformed with all 48 plasmids, transformation with pETMM41-PLCζ$^{29-583}$ failed on two occasions, so this plasmid was not further pursued. Expression was induced in 100 ml of bacterial culture, and crude lysates were separated by SDS-PAGE as shown in Figure 3-16. All hPLCζ fusion proteins showed high levels of expression except those terminating in Valine (Val) at 602

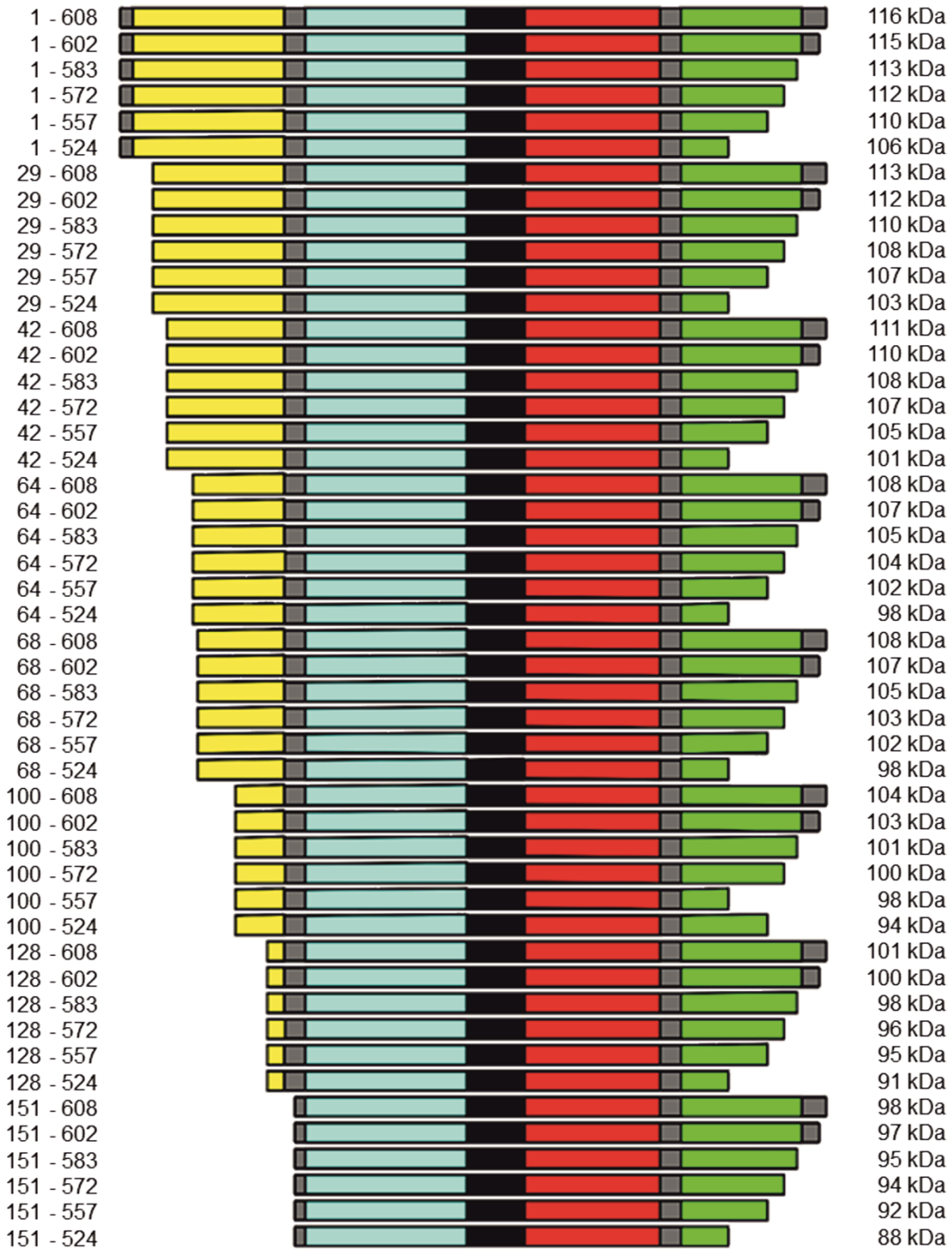

Figure 3-14 PLCζ N-Terminal and C-Terminal Deletion Mutants

PLCζ (EF hands yellow, X blue, XY linker black, Y red and C2 green) deletion mutants, of given coordinates, expressed with an N-terminal MBP tag not shown but included in expected size.

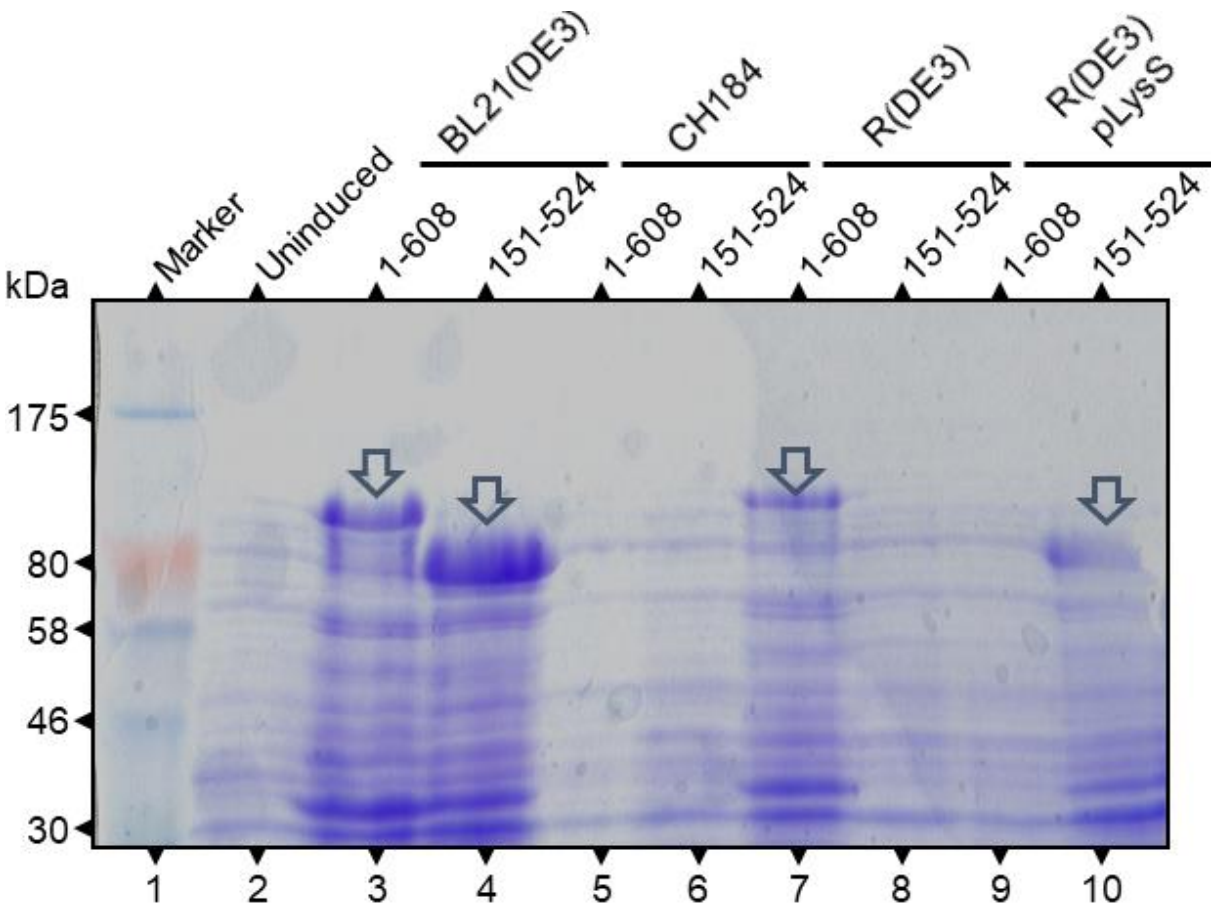

Wang Zhixin

Figure 3-15 Expression of hPLCζ$^{1-608}$ and hPLCζ$^{151-524}$ Varied with *E.coli* Strain

Expression of hPLCζ$^{1-608}$ and hPLCζ$^{151-524}$ with an MBP tag was induced in various *E.coli* strains with 0.1 mM IPTG. Crude lysates were separated using 7 % (w/v) SDS-PAGE and stained with Coomassie. Lane 1: Color Plus Prestained Protein Marker (NEB), Lane 2: Uninduced BL21(DE3)/pETMM41 hPLCζ$^{1-608}$, Lanes 3-10: crude lysate samples from induced cultures, Lane 3: BL21(DE3)/pETMM41-hPLCζ$^{1-608}$, Lane 4: BL21(DE3)/pETMM41-hPLCζ$^{151-524}$, Lane 5: CH184/pETMM41-hPLCζ$^{1-608}$, Lane 6: CH184/pETMM41-hPLCζ$^{151-524}$, Lane 7: R(DE3)/pETMM41-hPLCζ$^{1-608}$, Lane 8: R(DE3)/pETMM41-hPLCζ$^{151-524}$, Lane 9: R(DE3)pLysS/pETMM41-hPLCζ$^{1-608}$, Lane 10: R(DE3)pLysS/pETMM41-hPLCζ$^{151-524}$

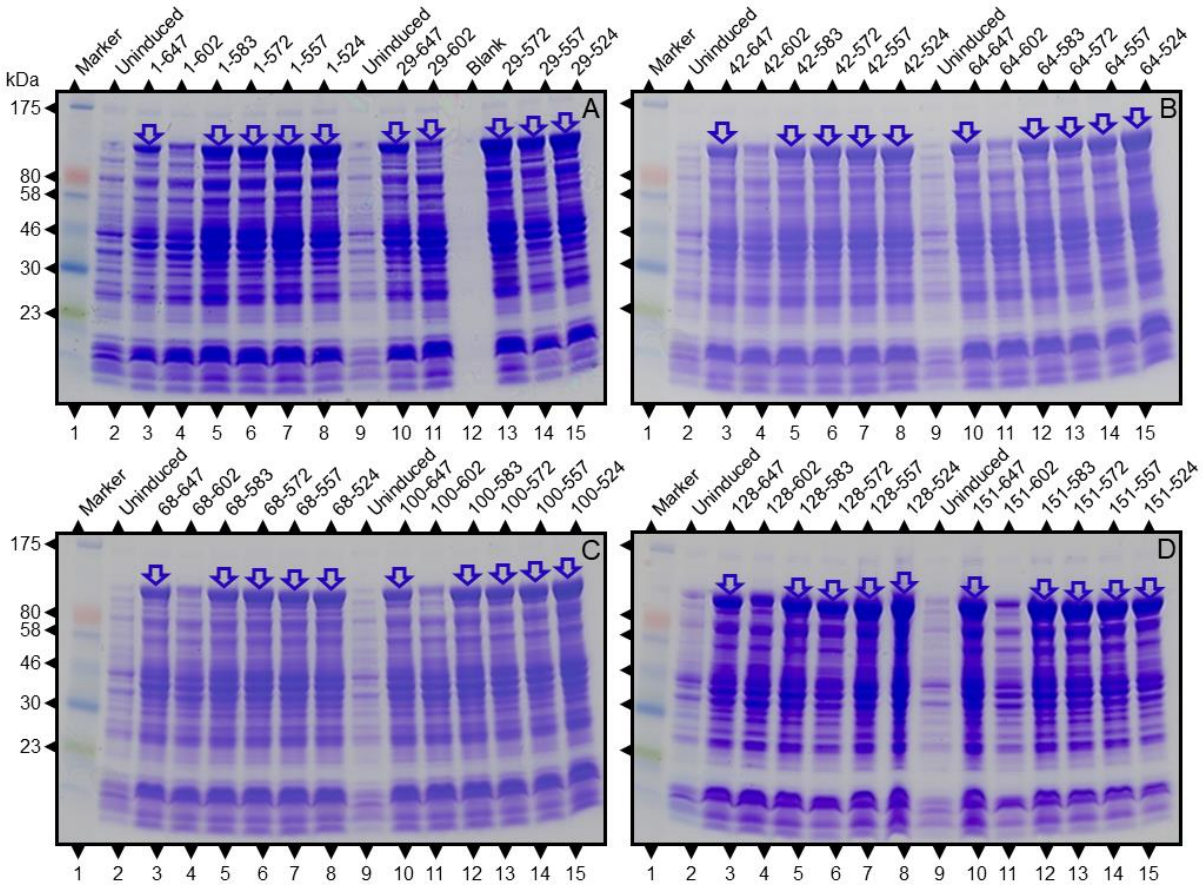

Figure 3-16 Expression of hPLCζ Deletion Mutants Can Vary with Amino Acid Coordinates.

Expression of hPLCζ deletion mutants with an MBP tag was induced in BL21(DE3) with 0.1 mM IPTG. Crude lysates were separated using 4-20 % (w/v) SDS-PAGE and stained with Coomassies All panels .Lane 1, ColorPlus Prestained Protein Marker (NEB), Lanes 2&9,: un-induced sample of the next lane. Remaining lanes: induced cultures co-ordinates of expressed protein are shown on the gel.Panel A. Note Panel A Lane 12: blank.

3.3.5.2 Screening Solubility of hPLCζ Deletion Mutants

An initial assessment of the solubility of selected deletion mutants was made by separating soluble and insoluble fractions using SDS-PAGE, as can be seen in

Figure 3-17. Although soluble protein was observed of the correct size, it is mainly restricted to the insoluble fraction. Only MBP-PLCζ$^{151-572}$ occurred in a sizeable quantity in the soluble fraction, but the majority was restricted to the insoluble fraction. Insufficient soluble protein for any deletion mutation was produced for crystallographic studies.

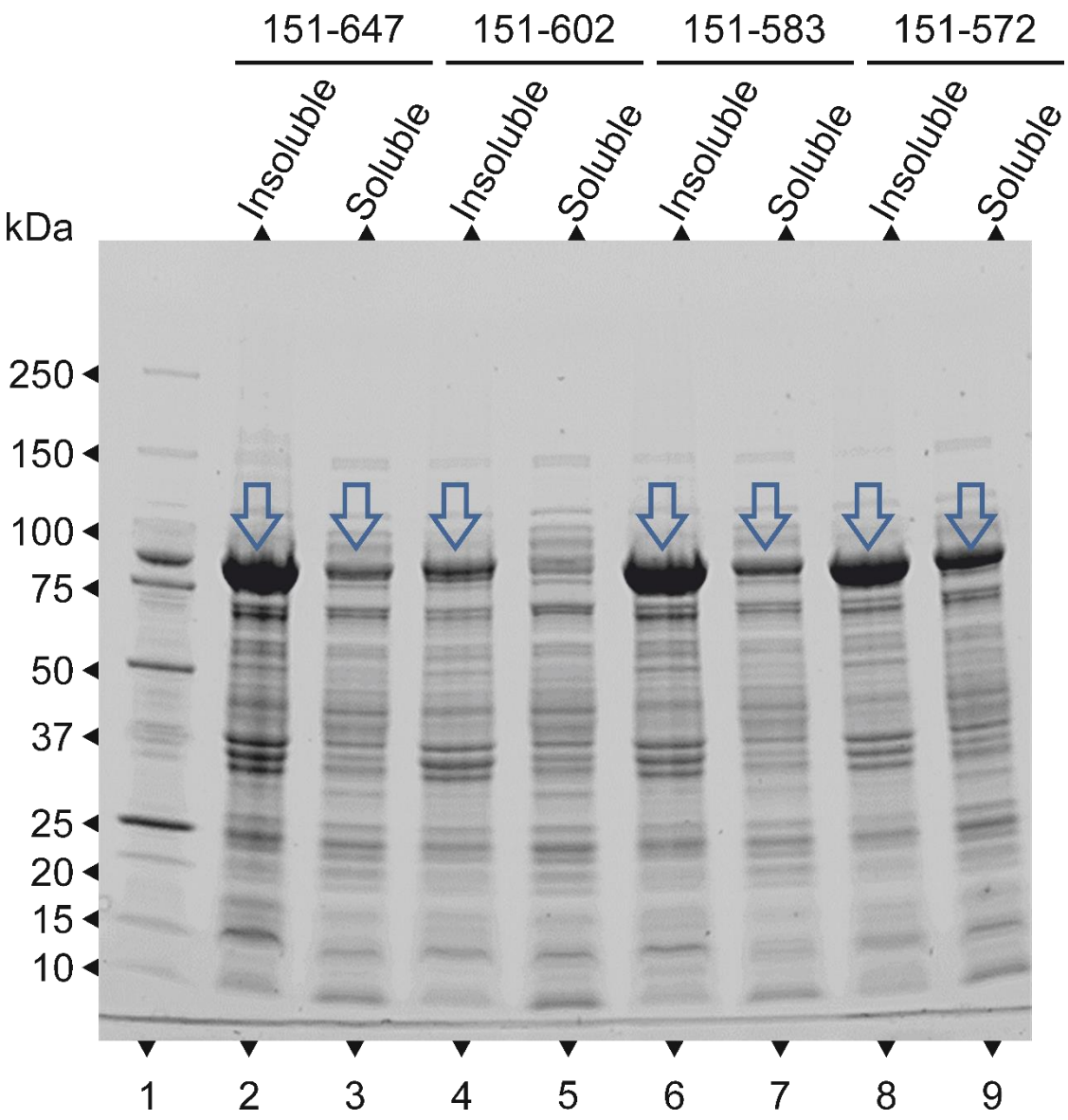

Figure 3-17 Deletion Mutants of hPLCζ Are Mainly Restricted to the Insoluble Fractions

Expression of hPLCζ deletion mutants fused to MBP was induced in BL21(DE3) with 0.1 mM IPTG. The insoluble fractions, re-suspended pellet (even lanes) and soluble fraction, clarified lysate (odd lanes), were separated by 4-20 % (w/v) SDS-PAGE and stained with Coomassie. Lane 1: Precision Plus Protein™ All Blue Prestained Protein Standards (BioRad), Lanes 2&3: pETMM41-hPLCζ$^{151-647}$, Lanes 4&5: pETMM41-hPLCζ$^{151-602}$, Lanes 6&7: pETMM41-hPLCζ$^{151-583}$, Lanes 8&9: pETMM41-hPLCζ$^{151-572}$

3.4 Discussion

Expression of recombinant PLCζ^{D210R} with eight different fusion partners was induced in two different *E.coli* strains. Expression levels varied between strains with expression levels being superior in R(DE3). Consequently, recombinant proteins expressed in R(DE3) were chosen for further analysis. Both SDS-PAGE and immunoblotting revealed that although PLCζ^{D210R} was expressed when fused with 6xHis, TrxA and GST most (or all) the protein was confined to the insoluble fraction. Immunoblotting also showed no detectable DsbA-PLCζ^{D210R}, DsbC-PLCζ^{D210R} and CBP-PLCζ^{D210R} expression in the soluble fraction.

Meanwhile, a significant proportion of the expressed MBP-PLCζ^{D210R} and PLCζ^{D210R}, cleaved from NusA, were detected in the soluble fractions. Therefore, MBP and NusA were selected for further assessment as fusion partners for PLCζ. Proteolysis of NusA-PLCζ^{D210R} was potentially the result of heat generated during sonication. Consequently, the lysis method to generate the lysates was modified to use the French press instead.

MBP-PLCζ^{D210R} and NusA-PLCζ^{D210R} were purified using the appropriate affinity resins. Common buffers prepared according to manufacturer's guidelines were used for the purification. SDS-PAGE revealed that the purification yield from the same volume of culture was greater for MBP-PLCζ^{D210R} than NusA-PLCζ^{D210R}. Therefore, MBP- PLCζ^{D210R} was chosen for large-scale purification.

MBP-PLCζ^{D210R} contains two N-terminal affinity tags, MBP and 6xHis. Both co-purify with idiosyncratic contaminants, which could be eliminated with a two-step

purification. To determine the optimal first step a lysate was split into two aliquots which were purified in parallel using Ni-NTA and amylose resin. The amylose column yielded sufficient protein for a 6xHis tag purification while the Ni-NTA column did not yield sufficient protein to attempt an MBP tag purification. Therefore, to assess polishing and remove contaminants all elution fractions containing recombinant protein were pooled, dialysed and concentrated for SEC. SDS-PAGE analysis of the fractions corresponding to the significant peaks revealed MBP-PLCζ^{D210R} in the void volume and MBP eluting separately. MBP eluting and MBP-PLCζ^{D210R} in the void volume suggests that MBP-PLCζ^{D210R} had undergone proteolysis releasing MBP, which remained soluble while intact MBP-PLCζ^{D210R} had aggregated.

Aggregation appears to be a feature of the domains of mPLCζ (unpublished data, laboratory communication). Another possibility is dimerisation, which has been observed in recombinant mPLCζ but not investigated (unpublished data, laboratory communication). While unsuitable for use in structural studies both MBP-PLCζ^{D210R} and NusA-PLCζ^{D210R} may be utilised as controls in other studies. Additionally, 6xHis-PLCζ^{D210R}, TrxA-PLCζ^{D210R} and GST-PLCζ^{D210R} could be used in studies for which crude lysate is sufficient or under conditions where purification of the protein could be carried out under native conditions, although a potential issue is whether the correct refolding of the protein would occur.

Following the observation of mPLCζ protein aggregating, to improve the likelihood of generating soluble recombinant PLCζ protein the emphasis was switched to the human isoform. Systematic N- and C-terminal deletion mutations of hPLCζ were

designed as this strategy had been shown to be successful in expressing and purifying soluble PLCδ1 protein to a level that should be suitable to produce protein crystals.

The series of hPLCζ-containing expression plasmids were generated and validated by the presence of an appropriately sized insert (confirmed by PCR) that would correctly correspond to the hPLCζ insert. However, to ensure that the constructs terminated at the correct residues and that differences in expression were not due to sequence mutations, DNA sequencing through the cloning region was used to confirm the correct inserts. Initial screening revealed variation in the levels of protein expression within the different constructs and bacterial strains used. A screen of the expression of all constructs in BL21(DE3) showed a pattern where specific co-ordinates expressed at a stronger level than others. An initial assessment indicated that solubility was improved by removing large portions of the N- and C- terminal. However, the improvement on expression was insufficient to enhance the yield of soluble protein to a level that would be required for crystallisation trials.

In order to have sufficient recombinant protein for biophysical and crystallographic studies, it is necessary to optimise the yield. The optimisation parameters for recombinant protein expression and solubility include the presence and identity of solubility partners, the coordinates expressed, *E.coli* strains, and additional parameters, e.g., chaperone co-expression and media composition. The plasmids and expression systems described in this chapter, while improving in the expression of PLCζ, was not sufficient to improve expression and solubility for a crystallisation study.

The variable influence of fusion partners on protein expression and solubility demonstrates that screening additional fusion partners, e.g., Small Ubiquitin-like Modifier (SUMO) may offer the potential for further improvements. MBP was observed to improve protein expression and solubility. Previously NusA was used, but it is significantly bigger when compared to other fusion partners. Furthermore, NusA does not provide any additional advantages compared to the purification method with the 6xHis tag fusion partner, which requires further washing steps during purification to remove contaminating proteins rich in His residues (Bolanos-Garcia and Davies, 2006). Currently, MBP-hPLCζ is being investigated for clinical use in cases of male factor infertility (unpublished data, laboratory communication). While NusA-hPLCζ has been shown to rescue failed oocyte activation caused by male factor infertility, MBP could be a more suitable fusion partner in a therapeutic agent. The use of the smaller MBP would reduce the total protein dose required. Although both NusA and MBP are prokaryotic proteins, the use of NusA the precise function of which is uncertain could cause regulatory issues. Use of MBP offers the option of two affinity purification steps in a production process enabling an additional purification stage to remove all contaminating prokaryotic proteins. The long-term side-effects of either NusA or MBP on development will also have to be trialled.

The use of deletion mutants demonstrated that the coordinates chosen can be expressed, and some can improve protein solubility. The crystal structure of PLCδ1 was determined using a deletion construct lacking the lipid-binding PH domain, which was expressed and crystallised separately. Another possibility is the expression of single domains or domain deletion mutants. Unpublished data has shown that the

mPLCζ C2 domain appears to cause aggregation or dimerisation while PLCδ1 C2 does not. Therefore, a mPLCζ C2 deletion mutant and the mPLCζ C2 domain could also be expressed separately, structures determined and potential dimerisation investigated. Additionally, the EF-hand and the XY domains could also be expressed separately for biophysical and structural studies. Deletion mutants of PLCζ are currently being used to map the epitope of anti-PLCζ polyclonal antibodies (unpublished data, laboratory communication).

Further investigation is required to obtain high fidelity pure recombinant PLCζ for structural studies and the current strategy may prove a powerful tool to achieve this goal when combined with additional optimisations. Different expression vectors could be investigated, e.g., with different combinations of solubility partners and affinity tags on both N- and C- terminals. Another strategy would be to identify binding partners for PLCζ which could potentially stabilise the protein as a complex and thus would prevent aggregation. The protein binding partners could be co-crystallised with PLCζ and the structure of PLCζ resolved if the structure of the protein binding partner is known. One potential candidate is CaM, the ubiquitous Ca^{2+} binding protein that associates with PLCζ (unpublished data, laboratory communication). CaM has been crystallised under a variety of conditions, and its 3D structure is well-described. Alternatively, the binding of PLCζ peptides to a binding partner could be determined, and those with high affinity identified. The PLCζ binding partners could theoretically be crystallised with pre-bound PLCζ peptides to investigate the structural binding interface between PLCζ and the binding partners.

3.5 Findings

In summary, the following novel findings were made in this chapter:

- Expression levels of an inactive mPLCζ mutant differ markedly dependent on the fusion partner and prokaryotic expression strain used.
    - Varying *E.coli* strain and affinity tag is a useful tool in optimising the heterologous expression of recombinant PLCζ proteins.
    - Of the combinations trialled an MBP affinity tag and *E.coli* bearing rare codon tRNAs showed the highest yield of expressed protein.
    - Aggregation observed in purified MBP- PLCζ^{D210R} further evidence of aggregation observed previously in mPLC.
    - Several of the fusion partners used could produce PLC recombinant protein for characterisation studies.
- Deletion mutants of hPLCζ corresponding to different amino acid coordinates were expressed with an MBP fusion partner.
    - Expression can potentially be further optimised at a larger scale to produce sufficient protein for biophysical studies.
    - Coordinates could also be used to produce deletion mutants to identify epitope locations in polyclonal antibodies.
    - Full-length MBP-hPLCζ could also be used as an alternative to NusA-hPLCζ as a therapeutic agent.

Chapter 4 - EXPRESSION, PURIFICATION AND MOLECULAR ANALYSIS OF RECOMBINANT WILD-TYPE HUMAN CALMODULIN PROTEIN

4.1 Chapter Summary

Calmodulin (CaM) has been identified as a novel binding partner for PLCζ. Functional and structural studies to investigate the interaction of CaM with PLCζ require sizable quantities of pure, soluble high-fidelity recombinant human protein. An untagged protein would be ideal for interaction assays. Recombinant human CaM is available commercially, but the cost of quantities required would be prohibitive. The current methods for expressing recombinant CaM protein typically produce a protein with fusion partners. These methods require multiple steps for purification, tag removal and polishing. While the structure of CaM is well described, the data was produced from crystals of the native protein of several species and recombinant proteins from the sequences of various species and a consensus vertebrate sequence. This chapter describes the construction of a plasmid for the prokaryotic expression of human CaM DNA sequence as a fusion protein. A one-step purification method yields large quantities of pure, soluble, untagged protein. The purified protein is very homogenous, has the mobility of CaM, is recognised by anti-CaM IgG, has a secondary structure conforming to that published for CaM. The recombinant CaM protein performs as expected in functional assays measuring the binding affinity of Ca^{2+}, and interaction with and modulation of RyR2. Therefore, the protein is correctly folded human CaM. Crystallisation experiments with this protein are currently ongoing.

4.2 Introduction

4.2.1 Background

Recent data have demonstrated binding between CaM and PLCζ (Nomikos, Thanassoulas, *et al.*, 2017). The novel binding observed presents opportunities to investigate the structure and function of PLCζ. The kinetics of the binding can be determined quantitatively using Isothermal Titration Calorimetry. Binding could stabilise PLCζ. Pre-bound CaM/PLCζ proteins and CaM protein/PLCζ peptide could be crystallised and both the structure of PLCζ and location of binding could be determined.

The amino acid sequence of CaM is highly conserved across vertebrates with 100 % sequence identity in mammals. As can be seen in Figure 4-1**.** CaM consists of two lobes separated by a flexible linker. The lobes are comprised of similar globular domain one at the amino lobe (N-lobe) and the other at the carboxyl lobe (C-lobe). Each domain consists of two pairs of EF-hand motifs with a Ca^{2+} binding site in each. So CaM contains four Ca^{2+} binding sites. In mammals, CaM is encoded by three separate non-identical genes which all produce identical proteins. Native and recombinant CaM from several species has been successfully crystallised under a variety of conditions, Table 4-1. The crystals produced have been used to generate structural data. Generally, the solvent the crystals were grown contained sodium cacodylate or sodium acetate buffer and either PEG-6000 or MPD as precipitating agents/cryopreservatives.

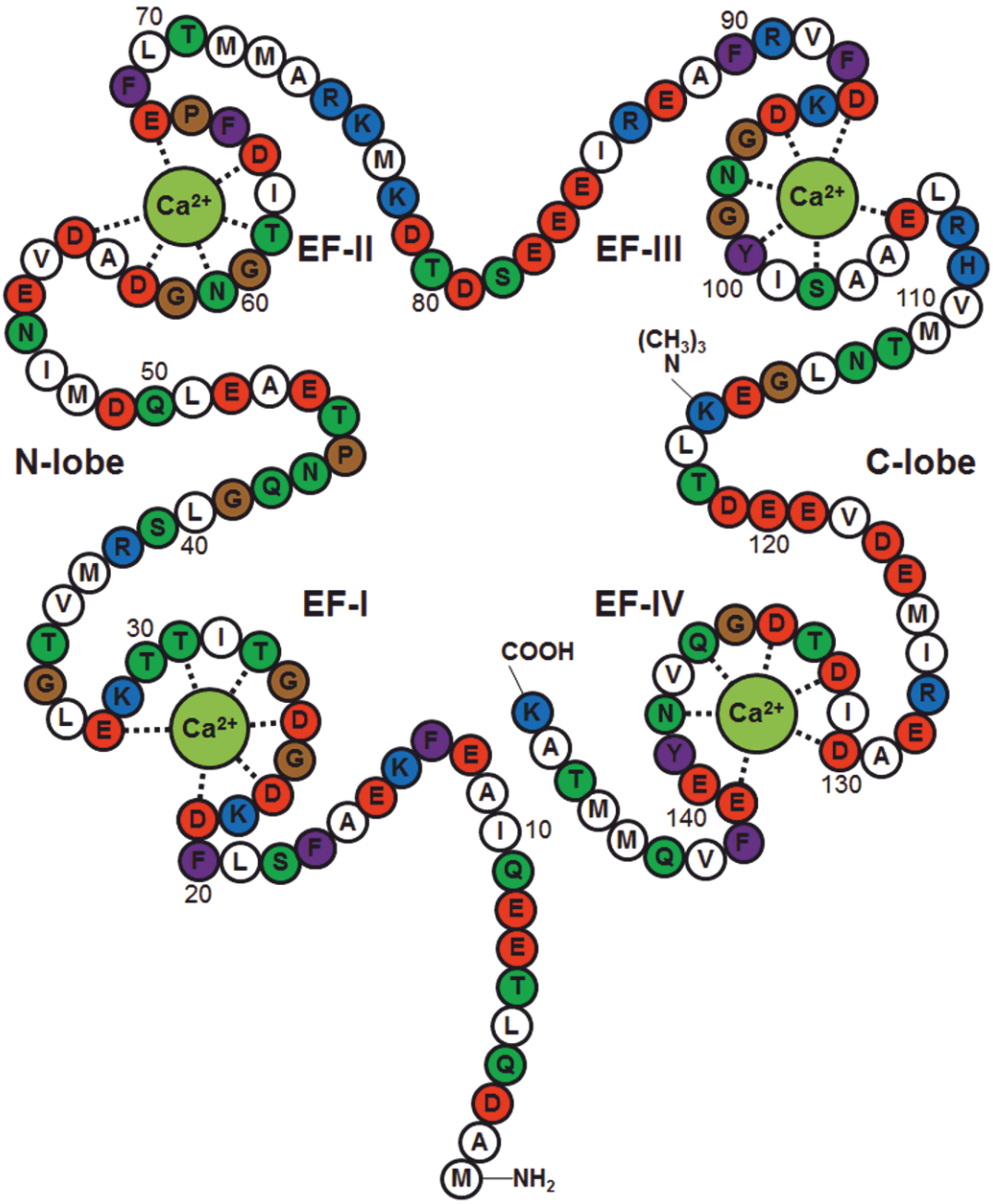

Figure 4-1 CaM Contains Four Ca^{2+} Binding Sites Across Two Lobes

The primary structure of human CaM expressed by *CALM1*.adapted from (Cheung, 1982) amino acid identified with single letter code. CaM consists of 148 residues in two lobes separated by a flexible linker. Each lobe contains two EF-hands motifs. Ca^{2+} binding sites are 12 residue sequences between D^{21}-E^{32}, D^{57}-E^{68}, D^{94}-E^{105} and D^{130}-E^{141} containing ligands which co-ordinate Ca^{2+} particularly the negative side chains of Asp (D) and Glu (E) (Red).

Table 4-1 Summary of Crystallisation of CaM

Protein source	Conditions	Reference
Purified from bovine brain	5-8 % PEG-6000, 5 mM sodium cacodylate or PIPES pH5.1-5.3, 5-20 mM $CaCl_2$, 0-10 mM $MgCl_2$	(Kretsinger *et al.*, 1980)
Purified from rat testis	55 % MPD, 50 mM sodium cacodylate pH6	(Cook *et al.*, 1980)
	22-30% MPD, 25 mM sodium cacodylate pH5.8-6.2	(Cook and Sack, 1983)
	5-8% PEG-6000, 10 mM sodium cacodylate pH5.1-5.3, 5 mM $CaCl_2$	
	MPD/sodium cacodylate pH5.6 (Cook and Sack, 1983)	(Babu *et al.*, 1985; Babu, Bugg and Cook, 1987, 1988)
Purified from bovine brain	6.7 % PEG-6000, 6.7 % MPD, 10 mM sodium cacodylate pH5.7, 10 mM $CaCl_2$	(Kretsinger, Rudnick and Weissman, 1986)
	25 % MPD, 10 mM sodium acetate pH4, 15 % ethanol, 5 mM $CaCl_2$	(Barford, Gilliland and Morgan, 1986)
Recombinant *D.melangostar* expressed in *E.coli*	25% MPD, 10 mM sodium acetate pH4, 15% ethanol, 5 mM $CaCl_2$	(Taylor *et al.*, 1991)

Protein source	Conditions	Reference
Recombinant vertebrate consensus sequence expressed in *E.coli*	17.5 % MPD, 50 mM sodium acetate pH5, 7.5% ethanol, 10 mM $CaCl_2$, 50 mM $MgCl_2$	(Chattopadhyaya *et al.*, 1992)
	12.5 % PEG-6000, 25 mM sodium acetate pH4.6, 2.5 mM $CaCl_2$	(Meador, Means and Quiocho, 1992)
Recombinant *P.tetraurelia* expressed in *E.coli*	55 % MPD, 50 mM sodium cacodylate pH5, 5 mM $CaCl_2$	(Rao *et al.*, 2008)
	20 % MPD, 40 mM sodium cacodylate pH5, 4 mM $CaCl_2$	(Wilson and Brunger, 2000)

The published structures for human CaM were produced using recombinant protein expressed from a vertebrate consensus nucleotide sequence (Chattopadhyaya *et al.*, 1992; Meador, Means and Quiocho, 1992). However, there are discrepancies between structural information for CaM obtained from CD and nuclear magnetic resonance (NMR) or X-ray data. These have been attributed to differences in the secondary structure of the proteins depending on the buffer in which the protein is dissolved (Bayley and Martin, 1992; Protasevich *et al.*, 1997).

The function and biological significance of CaM/PLCζ binding is currently unknown. However, biophysical and structural data on recombinant CaM protein derived from the human sequence would be novel and clinically relevant; especially

X-ray data obtained from crystals grown in new conditions. Also, the interaction of CaM with other human proteins could be investigated using recombinant human CaM.

RyR2 is a major binding partner of CaM in cardiac tissue (Yang *et al.*, 2014). One CaM molecule binds directly to one RyR2 molecule. So CaM binds to the tetrameric RyR2 channel at a ratio of four CaM molecules per channel and binding is associated with inhibition of channel function (Meissner and Henderson, 1987; Fruen *et al.*, 2000). Recent genetic studies have identified mutations in the genes encoding CaM in clinical cases of ventricular arrhythmia. A potential pathophysiological mechanism is that RyR2/CaM binding is altered, so regulation of the channel is changed. These mutations could be recreated in the human sequence using site-directed mutagenesis and recombinant mutant CaM protein produced. The parameters of the recombinant mutant CaM proteins would be comparable to those of wild-type protein produced using the same protocol. Conditions for crystallisation could also be screened for mutant CaM.

4.2.2 Rationale and Experimental Plan

To investigate the interaction of CaM with PLCζ and RyR2 it is desirable to produce recombinant human CaM in the quantities required for biophysical and structural studies. Commercial preparations of native and recombinant CaM are available. The purchase of enough commercial recombinant CaM would be prohibitively expensive. Commercial recombinant proteins are commonly produced as a fusion protein. As shown in Chapter 3, expressing proteins of interest as fusion proteins can improve heterologous expression and solubility.

However, it is desirable to remove the fusion partners, particularly before binding assays. Binding to the fusion partner will have to be controlled for, or the fusion partner could hinder the binding being measured. The plasmids used in Chapter 3 all expressed fusion proteins with a TEV cleavage site to facilitate cleaving of the fusion partner. Different plasmids can express fusion proteins with sites for other proteases, i.e. Thrombin and Factor Xa. There are disadvantages which apply to these proteases. Protein folding could conceal the protease site or hinder protease activity by steric interference. The recognition sites are degenerate sequences, and there is the risk of non-specific proteolysis. Time-consuming buffer changes and additional steps are often required for optimal protein cleavage and separation of the target protein from the protease and cleaved fusion partner with the risk of loss of product at each step.

The identity, functional activity and biophysical parameters of recombinant human CaM protein produced must be established. Specific antibodies for CaM are available, and biophysical parameters have been published. Examining the interaction of recombinant human CaM protein with a known CaM target would establish the functional activity of the protein produced. The ability of CaM to bind and regulate the known target RyR2 is known. Activity assays for RyR2 in the presence of recombinant human CaM would establish the functional activity of the protein produced.

A prokaryotic expression system and simple purification protocol which produced a high yield of correctly folded, soluble, untagged human CaM protein would be advantageous.

4.2.3 Alternative Fusion Partners and Purification Methods.

4.2.3.1 SUMO

An alternative cleavage target and fusion partner is the eukaryotic protein Small Ubiquitin-like Modifier (SUMO) (Butt *et al.*, 2005). In vertebrates, there are three SUMO proteins SUMO1 and the closely related SUMOs 2 and 3 (Saitoh and Hinchey, 2000). SUMOs are members of the family of ubiquitin-like proteins which are conjugated to proteins to be targeted for post-translational modification (Jentsch and Pyrowolakis, 2000). Use of yeast SUMO protein as a fusion partner can improve heterologous expression of difficult to express proteins and can be efficiently removed by SUMO protease yielding the native amino acid sequence (Zuo, Li, *et al.*, 2005; Zuo, Mattern, *et al.*, 2005). SUMO protease recognises the tertiary structure of SUMO (Reverter and Lima, 2004), so there is no non-specific proteolysis within the target protein, nor will proteolysis be hindered due to the recognition site being occluded (Malakhov *et al.*, 2004). SUMO improves the expression of eukaryotic proteins in *E.coli* compared to other fusion partners, and SUMO protease-mediated proteolysis can be induced over a wide range of conditions with an efficiency higher than that of other proteases/recognition sites (Marblestone *et al.*, 2006)

4.2.3.2 Inteins

An alternative cleavage method is to incorporate modified internal or intervening proteins (Inteins) into the fusion protein (Xu, Paulus and Chong, 2000; Elleuche and Pöggeler, 2010; Fong, Wu and Wood, 2010; Miraula *et al.*, 2015). Inteins are self-cleaving protein sequences involved in protein splicing (Perler *et al.*, 1994). During

post-translational modification, inteins self-excise from the precursor protein and re-ligate the two flanking sequences to produce the mature protein (Gogarten *et al.*, 2002; Shah and Muir, 2014). The process is autocatalytic and restricted to within the intein (Anraku, 1997; Anraku, Mizutani and Satow, 2005). Inteins have been used in the expression and purification of a variety of proteins (Chong *et al.*, 1997; Mathys *et al.*, 1999; Southworth *et al.*, 1999; Wood *et al.*, 1999; Singleton *et al.*, 2002; Sharma, Chong and Harcum, 2006; Bastings *et al.*, 2008; Zhao *et al.*, 2008; Liu *et al.*, 2008; Gillies, Mahmoud and Wood, 2009; Srinivasa Babu *et al.*, 2009). Engineered versions of inteins have been developed capable of self-cleaving at the C- or N- terminals, leaving no additional residues, in response to the addition of thiols or increased pH and temperature (Chong *et al.*, 1998; Mathys *et al.*, 1999; Wood *et al.*, 1999).

An affinity tagged Intein fusion partner enables the purification of the target POI by on-column cleavage (Chong *et al.*, 1997). The fusion protein can be immobilised on an affinity column and then the column conditions can be altered to those optimal for intein self-cleavage. The POI can then be eluted untagged while the cleaved tag and any intact fusion protein remain bound to the column. Cleavage is site-specific and restricted to within the Intein, so there is no non-specific proteolysis within neighbouring sequences and between protein molecules.

4.2.3.3 Expression and Purification of Human Calmodulin

The protein expression vector pHSIE expresses target proteins with an N-terminal fusion partner consisting of 6xHis, human SUMO2 (hSUMO2) and a shortened mutant of the Intein from *M.tuberculosis* recA protein (ΔI-CM) (Z. Wang *et al.*, 2012). The 11

kDa hSUMO2 can enhance the solubility of heterologous expressed recombinant proteins (Wang *et al.*, 2010). ΔI-CM is 168 amino acids long, lacking residues 111-382 of the full-length recA Intein and contains three missense mutations ($Val^{67}Leu$, $Asp^{24}Gly$ and $Asp^{422}Gly$). The engineered intein self cleaves at the C-terminal rapidly in response to a change in pH and increase in temperature, leaving no overhanging amino acids (Wood *et al.*, 1999, 2000; Banki, Feng and Wood, 2005; Fong and Wood, 2010; Wu *et al.*, 2010; Warren, Coolbaugh and Wood, 2013). The target protein can be expressed as a fusion protein and purified using a single step purification to yield pure, untagged protein by inducing Intein self-cleavage (Z. Wang *et al.*, 2012).

This chapter describes the production of a protein expression plasmid which expresses human CaM with an N-terminal 6xHis-human SUMO2-Intein fusion partner. A one-step purification protocol will produce soluble untagged human CaM. SDS-PAGE of the purified protein reveals a single protein band of the expected size which has the same electrophoretic mobility as CaM and is recognised by anti-CaM. The biophysical analysis shows the secondary structure of the protein is comparable to that published for CaM. Functional analysis reveals that the protein interacts with a major binding partner as expected. DLS shows that the protein is homogenous. The single species detected has a H_R and estimated molecular weight comparable to CaM. The protein elutes from SEC in a single peak and at the volume observed for calibration protein of a similar H_R. Trials of optimal conditions for the crystallisation of this protein are ongoing..

4.3 Results

4.3.1 Molecular Cloning

PCR amplified the sequence encoding human liver CaM (Genbank accession number AAD45181.1) from the pAED4-hCaM plasmid (Tan, Mabuchi and Grabarek, 1996). Primers hCaMKpNF and hCaMNotIR were used to incorporate a 5'-*Kpn*I site and a 3'-*Not*I site to facilitate cloning into the pHSIE expression vector, see Figure 4-2. The resulting plasmid was termed pHSIE-CaM^{WT}, PCR containing the cloning oligos confirmed the presence of the insert. Figure 4-3 shows that the PCR containing pHSIE-CaM^{WT} yields a product matching the size of CaM^{WT} sequence while PCR containing pHSIE yields no product. The sequence of the insert was confirmed by sequencing.

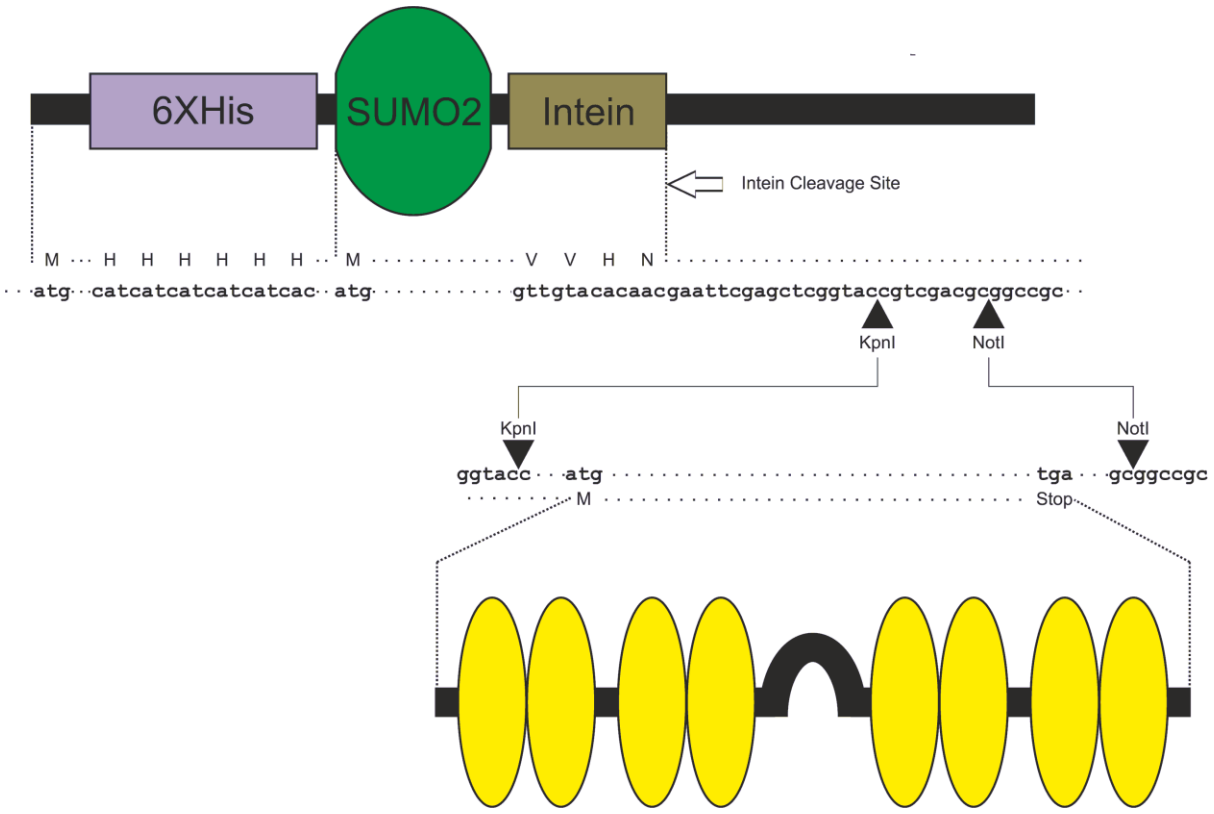

Figure 4-2 Cloning Strategy for the Construction of pHSIE-CaM^{WT}

Primers were designed to produce a 444 bp PCR product that encoded wild-type human CaM (CaM^{WT}) flanked by the recognition sites for *Kpn*I and *Not*I. Following digestion of the PCR product and pHSIE plasmid with both enzymes, the cut insert and vector were ligated to produce pSHIE-CaM^{WT}

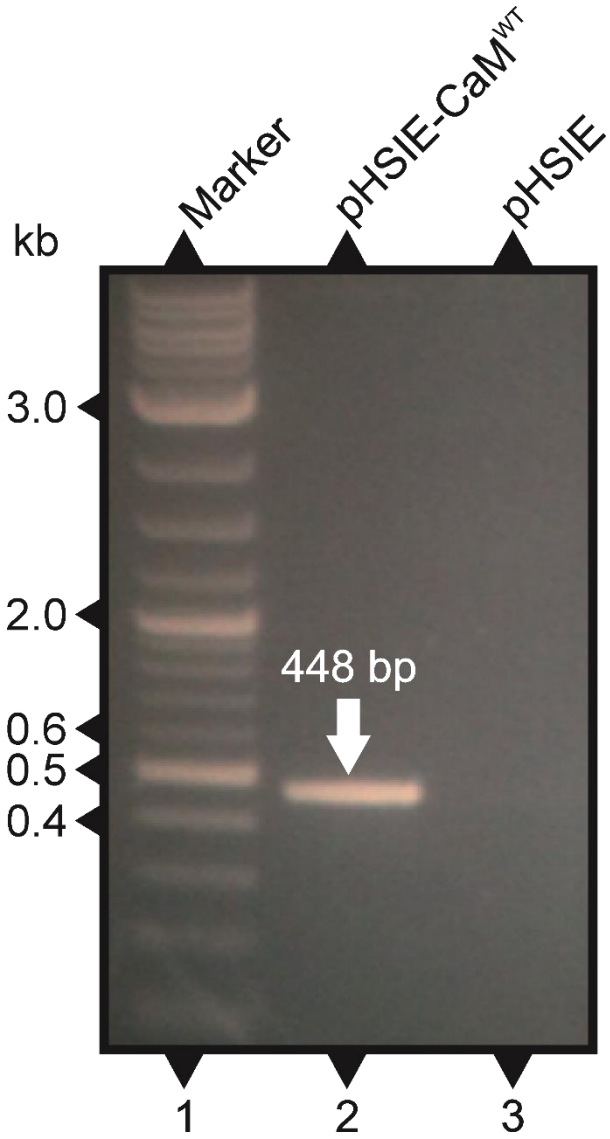

Figure 4-3 PCR of pHSIE-CaM^{WT} Yields Product of the Correct Size

Confirmation of successful sub-cloning of the pHSIE-CaM^{WT} plasmid. The products of PCRs containing hCaMKpNF and hCaMNotIR, with candidate clone and empty vector as templates were separated by 0.1 % (w/v) agarose gel electrophoresis. PCR from the candidate clone yielded a >500 bp product while the empty vector yielded no product. Lane 1: 2-Log DNA marker (NEB), Lane 2: 500 ng PCR product with candidate clone as template and Lane 3: Equivalent volume of PCR with empty vector as a template.

4.3.2 Expression and Purification of Recombinant Human Calmodulin

4.3.2.1 Expression of Calmodulin

Chemically competent BL21-CodonPlus(DE3)-RILP *E.coli* (BL21-CodonPlus) (Stratagene, UK) were transformed with pHSIE-CaM^{WT}. The expression of recombinant protein was induced using established conditions; the predicted expressed protein is shown in Figure 4-4. The crude lysates of samples of induced and uninduced cultures were separated by SDS-PAGE, Figure 4-5. The induced sample contains a band of approximately 47 kDa which is not visible in the un-induced sample.

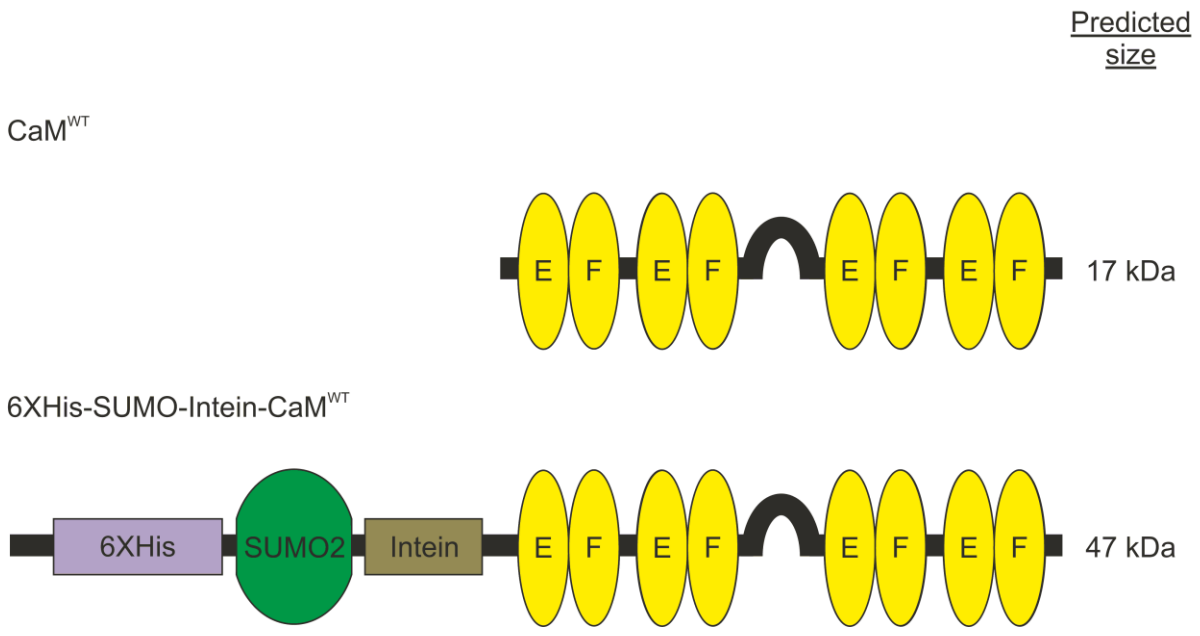

Figure 4-4 Wild-Type Human Calmodulin Expressed as a Fusion Protein

Induction of expression of competent *E.coli* transformed with pHSIE-CaM^{WT} yields a 47 kDa protein consisting of full-length CaM^{WT} with an N-terminal 6xHis, SUMO2, Intein fusion partner. Intein self-cleavage will yield a 17 kDa protein, untagged full-length CaM^{WT} protein.

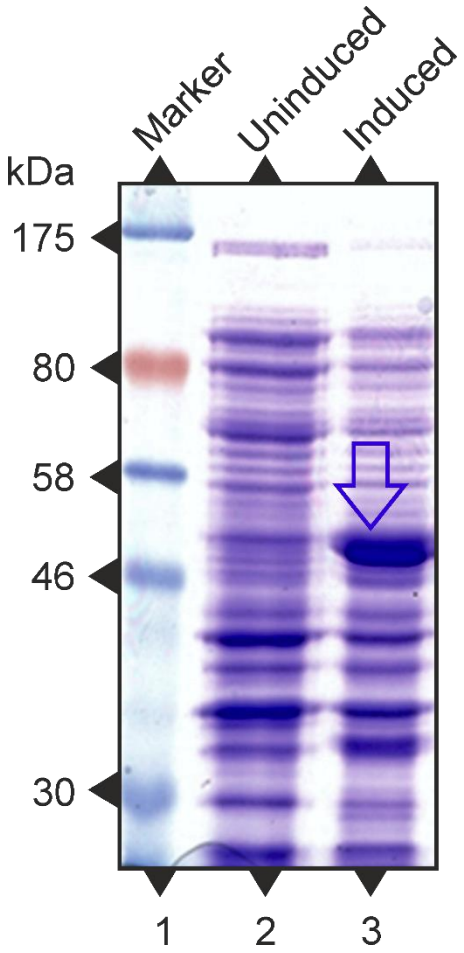

Figure 4-5 Expression of 6xHis-SUMO-CaM^{WT}

BL21-CodonPlus were transformed with pHSIE-CaMWT. Protein expression was induced with 0.1 mM IPTG. Crude lysates were separated 7 % (w/v) SDS-PAGE and stained with Coomassie.A 47 kDa band, highlighted, was visible in the induced sample only. Lane 1: Color Plus Prestained Protein Marker (NEB), Lane 2: Un-induced and Lane 3: Induced.

4.3.2.2 Purification of Calmodulin

Pellets representing 16 L of expression culture were re-suspended, pooled, lysed and clarified. Clarified lysate was applied to Ni-NTA as can be seen in Figure 4-4, the N-terminal 6xHis tag of 6xHis-SUMO2-Intein-CaM^{WT} will bind to Ni-NTA, isolating the recombinant protein. When the pH is lowered, and temperature increased the Intein moiety will undergo self-cleavage liberating CaM^{WT} while 6xHis-SUMO2-Intein remains immobilised. SDS-PAGE separated purification fractions, are shown in Figure 4-7. While the clarified bacterial lysate and flow-through fractions contain multiple bands, one of the strongest is a 47 kDa protein which is diminished in the flow-through fraction. The number of protein bands is reduced in the first wash fraction, and the 47 kDa band is still present. The second wash fraction of cleaving buffer contained no proteins. However, following incubation at room temperature a protein of approximately 17 kDa is present. The final fraction, collected when the imidazole concentration was increased to 250 mM, contains a 47 kDa protein and 30 kDa protein.

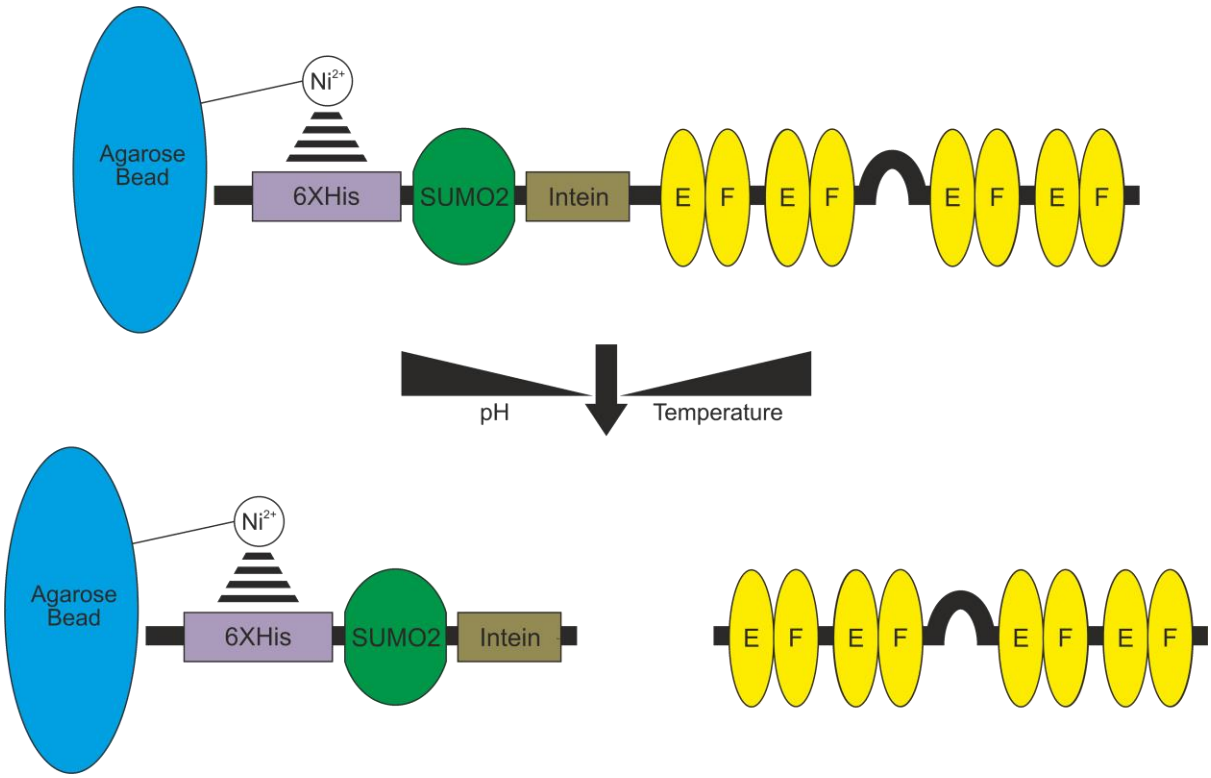

Figure 4-6 Changing Ni-NTA Affinity Column Conditions Yields Untagged CaM^{WT}

The 6xHis of 6xHis-SUMO2-Intein-CaM^{WT} will bind to the immobilised Ni^{2+} ions in Ni-NTA resin. Increasing temperature and reducing pH will initiate auto-cleavage of Intein, liberating untagged CaM^{WT} while 6xHis-SUMO2-Intein remains bound to the column.

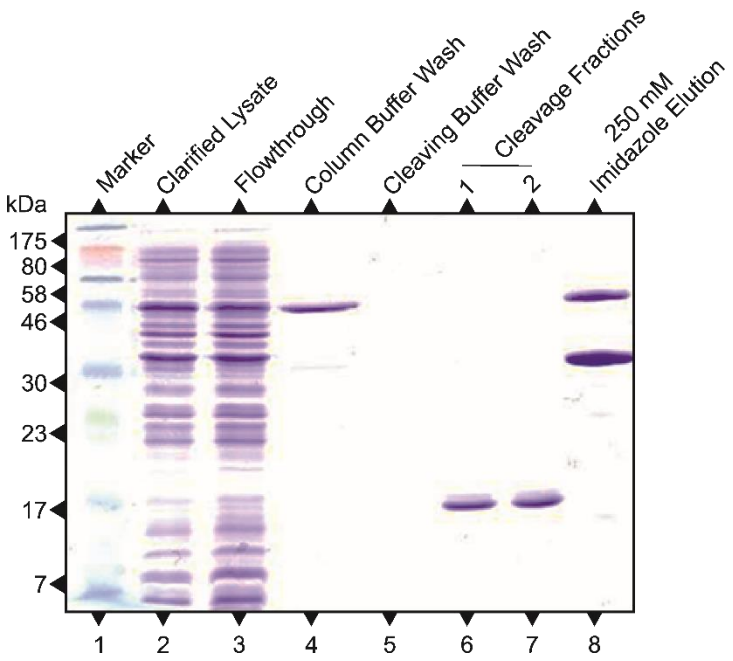

Figure 4-7 Changing Column Conditions Liberates CaM^{WT} from 6xHis-SUMO2-Intein-CaM^{WT} Immobilised on Ni-NTA

BL21-CodonPlus /pHSIE-CaMWT induced with 0.1 mM IPTG were lysed and applied to Ni-NTA resin column. The column was washed, and conditions were altered to those optimal for Intein self-cleavage. Following this, increasing the imidazole concentration released any protein still bound to the column. Fractions collected at every step were separated by 15 % (w/v) SDS-PAGE and stained with Coomassie. Lane 1: Colorplus Marker (NEB). Lane 2: 5 µl clarified lysate. Lane 3: 5 µl of flowthrough. Lane 4: 15 µl of wash 1. Lane 5: 15 µl of wash 2. Lane 6: and 7 10 µl of cleavage fractions Lane 8: 250 mM imidazole elution fraction

4.3.2.3 Immunoblotting of Calmodulin

The fractions containing the 17 kDa protein were pooled. The pooled protein sample was separated by SDS-PAGE, Figure 4-8. Coomassie staining, Figure 4-8 Panel A, revealed a single observable band of 17 kDa, plotting the lane profile revealed a single peak, Figure 4-8 Panel B. Immunoblotting with anti-CaM detected only one band at 17 kDa confirming the identity of the protein as CaM^{WT}, Figure 4-8 Panel C. Based on these results the protein was estimated to be ≥95% pure. The pooled fractions, typically 10 ml, were dialysed against PBS and stored at 4°C until required.

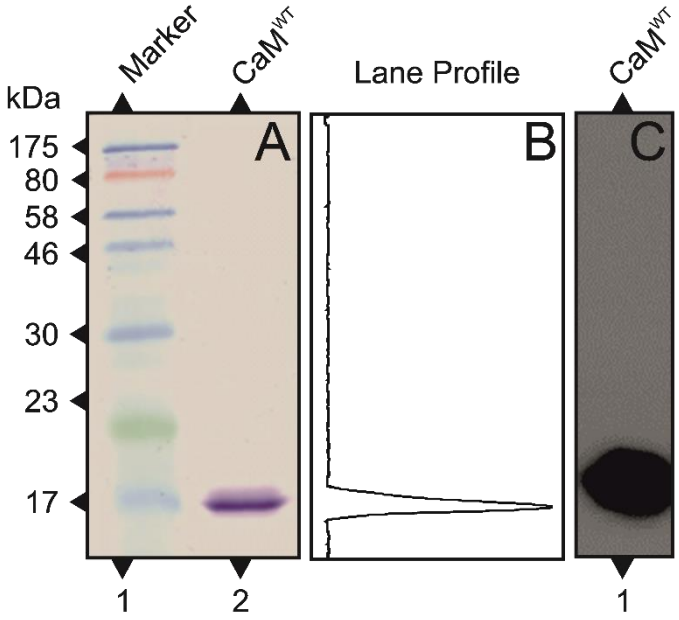

Figure 4-8 Purified CaM^{WT} Resolves as a Single Band of the Correct Size and Recognised by the Specific Monoclonal Antibody

Cleavage fractions from Ni-NTA resin column purification were pooled and separated by SDS-PAGE in duplicate. **(A)** Coomassie stained 4-20 % (w/v) SDS-PAGE gel Lane 1: ColorPlus Prestained Protein Marker (NEB), Lane 2: Purified protein. (B) Corresponding Immunoblot Primary Mouse anti-CaM monoclonal (1:10,000) Secondary HRP anti Mouse polyclonal (1:10,000). Exposure 20s. Lane 1: purified protein

4.3.3 Circular Dichroism Spectroscopy of Recombinant Human Calmodulin

4.3.3.1 Confirmation of the Secondary Structure of Calmodulin

The far UV CD spectra of CaM^{WT} was recorded at a low and high temperature in the presence and absence of Ca^{2+}. The measured spectra are shown in Figure 4-9, Panel A. For reference a CD spectra for CaM available in the Protein CD Data Bank is shown in Figure 4-9 Panel B (Lees *et al.*, 2006; Whitmore *et al.*, 2017). As can be seen in Figure 4-9 Panel A, the CD spectra of CaM^{WT} at 4 °C have positive maxima at 192 nm and two negative maxima at 208 and 221 nm. The two negative maxima are consistent with that of a protein containing α-helices and with the published CD spectra (Hennessey *et al.*, 1987; Lees *et al.*, 2006; Wang *et al.*, 2011). The comparable CD spectra indicate that the secondary structures of native CaM and CaM^{WT} are the same.

Additionally, there a transition in the CD spectra when Ca^{2+} is present compared to when it is absent; as can be seen in Figure 4-9. In the presence of Ca^{2+} the CD amplitude at both negative maxima is greater and the ratio of $\Delta\varepsilon_{208\ nm}/\Delta\varepsilon_{221\ nm}$ is decreased compared to when Ca^{2+} is absent which is in good agreement with published data (Hennessey *et al.*, 1987; Wang *et al.*, 2011). The transition corresponds to a conformational change in response to the binding of Ca^{2+} probably due to the spatial rearrangement of the α-helices within CaM^{WT} upon Ca^{2+} binding (Protasevich *et al.*, 1997). At high temperature, the negative maxima in CD amplitude at 208 and 221 nm are reduced which corresponds to a decrease in the proportion of residues involved in α-helices as the protein unfolds. However, as can be seen in Figure 4-9 the reduction is less at 221 nm in the presence of Ca^{2+} at 99 °C compared to when Ca^{2+} is absent at 90 °C.

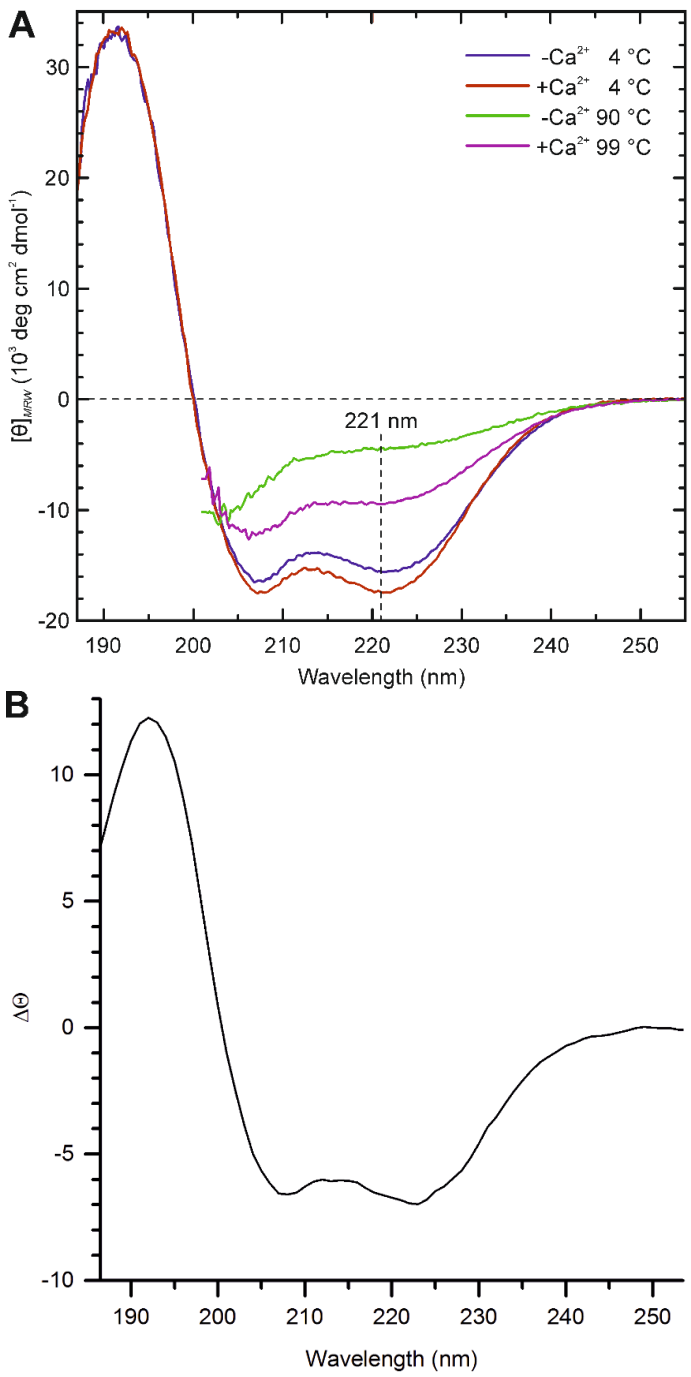

Figure 4-9 Secondary Structure of CaM^{WT} Corresponds to Native CaM

The far-UV CD of CaM^{WT} in pH 6.5, 10 mM MES, 50 mM KCl with Ca^{2+} (1 mM $CaCl_2$) or without Ca^{2+} (1mM EDTA), at 4 °C and 99 °C (with Ca^{2+}) and 90 °C (without Ca^{2+}) **A)** CD Spectra for CaM^{WT} measured at low and high temperature in the presence and absence of Ca^{2+}. **B)** Illustrative CD spectra for native bovine CaM at 4 °C is shown for comparison (Lees *et al.*, 2006)

4.3.3.2 Thermal Denaturation of Calmodulin

Thermal unfolding of CaM^{WT} was measured by recording changes in CD at 221 nm with increasing temperature in the presence and absence of Ca^{2+}. In Figure 4-10 Panel A, molar ellipticity ([θ]) is plotted against temperature. An increased degree of [θ] indicates a higher proportion of residues in α-helical conformation and so more folding. For reference, the CD monitored at 221 nm between 5 °C to 90 °C is shown in Figure 4-10 Panel B (Wang *et al.*, 2011).

In the absence of Ca^{2+} as temperature increases from 4 °C to 90 °C unfolding begins with a gradual decrease in helical content followed by a rapid reduction and then plateauing decrease as the protein entirely unfolds. The observed unfolding is complex and does not precisely fit a two or three state unfolding process. However, this in keeping with previous reports that the interdomain interaction contributes to the thermostability of CaM (Sorensen and Shea, 1998; Wang *et al.*, 2011). Assuming a two-state model the melting temperature (T_M) and van't Hoff enthalpy (ΔHvH) were calculated to be 53.8±0.2 °C and -112 kJ/mol. Meanwhile, when a three-state model was assumed, the T_M and ΔH_{Vh} were 45.6±1.1 °C and -133±10 kJ/mol for the initial transition and 60.2±0.7 °C 212±15 kJ/mol for the second. These figures and observed relationship between [θ] and temperature agree well with those reported for apoCaM (Sorensen and Shea, 1998).

The thermal unfolding of CaM^{WT} in the presence of Ca^{2+} was monitored from 4 °C to 99 °C. At 4 °C when Ca^{2+} is present [θ] is greater than in the absence of Ca^{2+}; corresponding to the different conformation of CaM^{WT} in the presence of Ca^{2+} which

could be expected following Figure 4-9. As temperature increases, [θ] decreases as the protein unfolds although not at the same rate and does not fully unfold as in the absence of Ca^{2+}. The plotted data better fit a two-state unfolding model, this and the calculated parameters of an increased T_M of 105 °C and ΔH_{Vh} of -105 kJ/moll agree well with those reported for holo-CaM (Sorensen and Shea, 1998; Wang *et al.*, 2011).

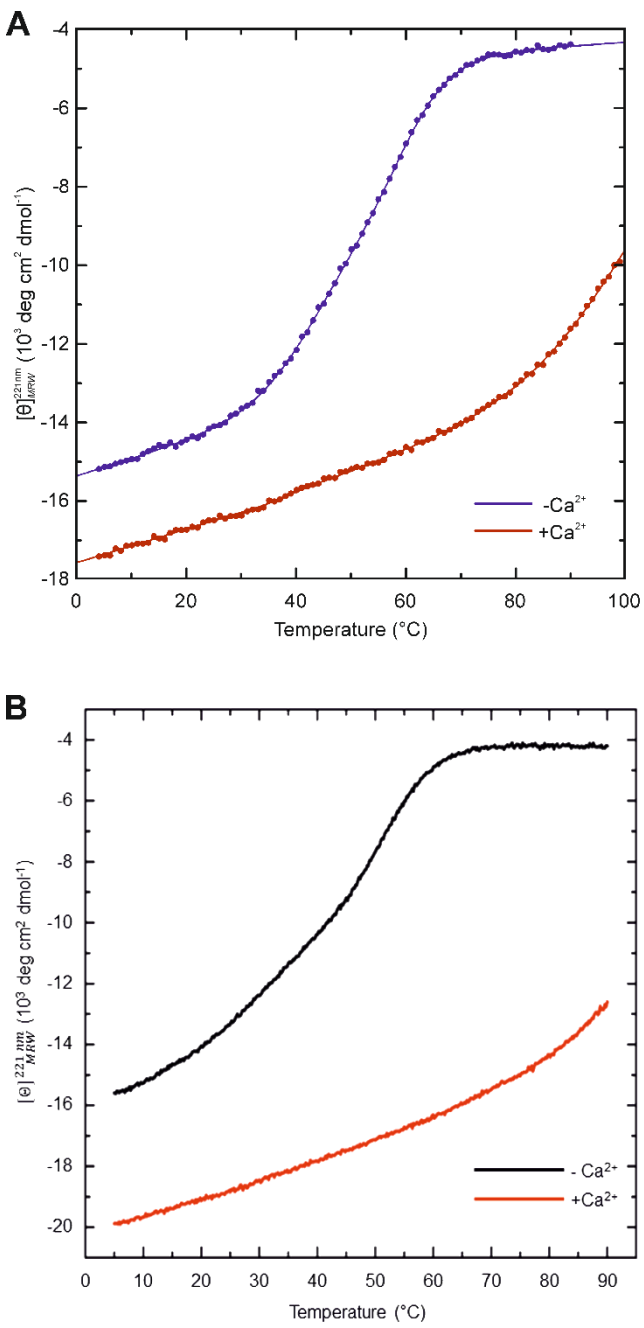

Figure 4-10 Thermostability of CaM^{WT} Increases with Ca^{2+} Binding

The far-UV CD of CaM^{WT} in pH 6.5, 10 mM MES, 50 mM KCl with Ca^{2+} (1 mM $CaCl_2$) or without Ca^{2+} (1mM EDTA) was recorded at 221 nm CD of CaM^{WT} at 221 nm increasing temperature (0.5 °C increments). **A)** A fitted curve plot of CD in the presence and absence of $Ca^{2+}$is plotted against temperature, at each increment the plotted measurement is the mean of 120 data points taken at 0.1 s intervals over 12 s. For clarity, only the measurements at 1 °C increments are shown. **B)** An illustrative plot of CD signal at 221 nm for synthetic CaM between 5 °C to 90 °C is shown for comparison (Wang *et al.*, 2011)

4.3.4 Functional Studies of Recombinant Human Calmodulin

4.3.4.1 Co-Immunoprecipitation of Calmodulin

The ability of CaM^{WT} to bind RyR2 was assessed by co-immunoprecipitation at three different free Ca^{2+} concentrations, 0 µM, 10 µM and 100 µM. Native cardiac RyR2 was immunoprecipitated with anti-RyR2 in the presence of 1 µM of exogenous CaM^{WT}. Sepharose beads were labelled with RyR2-specific Ab^{1093} and incubated with CHAPS-solubilised cardiac SR vesicle preparation (SR prep) and CaM^{WT}. Following recovery of the beads, the presence of CaM^{WT} was detected by SDS-PAGE and immunoblotting with rabbit anti-CaM monoclonal antibody. Representative immunoblots are shown in Figure 4-11. As can be seen in Figure 4-11 the anti-CaM can detect a band in the sample containing Sepharose beads labelled with anti RyR2.

Levels of endogenous CaM in the SR preps were probed by immunoblotting with anti-CaM monoclonal. As can be seen in Figure 4-12, CaM was not detected in 50 µg of total protein from the SR preps while 10 ng of purified CaM^{WT} was. Therefore, the SR preps used in the functional studies contain less than 10 ng of CaM per 50 µg of total protein.

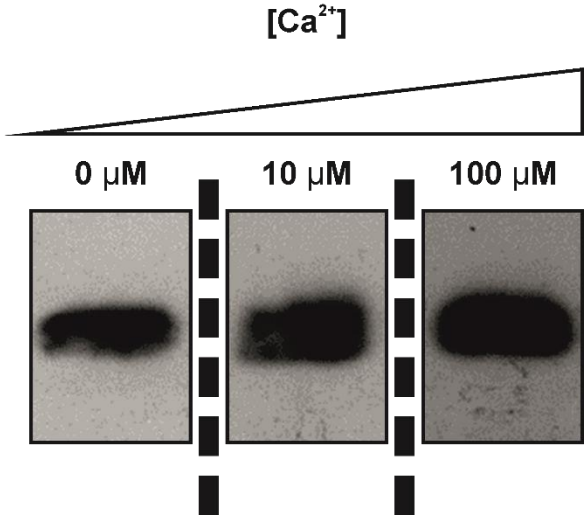

Figure 4-11 CaM^{WT} Associates with RyR2 in a Ca^{2+} Dependent Manner

SR prep and CaM^{WT} were incubated with rabbit anti-human RyR2 Ab^{1093} (in-house) pre-bound to nProtein-A-Sepharose beads (GE Healthcare) at three different free Ca^{2+} concentrations. Following recovery by centrifugation, the recovered beads were washed and re-suspended in SDS-PAGE loading buffer and separated using 18 % (w/v) SDS–PAGE. The presence of RyR2-coprecipitated CaM^{WT} was detected by immunoblotting with mouse anti-CaM monoclonal primary (1:7,500) (Source Bioscience), and secondary HRP anti Mouse polyclonal (1:10,000) (Santa Cruz). Immunoblots were developed by enhanced chemiluminescence (GE Healthcare) with exposure of 20 s. The experiment was repeated on three occasions, on each occasion a different cardiac SR prep was used. Representative immunoblots from the same occasion at 0, 10 and 100 µM free Ca^{2+} are shown.

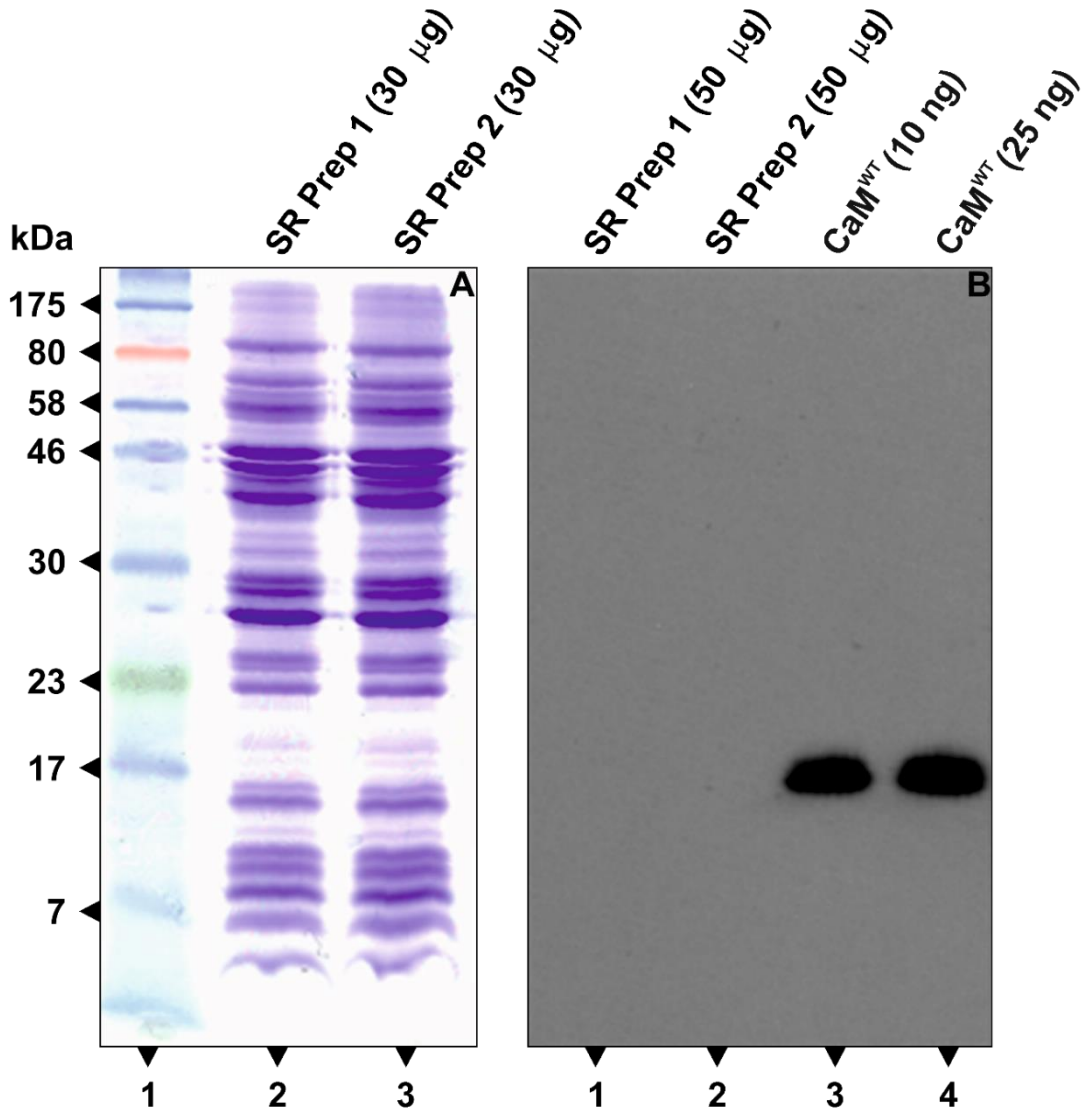

Figure 4-12 SR Preparations Do Not Contain Detectable Endogenous CaM

Two of the SR Preps used in these studies, each from a different heart, were separated by SDS-PAGE in duplicate. **(A)** Coomassie stained 4-20 % (w/v) SDS-PAGE gel. Lane 1: ColorPlus Prestained Protein Marker (NEB), Lane 2: SR Prep 1 (30 μg total protein) Lane 3: SR Prep 2 (30 μg total protein). **(B)** Corresponding Immunoblot. Primary mouse anti-CaM monoclonal (1:10,000) (Source Bioscience). Secondary HRP anti Mouse polyclonal (1:10,000) (Santa Cruz). Developed by enhanced chemiluminescence (GE Healthcare) exposure of 20 s. Lane 1: SR Prep 1 (50 ng total protein). Lane 2: SR Prep 2 (50 ng total protein). Lane 3: CaM^{WT} (10 ng protein). Lane 4: CaM^{WT} (25 ng protein).

4.3.4.2 Binding of Ryanodine to the Ryanodine Receptor in the Presence of Calmodulin

RyR2 channel conformation can be modulated by binding partners, e.g. CaM which inhibits RyR2 open conformation. The conformational state of RyR2, whether it is open or closed, can be assessed by measuring the binding of ryanodine radiolabelled with tritium ([^{3}H]ryanodine) to solubilised cardiac RyR2. RyR2 open conformation is Ca^{2+} dependent; the channel is closed in the absence of Ca^{2+}, and P_O increases with Ca^{2+}. Ryanodine will only bind to RyR2 when it is an open conformation. Measuring [^{3}H]ryanodine binding in the absence and presence of a RyR2 binding partner at different Ca^{2+} concentrations assesses the effect of the binding partner on channel conformation. Therefore, the [^{3}H]ryanodine binding assay can assess the ability of CaM^{WT} to modulate the conformational state of RyR2 channels in response to Ca^{2+}.

The binding of [^{3}H]ryanodine to RyR2 in the presence and absence of CaM^{WT} was measured at a range of [Ca^{2+}] between 10 nM and 1 mM free Ca^{2+}. Binding was expressed as a percentage of maximal [^{3}H]ryanodine binding and plotted against free Ca^{2+} concentration as shown in Figure 4-13. Minimal [^{3}H]ryanodine binding to RyR2 in the absence of CaM^{WT} is at 0.01 μM free Ca^{2+} while maximal binding occurs at 100 μM Ca^{2+}. However, at 100 μM free Ca^{2+} in the presence of CaM^{WT} [^{3}H]ryanodine binding to RyR2 is reduced by 20-30%.

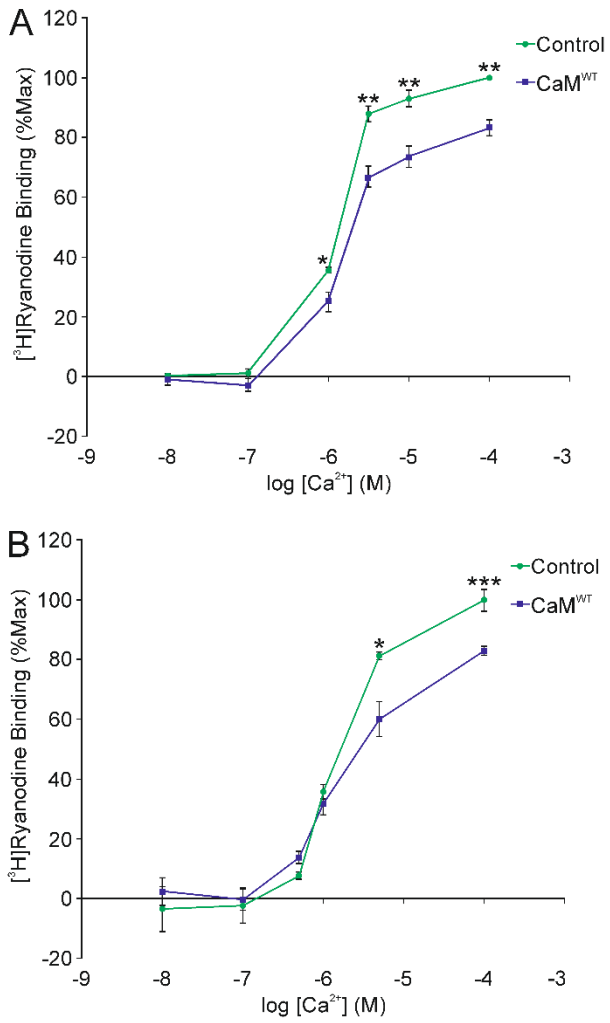

Figure 4-13 The Presence of CaM^{WT} Reduces the Binding of Ryanodine to RyR2

CHAPS-solubilised cardiac SR extract was incubated with [^{3}H]ryanodine in the presence and absence of CaM^{WT} (1 µM) in triplicate at a range of free Ca^{2+} concentrations ([Ca^{2+}]). SR vesicles were recovered by filtration and radioactivity present on filters was measured by scintillation and corrected for background and non-specific activity. Binding was expressed as a percentage of maximal activity at 100 µM Ca^{2+}. **A)** and **B)** are two independent experiments in which different batches of recombinant proteins, SR preps and buffers were used. Each experiment consisted of three occasions (n=3). In each occasion, a cardiac SR prep from a different heart was used. Mean binding (±SEM) was plotted against log [Ca^{2+}]. The difference in binding between the absence and presence of CaM^{WT} was calculated for each [Ca^{2+}] and compared using an unpaired Student's t-test (GraphPad, Prism 5). Statistically significant differences are shown, * $P<0.05$, ** $P<0.005$ and *** $P<0.001$.

4.3.5 Calcium Binding Affinity

The Ca2+-binding properties of CaMWT were measured in vitro by monitoring specific Ca2+-dependent changes in intrinsic fluorescence of CaMWT. Phe fluorescence and Tyr emission specifically indicate Ca2+ occupancy within the N-domain and C-domain of CaM respectively. The Ca2+-binding properties of each of the four sites within CaM can be measured specifically because C-domain Phe residues are non-emissive while Tyr emission from the C-domain does not interfere with fluorescence of N-domain Phe residues (VanScyoc and Shea, 2001; VanScyoc et al., 2002)

Mean binding data from three independent titration experiments was fitted using non-linear least squares. With increasing free [Ca2+], the intensity of fluorescence for C-domain Tyr residues increased and that of N-domain Phe residues decreased as expected. The C-domain binding sites have an apparent K_d almost three times greater than that of the N-domain binding sites (2.97 and 8.08 μM respectively). The free energy change that accompanies the binding of two Ca^{2+} at the C-domain binding sites was found to be -63.1 kJ/mol with a cooperative free energy change of -9.8 kJ/mol, while the corresponding values for the N-domain binding sites were -58.2 and -4.3 kJ/mol respectively.

The calculated K_d and free energy changes of Ca2+ binding CaM^{WT} are in good agreement with earlier studies under the same experimental conditions (Sorensen and Shea, 1998; Crotti *et al.*, 2013). Co-operative binding is required by CaM to change from apo- to holo- conformations over a narrow [Ca2+] range, ensuring efficienct function as a biological Ca2+ sensor. Loss of co-operatvity as a result of reduced binding affinities for Ca2+ may have profound biological implications.

4.3.6 Crystallisation Experiments

4.3.6.1 Protein Polishing

Elution fractions were pooled and concentrated to a total volume of approximately 1 ml. The purified protein was further purified using SEC, CaM^{WT} was further purified using SEC a representative trace is shown in Figure 4-14. The main elution peak occurred at an elution volume of approximately 90 ml, corresponding with the elution volume of carbonic anhydrase with adjoining peaks at 76 ml, and 82 ml. Separation of selected fractions by SDS-PAGE, inset Figure 4-14, showed a major protein band which could resolve as a double band of approximately 17 kDa was eluted in the main peak. The remaining peaks also contained 17 kDa protein bands, all corresponding to the molecular weight of CaM^{WT}. There were also minor low M_W bands present, potentially breakdown products of CaM as these were recognised by anti-CaM, Appendix Figure XI.

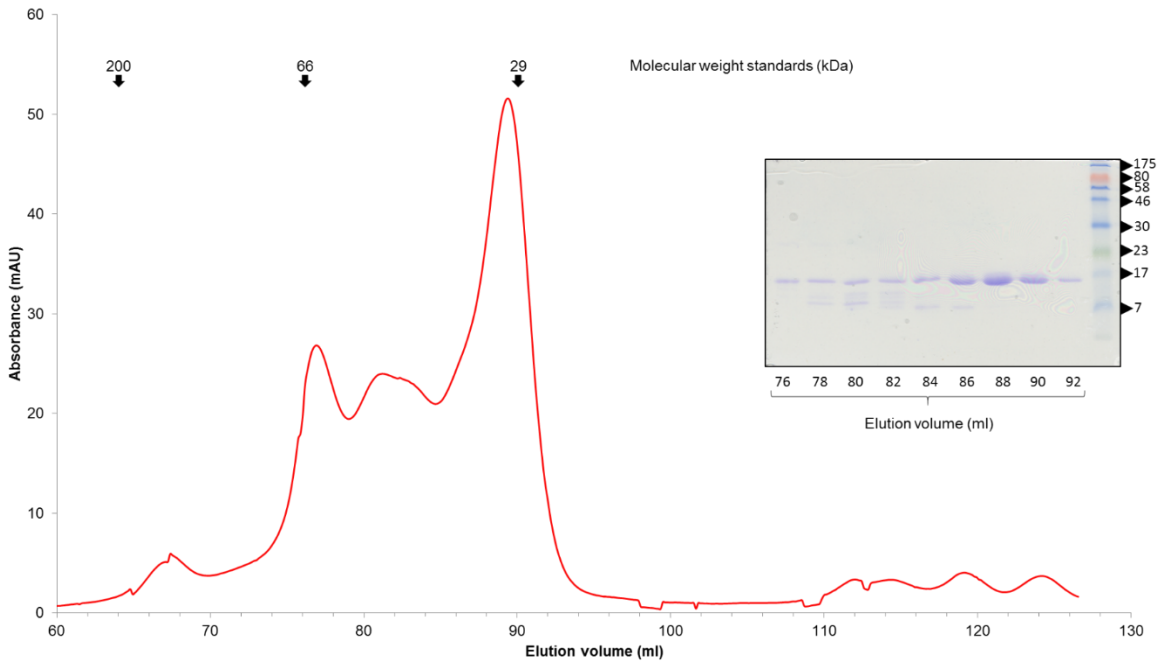

Figure 4-14 Gel Filtration of CaM^{WT} Yields Pure Protein in a Single Peak

Pooled and concentrated elution fractions were loaded onto a Superdex 200 SEC Column (GE Healthcare) with a 2 ml Superloop equilibrated with pH 7 10 mM HEPES, 50 mM KCl, 5 mM Ca^{2+}. One peak was observed. Elution fractions from beneath the main peak were collected and separated by SDS-PAGE. Main figure, UV trace of preparative SEC molecular weight standards are shown for comparison. Inset, Coomassie stained 15 % (w/v) SDS-PAGE gel elution fractions (volumes as shown) occurring around the volume of 88 ml, last lane ColorPlus Prestained Protein Marker (NEB).

Fractions beneath the main peak of the SEC elution profile, typically 86-92 ml elution volume, were separated by SDS-PAGE. Those containing only the 17 kDa protein were pooled and concentrated to ~20 mg/ml in a final volume, depending on yield, of at least 100 μl. The concentration was confirmed spectrophotometrically and by SDS-PAGE alongside known amounts of lysozyme, Figure 4-15. As can be seen in Figure 4-15, the purified protein occurs as a onemajor band migrating as a double band of approximately 17 kDa when upwards of 2 μg of total protein has been loaded. The protein was estimated to be ≥95% pure, with the minor contaminating bands observable in Figure 4-14 no longer visible potentially removed during ultrafiltration. The apparent double band has been previously observed in SDS-PAGE of native bovine CaM purified to a high degree of homogeneity and ascribed to incomplete saturation of CaM by Ca^{2+} (Burgess, Jemiolo and Kretsinger, 1980). A profile plot, Appendix Figure X, revealed only one major band in each lane. Immunoblotting IgG specific for CaM of increasing quantities of CaM^{WT}, revealed detectable double bands and minor contaminating bands confirming that anomalous bands are all CaM

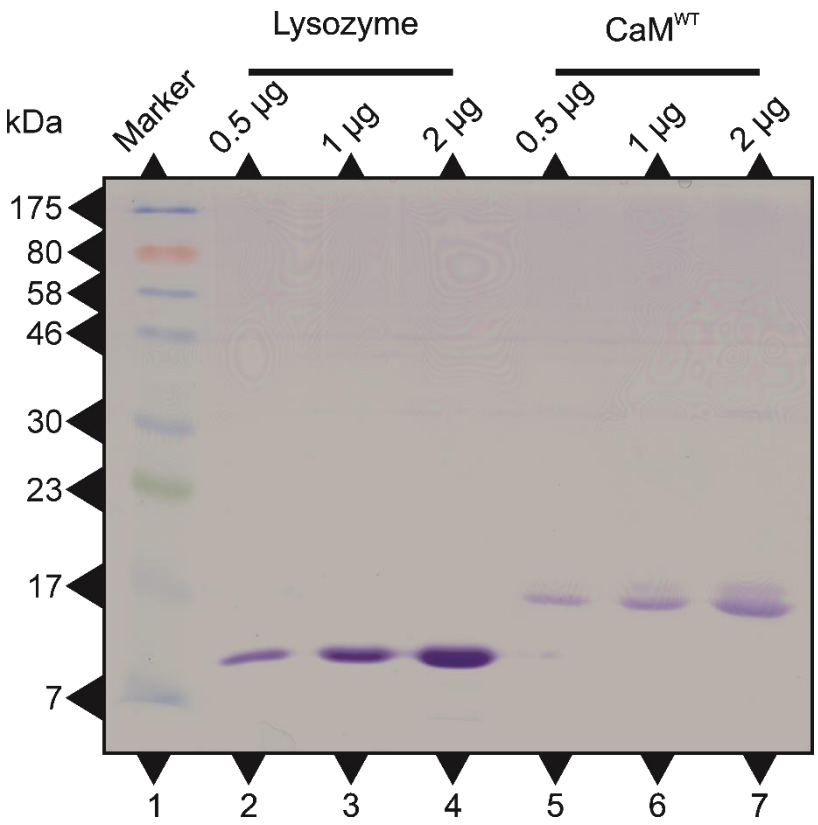

Figure 4-15 Concentrated CaM^{WT} at a High Level of Purity.

The concentration of purified CaM^{WT} was estimated spectrophotometrically and weighed crystallised lysozyme was dissolved in buffer. Known amounts of CaM^{WT} and lysozyme were separated by 15 % (w/v) SDS-PAGE and stained with Coomassie . Lane 1: ColorPlus Pre-Stained Protein Marker (NEB), Lane 2: 0.5 µg Lysozyme, Lane 3: 1 µg lysozyme, Lane 4: 2 µg lysozyme, Lane 5: 0.5 µg CaM^{WT}, Lane 6: 1 µg CaM^{WT}, Lane 7: 2 µg CaM^{WT}.

4.3.6.2 Dynamic Light Scattering

CaM^{WT} was analysed using dynamic light scattering (DLS), a mean representative peak is shown in Figure 4-16. A single species was observed which comprised 100% of the mass of the sample and the mode of the estimated molecular weight of the species was 19.7 kDa. The mean H_R (nm ±sd) was 2.08 nm ±0.22. The observed H_R is comparable but slightly smaller than those previously reported from earlier DLS studies, 2.5 nm ±0.1 for apoCaM and 3.0 nm ±0.1 for holoCaM and SAXS (Seaton *et al.*, 1985; Papish, Tari and Vogel, 2002). The observed H_R for CaM^{WT} does correlate with a calculated H_R and H_R measured by gel permeation chromatography (Sorensen and Shea, 1996).

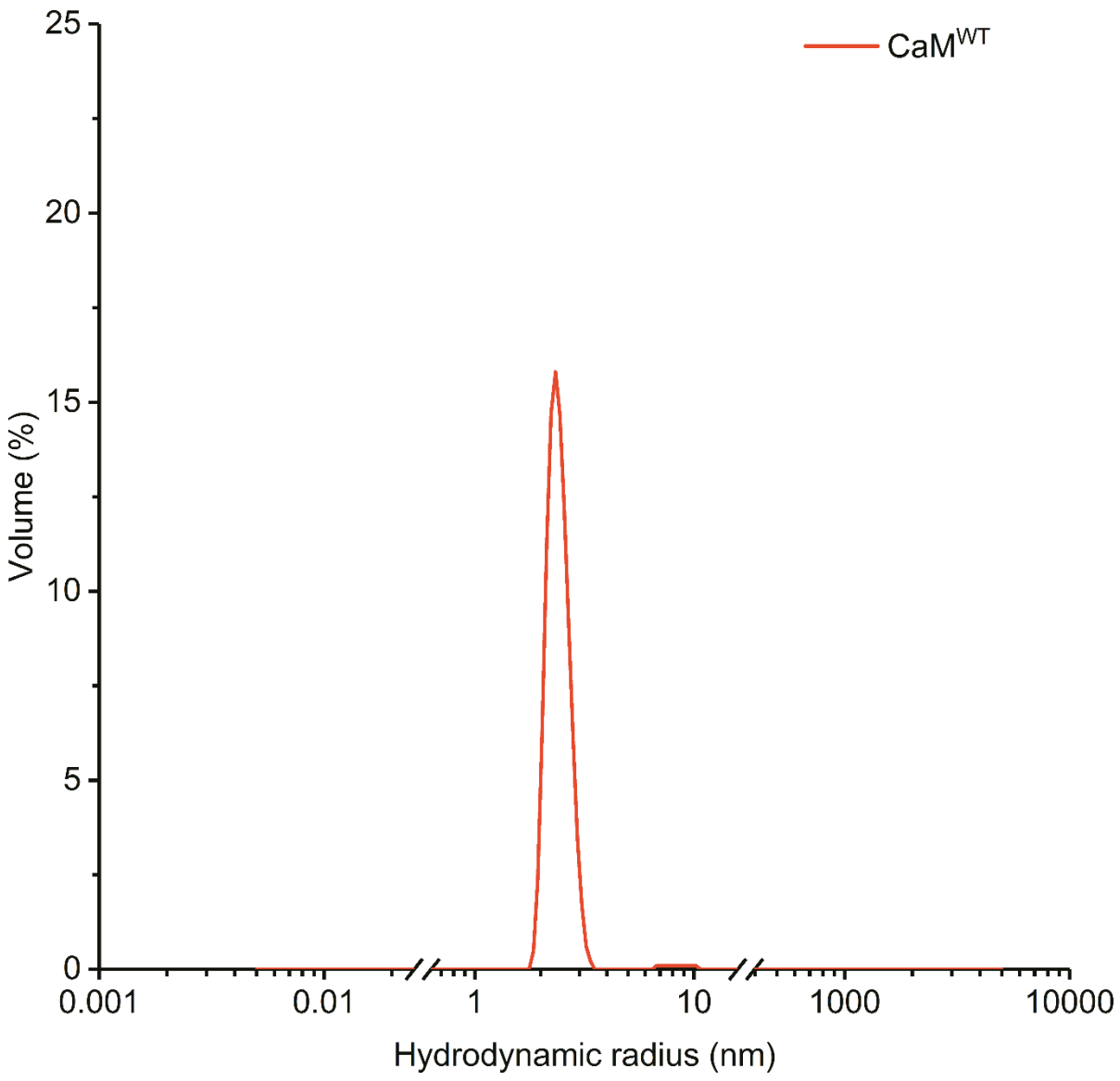

Figure 4-16 Purified Human CaM^{WT} Consists of a Single Monodisperse Species

DLS measured the hydrodynamic size of molecules in concentrated, purified CaM^{WT}, in triplicate. Histogram for mean (n=3) size distribution by volume of CaM^{WT} (20 mg/ml) in 10mM HEPES 50 mM KCl and 5mM Ca^{2+} at 20 °C is shown.

4.3.6.3 Protein Crystallisation Experiments

Crystals of CaM have been prepared in a variety of conditions from different sources, these are summarised in Table 4-1. Typically, the conditions are pH5 sodium cacodylate and 2-methyl-2,4-pentanediol (MPD) or pH5 sodium acetate and polyethylene glycol average M_n 6,000 (PEG-6000). A 96 well screen, Fine Screen 3 (FS3), was designed with these buffers and sequential increases in pH and precipitant. The range of conditions bracketed the conditions reported. The plate layout of Fine Screen 3 can be seen in Figure 2-1 and was obtained commercially (Molecular Dimensions, UK). Two commercial screens, JCSG+ and PACT (both Molecular Dimensions, UK) were also used. JCSG+ is a sparse matrix screen which encompasses conditions used to crystallise a range of proteins. PACT is a systematic grid screen which sequentially tests the effects on the protein of pH, anions and cations with precipitant PEG. The use of both in combination has been recommended as a technique for identifying new crystallisation conditions (Newman *et al.*, 2005).

Crystallisation experiments were set up using FS3, PACT and JCSG crystallisation screens as summarised in Table 2-10, to identify conditions for the crystallisation of CaM^{WT}. Concentrated CaM^{WT} was dissolved in buffer with low buffer concentration and low ionic strength. The plates were monitored at a regular interval, and observed crystals were harvested and taken to Diamond for X-ray analysis the plates continue to be monitored periodically.

A crystal was observed in well A1 of the JCSG screen, Figure 4-17. Consequently, a fine screen based on the conditions in A1 was designed and used to

set up further crystallisation experiments (Chapter 5). Subsequently, the crystal shown in Figure 4-17 was harvested, and X-ray diffraction data (data not shown) indicates that the crystal consisted of small molecules.

Increasing the amount of protein resulted in optically active crystals in wells A3, A10, D7 and G7 of JCSG as shown in Figure 4-18. However, X-ray diffraction (data not shown) indicated that all crystals harvested consisted of small molecules.

The presence of lysozyme has been shown to facilitate the formation of crystals (Liu *et al.*, 2012). Further experiments were set up increasing the amount of protein and including lysozyme in the crystallisation well. The presence of lysozyme in the wells resulted in crystals observable in A3, H11 and H12 of JCSG as shown in Figure 4-19. Following harvest X-ray diffraction data (data not shown) indicated that the crystals observed to date consist only of lysozyme.

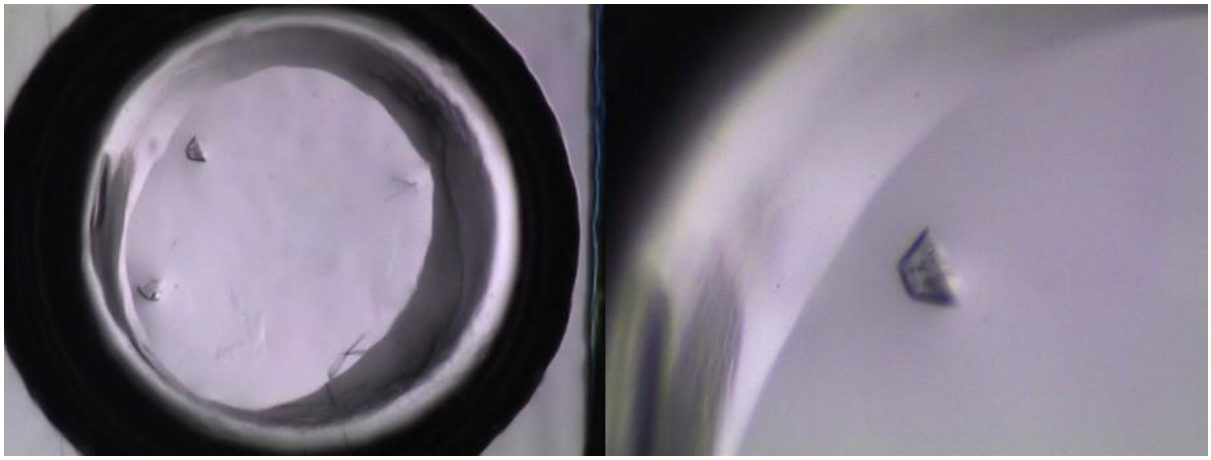

Figure 4-17 Crystal Obtained from JCSG Screen

Brightfield images of well containing 9 mg/ml CaM^{WT} 1:1 Reservoir solution on day 3 at 16 °C. Reservoir solution pH4.5 0.2 M lithium sulfate 0.1 M sodium acetate 50 % (w/v) PEG 400

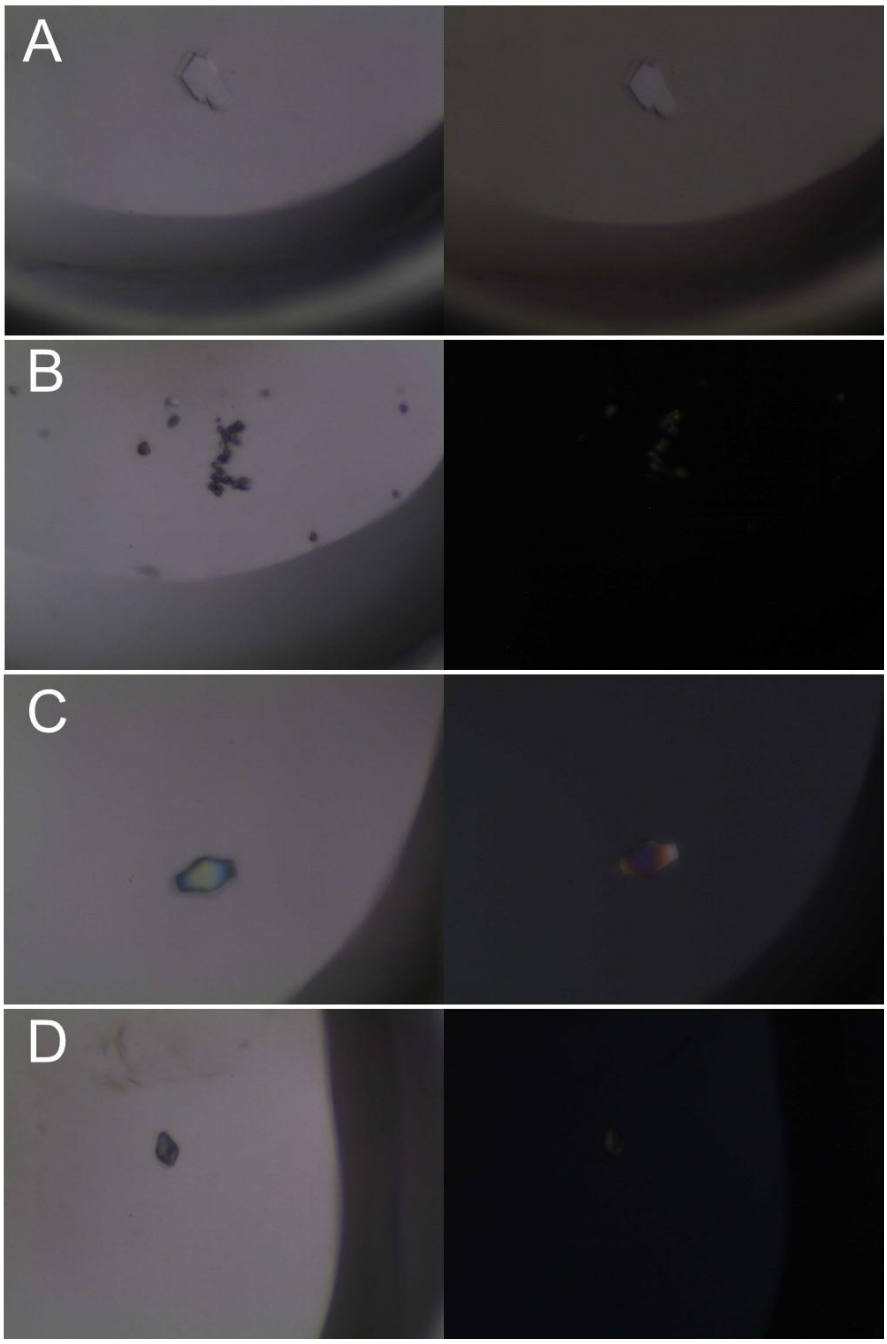

Figure 4-18 Crystals Obtained from the JCSG screen.

Brightfield (left) and polarised (right) images of wells containing 20mg/ml CaM^{WT} 2:1 with reservoir solution; **A)** 0.2M ammonium citrate dibasic 20% (w/v) PEG 3350, **B)** 0.2M potassium formate 20 % (w/v) PEG 3350, **C)** pH8.5 0.2M lithium sulfate 0.1M Tris 40% (v/v) PEG 400 **D)** 0.1M succinic acid 15% (w/v) PEG 3350

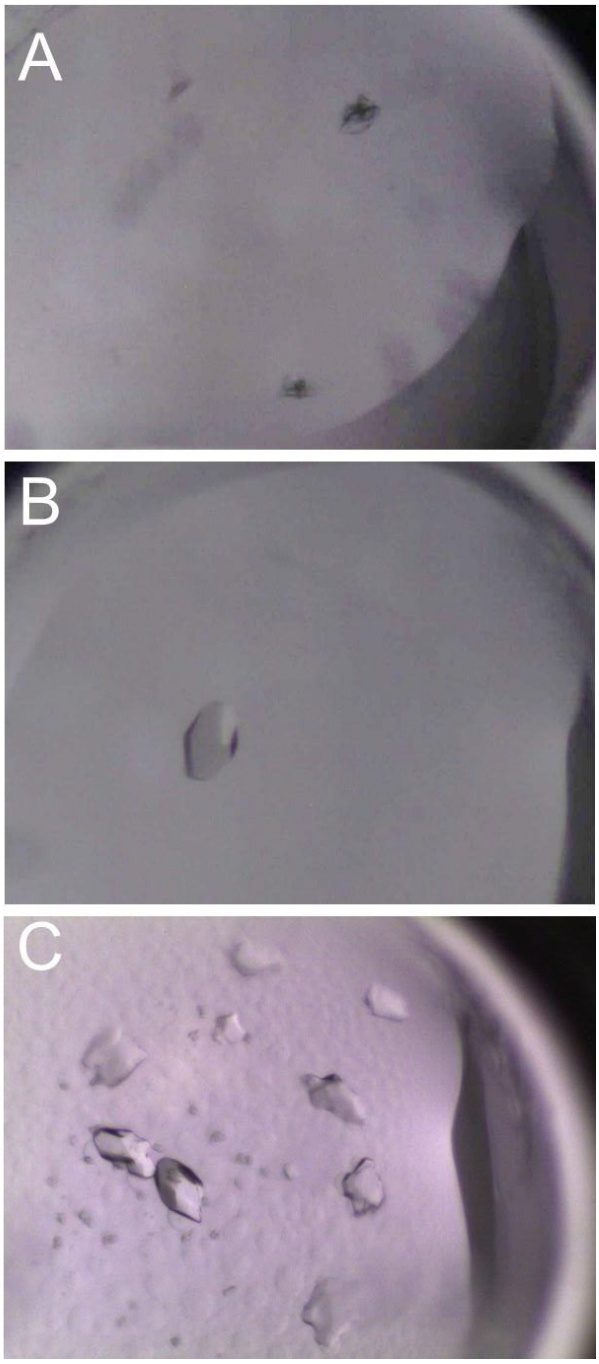

Figure 4-19 Crystals from PACT Screen of CaM^{WT} with Lysozyme

Bright-field images of wells containing 40 mg/ml CaM^{WT} and 20 mg/ml lysozyme 1:1 with reservoir solution; **A)** pH6.0 0.1 M SPG, 25 % (w/v) PEG 1500 **B)** pH8.5 0.2 M sodium citrate tribasic dihydrate 0.1 M Bis-Tris propane 20 % (w/v) PEG 3350 **C)** pH8.5 0.2 M sodium malonate dibasic monohydrate 0.1M Bis-Tris propane 20 % (w/v) PEG 3350

4.4 Discussion

In this chapter, the protein expression plasmid pHSIE-CaM^{WT} was produced which was designed to express a 47 kDa recombinant protein. The recombinant fusion protein consisted of human CaM^{WT} with an N-terminal 6xHis affinity tag and human SUMO2 solubility partner separated from CaM^{WT} by a self-cleaving Intein sequence. A PCR product of the expected size was ligated successfully into the pHSIE expression plasmid. Expression of 6xHis-SUMO2-Intein-CaM^{WT} was induced in *E.coli* transformed with pHSIE-CaM^{WT}. SDS-PAGE analysis of samples of un-induced and induced bacterial cells showed a protein band of the expected size overexpressed only in the induced sample. The expressed protein was separated from contaminant proteins and immobilised on Ni-NTA resin. The column was washed, and column conditions altered to those optimal for Intein self-cleavage. A single 17 kDa protein was subsequently eluted from the column. The protein had mobility matching the predicted molecular mass of CaM^{WT}. Meanwhile, protein matching the mobility of un-cleaved protein and cleaved tag remained bound to the resin and were eluted by increasing the imidazole concentration. The identity of the 17 kDa protein as CaM^{WT} was confirmed by immunoblotting with an antibody specific for CaM^{WT}.

The secondary structure and thermal stability of CaM^{WT} both in the absence and presence of Ca^{2+} was assessed using CD and compared to published data, see Figure 4-9 and Figure 4-10. The measured CD spectra indicate that CaM^{WT} has a similar overall structural conformation and thermal stability to wild-type CaM. Comparable CD spectra indicate that the recombinant protein is correctly folded,

stable and has a secondary structure comparable with native protein. Further, Ca^{2+} binding has a stabilising effect on the secondary structure of CaM^{WT}.

The ability of CaM^{WT} to bind RyR2 was assessed using a co-immunoprecipitation assay, as can be seen in Figure 4-11. CaM was detected in the fraction containing RyR2 immuno-precipitated from SR preps by an anti-RyR2 specific antibody bound to Sepharose resin. Levels of endogenous CaM in the SR preps (> 10 μM) are insufficient to account for the presence of CaM, see Figure 4-12. Therefore, the detected CaM is the exogenous CaM^{WT} co-precipitating with RyR2. The most plausible explanation is that the CaM^{WT} has bound to the immobilised RyR2. A visual inspection of the density of the bands indicated that a higher signal is observable as Ca^{2+} increases. However, this is not a quantifiable observation.

The ability of CaM^{WT} to modulate the function of the RyR2 channel was assayed using a [^{3}H]ryanodine binding assay, as can be seen in Figure 4-13. The binding of CaM to RyR2 reduces the P_O of the RyR2 channel. The binding affinity of ryanodine for RyR2 is highest when RyR2 is in an open conformation. Therefore, [^{3}H]ryanodine binding assay can be used to assess the functional effect of RyR2 channel modulators, i.e. CaM. In the control assay at low [Ca^{2+}] ryanodine binding was minimal indicating that RyR2 was in a closed conformation. With increasing [Ca^{2+}] the binding of ryanodine increased until plateauing when [Ca^{2+}] was 1 mM and greater, corresponding with maximal activation of the channel which is now fully open.

However, in the presence of CaM^{WT} binding of ryanodine to RyR2 was reduced compared to control. With increasing [Ca^{2+}] ryanodine binding was reduced indicating

a reduced P_O When [Ca^{2+}] was 1 mM the binding of ryanodine to RyR2 was reduced by 21 % compared to control indicating that the channel was not fully open. Therefore, CaM^{WT} was capable of significantly reducing the channel activation by approximately 20 % compared with control.

CaM^{WT} was further purified by SEC Figure 4-14, the protein eluted in a single peak at an elution volume of 90 ml indicating the species eluted is monodisperse and homogenous. According to the calibration curve for this column carbonic anhydrase which has a molecular weight of 29 kDa will elute at a volume of 90 ml. The discrepancy in size can be attributed to the mobility of native CaM being affected by its dumbbell conformation which is variable mainly due to conformational changes dependent on Ca^{2+} saturation. The Stokes radii of CaM^{WT} (23 nm) and carbonic anhydrase (20.1 nm) are comparable (Sorensen and Shea, 1996).

The purified protein was confirmed to be homogenous and mono-disperse by DLS which indicated the presence of single species as shown in Figure 4-16. The estimated size of the species observed does not match the correct size. The mismatch in size can be allowed for as the DLS analysis software assumes a uniform H_R, i.e. that the particle is a sphere. The H_R of CaM is not uniform due to the dumbbell conformation. Furthermore, unless Ca^{2+} is in excess any sample of CaM^{WT} is likely to have different proportions of apoCaM and holoCaM. The open or closed conformation dependent on Ca^{2+} saturation will result in different hydrodynamic radii.

The mean H_R (nm ±sd) was 2.08 nm ±0.22 which correlate with calculated H_R and H_R measured by gel permeation chromatography (Sorensen and Shea, 1996).

The observed H_R is comparable but slightly smaller than those previously reported from earlier DLS studies, 2.5 nm ±0.1 for apoCaM and 3.0 nm ±0.1 for holoCaM and SAXS (Seaton *et al.*, 1985; Papish, Tari and Vogel, 2002). However, in the DLS study buffer conditions and DLS instrument differ. Discrepancies between radii measured by SAXS and DLS are to be expected. The radius measured by SAXS is based on a direct measure of distance between points of scatter within the molecule and can be affected by hydration. DLS gives an approximate radius of a notional spherical particle based on indirect measurements of the radius by measuring the exterior of the molecule.

The purity and size of the protein were confirmed by SDS-PAGE, which showed a single band of the correct size (approximately 17 kDa) even when 2 µg of protein was separated. The discrepancy between the molecular weight indicated by DLS and SEC compared to SDS-PAGE and the known size of CaM can be ascribed to the dumbbell conformation of CaM protein and resulting difference in mobility of native CaM versus denatured CaM.

A fine screen was designed with conditions surrounding the range of conditions reported for crystallisation of CaM^{WT}. A screen was prepared by a commercial supplier to eliminate the possibility of an error in screen preparation. Higher ionic strengths of cacodylate and its use instead of HEPES can cause an increase in the α-helical content of CaM (Protasevich *et al.*, 1997). Also, the presence of MPD and PEG results in additional α-helices in CaM (Bayley and Martin, 1992). To identify additional conditions for crystallisation two commercial screens, PACT and JCSG were also used.

Some of the conditions in the commercial screens yielded harvestable crystals. All harvested crystals were subjected to X-ray diffraction, but the results indicate that these crystals were composed of either small molecules or lysozyme. CaM^{WT} and mutant proteins of the correct size have been isolated to a high degree of purity. The purified proteins are homogenous, mono-disperse, correctly folded and stable. Work continues to identify the conditions required for recombinant CaM protein produced by this system to crystallise.

In summary, the purified protein is soluble, homogenous and mono-disperse. The size, secondary structure and function of the protein matched that of previously published for native protein. So, CaM^{WT} is suitable for a range of biophysical and structural experiments. As will be seen in Chapters 5 and 6 pHSIE-CaM^{WT} and the one-step purification method developed in this chapter can be adapted to express mutants and the individual domains of CaM. Wild-type and mutant recombinant CaM protein can be used to investigate the pathophysiological mechanisms in clinical cardiac arrhythmia cases. Wild-type and domains of CaM can be used to investigate the regulation of PLCζ. by CaM and be used in structural studies of PLCζ.

4.5 Findings

In summary, the following novel findings were made in this chapter:

- Wild-type CaM can be expressed and purified as untagged protein using a one-step purification protocol without requiring a multiple stage purification with an enzymatic cleavage step.
- Purified CaM^{WT}

- conforms to the known biophysical parameters of CaM.
- conforms to the known functional activity of CaM

- CaM^{WT} can be used
  - to further study
    - interaction of CaM with PLCζ
    - the effects of CaM mutations on interaction with RyR2
    - regulation of RyR2 by CaM
  - as an aid in the crystallisation of PLCζ

Chapter 5 - EXPRESSION, PURIFICATION AND CHARACTERISATION OF ARRHYTHMOGENIC CALMODULIN MUTATIONS.

5.1 Chapter Summary

Recent genetic studies link mutations in genes expressing CaM to clinical cases of cardiac arrhythmia. The primary binding partner for CaM in cardiomyocytes is RyR2. Therefore, a potential pathophysiological mechanism of the mutations is a disruption of the inhibition of RyR2 by CaM. Characterisation of the CaM mutations and assessment of the impact on the regulatory interaction between CaM and RyR2 vary or have not been compared directly. The *in vitro* comparison of the mutations requires recombinant proteins expressed in the same system. The CaM^{WT} expression plasmid described in Chapter 4 is an ideal base for generating a set of plasmids that express soluble mutant CaM. This chapter describes the construction of plasmids for the prokaryotic expression of human CaM DNA sequences corresponding to genetic variants associated with cardiac arrhythmia as fusion proteins. The one-step purification method was found to yield significant quantities of pure, soluble, untagged proteins. The expressed proteins conform to structural characteristics of CaM^{WT} described in Chapter 4 so were correctly folded. Some CaM mutants displayed reduced thermal stability in the presence of Ca^{2+}. The CaM mutations had different biochemical effects compared to either CaM^{WT} or each other. The majority of CaM mutants showed altered RyR2 interaction and regulation and all bar one had reduced C-terminal domain Ca^{2+} binding affinity. Therefore, the dysfunctional Ca^{2+}-binding to CaM mediated by the mutations appears to play a crucial role in the aetiology of the associated arrhythmias. Crystallisation experiments with the CaM mutant proteins are ongoing.

5.2 Introduction

5.2.1 Background

Genetic studies have identified to date 15 different missense mutations of the three genes encoding CaM in clinical cases of arrhythmia. The patients were genotype negative for mutations in established susceptibility genes for cardiac arrhythmias. The initial reports identified mutations in *CALM1* and *CALM2*. (Nyegaard *et al.*, 2012; Crotti *et al.*, 2013; Marsman *et al.*, 2014). All were missense mutations and predicted to result in a single amino acid substitution in CaM. The mutations described in these reports are summarised in Table 5-1. Subsequent investigations of other arrhythmia cases identified *CALM2* and *CALM3* mutations each homologous to different *CALM1* Mutations (Makita *Et Al.*, 2014; Reed *Et Al.*, 2015).

Table 5-1 Summary of Arrhythmogenic Mutations of CaM Reported 2012-15

Substitution	Gene	Disease	Ca^{2+} binding affinity		Ryanodine binding
			N-domain	C-domain	
p.(N54I)	CALM1	CPVT	unreported	"Slight increase"	*In vitro* Unaffected
p.(F90L)	CALM1	IVT	unreported	unreported	unreported
p.(D96V)	CALM2	LQTS	"unaffected"	13.5 less	unreported
p.(N98S)	CALM1	CPVT	unreported	"Significant reduction"	"Aberrant" at low Ca^{2+}
	CALM2	LQTS	unaffected	unreported	unreported
p.(N98I)	CALM2	LQTS	unaffected	8-fold less	unreported
p.(D130G)	CALM1	LQTS	unaffected	53-fold less	unreported
	CALM3	LQTS	unaffected	unreported	unreported

Substitution	Gene	Disease	Ca^{2+} binding affinity		Ryanodine binding
			N-domain	C-domain	
p.(D132E)	CALM2	Mixed	unaffected	23-fold less	unreported
p.(D134H)	CALM2	LQTS	unaffected	13-fold less	unreported
p.(Q136P)	CALM2	Mixed	unaffected	6.5-fold less	unreported
p.(F142L)	CALM1	LQTS	unaffected	5-fold less	unreported

All the mutations cosegregated with severe ventricular arrhythmia and sudden cardiac death. The location of the mutations within CaM varied. The majority occurred in the C-lobe with some in Ca^{2+}-binding sites and others in the surrounding α-helices. The clinical presentations and phenotypes of the mutations were highly varied. Some were *de novo*, others inherited. Age of onset, co-morbidity, association with stress, and penetrance was highly varied. In some cases, there were varying degrees of developmental delay and cognitive impairment. Classification of the arrhythmias as CPVT, LQTS, mixed CPVT and LQTS, and IVT followed the analysis of ECG. The success of different therapeutic strategies to treat both arrhythmias and resulting cardiovascular symptoms varied. Novel mutations continue to be reported (Boczek *et al.*, 2016; Gomez-Hurtado *et al.*, 2016; Pipilas *et al.*, 2016; Takahashi *et al.*, 2017).

Mutations were identified in all three CaM genes, *CALM1*, *CALM2* or *CALM3* and shown to segregate with arrhythmias diagnosed as either LQTS, CPVT, unclear or a mixed disease. All three genes produce identical proteins, and relative expression levels vary with tissue type (Fischer *et al.*, 1988; MacManus *et al.*, 1989). In human cardiac tissue, the relative expression levels of *CALM1*:*CALM2*:*CALM3* is found at a ratio of 1:2:5 (Crotti *et al.*, 2013).

Therefore, all six alleles of CaM are expressed in the heart. In a heterozygous patient, five alleles producing wildtype CaM and one allele producing mutant CaM are expressed. The level of expression of the mutant allele will always be matched by that of at least one normal allele. Depending on the *CALM* gene, the mutant CaM protein could be at a greater or lesser proportion of total CaM expression. However, despite five CaM alleles producing normal protein, the presence in myocytes of a mutant CaM

protein product from one allele alone is sufficient to cause a disease phenotype. Despite this, all the mutations described to date display a dominant effect. Also given the wide-ranging role of CaM it is unclear why mutations of CaM have to date only been identified in cardiac arrhythmias.

The different relative expression levels could affect mutation penetrance as a mutant *CALM3* allele would have higher expression than *CALM1* or *CALM2* alleles. Due to the relatively higher expression of *CALM3 de novo* mutations are more likely to be fatal pre-term. Conversely, *CALM1* and *CALM2* mutation carriers may be relatively more likely to survive hence the higher number of *CALM1* and *CALM2* mutations observed. The particular affinity of CaM mutations and cardiac arrhythmia may be due to the binding of four CaM molecules to each RyR channel increasing the likelihood of at least one mutant being bound, which would be sufficient to cause dysfunction.

CaM directly or indirectly regulates the activity of essential proteins involved in E-CC (Hamilton, Serysheva and Strasburg, 2000; Tang, 2002). The cardiac-specific Ca^{2+} channel, RyR2, binds both apo- and holoCaM with high affinity and at nanomolar Ca^{2+} concentrations, binding inhibits channel activity (Balshaw *et al.*, 2001; Yamaguchi *et al.*, 2003). The binding of CaM to RyR2 reduces the P_O of the RyR2 channel (Xu and Meissner, 2004) In cardiomyocytes, CaM in the Z-line is predominately bound to RyR2 channels. Reduction in the binding of CaM to RyR2 occurs during HF and can induce arrhythmias (Yang *et al.*, 2014), revealing that normal cardiac function requires CaM and RyR2 binding. In animal models, reducing or eliminating CaM-RyR2 binding by mutagenesis of critical residues results in cardiovascular abnormalities and

premature death. (Yamaguchi *et al.*, 2007; Arnáiz-Cot *et al.*, 2013). Distinct reduction in binding between CaM and RyR2 in CPVT indicated that dysfunctional interaction between CaM and RyR2 might contribute on a molecular level to the aetiology of CPVT and other cardiac diseases (Xu *et al.*, 2010).

The recently identified CPVT causing mutations in *CALM1-3* are proposed to elicit a CPVT phenotype by modifying the association of CaM with the CaMBD of RyR2 (Nyegaard *et al.*, 2012; Crotti *et al.*, 2013; Hwang *et al.*, 2014; Makita *et al.*, 2014). CaM inhibits RyR2 channel opening in a Ca^{2+}-dependent manner (Yamaguchi *et al.*, 2003). There are multiple putative RyR2 CaM-binding regions, but only two to three are predicted to be accessible on surface-exposed domains (Huang *et al.*, 2013; Lau, Chan and Van Petegem, 2014). Apo- and holoCaM are believed to bind to adjacent discrete sequences and bridge different sites within RyR2 depending on Ca^{2+} saturation and in response to Ca^{2+}-binding. The best-characterised region is $RyR2^{3581-3608}$, which has been shown to be “grasped” by both lobes of CaM in the presence of Ca^{2+} (Maximciuc *et al.*, 2006). Therefore, mutation mediated changes to the binding of Ca^{2+} to CaM could alter the interaction of CaM with RyR2 in response to changes in Ca^{2+}. The changes to the interaction of CaM and RyR2 would impact the ability of CaM to stabilise the closed conformation of RyR2 leading aberrant Ca^{2+} release (Rodney *et al.*, 2000, 2001; Lau, Chan and Van Petegem, 2014).

The mutations in *CALM1-3* associated with LQTS identified in recent genetic studies potentially disrupt the interaction between CaM and the regulatory CaM binding regions of ion channels (Nyegaard *et al.*, 2012; Crotti *et al.*, 2013; Hwang *et al.*, 2014; Limpitikul *et al.*, 2014; Makita *et al.*, 2014; Reed *et al.*, 2015). The C terminus

cytoplasmic domains of $K_V7.1$ and $Na_V1.5$, also contain conserved IQ and 1–5–10 CaM-binding motifs (Yus-Nájera, Santana-Castro and Villarroel, 2002; Chagot and Chazin, 2011). An LQTS associated *KCNQ1* mutation is predicted to be located in the CaM-binding motifs of $K_V7.1$ (Ghosh, Nunziato and Pitt, 2006).

The ion channels RyR2, $Ca_V1.2$, $K_V7.1$ and $Na_V1.5$ all play critical roles in the movement of ions before, during and after an AP in cardiomyocytes. Mutations in the genes encoding these ion channels are associated with cardiac arrhythmias and SCD. Dysregulation could cause inappropriate ion release leading to arrhythmogenic disturbances of the transmembrane potential. All have more than one binding site for the ubiquitous Ca^{2+} sensitive regulatory protein CaM and will bind both apo- and holo-CaM. Included amongst the predicted changes are alterations to highly conserved sequences containing CaM-binding motifs.

The interactions of CaM and target proteins are complex, with multiple and diverse recognition, binding and regulatory mechanisms identified which can be either Ca^{2+}-dependent or Ca^{2+}-independent (Hoeflich and Ikura, 2002; Yamniuk and Vogel, 2004). Over 300 CaM-binding sequences in more than 100 proteins have been identified, (http://calcium.uhnres.utoronto.ca/ctdb) (Yap *et al.*, 2000). IQ motifs are consensus sequences that are recognised and bound to by apoCaM, which becomes tethered to the protein in a Ca^{2+} free state. Effectively, apoCaM prebound to a protein, e.g. an ion channel protein creates a Ca^{2+} binding domain. A mechanism has been proposed whereby the tethered apoCaM form localised Ca^{2+} signalling domains regulating ion channel activity in cardiomyocytes (Saucerman and Bers, 2012). Recently, in neuronal tissue apoCaM binding has been shown in the absence of Ca^{2+}

to directly stimulate the activity of voltage-gated Na^+ and Ca^{2+} channels (Adams *et al.*, 2014).

There is not a universal recognition or binding sequence for CaM; most holoCaM target sequences are α-helix-rich sequences interspersed with hydrophobic residues (Tidow and Nissen, 2013). Upon Ca^{2+}-binding, CaM undergoes conformational change exposing hydrophobic patches containing multiple Met residues (Chin and Means, 2000). The exposed residues combined with the flexible linker separating the N- and C-lobes enables CaM to bind to and interact with numerous proteins via a variety of recognition sequences (Yamniuk and Vogel, 2004). The linker permits the N- and C-lobes to grab then envelope a target α-helix sequence with the mode and orientation of binding believed to be dictated by the sequence of the CaM binding site (Tidow and Nissen, 2013).

Therefore, in addition to affecting the conformation and stability of CaM, the identity and position of mutations may alter the interaction of CaM with any of the binding domains found in target proteins. As can be seen in Figure 5-2 the arrhythmogenic mutations examined in this study are clustered mainly in the C-domain in the vicinity of Ca^{2+}-binding sites. Potentially, these mutations could alter Ca^{2+} sequestration by CaM and change the binding of CaM to recognition sequences. Previously, various studies described the structural changes and Ca^{2+}-binding properties of CaM mutations (Crotti *et al.*, 2013; Makita *et al.*, 2014; Nomikos *et al.*, 2014; Søndergaard, Sorensen, *et al.*, 2015).

5.2.2 Arrhythmogenic Mutations of Calmodulin

Several research manuscripts identify the location of mutated residues by numbering from the initiating Met residue (Crotti *et al.*, 2013; Marsman *et al.*, 2014; Reed *et al.*, 2015; Gomez-Hurtado *et al.*, 2016; Pipilas *et al.*, 2016). Other authors do not include the Met in the sequence numbering when identifying the position of the amino acid substitution as the initiating Met residue is absent from mature processed CaM (Nyegaard *et al.*, 2012; Søndergaard, Sorensen, *et al.*, 2015; Søndergaard, Tian, *et al.*, 2015; Berchtold *et al.*, 2016). Hence the same mutation, e.g. *CALM1* c.389C>G, can be described as causing an amino acid substitution occurring at position 129 in one paper and 130 in another (Hwang *et al.*, 2014; Berchtold *et al.*, 2016). All the notations of the CaM mutations discussed in this thesis include the initiating Met. The affected amino acid residues within the primary sequence of CaM are shown in Figure 5-1.

```
1   MADQLTEEQI AEFKEAFSLF DKDGDGTITT
31  KELGTVMRSL GQNPTEAELQ DMINEVDADG
61  NGTIDFPEFL TMMARKMKDT DSEEEIREAF
91  RVFDKDGNGY ISAAELRHVM TNLGEKLTDE
121 EVDEMIREAD IDGDGQVNYE EFVQMMTAK
```

Figure 5-1 Positions of Arrhythmogenic Mutants Within Calmodulin

The amino acid sequence of human CaM (GenBank: AAD45181.1) showing residues affected by mutations identified in patients with cardiac disease. The sequence is annotated with the positions of the 10 residues underlined in bold predicted to be substituted in protein expressed by mutated CALM genes outlined in Table 5-1. At position 98 two different mutations were predicted to substitute the Asp with Ser or Ile.

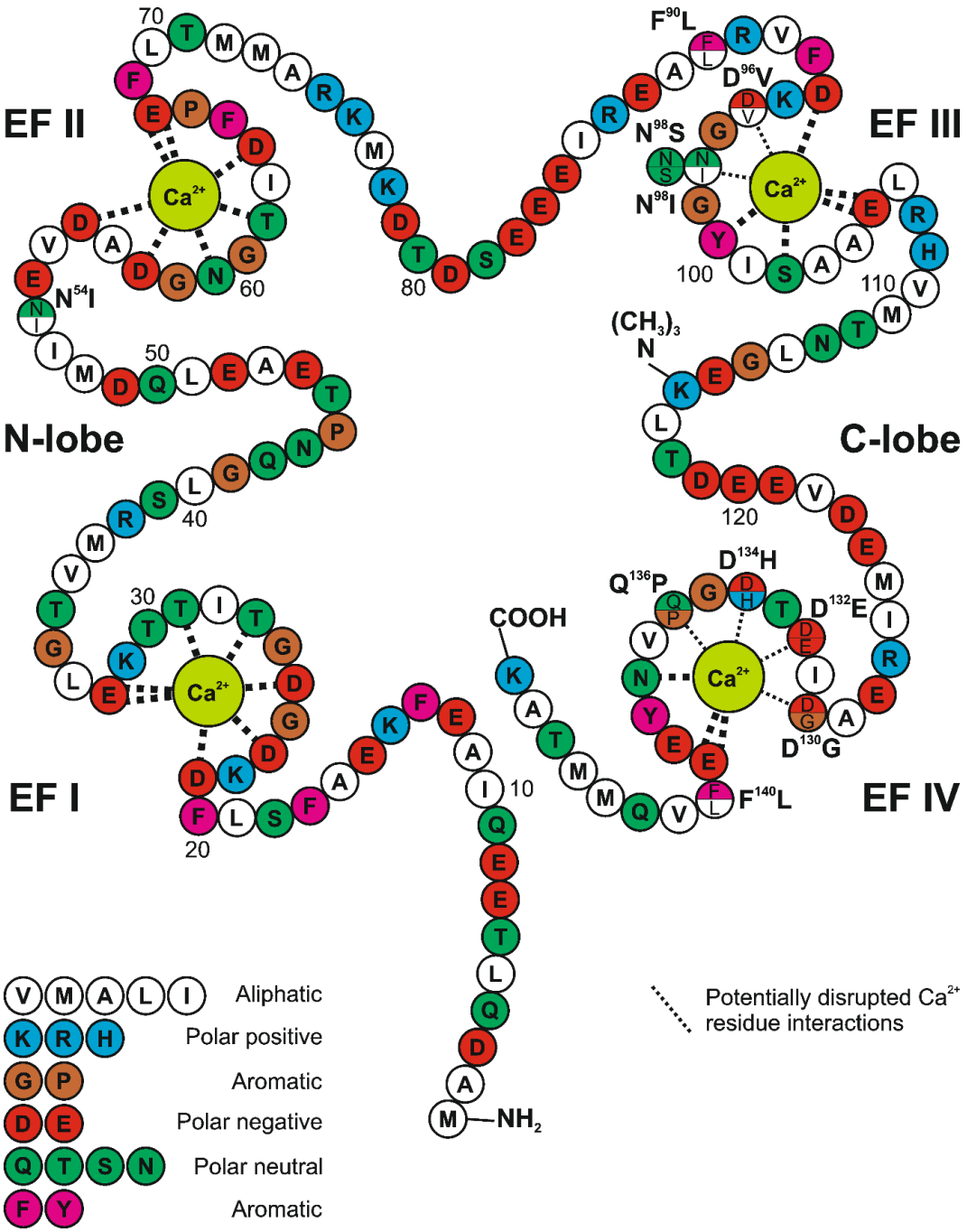

Figure 5-2 Arrhythmogenic Mutations Mainly Occur near Ca^{2+} Binding Sites

The primary structure of human CaM expressed by *CALM1* adapted from (Cheung, 1982) showing the location and identity of the predicted amino acid substitutions associated with cardiac arrhythmias described in this chapter.

5.2.2.1 Calmodulin N54I Mutation

A 42-year-old male of Swedish ethnic origin presented with a 30-year history characteristic of CPTV (Nyegaard *et al.*, 2012). The family history included multiple instances of ventricular arrhythmia, syncope, and sudden cardiac arrest and death associated with exercise or stress. All affected family members were negative for mutations in the genes encoding RyR2 and calsequestrin which are both associated with CPVT. Genetic studies revealed a heterozygous missense mutation in the coding sequence of *CALM1* c.161A>T, found only in affected family members. The mutation is predicted to result in the substitution of asparagine (Asn) at position 54 with Ile (p.(Asn54Ile)) (Nyegaard *et al.*, 2012). As can be seen in Figure 5-2, amino acid 54 is in the N-lobe of CaM that flanks the Ca^{2+}-binding site of EF-Hand II. Molecular modelling predicts p.(Asn54Ile) is located in an α-helix on a solvent-exposed surface which is in contact with Ca^{2+}, ligands, or domains of CaM (Nyegaard *et al.*, 2012). This mutation will result in a polar residue in an exposed position being replaced with a hydrophobic residue. Recombinant CaM protein bearing p.(Asn54Ile) displayed enhanced binding to Ca^{2+} and RyR2 at the C-lobe. However, biochemical characteristics at the N-lobe were not measured (Nyegaard *et al.*, 2012)

5.2.2.2 Calmodulin F90L Mutation

A 16-year-old male of Moroccan descent presented with cardiac arrest during physical exertion who then responded to defibrillation (Marsman *et al.*, 2014). Further investigation was inconclusive, and no further episodes were reported during the following 12 years. The family history contained a younger sibling who died suddenly

at 9-years-old. Subsequently, a 10-year-old sibling died suddenly. Another sibling, also at 10-years-old, was successfully treated initially for VF following exercise and on three more occasions over an 8 year follow up. Family members, including both affected individuals and asymptomatic parents and siblings, were negative for mutations in *RYR2* and *CASQ2*. ECG investigations were inconclusive but did reveal mild abnormalities in the mother and an asymptomatic sibling. A novel missense mutation was found in *CALM1* c.268C>T of both the affected individuals and mother and another sibling with mildly abnormal ECG. The mutation was not found in other family members with normal ECG. The mutation results in the replacement of phenylalanine (Phe) at position 90 with leucine (Leu) (p.(Phe90Leu)) in the C-lobe of CaM (Marsman *et al.*, 2014). As can be seen in Figure 5-2 amino acid 90 is located within the in the flexible region between the N- and C-lobes in an α helix preceding the Ca^{2+}-binding of EF-III in the C-lobe of CaM.

The unclear phenotype described in the initial report was not characteristic of either LQTS or CPVT and was classified as IVT (Marsman *et al.*, 2014). However, *in vitro* analysis of recombinant CaM protein bearing p.(Phe90Leu) revealed reduced binding to RyR2, inhibition of the ability of CaM to reduce channel activity and a reduced Ca^{2+}-binding affinity at the C-domain (Nomikos *et al.*, 2014).

5.2.2.3 Calmodulin D96V Mutation

A female of Hispanic origin presented at three-weeks-old with cardiac arrest and multiple episodes of VF treated successfully but had sustained a cerebral injury. Arrhythmia characteristic of LQTS was detected two hours after an uncomplicated

delivery. Heartbeat abnormalities had been detected *in utero*, but heart structure and function were unremarkable. During a 3 year follow up multiple episodes were noted of VF, seizure, and delayed development. The arrhythmias did not respond completely to treatment. The ECG of parents and an older sibling were normal. The family history contained no instances of seizures, sudden death or miscarriage. There were no mutations detected in the genes usually associated with LQTS. Genetic analysis revealed a novel *de novo* missense mutation in *CALM2*, c.287426A>T. The mutation causes aspartic acid (Asp) at position 96 to be substituted with valine (Val) (p.(Asp96Val)). As can be seen in Figure 5-2 amino acid 96 is a critical residue in the Ca^{2+}-binding site of EF-III on the C-lobe of CaM predicted to coordinate Ca^{2+}-binding (Chattopadhyaya *et al.*, 1992). The mutation results in a change of charge due to the replacement of the negatively charged Asp residue with a non-polar Val that will disrupt coordination of Ca^{2+}.

Recombinant mutant CaM protein bearing p.(Asp96Val) had 13-fold reduced Ca^{2+} affinity at the C-lobe compared to wild-type while Ca^{2+}-binding at the N-lobe of CaM^{D96V} was unaffected (Crotti *et al.*, 2013).

5.2.2.4 Calmodulin N98S Mutation

A 23-year-old female of Iraqi origin presented with a 19-year history of multiple cardiac events associated with exercise (Nyegaard *et al.*, 2012). ECGs appeared normal with no evidence of LQTS. There was no family history of ventricular arrhythmias. Both parents and the affected individual were negative for mutations in genes encoding RyR2, calsequestrin-2 and other proteins associated with arrhythmias including LQTS.

A *de novo* missense mutation in the coding region of *CALM1*, c.293A>G was detected in only the affected individual. The mutation is a single base substitution at position 98 of Asn with Ser (p.(Asn98Ser)) in the C-lobe of CaM (Nyegaard *et al.*, 2012).

The substitution is of a polar residue with another polar residue. However, as can be seen in Figure 5-2 amino acid 98 is in the Ca^{2+}-binding site of EF-III and is predicted to be a Ca^{2+}-coordinating residue directly involved in Ca^{2+}-binding by EF-III (Chattopadhyaya *et al.*, 1992). The Ca^{2+}-binding at the C-lobe of recombinant CaM protein bearing p.(Asn98Ser) was reduced. Also, the binding of recombinant CaM protein bearing p.(Asn98Ser) to the CaM Binding Domain (CBD) was reduced at a low cytosolic Ca^{2+} concentration (Nyegaard *et al.*, 2012).

Novel mutations in *CALM2*, c.293A>G, which result in the same amino acid substitution were detected in three unrelated cases. The first, a 5-year-old male of Japanese origin with a history of exercise-related syncope and seizures, and resting ECG characteristic of LQTS (Makita *et al.*, 2014). The second, a 7-year-old Spanish male with a posthumous diagnosis of CPVT following SCD associated with exercise (Jiménez-Jáimez *et al.*, 2016). The third, a 4-year-old Moroccan female treated for a cardiac arrest associated with emotional stress, the follow-up ECG was indicative of LQTS (Jiménez-Jáimez *et al.*, 2016).

None of the individuals with *CALM2* c.293A>G was positive for mutations in the genes commonly associated with LQTS. No cognitive or developmental problems were observed. In the living cases, arrhythmia was treated successfully. Family histories contained no instances of arrhythmias or cardiac death. Parents and any

siblings were all asymptomatic. The *CALM2* mutations in the first two cases were determined to be *de novo*, and no LQTS mutations were detected in the family members tested. (Makita *et al.*, 2014; Jiménez-Jáimez *et al.*, 2016).

5.2.2.5 Calmodulin N98I Mutation

A 2.5-year-old male from England, previously treated for VF at 17 months old, was treated for cardiac arrest (Makita *et al.*, 2014). An ECG indicated cardiac rhythm abnormalities and LQTS which were successfully managed. Both parents were asymptomatic and there no family history of arrhythmia. Genetic testing revealed no mutations in the genes generally associated with LQTS. A novel *de novo* mutation was detected in the child in *CALM2*, c.293A>T which results in another substitution at amino acid 98 but with a non-polar Ile residue (p.(Asn98Ile). Recombinant mutant CaM protein containing p.(Asn98Ile) had 8-fold reduced Ca^{2+} affinity at the C-lobe compared to wild-type (Makita *et al.*, 2014).

5.2.2.6 Calmodulin D130G Mutation

A Caucasian female infant from Italy presented with multiple episodes of VF since 6 months of age, and all episodes were treated successfully with defibrillation (Crotti *et al.*, 2013). Foetal heartbeat had been unremarkable, and the heart was structurally normal. However, following defibrillation ECG showed characteristics of LQTS. Treatment after initial cardiac arrest eventually reduced but did not prevent, the later episodes of VF and arrhythmia induced by stress. Additional mild impairment of neurodevelopment was noted. Both parents were asymptomatic with normal ECG, and the family history contained no instances of sudden cardiac death. A *de novo*

missense mutation in *CALM1*, c.389C>G, was detected only in the infant. The mutation is predicted to cause the substitution at amino acid 130 of Asp with Gly (p.(Asp130Gly)). Recombinant mutant CaM protein containing p.(Asp130Gly) had a 53-fold reduced Ca^{2+} affinity at the C-lobe when compared to the binding affinity of wild-type CaM (Crotti *et al.*, 2013).

The same mutation was subsequently identified in a 3-year-old Caucasian boy from Greece with a history of multiple cardiac arrests since 1-month-old (Crotti *et al.*, 2013). Also, a *de novo* missense mutation in *CALM3*, c.389A>G which also results in p.(Asp130Gly) was detected in a male infant of mixed ethnicity and limited family history with a postnatal diagnosis of LQTS and cardiac abnormalities (Reed *et al.*, 2015). No mutations were found in the genes customarily associated with LQTS in either of the cases. Genetic screening of LQTS patients negative for other known LQTS-susceptibility genes identified a novel *CALM2* missense mutation c.389A>G which also results in p.(Asp130Gly). The carrier was a female diagnosed with brachycardia at birth and successfully treated for VF since, with the last recorded episode at 14 years old (Boczek *et al.*, 2016).

As can be seen in Figure 5-2, amino acid 130 is located in the Ca^{2+}-binding site of EF IV and the residue substituted by both the *CALM1* and *CALM3* mutations is directly involved in the coordination of Ca^{2+} in EF IV (Chattopadhyaya *et al.*, 1992).

5.2.2.7 Calmodulin D132E Mutation

A 29-year-old female from Germany with a history since the birth of heartbeat irregularities exercise-induced syncope and arrhythmia under control with medication.

ECG at rest and exercise contained features of both LQTS and CPVT (Makita *et al.*, 2014). No mutations were detected in the genes commonly associated with either condition. The family history contained no instances of cardiac arrest or sudden death and both parents were asymptomatic. A *de novo* missense mutations in *CALM2* was detected, c.396T>G, which is predicted to result in single residue substitution at amino acid 132 of Asp with Glu (p.(Asp132Glu)). As can be seen in Figure 5-2 the amino acid at position 132 is involved in the coordination of Ca^{2+} in EF-IV. Recombinant CaM protein bearing p.(Asp132Glu) had 22-fold reduced Ca^{2+} affinity at the C-lobe when compared to wild-type (Makita *et al.*, 2014).

5.2.2.8 Calmodulin D134H Mutation

A 16-year-old Japanese female presented with a history including *in utero* and childhood cardiac rhythm abnormalities, syncope and exercise-related cardiac arrest. ECG was characteristic of LQTS (Makita *et al.*, 2014). There was no family history of arrhythmia or sudden death. Both parents and two siblings had no evidence of arrhythmia, and no mutations were found in the genes usually associated with LQTS. A novel *de novo* missense mutation was detected in *CALM2*, c.400G>C only in the affected individual. The mutation is predicted to result in a single amino acid substitution at position 134 of Asp with a His (p.D134H). As can be seen in Figure 5-2 the amino acid at position 134 is involved in the coordination of Ca^{2+} in EF-IV. Recombinant mutant CaM protein (CaM^{D134H}) had 12-fold reduced Ca^{2+} affinity at the C-lobe when compared to wild-type (Makita *et al.*, 2014).

5.2.2.9 Calmodulin Q136P Mutation

An 11-year-old female from Morocco died suddenly during physical exertion after presenting at 8 years old with syncope (Makita *et al.*, 2014). A Holter monitor recording at initial presentation indicated arrhythmia characteristic of LQTS which was controlled therapeutically. A genetic screen post-mortem revealed no mutations in the genes usually associated with either CPVT or LQTS. There was no family history of cardiac arrhythmia, and parents and siblings were asymptomatic. A *de novo* missense mutation in *CALM2* c.407A>C was identified only in the deceased. The mutation is predicted to result in the substitution at position 136 of Gln with Proline (Pro) (p.(Gln136Pro)). As can be seen in Figure 5-2 the amino acid at position 136 is involved in the coordination of Ca^{2+} in EF-IV. Recombinant mutant CaM protein containing p.(Gln136Pro) had 6-fold reduced Ca^{2+} affinity at the C-lobe compared to wild-type (Makita *et al.*, 2014).

5.2.2.10 Calmodulin F142L Mutation

A 14-year-old Caucasian male from Italy presented with arrhythmia, epilepsy, and cognitive and developmental disabilities (Crotti *et al.*, 2013). ECG indicated LQTS and family history was unavailable. Clinical information was limited but included multiple episodes of VF and seizures since birth. No mutations were identified in the genes associated with LQTS. A novel missense mutation not found in ethnically matched controls was identified in *CALM1* c.426C>G. The mutation is predicted to result in the substitution at position 142 of Phe with Leu (p.(Phe142Leu)). Recombinant mutant

CaM protein containing p.(Phe142Ala) had 5-fold reduced Ca^{2+} affinity at the C-lobe compared to wild-type (Crotti *et al.*, 2013).

The substitution is of an aromatic Phe residue with an aliphatic Leu residue as can be seen in Figure 5-2. Both Phe and Leu residues are non-polar but, the amino acid at position 142 is the first residue of the sequence that exits the Ca^{2+}-binding site of EF-IV. In Ca^{2+}-binding proteins containing EF-hands, the identity and location of aromatic residues in the α-helices that flank the Ca^{2+}-binding sites are predicted to modulate EF-hand function (Denessiouk *et al.*, 2014). Phe residues flanking the EF-hands of CaM are conserved and are required for the partner protein interaction, contributing to target binding and activation (Okano, Cyert and Ohya, 1998).

5.2.2.11 Characterisation of the Arrythmogenic Calmodulin Mutations

The initial reports contained limited functional data on the divergent effects and biochemical consequences of the CaM mutations. Recombinant CaM proteins bearing the mutations were expressed, purified and characterised in several different studies, Table 5-1. A variety of expression systems and fusion partners were used but no details of fusion partner removal were published (Nyegaard *et al.*, 2012; Crotti *et al.*, 2013; Makita *et al.*, 2014). , Charecterisation varied, and the effect of only two mutations, p.(Asn54Ile) and p.(Asn98Ser) on the interaction between CaM and RyR2 was reported (Nyegaard *et al.*, 2012).

All the mutations except p.(Asn54Ile) were reported as causing a reduction in Ca^{2+} binding affinity at the C-terminal. However, p.(Asn54Ile) and p.(Asn98Ser) were characterised by comparing the mutant CaM proteins with a wildtype protein, all of

which were expressed with MBP tags (Nyegaard *et al.*, 2012). The Ca^{2+} binding affinities of the wildtype and mutant CaM proteins were determined at the C-domain only and binding between RyR2 and the CaM proteins were assessed by monitoring intrinsic fluorescence of the C-domain at three [Ca2+] in the presence of a peptide corresponding to $RyR2^{3581–3611}$. The authors suggested that p.(Asn54Ile) caused an enhanced affinity at the C-domain for Ca^{2+} due to a mutation derived reduction in Ca2+ binding at the the N- terminal resulting in greater availability of Ca^{2+} (Nyegaard *et al.*, 2012).

Collectively the phenotypes displayed by individuals bearing the CaM mutations have been described as calmodulinopathies (Limpitikul *et al.*, 2014; Yin *et al.*, 2014). Also, some authors group the mutations according to the clinical classification of the phenotype, i.e., CPVT, LQTS, mixed or IVT. Mainly the paucity of the RyR studies is due to the classification of the phenotypes as LQTS indicating the minimal involvement of RyR2. No data describing the effect of the mutations on the tertiary structure has been published to date.

5.2.3 Rationale and Experimental Plan

Investigating the full aetiology of arrhythmias linked with CaM gene mutations requires establishing, compared to wild-type, the effects of the mutations on CaM protein and regulation of ion channels involved in E-CC by CaM. It is desirable to compare recombinant wildtype and mutant CaM proteins produced in the same system. This chapter discusses the functional and biophysical effects of the patient-derived mutations on CaM, with an emphasis on examining mutation mediated effects on regulation of RyR2 by CaM. Recombinant mutant CaM proteins bearing

arrhythmogenic mutations of CaM reported in published international studies between 2012-2015, will be produced and characterised using the same methods throughout.

Mutation of the CALM1 cDNA sequence using SDM and insertion of mutation bearing sequences into the pHSIE vector will create a series of protein expression plasmids expressing mutant human CaM with an N-terminal 6xHis-human SUMO2-Intein fusion partner. The one-step purification protocol described in Chapter 4 will produce soluble, untagged, CaM proteins bearing patient-derived mutations. Separation of the purified proteins by SDS-PAGE and immunoblotting with anti-CaM antibodies.will confirm the mobility and identity of the proteins as CaM recombinant proteins.

Analysis of CD spectra in the presence and absence of Ca2+will examine the effect of the mutations on the gross structure and inherent stability of CaM. Co-IP assays will assess the Ca2+ dependent capacity of CaM mutants to bind RyR2. Ryanodine binding assays will examine mutation mediated alterations in the ability of CaM to regulate RyR2 activity in a Ca2+-dependent manner. Comparing the Ca2+ binding affinity of mutant and wildtype CaM will measure mutation mediated changes in the ability of CaM to sequester Ca2+. To examine the effect of mutations on the tertiary structure of CaM optimisation trials of conditions for crystallisation of mutant and wildtype CaM based on conditions published for wildtype will be set up. Potentially, optimised conditions could be used to generate 3D structures of wild-type and mutant CaM pre-bound to target sequences comparison of which may reveal altered modes of binding.

5.3 Results

5.3.1 Molecular Cloning

Site-directed mutagenesis (SDM) of the pAED4-hCaM plasmid yielded plasmids containing CaM sequences bearing mutations linked with cardiac arrhythmias. The single base substitutions required to produce each mutation are shown in Figure 5-3. The primers used for each mutagenesis are outlined in Appendix Table I. The mutated sequences were cloned into the pHSIE expression vector as described in Chapter 4 for the wildtype sequence. Primers hCaMKpNF and hCaMNotIR were used to amplify each mutated CaM sequence with a 5'-*KpnI* site and a 3'-*NotI* site to facilitate cloning. Successful cloning for each CaM mutant was confirmed by PCR as can be seen in Figure 5-4. Sequencing confirmed the presence of the correct mutation. The mutant CaM (CaM^{MUT}) expressing plasmids were termed pHSIE-$CaMN^{54}I$, pHSIE-$CaMF^{90}L$, pHSIE-$CaMD^{96}V$, pHSIE-$CaMN^{98}S$, pHSIE-$CaMN^{98}I$, pHSIE-$CaMD^{130}G$, pHSIE-$CaMD^{132}E$, pHSIE-$CaMD^{134}H$, pHSIE-$CaMQ^{136}P$ and pHSIE-$CaMF^{142}L$.

```
1      atggctgatcagctgaccgaagaacagattgctgaattcaaggaagccttctccctattt
1       M  A  D  Q  L  T  E  E  Q  I  A  E  F  K  E  A  F  S  L  F

61     gataaagatggcgatggcaccatcacaacaaaggaacttggaactgtcatgaggtcactg
21      D  K  D  G  D  G  T  I  T  T  K  E  L  G  T  V  M  R  S  L

        .  .  .  .  .  .  .  .  .  .  .  .  .  I  .  .  .  .  .  .
       ........................................att..................
121    ggtcagaacccaacagaagctgaattgcaggatatgatcaatgaagtggatgctgatggt
41      G  Q  N  P  T  E  A  E  L  Q  D  M  I  N  E  V  D  A  D  G

181    aatggcaccattgacttccccgaatttttgactatgatggctagaaaaatgaaagataca
61      N  G  T  I  D  F  P  E  F  L  T  M  M  A  R  K  M  K  D  T

        .  .  .  .  .  .  .  .  .  .  .  .  .  .  .  .  .  I  .  .
       ......................................................att......
        .  .  .  .  .  .  .  .  .  L  .  .  .  .  .  V  .  S  .  .
       ............................ctc...............gtt...agt......
241    gatagtgaagaagaaatccgtgaggcattccgagtctttgacaaggatggcaatggttat
81      D  S  E  E  E  I  R  E  A  F  R  V  F  D  K  D  G  N  G  Y

301    atcagtgcagcagaactacgtcacgtcatgacaaacttaggagaaaaactaacagatgaa
101     I  S  A  A  E  L  R  H  V  M  T  N  L  G  E  K  L  T  D  E

        .  .  .  .  .  .  .  .  .  G  .  E  .  H  .  P  .  .  .  .
       ............................ggt...gag...cac...cca............
361    gaagtagatgaaatgatcagagaagcagatattgatggagacggacaagtcaactatgaa
121     E  V  D  E  M  I  R  E  A  D  I  D  G  D  G  Q  V  N  Y  E

        .  L  .  .  .  .  .  .
       ...tta..................
421    gaattcgtacagatgatgactgca
141     E  F  V  Q  M  T  A  K
```

Figure 5-3 Site-Directed Mutagenesis Can Be Used to Recreate Arrhythmogenic *CALM1* and *CALM2* Mutations in *CALM1.*

The translated mRNA sequence of *CALM1* (NCBI Reference Sequence: NM_006888.5) with codons found to contain missense mutations in cardiac arrhythmia patients highlighted. The single nucleotide substitution by SDM and resulting residue change to recreate the predicted amino acid substitution are in bold. Two different mutation reactions were required to produce the $N^{98}S$ and $N^{98}I$ mutants of CaM.

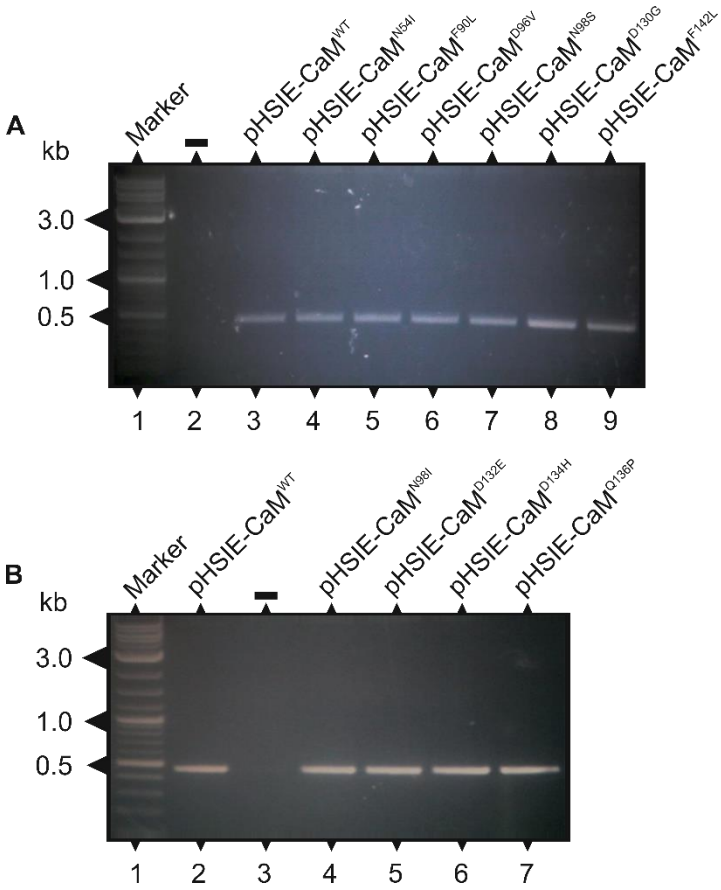

Figure 5-4 PCR Confirmation of Mutant pHSIE Plasmids.

A PCR product was amplified from a positive clone of each mutagenesis using cloning primers, hCaMKpNF and hCaMNotIR. pHSIE-CaMWT and pHSIE-were used as positive and negative controls. The lanes of 1.4 % (w/v) agarose gels were loaded with 500 ng of PCR product. The separated DNA was visualised under UV light, and a 0.5 kb band was observed in all reactions with the exception of the negative control. (A) Lane 1: 2 log DNA Marker (NEB), Lane 2: pHSIE, Lane 3: pHSIE-CaM^{WT}, Lane 4: pHSIE-CaM^{N54I}, Lane 5: pHSIE-CaM^{F90L}, Lane 6: pHSIE-CaM^{D96}V, Lane 7: pHSIE-CaM^{N98S}, Lane 8: pHSIE-CaM^{D130G}, Lane 9: pHSIE-CaM^{F142L}. (B) Lane 1: 2-log DNA Marker (NEB), Lane 2: pHSIE-CaM^{WT}, Lane 3: pHSIE, Lane 4: pHSIE-CaM^{N98I}, Lane 5: pHSIE-CaM^{D132E}, Lane 6: pHSIE-CaM^{D134H}, Lane 7: pHSIE-CaM^{Q136P}.

5.3.2 Expression and Purification of Recombinant Mutant Calmodulin Proteins

5.3.2.1 Expression of Mutant Calmodulin Proteins

Chemically competent BL21-CodonPlus were transformed with pHSIE CaM^{MUT} plasmids. The expression of recombinant protein was induced with IPTG using previously established conditions. The predicted expressed proteins will be similar to those in Chapter 4, with only a single amino acid residue difference. Crude lysates of induced and uninduced cultures were resolved on SDS-PAGE, as can be seen in Figure 5-5, which revealed a band of approximately 47 kDa in the induced but not in the control samples that were not induced.

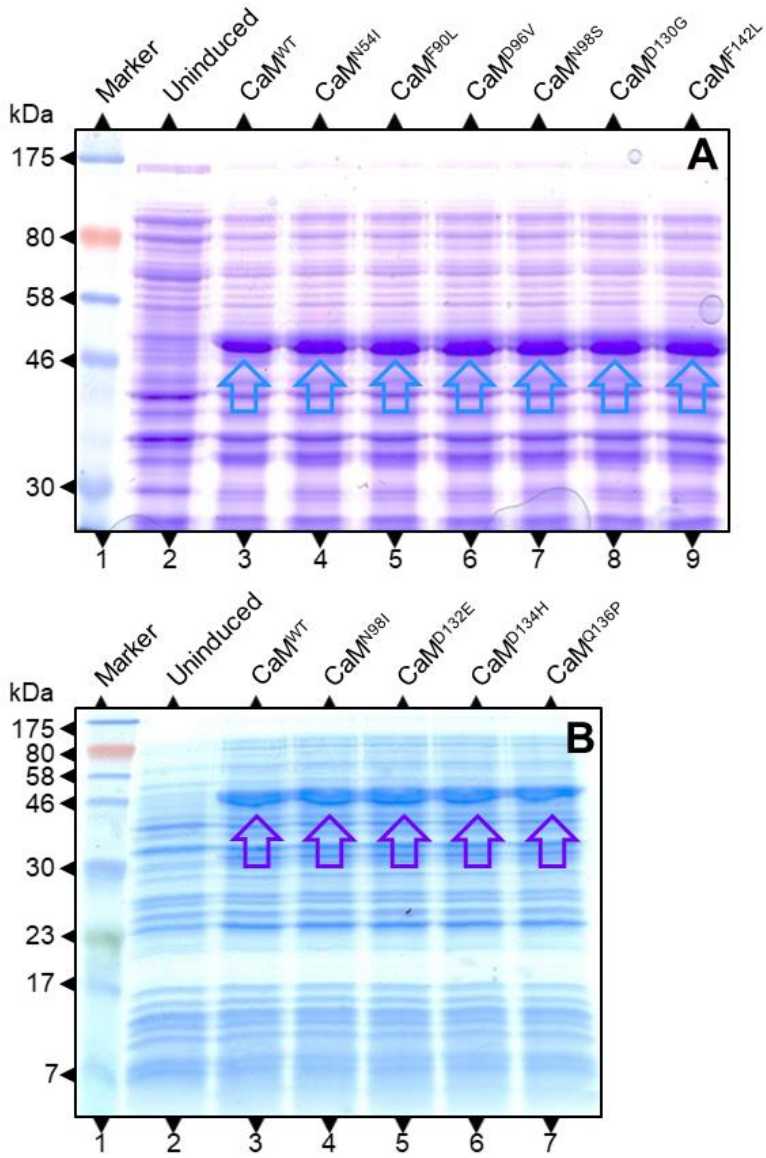

Figure 5-5 Expression of 6xHis SUMO CaM^{WT} and 6xHis SUMO CaM^{MUT} Proteins in *E.coli.*

BL21-CodonPlus were transformed with pHSIE-CaM^{WT}, and pHSIE-CaM^{MUT} plasmids. Protein expression was induced with 0.1 mM IPTG. Crude lysates of uninduced and induced cultures were separated using SDS-PAGE. A ~47 kDa band (arrow) was observed in the induced but not in uninduced samples. (A) Coomassie stained 15 % (w/v) SDS-PAGE gel. Lane 1: Colorplus marker (NEB), Lane 2: uninduced, Lane 3: pHSIE-CaM^{WT}, Lane 4: pHSIE-CaM^{N54I}, Lane 5: pHSIE-CaM^{F90L}, Lane 6: pHSIE-CaM^{D96V}, Lane 7: pHSIE-CaM^{N98S}, Lane 8: pHSIE-CaM^{D130G}, Lane 9: pHSIE-CaM^{F142L}. (B) Coomassie stained 10 % (w/v) SDS-PAGE, Lane 1: Colorplus marker (NEB), Lane 2: uninduced, Lane 3: pHSIE-CaM^{WT}, Lane 4: pHSIE-CaM^{N98I}, Lane 5: pHSIE-CaM^{D132E}, Lane 6: pHSIE-CaM^{D134H}, Lane 7: pHSIE-CaM^{Q136P}.

5.3.2.2 Purification of Mutant Calmodulin Proteins

Re-suspended pellets representing 16 L of expression culture were pooled, lysed and clarified. Recombinant protein was purified using the intein one-step purification method. The purified fractions were separated by SDS-PAGE, Figure 5-6 and Figure 5-7. There were multiple protein bands in the clarified bacterial lysate and flow-through fractions. The major protein band resolved at 47 kDa. Purified fractions were similar to those observed for CaM^{WT} as described in Chapter 4. Following incubation, at room temperature, a 17 kDa protein is present as highlighted in both Figure 5-6 and Figure 5-7. When the imidazole concentration increased to 250 mM, elution of two protein bands (at 47 kDa and 30 kDa) was observed.

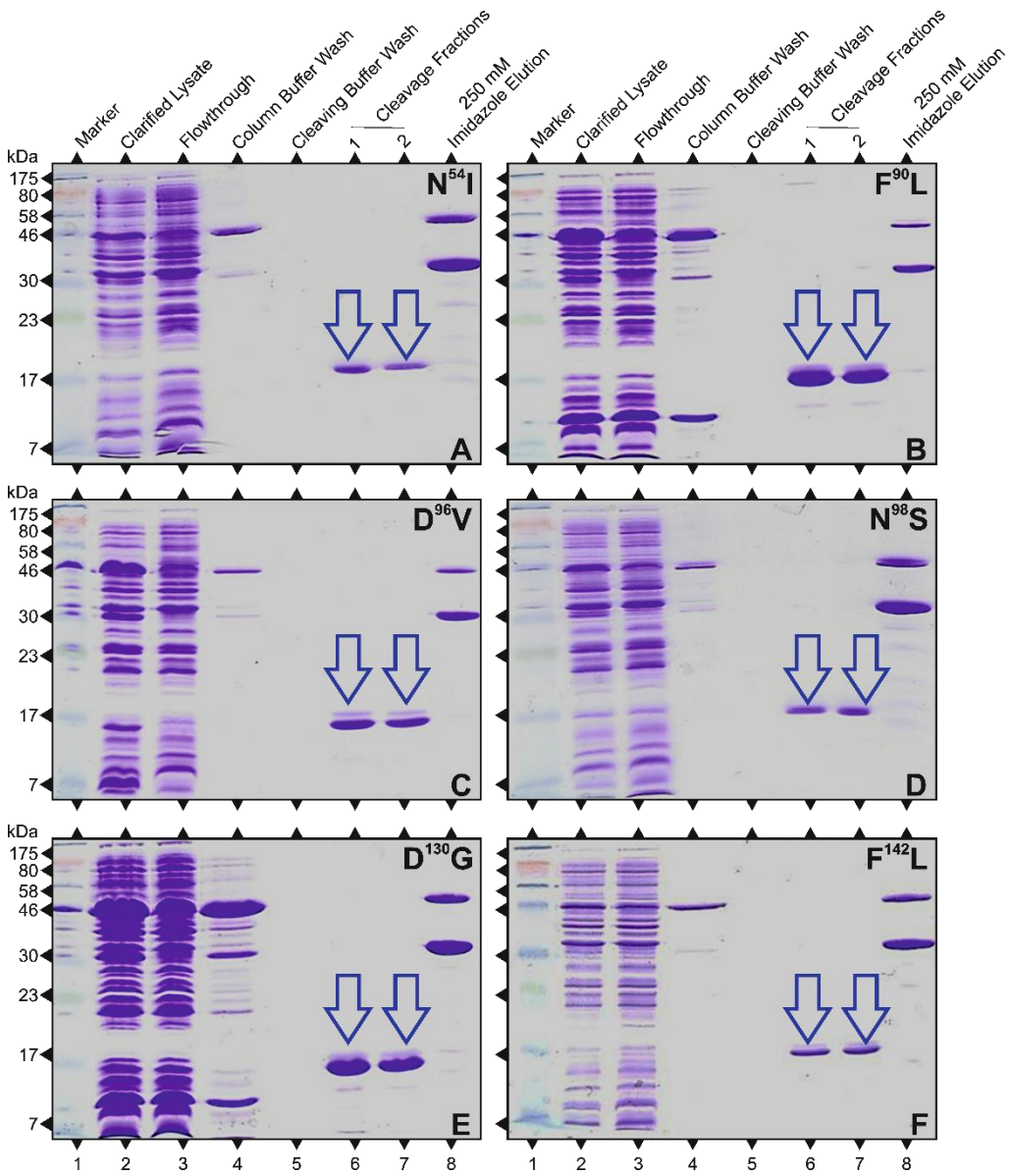

Figure 5-6 Recombinant CaM Proteins Bearing Mutations Associated with IVT, LQT and CPVT Are Liberated from Ni NTA by Changing Column Conditions.

BL21-CodonPlus /pHSIE CaM^{MUT} induced with 0.1 mM IPTG were lysed and applied to Ni-NTA resin column. After washing, column conditions were altered to those optimal for Intein self-cleavage. Lastly, the imidazole concentration was increased. Fractions collected at every step were separated by 15 % (w/v) SDS-PAGE and stained with Coomassie . Cleavage fractions contain only a 17 kDa band, indicated by the arrow. (A) CaM^{N54I}, (B) CaM^{F90L}, (C) CaM^{D96V}, (D) CaM^{N98S}, (E) CaM^{D130G}, (F) CaM^{F142L}. (A-F) Lane 1: Colorplus marker (NEB), Lane 2: 5 µl bacterial lysate supernatant, Lane 3: 5µl flowthrough, Lane 4: 15 µl Wash 1, Lane 5: 15 µl Wash 2, Lane 6: and 7: 10 µl of 3 ml cleavage fractions, and Lane 8: 10 µl of 250mM imidazole elution fraction.

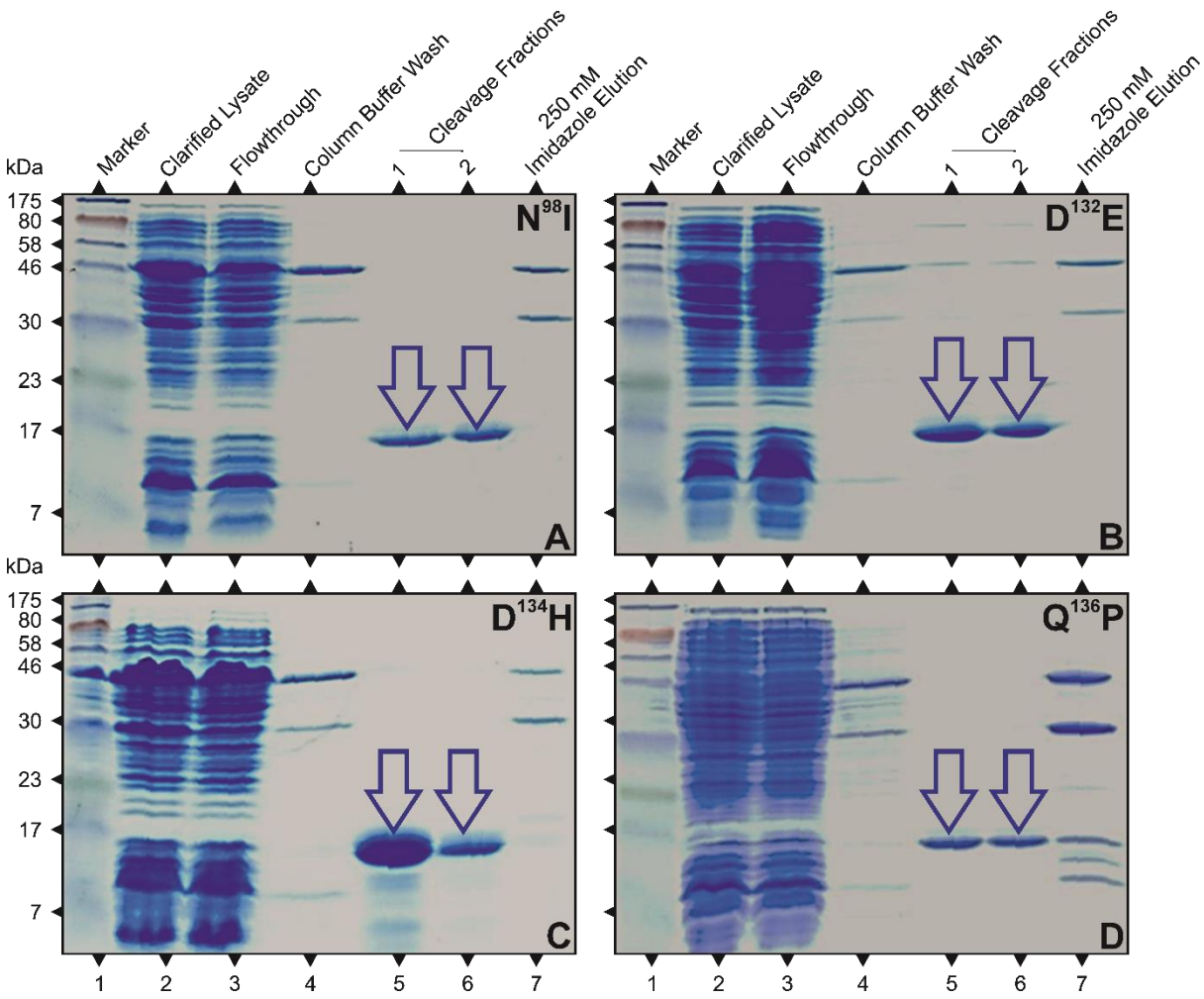

Figure 5-7 Recombinant CaM Proteins Bearing Mutations Associated with LQTS, CPVT and Cardiac Arrhythmias of Mixed Pathology Are Liberated from Ni-NTA by Changing Column Conditions

BL21-CodonPlus/pHSIE CaM^{MUT} induced with 0.1 mM IPTG were lysed and applied to Ni NTA resin column. The column was washed, and conditions were altered to those optimal for Intein self-cleavage. The imidazole concentration was increased. Fractions collected at every step were separated by 15 % (w/v) SDS-PAGE and stained with Coomassie . The cleavage fractions contain only a band of 17 kDa, indicated by the arrow. (A) CaM^{N98I}, (B) CaM^{D132E}, (C) CaM^{D134H}, (D) CaM^{Q136H}. (All panels) Lane 1: Colorplus marker (NEB), Lane 2: 5 µl bacterial lysate supernatant, Lane 3: 5 µl flowthrough, Lane 4: 15 µl Wash 1, Lane 5: 15 µl Wash 2, Lane 6: and 7: 10 µl of 3 ml cleavage fractions, and Lane 8: 10 µl of 250mM imidazole elution fraction.

5.3.2.3 Immunoblotting of Mutant Calmodulin Proteins

The cleavage fractions containing the 17 kDa protein were pooled and separated by SDS-PAGE, Figure 5-8 Panels A and D, the proteins had the same electrophoretic mobility as CaM^{WT} separated alongside. The plot of the lane profile did not reveal additional bands, Figure 5-8 Panels B and E. Immunoblotting with anti-CaM antibody detected only one band at 17 kDa, Figure 5-8, Panels B and D. This data confirms their identity as recombinant CaM proteins and the protein were estimated to be ≥95% pure. The pooled fractions, typically 10 mL, were dialysed against PBS and stored at 4 °C until required.

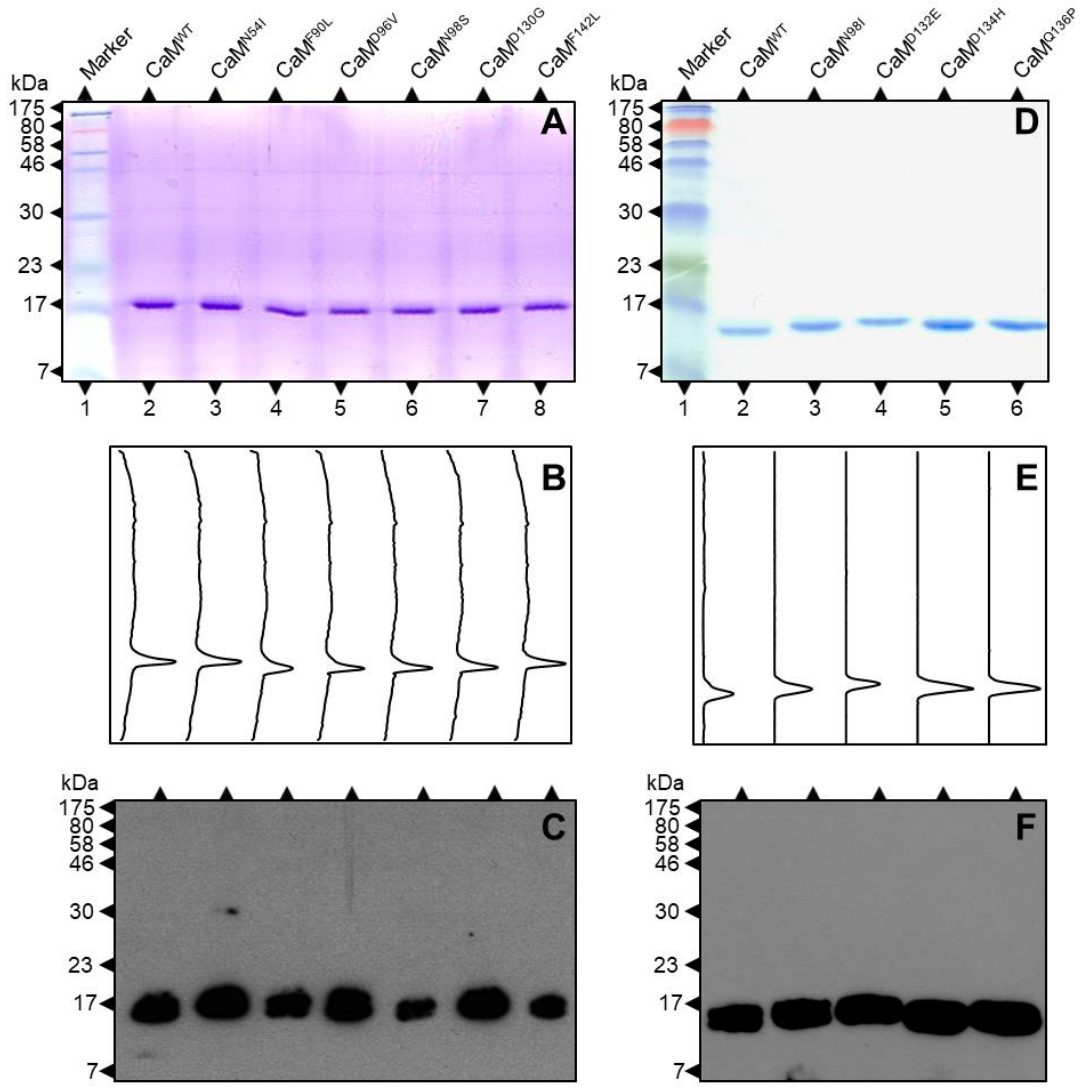

Figure 5-8 Purified Mutant CaM Proteins Resolve as Single Bands of the Correct Size and Recognised By the Specific Monoclonal Antibody

Cleavage fractions from Ni-NTA resin column purification were pooled and separated by 20 % (w/v) SDS-PAGE in duplicate. Both Coomassie staining and immunoblotting revealed only one band of approximately 17 kDa. (A) Coomassie stained gel, Lane 1: Colorplus marker (NEB), Lane 2: CaMWT, Lane 3: CaM^{N54I}, Lane 4: CaMF90L, Lane 5: CaM^{D96V}, Lane 6: CaM^{N98S}, Lane 7: CaM^{D130G}, Lane 8: CaM^{F142L}. (B) Lane profiles of (A). (C) Immunoblot corresponding to (A). (D) Coomassie stained gel, Lane 1: Colorplus marker (NEB), Lane 2: CaM^{WT}, Lane 3: CaM^{N98I}, Lane 4: CaM^{D132E}, Lane 5: CaM^{D134H}, Lane 6: CaM^{Q136P}. (E) Lane profiles of (D). (F) Immunoblot corresponding to (D). Primary antibody: anti-CaM (1:10,000), secondary antibody: anti-mouse HRP (1: 10,000). Exposure: 20 s.

5.3.3 Circular Dichroism Spectroscopy of Recombinant Mutant Calmodulin Proteins

5.3.3.1 Confirmation of the Secondary Structure of Mutant Calmodulin Proteins

The far UV CD spectra of CaM^{MUT} recorded at both low and high temperatures in the presence and absence of Ca^{2+}. The recorded spectra are shown in Figure 5-9 and Figure 5-10, As can be seen, at 4 °C in the absence (A) and presence (B) of Ca^{2+} the spectra are similar, all have positive maxima at 192 nm and two negative maxima at 208 and 221 nm. At 90 °C in the absence of Ca^{2+}, the negative maxima are absent. However, in the presence of Ca^{2+} at 99 °C the negative is reduced but still present, and there is a notable variance in the spectra both between mutants and wildtype and between mutants.

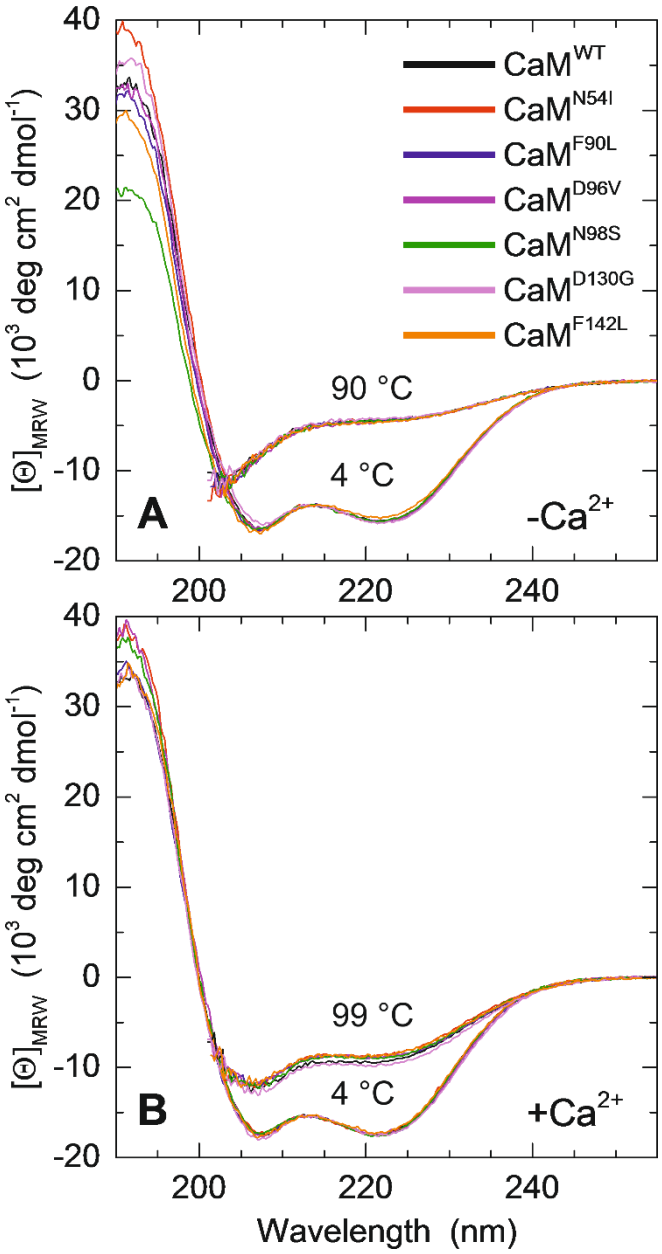

Figure 5-9 Secondary Structure of CaM^{MUT} Proteins Corresponds to CaM^{WT}.

The far UV CD spectra of CaM^{WT} and CaM^{MUT} proteins were recorded in the absence (1 mM EDTA), and presence (1 mM $CaCl_2$) of Ca^{2+} at low and high temperatures. The proteins were dissolved in pH 6.5, 10 mM MES, 50 mM KCl with either 1 mM EDTA or 1 mM $CaCl_2$. CD was measured at 4 °C and 90 °C without Ca^{2+} and at 4 °C and 99 °C with Ca^{2+}. (A) CD Spectra for CaM^{WT}, CaM^{N54I}, CaM^{F90L}, CaM^{D96V}, CaM^{N98S}, CaM^{D130G} and CaM^{F142L}, without Ca^{2+} at 4 °C and 90 °C. (B) CD Spectra for CaM^{WT}, CaM^{N54I}, CaM^{F90L}, CaM^{D96V}, CaM^{N98S}, CaM^{D130G} and CaM^{F142L}, with Ca^{2+} at 4 °C and 99 °C.

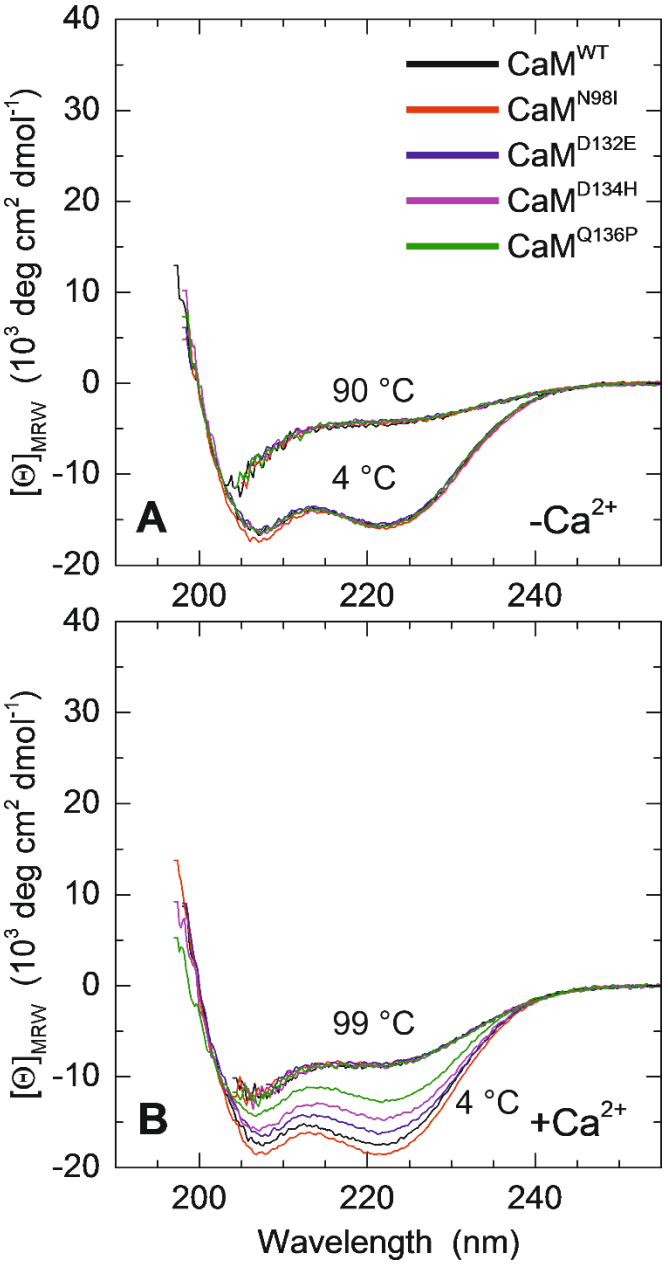

Figure 5-10 Secondary Structure of CaM^{MUT} Proteins Corresponds to CaM^{WT}

The far UV CD spectra of CaM^{WT} and CaM^{MUT} proteins were recorded in the absence (1 mM EDTA), and presence (1 mM $CaCl_2$) of Ca^{2+} at low and high temperatures. The proteins were dissolved in pH 6.5, 10 mM MES, 50 mM KCl with either 1 mM EDTA or 1 mM $CaCl_2$. CD was measured at 4 °C and 90 °C without Ca^{2+} and at 4 °C and 99 °C with Ca^{2+}. (A) CD Spectra for CaM^{WT}, CaM^{N98I}, CaM^{D132E}, CaM^{D134H}, CaM^{D130G} and CaM^{Q136P} without Ca^{2+} at 4 °C and 90 °C. (B) CD Spectra for CaM^{WT}, CaM^{N98I}, CaM^{D132E}, CaM^{D134H}, CaM^{D130G} and CaM^{Q136P}, with Ca^{2+} at 4 °C and 90 °C.

5.3.3.2 Thermal Denaturation of Mutant Calmodulin Proteins

Thermal unfolding of CaM^{MUT} proteins was measured by recording changes in CD at 221 nm with increasing temperature in the presence and absence of Ca^{2+}, as can be seen in Figure 5-11 and Figure 5-12. Like the observation of CaM^{WT} in Chapter 4, CaM^{MUT} proteins did not confirm definitively to a 2- or 3-state unfolding model. Thermodynamic parameters calculated from fitted curves are shown in Table 5-2. as shown in Panels A of Figure 5-11 and Figure 5-12 in the absence of Ca^{2+} with temperature increasing from 4 °C, the change in [θ] for all mutants was similar, comparable to CaM^{WT} and complete at 90 °C. As can be seen in Table 5-2 all the mutant proteins had similar values for T_M and ΔHvH compared with CaM^{WT} assuming either a 2- or 3- state unfolding.

In the presence of Ca^{2+} at 4 °C as shown in Panels B of Figure 5-11 and Figure 5-12 [θ] is greater than in the absence of Ca^{2+}, corresponding to a change in conformation by CaM^{MUT} in the presence of Ca^{2+} as observed in Chapter 4 for CaM^{WT}. Similarly, as temperature increases, [θ] decreases as the proteins unfold although not at the same rate and do not fully unfold as in the absence of Ca^{2+}. However, while the plotted data for most CaM^{MUT} proteins resembles that observed for CaM^{WT}, those of CaM^{D96V}, CaM^{D130G} and CaM^{F142L} do not. A two-state unfolding model could be assumed for all CaM^{MUT} proteins, except CaM^{D130G} which better fits a three-state unfolding model. The thermal profile of CaM^{D96V} and CaM^{F142L} differed from that observed for CaM^{WT}.

The differences in the thermal profiles are reflected in the thermodynamic parameters shown in Table 5-2. Most CaM^{MUT} proteins had similar values to CaM^{WT} for T_M and ΔHvH; except for CaM^{D96V} and CaM^{F142L} the values for which are reduced. A 3-state model had to be assumed to fit the curve for CaM^{D130G}. Compared to CaM^{WT}, the T_M and ΔHvH for the initial stage of CaM^{D130G} are much lower, and the values for the intermediate stage are much higher.

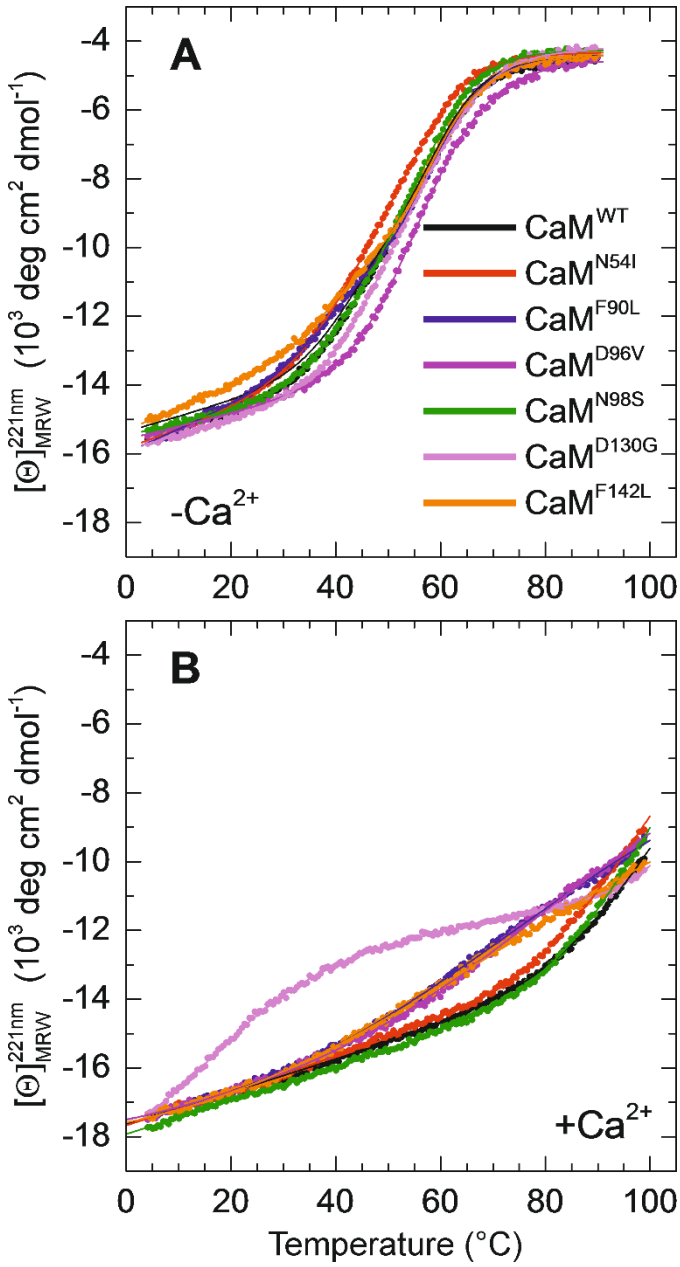

Figure 5-11 Thermostability of CaM in the Presence of Ca^{2+} is Altered in Some but Not All Mutations.

CD of CaM^{WT}, CaM^{N54I}, CaM^{F90L}, CaM^{D96V}, CaM^{N98S}, CaM^{D130G} and CaM^{F142L} proteins at 221 nm was recorded at increasing temperature (0.5 °C increments) in the absence (1 mM EDTA) and presence (1 mM $CaCl_2$) of Ca^{2+} as described in Chapter 4. (A) Thermal melting curve of CaM^{WT} and CaM^{MUT} proteins in the absence of Ca^{2+}. (B) The thermal melting curve of CaM^{WT} and CaM^{MUT} proteins in the presence of Ca^{2}.

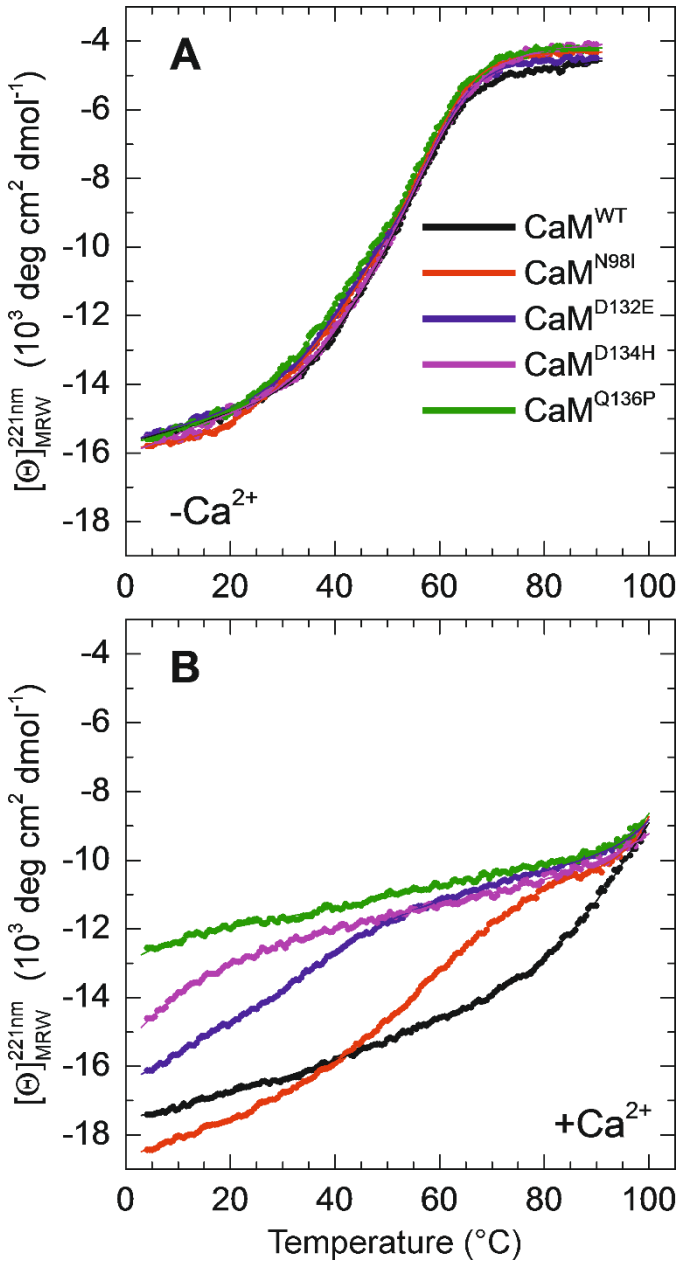

Figure 5-12 Thermostability of CaM in the Presence of Ca^{2+} Is Altered in Some but Not All Mutations

CD of CaM^{WT}, CaM^{N98I}, CaM^{D132E}, CaM^{D134H}, CaM^{D130G} and CaM^{Q136P} at 221 nm was recorded at increasing temperature (0.5 °C increments) in the absence (1 mM EDTA) and presence (1 mM $CaCl_2$) of Ca^{2+} as described in Chapter 4. (A) Thermal melting curve of CaM^{WT} and CaM^{MUT} in the absence of Ca^{2+}. (B) The thermal melting curve of CaM^{WT} and CaM^{MUT} proteins in the presence of Ca^{2+}.

Table 5-2 Thermodynamic Parameters in the Absence and Presence of Ca^{2+}

	$-Ca^{2+}$		$+Ca^{2+}$	
Protein	T_M (°C)	ΔHvH (kJ/mol)	T_M (°C)	ΔHvH (kJ/mol)
CaM^{WT}	53.8±0.2 °C	112 kJ/mol		
CaM^{WT}	45.6 ± 1.1	133 ± 10	105.5 ± 0.2	105 ± 2
	60.2 ± 0.7	212 ± 15		
CaM^{N54I}	47.0±1.7	110±9	101.3±0.1	105±2
	60.5±1.8	197±19		
CaM^{F90L}	58.0±0.2	126±2.9	87.3±1.5 °C	33±0.4
CaM^{D96V}	55.0±1.1	153±7	94.0±1.1	41±1
	73 ± 6	175 ± 24		
CaM^{N98I}	47.6±3.3	-100±3	70.8±3.6	-67±4
	59±12	-196±9	104.8±1.4	-198±23
CaM^{N98S}	46.9±1.8	119±11	102.0±0.1	113±1
	60.2 ± 1.3	180 ± 7		
CaM^{D130G}	48.7±2.4	136±11	12±7	63±4
	62.4 ± 2.6	162 ± 25	115±2	160±24

	$-Ca^{2+}$		$+Ca^{2+}$	
Protein	T_M (°C)	ΔHvH (kJ/mol)	T_M (°C)	ΔHvH (kJ/mol)
CaM^{D132E}	42.0±3.4	-129±9	44.8±1.0	-113±9
	59.4±1.3	-193±8	108.5±1.4	-182±33
CaM^{D134H}	46.4±0.6	-136±15	-11.2±0.9	-51±4
	60.3±0.3	-155±7	118.4±2.5	-123±17
CaM^{Q136P}	45.7±4.3	-112±10	-4.4±4.0	-80±26
	56.5±1.2	-191±6	106.1±1.2	-168±30
CaM^{F142L}	41.5±1.4	150±21	85±4	27±1
	58.4 ± 0.5	176 ± 11		

The parameters derived from both a two and three stage unfolding model are given for CaM^{WT} in the absence of Ca^{2+}. A 3-stage unfolding model was assumed for mutant proteins except for CaM^{F90L} in the absence of Ca^{2+}. While in the presence of Ca^{2+} a 2-stage model was assumed for mutant proteins except for CaM^{D130G}. Error quoted is SD derived from the multivariable curve fitting.

5.3.4 Dynamic Light Scattering

All purified recombinant CaM proteins were analysed using dynamic light scattering; representative peaks are shown in Figure 5-13 alongside that of CaM^{WT}. For each sample, a single monodisperse peak was observed. Each peak contained a single species with a molecular weight of 15-29 kDa, comprising approximately 100 % of the mass observed. As discussed in Chapter 4 the range of estimated molecular weights observed are to be expected. The mean and modal molecular weights, the percentage of the mass and the polydispersity of each recombinant protein are shown in Table 5-3.

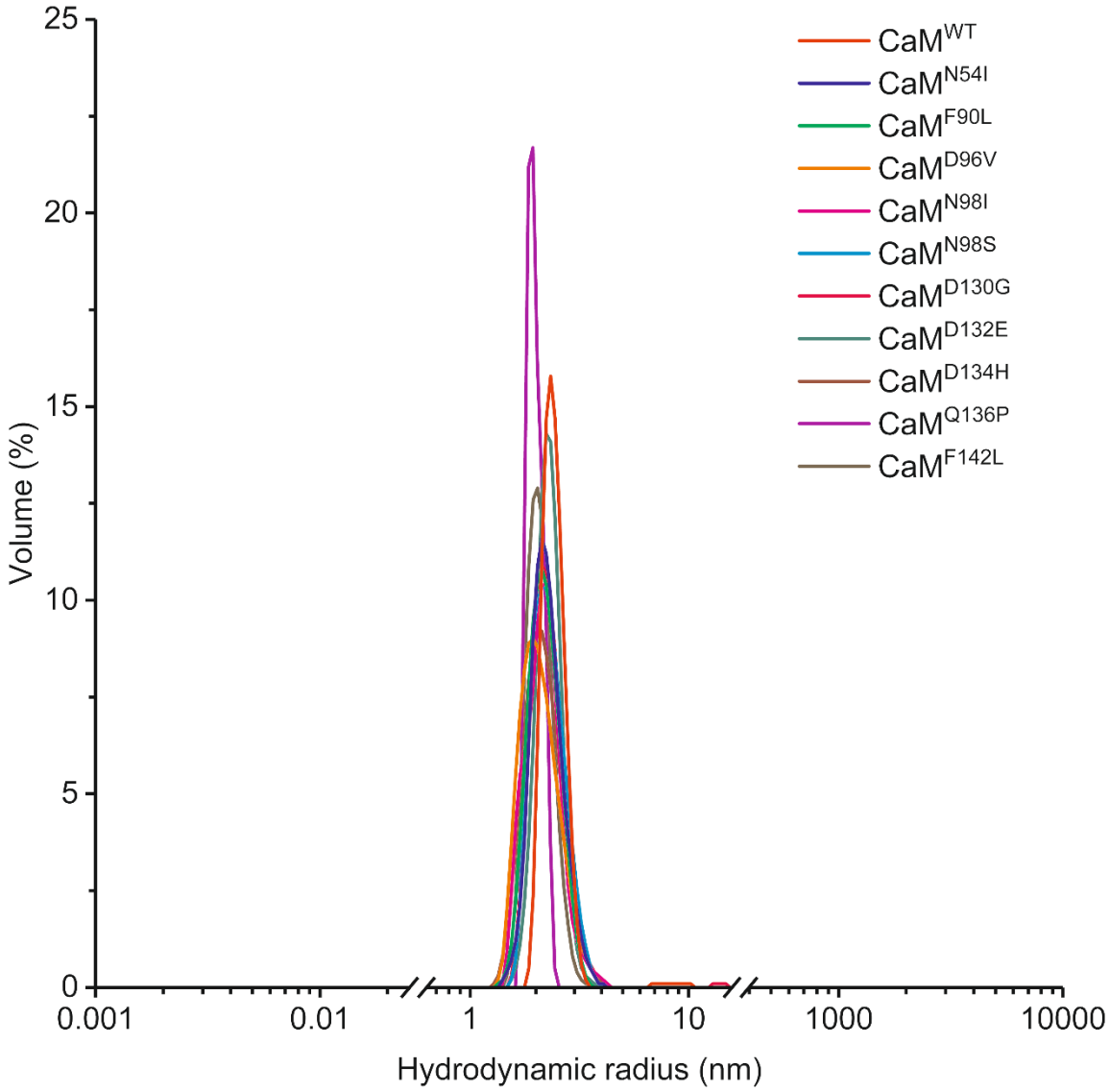

Figure 5-13 Purified CaM^{WT} and CaM^{MUT} Proteins Consist of a Single Monodisperse Species

Size Distribution of recombinant CaM proteins by DLS. The hydrodynamic size of molecules in samples of concentrated, purified CaM^{WT} and CaM^{MUT} were measured by DLS in triplicate. Histogram for mean (n=3) size distribution by volume of CaM^{WT} and CaM^{MUT} in 10 mM HEPES 50 mM KCl and 5 mM Ca^{2+} at 20 °C are shown.

Table 5-3 Summary of Dynamic Light Scattering Analysis

Protein	Estimated M_W (kDa)		% of mass	%PD
	mode±SD	mean±SD		
CaM^{WT}	19.7±2.4	20.2±2.4	100	11.8
CaM^{N54I}	24.4±5.3	28.1±5.3	100	19.0
CaM^{F90L}	24.4±4.1	25.4±4.1	100	16.1
CaM^{D96V}	24.4±5	26.6±5.9	100	22.2
CaM^{N98I}	24.4±3.1	27.6±3.1	99.6	22.8
CaM^{N98S}	27.2±5.2	29.4±5.2	100	17.7
CaM^{D130G}	24.4±11.7	28.8±11.7	99.2	20.1
CaM^{D132E}	24.4±9.8	26.6±9.8	99.8	14.1
CaM^{D134H}	24.4±6.1	27.9±6.1	100	21.8
CaM^{Q136P}	15.9±0.7	15.3±0.7	99.9	4.3
CaM^{F142L}	19.7±3.4	21.9±3.4	99.9	15.5

5.3.5 Functional Studies of Recombinant Mutant Calmodulin Proteins

A significant period separated the publication of the mutants. Therefore, the ryanodine binding assays and CoIP were performed in two batches each using a different set of cardiac SR microsome preparations. The first batch comprised “CPVT mutations” (CaM^{N54I}, CaM^{N98S}), “LQTS mutations” (CaM^{D96V}, CaM^{D130G}, CaM^{D142L}) and “IVT mutation” (CaM^{F90L}). The second batch comprised *CALM2* mutations associated with either LQTS (CaM^{N98I} CaM^{D134H}) or a mixed pathology (CaM^{D132E} & CaM^{Q136P}).

5.3.5.1 Co-Immunoprecipitation of Mutant Calmodulin Proteins.

The ability of CaMMUT proteins to bind with RyR2 was assessed by CoIP at three different free Ca2+ concentrations as discussed in Chapter 4. The resulting Co-IP immunoblots and densitometric analysis are shown in Figure 5-14 and Figure 5-15. The relative densities of the immunoreactive bands corresponding to CaM^{MUT} expressed as a percentage of the density of the band corresponding to CaM^{WT} indicate the relative amounts of CaM protein co-immunoprecipitated. A greater or lesser amount of CaM co-immunoprecipitation indicates the mutation alters the ability of CaM to associate and bind with the immobilised RyR2.

In the presence and absence of Ca^{2+}, the relative amount of CaM^{D130G}, CaM^{N98I}, CaM^{D132E}, CaM^{D134H} and CaM^{Q136P} co-immunoprecipitated was reduced, Figure 5-14 and Figure 5-15. In the absence of Ca^{2+}, the reduction in the amount of by CaM^{F90L}, CaM^{D130G}, CaM^{N98I} and CaM^{D134H} co-immunoprecipitated was statistically significant but the amounts of CaM^{N98I}, CaM^{D132E} and CaM^{Q136P} were not. However, in the presence of increasing Ca^{2+}, the reductions in CaM^{F90L}, CaM^{D130G}, CaM^{N98I}, CaM^{D132E},

CaM^{D134H} and CaM^{Q136P} co-immunoprecipitation by RyR2 all became statistically significant.

In both the absence and with increasing presence of Ca2+, more CaM^{N54I} and CaM^{D96V} were co-immunoprecipitated by RyR2 than CaM^{WT} at a statistically significant level, Figure 5-14. Furthermore, the relative amount of CaM^{N98S} and CaM^{F142L} that co-purified varied in both the presence and absence of Ca^{2+}, but no statistically significant difference with CaM^{WT} was observed, as can be seen in Figure 5-14, Generally the affects of the mutations on Co-IP are Ca^{2+} independent in the case of CaM^{N54I}, CaM^{D96V}, CaM^{N98S} CaM^{D130G}, CaM^{D134H} and CaM^{F142L}, and Ca^{2+} dependent in the case of CaM^{N98I}, CaM^{D132E}, and CaM^{Q136P}.

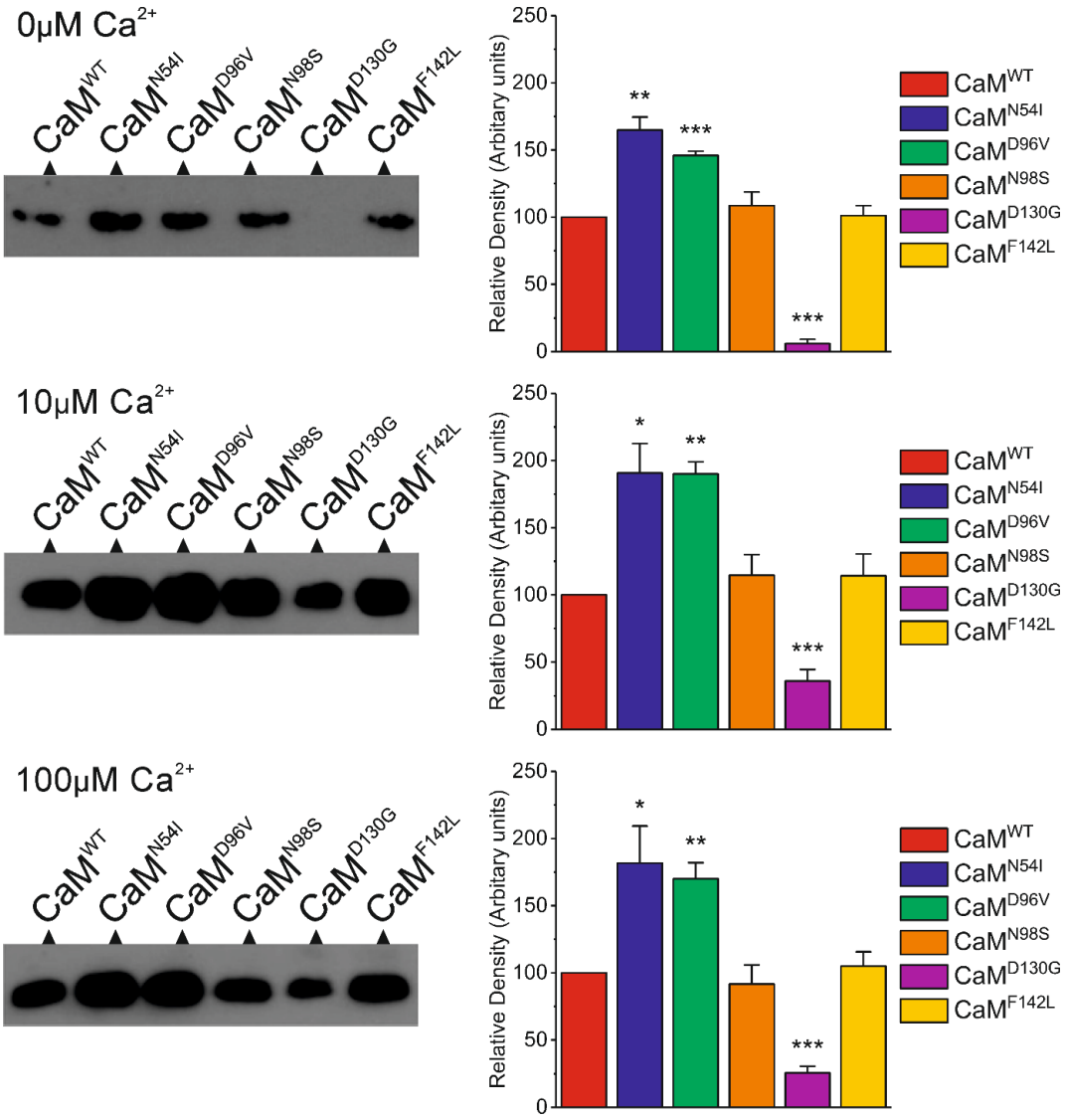

Figure 5-14 Ca^{2+}-Dependent Association of CaM and RyR2 Is Altered by the Presence of Mutations Linked to Both LQTS and CPVT Cardiac Arrhythmias

CoIP assays are measuring the association of CaM^{WT} and CaM^{MUT} proteins with cardiac RyR2 on three occasions at 0, 10 and 100 μM free Ca^{2+}, each with a different SR prep. Following densitometry analysis (Quantity One® 1-D analysis software, BioRad) for each occasion, the densities of the CaM^{MUT} bands were normalised to CaM^{WT}. Representative immunoblots from the same occasion are shown on the left and mean relative density (n=3 ±SEM) on the right. Differences in mean relative density between CaM^{WT} and CaM^{MUT} proteins were compared using unpaired Student's t-test (GraphPad, Prism 5). Statistically significant differences are shown, * P<0.05, ** P<0.005 and *** P<0.001.

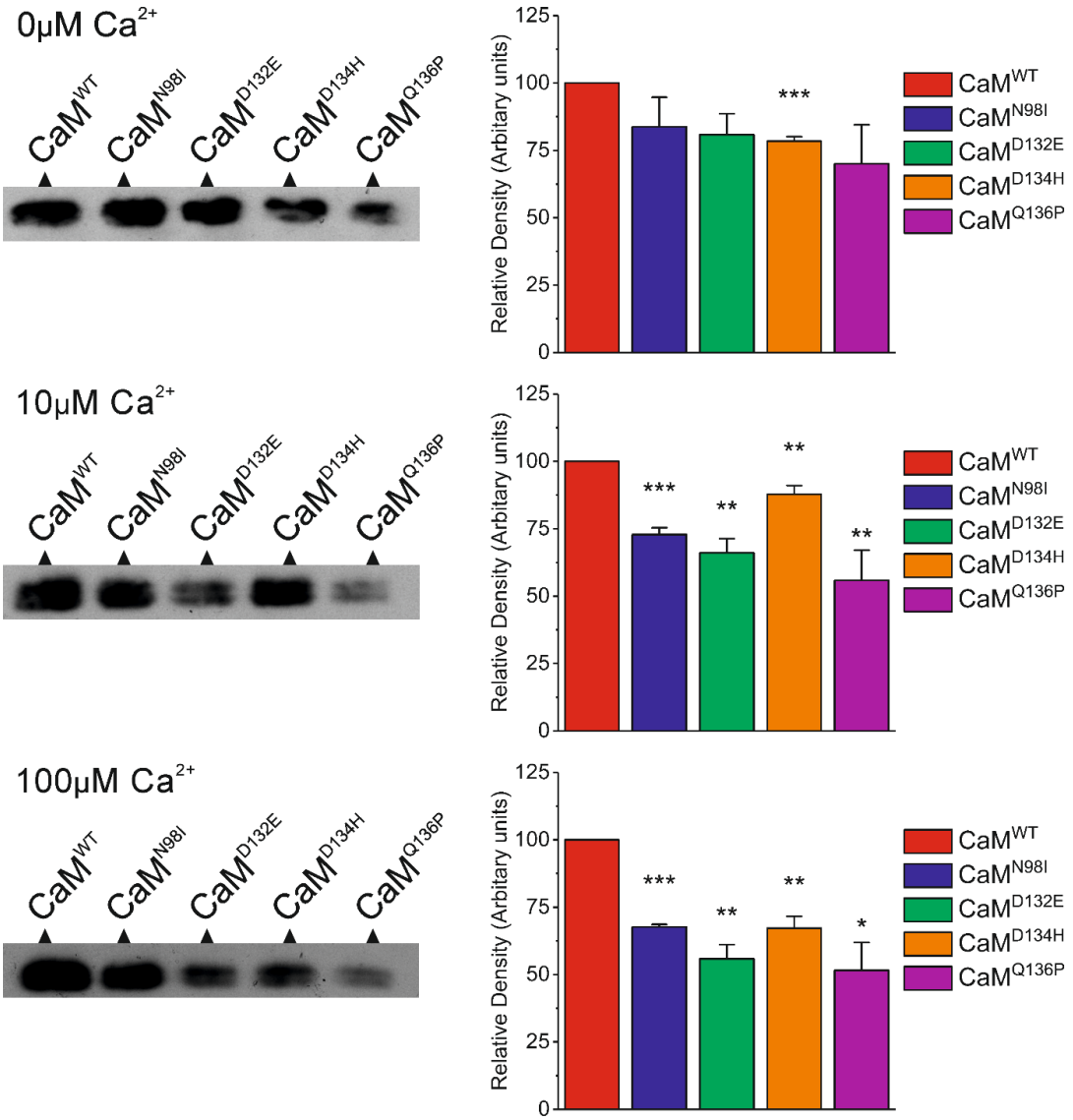

Figure 5-15 Ca2+ Dependent Association of CaM and RyR2 is Disrupted by the Presence of Mutations Linked to LQTS, CPVT and Mixed Pathology Arrhythmias

CoIP assays are measuring the association of CaMWT and CaMMUT proteins with cardiac RyR2 on three occasions at 0, 10 and 100 μM free Ca2+, each with a different SR prep. Following densitometry analysis (Quantity One® 1-D analysis software, BioRad) for each occasion, the densities of the CaMMUT bands were normalised to CaMWT. Representative immunoblots from the same occasion are shown on the left and mean relative density (n=3 ±SEM) on the right. Differences in mean relative density between CaMWT and CaMMUT proteins were compared using unpaired Student's t-test (GraphPad, Prism 5). Statistically significant differences are shown, * P<0.05, ** P<0.005 and *** P<0.001.

5.3.5.2 Binding of Ryanodine to the Ryanodine Receptor in the Presence of Mutant Calmodulin Proteins

Similarly to Chapter 4, measuring [^{3}H]ryanodine binding to cardiac SR microsomes in the presence and absence of CaM recombinant proteins at increasing Ca^{2+} concentrations were used to assess the ability of CaM^{MUT} proteins to modulate the activity of the RyR2 channel. The binding of [^{3}H]ryanodine is dependent on the functional state of the RyR2 channel, i.e., if it is open or closed. CaM inhibits the open conformation of RyR2, and so reduces the level of [^{3}H]ryanodine binding. Comparison of ryanodine binding in the presence of CaM^{MUT} and CaM^{WT} proteins reveal the effects of mutations on the ability of CaM to modulate RyR2 channel activity.

The binding of [^{3}H]ryanodine to solubilised cardiac RyR2 in the presence of CaM^{WT} and CaM^{MUT} and a set of controls without CaM present, was measured at a range of free Ca^{2+} concentrations. In the controls, the maximal binding of [^{3}H]ryanodine occurred at free [Ca^{2+}] of 1 mM. Binding of [^{3}H]ryanodine, expressed as a percentage of maximal control binding was plotted against free [Ca^{2+}] as shown in Figure 5-16, Figure 5-17, and Figure 5-18. As can be seen in both the presence and absence of CaM, minimal [^{3}H]ryanodine binding occurs at 0.01 μM as the channel is in a closed conformation and binding increases with free [Ca^{2+}] as the channel adopts an open conformation. In the presence of CaM^{WT} with increasing Ca^{2+}, [^{3}H]ryanodine binding is reduced compared to control as previously shown in Chapter 4. However, the presence of CaM^{MUT} altered the level of [^{3}H]ryanodine binding compared to CaM and control depending on the mutation present. The observed changes were not consistent between mutations associated with the same channelopathies.

The binding of [^{3}H]ryanodine in the presence of mutations associated with CPVT is shown in Figure 5-16. Compared to control, the presence of CaM^{N54I} results in a statistically significant increase in [^{3}H]ryanodine binding of ~9 15% with increasing Ca^{2+}. However, in the presence of CaM^{N98S}, [^{3}H]ryanodine binding is indistinguishable from CaM^{WT}.

Similarly, as can be seen in Figure 5-17, and Figure 5-18, the presence of CaM proteins bearing mutations associated with LQTS and a mixed phenotype including LQTS, had diverging effects on the binding of [^{3}H]ryanodine. While the level of [^{3}H]ryanodine binding in the presence of CaM^{F142L} was indistinguishable from that of CaM^{WT} with a statistically significant difference to control. The presence of CaM^{D96V} resulted in a statistically significant increase in [^{3}H]ryanodine binding compared to the control from 9 % to 13% with increasing Ca^{2+}. Conversely, at 1 mM Ca^{2+}, in the presence of the CaM^{D130G}, [^{3}H]ryanodine binding was 3 % lower than that of control and was significantly different from both control and CaM^{WT}. In the presence of the remaining mutations, CaM^{N98I} CaM^{D132E} CaM^{D134H} CaM^{Q136P} and CaM^{F142L}, the level of [^{3}H]ryanodine binding was indistinguishable from that of the control and was significantly different from CaM^{WT}.

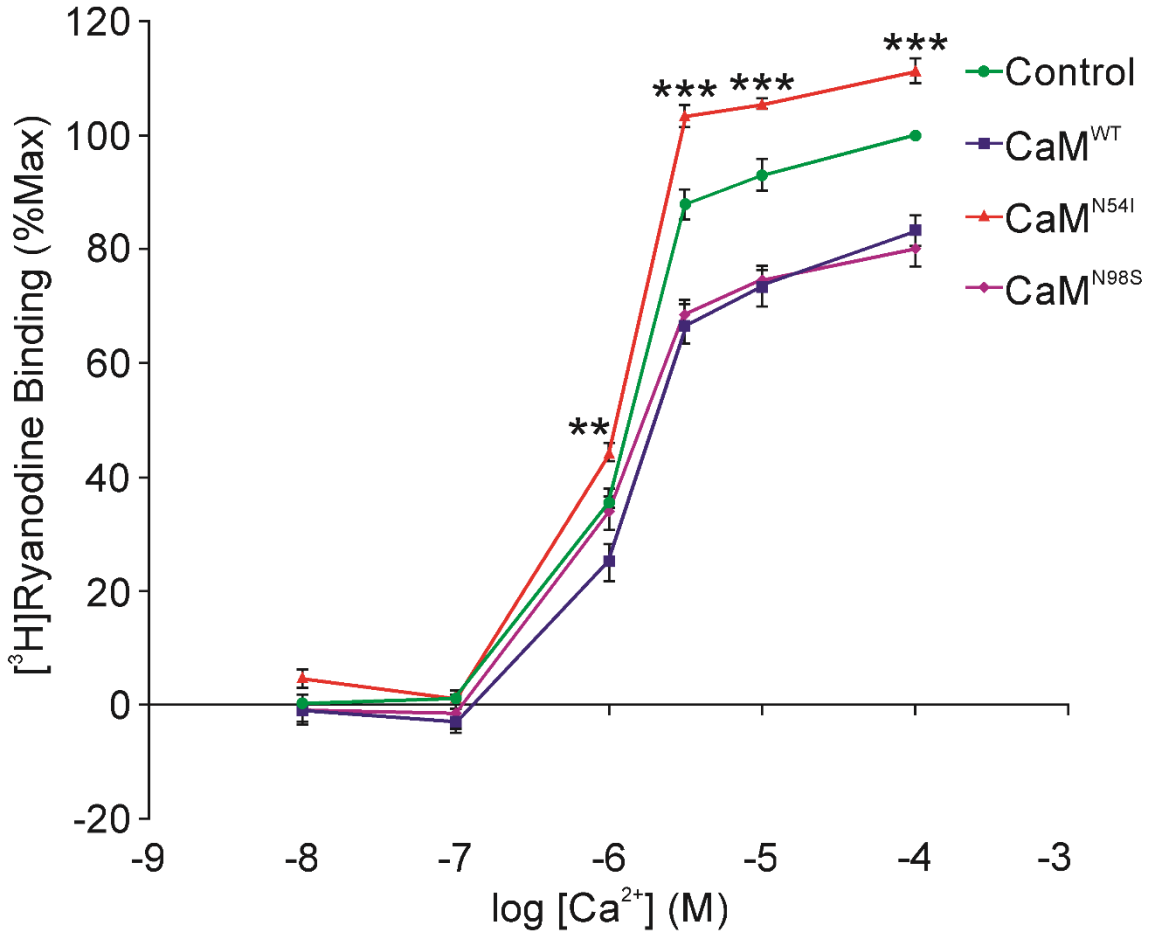

Figure 5-16 CaM Mutations Associated with CPVT Do Not Have a Consistent Effect on the Ability of CaM to Inhibit RyR2 Open Conformation

CHAPS solubilised cardiac SR extract was incubated with [^{3}H]-radiolabelled ryanodine in the presence of CaM^{WT}, CaM^{N54I}, CaM^{N98S} and in the absence of recombinant protein. Following incubation, SR vesicles were recovered by filtration. The radioactivity (cpm) present on filters was measured by scintillation and corrected for background. Assays were done in triplicate at a range of free Ca^{2+} concentrations ([Ca^{2+}]). Binding was expressed as a percentage of maximal activity at 100 μM Ca^{2+}. The experiment was repeated on three occasions with a different cardiac SR vesicle preparation used for each. Mean binding (n=3±SEM) plotted against log [Ca^{2+}]. The difference in binding between the absence and presence of CaM recombinant protein was calculated for each [Ca^{2+}] and compared using an unpaired Student's t-test (GraphPad, Prism 5). Statistically significant differences are shown, ** $P<0.005$, *** $P<0.001$.

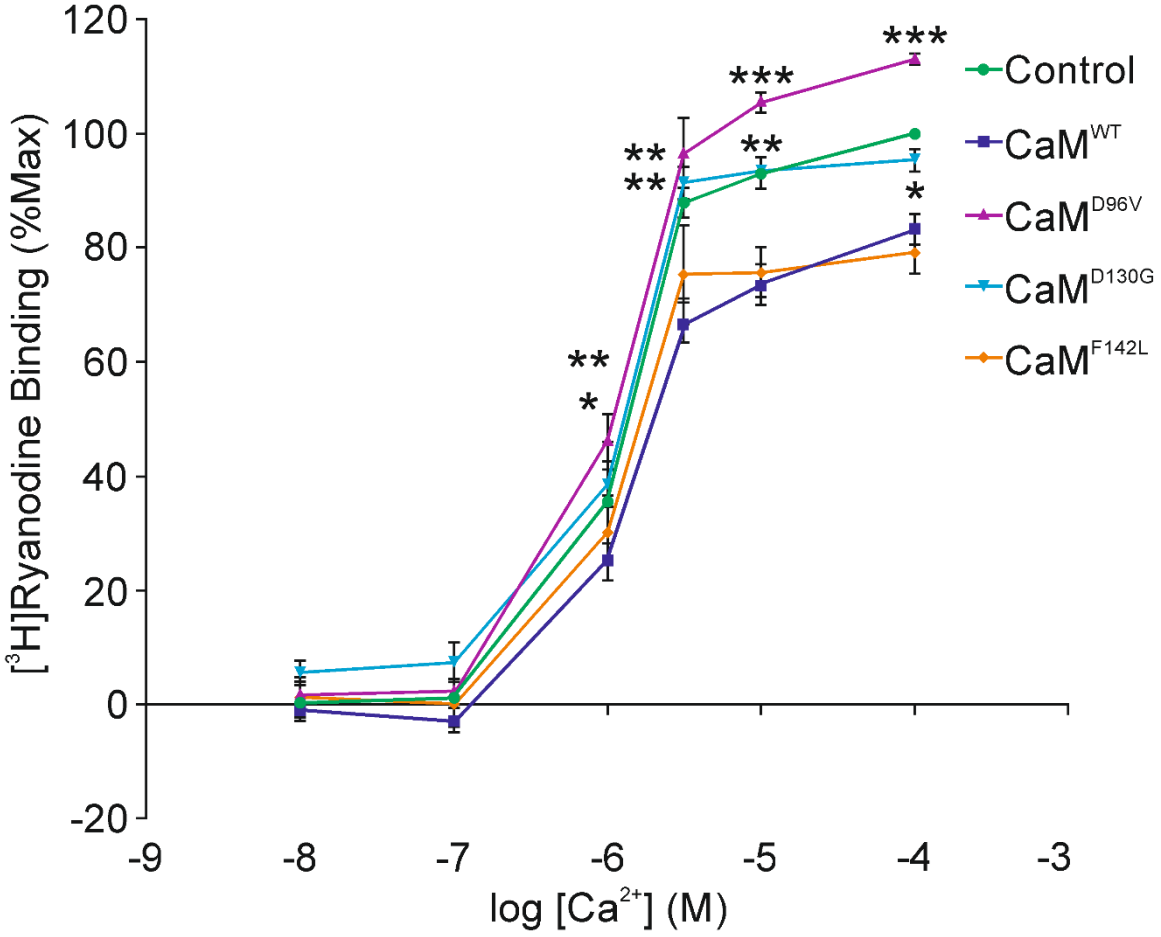

Figure 5-17 CaM Mutations Associated with LQTS Do Not Have a Consistent Effect on the Ability of CaM to Inhibit RyR2 Open Conformation

CHAPS solubilised cardiac SR extract was incubated with [^{3}H]-radiolabelled ryanodine in the presence of CaM^{WT}, CaM^{D96V}, CaM^{D130G}, CaM^{F142L} and in the absence of recombinant CaM protein. Following incubation, SR vesicles were recovered by filtration. The radioactivity (cpm) present on filters was measured by scintillation and corrected for background. Assays were done in triplicate at a range of free Ca^{2+} concentrations ([Ca^{2+}]). Binding was expressed as a percentage of maximal activity at 100 µM Ca^{2+}. The experiment was repeated on three occasions with a different cardiac SR vesicle preparation used for each. Mean binding (n=3±SEM.) was plotted against log [Ca^{2+}]. The difference in binding between the absence and presence of CaM recombinant protein was calculated for each [Ca^{2+}] concentration and compared using an unpaired Student's t-test (GraphPad, Prism 5). Statistically significant differences are shown, * $P<0.05$, ** $P<0.005$.

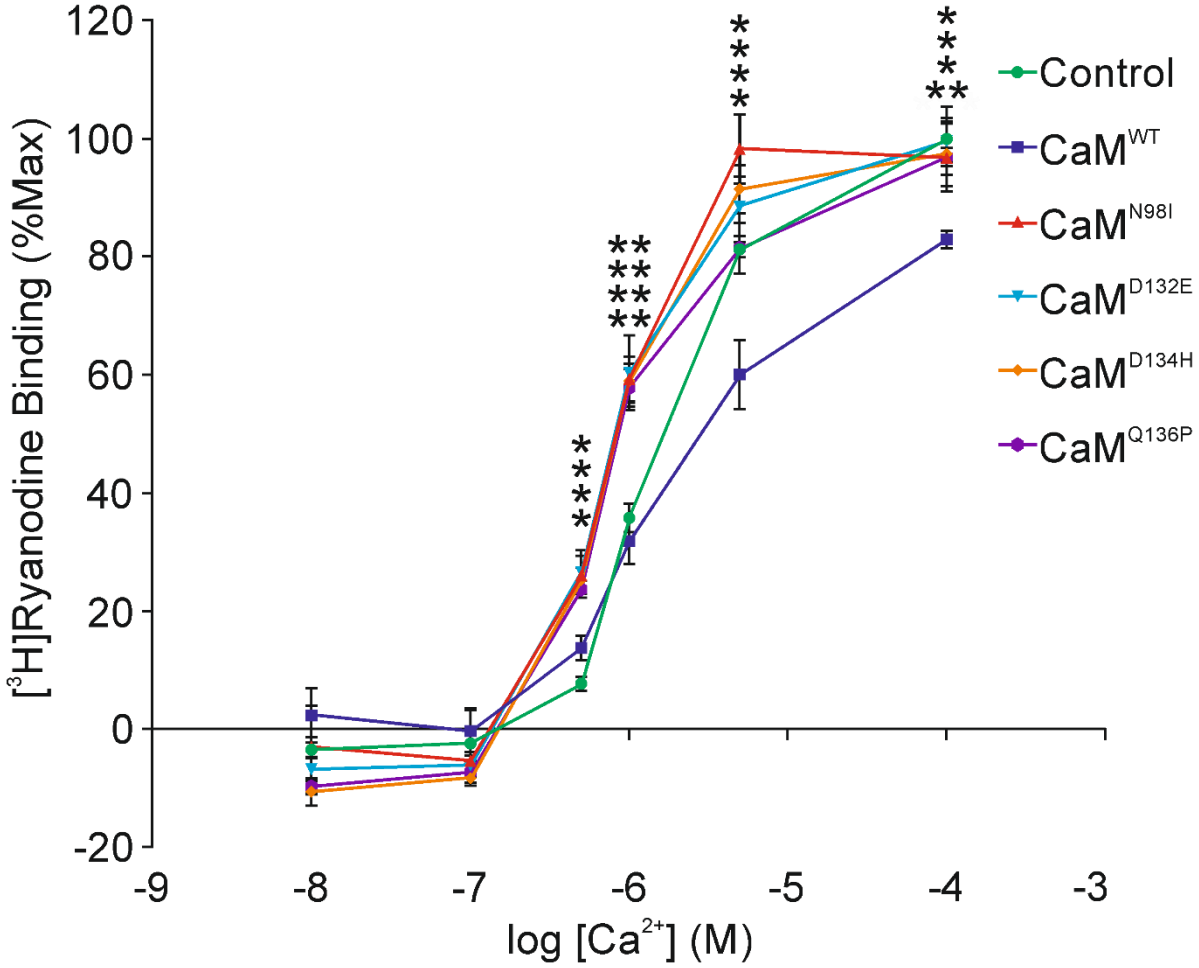

Figure 5-18 CaM Mutations Associated with LQTS, CPVT and Mixed Arrhythmias Impair the Ability of CaM to Inhibit RyR2 Open Conformation

CHAPS solubilised cardiac SR extract was incubated with [^{3}H]-radiolabelled ryanodine in the presence and absence of CaM^{WT} CaM^{N98I}, CaM^{D132E}, CaM^{D134H}, CaM^{Q136P} mutation associated with familial IVT. Following incubation, SR vesicles were recovered by filtration. The radioactivity (cpm) present on filters was measured by scintillation and corrected for background. Assays were done in triplicate at a range of free Ca^{2+} concentrations ([Ca^{2+}]). Binding was expressed as a percentage of maximal activity at 100 µM Ca^{2+}. The experiment was repeated on three occasions with a different cardiac SR vesicle preparation used for each. Mean binding (n=3±SEM.) was plotted against log [Ca^{2+}]. The difference in binding between the absence and presence of CaM recombinant protein was calculated for each [Ca^{2+}] concentration and compared using an unpaired Student's t-test (GraphPad, Prism 5). Statistically significant differences between control and CaM are shown, * P<0.05,** P<0.005.

5.3.5.3 Calcium Binding Affinity of Mutant Calmodulin Proteins

Measuring the intrinsic fluorescence of CaM^{WT} and CaM^{MUT} proteins in the presence of increasing [Ca^{2+}] was used to assess the effect of the mutations on the ability of CaM to bind Ca^{2+}. Domain-specific fluorescence of CaM^{WT} and CaM^{MUT} at increasing [Ca^{2+}] concentrations was monitored with selective residue excitation. Both CaM^{WT} and CaM^{MUT} displayed Tyr fluorescence intensity, which increased as a function of free [Ca^{2+}] at λ_{EX}=277 nm and λ_{EM}=320 nm, corresponding to Ca^{2+} binding at the C-domain. However, at λ_{EX}=250 nm and λ_{EM}=280 nm, the Phe fluorescence intensity decreases with increasing [Ca^{2+}], corresponding to Ca^{2+}-binding at the N-terminus. Data sets from four separate experiments were fitted using global nonlinear regression to a model-independent two site Adair function, and the results are summarised in Table 5-4, Figure 5-19 and Figure 5-20.

When compared to CaM^{WT} the N-domain binding sites of CaM^{MUT} proteins display little or no differences, Figure 5-19 and Figure 5-20. While unsurprising for the C-terminal mutations, the N-terminal CaM^{N54I} mutation appears not to affect the Ca^{2+}-binding affinity of CaM. Also as can be seen in Figure 5-19 and Figure 5-20, when compared to CaM^{WT} all the CaM mutations except CaM^{N54I} show reduced [Ca^{2+}]-binding affinities at the C-terminus. Furthermore, the values of K_d for each mutation shown in Table 5-4 reveals the scale of the impact on binding affinity varies with the mutation present.

Apart from CaM^{N54I}, which does not alter Ca^{2+} bindingthe mutations with the least effect on Ca^{2+}-binding at the C-terminal domain are CaM^{N98S} and CaM^{F142L},

which display 3.5 and 4.8 times greater K_d values than CaM^{WT}, respectively. The next least reduced C-terminal binding affinities are CaM^{Q136P} and CaM^{N98I} with K_d values that are 6.5 and 8.1 times greater than that of CaM^{WT}, respectively. Followed by CaM^{D134H}, CaM^{D96V} and CaM^{D132E}, with K_d values that were 10, 12 and 14 times greater than that of CaM^{WT}, respectively. The most severe reduction in the binding affinity of Ca^{2+} at the C-terminal domain was observed in CaM^{D130G}, with a K_d that was 46 times greater than that of CaM^{WT}.

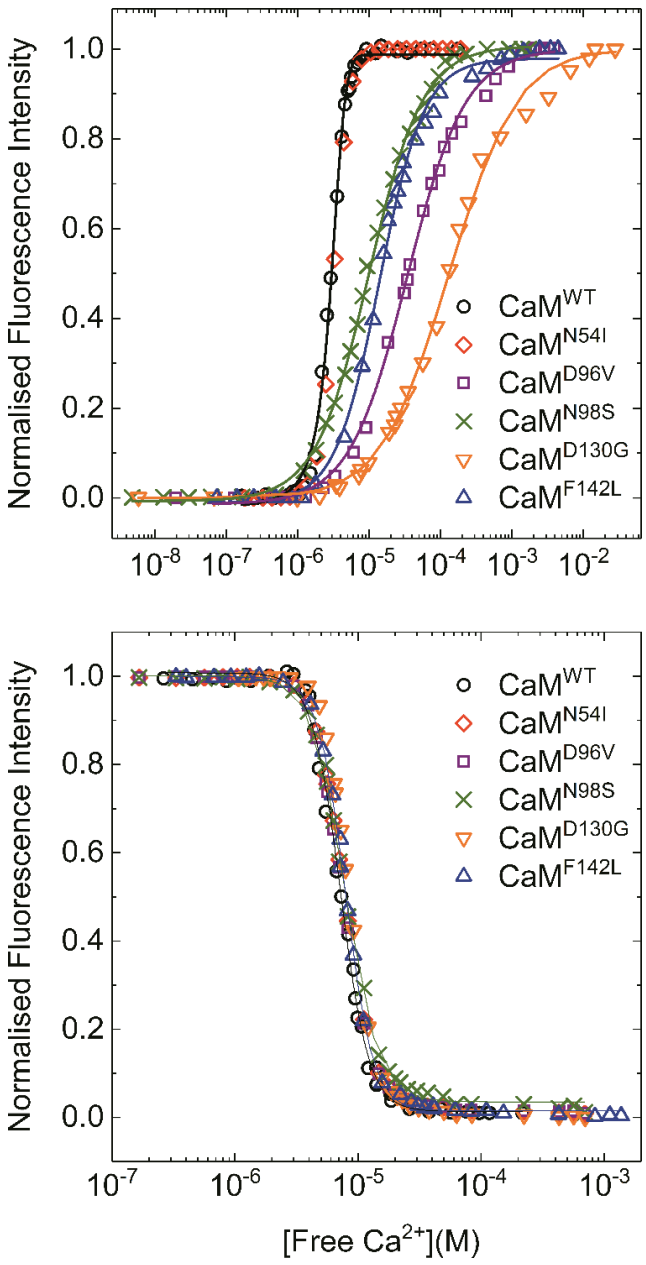

Figure 5-19 The Ca^{2+} Affinity at Only the C Domain of CaM Is Altered in the Presence of Mutations Associated with CPVT and LQTS

Intrinsic fluorescence of CaM^{WT} and CaM^{MUT} proteins, (A) Tyr fluorescence (λ_{ex}=277 nm, λ_{em}=300 nm) and (B) Phe fluorescence (λ_{ex}=250 nm, λ_{em}=280 nm) characteristic of the C- and N-domains respectively recorded in triplicate at increasing [Ca^{2+}]. Proteins were dissolved in 50 mM HEPES (pH 7.4), 100 mM KCl, 0.05 mM EGTA, 5 mM NTA, and 1 mM $MgCl_2$ and titrated with a Ca^{2+} rich solution. Normalised fluorescence intensity was plotted against determined free [Ca^{2+}]. Solid lines represent the nonlinear least square fit of a two-site model with independent Adair function to the collected data.

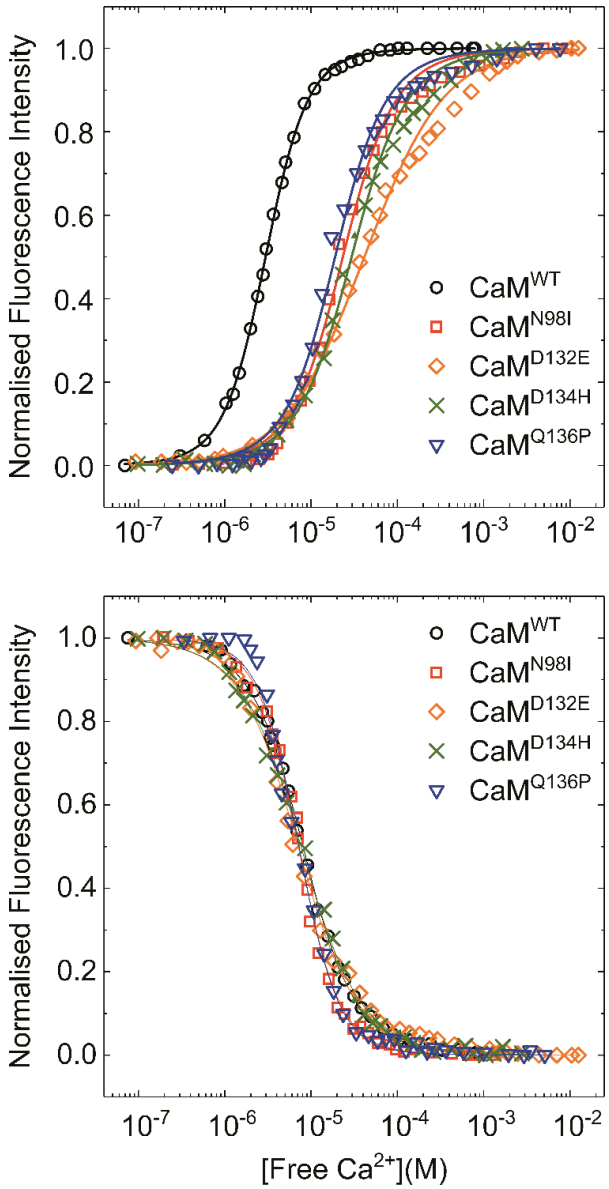

Figure 5-20 The Ca^{2+} Affinity at Only the C-Terminal Domain of CaM Is Altered in the Presence of Mutations Associated with CPVT and LQTS

Intrinsic fluorescence of CaM^{WT} and CaM^{MUT} proteins, (A) Tyr fluorescence (λ_{ex}=277 nm, λ_{em}=300 nm) and (B) Phe fluorescence (λ_{ex}=250 nm, λ_{em}=280 nm) characteristic of the C- and N-domains respectively recorded in triplicate at increasing [Ca^{2+}]. Proteins were dissolved in 50 mM HEPES (pH 7.4), 100 mM KCl, 0.05 mM EGTA, 5 mM NTA, and 1 mM $MgCl_2$ and titrated with a Ca^{2+} rich solution. Normalised fluorescence intensity was plotted against determined free [Ca^{2+}]. Solid lines represent the nonlinear least square fit of a two-site model with independent Adair function to the collected data.

Table 5-4 Ca^{2+} Binding Affinities at the Amino and Carboxyl Terminal Domains of CaM^{WT} and CaM^{MUT}

	Apparent K_d	
CaM protein	N-terminal domain (μM)	C-terminal domain (μM)
CaM^{WT}#1	7.2 ± 0.1	2.9 ± 0.1
CaM^{WT}#2	8.08 ± 0.09	2.97 ± 0.03
CaM^{N54I}	7.2 ± 0.1	2.9 ± 0.1
CaM^{D96V}	7.2 ± 0.1	34.3 ± 1.2
CaM^{N98S}	7.2 ± 0.1	10.1 ± 0.3
CaM^{D130G}	7.2 ± 0.1	132 ± 12
CaM^{F142L}	7.2 ± 0.1	13.9 ± 0.4
CaM^{N98I}	7.15 ± 0.12	23.40 ± 0.08
CaM^{D132E}	7.09 ± 0.23	41.55 ± 0.15
CaM^{D134H}	7.64 ± 0.19	29.56 ± 0.08
CaM^{Q136P}	7.24 ± 0.17	19.03 ± 0.07

Apparent K_d of Ca^{2+}-binding to C- and N-terminal domain sites at 25 °C resolved from the fitting of a model-independent two site Adair to function the experimental data. CaM^{WT}#1 and CaM^{WT}#2 refer to two batches of CaM^{WT} measured alongside either CaM^{N54I}, CaM^{N98S}, CaM^{D96V}, CaM^{D130G}, CaM^{D142L} or CaM^{N98I} CaM^{D134H}, CaM^{D132E}, CaM^{Q136P}, respectively.

5.3.6 Crystallisation Experiments

5.3.6.1 Protein Polishing

Five of the CaM^{MUT} proteins purified to date (CaM^{N54I}, CaM^{N98S}, CaM^{D96V}, CaM^{F90L}, and CaM^{F142L}) were further purified as previously described in Chapter 4. The mutants used were those for which sufficient starting material was available to produce the protein of sufficient quantity and quality for crystal trays. Representative traces from SEC are shown in Figure 5-21. For all proteins, the main elution peak occurred at an elution volume of ~90 ml. As discussed in Chapter 4 CaM proteins were predicted to elute from this column at 90 ml. Separation of the fractions by SDS-PAGE showed that one protein was eluted in the main peak of approximately 17 kDa. The other peaks either contained no protein or small amounts of protein not corresponding to the molecular weight of CaM (data not shown). These fractions were rejected.

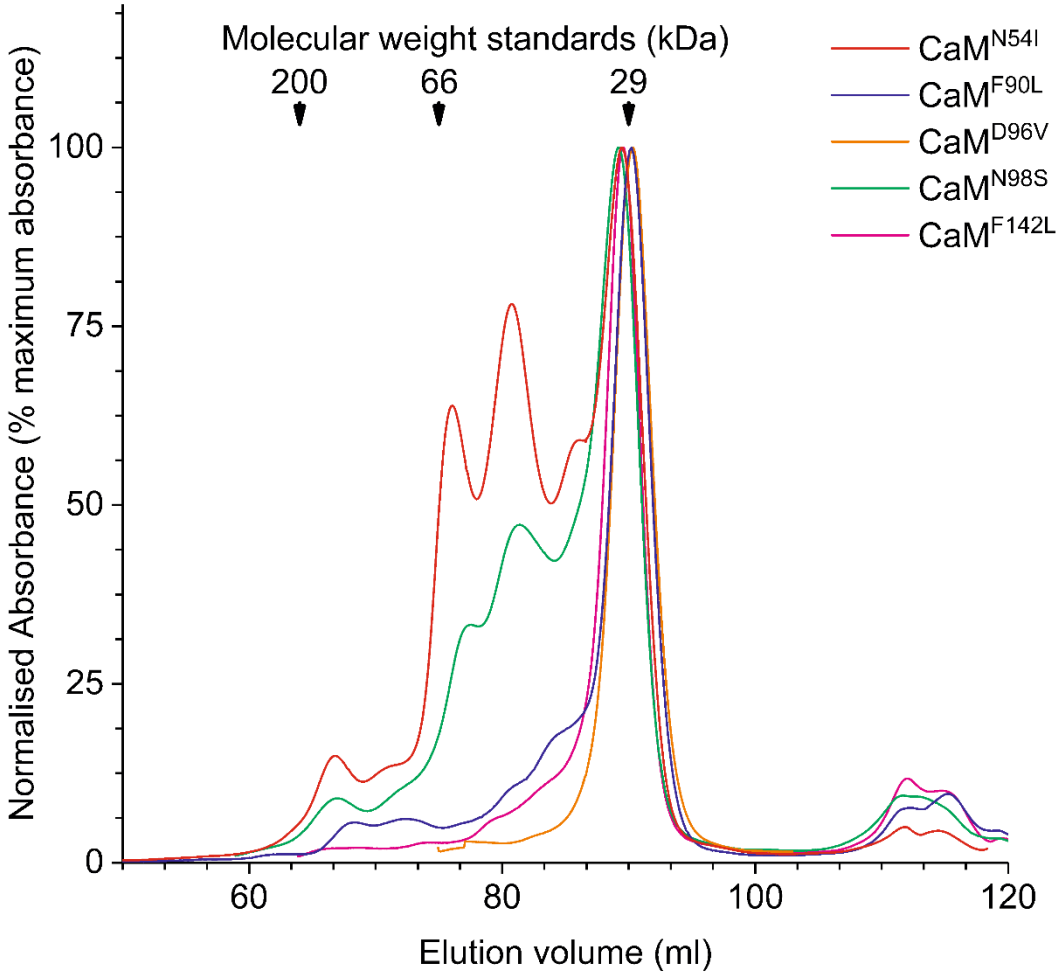

Figure 5-21 CaM^{MUT} Proteins Elute at the Same Elution volume as CaM^{WT}

Representative UV traces of SEC of CaM^{MUT} proteins. Pooled and concentrated elution fractions were loaded onto a Superdex 200 SEC Column (GE Healthcare) with a 2 mL Superloop equilibrated with 10 mM HEPES (pH 7), 50 mM KCl, 5 mM Ca^{2+}. Similar to CaM^{WT}, as seen in Chapter 4 one main peak occurring around an elution volume of 88 ml containing protein was observed. Elution fractions from beneath the main peak were collected and separated by SDS-PAGE. The elution volumes of SEC molecular weight standards are shown for comparison.

The fractions occurring beneath the main peak, typically an elution volume between 84-94 ml were separated by SDS-PAGE. Those containing CaM were pooled, and the buffer was exchanged by dialysis to one of low buffer concentration and low ionic strength. The protein was concentrated to ~20mg/ml in a final volume, depending on yield, of at least 100µl. The concentration was estimated spectrophotometrically. Based on estimation specified amounts of protein were separated by SDS-PAGE alongside known amounts of lysozyme, Figure 5-22. The estimated protein concentration was revised based on the observed band densities.

In Figure 5-22, the purified protein samples contained a major band of approximately 17 kDa when up to 5 µg of total protein has been loaded. Low M_W bands of potentially contaminating proteins and a doublet bands near the CaM bands were similar to those observed for CaM^{WT} in Figure 4-15. However, profile plots of the SDS-PAGE gel lanes in Figure 5-22 containing CaM proteins, Appendix Figure X; revealed only one major band in each lane. Therefore, the purity of the proteins was estimated at ≥ 95%.

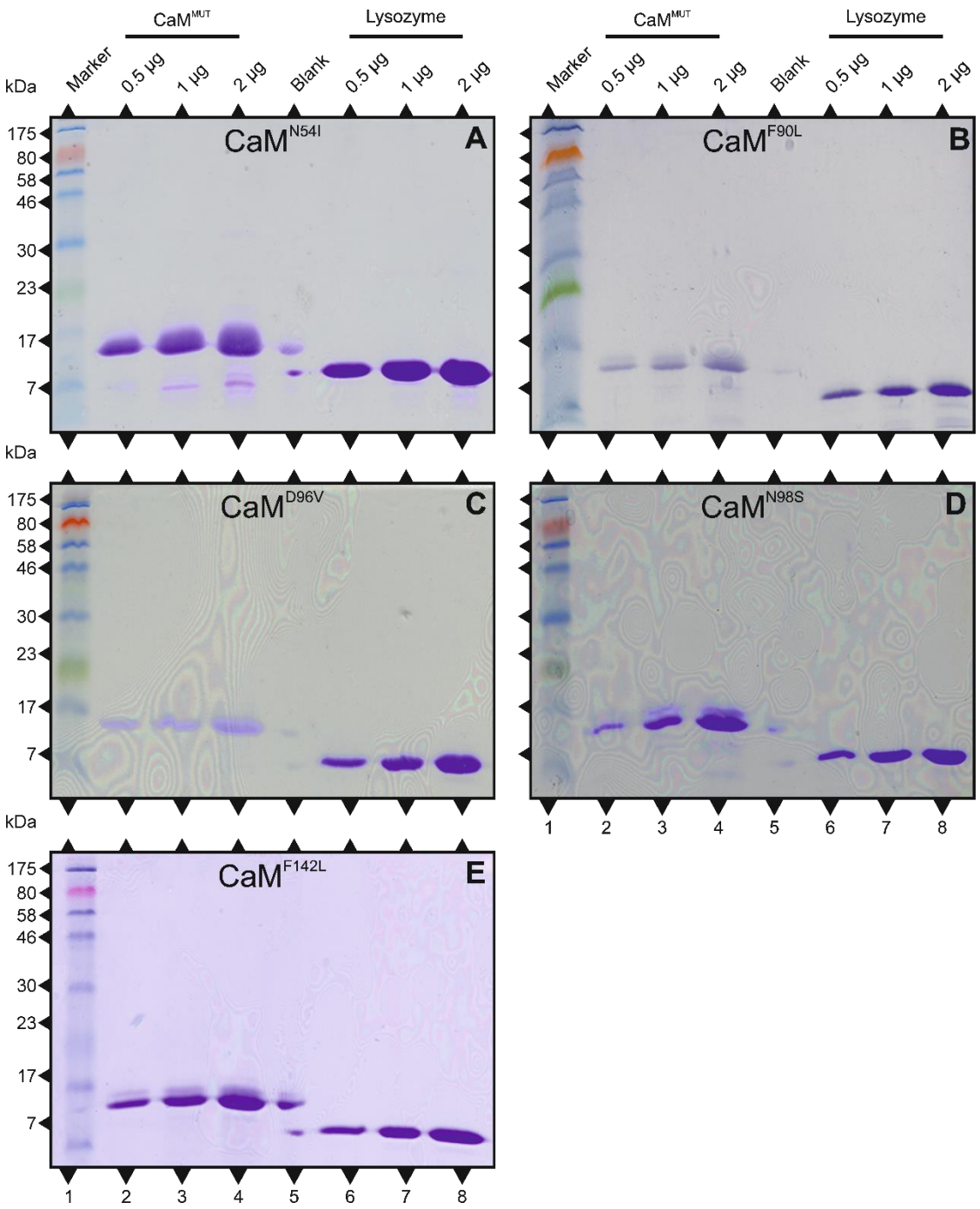

Figure 5-22 CaM^{MUT} Proteins Purified to a High Degree for Crystallisation

Concentrations of CaM^{MUT} proteins were estimated spectrophotometrically. Specific amounts of (A) CaM^{N54I}, (B) CaM^{F90L}, (C) CaM^{D96V}, (D) CaM^{N98S}, and (E) CaM^{F142L}, were separated alongside equivalent known amounts of lysozyme by 15 % (w/v) SDS-PAGE and stained with Coomassie . (A-E) Lane 1: Colorplus marker (NEB), Lanes 2-4: increasing CaM^{MUT} protein (1 µg, 2.5 µg and 5 µg), Lane 5: blanks, Lanes 6-8: increasing Lysozyme (1 µg, 2.5 µg and 5 µg).

5.3.6.2 Protein Crystallisation Experiments

Concentrated recombinant CaM proteins were aliquoted into crystallisation experiments using FS3, PACT and JCSG crystallisation screens as summarised in Table 2-11 to identify conditions for the crystallisation of CaM^{N54I}, CaM^{N98S}, CaM^{D96V}, CaM^{F90L}, and CaM^{F142L}.

The plates were monitored at regular intervals and continue to be monitored periodically. When crystals are harvested, the conditions yielding crystals from which diffraction data is obtained can be further optimised and used to synthesise crystals of the remaining mutants.

5.4 Discussion

This chapter describes the expression, purification and characterisation of patient-derived mutant CaM recombinant proteins associated with cardiac arrhythmias and SCD. Protein expression plasmids were designed to express 47 kDa CaM recombinant proteins. Each recombinant CaM fusion protein consisted of a different mutation of human CaM (CaM^{MUT}) with an N-terminal 6xHis affinity tag and human SUMO2 solubility partner separated from CaM by a self-cleaving intein sequence. PCR products of the expected size successfully ligated into the pHSIE expression plasmid. Expression of 6xHis-SUMO2-Intein-CaM^{MUT} proteins was induced in *E.coli* transformed with the pHSIE-CAM^{MUT} plasmids. SDS-PAGE analysis of samples of un-induced and induced bacterial cells showed protein bands of the expected size overexpressed only in the induced samples and functional characterisation were produced.

The expressed proteins were separated from contaminant proteins and immobilised on Ni-NTA resin. Following wash steps, altering the column conditions altered to those optimal for intein self-cleavage yielded a 17 kDa protein matching the predicted molecular mass of CaM. Meanwhile, proteins matching the mobility of un-cleaved protein and cleaved tag remained bound to the resin and until eluted by a 5-fold increase in imidazole concentration. Immunoblotting with an antibody specific for CaM confirmed the identity of the 17 kDa proteins as CaM.

The secondary structure of CaM^{MUT} proteins at high and low temperature both in the absence and presence of Ca^{2+} were assessed using CD. The CD spectra obtained for the mutants show high similarity with those for CaM^{WT} in Chapter 4 in

both the presence and absence of Ca^{2+} at 4 °C and in the absence of Ca^{2+} at 90 °C. The similarity in the CD spectrums indicates that the gross structures of CaM^{WT} and CaM^{MUT} are the same; so the protein is correctly folded in every case, and the secondary structure of CaM not perturbed by the presence of any of the mutations. No gross changes were observed in the secondary structure of CaM in the presence of any of the patient-derived mutations in this study. The unchanged structure has also been observed in the CPVT associated mutations, CaM^{N54I} and CaM^{N98S} (Søndergaard, Tian, *et al.*, 2015)

However, while the CD spectra are comparable in the presence of Ca^{2+} at 99 °C, there are differences between the spectra of CaM^{WT}, CaM^{N54I} and CaM^{N98S}, and the remaining CaM^{MUT} proteins. There is a degree of divergence in between the two maxima indicating that there is a difference in protein unfolding between the mutations. Therefore, most of the mutations reduced the thermal stability of CaM in the presence of Ca^{2+} to a varying degree.

The effect of the mutations on the thermal stability of CaM was further assessed by measuring the CD at 221 nm with increasing temperature in the presence and absence of Ca^{2+}. The thermal stability profiles of CaM^{WT} and CaM^{MUT} were similar in the absence of Ca^{2+}. However, in the presence of Ca^{2+}, compared to CaM^{WT} the profiles were markedly different for most of the CAM^{MUT} proteins with the exceptions of CaM^{N54I} and CaM^{N98S}. The presence of the mutations does not affect the thermal stability of apoCaM but the enhanced stability observed in the binding of Ca^{2+} is reduced. Therefore, most of the mutations result in a loss of function regarding thermal stability upon Ca^{2+}-binding of increasing severity. The effect of the mutations on overall

thermal stability can rank in order show decreasing thermal stability i.e. decreasing T_M, CaM^{WT} > CaM^{N98S} ≈ CaM^{N54I} > CaM^{D96V} > CaM^{F90L} ≈ CaM^{F142L} > CaM^{N98I} > CaM^{D132E} > CaM^{D130G} > CaM^{Q136P} > CaM^{D134H}. Interestingly, the CaM^{D130G} mutation displayed a LOF that would result in holoCaM unfolding partially at a core body temperature. The reduced thermal stability compared to CaM is a regularly occurring feature of the CaM mutations in patients and has been reported in other studies (Crotti *et al.*, 2013; Søndergaard, Sorensen, *et al.*, 2015).

Dysfunctional binding between RyR2 and CaM is arrhythmogenic. The IVT associated CaM^{F90L} mutation has reduced binding to RyR2 in the absence and presence of Ca^{2+}, impaired ability to inhibit RyR2 open conformation and reduced N-terminal Ca^{2+} affinity (Nomikos *et al.*, 2014). A Co-IP assay was used to assess the binding of RyR2 with CaM bearing CPVT and LQTS associated mutations relative to binding with CaM^{WT}. Ryanodine binding to SR vesicles in the presence of CAM^{MUT} proteins was assayed to assess the effect of the CaM mutations on RyR2 channel function. The level of ryanodine binding indirectly measures RyR2 channel opening.

RyR2 dysfunction is a common cause of arrhythmia, so altered binding between RyR2 and CPVT and LQTS associated CaM mutations is likely. The level of binding will indicate if the effect on channel function is a result of dissociation of CaM from RyR2. However, CaM also regulates the activity and function of other ion channels involved in the polarisation of the transmembrane potential including the L-type channels. LQTS and L-type channel dysfunction are linked so; it would not be unexpected if there were little or no difference to with RyR2 binding or channel opening in the presence of CaM mutants associated with LQTS.

Accordingly, both CaM^{N98S} and the LQTS associated CaM^{F142L} displayed no difference in interaction with RyR2 compared to CaM^{WT} and no detectable effect on CaM inhibition of RyR2 channel opening, both independent of Ca^{2+}. This indicates that the pathophysiological mechanism of CaM^{F142L} does not involve altered regulation of RyR2. However, *CALM1* c.293A>G that results in the CaM^{N98S} mutant protein associated with CPVT in the initial report. In three cases with symptoms varying between LQTS and CPVT, an equivalent *CALM2* mutation associated with the disease. A pathophysiological mechanism for arrhythmias is the leak of Ca^{2+} through defectively open RyR2 channels. Neither CaM^{F142L} or CaM^{N98S} causes enhanced or uninhibited channel opening and binding to RyR2 is unaltered. Therefore, the mechanism by which these patient mutations cause arrhythmias is unclear.

Recombinant proteins bearing LQTS mutations CaM^{D130G}, CaM^{N98I}, CaM^{D134H}, and mixed phenotype mutations CaM^{D132E} & CaM^{Q136P} all showed reduced association with RyR2. The interaction between RyR2 and CaM^{D130G} displayed a more significant reduction compared to CaM^{WT} than any other of the mutations tested. Correspondingly, the ability of all the mutations with reduced RyR2 interaction to inhibit channel opening was impaired so that the level of ryanodine binding was indistinguishable from that of the control. Therefore, the pathological mechanism of these mutations is likely to be dysfunctional regulation of RyR2 by CaM due to impaired binding of CaM to RyR2 leading to aberrant Ca^{2+} release. In the case of CaM^{D130G} impaired thermal stability could also play a role in impaired binding to, and effect on RyR2.

CaM containing the CPVT associated mutation, CaM^{N54I} and LQTS associated mutation CaM^{D96V} both had enhanced association with RyR2. The presence of the mutations resulted in channel opening greater than control indicating an agonist like effect on the channel. The arrhythmogenic mechanism in these mutations is likely to be an inappropriate release of Ca^{2+} due to CaM stimulating rather than inhibiting the opening of the channel.

Co-IP and ryanodine binding were assayed at different free Ca^{2+} levels because RyR2 and CaM are both Ca^{2+} responsive proteins. Overall binding between CaM and RyR2 and ryanodine binding to RyR2 increased with [Ca^{2+}] as to be expected. However, the mutation-specific differences were not Ca^{2+}-dependent although the differences lacked statistical difference at low Ca^{2+} levels.

Measurement of autofluorescence assayed the binding of Ca^{2+} at the N- and C- terminals of CaM^{MUT} proteins compared to CaM^{WT}. Previously, Ca^{2+}-binding at the C-terminus when bearing the N-terminal CaM^{N54I} mutation was shown to be enhanced compared to CaM^{WT} (Nyegaard *et al.*, 2012). The authors suggested altered co-operation between Ca^{2+}-binding sites in the C- and N-terminals mediated by the CaM^{N54I} mutation caused enhanced the Ca^{2+}-binding affinity at the C-terminus. However, in this study, the specific N- and C-terminal domain Ca^{2+}-binding affinities of CaM^{N54I} were both indistinguishable from CaM^{WT}. Other published data for this mutation supports this observation (Hwang *et al.*, 2014). Currently, all studies of arrhythmogenic CaM mutations show a Ca^{2+}-binding affinity at the N-terminal domain indistinguishable from that of CaM^{WT}. Apart from CaM^{N54I}, all patient-derived mutations display differing levels of reduction in Ca^{2+}-binding affinity at the C-terminal domain

compared to CaM^{WT} (Nyegaard *et al.*, 2012; Crotti *et al.*, 2013; Hwang *et al.*, 2014; Makita *et al.*, 2014; Nomikos *et al.*, 2014; Søndergaard, Sorensen, *et al.*, 2015).

The remaining mutations display reduced Ca^{2+} affinity at the C-terminal but intact at the N-terminal, which probably reflects the C-terminal location of these mutations. The reduction in Ca^{2+}-binding affinity can be ranked in decreasing order as $CaM^{WT} \approx CaM^{N54I} > CaM^{N98S} > CaM^{F142L} > CaM^{Q136P} > CaM^{N98I} > CaM^{D134H} > CaM^{D96V} > CaM^{D132E} > CaM^{D130G}$. The alteration of Ca^{2+} affinity indicates a possible disease mechanism where regulation of RyR2 by Ca^{2+} via CaM is altered due to the insensitivity of CaM to Ca^{2+}. However, it is unclear through the functional assays in this study how this occurs.

None of the assays used in this study directly examine the alteration of channel function, i.e. the release of Ca^{2+} in the presence of changes in [Ca^{2+}]. Single channel experiments would quantitatively measure differences in the activity of isolated channels in the presence of either CaM^{WT} or CaM^{MUT} with increased cytosolic and luminal [Ca^{2+}]. Imaging of Ca^{2+} in cells expressing transfected mutant and wildtype CaM constructs would show alterations in Ca^{2+} release events in the milieu of the cell.

CaM^{N98S} and CaM^{F142L} have similarly reduced Ca^{2+}-binding affinity, but do not affect CaM binding to and inhibiting the activity of RyR2. Potentially, the reduced Ca^{2+}-binding plays a role in the dysfunctional regulation by CaM of another component of the EC-C mechanism, e.g., L channels. However, different phenotypes observed might indicate different mechanisms.

Despite Ca^{2+} insensitivity, CaM^{N54I} and CaM^{D96V} enhance RyR2/CaM binding and channel opening. Maybe there is a mutation induced Ca^{2+}-independent conformational change which allows enhanced binding and interferes with the channel closing. The observed CPTV phenotype for CaM^{N54I} is consistent with enhanced RyR2 channel opening and reduced Ca^{2+} sensitivity leading to aberrant Ca^{2+} release regardless of [Ca^{2+}]. However, the same characteristics displayed by CaM^{D96V} do not fit the LQTS diagnosis but are also inconsistent with the characteristics of the other LQTS mutations.

Conversely, reduced Ca^{2+} affinity in CaM^{D130G} CaM^{N98I} CaM^{D134H} CaM^{D132E} & CaM^{Q136P} could explain reduced binding and increase in the opening of the channel which would lead to an arrhythmogenic phenotype which would be expected to have a CPVT phenotype. However, the observed phenotype is LQTS.

In this chapter, the mutations do not impart changes to the secondary structure of CaM, and both DLS and SEC data indicate that the overall size of CaM in the presence of Ca^{2+} is unaltered. The effect on the tertiary structure is unknown, and there is currently no information regarding tertiary structure available. Therefore, experiments were commenced to identify the conditions required to generate crystals of selected mutations of CaM. The protein produced was of sufficient quantity and quality for X-ray crystallography. Multiple conditions are currently under trial, while early timepoints yielded no crystals long-term time courses are underway.

A major cause of genetic arrhythmogenic is the aberrant release of Ca^{2+} from the SR by RyR2 channels mediated by mutations in either RyR2 itself or the proteins

that regulate its function (Ter Keurs and Boyden, 2007). Therefore, the functional assays provide potential disease mechanisms for all the arrhythmogenic CaM mutations in this study, bar CaM^{F142L} and CaM^{N98S}. Neither CaM^{N98S} and CaM^{F142L} appear to influence RyR2 but the increased Ca^{2+} insensitivity compared to CaM^{WT} suggests another interaction of CaM is altered perhaps due to failure to bind Ca^{2+}. The GOF displayed by CaM^{N54I} and CaM^{D96V} with increased binding to RyR2 and enhanced channel opening independent of Ca^{2+} which could lead to the uncontrolled release of Ca^{2+}. The remaining mutations all display LOF with reduced RyR2 binding and channel opening inhibition abolished, accompanied by a reduced affinity for Ca^{2+}. Potentially, the channel would remain open despite an increase in Ca^{2+}. How each mutation results in a disease phenotype are unclear. There is an overlap in the characteristics of mutations associated with specific channelopathies. Interestingly different substitutions at the same co-ordinate, CaM^{N98S} and CaM^{N98I}, resulted in both different and similar characteristics but had a similar disease diagnosis. Analogous to RYR2 mutations associated with channelopathies the observed phenotype differs dependent on the mutation present.

However, given the clinical challenges in diagnosing CPVT and LQTS correctly, comparison of ambiguous cases with novel mutations reported in different centres is difficult. Also, resolving disease aetiology in reported cases based on genotype is not reliable when mutations have been characterised using different methods and systems. An interaction between LQTS mutations and RyR2 does not preclude LQTS rather another altered interaction with LQTS aetiology “drowns out” the effect of aberrant Ca^{2+} release by RyR2. The increasing ability to screen the genome for

polymorphisms associated with disease will identify novel polymorphisms and susceptibility genes for arrhythmogenic channelopathies especially those which result in overlapping clinical features or uncharacteristic phenotypes (Devalla *et al.*, 2016).

To the best of the author's knowledge, this is the first study to characterise all of these patient-derived mutations side by side using the same experimental systems. Also, the methods used can be repeated to directly compare with novel arrhythmogenic CaM mutations that continue to be reported. The final phenotype may be the product of multiple altered interactions between CaM and multiple ion channels that consequently alter the flow of ions. To thoroughly dissect the aetiological mechanisms of arrhythmogenic CaM mutations; the interactions of mutant CaM with all target proteins involved in cardiac electrophysiology may be required. This chapter confirms the importance of *CALM1-3* as susceptibility genes in cardiac arrhythmia. Given the ability of CaM to affect multiple targets any course of treatment may have to be amended to reflect this despite a clear CPVT or LQTS phenotype. It also underscores the importance of genotyping both CPVT and LQTS susceptibility genes in clinical arrhythmia cases with ambiguous characteristics and cases which meet diagnosis guidelines but are genotype negative.

5.5 Findings

In summary, the following novel findings were made in this chapter:

- Mutant CaM can be expressed and purified as untagged protein using a one-step purification protocol without requiring a multiple stage purification with an enzymatic cleavage step.

- Arrhythmogenic mutants of CaM did not confer structural changes
    - a similar gross secondary structure to CaM^{WT}.
    - were recognised by anti-CaM IgG.
    - mobility and hydrodynamic radii matched CaM^{WT}.
- Arrhythmogenic mutants of CaM did confer divergent functional changes to CaM by having a range of effects on
    - Ca^{2+} binding affinity.
    - altered conformational change on the Ca^{2+} binding affinity.
    - the thermal stability in the presence of Ca^{2+}.
    - the binding of CaM to RyR2

Chapter 6 - THE INTERACTION BETWEEN CALMODULIN AND CALCIUM SIGNALLING PROTEINS

6.1 Summary of Chapter

In Chapter 5, mutations of CaM associated with cardiac arrhythmia were shown to have divergent effects on binding to and regulation of the RyR2 channel. However, measurement of binding was qualitative and prone to variation between experiments. ITC experiments have revealed that the lobes of CaM could bind up to three sites within RyR2 (Lau, Chan and Van Petegem, 2014). This chapter describes quantitative measurement of the binding between two sites in RyR2, and wildtype and mutant CaM using thermodynamic analysis. The CaM mutations had divergent effects on the capacity of CaM to bind the sites within RyR2. Recently, novel inhibition of activity and binding to PLCζ by CaM was observed, where this work had the potential of identifying a regulatory mechanism for PLCζ in sperm and oocytes (Nomikos, Thanassoulas, *et al.*, 2017). These *in silico* and *in vitro* experiments suggested that PLCζ and CaM bind via the C-lobe of CaM and the PLCζ XY linker. The CaM^{WT} expression plasmid described in Chapter 4 is an ideal base for generating plasmids that express the lobes of CaM. This chapter describes the construction of plasmids for the prokaryotic expression of human CaM DNA sequences corresponding to the individual lobes of CaM as fusion proteins. The one-step purification method yielded significant quantities of pure, soluble, untagged proteins. To confirm the bioinformatic predictions of binding between CaM and PLCζ, binding between full-length CaM and the N- and C-lobes of CaM to PLCζ were measured quantitatively using thermodynamic analysis. These

experiments showed that CaM and PLCζ bound at specific locations in a Ca^{2+}-dependent manner.

6.2 Introduction

6.2.1 The Interaction Between Calmodulin and PLCζ

Despite recent advances, the exact regulatory mechanism of PLCζ is still unclear. In contrast with the somatic PLC isoforms, the binding partners of PLCζ within the sperm or the oocyte are unknown. A previous study reported that CaM directly interacted with and regulated the activity of PLCδ1 (Sidhu, Clough and Bhullar, 2005). Recently, a novel interaction between PLCζ and CaM demonstrated that they regulated the activity of PLCζ (Nomikos, Thanassoulas, *et al.*, 2017). Bioinformatic analysis of the sequence of PLCζ revealed putative binding sites for CaM in the PLCζ XY linker. Purified, heterogeneously expressed recombinant proteins corresponding to full-length human PLCζ fused to MBP (MBP-PLCζ) and untagged CaM interacted in a Ca^{2+}-dependent manner. Peptides corresponding to the N-terminal (Peptide N PLCζ$^{289-308}$), middle (Peptide M PLCζ$^{310-328}$) and C-terminal (Peptide C PLCζ$^{338-353}$) of PLCζ XY linker were designed and synthesised (Lifetein, USA). Docking experiments simulating CaM interacting with Peptide C revealed the peptide bound to the central linker region of CaM between N- and C-terminal lobes. The work revealed that the majority of contacts between the protein and Peptide C stabilised the complex and involved the C-lobe of the protein. The presence of CaM significantly reduced the Ca^{2+}-dependent hydrolytic effect of MBP-PLCζ on PIP2 *in vitro*. CaM appeared to abolish the binding between MBP-PLCζ and PIP_2 in the presence of Ca^{2+}. HoloCaM associates with PLCζ and

inhibits PLCζ PIP_2 hydrolysis activity by altering the proper access of the enzyme active site to its substrate PIP_2 (Nomikos, Thanassoulas, *et al.*, 2017).

6.2.2 Mutation Mediated Derangement of Calmodulin and RyR2 Interaction

In Chapter 5, binding between RyR2 and CaM was shown to be disrupted by the presence of CaM mutations associated with arrhythmia in patients. Co-IP assays provided a relative measure of change in binding between RyR2 and CaM^{MUT} compared to CaM^{WT}. However, relative density is a qualitative rather than a quantitative measure, and the value obtained is likely to have a high degree of error due to variations between SR preps batches.

As discussed in Chapter 1, both RyR isoforms bind CaM at the conserved CaMBD2, $RyR1^{3614–3643}$ and $RyR2^{3583–3603}$ (Moore *et al.*, 1999; Yamaguchi, Xin and Meissner, 2001; Yamaguchi *et al.*, 2003). CaM appears to mediate isoform-specific Ca^{2+}-dependent regulation of the RyR channel by interacting with multiple binding sites in RyR (H. Zhang *et al.*, 2003; Yamaguchi *et al.*, 2004). Multiple proposed CaM binding regions in RyR2 were subsequently discounted (Yuchi, Lau and Van Petegem, 2012; Huang *et al.*, 2013). Currently, there are three CaM binding domain candidates in RyR2 with CaMBD2 being the most studied. In transgenic mice, disruption of binding between CaM and CaMBD2 resulted in cardiac hypertrophy, HF and early death (Yamaguchi *et al.*, 2007).

The stoichiometry of binding between RyR and CaM is one to one, so the regulatory mechanism of binding may involve the separate interaction of the lobes of CaM with different domains of RyR2. The regulation of ion channels by CaM has

previously been shown to involve dynamic, lobe-specific binding to different segments of the polypeptide sequence in response to Ca^{2+} (Alaimo *et al.*, 2014; Shao *et al.*, 2014; Marques-Carvalho *et al.*, 2016). Binding between CaM and peptides corresponding to the remaining CaMBDs was recently assessed quantitatively (Lau, Chan and Van Petegem, 2014). The regulation by CaM with multiple target protein entails a diverse and complex variety of binding mechanisms. The lobes of CaM binds both Ca^{2+} and target sequences independently (Kovalevskaya *et al.*, 2013). Therefore, CaM can simultaneously bind two discontiguous sequences in a target; binding is dynamic, bridging different sequences in response to the presence and absence of Ca^{2+}. Consequently, it would not be unexpected for CaM to bind more than one of the RyR2 CaMBD sequences in the presence and absence of Ca^{2+} or both.

As discussed in Chapter 1 the interdomain interaction between the N-terminal and central domains of RyR was suggested to regulate channel activity. Mutation hotspots in the N-terminal and central domains of both RyR1 and RyR2 display linkage with diseases of similar aetiology, i.e. MH and CPVT, respectively. Aberrant domain unzipping was the proposed pathological mechanism (Ikemoto, 2002). However, the binding of RyR agonists does not result in domain unzipping, so domain unzipping alone does not appear to account solely for regulation of RyR channel activation (Ono *et al.*, 2010; Walweel, Oo and Laver, 2017).

A recently proposed mechanism for regulation of RyR channel activity is an interaction between RyR domains associated with the binding of CaM to the channel. A peptide corresponding to RyR1 CaMBD2 was shown to bind to the RyR1 channel inducing a conformational change, channel activation and SR Ca^{2+} release

(Gangopadhyay, Grabarek and Ikemoto, 2004; Zhu *et al.*, 2004; Gangopadhyay and Ikemoto, 2006). The binding of CaMBD2 peptide recreates the conformational changes observed in RyR1 in a peptide corresponding to RyR1 3534–4271 encompassing both CaMBD2, CaMBD3 and CaMLD (Gangopadhyay and Ikemoto, 2006). The EF-hand-like CaMLD, a region with an amino acid sequence resembling CaM, capable of binding CaMBD2, occurs in both RyR1 and RyR2 (Xiong *et al.*, 2006; Gangopadhyay and Ikemoto, 2011). The interdomain interaction between CaMBD2 and CaMLD activates the RyR1 channel (Gangopadhyay and Ikemoto, 2008). The binding of CaM to RyR2 CaMBD2 is suggested to interfere with binding to CaMLD thus preventing channel activation. Interfering with CaMBD2 and CaMLD interaction in failing cardiomyocytes halts aberrant Ca^{2+} transients caused by the dissociation of CaM from RyR2 (Gangopadhyay and Ikemoto, 2011). A mutation resulting in CaMLD with increased affinity for CaMBD was believed to cause tightened interaction between the two domains resulting in CPVT like symptoms in transgenic animals (Nishimura *et al.*, 2018).

Crosstalk between the interdomain interactions of N-terminal and core domains, and CaMBD2 and CaMLD is hypothesised to regulate channel opening. In the proposed model domain unzipping alters the binding of CaM resulting in CaM dissociating from CaMBD2. In the absence of CaM, CaMBD2 and CaMLD interaction lead to channel opening (Ono *et al.*, 2010; Walweel, Oo and Laver, 2017). Prokaryotic expressed tagged peptides corresponding to rat RyR2 CaMDBD2, and CaMBD3 were both shown to bind human CaM in both the presence and absence of Ca^{2+} (Lau, Chan and Van Petegem, 2014). Peptide binding was also shown to be lobe-specific.

However, the mode of binding between CaM and CaMBD2 differed between the absence and presence of Ca^{2+}. Also, the specificity of CaM for CaMBD2 and CaMBD3 increased significantly in the presence compared to the absence of Ca^{2+} (Lau, Chan and Van Petegem, 2014).

6.2.3 Rationale and Experimental Plan

Calorimetric measurement of the energy changes associated with the binding of the protein and peptide can be analysed to quantify the parameters of a binding reaction. Measuring the heat changes while titrating known amounts of protein, i.e. CaM^{WT} or CaM^{MUT} with peptides corresponding to regions of PLCζ and RyR known to bind CaM could reveal the kinetics of the binding reaction.

Further investigation is required to elucidate the physiological role at mammalian fertilisation of the interaction between CaM and PLCζ. A critical piece of information that would develop our understanding is the confirmation of the location within CaM required for the interaction with PLCζ. While the interaction between the CaM C-lobe and the C-terminal portion of the PLCζ XY linker was shown *in silico,* to confirm the validity of this initial observation additional experimental evidence is required (Nomikos, Thanassoulas, *et al.*, 2017).

In this chapter, the binding kinetics of CaM^{WT} and peptides corresponding to putative CaM-binding sequences in PLCζ will be measured using ITC. Deletion mutations of human CaM lacking the N- and C-lobes will be constructed. The mutated CaM sequences will be inserted into the pHSIE vector to create expression plasmids expressing the N-lobe and C-lobe of human CaM with N-terminal 6xHis-human

SUMO2-Intein fusion partner. The expressed proteins can be purified using the one-step purification protocol described in Chapter 4 to produce soluble, untagged, proteins corresponding to the individual lobes of CaM. To further characterise the binding reactions of CaM and PLCζ the binding kinetics of the lobes of CaM and PLCζ peptides will also be measured using ITC. The peptides represent the N-terminal (Peptide N-hPLCζ$^{289-308}$) middle (Peptide M- hPLCζ$^{310-328}$) and C-terminal (Peptide C-hPLCζ$^{338-353}$) of the PLCζ XY linker.

During work with the second batch of CaM mutations, as part of a long-running collaboration, synthesised peptides representing the CaMBD2 of human RyR2 (hRyR2) (Peptide B-hRyR2$^{3581-3607}$) and CaMBD3 of hRyR2 (Peptide F-hRyR2$^{4255-4271}$) became available. The effect of arrhythmogenic CaM mutations on the interaction between RyR2 and CaM will be investigated further by titrating the peptides into CaM^{WT} and CaM^{MUT} proteins in the presence and absence of Ca^{2+}. Binding between recombinant CaM proteins and a peptide corresponding to RyR2 CaMBD2 was unaffected by p.(Asn54Ile) and aberrant at low [Ca2+] with p.(Asn98Ser). However, the RyR2 binding was assessed indirectly by measuring the change in Tyr fluorescence as binding of the peptide occludes the residue (Nyegaard *et al.*, 2012).

ITC experiments will reveal quantitative information on the kinetics of Ca^{2+} dependent and independent binding between human wildtype and mutant CaM to the CaMBD2 and CaMBD3 of human RyR2. The kinetics of the binding reactions would allow for a more detailed analysis of the arrhythmogenic CaM mutations and mechanisms by which CaM regulates RyR2. Previous ITC experiments included full length and the N- & C- lobes of CaM with peptides corresponding CaMBD1,2 and 3 of

rat RyR2 and rabbit RyR1 (Craig *et al.*, 1987). The mutation mediated changes in binding could be assessed quantitatively in a reproducible manner providing further information on the disease mechanism of the arrhythmia linked to these mutations.

6.3 Results

6.3.1 Molecular Cloning

6.3.1.1 Cloning of Deletion Mutants of Calmodulin into the pHSIE Expression Vector

Two deletion mutants of CaM were designed so that the expressed proteins corresponded to the amino acid sequence of CaM from Met^{1} to Lys^{78} and, from Asp^{79} to Lys^{149} preceded with a Met residue, i.e., the N- and C-lobes of CaM, respectively. DNA sequences encoding the two sets of coordinates were amplified from the pAED4-hCaM plasmid using primers NCaMf and NCaMr, and CCaMf and CCaMr. The cloning strategy is shown in Figure 6-1, as can be seen both sets of primers incorporated a 5'-*Kpn*I site and a 3'-*Not*I site to facilitate cloning into the pHSIE expression vector as previously described in Chapters 4&5. Additionally, CCaMf incorporated a codon for Met between the 5'-*Kpn*I cleavage site and the codon encoding Asp^{79}.

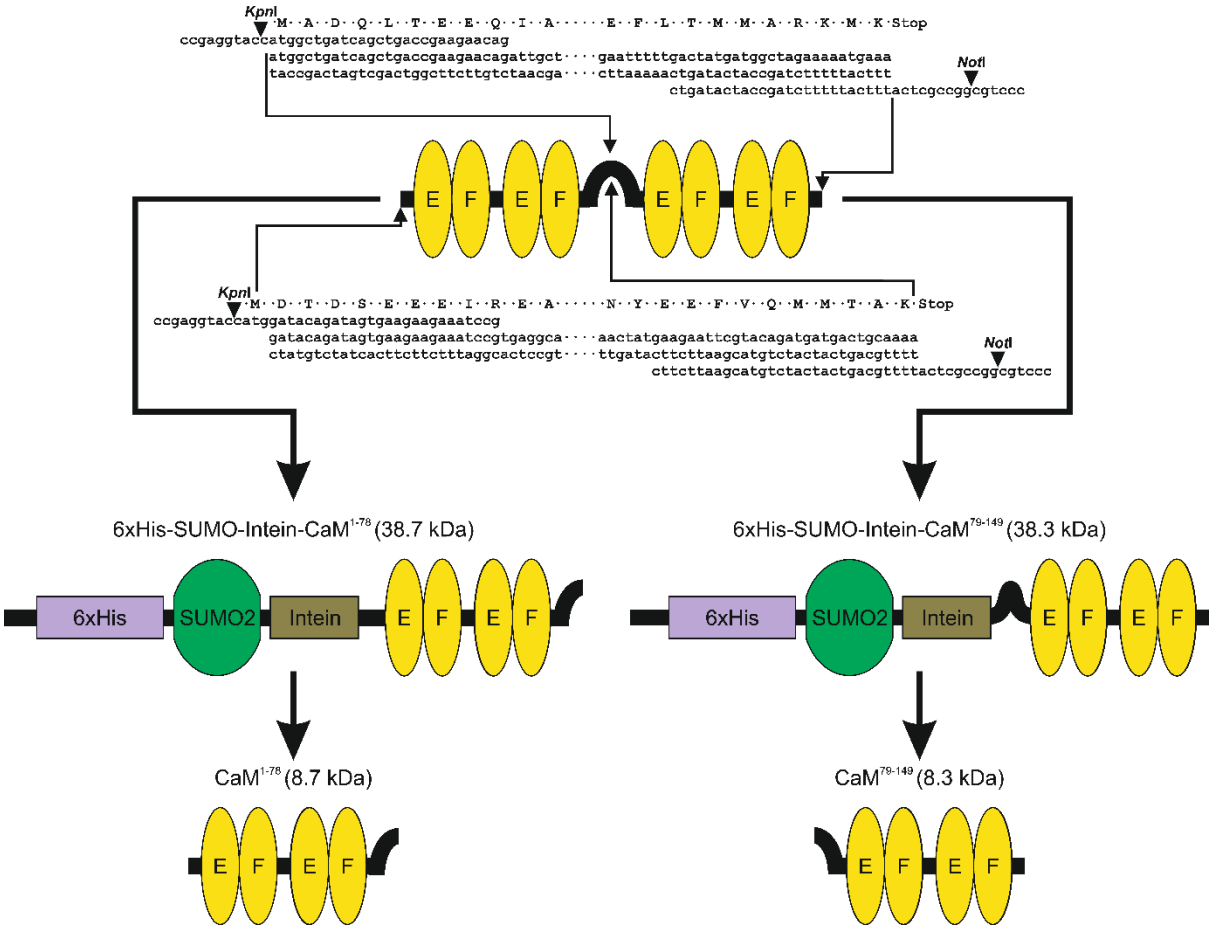

Figure 6-1 Cloning Strategy for Construction of CaM$^{1-78}$ and CaM$^{79-149}$

Primers were designed to produce two PCR products of 259 bp and 241 bp encoding Met^{1}-Lys^{78} and Asp^{79}-Lys^{149} amino acids of human CaM flanked by the recognition sites for *Kpn*I and *Not*I. Additionally, CCaMf was designed to incorporate a codon for Met between the codon encoding Asp^{79} and the *Kpn*I cleavage site. The PCR products and pHSIE plasmid were digested with both enzymes. The cut insert and vector were ligated to produce pSHIE-CaM$^{1-78}$ and pSHIE-CaM$^{79-149}$. Induction of expression of competent *E.coli* transformed with pHSIE-CaM1-78, and pHSIE-CaM79-149 yields ~38 kDa fusion proteins consisting of either the N-lobe or C-lobe of CaM^{WT} respectively with an N-terminal 6xHis, SUMO2, Intein fusion partner. Intein self-cleavage will yield a ~8 kDa protein, untagged N-lobe or C-lobe of CaM^{WT}

The resulting plasmids were termed pHSIE-CaM$^{1-78}$ and pHSIE-CaM$^{79-149}$. PCRs containing the cloning oligos confirmed the presence of the inserts. As can be seen in Figure 6-2, the PCRs containing pHSIE-CaM$^{1-78}$ and pHSIE-CaM$^{79-149}$ yields products matching the size of pHSIE-CaM$^{1-78}$ and pHSIE-CaM$^{79-149}$ sequences while PCR containing pHSIE yields no product. The sequence of the insert was confirmed by DNA sequencing.

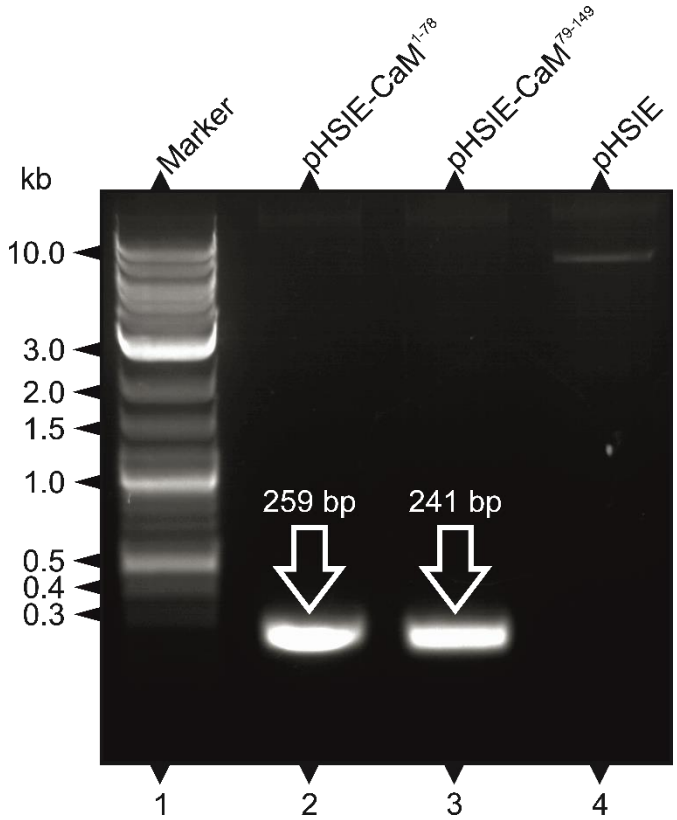

Figure 6-2 PCR of pHSIE-CaM$^{1-78}$ and pHSIE-CaM$^{79-149}$ Yield Products of the Correct Size

Confirmation of successful subcloning of pHSIE-CaM$^{1-78}$ and pHSIE-CaM$^{79-149}$ plasmids. The products of PCRs containing hCaMKpNF and hCaMNotIR with candidate clones and empty vector as templates were separated by 1 % (w/v) agarose gel electrophoresis. PCR from the candidate clones yielded a >300 bp product while the empty vector yielded no product. Lane 1: 2-Log DNA marker (NEB), Lanes 2 and 3: 500 ng PCR products with candidate clones for pHSIE-CaM$^{1-78}$ and pHSIE-CaM$^{79-149}$ plasmids as template respectively and Lane 4: Equivalent volume of PCR with empty vector as a template.

6.3.2 Expression and Purification of the Lobes of Calmodulin

6.3.2.1 Expression of Amino and Carboxyl Lobes of Calmodulin

Chemically competent BL21-CodonPlus were transformed with pHSIE-CaM$^{1-78}$ and pHSIE-CaM$^{79-149}$. The expression of recombinant proteins was induced using previously established conditions; the predicted expressed protein is shown in Figure 6-1. SDS-PAGE separated the crude lysates of samples of induced and uninduced cultures, as can be seen in Figure 6-3. The induced sample contains a band of approximately 38 kDa which is not present in the un-induced sample.

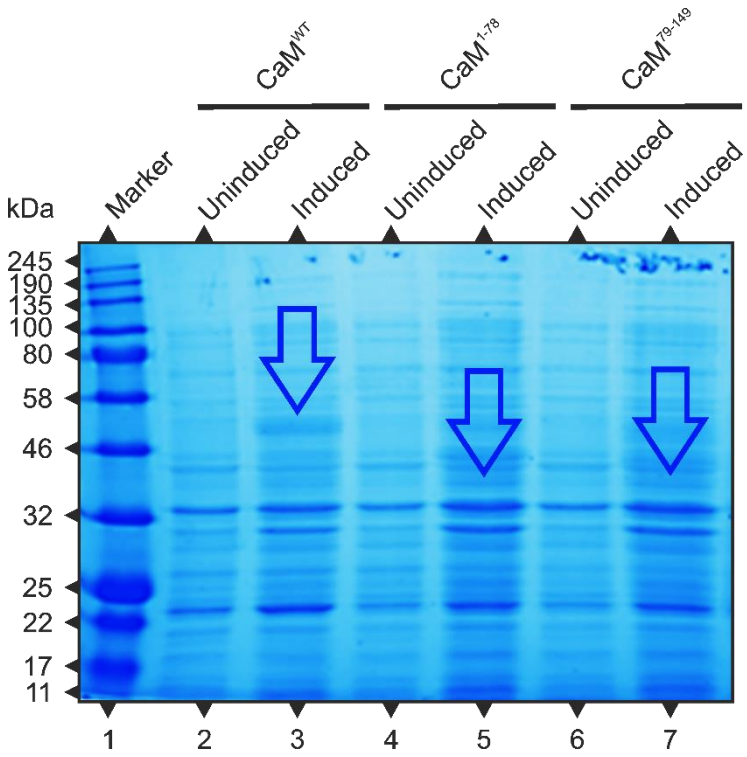

Figure 6-3 Expression of 6xHis SUMO CaM^{WT}, 6xHis SUMO CaM$^{1-78}$ and 6xHis SUMO CaM$^{79-149}$ Proteins in *E.coli*

BL21-CodonPlus were transformed with pHSIE-CaM$^{1-78}$ and pHSIE-CaM$^{79-149}$ plasmids. Protein expression was induced with 0.1 mM IPTG. Crude lysates of uninduced and induced cultures were separated using SDS-PAGE. Bands of ~>46 kDa and >32 kDa (highlighted by the boxes) were observed in the induced samples but not in the uninduced samples. Coomassie stained 15 % (w/v) SDS-PAGE gel. Lane 1: Color Prestained Protein Standard, Broad Range (11–245 kDa) (NEB), Lane 2: uninduced pHSIE-CaMWT, Lane 3: induced pHSIE-CaMWT, Lane 4: uninduced pHSIE-CaM$^{1-78}$, Lane 5: induced pHSIE-CaM$^{1-78}$, Lane 6: uninduced pHSIE-CaM$^{79-149}$, Lane 7: induced pHSIE-CaM$^{79-149}$.

6.3.2.2 Purification of Amino and Carboxyl Lobes of Calmodulin

Pellets representing 16 l of expression culture were re-suspended, pooled, lysed and clarified. Similar to the purification protocol outlined in Chapter 4 and 5, the clarified lysate was applied to Ni-NTA. The N-terminal 6xHis tag of 6xHis SUMO CaM^{1-78} and 6xHis SUMO CaM^{79-149} proteins allow for protein capture to Ni-NTA, isolating the recombinant proteins. Lowering the pH and increasing temperature induces the Intein moiety to undergo self-cleavage liberating CaM^{1-78} and CaM^{79-149} while 6xHis-SUMO2-Intein remains immobilised. Purification fractions were separated by SDS-PAGE, Figure 6-4. While the clarified bacterial lysate and flow-through fractions contain multiple bands, one of the strongest is a 38 kDa protein which diminishes in the flow-through fraction. There are fewer protein bands in the first wash fraction, and the 38 kDa band is still present. The second wash fraction of cleaving buffer contained very few proteins except a 38 kDa protein and 30 kDa protein. However, following incubation at room temperature a >11 kDa protein is present.

Fractions containing the >11 kDa protein were pooled. The pooled protein sample was separated by SDS-PAGE, Figure 6-5. The pooled fractions, typically 10 ml were dialysed against PBS and stored at 4°C until required.

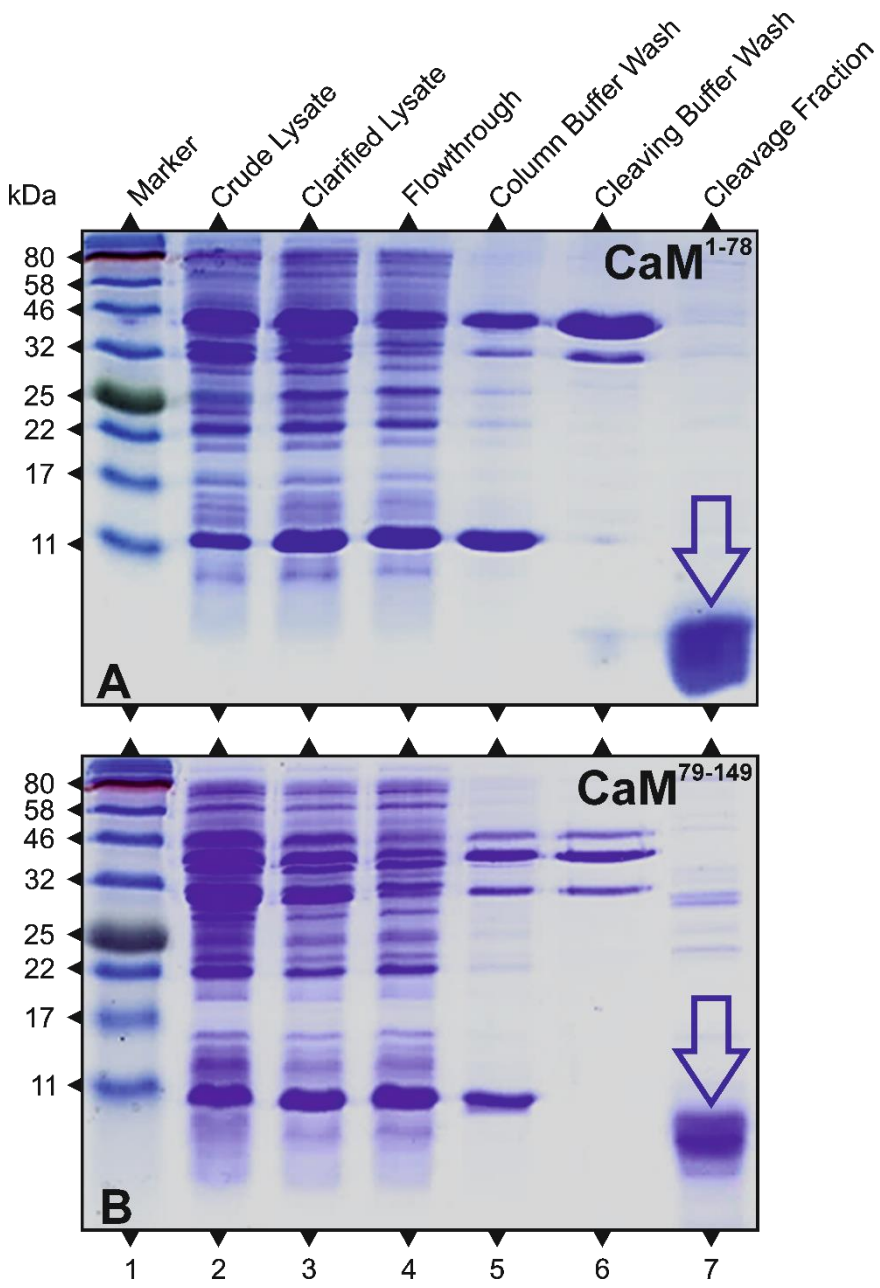

Figure 6-4 Changing Column Conditions Liberates the Lobes of CaM from 6xHis-SUMO-Intein-CaM Lobes Immobilised on Ni-NTA

BL21-CodonPlus were transformed with either pHSIE-CaM$^{1-78}$ (A) and pHSIE-CaM$^{79-149}$ (B) induced with 0.1 mM IPTG were lysed and applied to Ni-NTA resin column. The column was washed, and conditions were altered to those optimal for Intein self-cleavage. Fractions collected at every step were separated by 15 % (w/v) SDS-PAGE and stained with Coomassie . Lane 1: Color Prestained Protein Standard (NEB). Lane 2: 2 µl crude lysate. Lane 3: 5 µl clarified lysate. Lane 4: 5 µl of flowthrough. Lane 5: 15 µl of wash 1. Lane 6: 15 µl of wash 2. Lane 7: 10 µl of cleavage fraction.

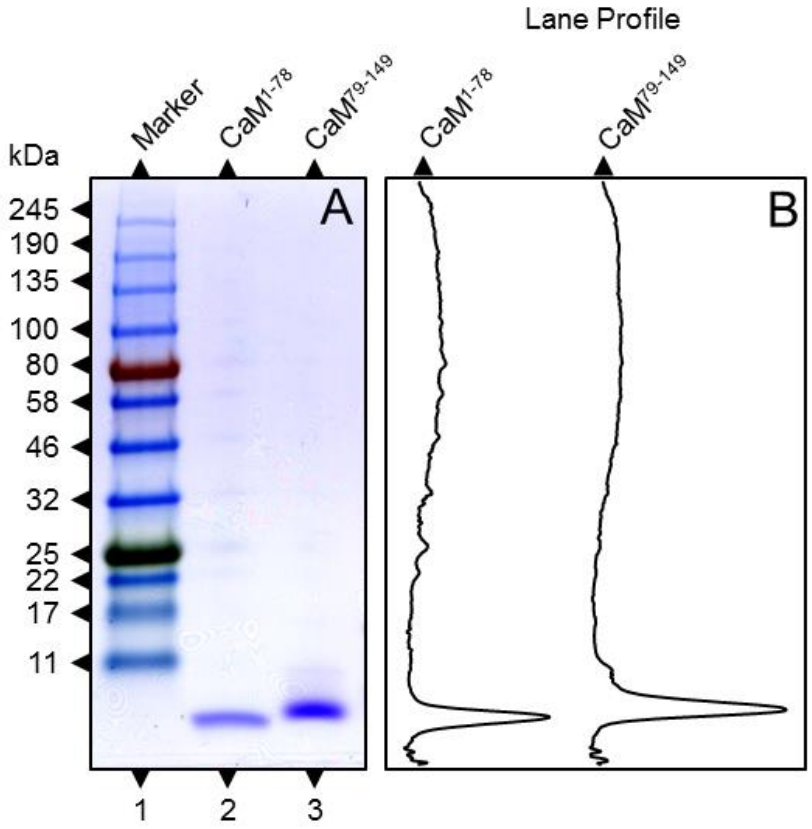

Figure 6-5 Purified Calmodulin Lobes Resolve as Major Bands of the Correct Apparent Molecular Weight

Cleavage fractions from Ni-NTA resin column purification were pooled and separated by SDS-PAGE. Coomassie staining revealed only one band of approximately 8 kDa. (A) Coomassie stained 20 % (w/v) SDS-PAGE gel, Lane 1: Color Prestained Protein Standard (NEB), Lane 2: CaM1-78, Lane 3: CaM79-149. (B) Profile of Lanes 1&2.

6.3.3 Isothermal Titration Calorimetry

Constant power was supplied to a heater keeping a calorimetric cell and reference cell isothermal. A feedback loop ensures the increase or decrease in power as required in response to temperature fluctuations. The power required during and after successive injections of titrant into the calorimetric cell containing analyte corresponds to heat changes associated with the interaction between the titrant and the analyte. Increased power supply corresponds to work by the calorimeter heater to keep the calorimetric cell isothermal as the temperature decreases due to heat absorbance during the titrant-analyte interaction. Therefore, the observed interaction is endothermic. However, reduced power supply indicates that the calorimeter is doing less work to keep the calorimetric cell isothermal as temperature increases due to heat production by the titrant-analyte interaction. Therefore, the observed interaction is exothermic. The power required plotted against time produces a heat graph which can be further analysed to provide a binding curve for the interaction.

In the following experiments, the titrant was peptide, and the analyte was recombinant CaM protein, both were dissolved in the same buffer containing either saturating Ca^{2+} or EDTA. For each peptide appropriate control experiments of peptide titrated into buffer were carried out. Subtracting the appropriate control heat graph from the experimental heat graph produced a net heat graph. The area under each injection was integrated and normalised to the molarity of the titrant. For each ITC experiment, the normalised heat was plotted against the molar ratio of titrant to the analyte. A non-linear least-square fit curve, assuming a model of 1:1 ligand-protein binding, was fitted to the titration data to provide a binding isotherm representative of

the interaction`s thermodynamic profile. The binding curve enables the precise determination of the thermodynamic parameters of the binding reaction, i.e., K_d, stoichiometry (N), enthalpy (ΔH) and entropy (ΔS).

6.3.4 Thermodynamic Studies of the Interaction of Calmodulin and PLCζ

6.3.4.1 Interaction Between Calmodulin and the XY Linker of PLCζ

The thermodynamics of the interaction between PLCζ XY linker and CaM were determined using ITC to investigate the specific region of the XY linker involved. ITC experiments, with the peptides corresponding to specific regions of PLCζ XY linker as titrants and CaM^{WT} as analyte, were performed in the presence and absence of Ca^{2+} at 298.15 K. Net heat graphs and binding isotherms for the interaction of peptides N, M and C with CaM in the presence and absence of Ca^{2+} are shown in Figure 6-6 and Figure 6-7 respectively. The derived thermodynamic parameters are shown in Table 6-1.

In the presence of Ca^{2+}, only the injection of peptide C into CaM^{WT} increases the required power supply, as shown in Figure 6-6, indicating that heat is absorbed. The absorption of heat indicates an endothermic binding reaction occurs between CaM and peptide C. No change in power was detected when peptides N and M were injected. Therefore, no interaction between CaM and either N or M was detected. CaM binds peptide C with high affinity at a 1:1 ratio as can be seen in Table 6-1 due to the low K_d value of 0.53 μM and N of ~1. The binding of CaM and peptide C is driven by entropy as indicated by the unfavourable positive value for binding enthalpy change

(ΔHb) being outweighed by the greater, more favourable negative value for the entropic term (-T·ΔSb).

However, in the absence of Ca^{2+} no change in power supply was detected when PLCζ peptides N, M or C were injected into CaM^{WT} as can be seen in Figure 6-7. The lack of change in power indicates no interaction occurred between any of the three peptides PLCζ and CaM.

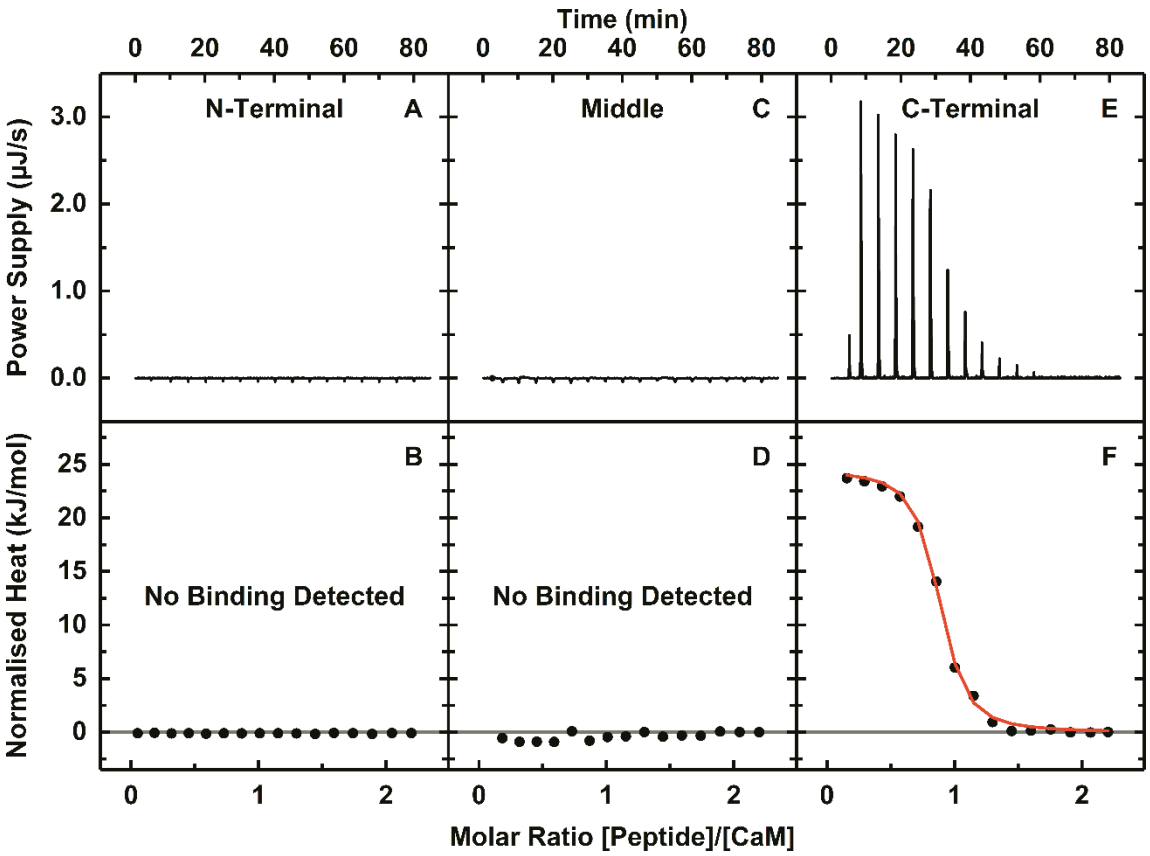

Figure 6-6 Full-Length Calmodulin Specifically Binds the C-Terminal of the XY Linker of PLCζ in the Presence of Ca^{2+}

Changes in the power supplied to an isothermal calorimetric cell containing 72 µM recombinant CaM protein accompanying successive injections of 750 µM peptide C were recorded. Both protein and peptides were dissolved in 10 mM HEPES pH 7.4, 100 mM KCl, 10 mM $CaCl_2$. Net heat graphs (Top) and concentration normalised enthalpograms (bottom) for the titration of (A&B): Peptide N, (C&D): Peptide M and (E&F): Peptide C into CaM^{WT} at 25 °C. The solid red line represents the best fit of a single-set-of-sites binding model to the ITC data. Positive signals indicate endothermic processes.

Table 6-1 Thermodynamic Properties of the Interaction Between Calmodulin and the XY Linker of PLCζ

	Kinetics of interaction with CaM^{WT} in the presence of Ca^{2+}				
Peptide	Dissociation Constant (μM)	Stoichiometry	Binding Enthalpy (kJ/mol)	Entropic Term (kJ/mol)	Gibbs Free Energy Change (kJ/mol)
C	0.53 ± 0.07	0.97 ± 0.01	17.4 ± 0.3	-53.3 ± 0.4	-35.9 ± 0.3
N	No Binding Detected				
M	No Binding Detected				

Dissociation Constant (K_d) Stoichiometry (N) binding enthalpy changes (ΔH_b), entropic term changes ($-T \cdot \Delta S_b$) and free energy changes (ΔG_b) for the binding of various peptides to CaM^{WT} at 25°C in Ca^{2+}-saturated buffer (n=3). Values and corresponding errors were derived from non-linear least square fit of the ITC data to a single set-of-sites binding model.

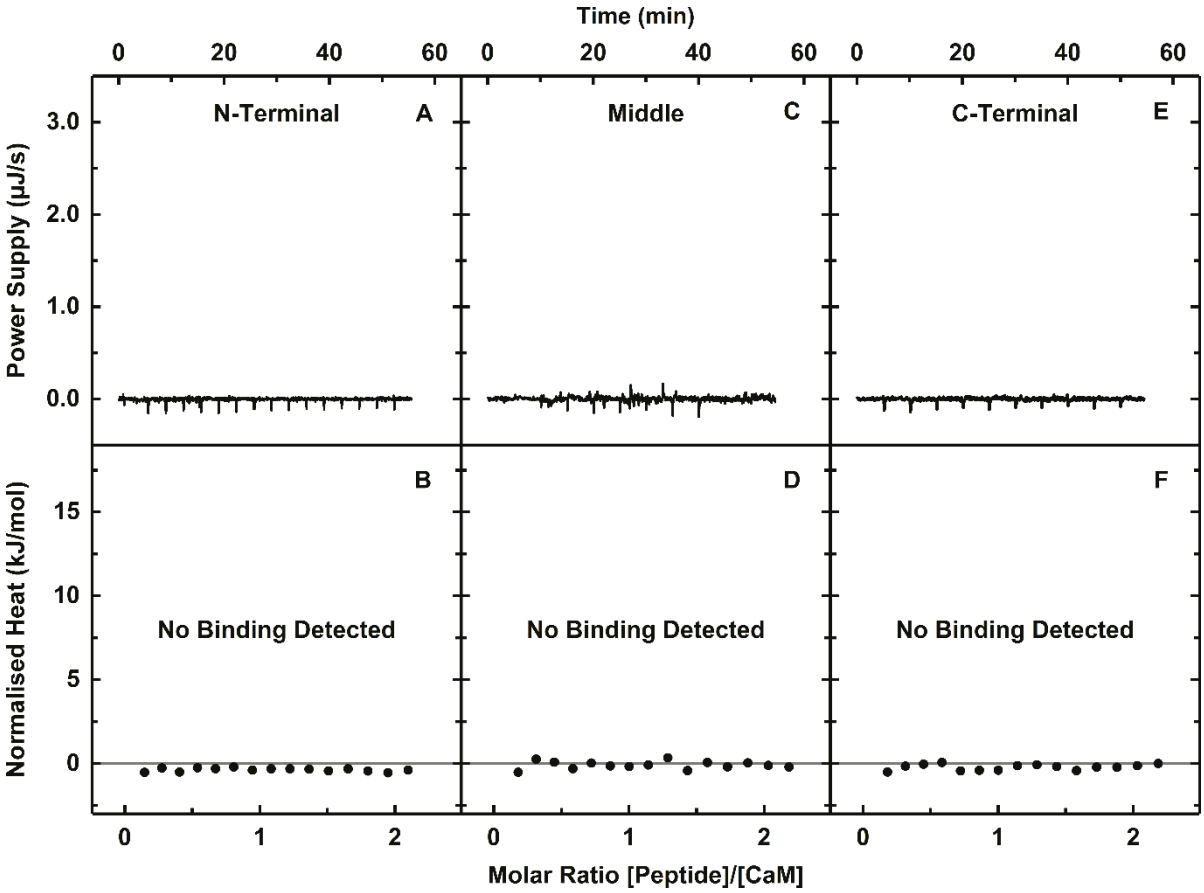

Figure 6-7 Full-Length Calmodulin Does Not Bind the XY Linker of PLCζ in the Absence of Ca^{2+}

Changes in the power supplied to an isothermal calorimetric cell containing 72 µM recombinant CaM protein accompanying successive injections of 750 µM peptide C were recorded. Both protein and peptides were dissolved in 10 mM HEPES pH 7.4, 100 mM KCl, 10 mM EDTA. Net heat graphs (Top) and concentration normalised enthalpograms (bottom) for the titration of (A&B): Peptide N, (C&D): Peptide M and (E&F): Peptide C into CaM^{WT} at 25 °C.

6.3.4.2 Interaction Between Calmodulin and the C-Terminal Region of the PLCζ XY Linker.

The thermodynamics of the interaction between PLCζ XY linker and CaM were further investigated using ITC to determine if a specific CaM lobe was involved in the binding of CaM to PLCζ XY linker C-terminal region the specific region of the XY linker involved. ITC experiments with PLCζ XY linker peptide C as titrant and CaM^{WT}, CaM^{1-78} and CaM^{79-149} as analytes were performed in the presence of Ca^{2+} at 298.15 K. Nett heat graphs and binding isotherms for the titration of CaM^{WT}, CaM^{1-78} and CaM^{79-149} with peptide C in the presence of Ca^{2+} are shown in Figure 6-8 and the derived thermodynamic parameters are shown in Table 6-2.

The injection of peptide C into CaM^{WT} and C-lobe of CaM elicited an increase in power required indicating that heat is absorbed. The absorption of heat indicates an endothermic binding reaction occurs between peptide C and both CaM^{WT} and C-lobe of CaM. The injection of peptide C into the N-lobe did not result in any change in the power supply. Therefore, no interaction between CaM N-lobe and peptide C occurred.

Like the interaction of CaM and peptide C, entropy drives C-lobe and peptide C binding. The negative -TΔSb value outweighed the unfavourable positive ΔHb value, as can be seen in Table 6-2. However, the binding affinity of peptide C and C-lobe is much reduced compared to CaM^{WT} with a 100-fold increase in K_d 0.53 versus 52.06 μM, Table 6-2.

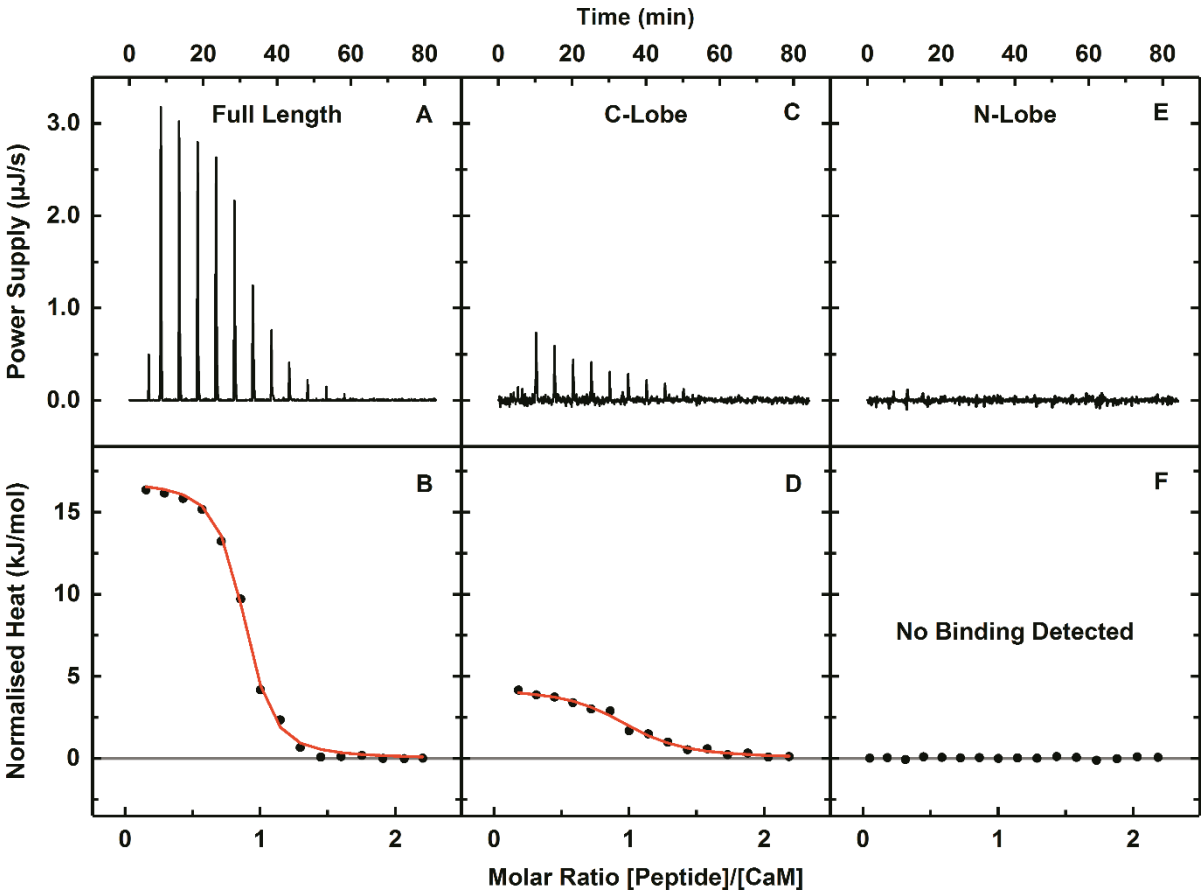

Figure 6-8 The C-Lobe of Calmodulin Specifically Binds the C-Terminal Region of PLCζ XY Linker but the N-Lobe Does Not

Changes in the power supplied to an isothermal calorimetric cell containing 72 µM recombinant CaM protein accompanying successive injections of 750 µM peptide C were recorded. Both protein and peptides were dissolved in 10 mM HEPES pH 7.4, 100 mM KCl, 10 mM $CaCl_2$. Net heat graphs (top) and concentration normalised enthalpograms (bottom) for the titration of Peptide C into (A&B): CaM^{WT}, (C&D): CaM^{79-149} and (E&F): CaM^{1-78} at 25 °C. The solid red line represents the best fit of a single-set-of-sites binding model to the ITC data. Positive signals indicate endothermic processes.

Table 6-2 Thermodynamic Properties of the Interaction Between Full Length, and the Amino and Carboxyl Lobes of Calmodulin and the Carboxyl-Terminal Region of the PLCζ XY Linker.

	Kinetics of interaction with Peptide C in the presence of Ca^{2+}				
Protein	Dissociation Constant (μM)	Stoichiometry	Binding Enthalpy (kJ/mol)	Entropic Term (kJ/mol)	Gibbs Free Energy Change (kJ/mol)
CaM^{WT}	0.53 ± 0.07	0.97 ± 0.01	17.4 ± 0.3	-53.3 ± 0.4	-35.9 ± 0.3
CaM^{1-78}	No binding				
CaM^{79-149}	52.06 ± 8.51	1.05 ± 0.02	9.9 ± 0.9	-34.3 ± 1.0	-24.4 ± 0.4

Dissociation Constant (K_d) Stoichiometry (N) binding enthalpy changes (ΔH_b), entropic term changes ($-T \cdot \Delta S_b$) and free energy changes (ΔG_b) for the binding of a PLCζ peptide C to CaM^{WT}, CaM^{79-149} and CaM^{1-78} proteins at 25°C in Ca^{2+}-saturated buffer (n=3). Values and error values were derived from non-linear least square fit of the ITC data to a single set-of-sites thermodynamic model of binding.

6.3.5 Thermodynamic Studies of the Interaction of Disease Associated Calmodulin Mutations and Ryanodine Receptor 2

6.3.5.1 Interaction Between Calmodulin and Calmodulin Binding Domain 2 of Ryanodine Receptor 2

The thermodynamics of the interaction between the CaMBD2 of RyR2, and wildtype CaM and mutants of CaM associated with disease were determined using ITC. ITC experiments with RyR2 peptide B as titrant and CaM^{WT} or CaM^{MUT} proteins as analytes were performed in the presence and absence of Ca^{2+} at 298.15 K. The CaM^{MUT} proteins were CaM^{N98I}, CaM^{D132E}, CaM^{D134H} and CaM^{Q136P}. Nett heat graphs and binding isotherms for the interaction of peptide B and CaM proteins in the presence and absence of Ca^{2+} are shown in Figure 6-9 and Figure 6-10, respectively. The derived thermodynamic parameters from Figure 6-9 and Figure 6-10 are shown in Table 6-3 and Table 6-4.

In the presence of Ca^{2+}, the injection of peptide B into both CaM^{WT} and CaM^{MUT} results in a reduction in the power supply required, as shown in Figure 6-9, indicating that heat is produced. The production of heat indicates an exothermic binding reaction between CaM and peptide B occurs regardless of arrhythmogenic mutations. Both CaM^{WT} and CaM^{MUT}, have significant binding affinities for RyR2 peptide B with K_d values of less than 1 μM, as can be seen in Table 6-3. However, K_d values for RyR2 peptide B binding to CaM^{D134H} and CaM^{Q136P} are slightly raised compared to WT indicating that the mutants have a slightly lower affinity for peptide B than WT. In contrast, CaM^{N98I} and CaM^{D132E} display values of K_d for peptide B lower than that of CaM^{WT} indicating that these mutants have a higher affinity for RyR2 peptide B than

WT. The stoichiometry each binding reaction is 1, so both wildtype and mutants bind to peptide B at ratio 1:1 and enthalpy drives the binding. In the absence of Ca^{2+}, an increase in demand for power accompanies the injection of peptide B into CaM^{WT} only, as shown in Figure 6-10. The increase in power indicated that heat is absorbed, so an endothermic binding reaction has occurred. No change in power was observed for the injections of RyR2 peptide B into CaM^{MUT} proteins, so no detectable binding of biologically significant level occurred between the mutations and peptide B in the absence of Ca^{2+}. The thermodynamics of the binding between CaM^{WT} and RyR2 peptide B in Ca^{2+} free conditions as can be seen in Table 6-4 and differ from those observed in the presence of Ca^{2+} shown in Table 6-3. The affinity of apoCaM for peptide B is weaker than that of holoCaM, K_d of 14.03 ± 2.40 μM versus 0.35 ± 0.03 μM. Also in contrast to holoCaM, the binding of apoCaM and peptide B is driven by entropy.

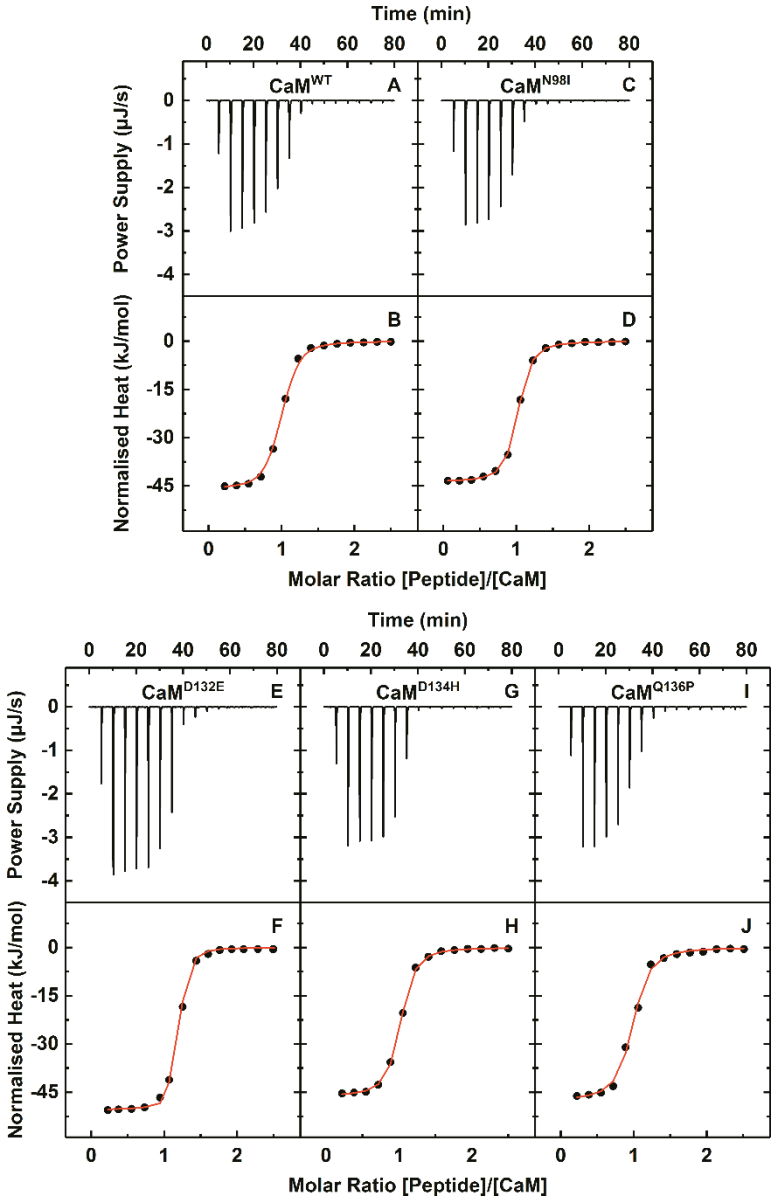

Figure 6-9 In the Presence of Ca^{2+} Binding Between Calmodulin and the CaMBD2 of Ryanodine Receptor 2 Occurs with Reduced Affinity in Mutants of CaM Associated with Arrhythmia

Changes in the power supply to an isothermal calorimetric cell containing 45 µM CaM^{WT} or CaM^{MUT} proteins accompanying successive injections of 450 µM peptide B were recorded. Both proteins and peptide were dissolved in 10 mM HEPES pH 7.4, 100 mM KCl, 10 mM CaCl2. Net heat graphs and concentration normalised enthalpograms respectively for the titration of Peptide B at 25 °C into (A & B) CaM^{WT}, (C & D) CaM^{N98I}, (E & F) CaM^{D132E}, (G & H) CaM^{D134H} and (I & J) CaM^{Q136P}. Solid red lines represent the non-linear least-square fit of the ITC data to a single-set-of-sites thermodynamic model.

Table 6-3 Thermodynamic Properties of the Interaction Between RyR2 peptide B and Wild-Type & Disease-associated Mutations of Calmodulin in the Presence of Ca^{2+}

	Kinetics of interaction with Peptide B in the presence of Ca^{2+}				
Protein	Dissociation Constant (μM)	Stoichiometry	Binding Enthalpy (kJ/mol)	Entropic Term (kJ/mol)	Gibbs Free Energy Change (kJ/mol)
CaM^{WT}	0.35 ± 0.03	0.93 ± 0.01	-45.9 ± 1.4	9.1 ± 1.4	0.35 ± 0.03
CaM^{N98I}	0.29 ± 0.01	0.94 ± 0.01	-43.8 ± 1.3	6.5 ± 1.3	0.29 ± 0.01
CaM^{D132E}	0.16 ± 0.01	1.09 ± 0.01	-50.8 ± 1.6	11.9 ± 1.6	0.16 ± 0.01
CaM^{D134H}	0.36 ± 0.03	0.97 ± 0.01	-46.2 ± 1.5	9.5 ± 1.6	0.36 ± 0.03
CaM^{Q136P}	0.42 ± 0.02	0.97 ± 0.01	-47.9 ± 1.5	11.5 ± 1.6	0.42 ± 0.02

Dissociation Constant (K_d) Stoichiometry (N) binding enthalpy changes (ΔH_b), entropic term changes ($-T\cdot\Delta S_b$) and free energy changes (ΔG_b) for the interaction of hRyR2 peptides and CaM^{WT}, CaM^{N98I}, CaM^{D132E}, CaM^{D134H}, and CaM^{Q136P}, at 25 °C in Ca^{2+}-saturated buffer (n=3). Values and errors values were derived from non-linear least square fit of the ITC data to a one-set-of-sites thermodynamic model.

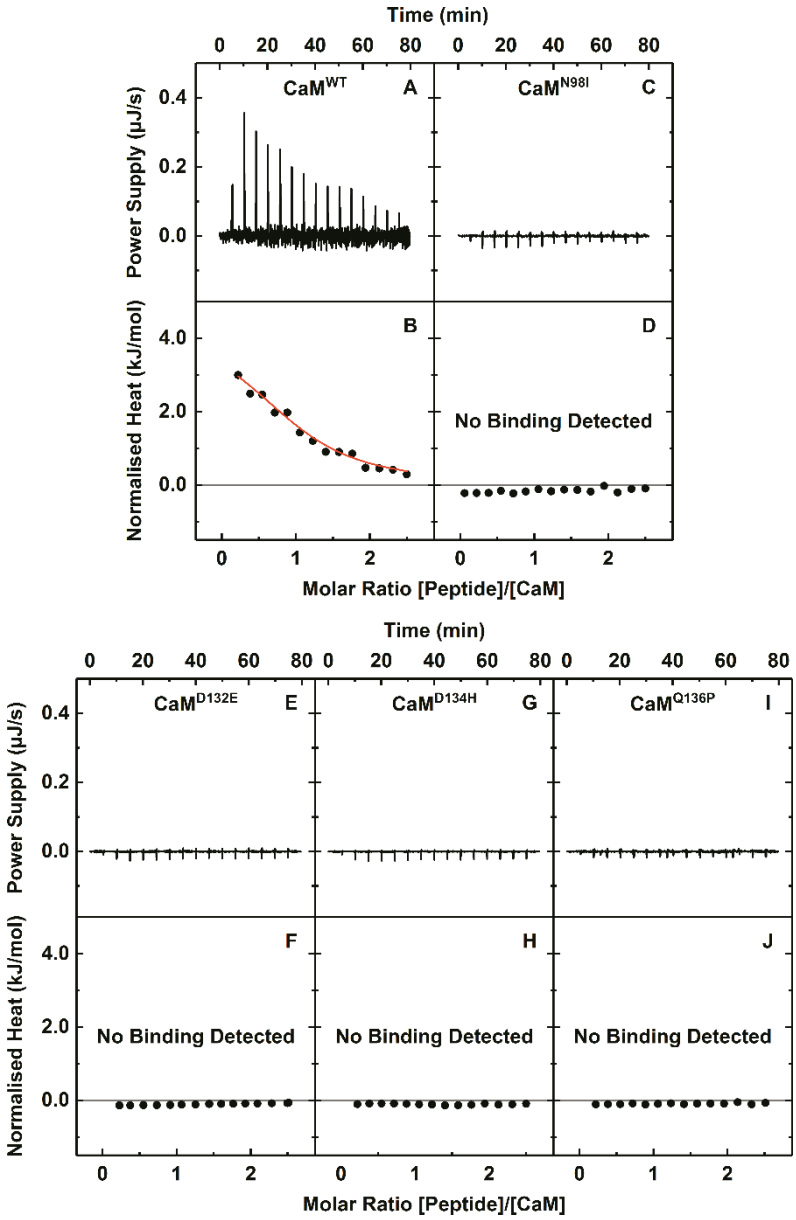

Figure 6-10 Arrhythmia Associated Calmodulin Mutations Abolish Binding Between Calmodulin and the CaMBD2 of Ryanodine Receptor 2 in the Absence of Ca^{2+}

Changes in the power supply to an isothermal calorimetric cell containing 45 µM CaM^{WT} or CaM^{MUT} proteins accompanying successive injections of 450 µM peptide B were recorded. Both proteins and peptide were dissolved in 10 mM HEPES pH 7.4, 100 mM KCl, 10 mM $CaCl_2$. Net heat graphs and concentration normalised enthalpograms respectively for the titration of Peptide B at 25 °C into (A & B) CaM^{WT}, (C & D) CaM^{N98I}, (E & F) CaM^{D132E}, (G & H) CaM^{D134H} and (I & J) CaM^{Q136P}. Solid red lines represent the non-linear least-square fit of the ITC data to a single-set-of-sites thermodynamic model.

Table 6-4 Thermodynamic Properties of the Interaction Between RyR2 Peptide B and Wild-type & Disease-Associated Mutations of Calmodulin in the Absence of Ca^{2+}

	Kinetics of interaction with Peptide B in the absence of Ca^{2+}				
Protein	Dissociation Constant (μM)	Stoichiometry	Binding Enthalpy (kJ/mol)	Entropic Term (kJ/mol)	Gibbs Free Energy Change (kJ/mol)
CaM^{WT}	14.03 ± 2.40	1.04 ± 0.01	6.3 ± 0.9	-34.0 ± 1.0	-27.7 ± 0.4
CaM^{N98I}	No binding detected				
CaM^{D132E}	No binding detected				
CaM^{D134H}	No binding detected				
CaM^{Q136P}	No binding detected				

Dissociation Constant (K_d) Stoichiometry (N) binding enthalpy changes (ΔH_b), entropic term changes ($-T\cdot\Delta S_b$) and free energy changes (ΔG_b) for the interaction of hRyR2 peptide B and CaM samples at 298.15 K in Ca^{2+}-chelating buffer (n=3). Values and error values were derived from non-linear least square fit of the ITC data to a one-set-of-sites thermodynamic model.

6.3.5.2 Interaction Between Calmodulin and Calmodulin Binding Domain 3 of Ryanodine Receptor 2

The thermodynamics of the interaction between the CaMBD3 of RyR2, and wildtype CaM and mutants of CaM associated with disease were determined using ITC. A series of ITC experiments with RyR2 peptide F as titrant and CaM^{WT} or CaM^{MUT} proteins as analytes were performed in the presence and absence of Ca^{2+} at 298.15 K. Net heat graphs and binding isotherms for the interaction of peptide F and CaM proteins in the presence and absence of Ca^{2+} are shown in Figure 6-11 and Figure 6-12 respectively. The derived thermodynamic parameters from Figure 6-11 and Figure 6-12 are shown in Table 6-5 and Table 6-6.

In the presence of Ca^{2+}, the injection of peptide F into both CaM^{WT} and CaM^{MUT} results in changes in the power supply required, as shown in Figure 6-11. The changes in power indicate alterations in temperature associated with binding of CaM^{WT} and CaM^{MUT} to peptide F. When CaM^{WT}, CaM^{N98I} or CaM^{D132E} are present power increases on the injection of peptide F indicating that heat is absorbed so the binding observed is endothermic. However, as can be seen in Figure 6-11, the power supply is reduced upon injection of peptide F when CaM^{D134H} or CaM^{Q136P} are present indicating that heat is released, so binding is exothermic.

In the absence of Ca^{2+}, an increase in demand for power accompanies only the injection of peptide F into CaM^{WT}, as shown in Figure 6-12. The increase in power indicated that heat is absorbed, so an endothermic binding reaction has occurred. No change in power was observed for the injections of RyR2 peptide F into CaM^{MUT}

proteins, so no detectable binding of a biologically significant level occurred between the mutations and peptide F in the absence of Ca^{2+}. The thermodynamic parameters of the binding between CaM^{WT} and RyR2 peptide F differ in the absence and presence of Ca^{2+} as can be seen in Table 6-5 and Table 6-6. The affinity of apoCaM for peptide F is weaker than that of holoCaM, K_d of 16.58 ± 3.22 μM versus 0.60 ± 0.05 μM. The binding of apoCaM and peptide B is at a ratio of 1:1 and driven by entropy.

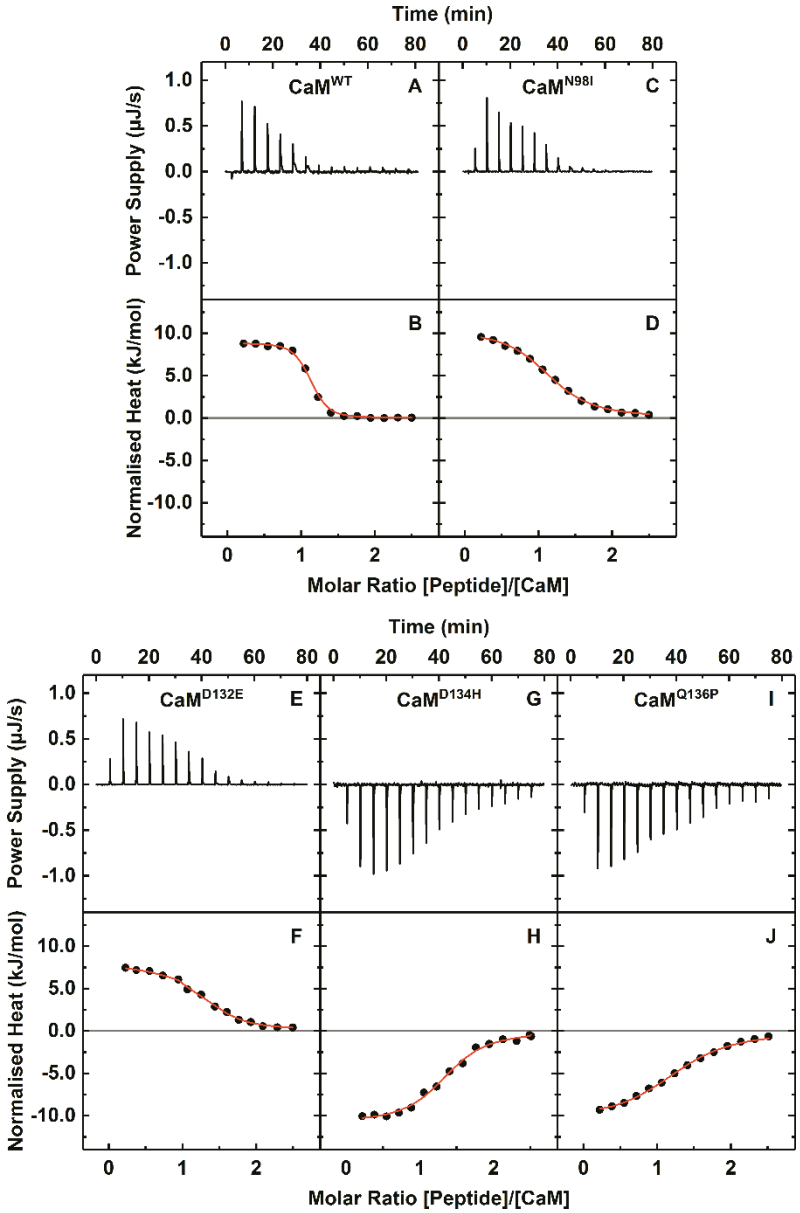

Figure 6-11 Mutations of Calmodulin Associated with Arrhythmia have Divergent Effects on the Binding of Calmodulin and the CaMBD3 of Ryanodine Receptor 2 in the Presence of Ca^{2+}

Changes in the power supply to an isothermal calorimetric cell containing 45 µM CaM^{WT} or CaM^{MUT} proteins accompanying successive injections of 450 µM peptide F were recorded. Both proteins and peptide were dissolved in 10 mM HEPES pH 7.4, 100 mM KCl, 10 mM $CaCl_2$. Net heat graphs and concentration normalised enthalpograms respectively for the titration of Peptide B at 25 °C into (A & B) CaM^{WT}, (C & D) CaM^{N98I}, (E & F) CaM^{D132E}, (G & H) CaM^{D134H} and (I & J) CaM^{Q136P}. Solid red lines represent the non-linear least-square fit of the ITC data to a single-set-of-sites thermodynamic model.

Table 6-5 Thermodynamic Properties of the Interaction Between Ryanodine Receptor 2 Peptide F and Wild-Type & Disease-Associated Mutations of Calmodulin in the Presence of Ca^{2+}

	Kinetics of interaction with Peptide F in the presence of Ca^{2+}				
Protein	Dissociation Constant (μM)	Stoichiometry	Binding Enthalpy (kJ/mol)	Entropic Term (kJ/mol)	Gibbs Free Energy Change (kJ/mol)
CaM^{WT}	0.60 ± 0.05	1.05 ± 0.01	8.9 ± 0.4	-44.4 ± 0.5	-35.5 ± 0.2
CaM^{N98I}	2.99 ± 0.28	1.04 ± 0.01	9.5 ± 0.4	-41.0 ± 0.5	-31.5 ± 0.3
CaM^{D132E}	2.13 ± 0.15	1.06 ± 0.01	8.1 ± 0.4	-40.5 ± 0.5	-32.4 ± 0.2
CaM^{D134H}	2.54 ± 0.39	1.16 ± 0.02	-10.9 ± 0.4	-21.1 ± 0.6	-31.9 ± 0.4
CaM^{Q136P}	5.92 ± 0.50	1.09 ± 0.01	-10.5 ± 0.4	-19.3 ± 0.5	-29.8 ± 0.2

Dissociation Constant (K_d) Stoichiometry (N) binding enthalpy changes (ΔH_b), entropic term changes ($-T \cdot \Delta S_b$) and free energy changes (ΔG_b) for the interaction of hRyR2 peptides and CaM samples at T = 298.15 K in Ca^{2+}-saturated buffer (n=3). Values and error values were derived from non-linear least square fit of the ITC data to a one-set-of-sites thermodynamic model.

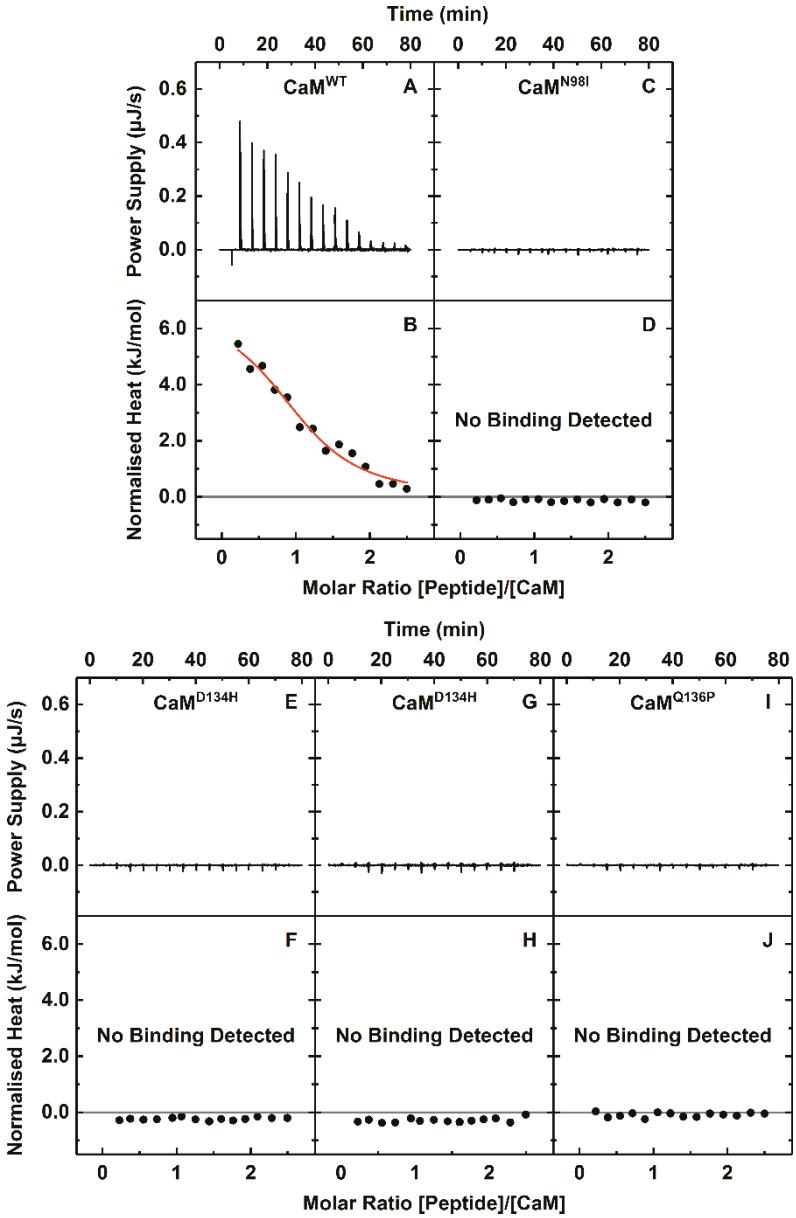

Figure 6-12 CaM Mutations Associated with Arrhythmias Abolish Binding Between Calmodulin and the CaMBD3 of Ryanodine Receptor 2 in the Absence of Ca^{2+}

Changes in the power supply to an isothermal calorimetric cell containing 45 µM CaM^{WT} or CaM^{MUT} proteins accompanying successive injections of 450 µM peptide F were recorded. Both proteins and peptide were dissolved in 10 mM HEPES pH 7.4, 100 mM KCl, 10 mM EDTA. Net heat graphs and concentration normalised enthalpograms respectively for the titration of Peptide B at 25 °C into (A & B) CaM^{WT}, (C & D) CaM^{N98I}, (E & F) CaM^{D132E}, (G & H) CaM^{D134H} and (I & J) CaM^{Q136P}. Solid red lines represent the non-linear least-square fit of the ITC data to a single-set-of-sites thermodynamic model.

Table 6-6 Thermodynamic Properties of the Interaction Between Ryanodine Receptor 2 Peptide F and Wild-type & Disease-Associated Mutations of Calmodulin in the Absence of Ca^{2+}

	Kinetics of interaction with Peptide F in the absence of Ca^{2+}				
Protein	Dissociation Constant (μM)	Stoichiometry	Binding Enthalpy (kJ/mol)	Entropic Term (kJ/mol)	Gibbs Free Energy Change (kJ/mol)
CaM^{WT}	16.58 ± 3.22	0.96 ± 0.01	6.6 ± 0.5	-33.9 ± 0.7	16.58 ± 3.22
CaM^{N98I}	No binding detected				
CaM^{D132E}	No binding detected				
CaM^{D134H}	No binding detected				
CaM^{Q136P}	No binding detected				

Dissociation Constant (K_d) Stoichiometry (N) binding enthalpy changes (ΔH_b), entropic term changes ($-T \cdot \Delta S_b$) and free energy changes (ΔG_b) for the interaction of hRyR2 peptide F and CaM samples at 298.15 K in Ca^{2+} chelating buffer (n=3). Values and error values were derived from non-linear least square fit of the ITC data to a one-set-of-sites thermodynamic model.

6.4 Discussion

This chapter describes the expression and purification of the isolated N- and C- lobes of CaM. Together with CaM^{WT} described in Chapter 4, the CaM lobes were used with peptides corresponding to PLCζ in ITC experiments to investigate the binding of CaM and PLCζ. Additionally, ITC experiments with CaM^{WT} and CaM^{MUT} proteins and peptides corresponding to RyR2 CaMBD2 and CaMBD3 probed the interaction of CaM with RyR2 and the effect of arrhythmogenic mutations on the interaction.

Of the three PLCζ peptides, only the peptide corresponding to the C-terminal residues of the XY linker bound to CaM^{WT} and only in the presence of Ca^{2+}. The binding was of high affinity, endothermic and driven by entropy. None of the peptides bound to CaM^{WT} in the absence of Ca^{2+}. Therefore, CaM^{WT} and PLCζ bind via the C-terminal region of the XY linker of PLCζ and binding is dependent on Ca^{2+}. The binding of Ca^{2+} to CaM induces a conformational change that exposes hydrophobic patches on both lobes to potential binding partners (Babu, Bugg and Cook, 1988; Finn and Forsén, 1995). Dehydration of hydrophobic patches at the interface between binding proteins is a typical entropy driven protein binding mechanism (Makhatadze and Privalov, 1995). Therefore, it appears that the binding of Ca^{2+} to the EF hands of CaM elicits conformational changes that expose regions of CaM to the solvent. The solvent-exposed areas enable recognition by PLCζ and the shielding of the solvent-exposed hydrophobic surface upon complex formation drives the binding.

Each lobe of CaM was titrated individually with peptide C in the presence of Ca^{2+} to investigate whether the observed binding between CaM^{WT} and peptide C

occurred via a specific lobe of CaM. In the ITC experiments, C-lobe and N-lobe solutions replaced WT CaM in Ca^{2+}-saturated conditions. Peptide interacted with C-lobe of CaM but not the N-lobe of CaM. Similar to binding between CaM^{WT} and peptide C the binding is endothermic and driven by entropy with binding affinity between peptide C and CaM C-lobe reduced 100-fold compared to peptide C and CaM^{WT}. The significant albeit reduced binding affinity between peptide C and CaM C-lobe alone indicates that the C-lobe of CaM is the primary binding site for PLCζ via the C-terminal region of the XY linker. However, the N-lobe of Ca^{2+} may also be required to help form a hydrophobic cleft enables the observed higher binding affinity observed between CaM^{WT} and peptide C. In docking simulation experiments the peptide bound to a central hydrophobic region between the two CaM lobes is the best-scoring structure of the Peptide C/CaM complex (Nomikos, Thanassoulas, *et al.*, 2017).

In summary, a peptide corresponding to the PLCζ XY linker C-terminal region bound to CaM^{WT} with high affinity and the C-lobe of CaM with reduced affinity but only in the presence of Ca^{2+}. The entropy driven binding is Ca^{2+}-dependent, presumably due to Ca^{2+} conformational changes enabling target recognition and binding. Therefore, it appears specific residues in PLCζ XY linker bind to residues in the C-lobe CaM exposed to the solvent upon Ca^{2+}-binding. The N-lobe of CaM does not bind PLCζ within the XY linker but does contribute to high-affinity binding possibly by forming a hydrophobic pocket to accommodate the PLCζ.

In the presence of $Ca^{2+,}$ both WT and mutant CaM proteins bind to RyR2 peptide B with high affinity at a 1:1 ratio. For both WT and mutant, the mode of binding is the same. Enthalpy driven binding indicates that hydrogen bonds and hydrophobic

interactions between multiple residues in the protein and peptide are responsible. However, D134H and Q136P mutants reduce the binding affinity of holo-CaM for peptide B compared to WT representing a LOF. The other mutants, N98I and D132E, display a GOF with a higher affinity for peptide B compared to WT with lower K_d values in the case of D132E the K_d is approximately 50 % that of WT.

In contrast in the absence of $Ca^{2+,}$ only CaM^{WT} binds to peptide B, and the binding is endothermic. The lack of binding indicates the mutations confer a LOF. The binding affinity of apoCaM is considerably weaker than holoCaM with a K_d value forty-fold greater. Entropy drives the binding of peptide B to CaM in the absence of Ca^{2+}. The different binding modes for the apo- and holo-CaM binding to peptide B are most likely the result of the Ca^{2+} induced conformational change. The conformational change alters the peptide-protein interface resulting in the formation of the protein/peptide complex driven by the occlusion of solvent-exposed hydrophobic residues on the binding. The lack of binding in mutants indicates that N98I, D132E, D134H and Q136P mutations do not adopt a Ca^{2+} free conformation that permits the entropy-driven binding of peptide B.

Both CaM and CaM proteins bind RyR2 peptide F at 1:1 ratio in the presence of Ca^{2+}. However mutant CaMs display a significantly decreased affinity for peptide F compared to WT. The 3- to 10-fold increase in K_d values can be ranked 132<134<98<136 and represents a diverged function. Notably, the binding of RyR2 peptide F to WT, N98I and D132E is endothermic while to D134H, and Q136P binding is exothermic. The drastic difference in thermodynamic signatures suggests a different

binding site or that D134H and Q136P are aligned to the peptide differently on complex formation with peptide F compared to WT, N98I and D132E.

Comparable to peptide B in the absence of Ca^{2+} peptide F only binds to CaM^{WT}, the binding is endothermic and entropically driven. In the absence of Ca^{2+} CaM has similar affinities for peptide B and peptide F. Entropy drives binding of peptide F with both holoCaM and apoCaM. However, with a 30-fold greater K_d the apo-CaM has a reduced affinity for peptide F compared to holoCaM, though it follows a similar entropically-driven process. The lower affinity of apoCaM for peptide F binding is due to the less favourable entropic term. The reduced entropic term on Ca^{2+}-binding could be due to conformational changes result in either altered peptide/protein complex flexibility, hydrophobic residues exposure or both. Structural data of the CaM/peptide F complex would clarify the mechanistic basis of the difference. Like peptide B, the mutations disrupt the binding of CaM to peptide F in the absence of Ca^{2+} representing a LOF.

In summary, CaM binds peptide B exothermically and peptide F endothermically with similar affinities in the presence of Ca^{2+}. In the absence of Ca^{2+} endothermic binding occurs between CaM and both peptide B and peptide F with similar binding affinities that are reduced compared to holoCaM. The presence of the mutations have divergent effects on the binding of CaM and peptides B and F. In the presence of Ca^{2+} the mutations alter the affinities of peptide B and F and can alter the mode of binding to peptide F. In the absence of Ca^{2+} the mutations appear to abolish the ability of CaM to bind the CaMBD and CaMLD of RyR2.

In the presence of Ca^{2+}, CaM specifically bound a peptide representing the C-terminal portion of the XY linker of PLCζ (Peptide C) with a high level of affinity at a ratio of 1:1. However, there was no detectable binding between CaM and peptides representing the N-terminal and middle of the XY linker of PLCζ.

Due to time and materials being limited it was not feasible to carry out all potential experiments using the peptides and recombinant proteins available. The individual lobes of CaM bearing arrhythmogenic mutations could be generated and used in further experiments.. Potential experiments include further examining the mechanisms behind RyR2 and CaM binding with ITC experiments of RyR2 peptides and the N- and C-lobes of CaM both mutant and wildtype. There is no data published regarding the effect of the CaM mutations on fertility and one mutation was inherited. However, ITC experiments coupled with PLCζ activity assays in the presence of CaM^{MUT} proteins,. both full length and the lobes, may yield informative data regarding the ability of CaM to regulate PLCζ activity.

6.5 Findings

In summary, the following novel findings were made in this chapter:

- N- and C-lobes of CaM can be expressed and purified as untagged proteins using a one-step purification protocol without requiring a multiple stage purification with an enzymatic cleavage step.
- CaM binds the C-terminal region of PLCζ XY linker via the C-lobe. However, high-affinity binding requires the N-lobe.

- Binding between human CaM and RyR2 CaMBDs is as previously published but with human sequence peptides.
- In the presence of Ca^{2+}, arrhythmogenic CaM mutations caused:
    - Reduced affinity for CaMBD2
    - Divergent effects on binding to CaMBD3
- In the absence of Ca^{2+}, arrhythmogenic CaM mutations abolished binding between CaM and both CaMBD2 and CaMBD3.

Chapter 7 - FINAL DISCUSSION

Initially, this thesis investigated methods to increase yields of PLCζ recombinant protein sufficiently for X-ray crystallography. The expression and solubility of the expressed proteins varied dependent on the fusion partners, amino acid coordinates and bacterial strain used. Several fusion partners were shown to increase expression levels. However, the quantity and solubility of recombinant proteins were insufficient for crystallisation experiments.

Nevertheless, some of the constructs could be useful in other studies and combined with the optimisation of other parameters, e.g. expression strain and inductions conditions. The results of the optimisation studies in this thesis re-enforced the utility of optimising multiple parameters when expressing problematic proteins and could be repeated with different fusion partners and affinity tags. High-throughput cloning and small-scale expression may be required to optimise expression of PLCζ further. Therefore, an application to access the MRC Oxford Protein Production Facility was prepared.

To further study a potential regulatory interaction between PLCζ and CaM an expression system to produce untagged, recombinant human CaM, CaM^{WT}, was developed. An antibody specific for CaM recognised CaM^{WT} which matched the established characteristics of CaM, e.g. mobility, size, secondary structure, thermal stability and Ca^{2+} binding affinity. The functional activity of CaM^{WT} with RyR2, i.e. binding to and inhibiting the activity of RyR2 was also as expected. Sufficient protein

was produced for ongoing experiments to establish optimal conditions for the crystallisation of the protein produced using this expression system.

The expression system for CaM^{WT} provided a suitable base for generating mutations of CaM recently identified in clinical cases of cardiac arrhythmias. None of the mutations affected the gross structure of CaM. All but one of the proarrhythmic CaM mutations were shown to alter the Ca^{2+}binding affinity of CaM. All the C-terminal mutations reduced the binding affinity for Ca^{2+} while the single N-terminal mutation did not. The thermal stability of CaM in the prescence of Ca^{2+} was reduced to varying degrees by the mutations with the exception of two. Generally, a decreased affinity for Ca^{2+} coincided with a reduction in thermal stability compared to CaM^{WT}. Altered interaction between RyR2 and CaM in the Co-IP assay coincided with greater [^{3}H]-ryanodine binding to RyR2 at high [Ca^{2+}]. Mutations linked with CPVT, LQTS and arrythmia with a mixture of characteristics were shown to have divergent effects on the ability of CaM to interact with RyR2. Additionally, in ITC experiments four CaM mutants with reduced RyR2 binding and inhibition, also had altered and abolished binding to RyR2 peptide sequences in the prescence and absence of Ca2+ respectively. The *in vitro* effects of the mutations on CaM, are summarised in Table 7-1.

Table 7-1 Summary of the *In Vitro* Effects of Arrhythmogenic Mutations on the Functional and Biophysical Charecterisitcs of Calmodulin

CaM Mutation	Ca^{2+} Binding Affinity*	Thermal Stability†	CaM binding to RyR2		RyR2 channel inhibition‖	CaM binding to CaMBD2¶		CaM binding to CaMBD3¶	
			Change‡	Ca^{2+} Dependent§		- Ca^{2+}	+ Ca^{2+}	- Ca^{2+}	+ Ca^{2+}
CaM^{N54I}	↔	1	↑	×	↓				
CaM^{D96V}	↓ 6	2	↑	×	↓				
CaM^{N98S}	↓ 1	1	↔	×	↔				
CaM^{N98I}	↓ 4	4	↓	✓	↓	×	↓ Affinity	×	↓ Affinity#
CaM^{D130G}	↓ 8	6	↓	×	↓				
CaM^{D132E}	↓ 7	5	↓	✓	↓	×	↓ Affinity	×	↓ Affinity#
CaM^{D134H}	↓ 5	8	↓	×	↓	×	↓ Affinity	×	↓ Affinity$^{\Delta}$
CaM^{Q136P}	↓ 3	7	↓	✓	↓	×	↓ Affinity	×	↓ Affinity$^{\Delta}$
CaM^{F142L}	↓ 2	3	↔	×	↔				

*C-Terminal Ca^{2+} Affinity Compared To CaM^{WT} the Difference Is Ranked With 1 Closest To the Value for CaM^{WT}

†T_M in the Presence of Ca^{2+} Ranked Compared to CaM^{WT}, With 1 Closest to the Value for CaM^{WT}

‡Compared to Binding of CaM^{WT}

§Significant Difference Only Observed at High [Ca^{2+}]

¶Compared to Binding of Peptide to CaM^{WT}

#Binding Remains Endothermic

$^{\Delta}$Binding Becomes Exothermic

Compared to CaM^{WT}, the affinity of Ca^{2+} binding, thermal stability, binding to RyR2 and inhibition of RyR2 activity were all reduced in CaM^{F90L}, recombinant protein corresponding to IVT linked p.(F90L) CaM mutation (Nomikos *et al.*, 2014). The combined effect of decreased domain stability and loss of co-operativity between binding sites in the C-domain could have a profound impact on the biological functions of CaM. The reduced ability of CaM^{F90L} to bind to RyR2 in CoIP assays and inhibit RyR2 channel opening in [^{3}H]-ryanodine binding assays compared to CaM^{WT} could be a result. These functional effects of the mutation combined with a reduced sensitivity to Ca^{2+} provide a potential pathophysiological mechanism in which reduced ability to inhibit RyR2 channel P_O in the presence of increased Ca^{2+} increases the likelihood of inappropriate SR Ca^{2+} sparks and leaks (Nomikos *et al.*, 2014).

In this study summarised in Table 7-1, reduced Ca^{2+} binding and thermal stability, and a similar pattern in altered binding to and regulation of RyR2 by CaM, were observed in CaM mutations associated with cardiac arrhythmias. Compared to CaM^{WT}, binding to RyR2 was reduced in five mutants, greater in two mutants and unaltered in the remaining two mutants in Co-IP experiments. All of the mutants with altered RyR2 binding had a reduced ability to inhibit RyR2 activity in [^{3}H]-ryanodine binding assays. Intriguingly, RyR2 channel activity was greater in the presence of mutations which displayed enhanced binding to RyR2 than when CaM was absent. Meanwhile, in the presence of mutations with an unaltered binding to RyR2, RyR2 channel activity was indistinguishable from when CaM^{WT} was present.

Interestingly, both the binding of CaM to RyR2 and inhibition of RyR2 activity by CaM were unaffected by CaM^{N98S} and CaM^{F142L} indicating a pathophysiological mechanism not involving altered binding to RyR2 and/or dysfunctional regulation of RyR2 channel activation.

Binding between the CaM binding domains of RyR2 and CaM^{WT} and four CaM^{MUT} proteins were examined In ITC experiments. Reduced binding of CaM mutants to RyR2 compared to wild type observed in Co-IP experiments was confirmed. Examination of the interaction between the four mutations and CaM binding domains of RyR2 showed that, regardless of clinical phenotype, the mutations abolished Ca^{2+} free binding of CaM and RyR2. Meanwhile, in the presence of Ca^{2+} binding between CaM mutants and CaMBD2 occurred with a reduced affinity compared to CaM^{WT}. The mutations also had divergent effects on the binding between CaM and CaMBD3 in the presence of Ca^{2+} with all mutants having a reduced binding affinity with CaMBD3 but with an altered binding mode in two mutations compared to CaM^{WT}.

In this study mutations of CaM result in both enhanced and reduced binding to RyR2. Both result in a reduction in the ability of CaM to inhibit channel opening. Mutations also have the capacity to diversely alter Ca^{2+} dependent binding at specific locations of RyR2 and the distinct mode of the binding. Dissociation of CaM and RyR2 is known to cause dysfunctional regulation of RyR2 and CaM which can be arrhythmogenic. However, it appears that enhanced binding between CaM and RyR2 may also be arrhythmogenic by also abolishing the ability of CaM to inhibit RyR2 channel opening. In this thesis select CaM mutations have been shown to have the

capacity to alter the thermodynamics and specific location of CaM RyR2 binding in response to Ca2+. Increased binding between CaM and a specific region of RyR2 may occur at the expense of binding to another region in the response to Ca2+ or due to changes in relative affinities.

In the case of mutations which did not alter binding of CaM, inhibition of channel activation to RyR2 was indistinguishable from CaM^{WT}. However, this does not preclude the possibility that these CaM mutations are not perturbing other parameters of RyR2 channel function e.g. number and length of channel opening events which were not examined in this thesis. The role CaM plays in regulating RyR2 activity is still under active investigation and these mutations may cause subtle alterations to CaM RyR2 binding e.g. binding mode and location, which also result in dysfunctional channel regulation. These results reinforce that the interaction between CaM and distinct separate regions of RyR2 are key in channel regulation. Further studies of the mutations may provide both insight into RyR2 channel function and therapeutic targets in treatment of cardiac arrthymia.

The presence of a mutation in CaM has the potential to disrupt one or more of the CaM target proteins involved in regulating the flow of ions during the cardiac cycle. After the initial reports, functional and structural studies of six of CaM mutants in this thesis p.(N54I), p.(F90L), p.(D96V), p.(N98S), p.(D130G), and p.(F142L) have been published. The published data presents a complex picture of proarrhythmic CaM mutations with diverse, overlapping consequences on the activity of several essential proteins resulting in converging clinical manifestations. Studies have also highlighted

potentially distinct molecular mechanisms for LQTS and CPVT associated with CaM mutations p.(N98S) and p.(F142L) respectively, that may not involve RyR2.

The effect of the mutations on the ability of CaM to activate CaMKII varied from no effect to reduced activation to inhibition of CaMKII function (Berchtold *et al.*, 2016). Compared to wildtype and other mutants one LQTS associated mutation, p.(D130G), was unable to support cell growth and viability or activate CaMKII (Berchtold *et al.*, 2016). LQTS associated CaM mutations alter the interaction between CaM and L-type VGCCs, inhibiting Ca^{2+} dependent inactivation and causing proarrhythmic changes in Ca^{2+} handling (Limpitikul *et al.*, 2014). Novel LQTS associated *CALM2* mutations, including p.(D132H), were also shown to impair CDI of L-type VGCCs (Pipilas *et al.*, 2016).

Both LQTS and CPVT associated CaM mutations alter regulation of RyR2 by CaM in response to Ca^{2+} either via changed interaction with CaMBD2 or an alternative mechanism due to altered Ca^{2+} binding affinity (Søndergaard, Tian, *et al.*, 2015). The presence of CaM mutations p.(N54I), p.(D96V), p.(D130G) and p.(N98S), increased spontaneous Ca^{2+} release by reducing the initiation and termination thresholds of SOICR; while in the presence of p.(F142L) SOICR is not adversely affected (Søndergaard, Tian, *et al.*, 2015; Søndergaard *et al.*, 2017).

In a cell model derived from a LQTS patient bearing the p.(F142L) CaM mutation, Ca^{2+} dependent inactivation of the L-type VGCCs was severely impaired during the plateau phase causing a prolonged repolarisation (Rocchetti *et al.*, 2017). These results indicate that the pathophysiological mechanism of p.(F142L) linked

arrhythmias is distinct and does not involve disrupted interaction with RyR2. However, low and Ca^{2+} free binding of RyR2 and CaM p.(F142L) via CaMBD was shown to be thermodynamically and structural distinct to that of wildtype CaM (Søndergaard *et al.*, 2017).

Animal models of two CPVT linked mutations, p.(N54I) and p.(N98S), display similar arrhythmic phenotypes despite pronounced opposed effects on biophysical and functional properties of CaM, indicating distinct molecular mechanisms of disease (Søndergaard, Sorensen, *et al.*, 2015). Recent experiments *in silico* have shown that due to the flexibility of CaM, the structural effects of the C-lobe EF hands mutations are limited, but mutations will disrupt the Ca^{2+} binding affinity of the domains (Shaik *et al.*, 2018). With one exception all the proarrhythmic CaM mutations described in this thesis confer a reduced Ca^{2+} binding affinity. The resulting reduced sensitivity to Ca^{2+} appears to result in divergent aberrations of function regulating Ca^{2+} signalling pathway proteins which cause converging proarrhythmic phenotypes.

The clinical importance of CaM in cardiology has been reinforced by recent studies proposing *CALM3* polymorphisms as cardiomyopathy disease modifiers and CaM deficient RyR2 as a therapeutic target in HF (Klipp *et al.*, 2018; Kumar *et al.*, 2018). Also, the normal phenotype was rescued in an arrhythmia cell model derived from an LQTS patient bearing a p.(N98S) *CALM2* mutation (Yamamoto *et al.*, 2017). Establishing causative mutations and associated mechanisms will aid in both disease screening, drug development and offers the opportunity to develop gene-specific treatments for inherited cardiac arrhythmias.

A key element of understanding the pathophysiological mechanisms of CaM mutations in cardiac arrhythmias is to directly compare the effects of each mutation on RyR2 function within the same systems. The contribution to the disease phenotype by CaM mutations disrupting the regulation of other target proteins, e.g. CaMKII and L-type VGCCs must also be considered. Ideally, *in vitro* studies would use recombinant mutant CaM proteins from the same expression system. This study sought to compare and contrast the mutations biophysical and functional effects on recombinant CaM proteins expressed in the same system.

Ongoing structural studies may reveal alterations in the tertiary protein structure and could be used for further studies of the structural interaction between CaM and target sequences, e.g. CaMBD2 and CaMBD3 which this study reveal to be functionally different. Thermodynamic studies of Ca^{2+} binding to wildtype and mutant CaM would reveal mutant conferred alterations in the kinetics of the Ca^{2+} binding reaction. Initial studies have revealed variation between the mutants and changes in a binding mode with Ca^{2+} saturation.

Single channel experiments in the presence of mutant recombinant CaM proteins from this thesis are planned to study the effect on the gating properties of RyR2 (Mukherjee, Thomas and Williams, 2012). Expression of mutant CaM in RyR2 cell lines is under development for single cell Ca^{2+} imaging which was used previously to study the impact of CPVT associated RyR2 mutations on cardiomyocyte phenotype (George, Higgs and Lai, 2003). Also, transgenic zebrafish expressing new and established CaM mutations are being developed (Da'as *et al.*, 2019). When *in vitro* and *in vivo* data are considered together a complete picture may emerge of how each

mutation effects channel gating, Ca^{2+} handling in cardiomyocytes and disease phenotype. It may then be possible to group mutations according to common and related mechanisms rather than clinical manifestation alone.

This thesis also examined a novel interaction between PLCζ and CaM. Thermodynamic studies revealed that PLCζ binds specifically to CaM via the C-lobe of CaM with a contribution by the N-lobe. The biological significance of this interaction is currently unclear although regulatory mechanisms involving both the substrate of PLCζ, PIP_2 and holoCaM have been described. Several studies have reported competition for binding between CaM and PIP_2 at regulatory sites of ion channels and that a mutation at one such site is associated with LQTS (Grycova *et al.*, 2015; Tobelaim *et al.*, 2017a, 2017b).

Potential roles for an interaction between PLCζ and CaM include: inhibition of activity in the sperm which lifts when CaM dissociates from PLCζ in the low [Ca^{2+}] of the oocyte, and CaM remaining bound to PLCζ in the oocyte, perhaps at the C-lobe, in order to target PLC to the specific target pool of substrate. Further experiments are required to further elucidate the role of the interaction between PLCζ and CaM.

Ongoing crystallisation experiments of CaM and PLCζ could reveal structural information on the binding between CaM and PLCζ and lead to co-crystallisation of full-length PLCζ bound to CaM. Expression in oocytes of luciferase-tagged PLCζ mRNAs that bear mutations in the CaM binding site could reveal if abolishing CaM interaction effects the ability of PLCζ to target specific PIP_2 stores and to elicit Ca^{2+} oscillations (Swann *et al.*, 2009). Immunofluorescence microscopy of whole sperm

may reveal if CaM and PLCζ co-localise in functionally important subcellular compartments (Kashir *et al.*, 2017). Here, CaM binding may assist with protein stabilisation of the heat-sensitive PLCζ.

Recombinant PLCζ may require a stabilising agent to be of practical use as a therapeutic agent in IVF clinics. CaM could play this role. Clinical applications for PLCζ include an alternative to ionophores as an oocyte activation reagent to induce physiological Ca^{2+} oscillations at IVF and to treat male infertility which is resistant to ICSI.

This thesis has explored two emerging areas of research with a clinical application involving the role played by CaM in the regulation of two important Ca^{2+} signalling proteins in health and disease. This thesis shows improvements to recombinant PLCζ expression, a new method for expressing and purifying human CaM, how CaM mutants effect RyR function and demonstrates a novel specific binding between CaM and PLCζ. Further work will be required to optimise PLCζ expression and investigate the role played by binding between PLCζ and CaM. However, the interaction with CaM provides a new avenue for PLCζ crystallisation experiments. Due to the complexity of the results of the effect of CaM mutants on RyR2 activity, additional studies will be required to resolve how point CaM mutations contribute to CPVT and LQTS. The studies described have produced both original data and new tools which will contribute to these future studies.

BIBLIOGRAPHY

Abbott, Allison, L. (2001) ‘Calcium and The Control of Mammalian Cortical Granule Exocytosis’, *Frontiers in Bioscience*, 6(1), p. d792. doi: 10.2741/Abbott.

Abriel, H. and Zaklyazminskaya, E. V. (2013) ‘Cardiac channelopathies: Genetic and molecular mechanisms’, *Gene*, 517(1), pp. 1–11. doi: 10.1016/j.gene.2012.12.061.

Ackerman, M. J. *et al.* (2011) ‘HRS/EHRA Expert Consensus Statement on the State of Genetic Testing for the Channelopathies and Cardiomyopathies’, *Heart Rhythm*, 8(8), pp. 1308–1339. doi: 10.1016/j.hrthm.2011.05.020.

Adams, P. J. *et al.* (2014) ‘Apocalmodulin Itself Promotes Ion Channel Opening and Ca2+ Regulation’, *Cell*, 159(3), pp. 608–622. doi: 10.1016/j.cell.2014.09.047.

Alaimo, A. *et al.* (2014) ‘Pivoting between Calmodulin Lobes Triggered by Calcium in the Kv7.2/Calmodulin Complex’, *PLoS ONE*. Edited by A. Guerrero-Hernandez, 9(1), p. e86711. doi: 10.1371/journal.pone.0086711.

Anderson, K. *et al.* (1989) ‘Structural and functional characterization of the purified cardiac ryanodine receptor-Ca2+ release channel complex’, *Journal of Biological Chemistry*, 264(2), pp. 1329–1335.

Anraku, Y. (1997) ‘Protein splicing: its chemistry and biology’, *Genes to Cells*, 2(6), pp. 359–367. doi: 10.1046/j.1365-2443.1997.1270325.x.

Anraku, Y., Mizutani, R. and Satow, Y. (2005) ‘Protein Splicing: Its Discovery and Structural Insight into Novel Chemical Mechanisms’, *IUBMB Life (International Union of Biochemistry and Molecular Biology: Life)*, 57(8), pp. 563–574. doi:

10.1080/15216540500215499.

Antal, C. E. and Newton, A. C. (2014) ‘Tuning the signalling output of protein kinase C’, *Biochemical Society Transactions*, 42(6), pp. 1477–1483. doi: 10.1042/BST20140172.

Anyatonwu, G. and Joseph, S. K. (2009) ‘Surface Accessibility and Conformational Changes in the N-terminal Domain of Type I Inositol Trisphosphate Receptors’, *Journal of Biological Chemistry*, 284(12), pp. 8093–8102. doi: 10.1074/jbc.M806932200.

Arcaro, A. *et al.* (1998) ‘Human Phosphoinositide 3-Kinase C2β, the Role of Calcium and the C2 Domain in Enzyme Activity’, *Journal of Biological Chemistry*, 273(49), pp. 33082–33090. doi: 10.1074/jbc.273.49.33082.

Arnáiz-Cot, J. J. *et al.* (2013) ‘Cardiac calcium signalling pathologies associated with defective calmodulin regulation of type 2 ryanodine receptor’, *The Journal of Physiology*, 591(17), pp. 4287–4299. doi: 10.1113/jphysiol.2013.256123.

Ashcroft, F. M. (2006) ‘From molecule to malady’, *Nature*, 440(7083), pp. 440–447. doi: 10.1038/nature04707.

Asmara, H. *et al.* (2010) ‘Interactions of Calmodulin With the Multiple Binding Sites of Cav1.2 Ca2+ Channels’, *Journal of Pharmacological Sciences*, 112(4), pp. 397–404. doi: 10.1254/jphs.09342FP.

Austin, C. and Braden, A. (1956) ‘Early reaction of the rodent egg to spermatozoon penetration’, *J Exp Biol*, 33, pp. 358–365.

Avila, G., O'Brien, J. J. and Dirksen, R. T. (2001) 'Excitation-contraction uncoupling by a human central core disease mutation in the ryanodine receptor', *Proceedings of the National Academy of Sciences*, 98(7), pp. 4215–4220. doi: 10.1073/pnas.071048198.

Axelsen, K. B. and Palmgren, M. G. (1998) 'Evolution of Substrate Specificities in the P-Type ATPase Superfamily', *Journal of Molecular Evolution*, 46(1), pp. 84–101. doi: 10.1007/PL00006286.

Babu, Y. S. *et al.* (1985) 'Three-dimensional structure of calmodulin', *Nature*, 315(6014), pp. 37–40. doi: 10.1038/315037a0.

Babu, Y. S., Bugg, C. E. and Cook, W. J. (1987) 'X-Ray diffraction studies of calmodulin', in *Methods in Enzymology*. Elsevier Inc., pp. 632–642. doi: 10.1016/0076-6879(87)39116-5.

Babu, Y. S., Bugg, C. E. and Cook, W. J. (1988) 'Structure of calmodulin refined at 2.2 Å resolution', *Journal of Molecular Biology*, 204(1), pp. 191–204. doi: 10.1016/0022-2836(88)90608-0.

Van Baelen, K. *et al.* (2004) 'The Ca2+/Mn2+ pumps in the Golgi apparatus', *Biochimica et Biophysica Acta (BBA) - Molecular Cell Research*, 1742(1–3), pp. 103–112. doi: 10.1016/j.bbamcr.2004.08.018.

Bai, X. C. *et al.* (2016) 'The Central domain of RyR1 is the transducer for long-range allosteric gating of channel opening', *Cell Research*, 26(9), pp. 995–1006. doi: 10.1038/cr.2016.89.

Bai, X., McMullan, G. and Scheres, S. H. . (2015) 'How cryo-EM is revolutionizing

structural biology', *Trends in Biochemical Sciences*, 40(1), pp. 49–57. doi: 10.1016/j.tibs.2014.10.005.

Baker, M. R., Fan, G. and Serysheva, I. I. (2017) 'Structure of IP3R channel: high-resolution insights from cryo-EM', *Current Opinion in Structural Biology*, 46, pp. 38–47. doi: 10.1016/j.sbi.2017.05.014.

Balshaw, D. M. *et al.* (2001) 'Calmodulin Binding and Inhibition of Cardiac Muscle Calcium Release Channel (Ryanodine Receptor)', *Journal of Biological Chemistry*, 276(23), pp. 20144–20153. doi: 10.1074/jbc.M010771200.

Banki, M. R., Feng, L. and Wood, D. W. (2005) 'Simple bioseparations using self-cleaving elastin-like polypeptide tags', *Nature Methods*, 2(9), pp. 659–662. doi: 10.1038/nmeth787.

Bannister, R. A. and Beam, K. G. (2013) 'CaV1.1: The atypical prototypical voltage-gated Ca2+ channel', *Biochimica et Biophysica Acta (BBA) - Biomembranes*, 1828(7), pp. 1587–1597. doi: 10.1016/j.bbamem.2012.09.007.

Barford, A. M., Gilliland, G. L. and Morgan, D. W. (1986) 'Growing calmodulin crystals for X-ray diffraction studies at room temperature in 2 days', *Analytical Biochemistry*, 158(2), pp. 361–364. doi: 10.1016/0003-2697(86)90561-0.

Bartos, D. C., Grandi, E. and Ripplinger, C. M. (2015) 'Ion Channels in the Heart', in *Comprehensive Physiology*. Hoboken, NJ, USA: John Wiley & Sons, Inc., pp. 1423–1464. doi: 10.1002/cphy.c140069.

Bastiaenen, R. and Behr, E. R. (2011) 'Sudden death and ion channel disease: pathophysiology and implications for management', *Heart*, 97(17), pp. 1365–1372.

doi: 10.1136/hrt.2011.223883.

Bastings, M. M. *et al.* (2008) 'One-step refolding and purification of disulfide-containing proteins with a C-terminal MESNA thioester', *BMC Biotechnology*, 8(1), p. 76. doi: 10.1186/1472-6750-8-76.

Baughman, J. M. *et al.* (2011) 'Integrative genomics identifies MCU as an essential component of the mitochondrial calcium uniporter', *Nature*, 476(7360), pp. 341–345. doi: 10.1038/nature10234.

Bayley, P. M. and Martin, S. R. (1992) 'The α-helical content of calmodulin is increased by solution conditions favouring protein crystallisation', *Biochimica et Biophysica Acta (BBA) - Protein Structure and Molecular Enzymology*, 1160(1), pp. 16–21. doi: 10.1016/0167-4838(92)90034-B.

Bedford, J. M. (2011) 'Site of the mammalian sperm physiological acrosome reaction', *Proceedings of the National Academy of Sciences*, 108(12), pp. 4703–4704. doi: 10.1073/pnas.1102296108.

Behere, S. P. and Weindling, S. N. (2016) 'Catecholaminergic polymorphic ventricular tachycardia: An exciting new era', *Annals of Pediatric Cardiology*, 9(2), pp. 137–146. doi: 10.4103/0974-2069.180645.

Behr, E. R. *et al.* (2008) 'Sudden arrhythmic death syndrome: familial evaluation identifies inheritable heart disease in the majority of families', *European Heart Journal*, 29(13), pp. 1670–1680. doi: 10.1093/eurheartj/ehn219.

Bejarano, I. *et al.* (2012) 'Apoptosis, ROS and Calcium Signaling in Human Spermatozoa: Relationship to Infertility', in *Male Infertility*. InTech, pp. 51–76. doi:

10.5772/32617.

Berchtold, M. W. *et al.* (2016) 'The Arrhythmogenic Calmodulin Mutation D129G Dysregulates Cell Growth, Calmodulin-dependent Kinase II Activity, and Cardiac Function in Zebrafish', *Journal of Biological Chemistry*, 291(52), pp. 26636–26646. doi: 10.1074/jbc.M116.758680.

Berchtold, M. W. and Villalobo, A. (2014) 'The many faces of calmodulin in cell proliferation, programmed cell death, autophagy, and cancer', *Biochimica et Biophysica Acta (BBA) - Molecular Cell Research*, 1843(2), pp. 398–435. doi: 10.1016/j.bbamcr.2013.10.021.

Berman, H. M. (2000) 'The Protein Data Bank', *Nucleic Acids Research*, 28(1), pp. 235–242. doi: 10.1093/nar/28.1.235.

Berridge, M. J. *et al.* (1983) 'Changes in the levels of inositol phosphates after agonist-dependent hydrolysis of membrane phosphoinositides', *Biochemical Journal*, 212(2), pp. 473–482. doi: 10.1042/bj2120473.

Berridge, M. J. (1984) 'Inositol trisphosphate and diacylglycerol as second messengers', *Biochemical Journal*, 220(2), pp. 345–360. doi: 10.1042/bj2200345.

Berridge, M. J. (1993) 'Inositol trisphosphate and calcium signalling', *Nature*, 361(6410), pp. 315–325. doi: 10.1038/361315a0.

Berridge, M. J. (2002) 'The endoplasmic reticulum: A multifunctional signaling organelle', *Cell Calcium*, 32(5–6), pp. 235–249. doi: 10.1016/S0143416002001823.

Berridge, M. J. (2009) 'Inositol trisphosphate and calcium signalling mechanisms',

Biochimica et Biophysica Acta (BBA) - Molecular Cell Research, 1793(6), pp. 933–940. doi: 10.1016/j.bbamcr.2008.10.005.

Berridge, M. J. (2012) 'Calcium signalling remodelling and disease', *Biochemical Society Transactions*, 40(2), pp. 297–309. doi: 10.1042/BST20110766.

Berridge, M. J., Bootman, M. D. and Roderick, H. L. (2003) 'Calcium signalling: dynamics, homeostasis and remodelling', *Nature Reviews Molecular Cell Biology*, 4(7), pp. 517–529. doi: 10.1038/nrm1155.

Berridge, M. J. and Dupont, G. (1994) 'Spatial and temporal signalling by calcium', *Current Opinion in Cell Biology*, 6(2), pp. 267–274. doi: 10.1016/0955-0674(94)90146-5.

Berridge, M. J. and Irvine, R. F. (1984) 'Inositol trisphosphate, a novel second messenger in cellular signal transduction', *Nature*, 312(5992), pp. 315–321. doi: 10.1038/312315a0.

Berridge, M. J. and Lipke, H. (1979) 'Changes in calcium transport across Calliphora salivary glands induced by 5-hydroxytryptamine and cyclic nucleotides', *Journal of Experimental Biology*, 78, pp. 137–148.

Berridge, M. J., Lipp, P. and Bootman, M. D. (2000) 'The versatility and universality of calcium signalling', *Nature Reviews Molecular Cell Biology*, 1(1), pp. 11–21. doi: 10.1038/35036035.

Berrie, C. P. *et al.* (1996) 'A cytosolic sperm factor triggers calcium oscillations in rat hepatocytes', *Biochemical Journal*, 313(2), pp. 369–372. doi: 10.1042/bj3130369.

Bers, Donald M (2002) ‘Cardiac excitation–contraction coupling’, *Nature*. Elsevier, 415(6868), pp. 198–205. doi: 10.1038/415198a.

Bers, Donald M. (2002) ‘Cardiac excitation–contraction coupling’, *Nature*, 415(6868), pp. 198–205. doi: 10.1038/415198a.

Betzenhauser, M. J. and Marks, A. R. (2010) ‘Ryanodine receptor channelopathies’, *Pflügers Archiv - European Journal of Physiology*, 460(2), pp. 467–480. doi: 10.1007/s00424-010-0794-4.

Bezprozvanny, Ilya, Watras, J. and Ehrlich, B. E. (1991) ‘Bell-shaped calcium-response curves of Ins(l,4,5)P3- and calcium-gated channels from endoplasmic reticulum of cerebellum’, *Nature*, 351(6329), pp. 751–754. doi: 10.1038/351751a0.

Bhuiyan, Z. A. *et al.* (2007) ‘A Novel Early Onset Lethal Form of Catecholaminergic Polymorphic Ventricular Tachycardia Maps to Chromosome 7p14-p22’, *Journal of Cardiovascular Electrophysiology*, 18(10), pp. 1060–1066. doi: 10.1111/j.1540-8167.2007.00913.x.

Bianchi, E. and Wright, G. J. (2016) ‘Sperm Meets Egg: The Genetics of Mammalian Fertilization’, *Annual Review of Genetics*, 50(1), pp. 93–111. doi: 10.1146/annurev-genet-121415-121834.

Bird, L. E. (2011) ‘High throughput construction and small scale expression screening of multi-tag vectors in Escherichia coli’, *Methods*, 55(1), pp. 29–37. doi: 10.1016/j.ymeth.2011.08.002.

Blaich, A. *et al.* (2012) ‘Mutation of the Calmodulin Binding Motif IQ of the L-type Ca v 1.2 Ca 2+ Channel to EQ Induces Dilated Cardiomyopathy and Death’, *Journal of*

Biological Chemistry, 287(27), pp. 22616–22625. doi: 10.1074/jbc.M112.357921.

Blaustein, M. P. and Lederer, W. J. (1999) 'Sodium/Calcium Exchange: Its Physiological Implications', *Physiological Reviews*, 79(3), pp. 763–854. doi: 10.1152/physrev.1999.79.3.763.

Blondel, O. *et al.* (1994) 'Localization of inositol trisphosphate receptor subtype 3 to insulin and somatostatin secretory granules and regulation of expression in islets and insulinoma cells.', *Proceedings of the National Academy of Sciences*, 91(16), pp. 7777–7781. doi: 10.1073/pnas.91.16.7777.

Boal, D. (2012) *Mechanics of the Cell*. 2nd editio. Cambridge: Cambridge University Press. doi: 10.1017/CBO9781139022217.

Boczek, N. J. *et al.* (2013) 'Exome Sequencing and Systems Biology Converge to Identify Novel Mutations in the L-Type Calcium Channel, CACNA1C , Linked to Autosomal Dominant Long QT Syndrome', *Circulation: Cardiovascular Genetics*, 6(3), pp. 279–289. doi: 10.1161/CIRCGENETICS.113.000138.

Boczek, N. J. *et al.* (2016) 'Spectrum and Prevalence of CALM1 -, CALM2 -, and CALM3 -Encoded Calmodulin Variants in Long QT Syndrome and Functional Characterization of a Novel Long QT Syndrome–Associated Calmodulin Missense Variant, E141G', *Circulation: Cardiovascular Genetics*, 9(2), pp. 136–146. doi: 10.1161/CIRCGENETICS.115.001323.

Boehning, D. (2000) 'Direct association of ligand-binding and pore domains in homo- and heterotetrameric inositol 1,4,5-trisphosphate receptors', *The EMBO Journal*, 19(20), pp. 5450–5459. doi: 10.1093/emboj/19.20.5450.

Boehning, D. *et al.* (2001) 'Single-Channel Recordings of Recombinant Inositol Trisphosphate Receptors in Mammalian Nuclear Envelope', *Biophysical Journal*, 81(1), pp. 117–124. doi: 10.1016/S0006-3495(01)75685-8.

Bojarski, L., Herms, J. and Kuznicki, J. (2008) 'Calcium dysregulation in Alzheimer's disease', *Neurochemistry International*, 52(4–5), pp. 621–633. doi: 10.1016/j.neuint.2007.10.002.

Bolanos-Garcia, V. M. and Davies, O. R. (2006) 'Structural analysis and classification of native proteins from E. coli commonly co-purified by immobilised metal affinity chromatography', *Biochimica et Biophysica Acta (BBA) - General Subjects*, 1760(9), pp. 1304–1313. doi: 10.1016/j.bbagen.2006.03.027.

Bootman, M. D. *et al.* (2012) 'Calcium Signalling and Regulation of Cell Function', in *eLS*. Chichester, UK: John Wiley & Sons, Ltd, pp. 590–601. doi: 10.1002/9780470015902.a0001265.pub3.

Bootman, M. D., Berridge, M. J. and Roderick, H. L. (2002) 'Calcium Signalling: More Messengers, More Channels, More Complexity', *Current Biology*, 12(16), pp. R563–R565. doi: 10.1016/S0960-9822(02)01055-2.

Bootman, M. D., Lipp, P. and Berridge, M. J. (2001) 'The organisation and functions of local Ca(2+) signals.', *Journal of Cell Science*, 114(Pt 12), pp. 2213–22. Available at: http://www.jgp.org/lookup/doi/10.1085/jgp.116.5.697.

Borges, E. *et al.* (2009) 'Artificial oocyte activation using calcium ionophore in ICSI cycles with spermatozoa from different sources', *Reproductive BioMedicine Online*, 18(1), pp. 45–52. doi: 10.1016/S1472-6483(10)60423-3.

Bovo, E. *et al.* (2017) 'The effect of PKA-mediated phosphorylation of ryanodine receptor on SR Ca2+ leak in ventricular myocytes', *Journal of Molecular and Cellular Cardiology*. Elsevier Ltd, 104, pp. 9–16. doi: 10.1016/j.yjmcc.2017.01.015.

Brailoiu, E. *et al.* (2009) 'Essential requirement for two-pore channel 1 in NAADP-mediated calcium signaling', *The Journal of Cell Biology*, 186(2), pp. 201–209. doi: 10.1083/jcb.200904073.

Braun, A. P. and Schulman, H. (1995) 'The Multifunctional Calcium/Calmodulin-Dependent Protein Kinase: From Form to Function', *Annual Review of Physiology*, 57(1), pp. 417–445. doi: 10.1146/annurev.ph.57.030195.002221.

Brenker, C. *et al.* (2012) 'The CatSper channel: a polymodal chemosensor in human sperm', *The EMBO Journal*, 31(7), pp. 1654–1665. doi: 10.1038/emboj.2012.30.

Brillantes, A.-M. B. *et al.* (1994) 'Stabilization of calcium release channel (ryanodine receptor) function by FK506-binding protein', *Cell*, 77(4), pp. 513–523. doi: 10.1016/0092-8674(94)90214-3.

Brind, S., Swann, K. and Carroll, J. (2000) 'Inositol 1,4,5-Trisphosphate Receptors Are Downregulated in Mouse Oocytes in Response to Sperm or Adenophostin A but Not to Increases in Intracellular Ca2+ or Egg Activation', *Developmental Biology*, 223(2), pp. 251–265. doi: 10.1006/dbio.2000.9728.

Brini, M. *et al.* (2005) 'Ca 2+ Signaling in HEK-293 and Skeletal Muscle Cells Expressing Recombinant Ryanodine Receptors Harboring Malignant Hyperthermia and Central Core Disease Mutations', *Journal of Biological Chemistry*, 280(15), pp. 15380–15389. doi: 10.1074/jbc.M410421200.

Brini, M. *et al.* (2013) 'The plasma membrane calcium pump in health and disease', *FEBS Journal*, 280(21), pp. 5385–5397. doi: 10.1111/febs.12193.

Brostrom, C. O. and Wolff, D. J. (1981) 'Properties and functions of calmodulin', *Biochemical Pharmacology*, 30(12), pp. 1395–1405. doi: 10.1016/0006-2952(81)90358-0.

Bultynck, G. *et al.* (2004) 'Thimerosal stimulates Ca 2+ flux through inositol 1,4,5-trisphosphate receptor type 1, but not type 3, via modulation of an isoform-specific Ca 2+ -dependent intramolecular interaction', *Biochemical Journal*, 381(1), pp. 87–96. doi: 10.1042/BJ20040072.

Bunney, T. D. and Katan, M. (2011) 'PLC regulation: emerging pictures for molecular mechanisms', *Trends in Biochemical Sciences*. Elsevier Ltd, 36(2), pp. 88–96. doi: 10.1016/j.tibs.2010.08.003.

Burgess, G. M. *et al.* (1984) 'Actions of inositol phosphates on Ca2+ pools in guinea-pig hepatocytes', *Biochemical Journal*, 224(3), pp. 741–746. doi: 10.1042/bj2240741.

Burgess, W. H., Jemiolo, D. K. and Kretsinger, R. H. (1980) 'Interaction of calcium and calmodulin in the presence of sodium dodecyl sulfate', *Biochimica et Biophysica Acta (BBA) - Protein Structure*, 623(2), pp. 257–270. doi: 10.1016/0005-2795(80)90254-8.

Burnstock, G. (2000) 'P2X receptors in sensory neurones', *British Journal of Anaesthesia*, 84(4), pp. 476–488. doi: 10.1093/oxfordjournals.bja.a013473.

Burnstock, G. (2013) 'Introduction to Purinergic Signalling in the Brain', in Barańska, J. (ed.) *Glioma Signaling*. Dordrecht: Springer Netherlands, pp. 1–12. doi:

10.1007/978-94-007-4719-7_1.

Burnstock, G. (2017) ‘Purinergic Signaling in the Cardiovascular System’, *Circulation Research*, 120(1), pp. 207–228. doi: 10.1161/CIRCRESAHA.116.309726.

Burnstock, G. and Ralevic, V. (2013) ‘Purinergic Signaling and Blood Vessels in Health and Disease’, *Pharmacological Reviews*, 66(1), pp. 102–192. doi: 10.1124/pr.113.008029.

Butt, T. R. *et al.* (2005) ‘SUMO fusion technology for difficult-to-express proteins’, *Protein Expression and Purification*, 43(1), pp. 1–9. doi: 10.1016/j.pep.2005.03.016.

Cabrita, L. D., Dai, W. and Bottomley, S. P. (2006) ‘A family of E. coli expression vectors for laboratory scale and high throughput soluble protein production.’, *BMC Biotechnology*, 6(Lic), p. 12. doi: 10.1186/1472-6750-6-12.

Cai, X. and Lytton, J. (2004) ‘The Cation/Ca2+ Exchanger Superfamily: Phylogenetic Analysis and Structural Implications’, *Molecular Biology and Evolution*, 21(9), pp. 1692–1703. doi: 10.1093/molbev/msh177.

Calcraft, P. J. *et al.* (2009) ‘NAADP mobilizes calcium from acidic organelles through two-pore channels’, *Nature*, 459(7246), pp. 596–600. doi: 10.1038/nature08030.

Campbell, A. K. (1987) ‘Intracellular calcium: Friend or foe?’, *Clinical Science*, 72(1), pp. 1–10. doi: 10.1042/cs0720001.

Campbell, K. P. *et al.* (1987) ‘Identification and characterization of the high affinity [3H]ryanodine receptor of the junctional sarcoplasmic reticulum Ca2+ release channel.’, *Journal of Biological Chemistry*, 262(14), pp. 6460–3. Available at:

http://www.ncbi.nlm.nih.gov/pubmed/2437119.

Campbell, K. P., Franzini-Armstrong, C. and Shamoo, A. E. (1980) 'Further characterization of light and heavy sarcoplasmic reticulum vesicles. Identification of the "sarcoplasmic reticulum feet" associated with heavy sarcoplasmic reticulum vesicles', *Biochimica et Biophysica Acta (BBA) - Biomembranes*, 602(1), pp. 97–116. doi: 10.1016/0005-2736(80)90293-X.

Cancela, J. M. *et al.* (2000) 'Two different but converging messenger pathways to intracellular Ca2+ release: the roles of nicotinic acid adenine dinucleotide phosphate, cyclic ADP-ribose and inositol trisphosphate', *The EMBO Journal*, 19(11), pp. 2549–2557. doi: 10.1093/emboj/19.11.2549.

Cancela, J. M. (2001) 'Specific Ca 2+ Signaling Evoked by Cholecystokinin and Acetylcholine: The Roles of NAADP, cADPR, and IP 3', *Annual Review of Physiology*, 63(1), pp. 99–117. doi: 10.1146/annurev.physiol.63.1.99.

Capel, R. A. and Terrar, D. A. (2015) 'The importance of Ca2+-dependent mechanisms for the initiation of the heartbeat', *Frontiers in Physiology*, 6(MAR), pp. 1–19. doi: 10.3389/fphys.2015.00080.

Carafoli, E. *et al.* (2001) 'Generation, Control, and Processing of Cellular Calcium Signals', *Critical Reviews in Biochemistry and Molecular Biology*, 36(2), pp. 107–260. doi: 10.1080/20014091074183.

Carafoli, E. and Klee, C. B. (1992) 'Preface', *Cell Calcium*, 13(6–7), pp. 353–354. doi: 10.1016/0143-4160(92)90048-W.

Case, R. M. *et al.* (2007) 'Evolution of calcium homeostasis: From birth of the first

cell to an omnipresent signalling system', *Cell Calcium*, 42(4–5), pp. 345–350. doi: 10.1016/j.ceca.2007.05.001.

Catterall, W. A. (2011) 'Voltage-Gated Calcium Channels', *Cold Spring Harbor Perspectives in Biology*, 3(8), pp. a003947–a003947. doi: 10.1101/cshperspect.a003947.

Catterall, W. A., Wisedchaisri, G. and Zheng, N. (2017) 'The chemical basis for electrical signaling', *Nature Chemical Biology*, 13(5), pp. 455–463. doi: 10.1038/nchembio.2353.

Catterall, W. a (2000) 'Structure and Regulation of Voltage-Gated Ca 2+ Channels', *Annual Review of Cell and Developmental Biology*, 16(1), pp. 521–555. doi: 10.1146/annurev.cellbio.16.1.521.

Chagot, B. and Chazin, W. J. (2011) 'Solution NMR Structure of Apo-Calmodulin in Complex with the IQ Motif of Human Cardiac Sodium Channel NaV1.5', *Journal of Molecular Biology*, 406(1), pp. 106–119. doi: 10.1016/j.jmb.2010.11.046.

Chan, J. *et al.* (2007) 'Ligand-induced Conformational Changes via Flexible Linkers in the Amino-terminal region of the Inositol 1,4,5-Trisphosphate Receptor', *Journal of Molecular Biology*, 373(5), pp. 1269–1280. doi: 10.1016/j.jmb.2007.08.057.

Chan, J. *et al.* (2010) 'Structural Studies of Inositol 1,4,5-Trisphosphate Receptor', *Journal of Biological Chemistry*, 285(46), pp. 36092–36099. doi: 10.1074/jbc.M110.140160.

Chandrasekhar, R., Alzayady, K. J. and Yule, D. I. (2015) 'Using concatenated subunits to investigate the functional consequences of heterotetrameric inositol

1,4,5-trisphosphate receptors', *Biochemical Society Transactions*, 43(3), pp. 364–370. doi: 10.1042/BST20140287.

Chattopadhyaya, R. *et al.* (1992) 'Calmodulin structure refined at 1.7 A resolution.', *Journal of molecular biology*, 228(4), pp. 1177–92. Available at: http://www.ncbi.nlm.nih.gov/pubmed/1474585 (Accessed: 6 August 2015).

Cheek, T. R. *et al.* (1993) 'Fertilisation and thimerosal stimulate similar calcium spiking patterns in mouse oocytes but by separate mechanisms.', *Development*, 119(1), pp. 179–189.

Chen, H. *et al.* (2013) 'Mechanism of calsequestrin regulation of single cardiac ryanodine receptor in normal and pathological conditions', *The Journal of General Physiology*, 142(2), pp. 127–136. doi: 10.1085/jgp.201311022.

Chen, W. *et al.* (2014) 'The ryanodine receptor store-sensing gate controls Ca2+ waves and Ca2+-triggered arrhythmias', *Nature Medicine*, 20(2), pp. 184–192. doi: 10.1038/nm.3440.

Cheung, W. Y. (1982) 'Calmodulin: an overview.', *Federation Proceedings*, 41(7), pp. 2253–2257.

Chin, D. and Means, A. R. (2000) 'Calmodulin: a prototypical calcium sensor', *Trends in Cell Biology*, 10(8), pp. 322–328. doi: 10.1016/S0962-8924(00)01800-6.

Chizh, B. A. and Illes, P. (2001) 'P2X Receptors and Nociception', *Pharmacological Reviews*, 53(4), pp. 553 LP – 568. Available at: http://pharmrev.aspetjournals.org/content/53/4/553.abstract.

Chong, S. *et al.* (1997) ‘Single-column purification of free recombinant proteins using a self-cleavable affinity tag derived from a protein splicing element’, *Gene*, 192(2), pp. 271–281. doi: 10.1016/S0378-1119(97)00105-4.

Chong, S. *et al.* (1998) ‘Modulation of Protein Splicing of the Saccharomyces cerevisiae Vacuolar Membrane ATPase Intein’, *Journal of Biological Chemistry*, 273(17), pp. 10567–10577. doi: 10.1074/jbc.273.17.10567.

Chou, J. J. *et al.* (2001) ‘Solution structure of Ca(2+)-calmodulin reveals flexible hand-like properties of its domains.’, *Nature Structural & Molecular Biology*, 8(11), pp. 990–7. doi: 10.1038/nsb1101-990.

Chung, J.-J. *et al.* (2014) ‘Structurally Distinct Ca2+ Signaling Domains of Sperm Flagella Orchestrate Tyrosine Phosphorylation and Motility’, *Cell*, 157(4), pp. 808–822. doi: 10.1016/j.cell.2014.02.056.

Ciapa, B. *et al.* (1994) ‘Cell-cycle calcium transients driven by cyclic changes in inositol trisphosphate levels’, *Nature*, 368(6474), pp. 875–878. doi: 10.1038/368875a0.

Clapham, D. E. (2003) ‘TRP channels as cellular sensors’, *Nature*, 426(6966), pp. 517–524. doi: 10.1038/nature02196.

Clapham, D. E. (2007) ‘Calcium Signaling’, *Cell*, 131(6), pp. 1047–1058. doi: 10.1016/j.cell.2007.11.028.

Clusin, W. T. (2003) ‘Calcium and Cardiac Arrhythmias: DADs, EADs, and Alternans’, *Critical Reviews in Clinical Laboratory Sciences*, 40(3), pp. 337–375. doi: 10.1080/713609356.

Collins-Racie, L. A. *et al.* (1995) 'Production of Recombinant Bovine Enterokinase Catalytic Subunit in Escherichia coli Using the Novel Secretory Fusion Partner DsbA', *Nature Biotechnology*, 13(9), pp. 982–987. doi: 10.1038/nbt0995-982.

Conner, S. and Hughes, D. (2003) 'Analysis of fish ZP1/ZPB homologous genes--evidence for both genome duplication and species-specific amplification models of evolution', *Reproduction*, 126(3), pp. 347–352. doi: 10.1530/rep.0.1260347.

Conner, S. J. *et al.* (2005) 'Cracking the egg: increased complexity in the zona pellucida', *Human Reproduction*, 20(5), pp. 1148–1152. doi: 10.1093/humrep/deh835.

Contreras, L. *et al.* (2010) 'Mitochondria: The calcium connection', *Biochimica et Biophysica Acta (BBA) - Bioenergetics*, 1797(6–7), pp. 607–618. doi: 10.1016/j.bbabio.2010.05.005.

Cook, W. J. *et al.* (1980) 'Crystallization and preliminary X-ray investigation of calmodulin.', *Journal of Biological Chemistry*, 255(17), pp. 8152–3. Available at: http://www.ncbi.nlm.nih.gov/pubmed/7410353 (Accessed: 6 August 2015).

Cook, W. J. and Sack, J. S. (1983) 'Preparation of calmodulin crystals', in *Methods in Enzymology*. Elsevier Inc., pp. 143–147. doi: 10.1016/S0076-6879(83)02015-7.

Cordeiro, J. M. *et al.* (2010) 'Overlapping LQT1 and LQT2 phenotype in a patient with long QT syndrome associated with loss-of-function variations in KCNQ1 and KCNH2', *Canadian Journal of Physiology and Pharmacology*, 88(12), pp. 1181–1190. doi: 10.1139/Y10-094.

Correa, A. *et al.* (2014) 'Generation of a vector suite for protein solubility screening',

Frontiers in Microbiology, 5, p. 67. doi: 10.3389/fmicb.2014.00067.

Corsini, L. *et al.* (2008) 'Thioredoxin as a fusion tag for carrier-driven crystallization', *Protein Science*, 17(12), pp. 2070–2079. doi: 10.1110/ps.037564.108.

Costa, S. *et al.* (2014) 'Fusion tags for protein solubility, purification and immunogenicity in Escherichia coli: the novel Fh8 system', *Frontiers in Microbiology*, 5, p. 63. doi: 10.3389/fmicb.2014.00063.

Couchonnal, L. F. and Anderson, M. E. (2008) 'The Role of Calmodulin Kinase II in Myocardial Physiology and Disease', *Physiology*, 23(3), pp. 151–159. doi: 10.1152/physiol.00043.2007.

Courtot, A.-M., Pesty, A. and Lefèvre, B. (1999) 'Calmodulin, gametes and fertilisation', *Zygote*, 7(2), pp. 95–104. doi: 10.1017/S0967199499000441.

Cox, L. J. *et al.* (2002) 'Sperm phospholipase Czeta from humans and cynomolgus monkeys triggers Ca2+ oscillations, activation and development of mouse oocytes', *Reproduction*, 124(5), pp. 611–623. doi: 10.1530/reprod/124.5.611.

Craig, T. A. *et al.* (1987) 'Site-specific mutagenesis of the alpha-helices of calmodulin. Effects of altering a charge cluster in the helix that links the two halves of calmodulin.', *Journal of Biological Chemistry*, 262(7), pp. 3278–3284.

Cran, D. G. G., Moor, R. M. M. and Irvine, R. F. F. (1988) 'Initiation of the cortical reaction in hamster and sheep oocytes in response to inositol trisphosphate.', *Journal of Cell Science*, 91 (Pt 1), pp. 139–44. Available at: http://www.ncbi.nlm.nih.gov/pubmed/3267017.

Crotti, L. *et al.* (2013) ‘Calmodulin Mutations Associated With Recurrent Cardiac Arrest in Infants’, *Circulation*, 127(9), pp. 1009–1017. doi: 10.1161/CIRCULATIONAHA.112.001216.

Crouchl, T. H. and Klee, C. B. (1980) ‘Positive Cooperative Binding of Calcium to Bovine Brain Calmodulin’, *Biochemistry*, 19(16), pp. 3692–3698. doi: 10.1021/bi00557a009.

Curran, M. E. *et al.* (1995) ‘A molecular basis for cardiac arrhythmia: HERG mutations cause long QT syndrome’, *Cell*, 80(5), pp. 795–803. doi: 10.1016/0092-8674(95)90358-5.

Currie, K. P. *et al.* (1992) ‘Activation of Ca(2+)-dependent currents in cultured rat dorsal root ganglion neurones by a sperm factor and cyclic ADP-ribose.’, *Molecular Biology of the Cell*, 3(12), pp. 1415–1425. doi: 10.1091/mbc.3.12.1415.

Cuthbertson, K. S. R. and Cobbold, P. H. (1985) ‘Phorbol ester and sperm activate mouse oocytes by inducing sustained oscillations in cell Ca2+’, *Nature*, 316(6028), pp. 541–542. doi: 10.1038/316541a0.

Czech, M. P. (2000) ‘PIP2 and PIP3: complex roles at the cell surface.’, *Cell*, 100(6), pp. 603–6. doi: 10.1016/S0092-8674(00)80696-0.

Da’as, S. I. *et al.* (2019) ‘Arrhythmogenic calmodulin E105A mutation alters cardiac RyR2 regulation leading to cardiac dysfunction in zebrafish.’, *Annals of the New York Academy of Sciences*. Edited by M. Zaidi, MARROW, pp. 1–11. doi: 10.1111/nyas.14033.

Davis, G. D. *et al.* (1999) ‘New fusion protein systems designed to give soluble

expression in Escherichia coli', *Biotechnology and Bioengineering*, 65(4), pp. 382–388. doi: 10.1002/(SICI)1097-0290(19991120)65:4<382::AID-BIT2>3.0.CO;2-I.

Davis, T. N. *et al.* (1986) 'Isolation of the yeast calmodulin gene: Calmodulin is an essential protein', *Cell*, 47(3), pp. 423–431. doi: 10.1016/0092-8674(86)90599-4.

Delvendahl, I. *et al.* (2015) 'Reduced endogenous Ca^{2+} buffering speeds active zone Ca^{2+} signaling', *Proceedings of the National Academy of Sciences*, 112(23), pp. E3075–E3084. doi: 10.1073/pnas.1508419112.

Dempsey, E. C. *et al.* (2000) 'Protein kinase C isozymes and the regulation of diverse cell responses', *American Journal of Physiology-Lung Cellular and Molecular Physiology*, 279(3), pp. L429–L438. doi: 10.1152/ajplung.2000.279.3.L429.

Denessiouk, K. *et al.* (2014) 'Two Structural Motifs within Canonical EF-Hand Calcium-Binding Domains Identify Five Different Classes of Calcium Buffers and Sensors', *PLoS ONE*. Edited by M. Helmer-Citterich, 9(10), p. e109287. doi: 10.1371/journal.pone.0109287.

Deng, M. Q. and Sun, F. Z. (1996) 'The fertilization-induced Ca2+ oscillation in mouse oocytes is cytoplasmic maturation dependent1', *Cell Research*, 6(2), pp. 167–175. doi: 10.1038/cr.1996.18.

Derewenda, Z. S. (2004) 'The use of recombinant methods and molecular engineering in protein crystallization', *Methods*, 34(3), pp. 354–363. doi: 10.1016/j.ymeth.2004.03.024.

Devalla, H. D. *et al.* (2016) 'TECRL , a new life-threatening inherited arrhythmia gene associated with overlapping clinical features of both LQTS and CPVT', *EMBO*

Molecular Medicine, 8(12), pp. 1390–1408. doi: 10.15252/emmm.201505719.

de Diego, I. *et al.* (2010) 'Molecular Basis of the Death-Associated Protein Kinase-Calcium/Calmodulin Regulator Complex', *Science Signaling*, 3(106), pp. ra6–ra6. doi: 10.1126/scisignal.2000552.

Diercks, D. B. *et al.* (2004) 'Electrocardiographic manifestations: electrolyte abnormalities', *The Journal of Emergency Medicine*, 27(2), pp. 153–160. doi: 10.1016/j.jemermed.2004.04.006.

Dirksen, R. T. and Avila, G. (2004) 'Distinct effects on Ca2+ handling caused by malignant hyperthermia and central core disease mutations in RyR1', *Biophysical Journal*, 87(5), pp. 3193–3204. doi: 10.1529/biophysj.104.048447.

Doi, M. *et al.* (2002) 'Propranolol Prevents the Development of Heart Failure by Restoring FKBP12.6-Mediated Stabilization of Ryanodine Receptor', *Circulation*, 105(11), pp. 1374–1379. doi: 10.1161/hc1102.105270.

Domínguez, D. C., Guragain, M. and Patrauchan, M. (2015) 'Calcium binding proteins and calcium signaling in prokaryotes', *Cell Calcium*, 57(3), pp. 151–165. doi: 10.1016/j.ceca.2014.12.006.

Dowler, S. *et al.* (2000) 'Identification of pleckstrin-homology-domain-containing proteins with novel phosphoinositide-binding specificities', *Biochemical Journal*, 351(1), pp. 19–31. doi: 10.1042/bj3510019.

Du, G. G. *et al.* (2004) 'Central core disease mutations R4892W, I4897T and G4898E in the ryanodine receptor isoform 1 reduce the Ca 2+ sensitivity and amplitude of Ca 2+ -dependent Ca 2+ release', *Biochemical Journal*, 382(2), pp.

557–564. doi: 10.1042/BJ20040580.

Ducibella, T. *et al.* (1993) ‘Regulation of the Polyspermy Block in the Mouse Egg: Maturation-Dependent Differences in Cortical Granule Exocytosis and Zona Pellucida Modifications Induced by Inositol 1,4,5-Trisphosphate and an Activator of Protein Kinase C1’, *Biology of Reproduction*, 48(6), pp. 1251–1257. doi: 10.1095/biolreprod48.6.1251.

Ducibella, T. (1996) ‘The cortical reaction and development of activation competence in mammalian oocytes’, *Human Reproduction Update*, 2(1), pp. 29–42. doi: 10.1093/humupd/2.1.29.

Ducibella, T. *et al.* (2002) ‘Egg-to-Embryo Transition Is Driven by Differential Responses to Ca2+ Oscillation Number’, *Developmental Biology*, 250(2), pp. 280–291. doi: 10.1016/S0012-1606(02)90788-8.

Ducibella, T., Schultz, R. M. and Ozil, J.-P. (2006) ‘Role of calcium signals in early development’, *Seminars in Cell & Developmental Biology*, 17(2), pp. 324–332. doi: 10.1016/j.semcdb.2006.02.010.

Dummler, A., Lawrence, A.-M. and de Marco, A. (2005) ‘Simplified screening for the detection of soluble fusion constructs expressed in E. coli using a modular set of vectors’, *Microbial Cell Factories*, 4(1), p. 34. doi: 10.1186/1475-2859-4-34.

Dupré, A., Haccard, O. and Jessus, C. (2011) ‘Mos in the Oocyte: How to Use MAPK Independently of Growth Factors and Transcription to Control Meiotic Divisions’, *Journal of Signal Transduction*, 2011, pp. 1–15. doi: 10.1155/2011/350412.

Efremov, R. G. *et al.* (2015) ‘Architecture and conformational switch mechanism of

the ryanodine receptor', *Nature*, 517(7532), pp. 39–43. doi: 10.1038/nature13916.

Eichmann, T. O. *et al.* (2012) 'Studies on the Substrate and Stereo/Regioselectivity of Adipose Triglyceride Lipase, Hormone-sensitive Lipase, and Diacylglycerol- O -acyltransferases', *Journal of Biological Chemistry*, 287(49), pp. 41446–41457. doi: 10.1074/jbc.M112.400416.

Eisner, D. A. *et al.* (2017) 'Calcium and Excitation-Contraction Coupling in the Heart', *Circulation Research*, 121(2), pp. 181–195. doi: 10.1161/CIRCRESAHA.117.310230.

Elleuche, S. and Pöggeler, S. (2010) 'Inteins, valuable genetic elements in molecular biology and biotechnology', *Applied Microbiology and Biotechnology*, 87(2), pp. 479–489. doi: 10.1007/s00253-010-2628-x.

Ellis, M. V. *et al.* (1998) 'Catalytic Domain of Phosphoinositide-specific Phospholipase C (PLC)', *Journal of Biological Chemistry*, 273(19), pp. 11650–11659. doi: 10.1074/jbc.273.19.11650.

Ellis, M. V, Carne, A. and Katan, M. (1993) 'Structural requirements of phosphatidylinositol-specific phospholipase C delta1 for enzyme activity', *European Journal of Biochemistry*, 213(1), pp. 339–347. doi: 10.1111/j.1432-1033.1993.tb17767.x.

Emsley, P. *et al.* (2010) 'Features and development of Coot', *Acta Crystallographica Section D Biological Crystallography*, 66(4), pp. 486–501. doi: 10.1107/S0907444910007493.

Entman, M. L. *et al.* (1979) 'Spontaneous calcium release from sarcoplasmic reticulum. A re-examination', *Biochimica et Biophysica Acta (BBA) - Biomembranes*,

551(2), pp. 382–388. doi: 10.1016/0005-2736(89)90014-X.

Esposito, D. and Chatterjee, D. K. (2006) 'Enhancement of soluble protein expression through the use of fusion tags', *Current Opinion in Biotechnology*, 17(4), pp. 353–358. doi: 10.1016/j.copbio.2006.06.003.

Essen, L.-O. *et al.* (1996) 'Crystal structure of a mammalian phosphoinositide-specific phospholipase Cδ', *Nature*, 380(6575), pp. 595–602. doi: 10.1038/380595a0.

Essen, L. O. *et al.* (1997) 'Structural mapping of the catalytic mechanism for a mammalian phosphoinositide-specific phospholipase C', *Biochemistry*, 36(7), pp. 1704–1718. doi: 10.1021/bi962512p.

Evans, P. (2006) 'Scaling and assessment of data quality', *Acta Crystallographica Section D Biological Crystallography*, 62(1), pp. 72–82. doi: 10.1107/S0907444905036693.

Faas, G. C. *et al.* (2007) 'Resolving the Fast Kinetics of Cooperative Binding: Ca2+ Buffering by Calretinin', *PLoS Biology*. Edited by R. W. Aldrich, 5(11), p. e311. doi: 10.1371/journal.pbio.0050311.

Fabiato, A. and Fabiato, F. (1975) 'Contractions induced by a calcium-triggered release of calcium from the sarcoplasmic reticulum of single skinned cardiac cells.', *The Journal of Physiology*, 249(3), pp. 469–495. doi: 10.1113/jphysiol.1975.sp011026.

Fabiato, A. and Fabiato, F. (1978) 'Calcium-induced release of calcium from the sarcoplasmic reticulum of skinned cells from adult human, dog, cat, rabbit, rat, and

frog hearts and from fetal and new-born rat ventricles.', *Annals of the New York Academy of Sciences*, 307, pp. 491–522. Available at: http://www.ncbi.nlm.nih.gov/pubmed/360947.

Faggioni, M., Kryshtal, D. O. and Knollmann, B. C. (2012) 'Calsequestrin Mutations and Catecholaminergic Polymorphic Ventricular Tachycardia', *Pediatric Cardiology*, 33(6), pp. 959–967. doi: 10.1007/s00246-012-0256-1.

Fairhurst, A. (1974) 'A ryanodine-caffeine-sensitive membrane fraction of skeletal muscle', *American Journal of Physiology-Legacy Content*, 227(5), pp. 1124–1131. doi: 10.1152/ajplegacy.1974.227.5.1124.

Fairhurst, A. S. and Hasselbach, W. (1970) 'Calcium Efflux from a Heavy Sarcotubular Fraction. Effects of Ryanodine, Caffeine and Magnesium', *European Journal of Biochemistry*, 13(3), pp. 504–509. doi: 10.1111/j.1432-1033.1970.tb00953.x.

Fairhurst, A. S. and Jenden, D. J. (1966) 'The distribution of a ryanodine-sensitive Calcium pump in skeletal muscle fractions', *Journal of Cellular Physiology*, 67(2), pp. 233–238. doi: 10.1002/jcp.1040670205.

Fallon, J. L. *et al.* (2005) 'Structure of Calmodulin Bound to the Hydrophobic IQ Domain of the Cardiac Cav1.2 Calcium Channel', *Structure*, 13(12), pp. 1881–1886. doi: 10.1016/j.str.2005.09.021.

Fan, G. *et al.* (2015) 'Gating machinery of InsP3R channels revealed by electron cryomicroscopy', *Nature*, 527(7578), pp. 336–341. doi: 10.1038/nature15249.

Fedorenko, O. A. *et al.* (2014) 'Intracellular calcium channels: Inositol-1,4,5-

trisphosphate receptors', *European Journal of Pharmacology*, 739(C), pp. 39–48. doi: 10.1016/j.ejphar.2013.10.074.

Ferguson, K. M. *et al.* (1995) 'Structure of the high affinity complex of inositol trisphosphate with a phospholipase C pleckstrin homology domain', *Cell*, 83(6), pp. 1037–1046. doi: 10.1016/0092-8674(95)90219-8.

Fernández-Falgueras, A. *et al.* (2017) 'Cardiac Channelopathies and Sudden Death: Recent Clinical and Genetic Advances', *Biology*, 6(4), p. 7. doi: 10.3390/biology6010007.

Ferris, C. D. *et al.* (1989) 'Purified inositol 1,4,5-trisphosphate receptor mediates calcium flux in reconstituted lipid vesicles', *Nature*, 342(6245), pp. 87–89. doi: 10.1038/342087a0.

Fessenden, J. D. *et al.* (2004) 'Mutational Analysis of Putative Calcium Binding Motifs within the Skeletal Ryanodine Receptor Isoform, RyR1', *Journal of Biological Chemistry*, 279(51), pp. 53028–53035. doi: 10.1074/jbc.M411136200.

Fierro, L. and Llano, I. (1996) 'High endogenous calcium buffering in \protect{P}urkinje cells from rat cerebellar slices', *J. Physiol.*, 496, pp. 617–625.

Fill, M. and Copello, J. A. (2002) 'Ryanodine Receptor Calcium Release Channels', *Physiological Reviews*, 82(4), pp. 893–922. doi: 10.1152/physrev.00013.2002.

Finch, E., Turner, T. and Goldin, S. (1991) 'Calcium as a coagonist of inositol 1,4,5-trisphosphate-induced calcium release', *Science*, 252(5004), pp. 443–446. doi: 10.1126/science.2017683.

Finn, B. E. and Forsén, S. (1995) ‘The evolving model of calmodulin structure,function and activation’, *Structure*, 3(1), pp. 7–11. doi: 10.1016/S0969-2126(01)00130-7.

Fischer, R. *et al.* (1988) ‘Multiple divergent mRNAs code for a single human calmodulin’, *Journal of Biological Chemistry*, 263(32), pp. 17055–17062.

Fischer, T. H., Maier, L. S. and Sossalla, S. (2013) ‘The ryanodine receptor leak: how a tattered receptor plunges the failing heart into crisis’, *Heart Failure Reviews*, 18(4), pp. 475–483. doi: 10.1007/s10741-012-9339-6.

Fissore, R. A. *et al.* (1992) ‘Patterns of Intracellular Ca2+ Concentrations in Fertilized Bovine Eggs1’, *Biology of Reproduction*, 47(6), pp. 960–969. doi: 10.1095/biolreprod47.6.960.

Fleischer, S. *et al.* (1985) ‘Localization of Ca2+ release channels with ryanodine in junctional terminal cisternae of sarcoplasmic reticulum of fast skeletal muscle.’, *Proceedings of the National Academy of Sciences*, 82(21), pp. 7256–7259. doi: 10.1073/pnas.82.21.7256.

Fliniaux, I. *et al.* (2018) ‘TRPs and Ca2+ in cell death and survival’, *Cell Calcium*, 69, pp. 4–18. doi: 10.1016/j.ceca.2017.07.002.

Fong, B. A. and Wood, D. W. (2010) ‘Expression and purification of ELP-intein-tagged target proteins in high cell density E. coli fermentation’, *Microbial Cell Factories*, 9(1), p. 77. doi: 10.1186/1475-2859-9-77.

Fong, B. A., Wu, W.-Y. and Wood, D. W. (2010) ‘The potential role of self-cleaving purification tags in commercial-scale processes’, *Trends in Biotechnology*, 28(5), pp.

272–279. doi: 10.1016/j.tibtech.2010.02.003.

da Fonseca, P. C. A. *et al.* (2003) ‘Domain organization of the type 1 inositol 1,4,5-trisphosphate receptor as revealed by single-particle analysis’, *Proceedings of the National Academy of Sciences*, 100(7), pp. 3936–3941. doi: 10.1073/pnas.0536251100.

Foskett, J. K. *et al.* (2007) ‘Inositol Trisphosphate Receptor Ca 2+ Release Channels’, *Physiological Reviews*, 87(2), pp. 593–658. doi: 10.1152/physrev.00035.2006.

Fowler, C. J., Griffiths, D. and de Groat, W. C. (2008) ‘The neural control of micturition’, *Nature Reviews Neuroscience*. Nature Publishing Group, 9, p. 453. Available at: https://doi.org/10.1038/nrn2401.

Franzini-Armstrong, C. (1970) ‘Studies of the Triad: Structure of the Junction in Frog Twitch Fibers’, *The Journal of Cell Biology*, 47(2), pp. 488–499. doi: 10.1083/jcb.47.2.488.

Friedberg, F. and Rhoads, A. R. (2001) ‘Evolutionary Aspects of Calmodulin’, *IUBMB Life*, 51, pp. 215–221.

Fruen, B. R. *et al.* (2000) ‘Differential Ca 2+ sensitivity of skeletal and cardiac muscle ryanodine receptors in the presence of calmodulin’, *American Journal of Physiology-Cell Physiology*, 279(3), pp. C724–C733. doi: 10.1152/ajpcell.2000.279.3.C724.

Fruen, B. R. *et al.* (2003) ‘Regulation of the RYR1 and RYR2 Ca2+ release channel isoforms by Ca2+-insensitive mutants of calmodulin’, *Biochemistry*, 42(9), pp. 2740–2747. doi: 10.1021/bi0267689.

Fujii, Y. *et al.* (2017) 'A type 2 ryanodine receptor variant associated with reduced Ca2+ release and short-coupled torsades de pointes ventricular arrhythmia', *Heart Rhythm*, 14(1), pp. 98–107. doi: 10.1016/j.hrthm.2016.10.015.

Fukuyama, M. *et al.* (2014) 'Long QT syndrome type 8: novel CACNA1C mutations causing QT prolongation and variant phenotypes', *Europace*, 16(12), pp. 1828–1837. doi: 10.1093/europace/euu063.

Futatsugi, A., Kuwajima, G. and Mikoshiba, K. (1998) 'Muscle-specific mRNA isoform encodes a protein composed mainly of the N-terminal 175 residues of type 2 Ins(1,4,5)P3 receptor', *Biochemical Journal*, 334(3), pp. 559–563. doi: 10.1042/bj3340559.

Gachet, C. (2006) 'Regulation of Platelet Functions by P2 Receptors', *Annual Review of Pharmacology and Toxicology*, 46(1), pp. 277–300. doi: 10.1146/annurev.pharmtox.46.120604.141207.

Galvan, D. L. *et al.* (1999) 'Subunit Oligomerization, and Topology of the Inositol 1,4,5-Trisphosphate Receptor', *Journal of Biological Chemistry*, 274(41), pp. 29483–29492. doi: 10.1074/jbc.274.41.29483.

Gangopadhyay, J. P., Grabarek, Z. and Ikemoto, N. (2004) 'Fluorescence probe study of Ca2+-dependent interactions of calmodulin with calmodulin-binding peptides of the ryanodine receptor', *Biochemical and Biophysical Research Communications*, 323(3), pp. 760–768. doi: 10.1016/j.bbrc.2004.08.154.

Gangopadhyay, J. P. and Ikemoto, N. (2006) 'Role of the Met3534-Ala4271 region of the ryanodine receptor in the regulation of Ca2+ release induced by calmodulin

binding domain peptide', *Biophysical Journal*, 90(6), pp. 2015–26. doi: 10.1529/biophysj.105.074328.

Gangopadhyay, J. P. and Ikemoto, N. (2008) 'Interaction of the Lys 3614 –Asn 3643 calmodulin-binding domain with the Cys 4114 -Asn 4142 region of the type 1 ryanodine receptor is involved in the mechanism of Ca 2+ /agonist-induced channel activation', *Biochemical Journal*, 411(2), pp. 415–423. doi: 10.1042/BJ20071375.

Gangopadhyay, J. P. and Ikemoto, N. (2011) 'Aberrant interaction of calmodulin with the ryanodine receptor develops hypertrophy in the neonatal cardiomyocyte', *Biochemical Journal*, 438(2), pp. 379–387. doi: 10.1042/BJ20110203.

Gardner, A. J. and Evans, J. P. (2006) 'Mammalian membrane block to polyspermy: new insights into how mammalian eggs prevent fertilisation by multiple sperm', *Reproduction, Fertility and Development*, 18(2), p. 53. doi: 10.1071/RD05122.

Geisow, M. J. *et al.* (1986) 'A consensus amino-acid sequence repeat in Torpedo and mammalian Ca2+-dependent membrane-binding proteins', *Nature*, 320(6063), pp. 636–638. doi: 10.1038/320636a0.

George, A. L. (2015) 'Calmodulinopathy: A genetic trilogy', *Heart Rhythm*, 12(2), pp. 423–424. doi: 10.1016/j.hrthm.2014.11.017.

George, C. H. *et al.* (2007) 'Ryanodine receptors and ventricular arrhythmias: Emerging trends in mutations, mechanisms and therapies', *Journal of Molecular and Cellular Cardiology*, 42(1), pp. 34–50. doi: 10.1016/j.yjmcc.2006.08.115.

George, C. H., Higgs, G. V. and Lai, F. A. (2003) 'Ryanodine Receptor Mutations Associated With Stress-Induced Ventricular Tachycardia Mediate Increased Calcium

Release in Stimulated Cardiomyocytes', *Circulation Research*, 93(6), pp. 531–540. doi: 10.1161/01.RES.0000091335.07574.86.

des Georges, A. *et al.* (2016) 'Structural Basis for Gating and Activation of RyR1', *Cell*, 167(1), pp. 145-157.e17. doi: 10.1016/j.cell.2016.08.075.

Gerasimenko, J. V. *et al.* (2003) 'NAADP mobilizes Ca 2+ from a thapsigargin-sensitive store in the nuclear envelope by activating ryanodine receptors', *The Journal of Cell Biology*, 163(2), pp. 271–282. doi: 10.1083/jcb.200306134.

Ghosh, S., Nunziato, D. A. and Pitt, G. S. (2006) 'KCNQ1 Assembly and Function Is Blocked by Long-QT Syndrome Mutations That Disrupt Interaction With Calmodulin', *Circulation Research*, 98(8), pp. 1048–1054. doi: 10.1161/01.RES.0000218863.44140.f2.

Giannini, G. *et al.* (1992) 'Expression of a ryanodine receptor-Ca2+ channel that is regulated by TGF-beta', *Science*, 257(5066), pp. 91–94. doi: 10.1126/science.1320290.

Giannini, G. *et al.* (1995) 'The ryanodine receptor/calcium channel genes are widely and differentially expressed in murine brain and peripheral tissues', *The Journal of Cell Biology*, 128(5), pp. 893–904. doi: 10.1083/jcb.128.5.893.

Gillies, A. R., Mahmoud, R. B. and Wood, D. W. (2009) 'PHB-Intein-Mediated Protein Purification Strategy', in Doyle SA. (ed.) *High Throughput Protein Expression and Purification. Methods in Molecular Biology*. Humana Press, pp. 173–183. doi: 10.1007/978-1-59745-196-3_12.

Glaser, T., Resende, R. R. and Ulrich, H. (2013) 'Implications of purinergic receptor-

mediated intracellular calcium transients in neural differentiation', *Cell Communication and Signaling*, 11(1), p. 12. doi: 10.1186/1478-811X-11-12.

Gogarten, J. P. *et al.* (2002) 'Inteins: Structure, Function, and Evolution', *Annual Review of Microbiology*, 56(1), pp. 263–287. doi: 10.1146/annurev.micro.56.012302.160741.

Goldenberg, I., Zareba, W. and Moss, A. J. (2008) 'Long QT Syndrome', *Current Problems in Cardiology*, 33(11), pp. 629–694. doi: 10.1016/j.cpcardiol.2008.07.002.

Gomez-Hurtado, N. *et al.* (2016) 'Novel CPVT-Associated Calmodulin Mutation in CALM3 (CALM3-A103V) Activates Arrhythmogenic Ca Waves and Sparks', *Circulation: Arrhythmia and Electrophysiology*, 9(8). doi: 10.1161/CIRCEP.116.004161.

Gomez, A. C. and Yamaguchi, N. (2014) 'Two regions of the ryanodine receptor calcium channel are involved in Ca2+-dependent inactivation', *Biochemistry*, 53(8), pp. 1373–1379. doi: 10.1021/bi401586h.

Goonasekera, S. A. and Molkentin, J. D. (2012) 'Unraveling the secrets of a double life: Contractile versus signaling Ca2+ in a cardiac myocyte', *Journal of Molecular and Cellular Cardiology*. Elsevier Ltd, 52(2), pp. 317–322. doi: 10.1016/j.yjmcc.2011.05.001.

Green, M. R. and Sambrook, J. (2012) *Molecular Cloning: A Laboratory Manual*. Fourth edi. Cold Spring Harbor Laboratory Press.

Groigno, L. and Whitaker, M. (1998) 'An Anaphase Calcium Signal Controls Chromosome Disjunction in Early Sea Urchin Embryos', *Cell*, 92(2), pp. 193–204.

doi: 10.1016/S0092-8674(00)80914-9.

Grycova, L. *et al.* (2015) ‘Ca2+Binding protein s100a1 competes with calmodulin and PIP2 for binding site on the c-terminus of the tprv1 receptor’, *ACS Chemical Neuroscience*, 6(3), pp. 386–392. doi: 10.1021/cn500250r.

Gu, M. *et al.* (2018) ‘Small-conductance Ca2+-activated K+ channels: insights into their roles in cardiovascular disease’, *Experimental & Molecular Medicine*, 50(4), p. 23. doi: 10.1038/s12276-018-0043-z.

Guo, W. *et al.* (2016) ‘The EF-hand Ca 2+ Binding Domain Is Not Required for Cytosolic Ca 2+ Activation of the Cardiac Ryanodine Receptor’, *Journal of Biological Chemistry*, 291(5), pp. 2150–2160. doi: 10.1074/jbc.M115.693325.

Haiech, J., Klee, C. B. and Demaille, J. G. (1981) ‘Effects of Cations on Affinity of Calmodulin for Calcium: Ordered Binding of Calcium Ions Allows the Specific Activation of Calmodulin-Stimulated Enzymes’, *Biochemistry*, 20(13), pp. 3890–3897. doi: 10.1021/bi00516a035.

Hamada, K., Terauchi, A. and Mikoshiba, K. (2003) ‘Three-dimensional Rearrangements within Inositol 1,4,5-Trisphosphate Receptor by Calcium’, *Journal of Biological Chemistry*, 278(52), pp. 52881–52889. doi: 10.1074/jbc.M309743200.

Hamilton, S. L. and Serysheva, I. I. (2009) ‘Ryanodine Receptor Structure: Progress and Challenges’, *Journal of Biological Chemistry*, 284(7), pp. 4047–4051. doi: 10.1074/jbc.R800054200.

Hamilton, S. L., Serysheva, I. and Strasburg, G. M. (2000) ‘Calmodulin and Excitation-Contraction Coupling’, *Physiology*, 15(6), pp. 281–284. doi:

10.1152/physiologyonline.2000.15.6.281.

Hammarström, M. *et al.* (2009) ‘Rapid screening for improved solubility of small human proteins produced as fusion proteins in Escherichia coli’, *Protein Science*, 11(2), pp. 313–321. doi: 10.1110/ps.22102.

Harrison, G. G. (1998) ‘Control of the malignant hyperpyrexic syndrome in MHS swine by dantrolene sodium. 1975’, *British Journal of Anaesthesia*, 81(4), pp. 626–629. doi: 10.1093/bja/81.4.626.

Harteneck, C., Klose, C. and Krautwurst, D. (2011) ‘Synthetic Modulators of TRP Channel Activity’, in, pp. 87–106. doi: 10.1007/978-94-007-0265-3_4.

Hayashi, Meiso *et al.* (2009) ‘Incidence and Risk Factors of Arrhythmic Events in Catecholaminergic Polymorphic Ventricular Tachycardia’, *Circulation*, 119(18), pp. 2426–2434. doi: 10.1161/CIRCULATIONAHA.108.829267.

Hennessey, J. P. *et al.* (1987) ‘Conformational transitions of calmodulin as studied by vacuum-UV CD’, *Biopolymers*, 26(4), pp. 561–571. doi: 10.1002/bip.360260409.

Her, C. *et al.* (2016) ‘Calcium-Dependent Structural Dynamics of a Spin-Labeled RyR Peptide Bound to Calmodulin’, *Biophysical Journal*, 111(11), pp. 2387–2394. doi: 10.1016/j.bpj.2016.10.025.

Heytens, E. *et al.* (2009) ‘Reduced amounts and abnormal forms of phospholipase C zeta (PLC) in spermatozoa from infertile men’, *Human Reproduction*, 24(10), pp. 2417–2428. doi: 10.1093/humrep/dep207.

Hilgemann, D. W. (1986) ‘Extracellular calcium transients and action potential

configuration changes related to post-stimulatory potentiation in rabbit atrium', *The Journal of General Physiology*, 87(5), pp. 675–706. doi: 10.1085/jgp.87.5.675.

Hilgemann, D. W., Delay, M. J. and Langer, G. A. (1983) 'Activation-dependent cumulative depletions of extracellular free calcium in guinea pig atrium measured with antipyrylazo III and tetramethylmurexide', *Circulation Research*, 53(6), pp. 779–93. doi: 10.1161/01.RES.53.6.779.

Hiraoki, T. and Vogel, H. J. (1987) 'Structure and function of calcium-binding proteins.', *Journal of Cardiovascular Pharmacology*, 10 Suppl 1, pp. S14-31. Available at: http://www.ncbi.nlm.nih.gov/pubmed/2442507.

Hoch, B. *et al.* (1999) 'Identification and Expression of δ-Isoforms of the Multifunctional Ca 2+ /Calmodulin-Dependent Protein Kinase in Failing and Nonfailing Human Myocardium', *Circulation Research*, 84(6), pp. 713–721. doi: 10.1161/01.RES.84.6.713.

Hochuli, E. *et al.* (1988) 'Genetic Approach to Facilitate Purification of Recombinant Proteins with a Novel Metal Chelate Adsorbent', *Nature Biotechnology*. Nature Publishing Company, 6(11), pp. 1321–1325. doi: 10.1038/nbt1188-1321.

Hochuli, E., Döbeli, H. and Schacher, A. (1987) 'New metal chelate adsorbent selective for proteins and peptides containing neighbouring histidine residues', *Journal of Chromatography A*, 411, pp. 177–184. doi: 10.1016/S0021-9673(00)93969-4.

Hoeflich, K. P. and Ikura, M. (2002) 'Calmodulin in action: diversity in target recognition and activation mechanisms.', *Cell*, 108(6), pp. 739–42. doi:

10.1016/S0092-8674(02)00682-7.

Hoffman, L. *et al.* (2014) 'Neurogranin Alters the Structure and Calcium Binding Properties of Calmodulin', *Journal of Biological Chemistry*, 289(21), pp. 14644–14655. doi: 10.1074/jbc.M114.560656.

Hogan, P. G. and Rao, A. (2015) 'Store-operated calcium entry: Mechanisms and modulation', *Biochemical and Biophysical Research Communications*, 460(1), pp. 40–49. doi: 10.1016/j.bbrc.2015.02.110.

Hokin, R.; Hokin, L. (1953) 'Enzyme secretion and into phospholipides', *J. Bio. Chem.*, 203, pp. 967–977.

Houdusse, A. *et al.* (2006) 'Crystal structure of apo-calmodulin bound to the first two IQ motifs of myosin V reveals essential recognition features', *Proceedings of the National Academy of Sciences*, 103(51), pp. 19326–19331. doi: 10.1073/pnas.0609436103.

Huang, C. L.-H. *et al.* (2016) 'Editorial: Ca2+ Signaling and Heart Rhythm', *Frontiers in Physiology*, 6(3), pp. 147–58. doi: 10.3389/fphys.2015.00423.

Huang, F. *et al.* (2006) 'Analysis of calstabin2 (FKBP12.6)-ryanodine receptor interactions: Rescue of heart failure by calstabin2 in mice', *Proceedings of the National Academy of Sciences*, 103(9), pp. 3456–3461. doi: 10.1073/pnas.0511282103.

Huang, P. *et al.* (2014) 'P2X4 Forms Functional ATP-activated Cation Channels on Lysosomal Membranes Regulated by Luminal pH', *Journal of Biological Chemistry*, 289(25), pp. 17658–17667. doi: 10.1074/jbc.M114.552158.

Huang, X. *et al.* (2013) ‘Two potential calmodulin-binding sequences in the ryanodine receptor contribute to a mobile, intra-subunit calmodulin-binding domain’, *Journal of Cell Science*, 126(19), pp. 4527–4535. doi: 10.1242/jcs.133454.

Huke, S. and Bers, D. M. (2008) ‘Ryanodine receptor phosphorylation at Serine 2030, 2808 and 2814 in rat cardiomyocytes’, *Biochemical and Biophysical Research Communications*, 376(1), pp. 80–85. doi: 10.1016/j.bbrc.2008.08.084.

Hunter, D. R., Haworth, R. A. and Berkoff, H. A. (1983) ‘Modulation of cellular calcium stores in the perfused rat heart by isoproterenol and ryanodine.’, *Circulation Research*, 53(5), pp. 703–712. doi: 10.1161/01.RES.53.5.703.

Hurley, J. H. and Misra, S. (2000) ‘Signaling and Subcellular Targeting by Membrane-Binding Domains’, *Annual Review of Biophysics and Biomolecular Structure*, 29(1), pp. 49–79. doi: 10.1146/annurev.biophys.29.1.49.

Hwang, H. S. *et al.* (2014) ‘Divergent Regulation of Ryanodine Receptor 2 Calcium Release Channels by Arrhythmogenic Human Calmodulin Missense Mutants’, *Circulation Research*, 114(7), pp. 1114–1124. doi: 10.1161/CIRCRESAHA.114.303391.

Hymel, L. *et al.* (1988) ‘Purified ryanodine receptor of skeletal muscle sarcoplasmic reticulum forms Ca2+-activated oligomeric Ca2+ channels in planar bilayers.’, *Proceedings of the National Academy of Sciences*, 85(2), pp. 441–445. doi: 10.1073/pnas.85.2.441.

Ikemoto, N. (2002) ‘Regulation of calcium release by interdomain interaction within ryanodine receptors’, *Frontiers in Bioscience*, 7(4), p. A803. doi: 10.2741/A803.

Ikemoto, N., Antoniu, B. and Mészáros, L. G. (1985) ‘Rapid flow chemical quench studies of calcium release from isolated sarcoplasmic reticulum.’, *Journal of Biological Chemistry*, 260(26), pp. 14096–100. Available at: http://www.ncbi.nlm.nih.gov/pubmed/2414290.

Ikura, M. and Ames, J. B. (2006) ‘Genetic polymorphism and protein conformational plasticity in the calmodulin superfamily: Two ways to promote multifunctionality’, *Proceedings of the National Academy of Sciences*, 103(5), pp. 1159–1164. doi: 10.1073/pnas.0508640103.

Imagawa, T. *et al.* (1987) ‘Purified ryanodine receptor from skeletal muscle sarcoplasmic reticulum is the Ca2+-permeable pore of the calcium release channel’, *J Biol Chem*, 262(34), pp. 16636–16643. Available at: http://www.ncbi.nlm.nih.gov/entrez/query.fcgi?cmd=Retrieve&db=PubMed&dopt=Citation&list_uids=2445748.

Inoue, R., Jian, Z. and Kawarabayashi, Y. (2009) ‘Mechanosensitive TRP channels in cardiovascular pathophysiology’, *Pharmacology & Therapeutics*, 123(3), pp. 371–385. doi: 10.1016/j.pharmthera.2009.05.009.

Inui, M., Saito, A. and Fleischer, S. (1987a) ‘Isolation of the ryanodine receptor from cardiac sarcoplasmic reticulum and identity with the feet structures’, *Journal of Biological Chemistry*, 262(32), pp. 15637–15642.

Inui, M., Saito, A. and Fleischer, S. (1987b) ‘Purification of the ryanodine receptor and identity with feet structures of junctional terminal cisternae of sarcoplasmic reticulum from fast skeletal muscle.’, *Journal of Biological Chemistry*, 262(4), pp.

1740–1747.

Islam, M. S. (2010) ‘Calcium Signaling in the Islets’, *Advances in Experimental Medicine and Biology*, 654, pp. 235–259. doi: 10.1007/978-90-481-3271-3_11.

Ito, M., Shikano, T., Oda, S., *et al.* (2008) ‘Difference in Ca2+ Oscillation-Inducing Activity and Nuclear Translocation Ability of PLCZ1, an Egg-Activating Sperm Factor Candidate, Between Mouse, Rat, Human, and Medaka Fish1’, *Biology of Reproduction*, 78(6), pp. 1081–1090. doi: 10.1095/biolreprod.108.067801.

Ito, M., Shikano, T., Kuroda, K., *et al.* (2008) ‘Relationship between nuclear sequestration of PLCζ and termination of PLCζ-induced Ca2+ oscillations in mouse eggs’, *Cell Calcium*, 44(4), pp. 400–410. doi: 10.1016/j.ceca.2008.02.003.

Iwai, M. *et al.* (2007) ‘Molecular Basis of the Isoform-specific Ligand-binding Affinity of Inositol 1,4,5-Trisphosphate Receptors’, *Journal of Biological Chemistry*, 282(17), pp. 12755–12764. doi: 10.1074/jbc.M609833200.

Jacobs, P. A. A. *et al.* (1978) ‘The origin of human triploids’, *Annals of Human Genetics*, 42(1), pp. 49–57. doi: 10.1111/j.1469-1809.1978.tb00930.x.

Jacobson, D. A. and Philipson, L. H. (2007) ‘TRP channels of the pancreatic beta cell.’, *Handbook of Experimental Pharmacology*. Berlin, Heidelberg: Springer Berlin Heidelberg, 179, pp. 409–24. doi: 10.1007/978-3-540-34891-7_24.

Jaffe, L. F. (1983) ‘Sources of calcium in egg activation: A review and hypothesis’, *Developmental Biology*, 99(2), pp. 265–276. doi: 10.1016/0012-1606(83)90276-2.

Jaffe, L. F. (1991) ‘The path of calcium in cytosolic calcium oscillations: a unifying

hypothesis.', *Proceedings of the National Academy of Sciences*, 88(21), pp. 9883–9887. doi: 10.1073/pnas.88.21.9883.

Jaiswal, J. K. (2001) 'Calcium — how and why?', *Journal of Biosciences*, 26(3), pp. 357–363. doi: 10.1007/BF02703745.

James, P., Vorherr, T. and Carafoli, E. (1995) 'Calmodulin-binding domains: just two faced or multi-faceted?', *Trends in Biochemical Sciences*, 20(1), pp. 38–42. doi: 10.1016/S0968-0004(00)88949-5.

Jellerette, T. *et al.* (2000) 'Down-regulation of the Inositol 1,4,5-Trisphosphate Receptor in Mouse Eggs Following Fertilization or Parthenogenetic Activation', *Developmental Biology*, 223(2), pp. 238–250. doi: 10.1006/dbio.2000.9675.

Jenden, D. J. and Fairhurst, A. S. (1969) 'The Pharmacology of Ryanodine', *Pharmacological Reviews*, 21(1), pp. 1–25.

Jentsch, S. and Pyrowolakis, G. (2000) 'Ubiquitin and its kin: how close are the family ties?', *Trends in Cell Biology*, 10(8), pp. 335–342. doi: 10.1016/S0962-8924(00)01785-2.

Jiang, D. *et al.* (2002) 'Enhanced Basal Activity of a Cardiac Ca 2+ Release Channel (Ryanodine Receptor) Mutant Associated With Ventricular Tachycardia and Sudden Death', *Circulation Research*, 91(3), pp. 218–225. doi: 10.1161/01.RES.0000028455.36940.5E.

Jiang, D. *et al.* (2004) 'RyR2 mutations linked to ventricular tachycardia and sudden death reduce the threshold for store-overload-induced Ca2+ release (SOICR)', *Proceedings of the National Academy of Sciences*, 101(35), pp. 13062–13067. doi:

10.1073/pnas.0402388101.

Jiang, D. *et al.* (2005) ‘Enhanced Store Overload–Induced Ca 2+ Release and Channel Sensitivity to Luminal Ca 2+ Activation Are Common Defects of RyR2 Mutations Linked to Ventricular Tachycardia and Sudden Death’, *Circulation Research*, 97(11), pp. 1173–1181. doi: 10.1161/01.RES.0000192146.85173.4b.

Jiang, D. *et al.* (2007) ‘Loss of luminal Ca2+ activation in the cardiac ryanodine receptor is associated with ventricular fibrillation and sudden death’, *Proceedings of the National Academy of Sciences*, 104(46), pp. 18309–18314. doi: 10.1073/pnas.0706573104.

Jiang, Q. *et al.* (2002) ‘Three-dimensional structure of the type 1 inositol 1,4,5-trisphosphate receptor at 24 A resolution’, *The EMBO Journal*, 21(14), pp. 3575–3581. doi: 10.1093/emboj/cdf380.

Jiménez-Jáimez, J. *et al.* (2016) ‘Calmodulin 2 Mutation N98S Is Associated with Unexplained Cardiac Arrest in Infants Due to Low Clinical Penetrance Electrical Disorders’, *PLoS ONE*. Edited by D. Laver. Public Library of Science, 11(4), p. e0153851. doi: 10.1371/journal.pone.0153851.

Jones, K. T. *et al.* (2000) ‘Different Ca2+-releasing abilities of sperm extracts compared with tissue extracts and phospholipase C isoforms in sea urchin egg homogenate and mouse eggs’, *Biochemical Journal*, 346(3), p. 743. doi: 10.1042/0264-6021:3460743.

Jones, K. T. and Nixon, V. L. (2000) ‘Sperm-Induced Ca2+ Oscillations in Mouse Oocytes and Eggs Can Be Mimicked by Photolysis of Caged Inositol 1,4,5-

Trisphosphate: Evidence to Support a Continuous Low Level Production of Inositol 1,4,5-Trisphosphate during Mammalian Fertilization', *Developmental Biology*, 225(1), pp. 1–12. doi: 10.1006/dbio.2000.9826.

Jones, L. R. *et al.* (1979) 'Ryanodine-Induced Stimulation of Net Ca2+ Uptake by Cardiac Sarcoplasmic Reticulum Vesicles.', *The Journal of Pharmacology and Experimental Therapeutics*, 209(1), pp. 48–55.

Jones, P. *et al.* (2008) 'Endoplasmic reticulum Ca 2+ measurements reveal that the cardiac ryanodine receptor mutations linked to cardiac arrhythmia and sudden death alter the threshold for store-overload-induced Ca 2+ release', *Biochemical Journal*, 412(1), pp. 171–178. doi: 10.1042/BJ20071287.

Jones, P. P., Guo, W. and Chen, S. R. W. (2017) 'Control of cardiac ryanodine receptor by sarcoplasmic reticulum luminal Ca 2+', *The Journal of General Physiology*, 149(9), pp. 867–875. doi: 10.1085/jgp.201711805.

Joseph, S. K. (1996) 'The inositol triphosphate receptor family', *Cellular Signalling*, 8(1), pp. 1–7. doi: 10.1016/0898-6568(95)02012-8.

Joseph, S. K. *et al.* (1997) 'Membrane Insertion, Glycosylation, and Oligomerization of Inositol Trisphosphate Receptors in a Cell-free Translation System', *Journal of Biological Chemistry*, 272(3), pp. 1579–1588. doi: 10.1074/jbc.272.3.1579.

Josephs, K. *et al.* (2017) 'Compound heterozygous CASQ2 mutations and long-term course of catecholaminergic polymorphic ventricular tachycardia', *Molecular Genetics & Genomic Medicine*, 5(6), pp. 788–794. doi: 10.1002/mgg3.323.

Jungbluth, H. *et al.* (2018) 'Congenital myopathies: disorders of excitation–

contraction coupling and muscle contraction', *Nature Reviews Neurology*. Nature Publishing Group, 14(3), pp. 151–167. doi: 10.1038/nrneurol.2017.191.

Jurado, L. A., Chockalingam, P. S. and Jarrett, H. W. (1999) 'Apocalmodulin', *Physiological Reviews*, 79(3), pp. 661–682. doi: 10.1152/physrev.1999.79.3.661.

Juranic, N. *et al.* (2010) 'Calmodulin Wraps around Its Binding Domain in the Plasma Membrane Ca 2+ Pump Anchored by a Novel 18-1 Motif', *Journal of Biological Chemistry*, 285(6), pp. 4015–4024. doi: 10.1074/jbc.M109.060491.

Kadamur, G. and Ross, E. M. (2013) 'Mammalian Phospholipase C', *Annual Review of Physiology*, 75(1), pp. 127–154. doi: 10.1146/annurev-physiol-030212-183750.

Kahl, C. R. and Means, A. R. (2003) 'Regulation of Cell Cycle Progression by Calcium/Calmodulin-Dependent Pathways', *Endocrine Reviews*, 24(6), pp. 719–736. doi: 10.1210/er.2003-0008.

Kapiloff, M. S., Jackson, N. and Airhart, N. (2001) 'mAKAP and the ryanodine receptor are part of a multi-component signaling complex on the cardiomyocyte nuclear envelope.', *Journal of cell science*, 114(Pt 17), pp. 3167–76.

Kapplinger, J. D. *et al.* (2009) 'Spectrum and prevalence of mutations from the first 2,500 consecutive unrelated patients referred for the FAMILION® long QT syndrome genetic test', *Heart Rhythm*, 6(9), pp. 1297–1303. doi: 10.1016/j.hrthm.2009.05.021.

Kapust, R. B. and Waugh, D. S. (1999) 'Escherichia coli maltose-binding protein is uncommonly effective at promoting the solubility of polypeptides to which it is fused', *Protein Science*, 8(8), pp. 1668–1674. doi: 10.1110/ps.8.8.1668.

Karacsonyi, C., Miguel, A. S. and Puertollano, R. (2007) ‘Mucolipin-2 Localizes to the Arf6-Associated Pathway and Regulates Recycling of GPI-APs’, *Traffic*, 8(10), pp. 1404–1414. doi: 10.1111/j.1600-0854.2007.00619.x.

Kashir, J. *et al.* (2012) ‘Characterization of two heterozygous mutations of the oocyte activation factor phospholipase C zeta (PLCζ) from an infertile man by use of minisequencing of individual sperm and expression in somatic cells’, *Fertility and Sterility*. Elsevier, 98(2), pp. 423–431. doi: 10.1016/j.fertnstert.2012.05.002.

Kashir, J. *et al.* (2017) ‘Antigen unmasking enhances visualization efficacy of the oocyte activation factor, phospholipase C zeta, in mammalian sperm’, *Molecular Human Reproduction*. England, 23(1), pp. 54–67. doi: 10.1093/molehr/gaw073.

Kashir, J., Nomikos, M. and Lai, F. A. (2018) ‘Phospholipase C zeta and calcium oscillations at fertilisation: The evidence, applications, and further questions’, *Advances in Biological Regulation*. Elsevier, 67(October 2017), pp. 148–162. doi: 10.1016/j.jbior.2017.10.012.

Kass, R. S. (1997) ‘Genetically Induced Reduction in Small Currents has Major Impact.’, *Circulation*, 96(6), pp. 1720–1. Available at: http://www.ncbi.nlm.nih.gov/pubmed/9323051.

Katan, M. (1998) ‘Families of phosphoinositide-specific phospholipase C: structure and function’, *Biochimica et Biophysica Acta (BBA) - Molecular and Cell Biology of Lipids*, 1436(1–2), pp. 5–17. doi: 10.1016/S0005-2760(98)00125-8.

Kato, T. *et al.* (2017) ‘Correction of impaired calmodulin binding to RyR2 as a novel therapy for lethal arrhythmia in the pressure-overloaded heart failure’, *Heart Rhythm*,

14(1), pp. 120–127. doi: 10.1016/j.hrthm.2016.10.019.

Kawano, A. *et al.* (2012) 'Involvement of P2X4 receptor in P2X7 receptor-dependent cell death of mouse macrophages', *Biochemical and Biophysical Research Communications*, 419(2), pp. 374–380. doi: 10.1016/j.bbrc.2012.01.156.

Kawasaki, H. and Kretsinger, R. H. (2017) 'Structural and functional diversity of EF-hand proteins: Evolutionary perspectives', *Protein Science*, 26(10), pp. 1898–1920. doi: 10.1002/pro.3233.

Kawate, T. *et al.* (2011) 'Ion access pathway to the transmembrane pore in P2X receptor channels', *The Journal of General Physiology*, 137(6), pp. 579–590. doi: 10.1085/jgp.201010593.

Ter Keurs, H. E. D. J. and Boyden, P. A. (2007) 'Calcium and Arrhythmogenesis', *Physiological Reviews*, 87(2), pp. 457–506. doi: 10.1152/physrev.00011.2006.

Khananshvili, D. (2014) 'Sodium-calcium exchangers (NCX): molecular hallmarks underlying the tissue-specific and systemic functions', *Pflügers Archiv - European Journal of Physiology*, 466(1), pp. 43–60. doi: 10.1007/s00424-013-1405-y.

Kilpatrick, B. S. *et al.* (2013) 'Direct mobilisation of lysosomal Ca 2+ triggers complex Ca 2+ signals', *Journal of Cell Science*, 126(1), pp. 60–66. doi: 10.1242/jcs.118836.

Kimlicka, L. *et al.* (2013) 'Disease mutations in the ryanodine receptor N-terminal region couple to a mobile intersubunit interface', *Nature Communications*. Nature Publishing Group, 4(1), p. 1506. doi: 10.1038/ncomms2501.

Kirchhefer, U. *et al.* (1999) 'Activity of cAMP-dependent protein kinase and

Ca2+/calmodulin-dependent protein kinase in failing and nonfailing human hearts', *Cardiovascular Research*, 42(1), pp. 254–261. doi: 10.1016/S0008-6363(98)00296-X.

Kirichok, Y., Navarro, B. and Clapham, D. E. (2006) 'Whole-cell patch-clamp measurements of spermatozoa reveal an alkaline-activated Ca2+ channel', *Nature*, 439(7077), pp. 737–740. doi: 10.1038/nature04417.

Kiselyov, K. *et al.* (2005) 'TRP-ML1 Is a Lysosomal Monovalent Cation Channel That Undergoes Proteolytic Cleavage', *Journal of Biological Chemistry*, 280(52), pp. 43218–43223. doi: 10.1074/jbc.M508210200.

Kline, D. and Kline, J. T. (1992) 'Repetitive calcium transients and the role of calcium in exocytosis and cell cycle activation in the mouse egg', *Developmental Biology*, 149(1), pp. 80–89. doi: 10.1016/0012-1606(92)90265-I.

Klipp, R. C. *et al.* (2018) 'EL20, a potent antiarrhythmic compound, selectively inhibits calmodulin-deficient ryanodine receptor type 2', *Heart Rhythm*, 15(4), pp. 578–586. doi: 10.1016/j.hrthm.2017.12.017.

Knott, J. G. *et al.* (2005) 'Transgenic RNA Interference Reveals Role for Mouse Sperm Phospholipase Cζ in Triggering Ca2+ Oscillations During Fertilization1', *Biology of Reproduction*, 72(4), pp. 992–996. doi: 10.1095/biolreprod.104.036244.

Kobayashi, S. *et al.* (2005) 'Dantrolene Stabilizes Domain Interactions within the Ryanodine Receptor', *Journal of Biological Chemistry*, 280(8), pp. 6580–6587. doi: 10.1074/jbc.M408375200.

Kobayashi, S. *et al.* (2009) 'Dantrolene, a Therapeutic Agent for Malignant

Hyperthermia, Markedly Improves the Function of Failing Cardiomyocytes by Stabilizing Interdomain Interactions Within the Ryanodine Receptor', *Journal of the American College of Cardiology*. American College of Cardiology Foundation, 53(21), pp. 1993–2005. doi: 10.1016/j.jacc.2009.01.065.

Kohno, Masateru *et al.* (2003) 'A new cardioprotective agent, JTV519, improves defective channel gating of ryanodine receptor in heart failure', *American Journal of Physiology-Heart and Circulatory Physiology*, 284(3), pp. H1035–H1042. doi: 10.1152/ajpheart.00722.2002.

Kono, T. *et al.* (1996) 'A cell cycle-associated change in Ca2+ releasing activity leads to the generation of Ca2+ transients in mouse embryos during the first mitotic division', *The Journal of Cell Biology*, 132(5), pp. 915–923. doi: 10.1083/jcb.132.5.915.

Koshimizu, T. *et al.* (2000) 'Characterization of Calcium Signaling by Purinergic Receptor-Channels Expressed in Excitable Cells', *Molecular Pharmacology*, 58(5), pp. 936–945. doi: 10.1124/mol.58.5.936.

Kouchi, Z. *et al.* (2004) 'Recombinant Phospholipase Cζ Has High Ca 2+ Sensitivity and Induces Ca 2+ Oscillations in Mouse Eggs', *Journal of Biological Chemistry*, 279(11), pp. 10408–10412. doi: 10.1074/jbc.M313801200.

Kouchi, Z. *et al.* (2005) 'The role of EF-hand domains and C2 domain in regulation of enzymatic activity of phospholipase Cζ', *Journal of Biological Chemistry*, 280(22), pp. 21015–21021. doi: 10.1074/jbc.M412123200.

Koulen, P. and Thrower, E. C. (2001) 'Pharmacological Modulation of Intracellular

Ca^{2+} Channels at the Single-Channel Level', *Molecular Neurobiology*, 24(1–3), pp. 065–086. doi: 10.1385/MN:24:1-3:065.

Kovalevskaya, N. V. *et al.* (2013) 'Structural analysis of calmodulin binding to ion channels demonstrates the role of its plasticity in regulation', *Pflügers Archiv - European Journal of Physiology*, 465(11), pp. 1507–1519. doi: 10.1007/s00424-013-1278-0.

Krahn, A. D. *et al.* (2009) 'Systematic Assessment of Patients With Unexplained Cardiac Arrest', *Circulation*, 120(4), pp. 278–285. doi: 10.1161/CIRCULATIONAHA.109.853143.

Kretsinger, R. H. *et al.* (1980) 'Calmodulin, S-100, and crayfish sarcoplasmic calcium-binding protein crystals suitable for X-ray diffraction studies.', *Journal of Biological Chemistry*, 255(17), pp. 8154–6. Available at: http://www.ncbi.nlm.nih.gov/pubmed/7410354 (Accessed: 6 August 2015).

Kretsinger, R. H. and Barry, C. D. (1975) 'The predicted structure of the calcium-binding component of troponin', *Biochimica et Biophysica Acta (BBA) - Protein Structure*, 405(1), pp. 40–52. doi: 10.1016/0005-2795(75)90312-8.

Kretsinger, R. H. and Nockolds, C. E. (1973) 'Carp muscle calcium-binding protein. II. Structure determination and general description.', *Journal of Biological Chemistry*, 248(9), pp. 3313–26. Available at: http://www.ncbi.nlm.nih.gov/pubmed/4700463.

Kretsinger, R. H., Rudnick, S. E. and Weissman, L. J. (1986) 'Crystal structure of calmodulin', *Journal of Inorganic Biochemistry*, 28(2–3), pp. 289–302. doi: 10.1016/0162-0134(86)80093-9.

Kron, J., Ellenbogen, K. and Abbate, A. (2015) ‘Recurrent ventricular fibrillation in a young female carrying a previously unidentified RyR2 gene mutation’, *International Journal of Cardiology*. Elsevier Ireland Ltd, 201, pp. 222–224. doi: 10.1016/j.ijcard.2015.08.044.

Kumar, A. *et al.* (2018) ‘ACE2, CALM3 and TNNI3K polymorphisms as potential disease modifiers in hypertrophic and dilated cardiomyopathies’, *Molecular and Cellular Biochemistry*, 438(1–2), pp. 167–174. doi: 10.1007/s11010-017-3123-9.

Kung, C. *et al.* (1992) ‘In vivo Paramecium mutants show that calmodulin orchestrates membrane responses to stimuli’, *Cell Calcium*, 13(6–7), pp. 413–425. doi: 10.1016/0143-4160(92)90054-V.

Kupker, W., Diedrich, K. and Edwards, R. G. (1998) ‘Principles of mammalian fertilization’, *Human Reproduction*, 13(suppl 1), pp. 20–32. doi: 10.1093/humrep/13.suppl_1.20.

Kurasawa, S., Schultz, R. M. and Kopf, G. S. (1989) ‘Egg-induced modifications of the zona pellucida of mouse eggs: Effects of microinjected inositol 1,4,5-trisphosphate’, *Developmental Biology*, 133(1), pp. 295–304. doi: 10.1016/0012-1606(89)90320-5.

Kuroda, K. *et al.* (2006) ‘The role of X/Y linker region and N-terminal EF-hand domain in nuclear translocation and Ca2+oscillation-inducing activities of phospholipase Cζ, a mammalian egg-activating factor’, *Journal of Biological Chemistry*, 281(38), pp. 27794–27805. doi: 10.1074/jbc.M603473200.

Kurokawa, H. *et al.* (2001) ‘Target-induced conformational adaptation of calmodulin

revealed by the crystal structure of a complex with nematode Ca 2+ /calmodulin-dependent kinase kinase peptide 1 1Edited by K. Morikawa', *Journal of Molecular Biology*, 312(1), pp. 59–68. doi: 10.1006/jmbi.2001.4822.

Kurokawa, M. *et al.* (2007) 'Proteolytic processing of phospholipase Cζ and [Ca2+]i oscillations during mammalian fertilization', *Developmental Biology*, 312(1), pp. 407–418. doi: 10.1016/j.ydbio.2007.09.040.

Kursula, P. (2014a) 'Crystallographic snapshots of initial steps in the collapse of the calmodulin central helix', *Acta Crystallographica Section D Biological Crystallography*. International Union of Crystallography, 70(1), pp. 24–30. doi: 10.1107/S1399004713024437.

Kursula, P. (2014b) 'The many structural faces of calmodulin: a multitasking molecular jackknife', *Amino Acids*, 46(10), pp. 2295–2304. doi: 10.1007/s00726-014-1795-y.

Kuźnicki, J., Kuźnicki, L. and Drabikowski, W. (1979) 'Ca2+-binding modulator protein in protozoa and myxomycete', *Cell Biology International Reports*, 3(1), pp. 17–23. doi: 10.1016/0309-1651(79)90064-X.

Kwon, C. H. and Kim, S.-H. (2017) 'Intraoperative management of critical arrhythmia', *Korean Journal of Anesthesiology*, 70(2), p. 120. doi: 10.4097/kjae.2017.70.2.120.

de la Fuente, S. *et al.* (2008) 'A Case of Catecholaminergic Polymorphic Ventricular Tachycardia Caused by Two Calsequestrin 2 Mutations', *Pacing and Clinical Electrophysiology*, 31(7), pp. 916–919. doi: 10.1111/j.1540-8159.2008.01111.x.

Lahat, H., Pras, E., *et al.* (2001) 'A Missense Mutation in a Highly Conserved Region of CASQ2 Is Associated with Autosomal Recessive Catecholamine-Induced Polymorphic Ventricular Tachycardia in Bedouin Families from Israel', *The American Journal of Human Genetics*, 69(6), pp. 1378–1384. doi: 10.1086/324565.

Lahat, H., Eldar, M., *et al.* (2001) 'Autosomal Recessive Catecholamine- or Exercise-Induced Polymorphic Ventricular Tachycardia', *Circulation*, 103(23), pp. 2822–2827. doi: 10.1161/01.CIR.103.23.2822.

Lai, F. A. *et al.* (1988) 'Purification and reconstitution of the calcium release channel from skeletal muscle', *Nature*, 331(6154), pp. 315–319. doi: 10.1038/331315a0.

Laitinen, P. J. *et al.* (2001) 'Mutations of the Cardiac Ryanodine Receptor (RyR2) Gene in Familial Polymorphic Ventricular Tachycardia', *Circulation*, 103(4), pp. 485–490. doi: 10.1161/01.CIR.103.4.485.

Landstrom, A. P., Dobrev, D. and Wehrens, X. H. T. (2017) 'Calcium Signaling and Cardiac Arrhythmias', *Circulation Research*, 120(12), pp. 1969–1993. doi: 10.1161/CIRCRESAHA.117.310083.

Lanner, J. T. *et al.* (2010) 'Ryanodine Receptors: Structure, Expression, Molecular Details, and Function in Calcium Release', *Cold Spring Harbor Perspectives in Biology*, 2(11), pp. a003996–a003996. doi: 10.1101/cshperspect.a003996.

Larman, M. G. *et al.* (2004) 'Cell cycle-dependent Ca2+ oscillations in mouse embryos are regulated by nuclear targeting of PLC', *Journal of Cell Science*, 117(12), pp. 2513–2521. doi: 10.1242/jcs.01109.

Larsen, M. K. *et al.* (2013) 'Postmortem genetic testing of the ryanodine receptor 2

(RYR2) gene in a cohort of sudden unexplained death cases', *International Journal of Legal Medicine*, 127(1), pp. 139–144. doi: 10.1007/s00414-011-0658-2.

Lattanzio, F. A. *et al.* (1987) 'The effects of ryanodine on passive calcium fluxes across sarcoplasmic reticulum membranes', *Journal of Biological Chemistry*, 262(6), pp. 2711–2718.

Lau, K., Chan, M. M. Y. and Van Petegem, F. (2014) 'Lobe-specific calmodulin binding to different ryanodine receptor isoforms', *Biochemistry*, 53(5), pp. 932–946. doi: 10.1021/bi401502x.

Lau, K. and Van Petegem, F. (2014) 'Crystal structures of wild type and disease mutant forms of the ryanodine receptor SPRY2 domain', *Nature Communications*. Nature Publishing Group, 5(1), p. 5397. doi: 10.1038/ncomms6397.

Lau, S.-Y., Procko, E. and Gaudet, R. (2012) 'Distinct properties of Ca 2+ – calmodulin binding to N- and C-terminal regulatory regions of the TRPV1 channel', *The Journal of General Physiology*, 140(5), pp. 541–555. doi: 10.1085/jgp.201210810.

LaVallie, E. R. *et al.* (1993) 'A Thioredoxin Gene Fusion Expression System That Circumvents Inclusion Body Formation in the E. coli Cytoplasm', *Nature Biotechnology*, 11(2), pp. 187–193. doi: 10.1038/nbt0293-187.

LaVallie, E. R. *et al.* (2000) 'Thioredoxin as a fusion partner for production of soluble recombinant proteins in Escherichia coli', in *Methods in Enzymology*. Elsevier Inc., pp. 322–340. doi: 10.1016/S0076-6879(00)26063-1.

Ledbetter, M. W. *et al.* (1994) 'Tissue distribution of ryanodine receptor isoforms and

alleles determined by reverse transcription polymerase chain reaction.', *Journal of Biological Chemistry*, 269(50), pp. 31544–51. Available at: http://www.ncbi.nlm.nih.gov/pubmed/7989322.

Lee, S.-H. *et al.* (2000) 'Differences in Ca 2+ buffering properties between excitatory and inhibitory hippocampal neurons from the rat', *The Journal of Physiology*, 525(2), pp. 405–418. doi: 10.1111/j.1469-7793.2000.t01-3-00405.x.

Leenhardt, A. *et al.* (1995) 'Catecholaminergic Polymorphic Ventricular Tachycardia in Children : A 7-Year Follow-up of 21 Patients', *Circulation*, 91(5), pp. 1512–1519. doi: 10.1161/01.CIR.91.5.1512.

Lees, J. G. *et al.* (2006) 'A reference database for circular dichroism spectroscopy covering fold and secondary structure space', *Bioinformatics*, 22(16), pp. 1955–1962. doi: 10.1093/bioinformatics/btl327.

Lehnart, S. E. *et al.* (2005) 'Phosphodiesterase 4D Deficiency in the Ryanodine-Receptor Complex Promotes Heart Failure and Arrhythmias', *Cell*, 123(1), pp. 25–35. doi: 10.1016/j.cell.2005.07.030.

Leinonen, J. T. *et al.* (2018) 'The genetics underlying idiopathic ventricular fibrillation: A special role for catecholaminergic polymorphic ventricular tachycardia?', *International Journal of Cardiology*. Elsevier B.V., 250, pp. 139–145. doi: 10.1016/j.ijcard.2017.10.016.

Lemmon, M. A. *et al.* (1995) 'Specific and high-affinity binding of inositol phosphates to an isolated pleckstrin homology domain.', *Proceedings of the National Academy of Sciences*, 92(23), pp. 10472–10476. doi: 10.1073/pnas.92.23.10472.

Lewit-Bentley, A. and Réty, S. (2000) 'EF-hand calcium-binding proteins', *Current Opinion in Structural Biology*, 10(6), pp. 637–643. doi: 10.1016/S0959-440X(00)00142-1.

Leybaert, L. and Sanderson, M. J. (2012) 'Intercellular Ca 2+ Waves: Mechanisms and Function', *Physiological Reviews*, 92(3), pp. 1359–1392. doi: 10.1152/physrev.00029.2011.

Li, C. *et al.* (2013) 'CaBP1, a neuronal Ca2+ sensor protein, inhibits inositol trisphosphate receptors by clamping intersubunit interactions', *Proceedings of the National Academy of Sciences*, 110(21), pp. 8507–8512. doi: 10.1073/pnas.1220847110.

Li, N. *et al.* (2014) 'Ryanodine Receptor–Mediated Calcium Leak Drives Progressive Development of an Atrial Fibrillation Substrate in a Transgenic Mouse Model', *Circulation*, 129(12), pp. 1276–1285. doi: 10.1161/CIRCULATIONAHA.113.006611.

Li, P. and Chen, S. R. W. (2001) 'Molecular Basis of Ca 2 + Activation of the Mouse Cardiac Ca 2 + Release Channel (Ryanodine Receptor)', *The Journal of General Physiology*, 118(1), pp. 33–44. doi: 10.1085/jgp.118.1.33.

Liao, J. *et al.* (2012) 'Structural Insight into the Ion-Exchange Mechanism of the Sodium/Calcium Exchanger', *Science*, 335(6069), pp. 686–690. doi: 10.1126/science.1215759.

Limpitikul, W. B. *et al.* (2014) 'Calmodulin mutations associated with long QT syndrome prevent inactivation of cardiac L-type Ca2+ currents and promote proarrhythmic behavior in ventricular myocytes', *Journal of Molecular and Cellular*

Cardiology. Elsevier Ltd, 74, pp. 115–124. doi: 10.1016/j.yjmcc.2014.04.022.

Lin, C.-C., Baek, K. and Lu, Z. (2011) 'Apo and InsP3-bound crystal structures of the ligand-binding domain of an InsP3 receptor', *Nature Structural & Molecular Biology*, 18(10), pp. 1172–1174. doi: 10.1038/nsmb.2112.

Linse, S., Helmersson, A. and Forsen, S. (1991) 'Calcium binding to calmodulin and its globular domains', *Journal of Biological Chemistry*, 266(13), pp. 8050–8054.

Lips, M. B. and Keller, B. U. (1998) 'Endogenous calcium buffering in motoneurones of the nucleus hypoglossus from mouse', *The Journal of Physiology*, 511(1), pp. 105–117. doi: 10.1111/j.1469-7793.1998.105bi.x.

Lissandron, V. *et al.* (2010) 'Unique characteristics of Ca2+ homeostasis of the trans-Golgi compartment', *Proceedings of the National Academy of Sciences*. National Academy of Sciences, 107(20), pp. 9198–9203. doi: 10.1073/pnas.1004702107.

Liu, J.-R. *et al.* (2008) 'Cloning of a rumen fungal xylanase gene and purification of the recombinant enzyme via artificial oil bodies', *Applied Microbiology and Biotechnology*, 79(2), pp. 225–233. doi: 10.1007/s00253-008-1418-1.

Liu, M. (2011) 'The biology and dynamics of mammalian cortical granules', *Reproductive Biology and Endocrinology*. BioMed Central Ltd, 9(1), p. 149. doi: 10.1186/1477-7827-9-149.

Liu, N. and Priori, S. G. (2008) 'Disruption of calcium homeostasis and arrhythmogenesis induced by mutations in the cardiac ryanodine receptor and calsequestrin', *Cardiovascular Research*, 77(2), pp. 293–301. doi:

10.1093/cvr/cvm004.

Liu, W. *et al.* (2012) ‘Lysozyme contamination facilitates crystallization of a heterotrimeric cortactin–Arg–lysozyme complex’, *Acta Crystallographica Section F Structural Biology and Crystallization Communications*, 68(2), pp. 154–158. doi: 10.1107/S1744309111056132.

Liu, Y. *et al.* (2013) ‘The CPVT-associated RyR2 mutation G230C enhances store overloadinduced Ca $^{2+}$ release and destabilizes the N-terminal domains’, *Biochemical Journal*, 454(1), pp. 123–131. doi: 10.1042/BJ20130594.

Liu, Y. *et al.* (2017) ‘CPVT-associated cardiac ryanodine receptor mutation G357S with reduced penetrance impairs Ca2+ release termination and diminishes protein expression’, *PLoS ONE*. Edited by N. Beard, 12(9), p. e0184177. doi: 10.1371/journal.pone.0184177.

Lmyates16 (no date) *Own work, CC BY-SA 4.0,*. Available at: https://commons.wikimedia.org/w/index.php?curid=47268185.

Loaiza, R. *et al.* (2013) ‘Heterogeneity of Ryanodine Receptor Dysfunction in a Mouse Model of Catecholaminergic Polymorphic Ventricular Tachycardia’, *Circulation Research*, 112(2), pp. 298–308. doi: 10.1161/CIRCRESAHA.112.274803.

Loar, R. W. *et al.* (2015) ‘Sudden Cardiac Arrest During Sex in Patients with Either Catecholaminergic Polymorphic Ventricular Tachycardia or Long-QT Syndrome: A Rare But Shocking Experience’, *Journal of Cardiovascular Electrophysiology*, 26(3), pp. 300–304. doi: 10.1111/jce.12600.

Lopatin, A. N. and Nichols, C. G. (2001) ‘Inward Rectifiers in the Heart: An Update

on IK1', *Journal of Molecular and Cellular Cardiology*, 33(4), pp. 625–638. doi: 10.1006/jmcc.2001.1344.

Ludtke, S. J. *et al.* (2011) 'Flexible Architecture of IP3R1 by Cryo-EM', *Structure*. Elsevier Ltd, 19(8), pp. 1192–1199. doi: 10.1016/j.str.2011.05.003.

Ma, J. (1993) 'Block by ruthenium red of the ryanodine-activated calcium release channel of skeletal muscle', *The Journal of General Physiology*, 102(6), pp. 1031–1056. doi: 10.1085/jgp.102.6.1031.

MacLennan, D. H. and Chen, S. R. W. (2009) 'Store overload-induced Ca 2+ release as a triggering mechanism for CPVT and MH episodes caused by mutations in RYR and CASQ genes', *The Journal of Physiology*, 587(13), pp. 3113–3115. doi: 10.1113/jphysiol.2009.172155.

MacLennan, D. H. and Phillips, M. S. (1992) 'Malignant hyperthermia.', *Science*, 256(5058), pp. 789–94. doi: 10.1126/science.256.5058.789.

MacLennan, D. H. and Zvaritch, E. (2011) 'Mechanistic models for muscle diseases and disorders originating in the sarcoplasmic reticulum', *Biochimica et Biophysica Acta (BBA) - Molecular Cell Research*. Elsevier B.V., 1813(5), pp. 948–964. doi: 10.1016/j.bbamcr.2010.11.009.

MacManus, J. P. *et al.* (1989) 'Differential calmodulin gene expression in fetal, adult, and neoplastic tissues of rodents', *Biochemical and Biophysical Research Communications*, 159(1), pp. 278–282. doi: 10.1016/0006-291X(89)92434-0.

Maeda, N. *et al.* (1991) 'Structural and functional characterization of inositol 1,4,5-trisphosphate receptor channel from mouse cerebellum.', *Journal of Biological*

Chemistry, 266(2), pp. 1109–1116.

Maier, L. S. and Bers, D. M. (2002) 'Calcium, Calmodulin, and Calcium-Calmodulin Kinase II: Heartbeat to Heartbeat and Beyond', *Journal of Molecular and Cellular Cardiology*, 34(8), pp. 919–939. doi: 10.1006/jmcc.2002.2038.

Makhatadze, G. I. and Privalov, P. L. (1995) 'Energetics of Protein Structure', in *Advances in Protein Chemistry*. Elsevier, pp. 307–425. doi: 10.1016/S0065-3233(08)60548-3.

Makino, T., Skretas, G. and Georgiou, G. (2011) 'Strain engineering for improved expression of recombinant proteins in bacteria', *Microbial Cell Factories*, 10(1), p. 32. doi: 10.1186/1475-2859-10-32.

Makita, N. *et al.* (2014) 'Novel Calmodulin Mutations Associated With Congenital Arrhythmia Susceptibility', *Circulation: Cardiovascular Genetics*, 7(4), pp. 466–474. doi: 10.1161/CIRCGENETICS.113.000459.

Malakhov, M. P. *et al.* (2004) 'SUMO fusions and SUMO-specific protease for efficient expression and purification of proteins', *Journal of Structural and Functional Genomics*, 5(1/2), pp. 75–86. doi: 10.1023/B:JSFG.0000029237.70316.52.

Malcuit, C., Kurokawa, M. and Fissore, R. A. (2006) 'Calcium oscillations and mammalian egg activation', *Journal of Cellular Physiology*, 206(3), pp. 565–573. doi: 10.1002/jcp.20471.

Manning, B. M. *et al.* (1998) 'Identification of Novel Mutations in the Ryanodine-Receptor Gene (RYR1) in Malignant Hyperthermia: Genotype-Phenotype Correlation', *The American Journal of Human Genetics*, 62(3), pp. 599–609. doi:

10.1086/301748.

Marblestone, J. G. *et al.* (2006) ‘Comparison of SUMO fusion technology with traditional gene fusion systems: Enhanced expression and solubility with SUMO’, *Protein Science*, 15(1), pp. 182–189. doi: 10.1110/ps.051812706.

Marchant, J. S. and Parker, I. (2000) ‘Functional Interactions in Ca 2+ Signaling over Different Time and Distance Scales’, *The Journal of General Physiology*, 116(5), pp. 691–696. doi: 10.1085/jgp.116.5.691.

Marchant, J. S. and Taylor, C. W. (1997) ‘Cooperative activation of IP3 receptors by sequential binding of IP3 and Ca2+ safeguards against spontaneous activity’, *Current Biology*, 7(7), pp. 510–518. doi: 10.1016/S0960-9822(06)00222-3.

Marjamaa, A. *et al.* (2011) ‘Ryanodine receptor (RyR2) mutations in sudden cardiac death: Studies in extended pedigrees and phenotypic characterization in vitro’, *International Journal of Cardiology*. Elsevier Ireland Ltd, 147(2), pp. 246–252. doi: 10.1016/j.ijcard.2009.08.041.

Marques-Carvalho, M. J. *et al.* (2016) ‘Molecular Insights into the Mechanism of Calmodulin Inhibition of the EAG1 Potassium Channel’, *Structure*, 24(10), pp. 1742–1754. doi: 10.1016/j.str.2016.07.020.

Marquez, B., Ignotz, G. and Suarez, S. S. (2007) ‘Contributions of extracellular and intracellular Ca2+ to regulation of sperm motility: Release of intracellular stores can hyperactivate CatSper1 and CatSper2 null sperm’, *Developmental Biology*, 303(1), pp. 214–221. doi: 10.1016/j.ydbio.2006.11.007.

Marsman, R. F. *et al.* (2014) ‘A Mutation in CALM1 Encoding Calmodulin in Familial

Idiopathic Ventricular Fibrillation in Childhood and Adolescence', *Journal of the American College of Cardiology*. Elsevier Ltd, 63(3), pp. 259–266. doi: 10.1016/j.jacc.2013.07.091.

Martin, S. R. and Bayley, P. M. (1986) 'The effects of Ca 2+ and Cd 2+ on the secondary and tertiary structure of bovine testis calmodulin. A circular-dichroism study', *Biochemical Journal*, 238(2), pp. 485–490. doi: 10.1042/bj2380485.

Martonosi, A. N. (1984) 'Mechanisms of Ca2+ release from sarcoplasmic reticulum of skeletal muscle', *Physiological Reviews*, 64(4), pp. 1240–1320. doi: 10.1152/physrev.1984.64.4.1240.

Marx, J. (1980) 'Calmodulin: a protein for all seasons', *Science*, 208(4441), pp. 274–276. doi: 10.1126/science.6102798.

Marx, S. O. *et al.* (2000) 'PKA Phosphorylation Dissociates FKBP12.6 from the Calcium Release Channel (Ryanodine Receptor)', *Cell*, 101(4), pp. 365–376. doi: 10.1016/S0092-8674(00)80847-8.

Marx, S. O. *et al.* (2001) 'Coupled Gating Between Cardiac Calcium Release Channels (Ryanodine Receptors)', *Circulation Research*, 88(11), pp. 1151–1158. doi: 10.1161/hh1101.091268.

Marx, S. O., Ondrias, K. and Marks, A. R. (1998) 'Coupled Gating Between Individual Skeletal Muscle Ca2+ Release Channels (Ryanodine Receptors)', *Science*, 281(5378), pp. 818–821. doi: 10.1126/science.281.5378.818.

Masino, L., Martin, S. R. and Bayley, P. M. (2000) 'Ligand binding and thermodynamic stability of a multidomain protein, calmodulin', *Protein Science*, 9(8),

pp. 1519–1529. doi: 10.1110/ps.9.8.1519.

Mathys, S. *et al.* (1999) ‘Characterization of a self-splicing mini-intein and its conversion into autocatalytic N- and C-terminal cleavage elements: facile production of protein building blocks for protein ligation’, *Gene*, 231(1–2), pp. 1–13. doi: 10.1016/S0378-1119(99)00103-1.

Maury, P. *et al.* (2010) ‘Primary electrical diseases diagnosis, genetic and management.’, *Minerva cardioangiologica*, 58(4), pp. 449–83. Available at: http://www.ncbi.nlm.nih.gov/pubmed/20938412.

Maximciuc, A. A. *et al.* (2006) ‘Complex of Calmodulin with a Ryanodine Receptor Target Reveals a Novel, Flexible Binding Mode’, *Structure*, 14(10), pp. 1547–1556. doi: 10.1016/j.str.2006.08.011.

McCoy, A. J. *et al.* (2007) ‘Phaser crystallographic software’, *Journal of Applied Crystallography*. International Union of Crystallography, 40(4), pp. 658–674. doi: 10.1107/S0021889807021206.

Meador, W., Means, A. and Quiocho, F. (1992) ‘Target enzyme recognition by calmodulin: 2.4 A structure of a calmodulin-peptide complex’, *Science*, 257(5074), pp. 1251–1255. doi: 10.1126/science.1519061.

Means, A. R. *et al.* (1991) ‘Regulatory functions of calmodulin’, *Pharmacology & Therapeutics*, 50(2), pp. 255–270. doi: 10.1016/0163-7258(91)90017-G.

Medeiros-Domingo, A. *et al.* (2007) ‘SCN4B -Encoded Sodium Channel β4 Subunit in Congenital Long-QT Syndrome’, *Circulation*, 116(2), pp. 134–142. doi: 10.1161/CIRCULATIONAHA.106.659086.

Medeiros-Domingo, A. *et al.* (2009) 'The RYR2-Encoded Ryanodine Receptor/Calcium Release Channel in Patients Diagnosed Previously With Either Catecholaminergic Polymorphic Ventricular Tachycardia or Genotype Negative, Exercise-Induced Long QT Syndrome', *Journal of the American College of Cardiology*. Elsevier Inc., 54(22), pp. 2065–2074. doi: 10.1016/j.jacc.2009.08.022.

Meissner, G. (1986a) 'Evidence of a role for calmodulin in the regulation of calcium release from skeletal muscle sarcoplasmic reticulum', *Biochemistry*, 25(1), pp. 244–251. doi: 10.1021/bi00349a034.

Meissner, G. (1986b) 'Ryanodine activation and inhibition of the Ca2+ release channel of sarcoplasmic reticulum.', *Journal of Biological Chemistry*, 261(14), pp. 6300–6. Available at: http://www.ncbi.nlm.nih.gov/pubmed/2422165.

Meissner, G. (1994) 'Ryanodine Receptor/Ca2+ Release Channels and Their Regulation by Endogenous Effectors', *Annual Review of Physiology*, 56(1), pp. 485–508. doi: 10.1146/annurev.ph.56.030194.002413.

Meissner, G. *et al.* (1997) 'Regulation of Skeletal Muscle Ca 2+ Release Channel (Ryanodine Receptor) by Ca 2+ and Monovalent Cations and Anions', *Journal of Biological Chemistry*, 272(3), pp. 1628–1638. doi: 10.1074/jbc.272.3.1628.

Meissner, G. (2004) 'Molecular regulation of cardiac ryanodine receptor ion channel', *Cell Calcium*, 35(6), pp. 621–628. doi: 10.1016/j.ceca.2004.01.015.

Meissner, G. (2017) 'The structural basis of ryanodine receptor ion channel function', *The Journal of General Physiology*, 149(12), pp. 1065–1089. doi: 10.1085/jgp.201711878.

Meissner, G., Darling, E. and Eveleth, J. (1986) ‘Kinetics of rapid Ca2+ release by sarcoplasmic reticulum. Effects of Ca2+, Mg2+, and adenine nucleotides.’, *Biochemistry*, 25(1), pp. 236–44. doi: 10.1021/bi00349a033.

Meissner, G. and Henderson, J. S. (1987) ‘Rapid calcium release from cardiac sarcoplasmic reticulum vesicles is dependent on Ca2+ and is modulated by Mg2+, adenine nucleotide, and calmodulin.’, *Journal of Biological Chemistry*, 262(7), pp. 3065–3073.

Melchionda, M. *et al.* (2016) ‘Ca 2+ /H + exchange by acidic organelles regulates cell migration in vivo’, *The Journal of Cell Biology*, 212(7), pp. 803–813. doi: 10.1083/jcb.201510019.

Meyer, T., Holowka, D. and Stryer, L. (1988) ‘Highly cooperative opening of calcium channels by inositol 1,4,5-trisphosphate’, *Science*, 240(4852), pp. 653–656. doi: 10.1126/science.2452482.

Miao, Y.-L. and Williams, C. J. (2012) ‘Calcium signaling in mammalian egg activation and embryo development: The influence of subcellular localization’, *Molecular Reproduction and Development*, 79(11), pp. 742–756. doi: 10.1002/mrd.22078.

Michelmann, H. W., Bonhoff, A. and Mettler, L. (1986) ‘Chromosome analysis in polyploid human embryos’, *Human Reproduction*, 1(4), pp. 243–246. doi: 10.1093/oxfordjournals.humrep.a136393.

Michikawa, T. *et al.* (1994) ‘Transmembrane Topology and Sites of N-Glyeosylation of Inositol 1,4,5-Trisphosphate Receptor’, *Journal of Biological Chemistry*, 269(12),

pp. 9184–9189.

Mignery, G. A. and Südhof, T. C. (1990) ‘The ligand binding site and transduction mechanism in the inositol-1,4,5-triphosphate receptor.’, *The EMBO Journal*, 9(12), pp. 3893–3898. doi: 10.1002/j.1460-2075.1990.tb07609.x.

Mignery, G. a *et al.* (1990) ‘Structure and expression of the rat inositol 1,4,5-trisphosphate receptor.’, *Journal of Biological Chemistry*, 265(21), pp. 12679–12685.

Miklavc, P. *et al.* (2010) ‘Fusion-Activated Ca2+ Entry: An “Active Zone” of Elevated Ca2+ during the Postfusion Stage of Lamellar Body Exocytosis in Rat Type II Pneumocytes’, *PLoS ONE*. Edited by R. E. Morty, 5(6), p. e10982. doi: 10.1371/journal.pone.0010982.

Mikoshiba, K. (2007) ‘The IP3 receptor/Ca2+ channel and its cellular function’, *Biochemical Society Symposium*, 74(1), p. 9. doi: 10.1042/BSS0740009.

Mikoshiba, K. (2015) ‘Role of IP3 receptor signaling in cell functions and diseases’, *Advances in Biological Regulation*. Elsevier Ltd, 57, pp. 217–227. doi: 10.1016/j.jbior.2014.10.001.

Miraula, M. *et al.* (2015) ‘Inteins—A Focus on the Biotechnological Applications of Splicing-Promoting Proteins’, *American Journal of Molecular Biology*, 05(02), pp. 42–56. doi: 10.4236/ajmb.2015.52005.

Miyakawa, T. *et al.* (2001) ‘Ca2+-sensor region of IP3 receptor controls intracellular Ca2+ signaling’, *The EMBO Journal*, 20(7), pp. 1674–1680. doi: 10.1093/emboj/20.7.1674.

Miyata, K. *et al.* (2018) ‘Bradycardia Is a Specific Phenotype of Catecholaminergic Polymorphic Ventricular Tachycardia Induced by *RYR2* Mutations’, *Internal Medicine*, 57(13), pp. 1813–1817. doi: 10.2169/internalmedicine.9843-17.

Miyawaki, A. *et al.* (1991) ‘Structure-function relationships of the mouse inositol 1,4,5-trisphosphate receptor.’, *Proceedings of the National Academy of Sciences*, 88(11), pp. 4911–4915. doi: 10.1073/pnas.88.11.4911.

Miyazaki, S.-I. *et al.* (1986) ‘Temporal and spatial dynamics of the periodic increase in intracellular free calcium at fertilization of golden hamster eggs’, *Developmental Biology*, 118(1), pp. 259–267. doi: 10.1016/0012-1606(86)90093-X.

Miyazaki, S. (1988) ‘Inositol 1,4,5-trisphosphate-induced calcium release and guanine nucleotide-binding protein-mediated periodic calcium rises in golden hamster eggs’, *The Journal of Cell Biology*, 106(2), pp. 345–353. doi: 10.1083/jcb.106.2.345.

Miyazaki, S. *et al.* (1992) ‘Block of Ca2+ wave and Ca2+ oscillation by antibody to the inositol 1,4,5-trisphosphate receptor in fertilized hamster eggs’, *Science*, 257(5067), pp. 251–255. doi: 10.1126/science.1321497.

Miyazaki, S. *et al.* (1993) ‘Essential Role of the Inositol 1,4,5-Trisphosphate Receptor/Ca2+ Release Channel in Ca2+ Waves and Ca2+ Oscillations at Fertilization of Mammalian Eggs’, *Developmental Biology*, 158(1), pp. 62–78. doi: 10.1006/dbio.1993.1168.

Mohler, P. J. *et al.* (2003) ‘Ankyrin-B mutation causes type 4 long-QT cardiac arrhythmia and sudden cardiac death’, *Nature*, 421(6923), pp. 634–639. doi:

10.1038/nature01335.

Mohler, P. J. *et al.* (2004) ‘A cardiac arrhythmia syndrome caused by loss of ankyrin-B function’, *Proceedings of the National Academy of Sciences*, 101(24), pp. 9137–9142. doi: 10.1073/pnas.0402546101.

Moiseenkova-Bell, V. and Wensel, T. G. (2011) ‘Functional and Structural Studies of TRP Channels Heterologously Expressed in Budding Yeast’, in, pp. 25–40. doi: 10.1007/978-94-007-0265-3_2.

Montell, C. (2001) ‘Physiology, Phylogeny, and Functions of the TRP Superfamily of Cation Channels’, *Science Signaling*, 2001(90), pp. re1–re1. doi: 10.1126/stke.2001.90.re1.

Moore, C. P. *et al.* (1999) ‘Apocalmodulin and Ca2+ calmodulin bind to the same region on the skeletal muscle Ca2+ release channel’, *Biochemistry*, 38(26), pp. 8532–8537. doi: 10.1021/bi9907431.

Morad, M. and Tung, L. (1982) ‘Ionic events responsible for the cardiac resting and action potential’, *The American Journal of Cardiology*, 49(3), pp. 584–594. doi: 10.1016/S0002-9149(82)80016-7.

Morgan, A. J. *et al.* (2013) ‘Bidirectional Ca 2+ signaling occurs between the endoplasmic reticulum and acidic organelles’, *The Journal of Cell Biology*, 200(6), pp. 789–805. doi: 10.1083/jcb.201204078.

Morgan, A. J. (2016) ‘Ca 2+ dialogue between acidic vesicles and ER’, *Biochemical Society Transactions*, 44(2), pp. 546–553. doi: 10.1042/BST20150290.

Mori, M. X. *et al.* (2008) 'Crystal Structure of the CaV2 IQ Domain in Complex with Ca2+/Calmodulin: High-Resolution Mechanistic Implications for Channel Regulation by Ca2+', *Structure*, 16(4), pp. 607–620. doi: 10.1016/j.str.2008.01.011.

Moss, A. J. (2005) 'Long QT syndrome: from channels to cardiac arrhythmias', *Journal of Clinical Investigation*, 115(8), pp. 2018–2024. doi: 10.1172/JCI25537.

Mukherjee, S., Thomas, N. L. and Williams, A. J. (2012) 'A mechanistic description of gating of the human cardiac ryanodine receptor in a regulated minimal environment', *The Journal of General Physiology*, 140(2), pp. 139–158. doi: 10.1085/jgp.201110706.

Murray, S. C. *et al.* (2013) 'Validation of Cryo-EM Structure of IP3R1 Channel', *Structure*. Elsevier Ltd, 21(6), pp. 900–909. doi: 10.1016/j.str.2013.04.016.

Murshudov, G. N. *et al.* (2011) 'REFMAC 5 for the refinement of macromolecular crystal structures', *Acta Crystallographica Section D Biological Crystallography*, 67(4), pp. 355–367. doi: 10.1107/S0907444911001314.

Muthukumar, G., Nickerson, A. W. and Nickerson, K. W. (1987) 'Calmodulin levels in yeasts and filamentous fungi', *FEMS Microbiology Letters*, 41(3), pp. 253–255. doi: 10.1111/j.1574-6968.1987.tb02206.x.

Nagasaki, K. and Fleischer, S. (1988) 'Ryanodine sensitivity of the calcium release channel of sarcoplasmic reticulum', *Cell Calcium*, 9(1), pp. 1–7. doi: 10.1016/0143-4160(88)90032-2.

Nagasaki, K. and Kasai, M. (1983) 'Fast release of calcium from sarcoplasmic reticulum vesicles monitored by chlortetracycline fluorescence.', *Journal of*

biochemistry, 94(4), pp. 1101–9. Available at: http://www.ncbi.nlm.nih.gov/pubmed/6654845.

Nakade, S., Maeda, N. and Mikoshiba, K. (1991) 'Involvement of the C -terminus of the inositol 1,4,5-trisphosphate receptor in Ca 2+ release analysed using region-specific monoclonal antibodies', *Biochemical Journal*, 277(1), pp. 125–131. doi: 10.1042/bj2770125.

Nakagawa, T., Shiota, C., *et al.* (1991) 'Differential localization of alternative spliced transcripts encoding inositol 1,4,5-trisphosphate receptors in mouse cerebellum and hippocampus - insitu hybridization study', *J. Neurochem.*, 57(5), pp. 1807–1810.

Nakagawa, T., Okano, H., *et al.* (1991) 'The subtypes of the mouse inositol 1,4,5-trisphosphate receptor are expressed in a tissue-specific and developmentally specific manner.', *Proceedings of the National Academy of Sciences*, 88(14), pp. 6244–6248. doi: 10.1073/pnas.88.14.6244.

Nakano, Y. and Shimizu, W. (2016) 'Genetics of long-QT syndrome', *Journal of Human Genetics*. Nature Publishing Group, 61(1), pp. 51–55. doi: 10.1038/jhg.2015.74.

Nalefski, E. A. and Falke, J. J. (1996) 'The C2 domain calcium-binding motif: Structural and functional diversity', *Protein Science*, 5(12), pp. 2375–2390. doi: 10.1002/pro.5560051201.

Napolitano, C. *et al.* (2005) 'Genetic Testing in the Long QT Syndrome', *Jama*, 294(23), p. 2975. doi: 10.1001/jama.294.23.2975.

National Library of Medicine (2018) *Catecholaminergic polymorphic ventricular*

tachycardia, *Genetics Home Reference [Internet]*. Available at: https://ghr.nlm.nih.gov/condition/catecholaminergic-polymorphic-ventricular-tachycardia.

Navarro, B. *et al.* (2008) 'Ion channels that control fertility in mammalian spermatozoa', *The International Journal of Developmental Biology*, 52(5–6), pp. 607–613. doi: 10.1387/ijdb.072554bn.

Nerbonne, J. M. and Kass, R. S. (2005) 'Molecular Physiology of Cardiac Repolarization', *Physiological Reviews*, 85(4), pp. 1205–1253. doi: 10.1152/physrev.00002.2005.

Newman, J. *et al.* (2005) 'Towards rationalization of crystallization screening for small- to medium-sized academic laboratories: the PACT/JCSG+ strategy', *Acta Crystallographica Section D Biological Crystallography*. International Union of Crystallography, 61(10), pp. 1426–1431. doi: 10.1107/S0907444905024984.

Newman, R. A. *et al.* (2014) 'Calcium-dependent energetics of calmodulin domain interactions with regulatory regions of the Ryanodine Receptor Type 1 (RyR1)', *Biophysical Chemistry*. Elsevier B.V., 193–194, pp. 35–49. doi: 10.1016/j.bpc.2014.07.004.

Newton, C. L., Mignery, G. A. and Südhof, T. C. (1994) 'Co-expression in vertebrate tissues and cell lines of multiple inositol 1,4,5-trisphosphate (InsP3) receptors with distinct affinities for InsP3', *Journal of Biological Chemistry*, 269(46), pp. 28613–28619.

Niki, I. *et al.* (1996) 'Ca2+ signaling and intracellular Ca2+ binding proteins.', *Journal*

of biochemistry, 120(4), pp. 685–98. Available at: http://www.ncbi.nlm.nih.gov/pubmed/8947828.

Nishimura, S. *et al.* (2018) 'Mutation-linked, excessively tight interaction between the calmodulin binding domain and the C-terminal domain of the cardiac ryanodine receptor as a novel cause of catecholaminergic polymorphic ventricular tachycardia', *Heart Rhythm*, 15(6), pp. 905–914. doi: 10.1016/j.hrthm.2018.02.006.

Nishizuka, Y. (1992) 'Intracellular signaling by hydrolysis of phospholipids and activation of protein kinase C', *Science*, 258(5082), pp. 607–614. doi: 10.1126/science.1411571.

Niwa, N. and Nerbonne, J. M. (2010) 'Molecular determinants of cardiac transient outward potassium current (Ito) expression and regulation', *Journal of Molecular and Cellular Cardiology*, 48(1), pp. 12–25. doi: 10.1016/j.yjmcc.2009.07.013.

Nomikos, M. *et al.* (2005) 'Role of Phospholipase C-ζ Domains in Ca 2+ -dependent Phosphatidylinositol 4,5-Bisphosphate Hydrolysis and Cytoplasmic Ca 2+ Oscillations', *Journal of Biological Chemistry*, 280(35), pp. 31011–31018. doi: 10.1074/jbc.M500629200.

Nomikos, M. *et al.* (2007) 'Binding of Phosphoinositide-specific Phospholipase C-ζ (PLC-ζ) to Phospholipid Membranes', *Journal of Biological Chemistry*, 282(22), pp. 16644–16653. doi: 10.1074/jbc.M701072200.

Nomikos, M., Elgmati, K., Theodoridou, M., Calver, Brian L., *et al.* (2011) 'Male infertility-linked point mutation disrupts the Ca 2+ oscillation-inducing and PIP 2 hydrolysis activity of sperm PLCζ', *Biochemical Journal*. England, 434(2), pp. 211–

217. doi: 10.1042/BJ20101772.

Nomikos, M., Elgmati, K., Theodoridou, M., Georgilis, A., *et al.* (2011) 'Novel regulation of PLCζ activity via its XY-linker', *Biochemical Journal*, 438(3), pp. 427–432. doi: 10.1042/BJ20110953.

Nomikos, M., Elgmati, K., Theodoridou, M., Calver, Brian L, *et al.* (2011) 'Phospholipase C binding to PtdIns(4,5)P2 requires the XY-linker region', *Journal of Cell Science*. England, 124(15), pp. 2582–2590. doi: 10.1242/jcs.083485.

Nomikos, M. *et al.* (2013) 'Phospholipase Cζ rescues failed oocyte activation in a prototype of male factor infertility', *Fertility and Sterility*. Elsevier Inc., 99(1), pp. 76–85. doi: 10.1016/j.fertnstert.2012.08.035.

Nomikos, M. *et al.* (2014) 'Altered RyR2 regulation by the calmodulin F90L mutation associated with idiopathic ventricular fibrillation and early sudden cardiac death', *FEBS Letters*. England, 588(17), pp. 2898–2902. doi: 10.1016/j.febslet.2014.07.007.

Nomikos, M. *et al.* (2015) 'Essential Role of the EF-hand Domain in Targeting Sperm Phospholipase Cζ to Membrane Phosphatidylinositol 4,5-Bisphosphate (PIP 2)', *Journal of Biological Chemistry*. United States, 290(49), pp. 29519–29530. doi: 10.1074/jbc.M115.658443.

Nomikos, M., Thanassoulas, A., *et al.* (2017) 'Calmodulin Interacts and Regulates Enzyme Activity of the Mammalian Sperm Phospholipase C', *Biophysical Journal*. Elsevier, 112(3), pp. 398a-399a. doi: 10.1016/j.bpj.2016.11.2162.

Nomikos, M., Stamatiadis, P., *et al.* (2017) 'Male infertility-linked point mutation reveals a vital binding role for the C2 domain of sperm PLCζ', *Biochemical Journal*.

England, 474(6), pp. 1003–16. doi: 10.1042/BCJ20161057.

Nomikos, M., Kashir, J. and Lai, F. A. (2017) 'The role and mechanism of action of sperm PLC-zeta in mammalian fertilisation', *Biochemical Journal*, 474(21), pp. 3659–3673. doi: 10.1042/BCJ20160521.

Nomikos, M., Swann, K. and Lai, F. A. (2012) 'Starting a new life: Sperm PLC-zeta mobilizes the Ca 2+ signal that induces egg activation and embryo development: An essential phospholipase C with implications for male infertility', *BioEssays*, 34(2), pp. 126–34. doi: 10.1002/bies.201100127.

North, R. A. (2002) 'Molecular Physiology of P2X Receptors', *Physiological Reviews*, 82(4), pp. 1013–1067. doi: 10.1152/physrev.00015.2002.

North, R. A. (2016) 'P2X receptors', *Philosophical Transactions of the Royal Society B: Biological Sciences*, 371(1700), p. 20150427. doi: 10.1098/rstb.2015.0427.

Nyegaard, M. *et al.* (2012) 'Mutations in Calmodulin Cause Ventricular Tachycardia and Sudden Cardiac Death', *The American Journal of Human Genetics*, 91(4), pp. 703–712. doi: 10.1016/j.ajhg.2012.08.015.

Oda, T. *et al.* (2005) 'Defective Regulation of Interdomain Interactions Within the Ryanodine Receptor Plays a Key Role in the Pathogenesis of Heart Failure', *Circulation*, 111(25), pp. 3400–3410. doi: 10.1161/CIRCULATIONAHA.104.507921.

Ohya, Y. and Botstein, D. (1994) 'Diverse essential functions revealed by complementing yeast calmodulin mutants', *Science*, 263(5149), pp. 963–966. doi: 10.1126/science.8310294.

Okano, H., Cyert, M. S. and Ohya, Y. (1998) 'Importance of Phenylalanine Residues of Yeast Calmodulin for Target Binding and Activation', *Journal of Biological Chemistry*, 273(41), pp. 26375–26382. doi: 10.1074/jbc.273.41.26375.

Olwin, B. B. and Storm, D. R. (1985) 'Calcium Binding to Complexes of Calmodulin and Calmodulin Binding Proteins', *Biochemistry*, 24(27), pp. 8081–8086. doi: 10.1021/bi00348a037.

Ono, K. *et al.* (2000) 'Altered interaction of FKBP12.6 with ryanodine receptor as a cause of abnormal Ca2+ release in heart failure', *Cardiovascular Research*, 48(2), pp. 323–331. doi: 10.1016/S0008-6363(00)00191-7.

Ono, M. *et al.* (2010) 'Dissociation of calmodulin from cardiac ryanodine receptor causes aberrant Ca2+ release in heart failure', *Cardiovascular Research*, 87(4), pp. 609–617. doi: 10.1093/cvr/cvq108.

van Oort, R. J. *et al.* (2010) 'Ryanodine Receptor Phosphorylation by Calcium/Calmodulin-Dependent Protein Kinase II Promotes Life-Threatening Ventricular Arrhythmias in Mice With Heart Failure', *Circulation*, 122(25), pp. 2669–2679. doi: 10.1161/CIRCULATIONAHA.110.982298.

Orta, G. *et al.* (2018) 'CatSper channels are regulated by protein kinase A', *Journal of Biological Chemistry*, 293(43), pp. 16830–16841. doi: 10.1074/jbc.RA117.001566.

Otsus, K. *et al.* (1990) 'Molecular cloning of cDNA encoding the Ca2+ release channel (ryanodine receptor) of rabbit cardiac muscle sarcoplasmic reticulum.', *Journal of Biological Chemistry*, 265(23), pp. 13472–83.

Pacheco, B. *et al.* (2012) 'A screening strategy for heterologous protein expression

in Escherichia coli with the highest return of investment', *Protein Expression and Purification*. Elsevier Inc., 81(1), pp. 33–41. doi: 10.1016/j.pep.2011.08.030.

Paech, C. *et al.* (2014) 'Ryanodine Receptor Mutations Presenting as Idiopathic Ventricular Fibrillation: A Report on Two Novel Familial Compound Mutations, c.6224T>C and c.13781A>G, With the Clinical Presentation of Idiopathic Ventricular Fibrillation', *Pediatric Cardiology*, 35(8), pp. 1437–1441. doi: 10.1007/s00246-014-0950-2.

Papish, A. L., Tari, L. W. and Vogel, H. J. (2002) 'Dynamic Light Scattering Study of Calmodulin–Target Peptide Complexes', *Biophysical Journal*, 83(3), pp. 1455–1464. doi: http://dx.doi.org/10.1016/S0006-3495(02)73916-7.

Parker, I., Choi, J. and Yao, Y. (1996) 'Elementary events of InsP3-induced Ca2+ liberation in Xenopus oocytes: hot spots, puffs and blips', *Cell Calcium*, 20(2), pp. 105–121. doi: 10.1016/S0143-4160(96)90100-1.

Parrington, J. *et al.* (2002) 'Phospholipase C isoforms in mammalian spermatozoa: potential components of the sperm factor that causes Ca2+ release in eggs', *Reproduction*, 123(1), pp. 31–39. doi: 10.1530/rep.0.1230031.

Patel, S. (2015) 'Function and dysfunction of two-pore channels', *Science Signaling*, 8(384), pp. re7–re7. doi: 10.1126/scisignal.aab3314.

Patel, S. and Brailoiu, E. (2012) 'Triggering of Ca 2+ signals by NAADP-gated two-pore channels: a role for membrane contact sites?', *Biochemical Society Transactions*, 40(1), pp. 153–157. doi: 10.1042/BST20110693.

Patel, S. and Docampo, R. (2010) 'Acidic calcium stores open for business:

expanding the potential for intracellular Ca2+ signaling', *Trends in Cell Biology*. Elsevier Ltd, 20(5), pp. 277–286. doi: 10.1016/j.tcb.2010.02.003.

Pedersen, P. L. and Carafoli, E. (1987) 'Ion motive ATPases. I. Ubiquity, properties, and significance to cell function', *Trends in Biochemical Sciences*, 12(C), pp. 146–150. doi: 10.1016/0968-0004(87)90071-5.

Pegues, J. C. and Friedberg, F. (1990) 'Multiple mRNAs encoding human calmodulin', *Biochemical and Biophysical Research Communications*, 172(3), pp. 1145–1149. doi: 10.1016/0006-291X(90)91567-C.

Peinelt, C. *et al.* (2009) 'IP3receptor subtype-dependent activation of store-operated calcium entry through ICRAC', *Cell Calcium*, 45(4), pp. 326–330. doi: 10.1016/j.ceca.2008.12.001.

Peng, W. *et al.* (2016) 'Structural basis for the gating mechanism of the type 2 ryanodine receptor RyR2', *Science*, 354(6310), p. aah5324. doi: 10.1126/science.aah5324.

Pepio, A. M., Fan, X. and Sossin, W. S. (1998) 'The Role of C2 Domains in Ca 2+ -activated and Ca 2+ -independent Protein Kinase Cs in Aplysia', *Journal of Biological Chemistry*, 273(30), pp. 19040–19048. doi: 10.1074/jbc.273.30.19040.

Periasamy, M. and Kalyanasundaram, A. (2007) 'SERCA pump isoforms: Their role in calcium transport and disease', *Muscle & Nerve*, 35(4), pp. 430–442. doi: 10.1002/mus.20745.

Perler, F. B. *et al.* (1994) 'Protein splicing elements: inteins and exteins — a definition of terms and recommended nomenclature', *Nucleic Acids Research*, 22(7),

pp. 1125–1127. doi: 10.1093/nar/22.7.1125.

Persechini, A., Stemmer, P. M. and Ohashi, I. (1996) 'Localization of Unique Functional Determinants in the Calmodulin Lobes to Individual EF Hands', *Journal of Biological Chemistry*, 271(50), pp. 32217–32225. doi: 10.1074/jbc.271.50.32217.

Pessah, I. N. *et al.* (1986) 'Calcium-ryanodine receptor complex. Solubilization and partial characterization from skeletal muscle junctional sarcoplasmic reticulum vesicles', *Journal of Biological Chemistry*, 261(19), pp. 8643–8648.

Pettersen, E. F. *et al.* (2004) 'UCSF Chimera-A visualization system for exploratory research and analysis', *Journal of Computational Chemistry*, 25(13), pp. 1605–1612. doi: 10.1002/jcc.20084.

Philipson, K. D. and Nicoll, D. A. (2000) 'Sodium-Calcium Exchange: A Molecular Perspective', *Annual Review of Physiology*, 62(1), pp. 111–133. doi: 10.1146/annurev.physiol.62.1.111.

Phillips, S. V. *et al.* (2011) 'Divergent effect of mammalian PLCζ in generating Ca 2+ oscillations in somatic cells compared with eggs', *Biochemical Journal*, 438(3), pp. 545–553. doi: 10.1042/BJ20101581.

Pinton, P., Pozzan, T. and Rizzuto, R. (1998) 'The Golgi apparatus is an inositol 1,4,5-trisphosphate-sensitive Ca2+ store, with functional properties distinct from those of the endoplasmic reticulum', *The EMBO Journal*, 17(18), pp. 5298–5308. doi: 10.1093/emboj/17.18.5298.

Pipilas, D. C. *et al.* (2016) 'Novel calmodulin mutations associated with congenital long QT syndrome affect calcium current in human cardiomyocytes', *Heart Rhythm*,

13(10), pp. 2012–2019. doi: 10.1016/j.hrthm.2016.06.038.

Plaster, N. M. *et al.* (2001) ‘Mutations in Kir2.1 Cause the Developmental and Episodic Electrical Phenotypes of Andersen’s Syndrome’, *Cell*, 105(4), pp. 511–519. doi: 10.1016/S0092-8674(01)00342-7.

Plattner, H. and Verkhratsky, A. (2015) ‘The ancient roots of calcium signalling evolutionary tree’, *Cell Calcium*. Elsevier Ltd, 57(3), pp. 123–132. doi: 10.1016/j.ceca.2014.12.004.

Pogwizd, S. (2004) ‘Cellular Basis of Triggered Arrhythmias in Heart Failure’, *Trends in Cardiovascular Medicine*, 14(2), pp. 61–66. doi: 10.1016/j.tcm.2003.12.002.

Postma, A. V. *et al.* (2002) ‘Absence of Calsequestrin 2 Causes Severe Forms of Catecholaminergic Polymorphic Ventricular Tachycardia’, *Circulation Research*, 91(8), pp. e21-6. doi: 10.1161/01.RES.0000038886.18992.6B.

Potter, J. D. *et al.* (1983) ‘Ca2+ binding to calmodulin’, in *Methods in Enzymology*. Elsevier Inc., pp. 135–143. doi: 10.1016/S0076-6879(83)02014-5.

Prakriya, M. (2009) ‘The molecular physiology of CRAC channels’, *Immunological Reviews*, 231(1), pp. 88–98. doi: 10.1111/j.1600-065X.2009.00820.x.

Prentki, M., Wollheim, C. B. and Lew, P. D. (1984) ‘Ca2+ homeostasis in permeabilized human neutrophils. Characterization of Ca2+-sequestering pools and the action of inositol 1,4,5-triphosphate.’, *Journal of Biological Chemistry*, 259(22), pp. 13777–82. Available at: http://www.ncbi.nlm.nih.gov/pubmed/6334080.

Priori, S. G. *et al.* (2001) ‘Mutations in the Cardiac Ryanodine Receptor Gene (

hRyR2) Underlie Catecholaminergic Polymorphic Ventricular Tachycardia', *Circulation*, 103(2), pp. 196–200. doi: 10.1161/01.CIR.103.2.196.

Priori, S. G. *et al.* (2003) 'Risk Stratification in the Long-QT Syndrome', *New England Journal of Medicine*, 348(19), pp. 1866–1874. doi: 10.1056/NEJMoa022147.

Priori, S. G. *et al.* (2013) 'HRS/EHRA/APHRS Expert Consensus Statement on the Diagnosis and Management of Patients with Inherited Primary Arrhythmia Syndromes', *Heart Rhythm*, 10(12), pp. 1932–1963. doi: 10.1016/j.hrthm.2013.05.014.

Priori, S. G. and Chen, S. R. W. (2011) 'Inherited Dysfunction of Sarcoplasmic Reticulum Ca 2+ Handling and Arrhythmogenesis', *Circulation Research*, 108(7), pp. 871–883. doi: 10.1161/CIRCRESAHA.110.226845.

Priori, S. G. and Napolitano, C. (2005) 'Cardiac and skeletal muscle disorders caused by mutations in the intracellular Ca2+ release channels', *Journal of Clinical Investigation*, 115(8), pp. 2033–2038. doi: 10.1172/JCI25664.

Priori, S. G. and Napolitano, C. (2014) 'Inheritable Phenotypes Associated With Altered Intracellular Calcium Regulation', in *Cardiac Electrophysiology: From Cell to Bedside*. Elsevier, pp. 521–528. doi: 10.1016/B978-1-4557-2856-5.00053-4.

Priori, S. G., Napolitano, C. and Schwartz, P. J. (1999) 'Low penetrance in the long-QT syndrome: clinical impact.', *Circulation*, 99(4), pp. 529–33. Available at: http://www.ncbi.nlm.nih.gov/pubmed/9927399.

Procita, L. (1958) 'Some Pharmacological Actions of Ryanodine in the Mammal', *The Journal of Pharmacology and Experimental Therapeutics*, 123(4), pp. 296–305.

Available at: http://www.ncbi.nlm.nih.gov/pubmed/13564409.

Protasevich, I. *et al.* (1997) ‘Conformation and thermal denaturation of apocalmodulin: Role of electrostatic mutations’, *Biochemistry*, 36(8), pp. 2017–2024. doi: 10.1021/bi962538g.

Pryor, K. D. and Leiting, B. (1997) ‘High-Level Expression of Soluble Protein inEscherichia coliUsing a His6-Tag and Maltose-Binding-Protein Double-Affinity Fusion System’, *Protein Expression and Purification*, 10(3), pp. 309–319. doi: 10.1006/prep.1997.0759.

Qi, H. *et al.* (2014) ‘Frequency and relative prevalence of calcium blips and puffs in a model of small IP3R clusters’, *Biophysical Journal*, 106(11), pp. 2353–2363. doi: 10.1016/j.bpj.2014.04.027.

Qureshi, O. S. *et al.* (2007) ‘Regulation of P2X4 receptors by lysosomal targeting, glycan protection and exocytosis’, *Journal of Cell Science*, 120(21), pp. 3838–3849. doi: 10.1242/jcs.010348.

Radermacher, M. *et al.* (1994) ‘Cryo-electron microscopy and three-dimensional reconstruction of the calcium release channel/ryanodine receptor from skeletal muscle’, *The Journal of Cell Biology*, 127(2), pp. 411–423. doi: 10.1083/jcb.127.2.411.

Ralevic, V. and Burnstock, G. (1998) ‘Receptors for Purines and Pyrimidines.’, *Pharmacological Reviews*, 50(3), pp. 413–92. Available at: http://www.ncbi.nlm.nih.gov/pubmed/9755289.

Rao, S. T. *et al.* (2008) ‘Structure of Paramecium tetraurelia calmodulin at 1.8 Å

resolution', *Protein Science*, 2(3), pp. 436–447. doi: 10.1002/pro.5560020316.

Rebecchi, M. J. and Pentyala, S. N. (2000) 'Structure, Function, and Control of Phosphoinositide-Specific Phospholipase C', *Physiological Reviews*, 80(4), pp. 1291–1335. doi: 10.1152/physrev.2000.80.4.1291.

Reddish, F. N. *et al.* (2017) 'Calcium Dynamics Mediated by the Endoplasmic/Sarcoplasmic Reticulum and Related Diseases', *International Journal of Molecular Sciences*, 18(5), p. 1024. doi: 10.3390/ijms18051024.

Reed, G. J. *et al.* (2015) 'CALM3 mutation associated with long QT syndrome', *Heart Rhythm*, 12(2), pp. 419–422. doi: 10.1016/j.hrthm.2014.10.035.

Reid, D. S. *et al.* (1975) 'Bidirectional tachycardia in a child. A study using His bundle electrography.', *Heart*, 37(3), pp. 339–344. doi: 10.1136/hrt.37.3.339.

Reiken, S. *et al.* (2001) 'β-Adrenergic Receptor Blockers Restore Cardiac Calcium Release Channel (Ryanodine Receptor) Structure and Function in Heart Failure', *Circulation*, 104(23), pp. 2843–2848. doi: 10.1161/hc4701.099578.

Reiken, S. *et al.* (2003) 'β-Blockers Restore Calcium Release Channel Function and Improve Cardiac Muscle Performance in Human Heart Failure', *Circulation*, 107(19), pp. 2459–2466. doi: 10.1161/01.CIR.0000068316.53218.49.

Ren, D. *et al.* (2001) 'A sperm ion channel required for sperm motility and male fertility', *Nature*, 413(6856), pp. 603–609. doi: 10.1038/35098027.

Respress, J. L. *et al.* (2012) 'Role of RyR2 Phosphorylation at S2814 During Heart Failure Progression', *Circulation Research*, 110(11), pp. 1474–1483. doi:

10.1161/CIRCRESAHA.112.268094.

Reverter, D. and Lima, C. D. (2004) ‘A Basis for SUMO Protease Specificity Provided by Analysis of Human Senp2 and a Senp2-SUMO Complex’, *Structure*, 12(8), pp. 1519–1531. doi: 10.1016/j.str.2004.05.023.

Rhoads, A. R. and Friedberg, F. (1997) ‘Sequence motifs for calmodulin recognition.’, *The FASEB Journal*, 11(5), pp. 331–340. doi: 10.1096/fasebj.11.5.9141499.

Rice, A. *et al.* (2000) ‘Mammalian Sperm Contain a Ca2+-Sensitive Phospholipase C Activity That Can Generate InsP3 from PIP2 Associated with Intracellular Organelles’, *Developmental Biology*, 228(1), pp. 125–135. doi: 10.1006/dbio.2000.9929.

Rizo, J. and Südhof, T. C. (1998) ‘C 2 -domains, Structure and Function of a Universal Ca 2+ -binding Domain’, *Journal of Biological Chemistry*, 273(26), pp. 15879–15882. doi: 10.1074/jbc.273.26.15879.

Rocchetti, M. *et al.* (2017) ‘Elucidating arrhythmogenic mechanisms of long-QT syndrome CALM1-F142L mutation in patient-specific induced pluripotent stem cell-derived cardiomyocytes’, *Cardiovascular Research*, 113(5), pp. 531–541. doi: 10.1093/cvr/cvx006.

Roden, D. M. (2008) ‘Long-QT Syndrome’, *New England Journal of Medicine*, 358(2), pp. 169–176. doi: 10.1056/NEJMcp0706513.

Roderick, H. L., Berridge, M. J. and Bootman, M. D. (2003) ‘Calcium-induced calcium release.’, *Current biology : CB*, 13(11), p. R425. Available at:

http://www.ncbi.nlm.nih.gov/pubmed/12781146.

Roderick, H. L. and Cook, S. J. (2008) 'Ca2+ signalling checkpoints in cancer: remodelling Ca2+ for cancer cell proliferation and survival', *Nature Reviews Cancer*, 8(5), pp. 361–375. doi: 10.1038/nrc2374.

Rodney, G. G. *et al.* (2000) 'Regulation of RYR1 activity by Ca2+ and calmodulin', *Biochemistry*, 39(26), pp. 7807–7812. doi: 10.1021/bi0005660.

Rodney, G. G. *et al.* (2001) 'Calcium Binding to Calmodulin Leads to an N-terminal Shift in Its Binding Site on the Ryanodine Receptor', *Journal of Biological Chemistry*, 276(3), pp. 2069–2074. doi: 10.1074/jbc.M008891200.

Rodríguez-Castañeda, F. *et al.* (2010) 'Modular architecture of Munc13/calmodulin complexes: dual regulation by Ca2+ and possible function in short-term synaptic plasticity', *The EMBO Journal*, 29(3), pp. 680–691. doi: 10.1038/emboj.2009.373.

Rogers, E. F. *et al.* (1948) 'Plant Insecticides. I. Ryanodine, A New Alkaloid from Ryania Speciosa Vahl.', *Journal of the American Chemical Society*, 70(9), pp. 3086–3088. doi: 10.1021/ja01189a074.

Rosano, G. L. and Ceccarelli, E. A. (2014) 'Recombinant protein expression in Escherichia coli: advances and challenges', *Frontiers in Microbiology*, 5, p. 172. doi: 10.3389/fmicb.2014.00172.

Rossi, A. M. *et al.* (2009) 'Synthetic partial agonists reveal key steps in IP3 receptor activation', *Nature Chemical Biology*, 5(9), pp. 631–639. doi: 10.1038/nchembio.195.

Rossi, D. and Sorrentino, V. (2002) 'Molecular genetics of ryanodine receptors Ca 2+

-release channels', *Cell Calcium*, 32(5), pp. 6–307. doi: 10.1016/S0143-4160(02)00198-7.

Roston, T. M. *et al.* (2017) 'A novel RYR2 loss-of-function mutation (I4855M) is associated with left ventricular non-compaction and atypical catecholaminergic polymorphic ventricular tachycardia', *Journal of Electrocardiology*. Elsevier Inc., 50(2), pp. 227–233. doi: 10.1016/j.jelectrocard.2016.09.006.

Roston, T. M. *et al.* (2018) 'The clinical and genetic spectrum of catecholaminergic polymorphic ventricular tachycardia: findings from an international multicentre registry', *Europace*, 20(3), pp. 541–547. doi: 10.1093/europace/euw389.

Rousseau, E. *et al.* (1986) 'Single channel and 45Ca2+ flux measurements of the cardiac sarcoplasmic reticulum calcium channel', *Biophysical Journal*. Elsevier, 50(5), pp. 1009–1014. doi: 10.1016/S0006-3495(86)83543-3.

Rousseau, E. *et al.* (1988) 'Activation of the Ca2+ release channel of skeletal muscle sarcoplasmic reticulum by caffeine and related compounds', *Archives of Biochemistry and Biophysics*, 267(1), pp. 75–86. doi: 10.1016/0003-9861(88)90010-0.

Rousseau, E., Smith, J. S. and Meissner, G. (1987) 'Ryanodine modifies conductance and gating behavior of single Ca2+ release channel', *American Journal of Physiology-Cell Physiology*, 253(3), pp. C364–C368. doi: 10.1152/ajpcell.1987.253.3.C364.

Roux-Buisson, N. *et al.* (2011) 'Germline and somatic mosaicism for a mutation of the ryanodine receptor type 2 gene: implication for genetic counselling and patient

caring', *Europace*, 13(1), pp. 130–132. doi: 10.1093/europace/euq331.

Roux-Buisson, N. *et al.* (2012) 'Absence of triadin, a protein of the calcium release complex, is responsible for cardiac arrhythmia with sudden death in human', *Human Molecular Genetics*, 21(12), pp. 2759–2767. doi: 10.1093/hmg/dds104.

Roux-Buisson, N. *et al.* (2014) 'Prevalence and significance of rare RYR2 variants in arrhythmogenic right ventricular cardiomyopathy/dysplasia: Results of a systematic screening', *Heart Rhythm*, 11(11), pp. 1999–2009. doi: 10.1016/j.hrthm.2014.07.020.

La Rovere, R. M. L. *et al.* (2016) 'Intracellular Ca 2+ signaling and Ca 2+ microdomains in the control of cell survival, apoptosis and autophagy', *Cell Calcium*, 60(2), pp. 74–87. doi: 10.1016/j.ceca.2016.04.005.

Runft, L. L., Jaffe, L. A. and Mehlmann, L. M. (2002) 'Egg Activation at Fertilization: Where It All Begins', *Developmental Biology*, 245(2), pp. 237–254. doi: 10.1006/dbio.2002.0600.

Sabourin, J., Robin, E. and Raddatz, E. (2011) 'A key role of TRPC channels in the regulation of electromechanical activity of the developing heart', *Cardiovascular Research*, 92(2), pp. 226–236. doi: 10.1093/cvr/cvr167.

Saimi, Y. and Kung, C. (2002) 'Calmodulin as an Ion Channel Subunit', *Annual Review of Physiology*, 64(1), pp. 289–311. doi: 10.1146/annurev.physiol.64.100301.111649.

Saito, A. *et al.* (1988) 'Ultrastructure of the calcium release channel of sarcoplasmic reticulum', *J Cell Biol*, 107(1), pp. 211–219. Available at: http://www.ncbi.nlm.nih.gov/pubmed/2455723.

Saitoh, H. and Hinchey, J. (2000) ‘Functional Heterogeneity of Small Ubiquitin-related Protein Modifiers SUMO-1 versus SUMO-2/3’, *Journal of Biological Chemistry*, 275(9), pp. 6252–6258. doi: 10.1074/jbc.275.9.6252.

Samsó, M. *et al.* (2009) ‘Coordinated movement of cytoplasmic and transmembrane domains of RyR1 Upon gating’, *PLoS Biology*, 7(4), pp. 0980–0995. doi: 10.1371-journal.pbio.1000085-S.

Samsó, M. and Wagenknecht, T. (2002) ‘Apocalmodulin and Ca2+-calmodulin bind to neighboring locations on the ryanodine receptor’, *Journal of Biological Chemistry*, 277(2), pp. 1349–1353. doi: 10.1074/jbc.M109196200.

Sandow, A. (1952) ‘Excitation-contraction coupling in muscular response.’, *The Yale Journal of Biology and Medicine*, 25(3), pp. 176–201. Available at: http://www.ncbi.nlm.nih.gov/pubmed/13015950.

Santana, L. F., Cheng, E. P. and Lederer, W. J. (2010) ‘How does the shape of the cardiac action potential control calcium signaling and contraction in the heart?’, *Journal of Molecular and Cellular Cardiology*, 49(6), pp. 901–903. doi: 10.1016/j.yjmcc.2010.09.005.

Sato, K., Pollock, N. and Stowell, K. M. (2010) ‘Functional Studies of RYR1 Mutations in the Skeletal Muscle Ryanodine Receptor Using Human RYR1 Complementary DNA’, *Anesthesiology*, 112(6), pp. 1350–1354. doi: 10.1097/ALN.0b013e3181d69283.

Saucerman, J. J. and Bers, D. M. (2012) ‘Calmodulin binding proteins provide domains of local Ca2+ signaling in cardiac myocytes’, *Journal of Molecular and*

Cellular Cardiology. Elsevier Ltd, 52(2), pp. 312–316. doi: 10.1016/j.yjmcc.2011.06.005.

Saunders, C. M. *et al.* (2002) 'PLC zeta: a sperm-specific trigger of Ca(2+) oscillations in eggs and embryo development.', *Development*, 129(15), pp. 3533–44. Available at: http://www.ncbi.nlm.nih.gov/pubmed/12117804 (Accessed: 6 November 2015).

Schlotthauer, K. and Bers, D. M. (2000) 'Sarcoplasmic Reticulum Ca 2+ Release Causes Myocyte Depolarization', *Circulation Research*, 87(9), pp. 774–780. doi: 10.1161/01.RES.87.9.774.

Schneider, M. F. (1981) 'Membrane charge movement and depolarization-contraction coupling.', *Annual review of physiology*, 43(49), pp. 507–17. doi: 10.1146/annurev.ph.43.030181.002451.

Schrodinger, L. (2015) 'The PyMOL Molecular Graphics System, Version 1.8'.

Schug, Z. T. and Joseph, S. K. (2006) 'The Role of the S4-S5 Linker and C-terminal Tail in Inositol 1,4,5-Trisphosphate Receptor Function', *Journal of Biological Chemistry*, 281(34), pp. 24431–24440. doi: 10.1074/jbc.M604190200.

Schultz, R. M. and Kopf, G. S. (1995) 'Molecular Basis of Mammalian Egg Activation', in *Current topics in developmental biology*. Elsevier Inc., pp. 21–62. doi: 10.1016/S0070-2153(08)60563-3.

Schwaller, B. (2009) 'The continuing disappearance of "pure" Ca2+ buffers', *Cellular and Molecular Life Sciences*, 66(2), pp. 275–300. doi: 10.1007/s00018-008-8564-6.

Schwaller, B. (2010) ‘Cytosolic Ca2+ Buffers’, *Cold Spring Harbor Perspectives in Biology*, 2(11), pp. a004051–a004051. doi: 10.1101/cshperspect.a004051.

Schwaller, B. (2012) ‘The Regulation of a Cell’s Ca2+ Signaling Toolkit: The Ca2+ Homeostasome’, in M., I. (ed.) *Calcium Signaling. Advances in Experimental Medicine and Biology,*. Springe, Dordrecht, pp. 1–25. doi: 10.1007/978-94-007-2888-2_1.

Schwartz, P. J. *et al.* (2009) ‘Prevalence of the Congenital Long-QT Syndrome’, *Circulation*, 120(18), pp. 1761–1767. doi: 10.1161/CIRCULATIONAHA.109.863209.

Schwartz, P. J., Periti, M. and Malliani, A. (1975) ‘The long Q-T syndrome’, *American Heart Journal*, 89(3), pp. 378–390. doi: 10.1016/0002-8703(75)90089-7.

Seaton, B. A. *et al.* (1985) ‘Calcium-Induced Increase in the Radius of Gyration and Maximum Dimension of Calmodulin Measured by Small-Angle X-ray Scattering’, *Biochemistry*, 24(24), pp. 6740–3. doi: 10.1021/bi00345a002.

Sengupta, B., Friedberg, F. and Detera-Wadleigh, S. D. (1987) ‘Molecular analysis of human and rat calmodulin complementary DNA clones. Evidence for additional active genes in these species.’, *Journal of Biological Chemistry*, 262(34), pp. 16663–70. Available at: http://www.ncbi.nlm.nih.gov/pubmed/2445749.

Seo, M.-D. *et al.* (2012) ‘Structural and functional conservation of key domains in InsP3 and ryanodine receptors’, *Nature*. Nature Publishing Group, 483(7387), pp. 108–112. doi: 10.1038/nature10751.

Serysheva, I. I. *et al.* (2003) ‘Structure of the Type 1 Inositol 1,4,5-Trisphosphate Receptor Revealed by Electron Cryomicroscopy’, *Journal of Biological Chemistry*,

278(24), pp. 21319–21322. doi: 10.1074/jbc.C300148200.

Serysheva, I. I. *et al.* (2005) ‘Structure of Ca2+ Release Channel at 14Å Resolution’, *Journal of Molecular Biology*, 345(3), pp. 427–431. doi: 10.1016/j.jmb.2004.10.073.

Serysheva, I. I. *et al.* (2008) ‘Subnanometer-resolution electron cryomicroscopy-based domain models for the cytoplasmic region of skeletal muscle RyR channel’, *Proceedings of the National Academy of Sciences*, 105(28), pp. 9610–9615. doi: 10.1073/pnas.0803189105.

Shah, N. H. and Muir, T. W. (2014) ‘Inteins: nature’s gift to protein chemists’, *Chem. Sci.*, 5(2), pp. 446–461. doi: 10.1039/C3SC52951G.

Shah, S. R., Park, K. and Alweis, R. (2019) ‘Long QT Syndrome: A Comprehensive Review of the Literature and Current Evidence’, *Current Problems in Cardiology*. Elsevier, 44(3), pp. 92–106. doi: 10.1016/j.cpcardiol.2018.04.002.

Shaik, N. A. *et al.* (2018) ‘Protein phenotype diagnosis of autosomal dominant calmodulin mutations causing irregular heart rhythms’, *Journal of Cellular Biochemistry*, 119(10), pp. 8233–8248. doi: 10.1002/jcb.26834.

Shamgar, L. *et al.* (2006) ‘Calmodulin Is Essential for Cardiac I KS Channel Gating and Assembly’, *Circulation Research*, 98(8), pp. 1055–1063. doi: 10.1161/01.RES.0000218979.40770.69.

Shan, J. *et al.* (2010) ‘Phosphorylation of the ryanodine receptor mediates the cardiac fight or flight response in mice’, *Journal of Clinical Investigation*, 120(12), pp. 4388–4398. doi: 10.1172/JCI32726.

Shannon, T. R., Ginsburg, K. S. and Bers, D. M. (2002) 'Quantitative Assessment of the SR Ca 2+ Leak-Load Relationship', *Circulation Research*, 91(7), pp. 594–600. doi: 10.1161/01.RES.0000036914.12686.28.

Shao, D. *et al.* (2014) 'The individual N- and C-lobes of calmodulin tether to the Cav1.2 channel and rescue the channel activity from run-down in ventricular myocytes of guinea-pig heart', *FEBS Letters*. Federation of European Biochemical Societies, 588(21), pp. 3855–3861. doi: 10.1016/j.febslet.2014.09.029.

Sharma, P. *et al.* (2012) 'Structural determination of the phosphorylation domain of the ryanodine receptor', *FEBS Journal*, 279(20), pp. 3952–3964. doi: 10.1111/j.1742-4658.2012.08755.x.

Sharma, S. S., Chong, S. and Harcum, S. W. (2006) 'Intein-mediated protein purification of fusion proteins expressed under high-cell density conditions in E. coli', *Journal of Biotechnology*, 125(1), pp. 48–56. doi: 10.1016/j.jbiotec.2006.01.018.

Shigetomi, E. and Kato, F. (2004) 'Action Potential-Independent Release of Glutamate by Ca2+ Entry through Presynaptic P2X Receptors Elicits Postsynaptic Firing in the Brainstem Autonomic Network', *The Journal of Neuroscience*, 24(12), pp. 3125–35. doi: 10.1523/JNEUROSCI.0090-04.2004.

Shimizu, W. (2008) 'Clinical Impact of Genetic Studies in Lethal Inherited Cardiac Arrhythmias', *Circulation Journal*, 72(12), pp. 1926–1936. doi: 10.1253/circj.CJ-08-0947.

Shimizu, W. *et al.* (2009) 'Genotype-Phenotype Aspects of Type 2 Long QT Syndrome', *Journal of the American College of Cardiology*. Elsevier Inc., 54(22), pp.

2052–2062. doi: 10.1016/j.jacc.2009.08.028.

Shtifman, A. *et al.* (2002) 'Interdomain Interactions within Ryanodine Receptors Regulate Ca 2 + Spark Frequency in Skeletal Muscle', *The Journal of General Physiology*, 119(1), pp. 15–32. doi: 10.1085/jgp.119.1.15.

Sidhu, R. S., Clough, R. R. and Bhullar, R. P. (2005) 'Regulation of Phospholipase C-δ1 through Direct Interactions with the Small GTPase Ral and Calmodulin', *Journal of Biological Chemistry*, 280(23), pp. 21933–21941. doi: 10.1074/jbc.M412966200.

Siegers, C. E. P. *et al.* (2014) 'Catecholaminergic polymorphic ventricular tachycardia (CPVT) initially diagnosed as idiopathic ventricular fibrillation: The importance of thorough diagnostic work-up and follow-up', *International Journal of Cardiology*. Elsevier Ireland Ltd, 177(2), pp. e81–e83. doi: 10.1016/j.ijcard.2014.10.005.

Sienaert, I. *et al.* (2002) 'Localization and function of a calmodulin–apocalmodulin-binding domain in the N-terminal part of the type 1 inositol 1,4,5-trisphosphate receptor', *Biochemical Journal*, 365(1), pp. 269–277. doi: 10.1042/bj20020144.

Siller, E. *et al.* (2010) 'Slowing Bacterial Translation Speed Enhances Eukaryotic Protein Folding Efficiency', *Journal of Molecular Biology*. Elsevier Ltd, 396(5), pp. 1310–1318. doi: 10.1016/j.jmb.2009.12.042.

Singh, A. P. and Rajender, S. (2015) 'CatSper channel, sperm function and male fertility', *Reproductive BioMedicine Online*, 30(1), pp. 28–38. doi: 10.1016/j.rbmo.2014.09.014.

Singleton, S. F. *et al.* (2002) 'Intein-mediated affinity-fusion purification of the Escherichia coli RecA protein', *Protein Expression and Purification*, 26(3), pp. 476–488. doi: 10.1016/S1046-5928(02)00571-5.

Smani, T. *et al.* (2015) 'Functional and physiopathological implications of TRP channels', *Biochimica et Biophysica Acta (BBA) - Molecular Cell Research*, 1853(8), pp. 1772–1782. doi: 10.1016/j.bbamcr.2015.04.016.

Smedler, E. and Uhlén, P. (2014) 'Frequency decoding of calcium oscillations', *Biochimica et Biophysica Acta (BBA) - General Subjects*. The Authors, 1840(3), pp. 964–969. doi: 10.1016/j.bbagen.2013.11.015.

Smith, D. B. and Johnson, K. S. (1988) 'Single-step purification of polypeptides expressed in Escherichia coli as fusions with glutathione S-transferase', *Gene*, 67(1), pp. 31–40. doi: 10.1016/0378-1119(88)90005-4.

Smith, J. S., Coronado, R. and Meissner, G. (1985) 'Sarcoplasmic reticulum contains adenine nucleotide-activated calcium channels', *Nature*, 316(6027), pp. 446–449. doi: 10.1038/316446a0.

Smith, J.S., Coronado, R. and Meissner, G. (1986) 'Single-channel calcium and barium currents of large and small conductance from sarcoplasmic reticulum', *Biophysical Journal*. Elsevier, 50(5), pp. 921–928. doi: 10.1016/S0006-3495(86)83533-0.

Smith, J. S., Coronado, R. and Meissner, G. (1986) 'Single channel measurements of the calcium release channel from skeletal muscle sarcoplasmic reticulum. Activation by Ca2+ and ATP and modulation by Mg2+', *The Journal of General*

Physiology, 88(5), pp. 573–588. doi: 10.1085/jgp.88.5.573.

Snutch, T. P. *et al.* (1990) 'Molecular Properties of Voltage-Gated Calcium Channels', in *Voltage-Gated Calcium Channels*. Boston, MA: Springer US, pp. 61–94. doi: 10.1007/0-387-27526-6_5.

Søndergaard, M. T., Tian, X., *et al.* (2015) 'Arrhythmogenic Calmodulin Mutations Affect the Activation and Termination of Cardiac Ryanodine Receptor-mediated Ca 2+ Release', *Journal of Biological Chemistry*, 290(43), pp. 26151–26162. doi: 10.1074/jbc.M115.676627.

Søndergaard, M. T., Sorensen, A. B., *et al.* (2015) 'Calmodulin mutations causing catecholaminergic polymorphic ventricular tachycardia confer opposing functional and biophysical molecular changes', *The FEBS Journal*, 282(4), pp. 803–816. doi: 10.1111/febs.13184.

Søndergaard, M. T. *et al.* (2017) 'The Arrhythmogenic Calmodulin p.Phe142Leu Mutation Impairs C-domain Ca 2+ Binding but Not Calmodulin-dependent Inhibition of the Cardiac Ryanodine Receptor', *Journal of Biological Chemistry*, 292(4), pp. 1385–1395. doi: 10.1074/jbc.M116.766253.

Sorensen, A. B., Søndergaard, M. T. and Overgaard, M. T. (2013) 'Calmodulin in a Heartbeat', *FEBS Journal*, 280(21), pp. 5511–5532. doi: 10.1111/febs.12337.

Sorensen, B. R. and Shea, M. A. (1998) 'Interactions between Domains of Apo Calmodulin Alter Calcium Binding and Stability †', *Biochemistry*, 37(12), pp. 4244–4253. doi: 10.1021/bi9718200.

Sorensen, B. and Shea, M. (1996) 'Calcium binding decreases the stokes radius of

calmodulin and mutants R74A, R90A, and R90G', *Biophysical Journal*. Elsevier, 71(6), pp. 3407–3420. doi: 10.1016/S0006-3495(96)79535-8.

Soulsby, M. D. *et al.* (2004) 'The contribution of serine residues 1588 and 1755 to phosphorylation of the type I inositol 1,4,5-trisphosphate receptor by PKA and PKG', *FEBS Letters*, 557(1–3), pp. 181–184. doi: 10.1016/S0014-5793(03)01487-X.

Southworth, M. W. *et al.* (1999) 'Purification of Proteins Fused to Either the Amino or Carboxy Terminus of the Mycobacterium xenopi Gyrase A Intein', *BioTechniques*, 27(1), pp. 110–120. doi: 10.2144/99271st04.

Splawski, I. *et al.* (2004) 'CaV1.2 Calcium Channel Dysfunction Causes a Multisystem Disorder Including Arrhythmia and Autism', *Cell*, 119(1), pp. 19–31. doi: 10.1016/j.cell.2004.09.011.

Splawski, I. *et al.* (2005) 'Severe arrhythmia disorder caused by cardiac L-type calcium channel mutations', *Proceedings of the National Academy of Sciences*, 102(23), pp. 8089–8096. doi: 10.1073/pnas.0502506102.

Srinivasa Babu, K. *et al.* (2009) 'Single step intein-mediated purification of hGMCSF expressed in salt-inducible E. coli', *Biotechnology Letters*, 31(5), pp. 659–664. doi: 10.1007/s10529-009-9921-8.

Stathopulos, P. B. *et al.* (2012) 'Themes and Variations in ER/SR Calcium Release Channels: Structure and Function', *Physiology*, 27(6), pp. 331–342. doi: 10.1152/physiol.00013.2012.

Stathopulos, P. B. and Ikura, M. (2017) 'Store operated calcium entry: From concept to structural mechanisms', *Cell Calcium*, pp. 3–7. doi: 10.1016/j.ceca.2016.11.005.

Stattin, E.-L. *et al.* (2012) ‘Founder mutations characterise the mutation panorama in 200 Swedish index cases referred for Long QT syndrome genetic testing’, *BMC Cardiovascular Disorders*, 12(1), p. 95. doi: 10.1186/1471-2261-12-95.

De Stefani, D. *et al.* (2011) ‘A forty-kilodalton protein of the inner membrane is the mitochondrial calcium uniporter’, *Nature*, 476(7360), pp. 336–340. doi: 10.1038/nature10230.

Steinhardt, R. A. (1990) ‘Intracellular free calcium and the first cell cycle of the sea-urchin embryo (Lytechinus pictus).’, *Journal of Reproduction and Fertility. Supplement*, 42, pp. 191–7. Available at: http://www.ncbi.nlm.nih.gov/pubmed/1963899.

Stitzel, M. L. and Seydoux, G. (2007) ‘Regulation of the Oocyte-to-Zygote Transition’, *Science*, 316(5823), pp. 407–408. doi: 10.1126/science.1138236.

Stofko-Hahn, R. E., Carr, D. W. and Scott, J. D. (1992) ‘A single step purification for recombinant proteins Characterization of a microtubule associated protein (MAP 2) fragment which associates with the type II cAMP-dependent protein kinase’, *FEBS Letters*, 302(3), pp. 274–278. doi: 10.1016/0014-5793(92)80458-S.

Streb, H. *et al.* (1983) ‘Release of Ca2+ from a nonmitochondrial intracellular store in pancreatic acinar cells by inositol-1,4,5-trisphosphate’, *Nature*, 306(5938), pp. 67–69. doi: 10.1038/306067a0.

Stricker, S. A. (1997) ‘Intracellular Injections of a Soluble Sperm Factor Trigger Calcium Oscillations and Meiotic Maturation in Unfertilized Oocytes of a Marine Worm’, *Developmental Biology*, 186(2), pp. 185–201. doi: 10.1006/dbio.1997.8594.

Stricker, S. A. (1999) ‘Comparative Biology of Calcium Signaling during Fertilization and Egg Activation in Animals’, *Developmental Biology*, 211(2), pp. 157–176. doi: 10.1006/dbio.1999.9340.

Suarez, S. S. and Pacey, A. A. (2006) ‘Sperm transport in the female reproductive tract’, *Human Reproduction Update*, 12(1), pp. 23–37. doi: 10.1093/humupd/dmi047.

Suh, P.-G. *et al.* (2008) ‘Multiple roles of phosphoinositide-specific phospholipase C isozymes’, *BMB Reports*, 41(6), pp. 415–434. doi: 10.5483/BMBRep.2008.41.6.415.

Suko, J. *et al.* (1993) ‘Phosphorylation of serine 2843 in ryanodine receptor-calcium release channel of skeletal muscle by cAMP-, cGMP- and CaM-dependent protein kinase’, *BBA - Molecular Cell Research*, 1175(2), pp. 193–206. doi: 10.1016/0167-4889(93)90023-I.

Sumitomo, N. (2003) ‘Catecholaminergic polymorphic ventricular tachycardia: electrocardiographic characteristics and optimal therapeutic strategies to prevent sudden death’, *Heart*, 89(1), pp. 66–70. doi: 10.1136/heart.89.1.66.

Sumitomo, N. (2016) ‘Current topics in catecholaminergic polymorphic ventricular tachycardia’, *Journal of Arrhythmia*. Elsevier, 32(5), pp. 344–351. doi: 10.1016/j.joa.2015.09.008.

Sun, X. *et al.* (2017) ‘The Catsper channel and its roles in male fertility: a systematic review’, *Reproductive Biology and Endocrinology*, 15(1), p. 65. doi: 10.1186/s12958-017-0281-2.

Supattapone, S. *et al.* (1988) ‘Solubilization, purification, and characterization of an inositol trisphosphate receptor’, *Journal of Biological Chemistry*, 263(3), pp. 1530–

1534.

Sutko, J. L. and Airey, J. A. (1996) ‘Ryanodine receptor Ca2+ release channels: does diversity in form equal diversity in function?’, *Physiological Reviews*, 76(4), pp. 1027–1071. doi: 10.1152/physrev.1996.76.4.1027.

Sutko, J. L. and Kenyon, J. L. (1983) ‘Ryanodine modification of cardiac muscle responses to potassium-free solutions. Evidence for inhibition of sarcoplasmic reticulum calcium release.’, *The Journal of General Physiology*, 82(3), pp. 385–404. doi: 10.1085/jgp.82.3.385.

Swann, K. (1990) ‘A cytosolic sperm factor stimulates repetitive calcium increases and mimics fertilization in hamster eggs.’, *Development*, 110(4), pp. 1295–302. Available at: http://www.ncbi.nlm.nih.gov/pubmed/2100264.

Swann, K. *et al.* (2006) ‘PLCζ(zeta): A sperm protein that triggers Ca2+ oscillations and egg activation in mammals’, *Seminars in Cell & Developmental Biology*, 17(2), pp. 264–273. doi: 10.1016/j.semcdb.2006.03.009.

Swann, K. *et al.* (2009) ‘Use of Luciferase Chimaera to Monitor PLCζ Expression in Mouse Eggs’, in *Methods in Molecular Biology*, pp. 17–29. doi: 10.1007/978-1-59745-202-1_2.

Swann, K. and Lai, F. A. (2013) ‘PLCζ and the initiation of Ca2+oscillations in fertilizing mammalian eggs’, *Cell Calcium*. Elsevier Ltd, 53(1), pp. 55–62. doi: 10.1016/j.ceca.2012.11.001.

Swann, K. and Ozil, J.-P. (1994) ‘Dynamics of the Calcium Signal That Triggers Mammalian Egg Activation’, in *International Review of Cytology*, pp. 183–222. doi:

10.1016/S0074-7696(08)62557-7.

Swann, K. and Yu, Y. (2008) ‘The dynamics of calcium oscillations that activate mammalian eggs’, *The International Journal of Developmental Biology*, 52(5–6), pp. 585–594. doi: 10.1387/ijdb.072530ks.

Swillens, S. *et al.* (1999) ‘From calcium blips to calcium puffs: Theoretical analysis of the requirements for interchannel communication’, *Proceedings of the National Academy of Sciences*, 96(24), pp. 13750–13755. doi: 10.1073/pnas.96.24.13750.

Swindells, M. B. and Ikura, M. (1996) ‘Pre-formation of the semi-open conformation by the apo-calmodulin C-terminal domain and implications for binding IQ-motifs’, *Nature Structural & Molecular Biology*, 3(6), pp. 501–504. doi: 10.1038/nsb0696-501.

Szlufcik, K. *et al.* (2006) ‘The suppressor domain of inositol 1,4,5-trisphosphate receptor plays an essential role in the protection against apoptosis’, *Cell Calcium*, 39(4), pp. 325–336. doi: 10.1016/j.ceca.2005.11.007.

Tadross, M. R., Dick, I. E. and Yue, D. T. (2008) ‘Mechanism of Local and Global Ca2+ Sensing by Calmodulin in Complex with a Ca2+ Channel’, *Cell*, 133(7), pp. 1228–1240. doi: 10.1016/j.cell.2008.05.025.

Takahashi, K. *et al.* (2017) ‘A novel de novo calmodulin mutation in a 6-year-old boy who experienced an aborted cardiac arrest’, *HeartRhythm Case Reports*. Elsevier, 3(1), pp. 69–72. doi: 10.1016/j.hrcr.2016.09.004.

Takeshima, H. *et al.* (1989) ‘Primary structure and expression from complementary DNA of skeletal muscle ryanodine receptor’, *Nature*, 339(6224), pp. 439–445. doi: 10.1038/339439a0.

Tan, H. L. *et al.* (2002) ‘A calcium sensor in the sodium channel modulates cardiac excitability’, *Nature*, 415(6870), pp. 442–447. doi: 10.1038/415442a.

Tan, R. Y., Mabuchi, Y. and Grabarek, Z. (1996) ‘Blocking the Ca2+-induced conformational transitions in calmodulin with disulfide bonds.’, *Journal of Biological Chemistry*, 271(13), pp. 7479–83. Available at: http://www.ncbi.nlm.nih.gov/pubmed/8631777 (Accessed: 23 September 2015).

Tanaka, Y. *et al.* (2015) ‘Catecholaminergic Polymorphic Ventricular Tachycardia with QT Prolongation’, *Pacing and Clinical Electrophysiology*, 38(12), pp. 1499–1502. doi: 10.1111/pace.12735.

Tang, L. *et al.* (2014) ‘Structural basis for Ca2+ selectivity of a voltage-gated calcium channel’, *Nature*. Nature Publishing Group, 505(7481), pp. 56–61. doi: 10.1038/nature12775.

Tang, W. (2002) ‘Calmodulin modulation of proteins involved in excitation-contraction coupling’, *Frontiers in Bioscience*, 7(1–3), p. d1583. doi: 10.2741/tang.

Taylor, C. W., da Fonseca, P. C. A. and Morris, E. P. (2004) ‘IP3 receptors: the search for structure’, *Trends in Biochemical Sciences*, 29(4), pp. 210–219. doi: 10.1016/j.tibs.2004.02.010.

Taylor, C. W., Genazzani, A. A. and Morris, S. A. (1999) ‘Expression of inositol trisphosphate receptors’, *Cell Calcium*, 26(6), pp. 237–251. doi: 10.1054/ceca.1999.0090.

Taylor, C. W. and Tovey, S. C. (2010) ‘IP3 Receptors: Toward Understanding Their Activation’, *Cold Spring Harbor Perspectives in Biology*, 2(12), pp. a004010–

a004010. doi: 10.1101/cshperspect.a004010.

Taylor, D. a *et al.* (1991) 'Structure of a Recombinant Calmodulin from Drosophila-Melanogaster Refined at 2.2-a Resolution', *J. Biol. Chem.*, 266(14), pp. 21375–21380.

Terpe, K. (2003) 'Overview of tag protein fusions: from molecular and biochemical fundamentals to commercial systems', *Applied Microbiology and Biotechnology*, 60(5), pp. 523–533. doi: 10.1007/s00253-002-1158-6.

Tester, D. J. *et al.* (2004) 'Targeted Mutational Analysis of the RyR2-Encoded Cardiac Ryanodine Receptor in Sudden Unexplained Death: A Molecular Autopsy of 49 Medical Examiner/Coroner's Cases', *Mayo Clinic Proceedings*, 79(11), pp. 1380–1384. doi: 10.4065/79.11.1380.

Tester, D. J. *et al.* (2005) 'Spectrum and prevalence of cardiac ryanodine receptor (RyR2) mutations in a cohort of unrelated patients referred explicitly for long QT syndrome genetic testing', *Heart Rhythm*, 2(10), pp. 1099–1105. doi: 10.1016/j.hrthm.2005.07.012.

Tester, D. J. *et al.* (2007) 'A mechanism for sudden infant death syndrome (SIDS): Stress-induced leak via ryanodine receptors', *Heart Rhythm*, 4(6), pp. 733–739. doi: 10.1016/j.hrthm.2007.02.026.

Tester, D. J. *et al.* (2012) 'Cardiac Channel Molecular Autopsy: Insights From 173 Consecutive Cases of Autopsy-Negative Sudden Unexplained Death Referred for Postmortem Genetic Testing', *Mayo Clinic Proceedings*, 87(6), pp. 524–539. doi: 10.1016/j.mayocp.2012.02.017.

Tester, D. J. and Ackerman, M. J. (2006) ‘The role of molecular autopsy in unexplained sudden cardiac death’, *Current Opinion in Cardiology*, 21(3), pp. 166–172. doi: 10.1097/01.hco.0000221576.33501.83.

Theodoridou, M. *et al.* (2013) ‘Chimeras of sperm PLC reveal disparate protein domain functions in the generation of intracellular Ca2+ oscillations in mammalian eggs at fertilization’, *Molecular Human Reproduction*. England, 19(12), pp. 852–864. doi: 10.1093/molehr/gat070.

Thiel, C., Weber, K. and Gerke, V. (1991) ‘Characterization of a Ca (2+)-binding site in human annexin II by site-directed mutagenesis.’, *Journal of Biological Chemistry*, 266(22), p. 14732. Available at: http://www.ncbi.nlm.nih.gov/entrez/query.fcgi?cmd=Retrieve&db=PubMed&dopt=Citation&list_uids=1830590 %5Cnhttp://www.jbc.org/content/266/22/14732.short.

Thomas, A. P. *et al.* (1996) ‘Spatial and temporal aspects of cellular calcium signaling.’, *The FASEB Journal*, 10(13), pp. 1505–1517. doi: 10.1096/fasebj.10.13.8940296.

Thomas, H. *et al.* (2018) ‘Global Atlas of Cardiovascular Disease 2000-2016’, *Global Heart*, 13(3), pp. 143–163. doi: 10.1016/j.gheart.2018.09.511.

Tian, X. *et al.* (2015) ‘A Voltage-Gated Calcium Channel Regulates Lysosomal Fusion with Endosomes and Autophagosomes and Is Required for Neuronal Homeostasis’, *PLOS Biology*. Edited by D. E. Clapham, 13(3), p. e1002103. doi: 10.1371/journal.pbio.1002103.

Tidow, H. and Nissen, P. (2013) ‘Structural diversity of calmodulin binding to its

target sites', *FEBS Journal*, 280(21), pp. 5551–5565. doi: 10.1111/febs.12296.

Tilgen, N. *et al.* (2001) 'Identification of four novel mutations in the C-terminal membrane spanning domain of the ryanodine receptor 1: association with central core disease and alteration of calcium homeostasis', *Human Molecular Genetics*, 10(25), pp. 2879–2887. doi: 10.1093/hmg/10.25.2879.

Tobelaim, W. S. *et al.* (2017a) 'Ca 2+ -Calmodulin and PIP2 interactions at the proximal C-terminus of Kv7 channels', *Channels*. Taylor & Francis, 11(6), pp. 686–695. doi: 10.1080/19336950.2017.1388478.

Tobelaim, W. S. *et al.* (2017b) 'Competition of calcified calmodulin N lobe and PIP 2 to an LQT mutation site in Kv7.1 channel', *Proceedings of the National Academy of Sciences*, 114(5), pp. E869–E878. doi: 10.1073/pnas.1612622114.

Toutenhoofd, S. L. *et al.* (1998) 'Characterization of the human CALM2 calmodulin gene and comparison of the transcriptional activity of CALM1, CALM2 and CALM3', *Cell Calcium*, 23(5), pp. 323–338. doi: 10.1016/S0143-4160(98)90028-8.

Tripathy, A. *et al.* (1995) 'Calmodulin activation and inhibition of skeletal muscle Ca2+ release channel (ryanodine receptor)', *Biophysical Journal*. Elsevier, 69(1), pp. 106–119. doi: 10.1016/S0006-3495(95)79880-0.

Tu, H. *et al.* (2003) 'Functional and biochemical analysis of the type 1 inositol (1,4,5)-trisphosphate receptor calcium sensor', *Biophysical Journal*. Elsevier, 85(1), pp. 290–299. doi: 10.1016/S0006-3495(03)74474-9.

Tung, C.-C. *et al.* (2010) 'The amino-terminal disease hotspot of ryanodine receptors forms a cytoplasmic vestibule', *Nature*. Nature Publishing Group, 468(7323), pp.

585–588. doi: 10.1038/nature09471.

Uchida, K. *et al.* (2003) ‘Critical Regions for Activation Gating of the Inositol 1,4,5-Trisphosphate Receptor’, *Journal of Biological Chemistry*, 278(19), pp. 16551–16560. doi: 10.1074/jbc.M300646200.

Uchinoumi, H. *et al.* (2010) ‘Catecholaminergic Polymorphic Ventricular Tachycardia Is Caused by Mutation-Linked Defective Conformational Regulation of the Ryanodine Receptor’, *Circulation Research*, 106(8), pp. 1413–1424. doi: 10.1161/CIRCRESAHA.109.209312.

Uchiyama, T. *et al.* (2002) ‘A Novel Recombinant Hyperaffinity Inositol 1,4,5-Trisphosphate (IP 3) Absorbent Traps IP 3 , Resulting in Specific Inhibition of IP 3 -mediated Calcium Signaling’, *Journal of Biological Chemistry*, 277(10), pp. 8106–8113. doi: 10.1074/jbc.M108337200.

Várnai, P. and Balla, T. (1998) ‘Visualization of Phosphoinositides That Bind Pleckstrin Homology Domains: Calcium- and Agonist-induced Dynamic Changes and Relationship to Myo-[3 H]inositol-labeled Phosphoinositide Pools’, *The Journal of Cell Biology*, 143(2), pp. 501–510. doi: 10.1083/jcb.143.2.501.

Vassort, G. (2001) ‘Adenosine 5′-Triphosphate: a P2-Purinergic Agonist in the Myocardium’, *Physiological Reviews*, 81(2), pp. 767–806. doi: 10.1152/physrev.2001.81.2.767.

Vasudevan, S. R., Galione, A. and Churchill, G. C. (2008) ‘Sperm express a Ca 2+ -regulated NAADP synthase’, *Biochemical Journal*, 411(1), pp. 63–70. doi: 10.1042/BJ20071616.

Vatta, M. *et al.* (2006) ‘Mutant Caveolin-3 Induces Persistent Late Sodium Current and Is Associated With Long-QT Syndrome’, *Circulation*, 114(20), pp. 2104–2112. doi: 10.1161/CIRCULATIONAHA.106.635268.

Vega, A. L. *et al.* (2009) ‘Protein Kinase A-Dependent Biophysical Phenotype for V227F-KCNJ2 Mutation in Catecholaminergic Polymorphic Ventricular Tachycardia’, *Circulation: Arrhythmia and Electrophysiology*, 2(5), pp. 540–547. doi: 10.1161/CIRCEP.109.872309.

Verkhratsky, A. (2005) ‘Physiology and Pathophysiology of the Calcium Store in the Endoplasmic Reticulum of Neurons’, *Physiological Reviews*, 85(1), pp. 201–279. doi: 10.1152/physrev.00004.2004.

Verkhratsky, A. and Parpura, V. (2014) ‘Calcium signalling and calcium channels: Evolution and general principles’, *European Journal of Pharmacology*. Elsevier, 739(C), pp. 1–3. doi: 10.1016/j.ejphar.2013.11.013.

Villarroel, A. *et al.* (2014) ‘The Ever Changing Moods of Calmodulin: How Structural Plasticity Entails Transductional Adaptability’, *Journal of Molecular Biology*. Elsevier Ltd, 426(15), pp. 2717–2735. doi: 10.1016/j.jmb.2014.05.016.

Visser, M. *et al.* (2016) ‘Idiopathic Ventricular Fibrillation’, *Circulation: Arrhythmia and Electrophysiology*, 9(5). doi: 10.1161/CIRCEP.115.003817.

Vogel, H. J. (1994) ‘Calmodulin: a versatile calcium mediator protein’, *Biochemistry and Cell Biology*, 72(9–10), pp. 357–376. doi: 10.1139/o94-049.

Wagenknecht, T. *et al.* (1994) ‘Localization of calmodulin binding sites on the ryanodine receptor from skeletal muscle by electron microscopy’, *Biophysical*

Journal. Elsevier, 67(6), pp. 2286–2295. doi: 10.1016/S0006-3495(94)80714-3.

Wagenknecht, T. *et al.* (1997) 'Locations of Calmodulin and FK506-binding Protein on the Three-dimensional Architecture of the Skeletal Muscle Ryanodine Receptor', *Journal of Biological Chemistry*, 272(51), pp. 32463–32471. doi: 10.1074/jbc.272.51.32463.

Walker, D. S. *et al.* (2009) 'Inositol 1,4,5-Trisphosphate Signalling Regulates the Avoidance Response to Nose Touch in Caenorhabditis elegans', *PLoS Genetics*. Edited by M. B. Goodman, 5(9), p. e1000636. doi: 10.1371/journal.pgen.1000636.

Walweel, K., Oo, Y. W. and Laver, D. R. (2017) 'The emerging role of calmodulin regulation of RyR2 in controlling heart rhythm, the progression of heart failure and the antiarrhythmic action of dantrolene', *Clinical and Experimental Pharmacology and Physiology*, 44(1), pp. 135–142. doi: 10.1111/1440-1681.12669.

Wang, C. *et al.* (2012) 'Crystal Structure of the Ternary Complex of a NaV C-Terminal Domain, a Fibroblast Growth Factor Homologous Factor, and Calmodulin', *Structure*. Elsevier Ltd, 20(7), pp. 1167–1176. doi: 10.1016/j.str.2012.05.001.

Wang, J. H. *et al.* (1980) 'On the mechanism of activation of cyclic nucleotide phosphodiesterase by calmodulin.', *Annals of the New York Academy of Sciences*, 356(1), pp. 190–204. doi: 10.1111/j.1749-6632.1980.tb29611.x.

Wang, Q. *et al.* (1995) 'SCN5A mutations associated with an inherited cardiac arrhythmia, long QT syndrome', *Cell*, 80(5), pp. 805–811. doi: 10.1016/0092-8674(95)90359-3.

Wang, Q. *et al.* (2011) 'The Effect of Macromolecular Crowding, Ionic Strength and

Calcium Binding on Calmodulin Dynamics', *PLoS Computational Biology*. Edited by J. M. Briggs, 7(7), p. e1002114. doi: 10.1371/journal.pcbi.1002114.

Wang, S. *et al.* (1987) 'Localization of Ryanodine Receptor (RyR) in a Subfraction of Cardiac Sarcoplasmic Reticulum (CSR)', *Biophysical Journal*, 51(Issue 2, Part 2), p. 354a.

Wang, Z. *et al.* (2012) 'Ubiquitin-intein and SUMO2-intein fusion systems for enhanced protein production and purification', *Protein Expression and Purification*, 82(1), pp. 174–178. doi: 10.1016/j.pep.2011.11.017.

Wang, Zhongyuan *et al.* (2010) 'Human SUMO fusion systems enhance protein expression and solubility', *Protein Expression and Purification*, 73(2), pp. 203–208. doi: 10.1016/j.pep.2010.05.001.

Wangüemert, F. *et al.* (2015) 'Clinical and molecular characterization of a cardiac ryanodine receptor founder mutation causing catecholaminergic polymorphic ventricular tachycardia', *Heart Rhythm*. Elsevier, 12(7), pp. 1636–1643. doi: 10.1016/j.hrthm.2015.03.033.

Warren, T. D., Coolbaugh, M. J. and Wood, D. W. (2013) 'Ligation-independent cloning and self-cleaving intein as a tool for high-throughput protein purification', *Protein Expression and Purification*. Elsevier Inc., 91(2), pp. 169–174. doi: 10.1016/j.pep.2013.08.006.

Watterson, D. M., Sharief, F. and Vanaman, T. C. (1980) 'The complete amino acid sequence of the Ca2+-dependent modulator protein (calmodulin) of bovine brain.', *Journal of Biological Chemistry*, 255(3), pp. 962–75. Available at:

http://www.ncbi.nlm.nih.gov/pubmed/7356670.

Waugh, D. S. (2005) ‘Making the most of affinity tags’, *Trends in Biotechnology*, 23(6), pp. 316–320. doi: 10.1016/j.tibtech.2005.03.012.

Wayman, G. A. *et al.* (2011) ‘Analysis of CaM-kinase signaling in cells’, *Cell Calcium*. Elsevier Ltd, 50(1), pp. 1–8. doi: 10.1016/j.ceca.2011.02.007.

Wehrens, X. H. T. *et al.* (2004) ‘Ca 2+ /Calmodulin-Dependent Protein Kinase II Phosphorylation Regulates the Cardiac Ryanodine Receptor’, *Circulation Research*, 94(6), pp. e61–e70. doi: 10.1161/01.RES.0000125626.33738.E2.

Wehrens, X. H. T. (2004) ‘Protection from Cardiac Arrhythmia Through Ryanodine Receptor-Stabilizing Protein Calstabin2’, *Science*, 304(5668), pp. 292–296. doi: 10.1126/science.1094301.

Wehrens, X. H. T. *et al.* (2005) ‘Enhancing calstabin binding to ryanodine receptors improves cardiac and skeletal muscle function in heart failure’, *Proceedings of the National Academy of Sciences*, 102(27), pp. 9607–9612. doi: 10.1073/pnas.0500353102.

Wei, R. *et al.* (2016) ‘Structural insights into Ca2+-activated long-range allosteric channel gating of RyR1’, *Cell Research*. Nature Publishing Group, 26(9), pp. 977–994. doi: 10.1038/cr.2016.99.

Wemhöner, K. *et al.* (2015) ‘Gain-of-function mutations in the calcium channel CACNA1C (Cav1.2) cause non-syndromic long-QT but not Timothy syndrome’, *Journal of Molecular and Cellular Cardiology*. Elsevier Ltd, 80, pp. 186–195. doi: 10.1016/j.yjmcc.2015.01.002.

van der Werf, C. and Wilde, A. A. M. M. (2013) ‘Catecholaminergic polymorphic ventricular tachycardia: from bench to bedside’, *Heart*, 99(7), pp. 497–504. doi: 10.1136/heartjnl-2012-302033.

Wewers, M. D. and Sarkar, A. (2009) ‘P2X7 receptor and macrophage function’, *Purinergic Signalling*, 5(2), pp. 189–195. doi: 10.1007/s11302-009-9131-9.

Whitmore, L. *et al.* (2017) ‘PCDDB: new developments at the Protein Circular Dichroism Data Bank’, *Nucleic Acids Research*, 45(D1), pp. D303–D307. doi: 10.1093/nar/gkw796.

Wijeyeratne, Y. D. and Behr, E. R. (2017) ‘Sudden death and cardiac arrest without phenotype: the utility of genetic testing’, *Trends in Cardiovascular Medicine*. Elsevier, 27(3), pp. 207–213. doi: 10.1016/j.tcm.2016.08.010.

Williams, R. L. (1999) ‘Mammalian phosphoinositide-specific phospholipase C’, *Biochimica et Biophysica Acta (BBA) - Molecular and Cell Biology of Lipids*, 1441(2–3), pp. 255–267. doi: 10.1016/S1388-1981(99)00150-X.

Wilson, M. a and Brunger, a T. (2000) ‘The 1.0 A crystal structure of Ca(2+)-bound calmodulin: an analysis of disorder and implications for functionally relevant plasticity.’, *Journal of molecular biology*, 301(5), pp. 1237–1256. doi: 10.1006/jmbi.2000.4029.

Winn, M. D. *et al.* (2011) ‘Overview of the CCP 4 suite and current developments’, *Acta Crystallographica Section D Biological Crystallography*. International Union of Crystallography, 67(4), pp. 235–242. doi: 10.1107/S0907444910045749.

Winter, G. (2010) ‘Xia2: An expert system for macromolecular crystallography data

reduction', *Journal of Applied Crystallography*. International Union of Crystallography, 43(1), pp. 186–190. doi: 10.1107/S0021889809045701.

Wong, C. C. *et al.* (2010) 'Non-invasive imaging of human embryos before embryonic genome activation predicts development to the blastocyst stage', *Nature Biotechnology*. Nature Publishing Group, 28(10), pp. 1115–1121. doi: 10.1038/nbt.1686.

Wood, D. W. *et al.* (1999) 'A genetic system yields self-cleaving inteins for bioseparations', *Nature Biotechnology*. Nature America Inc., 17(9), pp. 889–892. doi: 10.1038/12879.

Wood, D. W. *et al.* (2000) 'Optimized Single-Step Affinity Purification with a Self-Cleaving Intein Applied to Human Acidic Fibroblast Growth Factor', *Biotechnology Progress*, 16(6), pp. 1055–1063. doi: 10.1021/bp0000858.

Woods, N. M., Cuthbertson, K. S. R. and Cobbold, P. H. (1986) 'Repetitive transient rises in cytoplasmic free calcium in hormone-stimulated hepatocytes', *Nature*, 319(6054), pp. 600–602. doi: 10.1038/319600a0.

Wu, H. *et al.* (2001) 'Sperm Factor Induces Intracellular Free Calcium Oscillations by Stimulating the Phosphoinositide Pathway1', *Biology of Reproduction*, 64(5), pp. 1338–1349. doi: 10.1095/biolreprod64.5.1338.

Wu, W.-Y. *et al.* (2010) 'Self-cleaving purification tags re-engineered for rapid Topo® cloning', *Biotechnology Progress*, 26(5), pp. 1205–1212. doi: 10.1002/btpr.430.

Xiao, B. *et al.* (2002) 'Isoform-dependent Formation of Heteromeric Ca 2+ Release Channels (Ryanodine Receptors)', *Journal of Biological Chemistry*, 277(44), pp.

41778–41785. doi: 10.1074/jbc.M208210200.

Xiong, H. *et al.* (1998) 'Identification of a Two EF-Hand Ca 2+ Binding Domain in Lobster Skeletal Muscle Ryanodine Receptor/Ca 2+ Release Channel', *Biochemistry*, 37(97), pp. 4804–4814. doi: 10.1021/bi971198b.

Xiong, L. *et al.* (2006) 'A Ca2+-Binding Domain in RyR1 that Interacts with the Calmodulin Binding Site and Modulates Channel Activity', *Biophysical Journal*, 90(1), pp. 173–182. doi: 10.1529/biophysj.105.066092.

Xu, L. *et al.* (2006) 'Two rings of negative charges in the cytosolic vestibule of type-1 ryanodine receptor modulate ion fluxes', *Biophysical Journal*. Elsevier, 90(2), pp. 443–453. doi: 10.1529/biophysj.105.072538.

Xu, L. *et al.* (2017) 'Two EF-hand motifs in ryanodine receptor calcium release channels contribute to isoform-specific regulation by calmodulin', *Cell Calcium*, 66, pp. 62–70. doi: 10.1016/j.ceca.2017.05.013.

Xu, L., Jones, R. and Meissner, G. (1993) 'Effects of local anesthetics on single channel behavior of skeletal muscle calcium release channel', *The Journal of General Physiology*, 101(2), pp. 207–233. doi: 10.1085/jgp.101.2.207.

Xu, L. and Meissner, G. (2004) 'Mechanism of Calmodulin Inhibition of Cardiac Sarcoplasmic Reticulum Ca2+ Release Channel (Ryanodine Receptor)', *Biophysical Journal*. Elsevier, 86(2), pp. 797–804. doi: 10.1016/S0006-3495(04)74155-7.

Xu, M.-Q., Paulus, H. and Chong, S. (2000) 'Fusions to self-splicing inteins for protein purification', in *Methods in Enzymology*. Elsevier Inc., pp. 376–418. doi: 10.1016/S0076-6879(00)26066-7.

Xu, X. *et al.* (2010) 'Defective calmodulin binding to the cardiac ryanodine receptor plays a key role in CPVT-associated channel dysfunction', *Biochemical and Biophysical Research Communications*. Elsevier Inc., 394(3), pp. 660–666. doi: 10.1016/j.bbrc.2010.03.046.

Xu, Z., Kopf, G. S. S. and Schultz, R. M. M. (1994) 'Involvement of inositol 1,4,5-trisphosphate-mediated Ca2+ release in early and late events of mouse egg activation.', *Development*, 120(7), pp. 1851–1859.

Yamada, N. *et al.* (1994) 'Human inositol 1,4,5-trisphosphate type-1 receptor, Ins P 3 R1: structure, function, regulation of expression and chromosomal localization', *Biochemical Journal*, 302(3), pp. 781–790. doi: 10.1042/bj3020781.

Yamaguchi, N. *et al.* (2003) 'Molecular Basis of Calmodulin Binding to Cardiac Muscle Ca 2 + Release Channel (Ryanodine Receptor)', *Journal of Biological Chemistry*, 278(26), pp. 23480–23486. doi: 10.1074/jbc.M301125200.

Yamaguchi, N. *et al.* (2004) 'Different Regions in Skeletal and Cardiac Muscle Ryanodine Receptors Are Involved in Transducing the Functional Effects of Calmodulin', *Journal of Biological Chemistry*, 279(35), pp. 36433–36439. doi: 10.1074/jbc.M405834200.

Yamaguchi, N. *et al.* (2005) 'Calmodulin regulation and identification of calmodulin binding region of type-3 ryanodine receptor calcium release channel', *Biochemistry*, 44(45), pp. 15074–15081. doi: 10.1021/bi051251t.

Yamaguchi, N. *et al.* (2007) 'Early cardiac hypertrophy in mice with impaired calmodulin regulation of cardiac muscle Ca2+ release channel', *Journal of Clinical*

Investigation, 117(5), pp. 1344–1353. doi: 10.1172/JCI29515.

Yamaguchi, N., Xin, C. and Meissner, G. (2001) 'Identification of Apocalmodulin and Ca2+-Calmodulin Regulatory Domain in Skeletal Muscle Ca2+ Release Channel, Ryanodine Receptor', *Journal of Biological Chemistry*, 276(25), pp. 22579–22585. doi: 10.1074/jbc.M102729200.

Yamamoto-Hino, M. *et al.* (1994) 'Cloning and characterization of human type 2 and type 3 inositol 1,4,5-trisphosphate receptors.', *Receptors & Channels*. England, 2(1), pp. 9–22. Available at: http://www.ncbi.nlm.nih.gov/pubmed/8081734.

Yamamoto, T. (1999) 'Abnormal Ca2+ release from cardiac sarcoplasmic reticulum in tachycardia-induced heart failure', *Cardiovascular Research*, 44(1), pp. 146–155. doi: 10.1016/S0008-6363(99)00200-X.

Yamamoto, T. *et al.* (2008) 'Identification of Target Domains of the Cardiac Ryanodine Receptor to Correct Channel Disorder in Failing Hearts', *Circulation*, 117(6), pp. 762–772. doi: 10.1161/CIRCULATIONAHA.107.718957.

Yamamoto, T., El-Hayek, R. and Ikemoto, N. (2000) 'Postulated Role of Interdomain Interaction within the Ryanodine Receptor in Ca 2+ Channel Regulation', *Journal of Biological Chemistry*, 275(16), pp. 11618–11625. doi: 10.1074/jbc.275.16.11618.

Yamamoto, T. and Ikemoto, N. (2002) 'Spectroscopic monitoring of local conformational changes during the intramolecular domain-domain interaction of the ryanodine receptor', *Biochemistry*, 41(5), pp. 1492–1501. doi: 10.1021/bi015581z.

Yamamoto, Y. *et al.* (2017) 'Allele-specific ablation rescues electrophysiological abnormalities in a human iPS cell model of long-QT syndrome with a CALM2

mutation', *Human Molecular Genetics*, 26(9), pp. 1670–1677. doi: 10.1093/hmg/ddx073.

Yamauchi, T. (2005) 'Neuronal Ca2+/Calmodulin-Dependent Protein Kinase II—Discovery, Progress in a Quarter of a Century, and Perspective: Implication for Learning and Memory', *Biological & Pharmaceutical Bulletin*, 28(8), pp. 1342–1354. doi: 10.1248/bpb.28.1342.

Yamazaki, H. *et al.* (2010) 'Tyr-167/Trp-168 in Type 1/3 Inositol 1,4,5-Trisphosphate Receptor Mediates Functional Coupling between Ligand Binding and Channel Opening', *Journal of Biological Chemistry*, 285(46), pp. 36081–36091. doi: 10.1074/jbc.M110.140129.

Yamniuk, A. P. and Vogel, H. J. (2004) 'Calmodulin's Flexibility Allows for Promiscuity in Its Interactions with Target Proteins and Peptides', *Molecular Biotechnology*, 27(1), pp. 33–58. doi: 10.1385/MB:27:1:33.

Yan, Z. *et al.* (2015) 'Structure of the rabbit ryanodine receptor RyR1 at near-atomic resolution', *Nature*. Nature Publishing Group, 517(7532), pp. 50–55. doi: 10.1038/nature14063.

Yang, Y. *et al.* (2014) 'Cardiac Myocyte Z-Line Calmodulin Is Mainly RyR2-Bound, and Reduction Is Arrhythmogenic and Occurs in Heart Failure', *Circulation Research*. Lippincott Williams and Wilkins, 114(2), pp. 295–306. doi: 10.1161/CIRCRESAHA.114.302857.

Yang, Z. *et al.* (2006) 'The RyR2 central domain peptide DPc10 lowers the threshold for spontaneous Ca2+ release in permeabilized cardiomyocytes', *Cardiovascular*

Research, 70(3), pp. 475–485. doi: 10.1016/j.cardiores.2006.03.001.

Yang, Z. *et al.* (2015) 'The Golgi apparatus is a functionally distinct Ca 2+ store regulated by the PKA and Epac branches of the β 1 -adrenergic signaling pathway', *Science Signaling*, 8(398), pp. ra101–ra101. doi: 10.1126/scisignal.aaa7677.

Yano, M. *et al.* (2000) 'Altered Stoichiometry of FKBP12.6 Versus Ryanodine Receptor as a Cause of Abnormal Ca 2+ Leak Through Ryanodine Receptor in Heart Failure', *Circulation*, 102(17), pp. 2131–2136. doi: 10.1161/01.CIR.102.17.2131.

Yano, M. *et al.* (2003) 'FKBP12.6-Mediated Stabilization of Calcium-Release Channel (Ryanodine Receptor) as a Novel Therapeutic Strategy Against Heart Failure', *Circulation*, 107(3), pp. 477–484. doi: 10.1161/01.CIR.0000044917.74408.BE.

Yap, K. L. *et al.* (1999) 'Diversity of conformational states and changes within the EF-hand protein superfamily', *Proteins: Structure, Function, and Genetics*, 37(3), pp. 499–507. doi: 10.1002/(SICI)1097-0134(19991115)37:3<499::AID-PROT17>3.0.CO;2-Y.

Yap, K. L. *et al.* (2000) 'Calmodulin Target Database', *Journal of Structural and Functional Genomics*, 1(1), pp. 8–14. doi: 10.1023/A:1011320027914.

Yazawa, M. *et al.* (1987) 'Communication between two globular domains of calmodulin in the presence of mastoparan or caldesmon fragment. Ca2+ binding and 1H NMR.', *Journal of Biological Chemistry*, 262(23), pp. 10951–10954.

Yeste, M. *et al.* (2017) 'Oocyte Activation and Fertilisation: Crucial Contributors from

the Sperm and Oocyte', in Arur, S. (ed.) *Signaling-Mediated Control of Cell Division From Oogenesis to Oocyte-to-Embryo Development*. Springer, pp. 213–239. doi: 10.1007/978-3-319-44820-6_8.

Yin, G. *et al.* (2014) 'Arrhythmogenic Calmodulin Mutations Disrupt Intracellular Cardiomyocyte Ca 2+ Regulation by Distinct Mechanisms', *Journal of the American Heart Association*, 3(3), p. e000996. doi: 10.1161/JAHA.114.000996.

Yoda, A. *et al.* (2004) 'Ca2+ oscillation-inducing phospholipase C zeta expressed in mouse eggs is accumulated to the pronucleus during egg activation', *Developmental Biology*, 268(2), pp. 245–257. doi: 10.1016/j.ydbio.2003.12.028.

Yoo, S. H. *et al.* (2001) 'Localization of Three Types of the Inositol 1,4,5-Trisphosphate Receptor/Ca 2+ Channel in the Secretory Granules and Coupling with the Ca 2+ Storage Proteins Chromogranins A and B', *Journal of Biological Chemistry*, 276(49), pp. 45806–45812. doi: 10.1074/jbc.M107532200.

Yoon, S.-Y. *et al.* (2008) 'Human sperm devoid of PLC, zeta 1 fail to induce Ca2+ release and are unable to initiate the first step of embryo development', *Journal of Clinical Investigation*, 118(11), pp. 3671–3681. doi: 10.1172/JCI36942.

Yoshikawa, F. *et al.* (1996) 'Mutational Analysis of the Ligand Binding Site of the Inositol 1,4,5-Trisphosphate Receptor', *Journal of Biological Chemistry*, 271(30), pp. 18277–18284. doi: 10.1074/jbc.271.30.18277.

Yoshikawa, F. *et al.* (1999) 'Cooperative Formation of the Ligand-binding Site of the Inositol 1,4,5-Trisphosphate Receptor by Two Separable Domains', *Journal of Biological Chemistry*, 274(1), pp. 328–334. doi: 10.1074/jbc.274.1.328.

Young, C. L., Britton, Z. T. and Robinson, A. S. (2012) 'Recombinant protein expression and purification: A comprehensive review of affinity tags and microbial applications', *Biotechnology Journal*, 7(5), pp. 620–634. doi: 10.1002/biot.201100155.

Yu, Y. *et al.* (2007) 'Preimplantation development of mouse oocytes activated by different levels of human phospholipase C zeta', *Human Reproduction*, 23(2), pp. 365–373. doi: 10.1093/humrep/dem350.

Yu, Y. *et al.* (2012) 'PLCζ causes Ca 2+ oscillations in mouse eggs by targeting intracellular and not plasma membrane PI(4,5)P 2', *Molecular Biology of the Cell*. Edited by J. York, 23(2), pp. 371–380. doi: 10.1091/mbc.e11-08-0687.

Yuchi, Z. *et al.* (2015) 'Crystal structures of ryanodine receptor SPRY1 and tandem-repeat domains reveal a critical FKBP12 binding determinant', *Nature Communications*. Nature Publishing Group, 6(1), p. 7947. doi: 10.1038/ncomms8947.

Yuchi, Z., Lau, K. and Van Petegem, F. (2012) 'Disease Mutations in the Ryanodine Receptor Central Region: Crystal Structures of a Phosphorylation Hot Spot Domain', *Structure*. Elsevier Ltd, 20(7), pp. 1201–1211. doi: 10.1016/j.str.2012.04.015.

Yus-Nájera, E., Santana-Castro, I. and Villarroel, A. (2002) 'The Identification and Characterization of a Noncontinuous Calmodulin-binding Site in Noninactivating Voltage-dependent KCNQ Potassium Channels', *Journal of Biological Chemistry*, 277(32), pp. 28545–28553. doi: 10.1074/jbc.M204130200.

Zalk, R. *et al.* (2015) 'Structure of a mammalian ryanodine receptor', *Nature*,

517(7532), pp. 44–49. doi: 10.1038/nature13950.

Zalk, R., Lehnart, S. E. and Marks, A. R. (2007) 'Modulation of the Ryanodine Receptor and Intracellular Calcium', *Annual Review of Biochemistry*, 76(1), pp. 367–385. doi: 10.1146/annurev.biochem.76.053105.094237.

Zalk, R. and Marks, A. R. (2017) 'Ca 2+ Release Channels Join the "Resolution Revolution"', *Trends in Biochemical Sciences*. Elsevier Ltd, 42(7), pp. 543–555. doi: 10.1016/j.tibs.2017.04.005.

Zaragoza, M. V *et al.* (2000) 'Parental Origin and Phenotype of Triploidy in Spontaneous Abortions: Predominance of Diandry and Association with the Partial Hydatidiform Mole', *The American Journal of Human Genetics*, 66(6), pp. 1807–1820. doi: 10.1086/302951.

Zhang, H. *et al.* (2003) 'A Noncontiguous, Intersubunit Binding Site for Calmodulin on the Skeletal Muscle Ca 2+ Release Channel', *Journal of Biological Chemistry*, 278(10), pp. 8348–8355. doi: 10.1074/jbc.M209565200.

Zhang, J. *et al.* (2003) 'Three-dimensional Localization of Divergent Region 3 of the Ryanodine Receptor to the Clamp-shaped Structures Adjacent to the FKBP Binding Sites', *Journal of Biological Chemistry*, 278(16), pp. 14211–14218. doi: 10.1074/jbc.M213164200.

Zhang, J. *et al.* (2016) 'FKBPs facilitate the termination of spontaneous Ca2+ release in wild-type RyR2 but not CPVT mutant RyR2', *Biochemical Journal*, 473(14), pp. 2049–2060. doi: 10.1042/BCJ20160389.

Zhang, M., Tanaka, T. and Ikura, M. (1995) 'Calcium-induced conformational

transition revealed by the solution structure of apo calmodulin', *Nature Structural & Molecular Biology*, 2(9), pp. 758–767. doi: 10.1038/nsb0995-758.

Zhang, Z. *et al.* (2002) 'Overexpression of DsbC and DsbG markedly improves soluble and functional expression of single-chain Fv antibodies in Escherichia coli', *Protein Expression and Purification*, 26(2), pp. 218–228. doi: 10.1016/S1046-5928(02)00502-8.

Zhao, F. *et al.* (2001) 'Dantrolene inhibition of ryanodine receptor Ca2+release channels. Molecular mechanism and isoform selectivity', *Journal of Biological Chemistry*, 276(17), pp. 13810–13816. doi: 10.1074/jbc.M006104200.

Zhao, M. *et al.* (1999) 'Molecular Identification of the Ryanodine Receptor Pore-forming Segment', *Journal of Biological Chemistry*, 274(37), pp. 25971–25974. doi: 10.1074/jbc.274.37.25971.

Zhao, X., Li, G. and Liang, S. (2013) 'Several Affinity Tags Commonly Used in Chromatographic Purification', *Journal of Analytical Methods in Chemistry*, 2013, pp. 1–8. doi: 10.1155/2013/581093.

Zhao, Z. *et al.* (2008) 'Purification of green fluorescent protein using a two-intein system', *Applied Microbiology and Biotechnology*, 77(5), pp. 1175–1180. doi: 10.1007/s00253-007-1233-0.

Zheng, C.-F. *et al.* (1997) 'A new expression vector for high level protein production, one step purification and direct isotopic labeling of calmodulin-binding peptide fusion proteins', *Gene*, 186(1), pp. 55–60. doi: 10.1016/S0378-1119(96)00680-4.

Zheng, L. *et al.* (2000) 'Distinct Ca 2+ Binding Properties of Novel C2 Domains of

Plant Phospholipase Dα and β', *Journal of Biological Chemistry*, 275(26), pp. 19700–19706. doi: 10.1074/jbc.M001945200.

Zhou, Y., Xue, S. and Yang, J. J. (2013) 'Calciomics: integrative studies of Ca 2+ -binding proteins and their interactomes in biological systems', *Metallomics*, 5(1), pp. 29–42. doi: 10.1039/C2MT20009K.

Zhu, M., Dai, X. and Wang, Y.-P. (2016) 'Real time determination of bacterial in vivo ribosome translation elongation speed based on LacZα complementation system', *Nucleic Acids Research*, 44(20), p. gkw698. doi: 10.1093/nar/gkw698.

Zhu, X. *et al.* (2004) 'The calmodulin binding region of the skeletal ryanodine receptor acts as a self-modulatory domain', *Cell Calcium*, 35(2), pp. 165–177. doi: 10.1016/j.ceca.2003.09.002.

Zhu, X. *et al.* (2015) 'CaM and CML emergence in the green lineage', *Trends in Plant Science*. Elsevier Ltd, 20(8), pp. 483–489. doi: 10.1016/j.tplants.2015.05.010.

Zima, A. V. *et al.* (2014) 'Ca handling during excitation–contraction coupling in heart failure', *Pflügers Archiv - European Journal of Physiology*, 466(6), pp. 1129–1137. doi: 10.1007/s00424-014-1469-3.

Zucchi, R. and Ronca-Testoni, S. (1997) 'The Sarcoplasmic Reticulum Ca2+ Channel/Ryanodine Receptor: Modulation by Endogenous Effectors, Drugs and Disease States.', *Pharmacological Reviews*, 49(1), pp. 1–51. Available at: http://www.ncbi.nlm.nih.gov/pubmed/9085308.

Zuo, X., Li, S., *et al.* (2005) 'Enhanced Expression and Purification of Membrane Proteins by SUMO Fusion in Escherichia coli', *Journal of Structural and Functional*

Genomics, 6(2–3), pp. 103–111. doi: 10.1007/s10969-005-2664-4.

Zuo, X., Mattern, M. R., *et al.* (2005) ‘Expression and purification of SARS coronavirus proteins using SUMO-fusions’, *Protein Expression and Purification*, 42(1), pp. 100–110. doi: 10.1016/j.pep.2005.02.004.

APPENDICES TO THESIS

Appendix I Primers Used in Study

Appendix Table I

Name	Sequence
HZ1F	ACCAGTCGACATGGAAATGAGATGGTTTTTGTC
HZ29F	ACCAGTCGACGAAAAATTAGATATTCGGTGCAG
HZ42F	ACCAGTCGACCAGATTTTTAAGGACAATGACAGGC
HZ64F	ACCAGTCGACTATCGAATTATCACGCACAGAG
HZ68F	ACCAGTCGACACGCACAGAGAAGAAATTATTGAG
HZ100F	ACCAGTCGACCAATATGCAGCTGAGATGAG
HZ128F	CGCAGTCGACCAAATGTCATTAGAAGGT
HZ151F	CGCAGTCGACAGAAAAGTTTATCAAGATATGAC
HZ608R	CTAAGCGGCCGCTCATCTGACGTACCAAACATAAAC
HZ602R	GAGAGCGGCCGCTCAAACAAACAGTGAAGCAGGCTC
HZ583R	GAGAGCGGCCGCTCAACGATAACCTTTGTTCATGC

Name	Sequence
HZ572R	GAGAGCGGCCGCTCAAGTATATTGCCCAAGAAATTC
HZ557R	GAGAGCGGCCGCTCATTCAACAACAAAACGTATCAATGC
HZ524R	GAGAGCGGCCGCTCAAGTCTGCTGCTTCATTTGATC
MZSALIF	CCTAGTCGACATGGAAAGCCAACTTCATGAGC
MZNOTIR	CTAAGCGGCCGCTCACTCTCTGAAGTACCAAACATA
PMALEF	GGTCGTCAGACTGTCGATGAAGCC
MM41F	GCGCAGACTAATTCGAGCTCG
MMUR(2)	ACTCAGCTTCCTTTCGGGCTT
HCAMKPNF	GGAAGGTACCATGGCTGATCAGCTGACCGAAG
HCAMNOTIR	GCAAGCGGCCGCTCATTTTGCAGTCATCATCTGTAC
CAMN54IF	GCAGGATATGATCATTGAAGTGGATGCTG
CAMN54IR	CAGCATCCACTTCAATGATCATATCCTGC
CAMF90LF	GAAATCCGTGAGGCACTCCGAGTCTTTGAC

Name	Sequence
CAMF90LR	GTCAAAGACTCGGAGTGCCTCACGGATTTC
CAMD96VF	CCGAGTCTTTGACAAGGTTGGCAATGGTTATATCAG
CAMD96VR	CTGATATAACCATTGCCAACCTTGTCAAAGACTCGG
CAMN98SF	CTTTGACAAGGATGGCAGTGGTTATATCAGTGCAGC
CAMN98SR	GCTGCACTGATATAACCACTGCCATCCTTGTCAAAG
CAMD130GF	GATCAGAGAAGCAGGTATTGATGGAGACGG
CAMD130GR	CCGTCTCCATCAATACCTGCTTCTCTGATC
CAMF142LF	GTCAACTATGAAGAATTAGTACAGATGATGACTGC
CAMF142LR	GCAGTCATCATCTGTACTAATTCTTCATAGTTGAC
CAMF	GGAAGGTACCATGGCTGATCAGCTGACCGAAG
CAMR	GCAAGCGGCCGCTCATTTTGCAGTCATCATCTGTAC
CAMN98IF	CTTTGACAAGGATGGCATTGGTTATATCAGTGCAGC
CAMN98IR	GCTGCACTGATATAACCAATGCCATCCTTGTCAAAG

Name	Sequence
CAMD132EF	CAGAGAAGCAGATATTGAGGGAGACGGACAAGTC
CAMD132ER	GACTTGTCCGTCTCCCTCAATATCTGCTTCTCTG
CAMD134HF	GCAGATATTGATGGACACGGACAAGTCAACTATG
CAMD134HR	CATAGTTGACTTGTCCGTGTCCATCAATATCTGC
CAMQ136PF	GATATTGATGGAGACGGACCAGTCAACTATGAAGAATTCG
CAMQ136PR	CGAATTCTTCATAGTTGACTGGTCCGTCTCCATCAATATC
NCaMf	CCGAGGTACCATGGCTGATCAGCTGACCGAAGAACAG
NCaMr	CCCTGCGGCCGCTCATTTCATTTTTCTAGCCATCATAGTC
CCaMf	CCGAGGTACCATGGATACAGATAGTGAAGAAGAAATCCG
CCaMr	CCCTGCGGCCGCTCATTTTGCAGTCATCATCTGTACGAATTC TTC

Appendix II Vectors Used in this Study

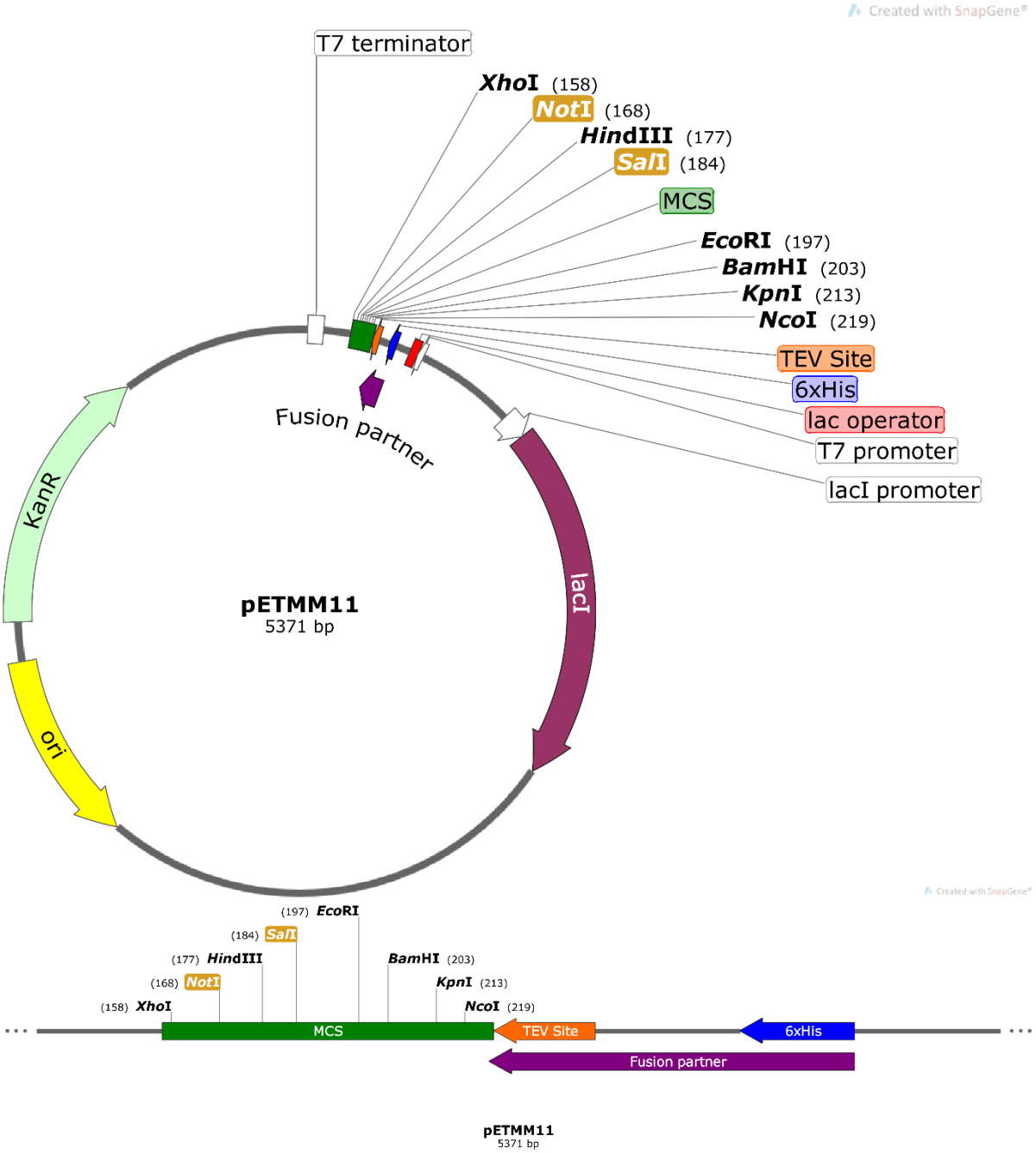

Appendix Figure I Plasmid Map of pETMM11

Vector pETMM11 contains the coding sequences for a hexahistidine tag (6xHis) followed by recognition site for Tobacco Etch Virus (TEV) protease at the 3' end of the (MCS). The vector also carries the

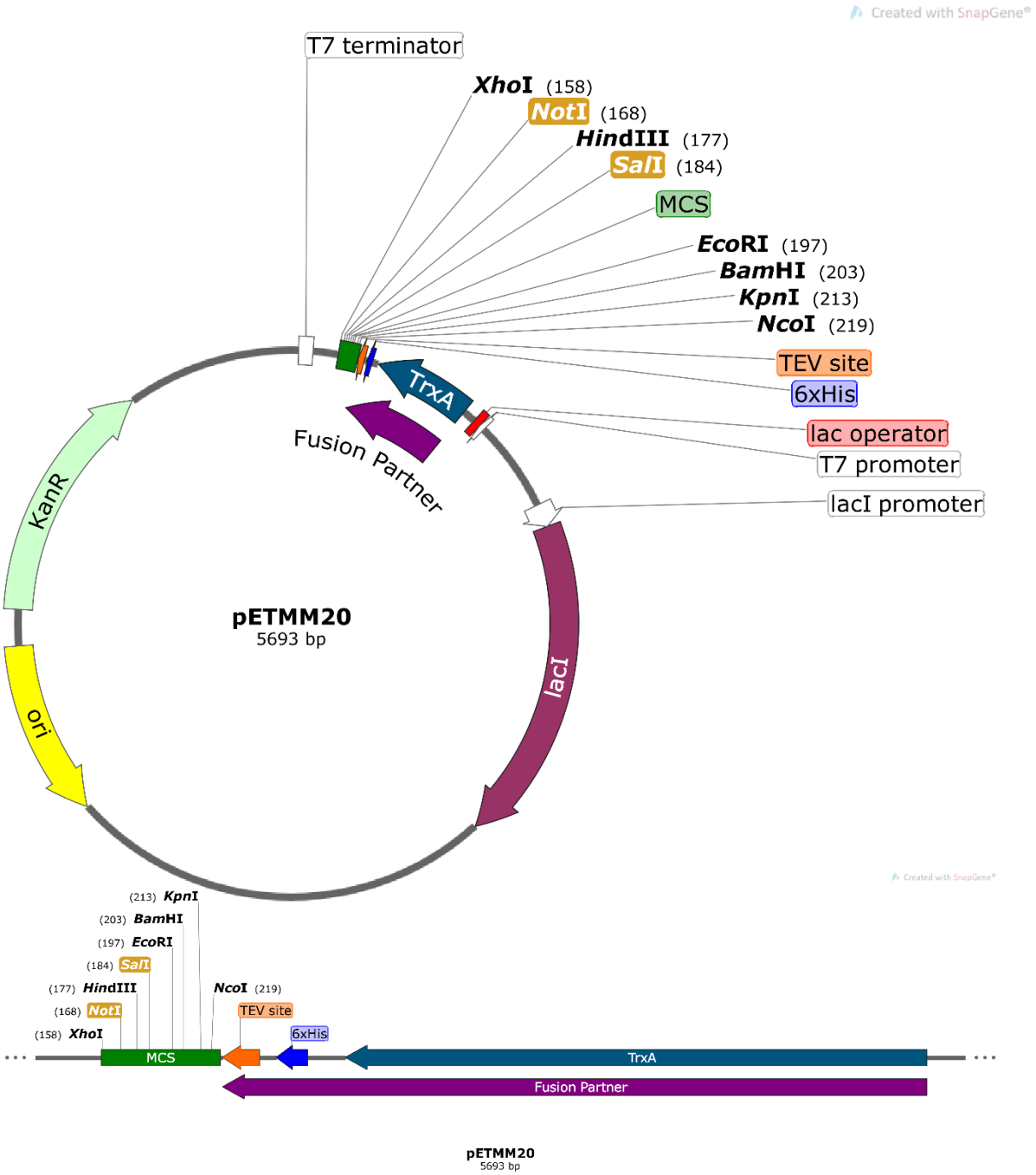

kanamycin resistance gene. Expression in this vector is anticlockwise and induced in *E. Coli* by addition of optimal IPTG to the growth media. The fusion partner in the expressed recombinant protein is 1 kDa

Appendix Figure II Plasmid Map of pETMM20

Vector pETMM20 encodes for 6xHis, followed by TEV recognition site then the coding sequence for *E. Coli* Thioredoxin A (TrxA) at the 3' end of the MCS. The vector also carries the kanamycin resistance gene. Expression in this vector is anticlockwise and induced in *E. Coli* by addition of optimal IPTG to the growth media. An expressed recombinant protein will contain a 12 kDa fusion partner.

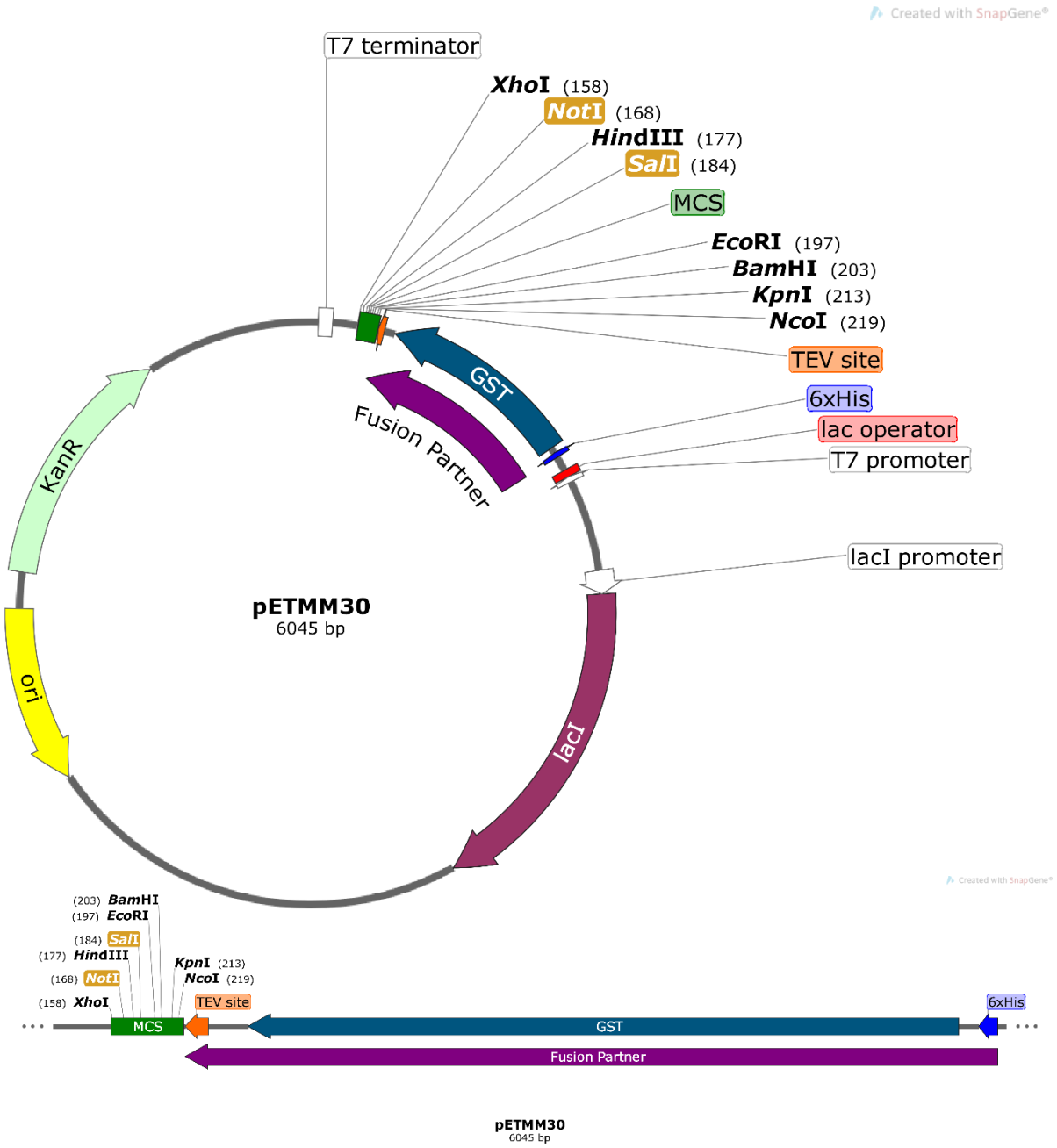

Appendix Figure III Plasmid Map of pETMM30

Vector pETMM30 encodes for 6xHis, followed by TEV recognition site then the coding sequence for Schistosoma japonicum glutathione S-transferase (GST) from at the 3'-end of the MCS. The vector also carries the kanamycin resistance gene. Expression in this vector is anticlockwise and induced in E. Coli by addition of optimal IPTG to the growth media. An expressed recombinant protein will contain a 26 kDa fusion partner.

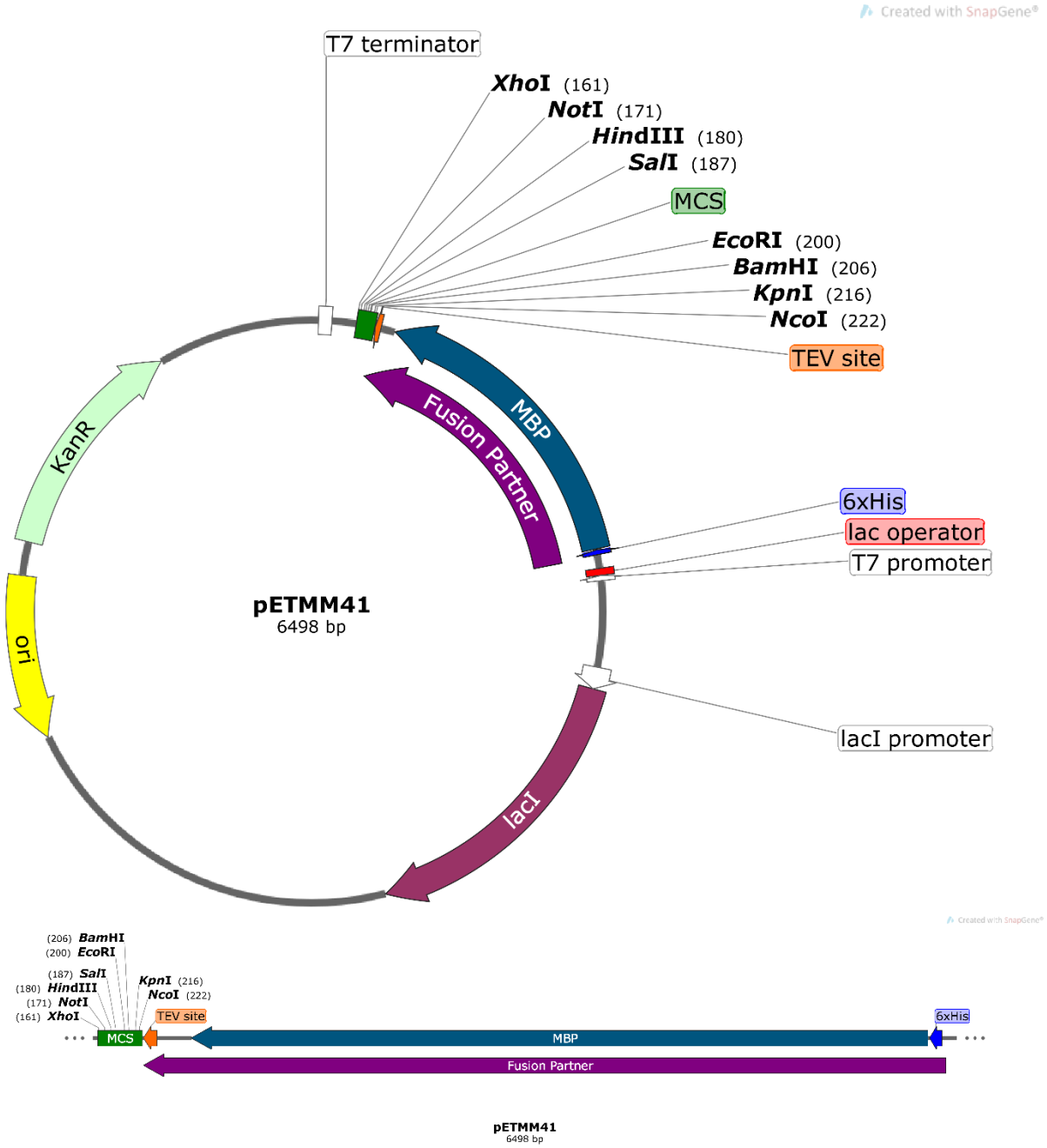

Appendix Figure IV Plasmid Map of pETMM41

Vector pETMM41 encodes for 6xHis, followed by TEV recognition site then the coding sequence for E. coli Maltose Binding Protein at the 3'-end of the MCS. The vector also carries the kanamycin resistance gene. Expression in this vector is anticlockwise and induced in E. Coli by addition of optimal IPTG to the growth media. An expressed recombinant protein will contain a 41 kDa fusion partner.

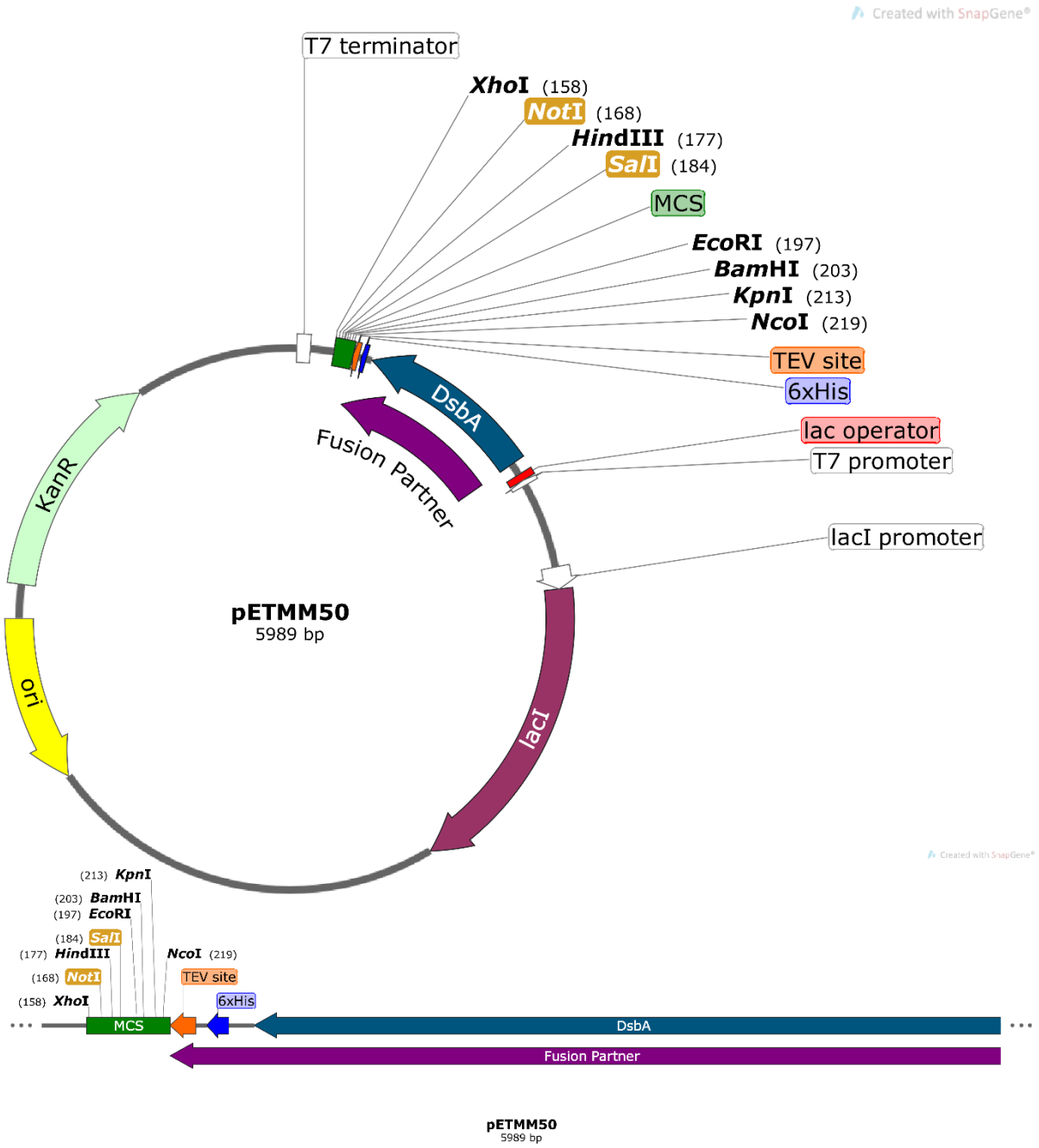

Appendix Figure V Plasmid Map of pETMM50

Vector pETMM50 encodes for DsbA followed by 6xHis then the TEV recognition site at the 3' end of the MCS. The vector also carries the kanamycin resistance gene. Expression in this vector is anticlockwise and induced in *E. Coli* by addition of optimal IPTG to the growth media. An expressed recombinant protein will contain a 21 kDa fusion partner.

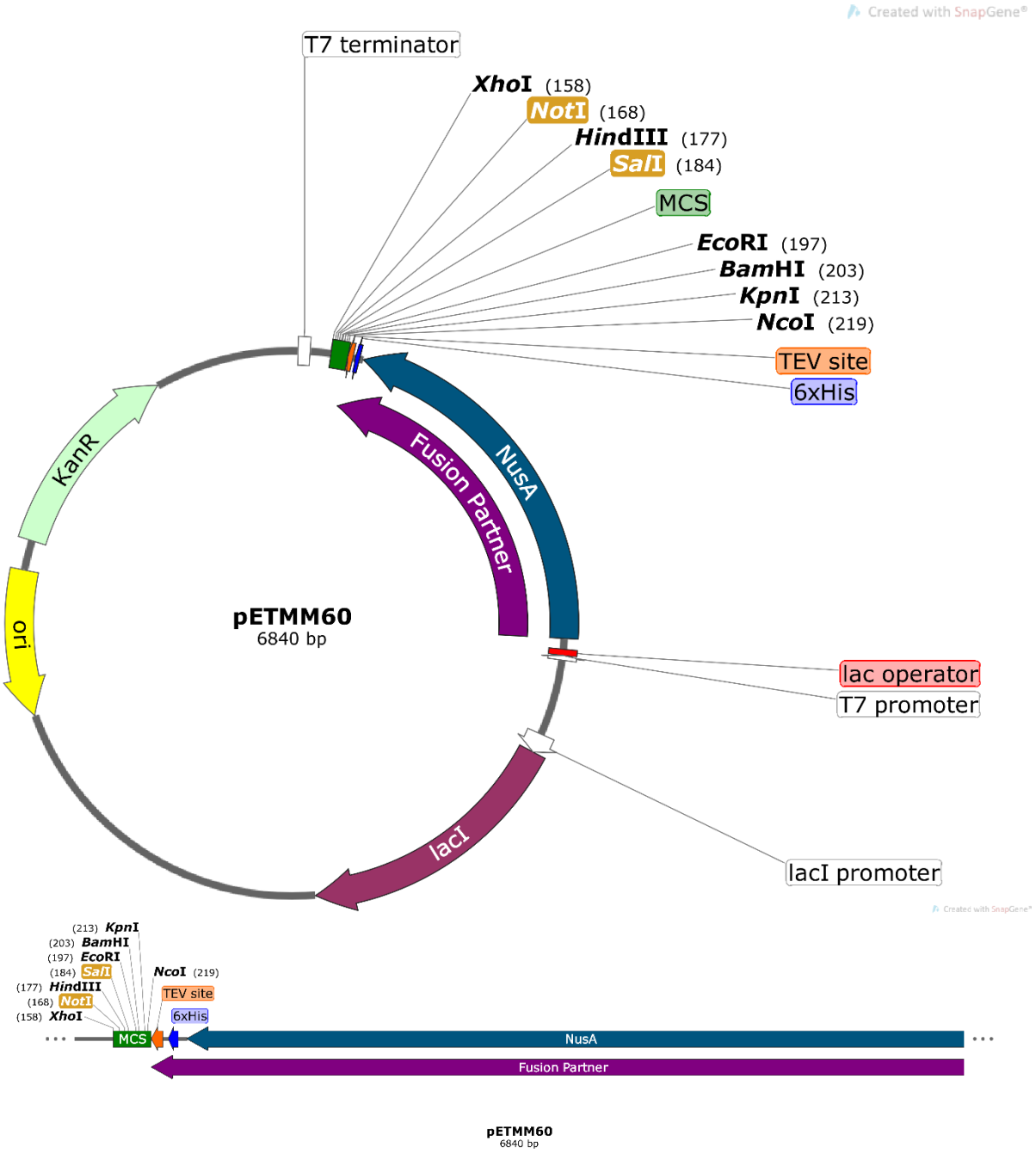

Appendix Figure VI Plasmid Map of pETMM60

Vector pETMM60 encodes for N utilisation substance protein A (NusA) followed by 6xHis then the TEV recognition site at the 3' end of the MCS. The vector also carries the kanamycin resistance gene. Expression in this vector is anticlockwise and induced in *E. Coli* by addition of optimal IPTG to the growth media. An expressed recombinant protein will contain a 55 kDa fusion partner.

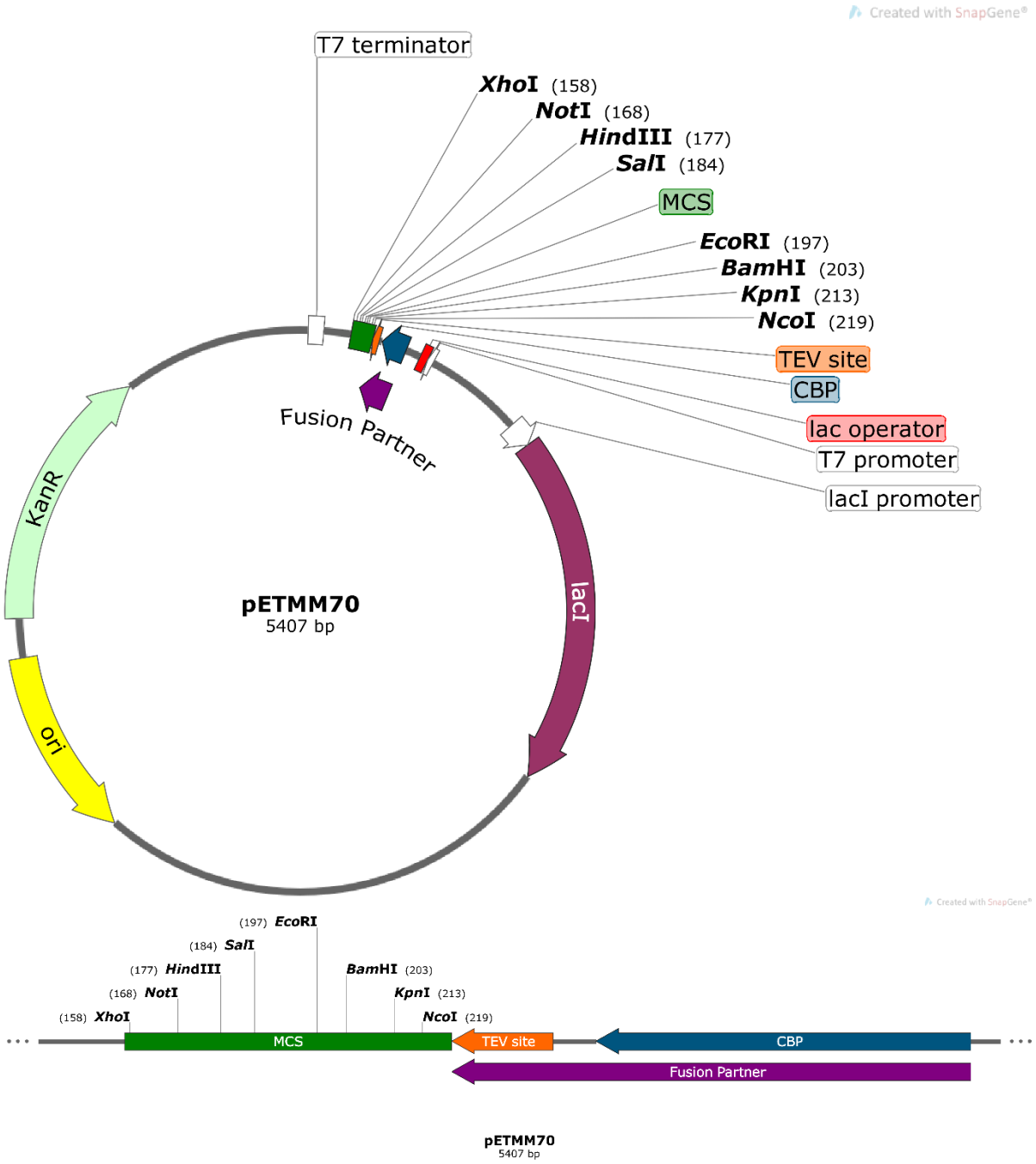

Appendix Figure VII Plasmid Map of pETMM70

Vector pETMM70 encodes for Calmodulin Binding Peptide (CBP) followed by the TEV recognition site at the 3'-end of the MCS. The vector also carries the kanamycin resistance gene. Expression in this vector is anticlockwise and induced in *E. Coli* by addition of optimal IPTG to the growth media. An expressed recombinant protein will contain a 4 kDa fusion partner.

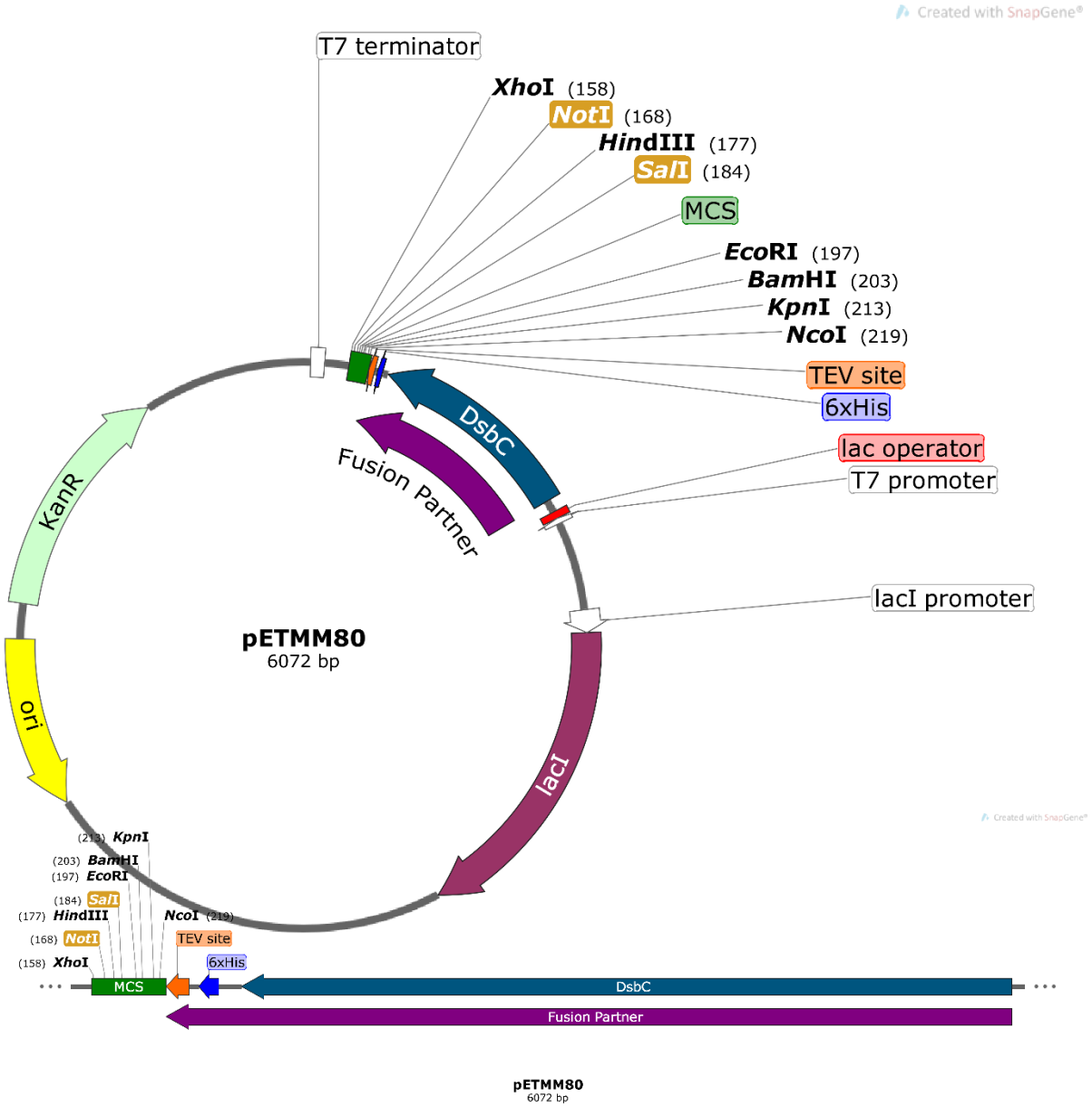

Appendix Figure VIII Plasmid Map of pETMM80

Vector pETMM80 encodes for DsbC followed by 6xHis then the TEV recognition site at the 3'-end of the MCS. The vector also carries the kanamycin resistance gene. Expression in this vector is anticlockwise and induced in *E. Coli* by addition of optimal IPTG to the growth media. An expressed recombinant protein will contain a 24 kDa fusion partner.

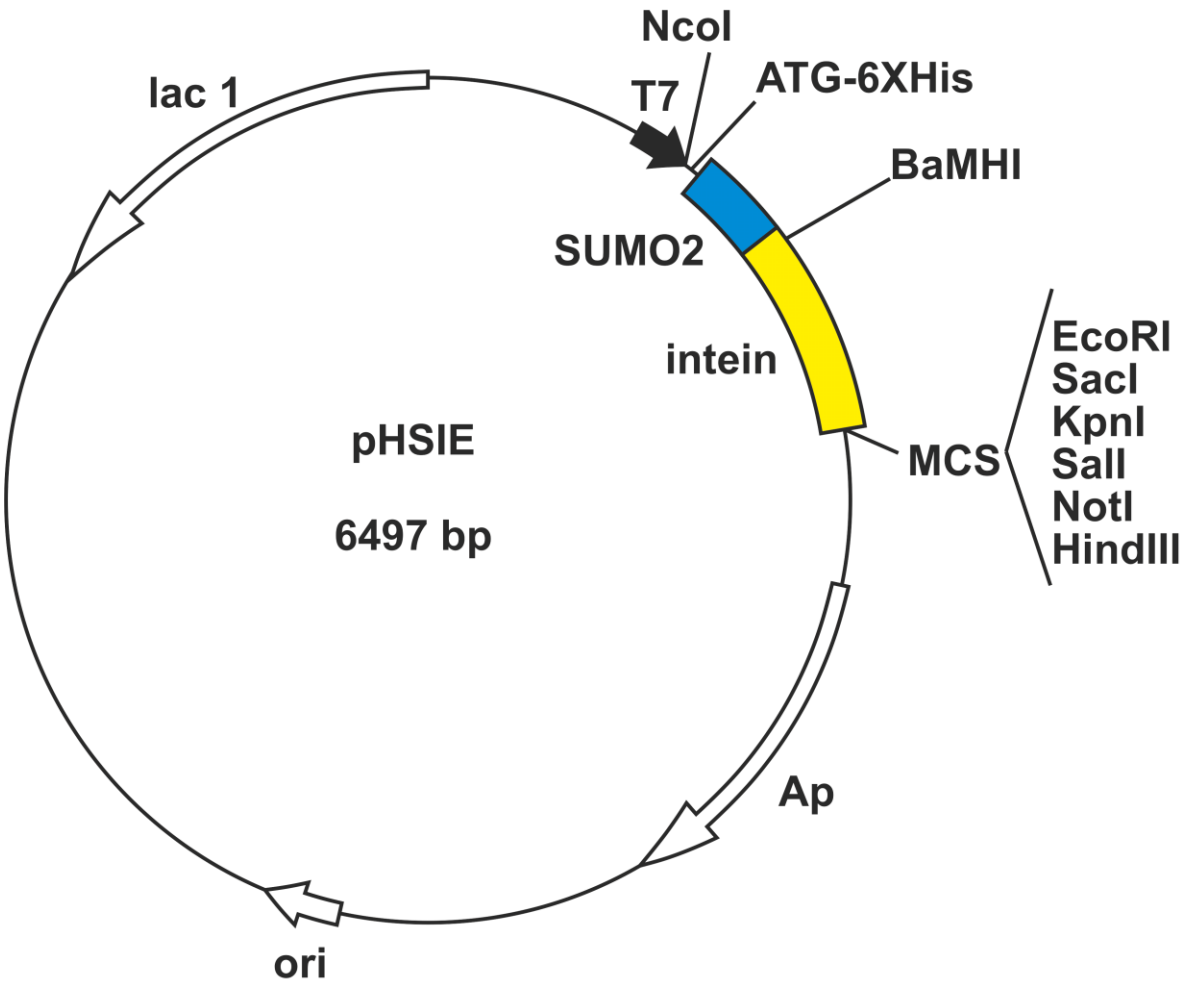

Appendix Figure IX Plasmid Map of pHSIE

Vector pHSIE encodes for 6xHis followed by SUMO2 then an Intein self-cleavage site at the 5' end of the MCS. The vector also carries the kanamycin ampicillin resistance gene. Expression in this vector is clockwise and induced in *E. Coli* by addition of optimal IPTG to the growth media. An expressed recombinant protein will contain a 26 kDa fusion partner.

Appendix III Confirmation of Purity of Proteins for Crystallisation Experiments

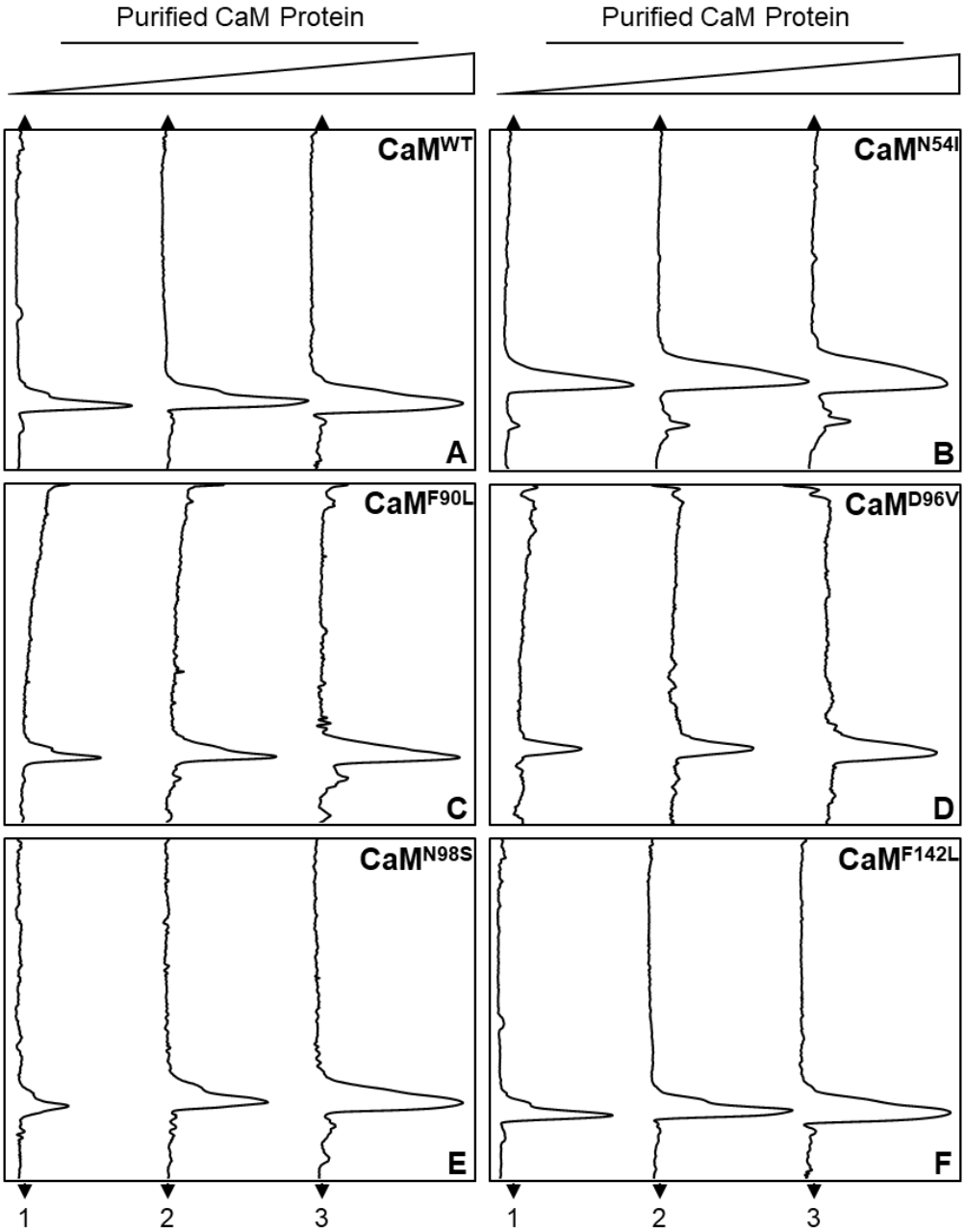

Appendix Figure X Calmodulin Proteins Purified for Crystallisation Studies contain only one major speices

Profile plots of the SDS-PAGE gels lanes in Figure 4-15 and Figure 5-22 containing increasing amounts purified CaM proteins **(A)** CaM^{WT}, **(B)** CaM^{N54I}, **(C)** CaM^{F90L}, **(D)** CaM^{D96V}, and **(E)** CaM^{N98S} **(F)** CaM^{F142L}. (A) Lanes 1-3: 0.5 µg, 1.0 µg and 2 µg protein. (B-F) Lanes 1-3 1 µg, 2.5 µg and 5 µg protein..

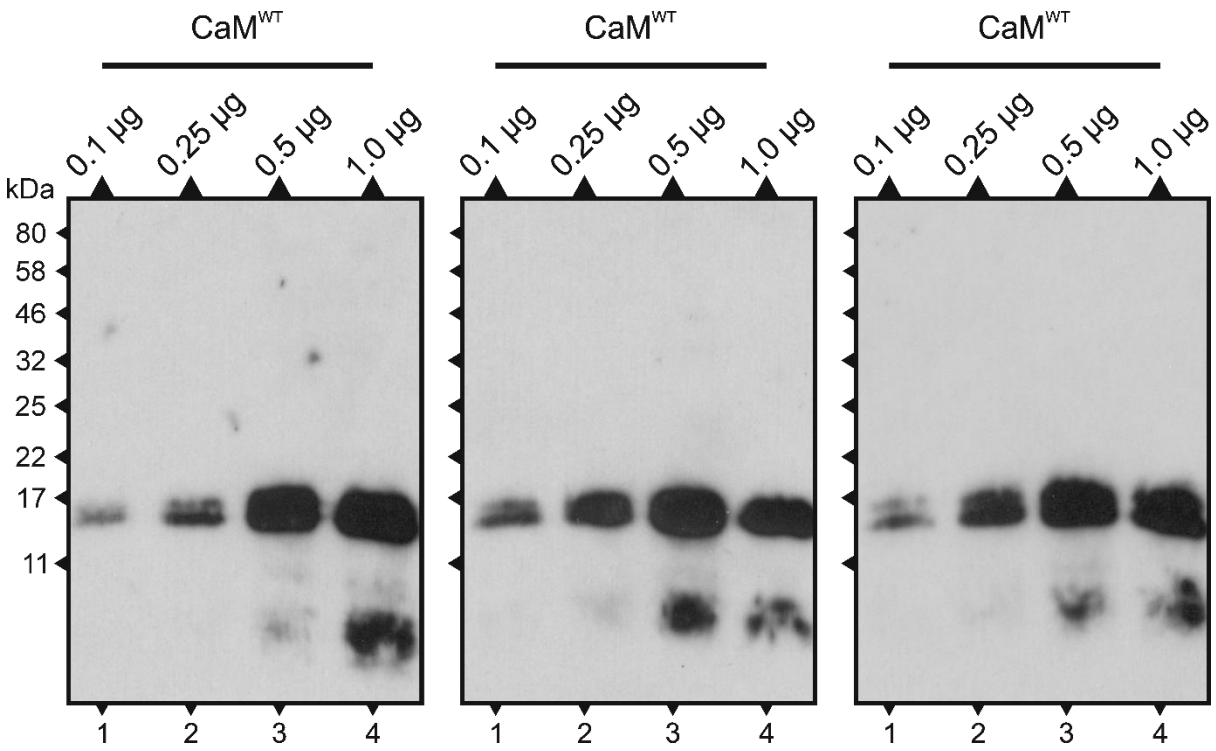

Appendix Figure XI Increased Quantities of CaM^{WT} Resolve as Several bands of Differing Molecular Weights All of which are Recognised by the Specific Monoclonal Antibody.

Increasing amounts of CaM^{WT} were separated with 7 % (w/v) SDS-PAGE gels alongside Color Prestained Protein Standard (NEB) on three occasions. All panels Lane 1: 0.1 µg CaM^{WT} Protein Marker (NEB), Lane 2: 0.25 µg CaM^{WT} Lane 2: 0.5 µg CaM^{WT} Lane 2: 1.0 µg CaM^{WT}. Primary Mouse anti-CaM monoclonal (1:10,000) Secondary HRP anti Mouse polyclonal (1:10,000). Exposure 20s.

Appendix IV Analysis of Protein Crystals

The plates were monitored for changes and crystal growth at increasing intervals using a CrysCam Digital Microscope (Art Robbins Instruments). Under magnification with a standard binocular microscope, each crystal was harvested with a CryoCap™ mounted LithoLoopTM (Molecular Dimensions) and frozen in liquid nitrogen. Remaining in liquid nitrogen the loop was placed in a pre-chilled Magnetic CryoVial which was then stored until use in a pre-chilled puck.

Harvested crystals were transferred to the National Synchrotron facility at Diamond Light Source, Oxfordshire. X-ray diffraction data at 100 K and a wavelength of 0.98 Å was collected using an ADSC Q315 CCD X-ray detector (Area Detector Systems Corp). Crystallographic software packages in the Collaborative Computational Project, Number 4, (CCP4) suite (Winn *et al.*, 2011) were used to collect and refine X-ray diffraction data to produce crystal structure models. The reflection intensities were estimated using XIA2 (Winter, 2010). SCALA (Evans, 2006) was used to scale, reduce and analyse the data. The structures were solved by molecular replacement with *Phaser* (McCoy *et al.*, 2007) and sequences were adjusted with COOT (Emsley *et al.*, 2010). The models were refined with REFMAC5 (Murshudov *et al.*, 2011). The PyMOL Molecular Graphics System (Schrodinger, 2015) was used to generate images of the crystal structures. X-ray diffraction, data collection and processing were performed by Dr.Pierre Riskallah (School of Medicine, Cardiff University).